

UNDERSTANDING THE RELATIONSHIPS BETWEEN LOCAL DYNAMICS AND
PHYSICAL STABILITY OF IgG1 ANTIBODIES: EFFECTS OF EXCIPIENTS, SALTS AND
MUTATIONS

By

Ranajoy Majumdar

M.S., Pharmaceutical Chemistry, 2011, The University of Kansas, Lawrence, Kansas.

M.S., Industrial Pharmacy, 2009, The University of Toledo, Toledo, Ohio.

B.S., Pharmaceutical Technology, 2007, Jadavpur University, Kolkata, India.

Copyright 2014

Submitted to the graduate degree program in Pharmaceutical Chemistry and the Graduate
Faculty of the University of Kansas in partial fulfillment of the requirements for the degree of
Doctor of Philosophy.

Chairperson - David B. Volkin, Ph.D.

David D. Weis, Ph.D.

Thomas Tolbert, Ph.D.

Teruna J. Siahaan, Ph.D.

Eric Deeds, Ph.D.

Date Defended: August 21, 2014

The Dissertation Committee for Ranajoy Majumdar
certifies that this is the approved version of the following dissertation:

UNDERSTANDING THE RELATIONSHIPS BETWEEN LOCAL DYNAMICS AND
PHYSICAL STABILITY OF IgG1 ANTIBODIES: EFFECTS OF EXCIPIENTS, SALTS AND
MUTATIONS

Chairperson - David B. Volkin, Ph.D.

Date approved: August 21, 2014

ABSTRACT

Immunoglobulins are large multi-domain and multi-functional proteins that are increasingly being developed as biologic drugs to bind to a wide variety of therapeutic targets. The immunoglobulin G1 class of molecules represents the largest class of therapeutic monoclonal antibodies (mAbs) currently under preclinical and clinical development. One of the major challenges in developing antibodies as drugs is their physical instability caused by various processing, storage and handling related stresses which can lead to aggregation and loss of efficacy. Immunoglobulins are dynamic molecules whose motions are important for their biological function and stability. It is currently difficult to predict the effects of minor process or formulation changes on the higher order structure and dynamics of mAbs using currently available analytical techniques. Hence new analytical techniques are needed to better understand the effects of such changes on the structure and dynamics of mAbs, especially within pharmaceutical dosage forms containing excipients. This dissertation work explored the effects of certain pharmaceutical excipients and three sodium salts from the Hofmeister series on the changes in thermal stability, storage stability and local dynamics of an IgG1 mAb. Changes in local dynamics of the mAb were explored at peptide level resolution using hydrogen-deuterium exchange mass spectrometry. Preliminary correlations were established between changes in dynamics of particular segments in the C_H2 domain of the IgG1 mAb and decreased thermal stability as well as higher aggregation propensity of the IgG1 mAb in presence of destabilizing excipients and salts. This dissertation work also explored the mechanism behind the relative decrease in physical stability due to YTE (M255Y/S257T/T259E) triple mutation in the C_H2 domain of a different IgG1 mAb (that was shown in previous work to result in extended in-vivo half-life due to changes in interaction with FcRn receptors). The YTE mutation induced

decreases in physical stability of the IgG1 mAb which correlated with changes in local dynamics of the same particular segment in the C_H2 domain described above in the presence of destabilizing excipients and salts. Hence, changes in dynamics of specific local segments within the C_H2 domain of IgG1 mAbs identified in this work may serve as a general indicator for changes in physical stability for other IgG mAb drug products. By better understanding the root causes of mAb physical destabilization, more rational design of antibody formulations and/or protein engineering approaches are now possible to improve the pharmaceutical stability properties of mAbs.

Dedicated to:

My parents

Rathindra Nath & Ranu Majumdar

and

my brother

Ranadeb Majumdar

ACKNOWLEDGEMENTS

The accomplishments described in this thesis would not have been possible without the direct or indirect support of several gifted folks. First and foremost, I would like to sincerely thank my thesis advisor, Dr. David Volkin for his support, patience, friendship and guidance throughout my dissertation research in the last four and half years. I have learnt immensely from interacting with him and I admire his organization skills, enthusiasm for science and willingness to share his scientific wisdom.

I would like to sincerely thank my thesis co-advisor, Dr. David Weis for his guidance and lessons in performing laboratory research as well as writing and presenting scientific findings. I have learnt a lot over the years from our regular conversations in and out of the lab and I admire his enthusiasm for science and attention to details in research and presentations.

I want to thank Dr. Thomas Tolbert, Dr. Teruna Siahaan, and Dr. Eric Deeds for agreeing to serve on my dissertation defense committee. Thank you very much for sparing time to evaluate my thesis research. I would like to thank all the faculty in the department of Pharmaceutical Chemistry for offering very good coursework that helped me master some of the basic scientific principles that I used later on in my research work. I would also thank Dr. Jianwen Fang and Dr. Yaping Fang of the Applied Bioinformatics laboratory KU for developing the R script used to generate the deuterium uptake curves shown in this thesis.

I would like to thank Dr. Russell Middaugh for his lessons on protein biophysics and protein science in general throughout my graduate study at KU. I have learnt immensely by interacting with him as well as from our lab meetings and coursework. I want to thank Dr. Sangeeta Joshi for her support, enthusiasm and friendship throughout my time at KU. I have learnt a lot by

interacting with the past and present members of the Macromolecule and Vaccine Stabilization Center (MVSC). I thank the past and present members of MVSC for the friendship and willingness we shared to support and learn from each other whenever needed. The wide variety of projects at MVSC over the last five years contributed to the richness of my learning about protein biotherapeutics and vaccines. I acknowledge financial support from MedImmune and Kansas Bioscience Authority for all the research work presented in this thesis.

It has been possible for me to pursue this research because of all the lessons I received from my earlier teachers. Hence, I thank my teachers from South Point School, and Jadavpur University at Kolkata, India and the University of Toledo, Ohio for my intellectual development.

Finally, I would like to thank my family for their unwavering support and inspiration for everything I have achieved to date. My parents taught me to value knowledge and opportunity. They always supported my endeavors and wanted me to succeed. I share a strong friendship with my brother who has always supported me through thin and thick. Thank you all for believing in me and allowing me to pursue my dreams. I dedicate this accomplishment to my family.

TABLE OF CONTENTS

Chapter 1: Hydrogen-deuterium exchange mass spectrometry as a new analytical tool for stabilization and formulation development of therapeutic monoclonal antibodies.....1

1.1 Introduction.....	2
1.2 Fundamentals of amide hydrogen exchange in proteins.....	5
1.3 Description of H/D-MS method applied to monoclonal antibodies.....	8
1.3.1 Automated sample preparation and data acquisition.....	9
1.3.2 H/D-MS Data Analysis.....	14
1.4 Case studies of the application of H/D-MS to formulation development of mAbs....	18
1.4.1 Impact of chemical modifications on mAb local dynamics.....	19
1.4.2 Impact of environmental stresses on mAb local dynamics.....	23
1.4.3 Impact of formulation additives on mAb local dynamics, conformational stability and aggregation.....	25
1.5 Aggregation hotspot identification in mAbs using H/D-MS.....	29
1.6 Challenges and opportunities for the H/D-MS technique as applied to mAb formulation development.....	31
1.6.1 Analytical technology challenges.....	31
1.6.2 MAb formulation development challenges.....	33
1.7 Conclusions.....	35
1.8 References.....	37

Chapter 2: Minimizing carry-over in an online pepsin digestion system used for the H/D exchange mass spectrometric analysis of an IgG1 monoclonal antibody.....63

2.1 Introduction.....64

2.2 Materials and Methods.....66

 2.2.1 Reagents and materials.....66

 2.2.2 Sample preparation.....66

 2.2.3 Chromatography and mass spectrometry.....66

 2.2.4 Peptide identification.....68

 2.2.5 Pepsin column washing.....69

 2.2.6 Pepsin column stress test.....69

 2.2.7 Data processing.....69

2.3 Results and Discussion.....69

 2.3.1 Online digestion is the major source of peptide carry-over.....71

 2.3.2 Pepsin column washing decreases peptide carry-over.....73

 2.3.3 Pepsin column washing does not degrade pepsin column performance.....74

 2.3.4 Basis of the carry-over.....74

2.4 Conclusions.....76

2.5 References.....78

Chapter 3: Correlating Excipient Effects on Conformational and Storage Stability of an IgG1 Monoclonal Antibody with Local Dynamics as Measured by Hydrogen-Deuterium Exchange Mass Spectrometry.....90

3.1 Introduction.....91

3.2 Materials and methods.....93

 3.2.1 Materials.....93

 3.2.2 Differential scanning calorimetry.....94

 3.2.3 Storage stability study.....94

 3.2.4 Size exclusion high performance liquid chromatography.....95

 3.2.5 Preparation of deuterated formulation buffers.....96

 3.2.6 Hydrogen/deuterium exchange mass spectrometry (H/D-MS).....98

 3.2.7 MS data processing and analysis.....99

 3.2.8 Construction of the homology map of mAb-B.....99

3.3 Results.....99

 3.3.1 Sucrose increases whereas arginine decreases the T_{onset} and T_m temperatures of mAb-B.....99

 3.3.2 Arginine decreases whereas sucrose increases the accelerated storage stability of mAb-B.....100

 3.3.3 Effect of excipients on the local flexibility of mAb-B in solution.....102

3.3.3.1 mAb-B in control sample (0.1 M NaCl).....	102
3.3.3.2 Identifying the effects of excipients on local backbone flexibility of mAb-B.....	103
3.3.3.3 Arginine alters the local flexibility of certain regions of mAb- B.....	105
3.3.3.4 Sucrose causes small global changes in the flexibility of the mAb- B.....	105
3.3.4 H/D exchange experiments in the presence of higher concentration of excipients.....	106
3.4 Discussion.....	107
3.4.1 Physical stability of mAb-B in the presence of arginine and sucrose.....	107
3.4.2 Effects of excipients on intrinsic exchange.....	108
3.4.3 Sucrose effects on mAb-B physical stability and local flexibility.....	110
3.4.4 Arginine effects on mAb-B physical stability and local flexibility.....	112
3.4.5 mAb-B physical stability and local flexibility of segments within the C _H 2 domain.....	114
3.5 References.....	117
Chapter 4: Effects of Salts from the Hofmeister Series on Conformational Stability, Aggregation Propensity, and Local Flexibility of an IgG1 Monoclonal Antibody.....	185
4.1 Introduction.....	186
4.2 Materials and Methods.....	189
4.2.1 Materials.....	189

4.2.2 Differential Scanning Calorimetry (DSC).....	189
4.2.3 Storage Stability and Analysis by Size Exclusion Chromatography (SEC).....	190
4.2.4 Deuterated labeling buffer preparation.....	190
4.2.5 H/D-MS.....	191
4.2.6 MS Data Analysis.....	192
4.2.7 Homology modeling of mAb-B.....	193
4.3 Results.....	193
4.3.1 Effect of salts on the conformational stability of mAb-B.....	193
4.3.2 Effect of salts on aggregation during storage of mAb-B.....	194
4.3.3 Backbone flexibility of mAb-B in 0.1 M NaCl.....	195
4.3.4 Identifying the effects of salts on local backbone flexibility of mAb-B...	196
4.3.5 The effects of 0.5 M chloride.....	198
4.3.6 The effects of 0.5 M sulfate.....	198
4.3.7 The effects of 0.5 M thiocyanate.....	199
4.3.8 Overlapping effects of anions.....	199
4.3.9 The effects of salt concentration on mAb-B local flexibility.....	199
4.3.10 Reproducibility of H/D-MS data	200
4.4 Discussion.....	201

4.5 References.....	209
Chapter 5: Correlations between changes in conformational dynamics and physical stability in a mutant IgG1 mAb engineered for extended serum half-life.....	304
5.1 Introduction.....	305
5.2 Materials and Methods.....	308
5.2.1 Materials.....	308
5.2.2 Differential scanning calorimetry (DSC).....	309
5.2.3 Accelerated storage stability study and analysis by size exclusion chromatography (SEC).....	309
5.2.4 Preparation of deuterated labeling buffers.....	310
5.2.5 Hydrogen/deuterium-exchange mass spectrometry.....	310
5.2.6 Mass spectrometry data analysis.....	311
5.2.7 Construction of the homology model.....	312
5.3 Results.....	312
5.3.1 YTE mutation decreased the conformational stability of only the C _{H2} domain.....	312
5.3.2 YTE mutation increased the aggregation propensity of mAb-E under accelerated storage conditions.....	313
5.3.3 Identifying the effects of YTE mutation on the backbone flexibility.....	314

5.3.4 The YTE mutation caused localized increases in backbone flexibility at pH 6.0.....	315
5.3.5 Mutation-induced differences in local flexibility at pH 7.4 were similar to differences at pH 6.0.....	316
5.3.6 Backbone flexibility of the peptide segments containing the YTE mutation.....	316
5.4 Discussion.....	317
5.5 References.....	322
Chapter 6: Conclusion and future work.....	396
6.1 Overview.....	397
6.2 Chapter summaries and future work.....	397
6.2.1 Chapter 2.....	398
6.2.2 Chapter 3.....	398
6.2.3 Chapter 4.....	400
6.2.4 Chapter 5.....	402
6.3 References.....	404

List of Tables

Table 2.1: Size distribution and number of IgG1 mAb peptic peptides ¹ before and after stress test of immobilized pepsin column.....	82
Table 3.1: Effect of excipient concentration on thermal onset temperature (T_{onset}) and thermal melting temperatures ($T_{\text{m}1}$, $T_{\text{m}2}$, and $T_{\text{m}3}$) for mAb-B as measured by DSC.....	129
Table 3.S1: Ordinal peptide numbers matched to their location identities.....	130
Table 4.1: Effect of salt type and concentration on thermal unfolding transitions (T_{m}) and onset of thermal unfolding (T_{onset}) for mAb-B as measured by DSC.....	223
Table 4.S1: Locations of peptides based on their ordinal numbers.....	224
Table 5.1: Thermal stability of mAb-A and mAb-E at pH 6.0 and pH 7.4 indicated by the melting onset temperature (T_{onset}) and the melting transitions ($T_{\text{m}1}$, $T_{\text{m}2}$, and $T_{\text{m}3}$) as measured by DSC.....	331
Table 5.S1: Segment location in the primary sequence of mAb-A or mAb-E corresponding to peptide numbers assigned based on segment midpoint calculated in ascending order from N-to-C termini of the heavy followed by the light chain of mAb-A/mAb-E.....	332
Table 5.S2: Possible glycoforms of mAb-A and mAb-E are shown according to the intact mass spectra of both the mAbs.....	337

List of Figures

Figure 1.1 Schematic representation of the H/D-MS experimental workflow for a typical IgG mAb.....	51
Figure 1.2 Schematic representation of the H/D-MS data processing workflow for a typical IgG mAb.....	53
Figure 1.3 Statistical analysis of H/D-MS data to identify significant changes in local dynamics of a mAb.....	55
Figure 1.4 H/D exchange differential plots for mAb1 heavy chain (HC, Panel A) and light chain (LC, Panel B).....	56
Figure 1.5 Representation of H/D exchange data mapped onto primary sequence.....	57
Figure 1.6 (A) Relative deuterium uptake differences for all peptide segments of an IgG1 mAb in the presence of different excipients and salts as measured by H/D-MS at each deuterium exposure time. (B) Effects of excipients and salts on the H/D exchange of the mAb plotted onto a homology model of the IgG1 mAb.....	59
Figure 1.7 Potential aggregation hotspot in the C _{H2} domain of IgG mAbs as identified by H/D-MS.....	61
Figure 2.1: Flow diagram of the LC/MS system for online digestion with an immobilized pepsin column used for carry-over studies.....	83
Figure 2.2: Carry-over from the online digestion of an IgG1 monoclonal antibody with an immobilized pepsin column arises from online digestion.....	84
Figure 2.3: Injections of different combinations of two wash cocktails decreased the number of consensus peptides (see Fig 2c) detected as carry-over in the digestion blanks.....	85

Figure 2.4: A pepsin column stress test consisting of 200 alternating injections of wash cocktails 1 and 2 did not cause a substantial decrease in the number of detected consensus peptides (see Fig 2c) in the online digestion of an IgG1 monoclonal antibody.....	86
Figure 2.5: A pepsin column stress test consisting of 200 alternating injections of wash cocktails 1 and 2 did not cause a substantial decrease in the MS response of the consensus peptides.....	87
Figure 2.6: Carried-over peptides are indistinguishable from peptides that were not carried over on the basis of (a) mass, (b) MS response, (c) pI, and (d) hydrophobicity.....	88
Figure 3.1: Representative DSC thermograms of mAb-B in different formulations (20 mM citrate-phosphate buffer, 0.1 M NaCl, pH 6.0) containing the indicated level of excipients.....	134
Figure 3.2: SEC analysis of mAb-B samples in different formulations before and after storage at 55 °C for 4 weeks.....	136
Figure 3.3: Effect of sucrose and arginine on accelerated and long term storage stability of mAb-B.....	138
Figure 3.4: Effect of presence and absence of arginine and sucrose on the deuterium uptake of six peptides from different regions of mAb-B as measured by H/D-MS.....	139
Figure 3.5: Mass difference plots of mAb-B in the presence of 0.5 M arginine and 0.5 M sucrose compared to the control as measured by H/D-MS.....	140
Figure 3.6: Effect of arginine and sucrose on the local flexibility of mAb-B as measured by H/D-MS.....	142
Figure 3.S1: Deuterium update curves for 137 peptides of mAb-B. The first set of curves is for mAb-B labeled in presence of arginine and the second set of curves is for mAb-B labeled in presence of sucrose.....	144

Figure 3.S2: Scatter plots of the mass increase for the 43 peptides of mAb-B with increasing concentration of either sucrose or arginine (0.5, 1.0, and 1.35 M) containing 0.1 M NaCl along with the control (0.1 M NaCl).....	182
Figure 4.1: Representative DSC thermograms of mAb-B in 20 mM citrate-phosphate buffer pH 6.0 containing indicated concentrations of different salts.....	228
Figure 4.2: MAb-B aggregation during storage at different temperatures as monitored by SE-HPLC.....	230
Figure 4.3: Effect of different salts on the deuterium uptake in six segments from different domains of mAb-B.....	232
Figure 4.4: Local flexibility of mAb-B, as measured by H/D exchange in 0.1 M NaCl at pH 6.0.....	233
Figure 4.5: Relative deuterium uptake differences for all 137 segments of mAb-B in the presence of 0.5 M concentration of the salts relative to the control solution (0.1 M sodium chloride) as measured by H/D-MS at each deuterium exposure time.....	235
Figure 4.6: Effects of salts on the flexibility of mAb-B relative to the control (0.1 M sodium chloride), as measured by H/D-MS plotted onto a homology model of mAb-B.....	237
Figure 4.S1: Primary sequence coverage map for (A) Heavy chain and (B) Light chain of mAb-B based on 137 identified peptides.....	239
Figure 4.S2: Distribution of number of replicates available across all data points.....	241

Figure 4.S3: Reproducibility of H/D-MS data from our experimental setup represented by the distribution of standard deviations for the mass increase across all time points and peptides of mAb-B from triplicate experiments (run on different days, N = 6473).....	242
Figure 4.S4: Standard deviation of deuterium uptake measurements does not depend on peptide size.....	243
Figure 4.S5: Deuterium uptake curves for the 137 segments from mAb-B in formulations containing 0.5 M chloride, sulfate or thiocyanate compared to the control (0.1 M chloride)....	244
Figure 4.S6: Plots of deuterium uptake vs. salt concentration for 43 segments of mAb-B.....	300
Figure 5.1: Representative overlay of DSC thermograms of mAb-A and mAb-E at (A) pH 6.0 and (B) pH 7.4.....	338
Figure 5.2: Accelerated storage stability of mAb-A and mAb-E after incubation at 50 °C for up to 28 days as measured by SEC.....	339
Figure 5.3: Effect of the YTE triple mutation on deuterium uptake of six peptide segments from mAb-A and mAb-E at (A) pH 6.0, and (B) pH 7.4.....	340
Figure 5.4: Differential deuterium uptake at five exposure times for 167 common peptide segments of mAb-E relative to mAb-A at pH 6.0.....	341
Figure 5.5: Differential deuterium uptake at five exposure times for 167 common peptide segments of mAb-E relative to mAb-A at pH 7.4.....	343
Figure 5.6: Effect of the YTE mutation (mAb-E) on the local flexibility of the native mAb (mAb-A) at pH 6.0 as measured by H/D-MS plotted on the homology models of (A) intact mAb-A and (B) Fc domain of mAb-A.....	345

Figure 5.7: Calculated intrinsic deuterium exchange rates of three peptide segments of mAb-A and mAb-E at pD 6.0 at 25 °C.....	347
Figure 5.S1: Peptide map of the (A) Heavy chain and (B) Light chain of mAb-A/mAb-E composed of 167 common segments covering the primary sequence of 96% of the HC and 92% of the LC.....	348
Figure 5.S2: Deuterium uptake plots of 167 common segments between mAb-A and mAb-E at pH 6.0.....	350
Figure 5.S3: Deuterium uptake plots of 167 common segments between mAb-A and mAb-E at pH 7.4.....	372
Figure 5.S4: Overlaid mass spectra of the two intact mAbs.....	394
Figure 5.S5: Reproducibility of H/D-MS data from our experimental setup as measured by pooling the standard deviations for mass increase measurement across all time points and peptides of mAb-B (chapters 3 and 4) and mAb-A (chapter 5).....	395

Chapter 1

**Hydrogen-deuterium exchange mass spectrometry as an emerging analytical tool for
stabilization and formulation development of therapeutic monoclonal antibodies**

1.1 Introduction

The IgG class of monoclonal antibodies (mAbs) represents the largest category of therapeutic protein candidates under clinical development.^{1,2} Antibodies are dynamic molecules with internal motions that are important for their biological function and stability. Monoclonal antibodies (mAbs) are large, multi-domain and multi-functional proteins that can be engineered to bind to a variety of therapeutic targets. An IgG molecule consists of two antigen binding (F_{ab}) regions, each containing a constant and variable domain from both the light and heavy chain, in the form of two arms attached by a proline-rich hinge region to the constant (F_c) region. The F_c region contains two constant Ig domains from each of two heavy chains including an N-linked glycosylation site. The F_c region is responsible for non-antigen binding biological activity and maintaining *in vivo* half-life. These regions are potentially flexible structures that lead to a wide range of possible conformations for IgG molecules. Dynamic motions of antibodies include whole molecule tumbling, rocking and breathing motions along with bending, flexing and rotational motions of the F_{ab} arms around the hinge region.³⁻⁶ However, the inter-relationships between regional and local dynamic motions and protein conformational stability are complex and is an active area of research.⁷

Therapeutic proteins such as mAbs are exposed to various environmental stresses during manufacturing, storage, and administration that can cause physical and chemical degradation. Hence, robust formulation strategies are needed to impart maximal stability to these proteins and to minimize degradation during long term storage (e.g., across the shelf life). From a pharmaceutical development perspective, it is also a major challenge to predict the effects of product or process changes on the higher-order structure and long term stability of mAb drug products as part of comparability assessments.⁸ One recent trend in the formulation development

field is to explore the interrelationships between antibody dynamics, conformational stability, and pharmaceutical stability.^{7,9-13} If direct relationships can be established between these variables, these relationships can lead to a better understanding of the implications of process and product changes on protein stability. This, in turn, would inform the design of improved mAb proteins and their formulations.

The global dynamics of monoclonal antibodies have been studied by various techniques such as high resolution ultrasonic spectroscopy, pressure perturbation calorimetry, red edge excitation shifts and time correlated single photon counting.^{7,9,14} Data visualization tools such as empirical phase diagrams have been used to compare changes to the dynamic states of antibodies as a function of solution pH and temperature.¹⁰ In addition, classical biophysical techniques such as circular dichroism, fluorescence spectroscopy, ultraviolet absorption spectroscopy, Fourier transform infrared spectroscopy and light scattering have been widely used to characterize the higher-order structural integrity and conformational stability of proteins.¹⁵ These biophysical methods provide global information about the overall dynamics and conformational stability of proteins.

One disadvantage of measuring global dynamics of antibodies is that there can be small-scale, local changes in dynamics due to a variety of factors that may go undetected when averaged across the entire molecule.¹² However, one or a few such local changes in dynamics may be important for the stability or biological functions of an antibody. Hence, higher resolution analytical techniques capable of detecting and localizing small scale changes in dynamics in an antibody are important for a more comprehensive assessment of changes in protein dynamics and stability. Two well-established high resolution techniques that have previously been used to investigate local structural changes in smaller therapeutic proteins are

nuclear magnetic resonance (NMR) spectroscopy^{16,17} and X-ray crystallography^{18,19}. Although great advances have been made in terms of applicability of these techniques to pharmaceutical development, practical limitations remain for the analysis of structural dynamics of an entire monoclonal antibody molecule under formulation conditions. For example, some of the challenges in NMR analysis of mAbs are the requirement for isotopic labelling (¹⁵N, ¹³C, or ¹⁹F) of the mAb and the difficulty of spectral crowding due to the large size of mAbs. X-ray crystallography data may not necessarily reflect antibody dynamics in complex solution buffers and the technique requires the generation of antibody crystals, which can sometimes be difficult to produce. Temperature factors for individual residues can be obtained as a measure of flexibility but are again limited to the solid state. Thus, there is a need for faster and more practical, higher resolution analytical techniques that are sensitive enough to detect changes in local structural dynamics in antibody molecules formulated in pharmaceutical dosage forms containing a wide range of protein concentrations and stabilizing excipients.

Hydrogen-deuterium exchange coupled to mass spectrometry (H/D-MS) potentially addresses this need.²⁰ This method utilizes the variable exchange rates of amide hydrogens along the protein backbone to provide information about the local dynamics of a protein. Hydrogen/deuterium exchange in proteins was first studied using gravimetric techniques by Hvidt and Linderstrom-Lang in the 1950s.²¹ Since then molecular sieve chromatography in tritiated water as well as several spectroscopic techniques such as infrared spectroscopy,²² NMR,^{23,24} and most recently mass spectrometry^{25,26} have been used to measure hydrogen exchange kinetics in proteins. H/D-MS has shown promising results for analysis of dynamics of large proteins such as IgG antibodies with high sensitivity, low sample requirements and the ability to analyze proteins in complex formulation buffers.^{12,13,20,27} Protease digestion using an

acid resistant protease such as pepsin along with reduction of disulfide bonds at low pH has enabled peptide level analysis of mAb structure at a resolution of 5-20 amino acids.²⁶

There has been a steady growth in the last five years in the number of reports describing the use of H/D-MS to explore dynamics of monoclonal antibodies and antibody fragments. For example, H/D-MS has recently been used to assess changes in higher order structure of mAbs as a result of deglycosylation,²⁰ freeze-thaw and thermal processing,²⁸ chemical modifications,^{29,30} post-translational modifications,²⁷ formulating with pharmaceutical excipients and salts from the Hofmeister series,^{12,13} targeted mutations,^{31,32} and drug conjugation to free inter-chain cysteine residues³³. This chapter summarizes the use of H/D-MS technique in advancing our understanding of the role of local dynamics in modulating antibody physical stability and implications for stabilization and formulation development of therapeutic mAbs.

1.2 Fundamentals of amide hydrogen exchange in proteins

When a protein is incubated in D₂O, its labile hydrogens will exchange with the solvent deuterium. There is nearly instantaneous exchange with deuterium by amine, carboxyl, and hydroxyl groups of amino acid residues, but these sites readily revert to hydrogen upon exposure to H₂O during LC separation (see below). In contrast, the amide hydrogens of the polypeptide backbone exchange much more slowly at rates strongly influenced by the folded structure of the protein.^{21,34-37} Amide hydrogens within the folded β -sandwich structure of Ig domains that are solvent shielded and strongly hydrogen bonded to neighboring hydrogen bond acceptors are expected to exchange slowly. In contrast, the amide hydrogens on the surface or in the unstructured loop regions of an antibody that are solvent exposed and weakly hydrogen bonded are expected to exchange faster. The fastest exchanging amide hydrogens in a mAb can exchange in milliseconds at physiological pH^{38,39} while the slowest exchanging amide hydrogen

may take many months to exchange because the central domain regions of mAbs are known to have a tightly folded and stable structure. Hence the difference in observed rates of deuterium exchange can provide valuable information about the local structure and dynamics of proteins such as mAbs.

Amide H/D exchange in the absence of any higher order structure is referred to as intrinsic or chemical exchange (*i.e.*, k_{ch} in equations 1-4). The rate of intrinsic exchange⁴⁰⁻⁴² can be expressed as

$$k_{\text{ch}} = k_A[\text{H}_3\text{O}^+] + k_B[\text{OH}^-] + k_W[\text{H}_2\text{O}] \quad (1)$$

where k_A , k_B and k_W are the rate constants for acid-, base- and water-catalyzed amide deuterium exchange reactions. The rate of intrinsic exchange is strongly influenced by solution pH, temperature, neighboring side chains and solution components such as salts.^{38,39} The intrinsic exchange rate is predominantly base-catalyzed above pH 3.0 and predominantly acid-catalyzed below pH 2.3. Moving away from the minimum at a pH of approximately 2.5, the rate increases ten-fold for every unit of pH increase. A temperature increase of ~ 22 °C has a similar effect.⁴³

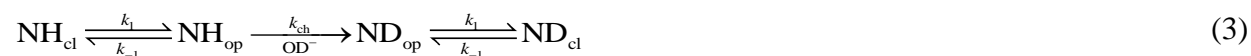
Proteins are known to exist as an ensemble of interconverting conformations in solution,⁴⁴⁻⁴⁶ and each amide hydrogen may therefore exist in folded and unfolded conformations at any point in time. Amide hydrogen exchange by folded proteins can be described by one of two distinct models: the two-process model and the local unfolding model. The two-process model,³⁷ proposes that amides in both folded and unfolded states can exchange. Amides in the folded state exchange due to very small-scale fluctuations in the protein's native state. These fluctuations, though small, are sufficient to bring solvent and catalyst (OD^- under physiological conditions) to the amide. Amides in globally unfolded states can also exchange. Hence, under the two-process model, the observed exchange rate (k_{obs}) for individual amide hydrogens in a protein

would be a sum of the exchange rate contributions from its folded (k_f) and unfolded (k_u) forms⁴⁷ as shown in Equation 2.

$$k_{\text{obs}} = k_f + k_u = (\beta + K_u) k_{\text{ch}} \quad (2)$$

Here β represent the probability of exchange from the folded state that is influenced by the strength of hydrogen bonding and solvent accessibility. K_u is the equilibrium rate constant for unfolding. k_{ch} is the chemical exchange rate constant for the particular amide hydrogen in the absence of any form of higher order protein structure (equation 1).

In contrast, the local unfolding model⁴⁸ proposes that the protein transiently occupies a locally unfolded state that fully exposes the amide to solvent and catalyst. The mechanism is illustrated in Equation 3. Breathing motions in proteins can transiently break amide hydrogen bonds in the folded state (NH_{cl}) allowing access of the catalyst (OD^- under physiological conditions) to the open backbone amide hydrogens in a locally unfolded conformation (NH_{op}).



$$k_{\text{obs}} = \frac{k_1}{k_{-1}} k_{\text{ch}} = K_{\text{op}} k_{\text{ch}} \quad (4)$$

The observed rate of exchange, as illustrated in Equation 3, depends on the dynamic equilibrium (K_{op}) between the open and closed H-bonded states and on the rate of intrinsic exchange (k_{ch}). The mechanism for exchange may not be universal for all amide hydrogens in a protein and can vary for individual amide hydrogens depending upon local fluctuation or unfolding reactions that present the individual amide hydrogen in the exchange competent state.³⁶ Furthermore, the mechanisms described here apply to proteins that undergo two-state unfolding. If there are long-lived unfolding intermediates in proteins, then their role would also need to be considered for a detailed mechanistic understanding of the observed deuterium exchange.

Under the local unfolding model, when $k_{ch} \gg k_{-1}$, the intrinsic exchange step is rate-limiting. This mechanism is referred to as the EX1 limit. EX1 exchange is often interpreted as evidence that deuterium exchange proceeds through global or subglobal unfolding of the protein. Although only a few proteins exchange by an EX1 mechanism under native conditions,⁴⁹ many proteins can be induced to undergo deuterium exchange by an EX1 mechanism by exposing the protein to denaturants.⁵⁰ Under native conditions, most proteins undergo exchange under the limit $k_{-1} \gg k_{ch}$, known as the EX2 limit. This kinetic limit implies that the opening and closing of a H-bond occurs many times before a successful deuterium chemical exchange. Deuterium exchange under the two types of kinetic regimes can easily be distinguished experimentally by their unique peptide mass spectral signatures.⁵¹ Under the EX2 exchange regime, a gradual increase in m/z of a peptide segment can be seen with increasing deuterium exposure. Upon EX1 exchange, two distinct spectral envelopes can be seen on the m/z scale.⁴⁹

1.3 Description of the H/D-MS method applied to monoclonal antibodies

H/D exchange experiments are typically performed to compare the effects of two or more conditions that can alter the local conformational dynamics of mAbs (e.g., physicochemical modifications, addition of perturbants, alteration of solution conditions, protein-protein or protein-ligand interactions, etc.). Protein amide hydrogen exchange reactions are typically performed at neutral or near-neutral pH for different lengths of time in either a continuous labeling protocol or for a single interval of time in a pulsed labeling experiment. In either case, a stock solution of protein, in H₂O solution, is rapidly diluted with a large excess of a D₂O solution to initiate exchange. After a predefined period of exchange, the H/D exchange reaction is quenched by reducing the pH to around 2.5 and lowering the temperature to ~0 °C where the intrinsic exchange rate is at a minimum. The half-life of intrinsic exchange under these quench

conditions is approximately 5000-fold slower than typical labeling conditions, pH 6.5 at 22 °C. In a continuous labeling experiment, the incorporation of deuterium into the protein is followed as a function of time by measuring deuterium uptake intervals in response to external perturbants.⁵² In a pulsed labeling experiment, the interval of exposure to D₂O is fixed. In the case of a rapid pulse (µsec – msec), such as in a protein refolding experiment, two or more distinct protein populations that are either folded, unfolded, or partially folded in response to the perturbant can be detected.⁵³ Continuous labeling experiments are used more widely than pulsed labeling primarily because the labeling time where differences will be most apparent between protein states can be difficult to predict *a priori*. Thus, casting a broad net of widely-spaced labeling times, typically spanning a range between ~10¹ and ~10⁵ seconds (i.e., over ~1 day), maximizes the probability of detecting differences between two protein states. When another experimental parameter such as ligand or perturbant concentration is varied, pulsed labeling is often used.

1.3.1 Automated sample preparation and data acquisition

A schematic representation of a typical H/D-MS experimental workflow to analyze the local dynamics of a mAb is shown in Figure 1.1. In the first step, the H/D exchange reaction is initiated by mixing mAb stock solution (panel A) in an excess of deuterated formulation buffer at a precisely regulated temperature (ideally ± 0.1 °C). The deuterated solution can contain excipients whose concentrations should be adjusted such that the mixed mAb-labeling buffer solution contains the same formulation composition that is used in parallel for mAb conformational and pharmaceutical stability studies. The only difference is that D₂O has replaced H₂O. Excipients containing exchangeable hydrogens such as sugars or amino acids either need to be deuterated beforehand, or the number of exchangeable hydrogens needs to be accounted for

while preparing deuterated buffers to maintain uniform deuterium content across all conditions being compared.¹³ Moreover, the pH of all deuterated buffers should be carefully checked and reported either directly from a pH meter or after correction for the deuterium isotope effect.⁵⁴ Since the formulation components are subsequently washed out during LC-MS analysis, there is no limitation on their use with a few notable exceptions. For example, surfactants such polysorbates should not be included in the deuterium labeling buffer, or ideally even the protein stock solution, since they are difficult to remove from reversed-phase columns and traps and even trace amounts tend to suppress ionization at the ESI source of mass spectrometers. A recent report, however, describes a removal technique for non-ionic surfactants prior to MS analysis that is compatible with H/D-MS workflow.⁵⁵

The deuterium labeling continues for various times usually ranging from a few tens of seconds to many hours. Since mAbs are well-folded proteins, some regions of a mAb may not be fully deuterated even after a day of incubation in deuterated buffers at room temperature.^{12,13} In the second step of Figure 1.1, mAb H/D exchange labeling (panel B) is quenched by reducing the pH of the final mixture to 2.5 by addition of concentrated acid such as hydrochloric, trifluoroacetic, or formic acids or a strong buffer such as phosphate. The temperature of the mixture is also lowered to ~ 0 °C. A denaturing agent (ex. guanidine HCl ~ 4 M for mAbs) and a reducing agent (ex. TCEP ~ 0.5 M for mAbs) are also included in the acidic quench buffer to unfold the mAb and rapidly reduce the disulfide bonds.

All of these steps are best accomplished with robotic autosamplers (such as the HDX-PAL from LEAP Technologies, NC) now widely used for protein H/D exchange sample preparation. These devices feature at least two independently temperature-controlled drawers, one for labeling (variable temperature) and the other for quenching (usually held just above 0

°C). Typically, each drawer can hold several trays containing 50-100 individual 0.5-2 mL autosampler vials. One tray each is used to hold vials containing the mAb stock solution, the deuterated labeling buffers, the labeling vials, and the quench buffer. Precise mixing and transfer of solutions from one vial to another are achieved by robotically controlled syringes. The quenched mAb solution is injected into a sample loop housed inside a refrigerated column compartment. The software that handles such autosamplers is capable of precisely performing any sequence of events for sample preparation such as syringe cleaning, dispensing protein into a vial, adding D₂O label, mixing, waiting for preset amounts of labeling time, transferring solution to a different vial containing quench solution, injection into the LC loop, and sending the signal to the LC-MS to start sample analysis. A schedule is built by the software that optimizes the time management during various steps of sample preparation thereby ensuring that the labeling for a comparatively long deuteration time point is started before initiating the labeling of a much shorter time point.

In the third step of Figure 1.1, the quenched, reduced, and denatured mAb (panel C) is digested using an acid resistant protease with high activity, the most popular being pepsin. This is achieved using a loading pump to carry the mAb sample from the sample loop, through an immobilized protease column^{56,57}, and then onto a reversed-phase peptide trap for concentration and desalting. Digestion with an immobilized pepsin column offers higher efficiency of digestion than in-solution digestion.⁵⁶ Typically, mAbs are completely digested during an approximately one minute passage through an immobilized pepsin column. A disadvantage of non-specific proteases is that they tend to produce many more peptides than specific proteases; the resulting peptides often have overlapping cleavage sites. However, reproducible digestion conditions yield reproducible peptide maps.⁵⁸

In the fourth step of Figure 1.1, a gradient pump (HPLC or UHPLC) is used to elute the peptides (panel D) from the trap, through a reversed phase column for peptide separation, and into a mass spectrometer for peptide mass analysis. The valves, columns, and tubing are housed inside a refrigerated compartment maintained at $\sim 0\text{ }^{\circ}\text{C}$. The mAb sample digestion, trapping, separation and elution are achieved using precooled ($\sim 0\text{ }^{\circ}\text{C}$) mobile phase at pH ~ 2.5 (e.g., 0.1 vol% formic acid has a pH of 2.5). The low temperature and pH ~ 2.5 throughout pepsin digestion, peptide trapping, and separation minimize peptide back-exchange, i.e. amide D to H conversion, during sample analysis. Following data acquisition by the mass spectrometer, the raw data for all peptides, as shown in the representative example in panel E, are provided in the form of a total ion chromatogram (TIC) which is a plot of ion count vs. retention time and mass spectra in the form of ion counts vs. mass to charge ratio (m/z).

Several experimental challenges are commonly faced during method development for the third and fourth steps. One such problem is resistance of a particular mAb towards pepsin digestion at $0\text{ }^{\circ}\text{C}$. In such cases, mAb digestion efficiency can be increased by increasing the temperature of the immobilized pepsin column either by placing it outside the refrigerated box at room temperature or placing it inside a protease column oven inside the refrigerated box.⁵⁹ However, increasing the temperature of the solution during pepsin digestion will lead to faster peptide back-exchange.

Another common challenge is carry-over of peptic peptides. Carry-over here refers to appearance of peptic peptides in subsequent blank LC runs following a sample injection. Carry-over is particularly problematic in H/D-MS measurements because the carried-over peptides undergo nearly complete back-exchange between LC-MS injections. Thus these carried-over peptides will appear as undeuterated features in subsequent LC-MS runs.⁶⁰ Carry-over can arise

from either the pepsin column⁶¹ or the reversed-phase trap and column.⁶⁰ Although an immobilized pepsin column offers better digestion efficiency than in-solution digestion, pepsin columns can also give rise to carry-over problems.⁶¹ Wash cocktails may be required to minimize carry-over originating from mAb digestion using an immobilized protease column; these solutions are designed to remove retained peptides while not degrading the enzymatic activity of the pepsin enzyme.⁶¹ In the fourth step, as shown in Figure 1.1, reversed-phase HPLC separation of hundreds of mAb peptic peptides is typically carried out using a steep gradient of acetonitrile over 5-10 min to minimize back-exchange. This type of gradient is unlike routine peptide mapping used for mAbs, where gradients are much shallower. Steep gradients increase the chance of carry-over on the trap and column. Hence, the chromatography cycle might require additional wash cycles at the end of the gradient to clean the reversed phase column to minimize carry-over.⁶⁰

Several experimental parameters discussed earlier determine the total amount of back-exchange after quenching the H/D exchange reaction and during LC-MS analysis. Back-exchange levels, when reported, usually vary between 5 and 40% depending on the peptide sequence.^{12,27,59} Higher deuterium loss may be unacceptable because valuable information about protein dynamics embedded in the amount of deuterium attached to amide nitrogen atoms may be lost. Back-exchange correction to normalize exchange to 100% can be applied by measuring back-exchange levels of fully deuterated mAb peptides under identical experimental conditions to the mAb H/D-MS experiments. The corrected average number of deuterons (D_0) gained by a peptide segment during an H/D exchange experiment is

$$D_0 = \frac{m - m_{0\%}}{m_{100\%} - m_{0\%}} \times N \quad (5)$$

where $m_{0\%}$, m , and $m_{100\%}$ denote the centroid m/z values of the undeuterated, partially deuterated, and fully deuterated peptide segment, respectively, and N denotes the number of exchangeable amide hydrogens.²⁶ Other approaches to correct for back-exchange include the use of reference peptides or internal standards to correct for deuterium loss.⁶² Correcting for back exchange, however, seems to offer only modest benefit. In practice, back-exchange is often monitored but not corrected for if the levels are within an acceptable range, since many H/D-MS experiments with mAbs compare two or more conditions “head to head”. Thus, the compared peptides generated from the mAb will have the same back-exchange levels and relative comparisons can be made without corrections.

1.3.2 H/D-MS Data Analysis

H/D exchange data analysis is illustrated schematically in Figure 1.2. In the first step, the raw LC-MS data (panel A) is processed to develop a peptic peptide map (panel B) for the mAb, ideally with high sequence coverage across all regions. The peptides from pepsin digestion are generally identified using a combination of accurate mass measurements and peptide fragmentation-based tandem MS measurements. Medium and high resolution mass spectrometers such as time-of-flight, quadrupole-time-of-flight, ion cyclotron resonance (ICR), or orbitrap mass spectrometers are beneficial for H/D exchange measurements because of their ability to resolve the isotopic structure of highly-charged ions and because of their high mass accuracy. It should be noted that the spectra of peptides that elute at nearly identical retention time and very close m/z values tend to partly or fully overlap upon deuteration. An additional benefit of high-resolution mass analyzers is their ability to resolve partially overlapping isotope profiles.

Some peptides may lose MS signal intensity due to ion suppression. If spectral quality is poor, such peptides get excluded from later steps of H/D-MS data processing. It is therefore

beneficial to have a fairly large number of redundant peptides (e.g., greater than 200 peptides for a mAb) with overlapping sequence and high total primary sequence coverage (> 95%) when constructing the initial peptide map in the first step. This helps to preserve relatively high primary sequence coverage across all regions at the end of H/D-MS data processing (for example, >85-90% coverage with ~100-200 peptides). High sequence coverage allows analysis of H/D exchange data for the majority of the protein's primary sequence. Moreover, it is typical to have peptides spanning 3 to 25 residues in the peptide map. Peptides larger than ~30 residues are less useful because the spatial resolution is poor. At the end of the first step (shown in Panel B), peptide retention time, mass and/or sequence are tabulated for all of the peptic peptides of the mAb that will be used in the peptide map.

The second step of data processing involves identification of deuterated peptides based on the retention time of the undeuterated peptide and range of possible m/z values. As shown in panel C of Figure 1.2, individual peptide spectra stacked with increasing deuterium exposure times show EX2 kinetics, i.e., a gradual shift of the spectral envelop towards higher m/z values (peptides that exhibit EX1 kinetics will have a bimodal profile.)⁴⁹ In the third step, the average masses of the deuterated peptide segments are calculated after peak picking (as shown by red dots in panel D) across the expected m/z range and retention time window. The second and third steps are generally accomplished using software specifically designed for H/D exchange mass spectrometry. Available software options include commercial products such as HDExaminer (Sierra Analytics) and DynamX (Waters), and free software such as HDX-Analyzer⁶³, HX-Express,⁶⁴ Hydra⁶⁵ and HDX WorkBench⁶⁶, some of which are also open-source. Programs such as DynamX are compatible with LC-MS data from one vendor only. Programs such as HDExaminer read all common vendor formats and other programs like Hydra read open-source

data formats such as mzXML, making all of these compatible with data from multiple types of instruments. In general, the information required for processing H/D-MS data are a list of peptides, retention times, and the sequence of the protein. The LC-MS data files need to be uploaded to the software along with assignment of labeling times for each data file. While most MS measurements of peptides focus on the monoisotopic peak, incorporation of deuterium obscures this feature, as shown in panel C of Figure 1.2. For this reason, the average or centroid m/z value of peptide isotopic clusters is measured:

$$\frac{\sum_i \left(\frac{m}{z}\right)_i I_i}{\sum_i I_i} \quad (6)$$

where I_i represents the spectral intensity of the i th channel in the peptide spectrum, averaged across the chromatographic band.

Although the peak picking feature is fully automated in most software packages, all of them allow some level of manual peak picking or manual adjustment of the retention time window and isotopic envelope used for centroid m/z calculation. These features allow an analyst to correct processing errors. In a typical H/D-MS workflow, a large number of peptides are separated chromatographically in a relatively short time window (usually 5-10 min). Hence there is always a possibility that two or more peptides with similar m/z will co-elute. The result is totally or partially overlapped mass spectra. Although software can usually identify such cases of spectral overlap using a scoring algorithm, they are in practice not completely reliable. Hence, as shown in the fourth step of Figure 1.2, the data must be inspected and curated by experts in order to have full confidence in peak picking and centroid m/z calculation for all peptides. Curating the data generally involves peptide retention time alignment to get better matching of calculated and observed mass spectra and exclusion of peptides that have spectral overlap or poor spectral

quality. It should be noted that many of the peptides that are excluded during manual curation of the data can be detected reliably and reproducibly in the undeuterated sample. Exclusion of peptides from the data set during H/D exchange data processing may lead to lower mAb sequence coverage compared to the initial peptide map of the mAb. The mass increase values (panel E) for each peptide segment are automatically calculated. In the fifth step, the mass increase values for each peptide are plotted (panel F) corresponding to predefined deuterium exposure times or displayed as a deuteration percent heat map using the protein sequence.

Ultimately, the goal in most H/D exchange efforts is to identify specific peptides that exhibit altered H/D exchange in response to some change in the protein or its solution conditions. To identify significant changes, statistical analysis usually needs to be performed. A complete review of all the statistical approaches used is beyond the scope of this chapter. Some examples include the use of pair-wise t tests,⁶⁷ analysis of covariance,⁶³ and Tukey's test for multiple comparisons.⁶⁸ The method outlined by Houde et. al.⁶⁷ to assess comparability of mAb local dynamics in multiple formulations or different processing conditions is illustrated in Figure 1.3. In the first step, variances in replicate measurements of deuterium uptake (Panel A) are pooled to define a confidence interval at the desired level (*e.g.*, 99%) for significant differences in deuterium incorporation in a specific peptide segment at a certain deuterium exposure time. First, the 99th percentile (or another confidence level) of variance is determined ($s_{99\%}^2$). Next, random error propagation is applied to estimate the 99% confidence interval for a deuterium uptake difference between two conditions, for example one test formulation and a control formulation: $s_{CI}^2 = s_{99\%}^2 + s_{99\%}^2$. This method was used in our laboratories to compare the effects of different excipients and salts on the local dynamics of an IgG1 mAb.^{12,13} Panel B in Figure 1.3 shows the deuterium uptake differences between two conditions plotted as bar charts and the 99%

confidence interval as dotted lines. Mass difference values exceeding the 99% confidence interval are regarded as significant.

To better visualize differences in deuterium uptake across the ~100-200 individual peptides from the mAb, the significant differences can be qualitatively mapped (third step in Figure 1.3) onto a homology model (Panel C in Figure 1.3) based on a known X-ray crystal structure. A simple mAb homology model can be obtained by simply aligning the mAb sequence against the solved mAb structure. Homology models for mAbs can also be prepared using software such as Modeller⁶⁹ (freely available) or Discovery Studio (commercially available from Accelrys, San Diego, CA). In case of significant differences between the sequence of the specific mAb being analyzed and the sequence of the antibody in the homology model, structure prediction features available in these programs can be used to address the gaps. These programs first thread the primary sequence of the mAb onto the structure of a homologous mAb or structures of separated F_{ab} and F_c domains that can then be ligated. The programs then use some form of energy minimization to optimize the structure of the homology model. Readjustments can be made to correct for missing sequence or secondary structure.¹³ Homology models may be displayed in PyMOL or similar modeling software to denote segments that exhibit changes in deuterium uptake.

1.4 Case studies of the application of H/D-MS to formulation development of mAbs

Monoclonal antibodies share high sequence similarity within an immunoglobulin subclass, yet they can have dramatically different physical and chemical stability properties unique to a specific mAb. Hence individual formulation strategies are needed to address different types of physical and chemical instabilities observed for different mAbs formulated in various dosage forms.⁷⁰ Stabilization strategies depend on an assessment of the impact of degradation

pathways on the structural integrity, stability and biological activity of a mAb. Experimentally, this often includes forced degradation studies as well as accelerated and long-term stability studies. However, standard quality control assays and lower resolution biophysical techniques are not always capable of detecting subtle changes in the higher order structure and local dynamics of mAbs, and hence may be limited in their ability to monitor and predict the ability of different formulations to provide long-term stability of therapeutic mAbs.

H/D-MS is emerging as a promising new analytical tool to explore the effect of chemical and physical modifications on the local structural dynamics of mAbs. Changes in local dynamics may better correlate with the short-term or long-term pharmaceutical stability of some or perhaps many different mAbs than data obtained from other biophysical measurements. Alterations in mAb local dynamics can therefore be of interest during many aspects of pharmaceutical development including elucidating degradation pathways, designing stable formulations, assessing biopharmaceutical comparability due to process or product changes,⁶⁷ and potentially assessing mechanisms of self-association and high viscosity in certain mAbs.⁷¹ Here we review the application of H/D-MS to formulation development of mAbs by exploring the effects of chemical modifications, environmental stresses, and formulation additives on the local dynamics of IgG1 mAbs and their interrelationships with conformational and pharmaceutical stability.

1.4.1 Impact of chemical modifications on mAb local dynamics.

A typical IgG1 monoclonal antibody is made up of approximately 1300 amino acid residues, along with post translational modifications such as glycans attached at a specific asparagine in the C_H2 domain. The result is a heterogeneous mixture of glycoforms with an average molecular weight around 150 kDa. Only a few of the twenty naturally-occurring amino acid residues are commonly prone to chemical modifications under conditions routinely

encountered during protein production, purification, long-term storage and administration.⁷² The effects of methionine oxidation, asparagine deamidation, and aspartic acid isomerization on mAb higher order structure and dynamics have been studied using H/D-MS and are discussed in the following paragraphs. Many other chemical modifications are possible in mAbs and need to be considered including light and free radical induced tryptophan and histidine oxidations (and their related byproducts),⁷³ C-terminal lysine cleavage, N-terminal pyroglutamate formation, hinge region fragmentation, and proteolysis.⁷² However, these modifications are not the focus of this chapter as we are not aware of any published literature to-date studying the effect of these modifications on mAb's higher order structure and dynamics using H/D-MS. While the impact of other chemical modifications such as deglycosylation,²⁰ cytotoxic drug conjugation to free cysteines,³³ and amino acid substitutions^{31,32} on the higher order structure and dynamics of mAbs have been explored using H/D-MS, they are also outside the scope of this chapter which focuses on stabilization and formulation development of "standard" therapeutic mAbs.

For Met oxidation, Asn deamidation and Asp isomerization, the probability and extent of occurrence of these chemical modifications can be dependent on the presence of specific neighboring amino acids (e.g., NG motif for deamidation and DG motif for Asp isomerization), location within the protein's higher order structure, solution pH and temperature as well as formulation composition. It is common to accumulate small fractions of these modifications in mAb drug products during manufacturing and long-term storage. The impact of these modifications on the higher order structure, conformational dynamics, and pharmaceutical properties (stability as well as functional attributes such as antigen binding or F_c effector functions) of the mAb drug product varies with the specific antibody, its mechanism of action, and the location of the modified amino acid residue within the mAb. For example, two specific

methionine residues, Met 257 in the C_{H2} domain and Met 433 in the C_{H3} domain, located in the F_c region and conserved across all human IgG1 and IgG2 mAbs, have been found to have a much higher propensity towards oxidation compared to other methionine residues located in other regions of mAbs.^{29,30} Furthermore, oxidation of these two methionine residues has been shown to result in decreased FcRn binding,^{74,75} protein A binding,⁷⁴ in vivo half-life,⁷⁶ thermal stability,⁷⁷ and increased aggregation propensity.²⁷

For experimental purposes, methionine oxidation can be induced under accelerated conditions by adding a molar excess of hydrogen peroxide followed by incubation for a few hours.⁷⁷ The impact of methionine oxidation on the conformational dynamics of six different IgG1 mAbs has been studied by H/D-MS in three different laboratories.^{27,30,77} All the studies reported increased deuterium uptake in an eleven residue segment (FLFPPKPKDTL) located immediately before Met 257. The numbering of the residues varies slightly across studies due to differences in total number of amino acids in the specific IgG1 mAbs used in these studies.^{27,30,77} Figure 1.4 A shows increased deuterium uptake in this peptide segment (HC 246-256) in the form of the H/D exchange mass difference plots for the mAb heavy chain as described in the previous section of this chapter.⁷⁷ The mAb light chain did not show any difference in H/D exchange kinetics (Figure 1.4 B). Similar results for the HC 246-256 segment due to methionine oxidation were also reported for five other IgG1 mAbs by Zhang et. al.,⁷⁷ Houde et. al.²⁷ and Burkitt et. al.³⁰ In one of these studies, Zhang et. al.⁷⁷ used structural modeling to better understand local environments of Met 257 and Met 433. As illustrated in Figure 1.4 C, D, and E, it was found that these two methionine residues are closely packed in 3D space allowing hydrophobic interactions between the two methionine residues thereby stabilizing the local conformation as well as the C_{H2}-C_{H3} interface.⁷⁷ Oxidation increases the distance between the

two sulfur atoms of the methionine residues, thereby disrupting the hydrophobic packing and increasing local dynamics. Segments in the C_H2-C_H3 interface also exchanged faster in oxidized mAbs, although the extent of exchange was lower than the segment adjacent to Met 257. Hence H/D-MS was successfully used to identify perturbations in local dynamics due to methionine oxidation in IgG1 mAbs that may be the underlying mechanism behind changes in mAb physical stability or receptor binding.

Asn deamidation and Asp isomerization can result in formation of aspartate and isoaspartate through a succinimide intermediate, and in contrast to methionine oxidation, have been found to occur at multiple locations within mAbs.⁷⁸ Deamidation and isomerization in two CDR locations within the variable domains of certain mAbs, i.e. Asn 55⁷⁹ and Asp 102⁸⁰, respectively, have been shown to decrease antigen binding depending on the location of the amino acid residue in the CDR. However, deamidation of Asn residues located in constant domains (Asn 389 and Asn 434) did not affect F_c receptor binding.⁸¹ The impact of these modifications on local dynamics of an IgG1 mAb was studied by H/D-MS recently by Zhang et al.⁷⁷ Various pH and temperature stresses were used to initiate deamidation and isomerization reactions in mAb samples which were then analyzed by H/D-MS experiments. Significant deamidation was detected at Asn 389 and isomerization was detected at Asp 55 and Asp 104. The mAb used in this work had Asp 55⁷⁷ in CDR 2 as opposed to Asn 55 residue.⁷⁹ H/D-MS experiments revealed no significant differences in local dynamics between the native mAb and either deamidated or isomerized mAb samples, likely because only a small fraction of mAbs underwent deamidation and isomerization at these sites. Since the observed kinetics of H/D exchange are essentially a weighted average of all protein forms present in solution, enriched fractions of deamidated and isomerized species of a mAb would need to be generated and/or

isolated to more fully assess the effects of these modifications on mAb structural dynamics. However, subtle changes in deuterium uptake compared to the control were observed in peptide segments covering Asp 55 and Asp 104 where the succinimide intermediate formed.

1.4.2 Impact of environmental stresses on mAb local dynamics.

Antibody drugs may be exposed to a variety of environmental stresses during processing such as freeze-thaw, elevated temperatures, pH changes, and agitation. These stresses may generate variable amounts and types of protein aggregates. For example, elevated temperature or agitation stress have been shown to induce aggregation by F_{ab} - F_{ab} interaction^{82,83} while pH changes may induce aggregation by F_c - F_c interaction.⁸² The aggregates formed by different conditions may thus contain protein molecules which have different types of structures which in turn may affect their immunogenic potential.⁸⁴ High-resolution analytical techniques such as H/D-MS may be valuable tools for deciphering the alterations in higher-order structure and dynamics of protein molecules found in process-induced mAb aggregates. For example, H/D-MS has been used to explore changes in the structural dynamics of Bevacizumab (Avastin) aggregates induced by both freeze/thaw cycles and by exposure to high temperature.²⁸

Thermally-induced Bevacizumab aggregates were produced by incubation at 70 °C for 10 min and then isolated by centrifugation. The thermally induced aggregates showed widely different dynamics by HD-MS analysis, primarily in the F_{ab} region compared to the control. Figure 1.5 shows a summary of the deuterium incorporation kinetics in the light chain (A) and the heavy chain (B) of both thermally-induced mAb aggregates and in the native mAb. Widely different deuteration rates were observed in the F_{ab} region of aggregated IgG, primarily showing increased deuterium uptake across most regions of the F_{ab} , but resulting in decreased deuteration in three segments of the CDRs (LC 48-54, HC 27-35, and HC 54-64). Only one segment in the

F_c region of the aggregated mAb (HC 430-452) had increased deuteration while the rest of the peptide segments from the F_c region were unaffected. Previous studies indicated the critical role of the F_{ab} region in thermally-induced mAb aggregation by correlating F_{ab} thermal stability with molecular aggregation propensity⁸⁵ and by correlating similarities observed in aggregation behavior between intact mAbs and isolated F_{ab} fragments.^{82,83} The H/D exchange data in this case study revealed substantial changes in local structural dynamics of the F_{ab} portion only in mAb aggregates, thereby demonstrating the critical role of the F_{ab} in thermally-induced mAb aggregation. Furthermore, the exchange protected segments in the CDRs of aggregated Bevacizumab are probably the locations of intermolecular contacts in the thermally-induced aggregates.⁸⁶ Extensive structural perturbations in thermally-induced aggregates detected by H/D-MS are consistent with a dramatic increase in the intensity and red-shift of intrinsic tryptophan fluorescence and by increased intensity and blue-shift of ANS fluorescence in the same mAb aggregates.²⁸

In contrast to thermally induced aggregates, isolated aggregates of Bevacizumab produced by up to 30 freeze/thaw cycles showed little change in H/D kinetics.²⁸ In this case, there was also no appreciable change in intrinsic tryptophan fluorescence or ANS fluorescence between the freeze-thaw induced aggregate and the control mAb. Results from H/D-MS analysis in this study correlated well with fluorescence measurements, and the fluorescence results were consistent with observations in a complementary freeze-thaw and thermally-induced aggregate study with another mAb.⁸³

As an additional example, dimers produced during production and storage of two different IgG1 mAbs were analyzed using H/D-MS and complimentary biophysical tools.⁸⁷ One of the mAb dimers showed no difference in local structural dynamics by H/D-MS but differential

scanning calorimetry (DSC) analysis indicated a decrease in thermal stability of the C_{H2} domain and small angle x-ray solution scattering (SAXS) analysis indicated a heterogeneous mixture of dimer species in solution. Since H/D-MS did not detect differences in the mAb aggregate, the authors concluded that the structural changes were mediated by the amino acid side chains. In the other mAb dimer, H/D-MS detected significant differences in the C_{H2} domain where more protection against exchange in the hinge region as well as less protection in a segment adjacent to the hinge region were observed in the dimer compared to native mAb. Biophysical measurements suggested that a collection of mechanisms including disulfide scrambling, domain swapping and surface interactions can play important roles in dimerization of the mAb. Hence complimentary biophysical tools may be valuable to help interpret or extrapolate the results obtained from H/D-MS experiments to better understand the degradation pathways leading to formation of aggregated mAbs.

1.4.3 Impact of formulation additives on mAb local dynamics, conformational stability and aggregation.

Since mAbs are prone to physical and/or chemical degradation due to various stress conditions, a variety of pharmaceutical excipients (such as buffering agents, sugars, sugar alcohols, surfactants, amino acids, salts, etc.) are routinely introduced into protein formulations to increase the solubility and/or stability during manufacturing, storage, distribution and administration.⁸⁸ The various mechanisms by which these excipients and salts interact with and/or stabilize proteins at the molecular level are an area of active investigation.⁸⁸⁻⁹¹ The identification of pharmaceutical excipients to stabilize mAb drugs during long term storage is often empirically determined. This is reflected in the wide spread interest in using high throughput screening technologies to identify stabilizing agents as part of protein formulation

development.^{92,93} Each class and type of excipient, along with their combinations, are generally evaluated for their ability to protect a mAb against physicochemical degradation pathways leading to inactivation and loss of potency specific to each mAb. By utilizing higher resolution analytical techniques, an improved mechanistic understanding of how different excipients can affect the pharmaceutical stability of multi-domain proteins such as mAbs is expected, and thus, more rationale strategies can be developed to design excipient mixtures to provide stable mAb formulations.

To this end, recent work in our laboratories has explored the inter-relationships of pharmaceutical excipients, physical stability and local dynamics in an IgG1 mAb.^{12,13} Arginine and sucrose were used as model excipients, while salts from the Hofmeister series (sodium salts of sulfate, chloride and thiocyanate) were also examined. The conformational stability of the mAb in different formulations was monitored using the thermal melting onset temperature and three different melting transitions obtained from DSC. The rate of aggregate formation was measured by size exclusion chromatography (SEC) following incubation at various temperatures. While both sucrose (0.5 M) and sodium sulfate (0.5 M) increased the conformational stability of the mAb as evidenced by DSC (T_m values), sucrose increased the T_{onset} temperature and sulfate decreased it. Both sucrose and sulfate slowed the rate of mAb monomer loss during storage as measured by SEC. Sucrose addition resulted in formation of soluble aggregates while sulfate led to formation of both soluble and insoluble aggregates. In contrast, arginine (0.5 M) moderately and sodium thiocyanate (0.5 M) substantially decreased the mAb's conformational stability as is evident from the decrease in T_m and T_{onset} values. The largest effects were observed for T_{m1} which corresponds to thermal unfolding of the C_H2 domain.⁹⁴ Both arginine and thiocyanate increased the rate of mAb aggregation as measured by monomer loss including elevated levels of

predominantly insoluble aggregate formation over time. These destabilizing effects on the IgG1 mAb were much more prominent in the presence of thiocyanate than arginine.

H/D-MS analysis of the IgG1 mAb in the presence of these additives was then performed. Figure 1.6 A is a summary of the changes in deuterium uptake observed by various peptide segments across the IgG1 mAb in the presence of the five different additives compared to the control (0.1 M NaCl in 20 mM citrate phosphate at pH 6.0) at four deuterium exchange times (120, 10^3 , 10^4 , and 10^5 s). The vertical axes in these plots indicate deuterium uptake differences for each peptide segment when the mAb was labeled in the presence of an excipient compared to the control condition. The horizontal axes indicate the ordinal peptide number arranged in ascending order from the N to C terminus of the protein based on the peptide midpoint. The domain locations of the peptides are indicated at the top of the plots. A positive difference in Figure 1.6 A indicates increased H/D exchange while a negative difference indicates decreased exchange by a peptide in the presence of the two excipients or three different salts. Only differences that exceed the 99% confidence interval indicated by the dotted lines in the difference charts are considered to be significant. These significant changes in dynamics are colored in yellow, for faster exchange, or blue, for slower exchange, in each of the corresponding mAb homology models shown in Figure 1.6 B.

Deuterium exchange experiments in the presence of 0.5 M sucrose revealed a global trend of small decreases in local dynamics across most regions of the mAb as shown in the mass difference charts for sucrose in Figure 1.6 A. Individually, the small decreases in dynamics were generally not statistically significant vs. the 99% CI, but collectively show a global trend which supports the preferential exclusion mechanism by which certain additives are believed to stabilize proteins in solution.^{95,96} For example, sugars have been shown to be preferentially

excluded from a protein's surface thus increasing the chemical potential of the solution. In response to this thermodynamically unfavorable condition, proteins adopt smaller, more compact structures to decrease the relative surface area exposure (compared to unfolded forms of the protein). The H/D exchange results in this work with 0.5 M sucrose and 0.5 M NaCl are consistent with this model of global protein structural rigidification caused by preferential hydration due to addition of certain excipients to the protein solution. Sodium sulfate, on the other hand, even though it was observed to physically stabilize the mAb, increased the dynamics of local segments in the C_{H1}, C_L, V_H and V_L domains of the mAb (Figure 1.6 A and B). Thus its stabilizing effects on the mAb are likely due to a different mechanism. These two stabilizers did not cause any consensus change in any segment of the IgG1 mAb in terms of local dynamics of the amide backbone which points to the varying mechanisms by which sucrose and sulfate interact with and stabilize proteins. However, both sulfate and sucrose shared a common feature in terms of their effects on the local dynamics of this IgG1: both additives did not affect the local flexibility of the C_{H2} domain of the mAb. The importance of this observation is described below.

The destabilizing additives, arginine and thiocyanate, significantly increased the local dynamics of specific segments of the mAb. Effects of arginine on local dynamics were found to be limited to only a few segments of the mAb, while thiocyanate increased dynamics of several segments from all domains. Although arginine and thiocyanate seemed to have differential effects at various regions of the mAb, both substantially increased the dynamics of the 241-251 segment of the heavy chain in the C_{H2} domain. This effect is evident from the mass increase of several overlapping peptide segments representing this common segment (Figure 1.6 A and B). These results indicate that local dynamics of key regions within the C_{H2} domain correlate well

with the observed overall physical stability of this IgG1 mAb in the presence of the excipients and salts used in these studies.^{12,13}

1.5 Aggregation hotspot identification in mAbs using H/D-MS

Antibody aggregation is a complex, multi-step process that results in formation of soluble or insoluble aggregates of varying sizes containing protein with varying levels of structural alterations.⁹⁷ Aggregation of mAbs can proceed via several different mechanisms depending on factors such as the structural integrity of the protein, effective charge of the protein, nature of protein-protein interactions, colloidal properties of the protein solution, and the type of environmental stress (e.g., heat, agitation, freeze-thaw).⁹⁸ While each mAb has its unique CDRs that can contribute to aggregation, the sequence of the constant domains in the F_{ab} and F_c regions are highly similar across one source and class of antibody (e.g., human IgG1). Hence there could be more “universal” aggregation-prone sequences in the constant domains that affect mAb stability across one source and class of antibodies, e.g., human IgG1 mAbs.⁹⁹

Despite the heterogeneous nature of protein aggregates, their formation proceeds via some common steps as illustrated in Figure 1.7 A (from Roberts and Sahin, 2011). These steps are (i) a certain degree of structural alteration of the protein monomer (F) to reversible intermediate (R), (ii) reversible self-association of the partially unfolded monomers (R) to an oligomeric Rx species, and (iii) conformational rearrangement of reversible species to form irreversible intermolecular associations that act as the aggregating nucleus (Ax).^{98,100} Detection of these reversibly conformationally altered species remains an important analytical challenge for the better understanding of aggregation pathways. Recent work with the molecular chaperone protein GroEL linked to bilayer interferometry biosensors has shown the capability to trap

structurally altered pre-aggregate and early aggregated species (schematically shown in Figure 1.7 A) of several pharmaceutically relevant proteins including an IgG1 mAb.¹⁰¹

Recent results have indicated that H/D-MS may also be capable of detecting these pre-aggregate species in mAbs by localizing unfolding to particular sequence locations that act as hotspots to trigger aggregation under stressed conditions. For example, significant increases in flexibility of a highly conserved sequence in the C_H2 domain of IgG1 monoclonal antibodies have been identified in response to a variety of stress conditions such as the presence of destabilizing additives (thiocyanate and arginine),^{12,13} methionine oxidation,^{27,30,77} deglycosylation,²⁰ as well as point mutations in the C_H2 domain introduced to modulate the pharmacokinetic profile of a mAb.³¹ The shapes of the deuterium uptake curves for this segment in the C_H2 domain across a variety of mAbs measured by H/D-MS in many different labs, are remarkably similar as shown in Figure 1.7 B to G. Hence this segment not only appears to exhibit similar local dynamics in many IgG1 mAbs, but shows similar increases in local flexibility when exposed to a variety of stresses and alterations (although the sequence numbering differs in each plot due to amino acid differences between the mAbs, all of the plots correspond to the same peptide segment). This segment has two aliphatic side-chains (valine and leucine) and two phenylalanine residues. The phenyl rings pack tightly with the glycans in the crystal structure of an IgG1 mAb.¹⁰² Stress conditions accelerate H/D exchange in this region suggesting that stress causes an increase in the flexibility of this hydrophobic segment. The resulting increase in flexibility disrupts the packing of the hydrophobic side-chains with the glycans, thereby transiently unfolding this particular segment. The exposure of this hydrophobic patch could then trigger conformational instability and aggregation.^{99,103} The similarity of deuterium uptake kinetic profiles of this segment across multiple studies and IgG1 mAbs also

points to the high inter-laboratory reproducibility in analyzing this aspect of local dynamics by H/D-MS.

1.6 Challenges and opportunities for the H/D-MS technique as applied to mAb formulation development

The technology for H/D-MS both, hardware and software, has seen revolutionary improvements in the last decade allowing for more wide spread use with larger, more complex protein molecules.^{104,105} The utility of this technique for assessing higher order protein structural and dynamic changes of mAbs has been established by numerous publications in recent years. As a result, the technique is becoming widely-adopted in both academic and industrial laboratories. In spite of all this recent progress, there still remain more challenges to overcome to make this technique more widely available and acceptable especially in the biopharmaceutical industry. First, we examine some of the current challenges with the analytical technology, and then evaluate some of remaining hurdles to implement H/D-MS technology as part of standard formulation development activities.

1.6.1 Analytical technology challenges

Advances in both hardware and software to control robotic autosamplers designed especially for H/D-MS experiments have made the technology amenable to customization for a wide variety of experiments. It is possible to do the entire H/D exchange reaction, liquid handling, mixing and moving, and sample analysis by LC-MS for hundreds of samples in a fully automated manner. Robotic liquid handling allows high accuracy and precision in deuterium labeling experiments that is difficult to achieve in long, labor-intensive manual labeling experiments. To-date, however, commercial solutions for automated H/D exchange are not

seamlessly integrated with LC-MS platforms. Typically, experiments need to be set up in parallel on both platforms with limited communication between the instrument platforms to handle errors.

While there is the promise of fully-automated data analysis, the current reality is that considerable user review and correction is still required. Hence, data processing is still the rate-limiting step in bottom up H/D-MS analysis of large proteins such as mAbs. This is primarily because no perfect scoring algorithm exists so far that can predict the match of calculated isotopic envelopes with experimentally observed envelopes with 100% accuracy for every peptide and every exchange time point in a large H/D-MS data set. In our hands using HDExaminer, for example, to process H/D-MS data for a mAb, only ~ 10% of the peptide mass spectra need to be manually corrected. To date, there is no completely reliable algorithm to identify data that requires manual correction. Hence, manual review and correction to correctly identify the peaks in a peptide isotopic cluster is still necessary to improve accuracy. Thus, there is currently no satisfactory alternative available to avoid manually reviewing and correcting at least some of the data.

Because of the subjective nature of data processing and because different levels of back-exchange are obtained using different H/D-MS instrumental setups, some more formal assessment of inter-laboratory comparison of H/D-MS data would be highly beneficial to gain more confidence in the reproducibility of H/D-MS results. This may be achieved by performing H/D-MS experiments using the same protein under similar experimental conditions in multiple laboratories. To meet this need, the US National Institute of Standards and Technology recently announced a round-robin H/D-MS study of a reference protein.

Finally, H/D-MS data have been summarized and presented in various ways such as deuterium incorporation heat maps, bar charts, line diagrams, scatter plots, etc. Some of these different modes of data visualization are shown in Figures 1.4, 1.5, and 1.6 of this chapter. A consensus mode of data presentation that will be informative for most types of experiments has the potential for better comprehension and comparison of H/D-MS data generated across laboratories.

1.6.2 MAb formulation development challenges

There are several challenges in implementing bottom up H/D exchange experiments for more routine formulation development of mAbs. First, excipients can potentially change intrinsic exchange rates. Zhang et al.⁶² described the use of a poly-proline and isoleucine peptide as an internal standard in a protein stock solution to track and correct for changes in intrinsic exchange during deuterium labeling due to the presence of various amounts of guanidine salt in solution. However, introducing such control peptides in solution requires testing to establish that no form of interaction occurs between the control peptide and the protein. Second, as described below, although H/D-MS has the potential to provide better mechanistic understanding of mAb pharmaceutical stability profiles, some additional challenges remain as discussed below.

The effects of chemical degradation on local flexibility of IgG mAbs as measured by H/D-MS has now been investigated by several groups including studies of methionine oxidation, asparagine deamidation, and aspartic acid isomerization.^{27,30,77} In these studies, methionine oxidation caused significant changes in H/D exchange kinetics in some regions and peptide segments of the mAb, but no significant effects were detected for asparagine deamidation or

aspartic acid isomerization.^{27,30,77} The absence of effects as detected by H/D-MS, however, may have been due to the small fraction of chemically-modified protein present in solution. The observed kinetics of H/D exchange are the weighted average of all protein forms present in solution. Hence, H/D-MS analysis may be more useful for detailed characterization of enriched, isolated fractions of such chemically altered samples, but less useful for probing their nature directly in protein formulations when present at low levels. H/D-MS experiments planned at different concentrations of chemically modified mAb species may be required to establish whether H/D-MS is sufficiently sensitive to detect changes in higher order structure, if present, due to the minor amounts of chemically modified mAb species present in solution.

In terms of characterization of mAb aggregates by H/D-MS, the impact of freeze-thaw and heating on the nature of the higher order structure and dynamics of protein within the mAb aggregate has been explored using H/D-MS.²⁸ It will be interesting to explore the impact of similar stresses on different IgG1 molecules as well as other classes of IgG molecules. In addition, the impact of other types of processing stresses such as shaking, stirring, and lyophilization/reconstitution on the local dynamics of mAb molecules may also potentially be explored by H/D-MS.

The work reviewed in the preceding section suggests that H/D-MS could be used to screen excipients and additives for their effects on dynamics of specific aggregation-prone regions in mAbs. For example, it was shown that changes in the local dynamics of specific sequences in the C_H2 domain caused by destabilizing excipients and salts correlated with decreased storage stability and conformational stability of an IgG1 mAb.^{12,13} Hence, a large number of different formulations could be screened using H/D-MS for their effects on specific peptides that have been identified as markers of instability. By focusing on a subset of peptide

segments, H/D-MS experiments including data analysis could be performed more rapidly offering the possibility of a high-throughput excipient screening H/D-MS assay to identify stabilizing excipients. Such changes in dynamics could potentially serve as indicators of long-term stability of different mAbs in different formulations. Results from such experiments may also improve our basic understanding of the relationships between changes in protein flexibility and stability. Such experiments are currently underway in our laboratories.

Therapeutic mAbs are more frequently being formulated in high concentration solution dosage forms to facilitate subcutaneous self-administration by patients. Some mAbs however undergo reversible self-association^{71,106} in a concentration dependent manner resulting in high viscosity,^{107,108} opalescence¹⁰⁹ or liquid-liquid phase separation¹¹⁰. High viscosity, for example, can pose major problems for manufacturing (filtration), stability (aggregation) and administration (syringeability).¹¹¹ The interfacial contacts involved in self-association of such mAb candidates could potentially be identified using H/D-MS to gain mechanistic insights into the molecular origin of self-association of mAbs. Such insights may guide design of appropriate strategies to minimize or mitigate self-association behavior of specific mAbs using selected excipients or protein engineering. Such experiments are also currently underway in our laboratories.

1.7 Conclusions

H/D-MS is a promising technique for more expanded use in formulation development of mAbs, especially in terms of analysis of higher order structure and dynamics of mAbs in response to various external stress conditions, changes in formulation composition, or specific physicochemical modifications. This chapter not only presented an overview of the method as applied to mAb formulation development (i.e., sample preparation, sample analysis, data

acquisition, and data processing), but also presented illustrative case studies using the of H/D-MS technique to analyze mAbs as part of formulation development. Furthermore, the utility of using H/D-MS in identifying transient locally unfolded mAb monomeric species that can act as aggregation hotspots under stress conditions has been demonstrated with the example of a specific sequence in the C_{H2} domain of IgG1 mAbs. This chapter also highlights the current challenges in using this technique, opportunities for further advances in H/D-MS technology and potential future applications during formulation development of mAb biotherapeutics.

1.8 References

1. Reichert JM 2011. Antibody-based therapeutics to watch in 2011. *mAbs* 3(1):76-99.
2. Reichert JM 2014. Antibodies to watch in 2014. *mAbs* 6(1):5-14.
3. Saphire EO, Stanfield RL, Max Crispin MD, Parren PWHI, Rudd PM, Dwek RA, Burton DR, Wilson IA 2002. Contrasting IgG Structures Reveal Extreme Asymmetry and Flexibility. *J Mol Biol* 319(1):9-18.
4. Hanson DC, Yguerabide J, Schumaker VN 1985. Rotational dynamics of immunoglobulin G antibodies anchored in protein A soluble complexes. *Mol Immunol* 22(3):237-244.
5. Bongini L, Fanelli D, Piazza F, De Los Rios P, Sandin S, Skoglund U 2005. Dynamics of antibodies from cryo-electron tomography. *Biophys Chem* 115(2-3):235-240.
6. Roux KH, Strelets L, Michaelsen TE 1997. Flexibility of human IgG subclasses. *J Immunol* 159(7):3372-3382.
7. Kamerzell TJ, Ramsey JD, Middaugh CR 2008. Immunoglobulin Dynamics, Conformational Fluctuations, and Nonlinear Elasticity and Their Effects on Stability. *The Journal of Physical Chemistry B* 112(10):3240-3250.
8. Alsenaidy MA, Jain NK, Kim JH, Middaugh CR, Volkin DB 2014. Protein comparability assessments and potential applicability of high throughput biophysical methods and data visualization tools to compare physical stability profiles. *Frontiers in pharmacology* 5:39.
9. Kamerzell TJ, Middaugh CR 2007. Two-Dimensional Correlation Spectroscopy Reveals Coupled Immunoglobulin Regions of Differential Flexibility that Influence Stability. *Biochemistry* 46(34):9762-9773.

10. Ramsey JD, Gill ML, Kamerzell TJ, Price ES, Joshi SB, Bishop SM, Oliver CN, Middaugh CR 2009. Using empirical phase diagrams to understand the role of intramolecular dynamics in immunoglobulin G stability. *J Pharm Sci* 98(7):2432-2447.
11. Thakkar SV, Kim JH, Samra HS, Sathish HA, Bishop SM, Joshi SB, Volkin DB, Middaugh CR 2012. Local dynamics and their alteration by excipients modulate the global conformational stability of an IgG1 monoclonal antibody. *J Pharm Sci* 101(12):4444-4457.
12. Majumdar R, Manikwar P, Hickey JM, Samra HS, Sathish HA, Bishop SM, Middaugh CR, Volkin DB, Weis DD 2013. Effects of salts from the Hofmeister series on the conformational stability, aggregation propensity, and local flexibility of an IgG1 monoclonal antibody. *Biochemistry* 52(19):3376-3389.
13. Manikwar P, Majumdar R, Hickey JM, Thakkar SV, Samra HS, Sathish HA, Bishop SM, Middaugh CR, Weis DD, Volkin DB 2013. Correlating excipient effects on conformational and storage stability of an IgG1 monoclonal antibody with local dynamics as measured by hydrogen/deuterium-exchange mass spectrometry. *J Pharm Sci* 102(7):2136-2151.
14. Thakkar SV, Joshi SB, Jones ME, Sathish HA, Bishop SM, Volkin DB, Middaugh CR 2012. Excipients differentially influence the conformational stability and pretransition dynamics of two IgG1 monoclonal antibodies. *J Pharm Sci* 101(9):3062-3077.
15. Alsenaidy MA, Kim JH, Majumdar R, Weis DD, Joshi SB, Tolbert TJ, Middaugh CR, Volkin DB 2013. High-throughput biophysical analysis and data visualization of conformational stability of an IgG1 monoclonal antibody after deglycosylation. *J Pharm Sci* 102(11):3942-3956.
16. Panjwani N, Hodgson DJ, Sauve S, Aubin Y 2010. Assessment of the effects of pH, formulation and deformulation on the conformation of interferon alpha-2 by NMR. *J Pharm Sci* 99(8):3334-3342.

17. Amezcua CA, Szabo CM 2013. Assessment of higher order structure comparability in therapeutic proteins using nuclear magnetic resonance spectroscopy. *J Pharm Sci* 102(6):1724-1733.
18. Favero-Retto MP, Palmieri LC, Souza TA, Almeida FC, Lima LM 2013. Structural meta-analysis of regular human insulin in pharmaceutical formulations. *Eur J Pharm Biopharm* 85(3 Pt B):1112-1121.
19. Norrman M, Schluckebier G 2007. Crystallographic characterization of two novel crystal forms of human insulin induced by chaotropic agents and a shift in pH. *BMC Struct Biol* 7:83.
20. Houde D, Arndt J, Domeier W, Berkowitz S, Engen JR 2009. Characterization of IgG1 Conformation and Conformational Dynamics by Hydrogen/Deuterium Exchange Mass Spectrometry. *Anal Chem* 81(7):2644-2651.
21. Hvidt A, Linderstrom-Lang K 1954. Exchange of hydrogen atoms in insulin with deuterium atoms in aqueous solutions. *Biochim Biophys Acta* 14(4):574-575.
22. Kim YS, Randolph TW, Manning MC, Stevens FJ, Carpenter JF 2003. Congo red populates partially unfolded states of an amyloidogenic protein to enhance aggregation and amyloid fibril formation. *J Biol Chem* 278(12):10842-10850.
23. Paterson Y, Englander SW, Roder H 1990. An antibody binding site on cytochrome c defined by hydrogen exchange and two-dimensional NMR. *Science* 249(4970):755-759.
24. Jeng MF, Englander SW, Elove GA, Wand AJ, Roder H 1990. Structural description of acid-denatured cytochrome c by hydrogen exchange and 2D NMR. *Biochemistry* 29(46):10433-10437.

25. Katta V, Chait BT, Carr S 1991. Conformational changes in proteins probed by hydrogen exchange electrospray ionization mass spectrometry. *Rapid Commun Mass Spectrom* 5(4):214-217.
26. Zhang Z, Smith DL 1993. Determination of amide hydrogen exchange by mass spectrometry: A new tool for protein structure elucidation. *Protein Sci* 2(4):522-531.
27. Houde D, Peng Y, Berkowitz SA, Engen JR 2010. Post-translational Modifications Differentially Affect IgG1 Conformation and Receptor Binding. *Molecular & Cellular Proteomics* 9(8):1716-1728.
28. Zhang A, Singh S, Shirts M, Kumar S, Fernandez E 2012. Distinct Aggregation Mechanisms of Monoclonal Antibody Under Thermal and Freeze-Thaw Stresses Revealed by Hydrogen Exchange. *Pharm Res* 29(1):236-250.
29. Zhang A, Hu P, MacGregor P, Xue Y, Fan H, Suchecki P, Olszewski L, Liu A 2014. Understanding the conformational impact of chemical modifications on monoclonal antibodies with diverse sequence variation using hydrogen/deuterium exchange mass spectrometry and structural modeling. *Anal Chem* 86(7):3468-3475.
30. Burkitt W, Domann P, O'Connor G 2010. Conformational changes in oxidatively stressed monoclonal antibodies studied by hydrogen exchange mass spectrometry. *Protein Sci* 19(4):826-835.
31. Majumdar R, Esfandiary R, Bishop SM, Middaugh CR, Volkin DB, Weis DD 2014. Correlations between changes in conformational dynamics and physical stability in a mutant IgG1 mAb engineered for extended serum half-life. *mAbs* (Submitted).

32. Rose RJ, van Berkel PHC, van den Bremer ETJ, Labrijn AF, Vink T, Schuurman J, Heck AJR, Parren PWHI 2013. Mutation of Y407 in the CH3 domain dramatically alters glycosylation and structure of human IgG. *mAbs* 5(2):219-228.
33. Pan LY, Salas-Solano O, Valliere-Douglass JF 2014. Conformation and dynamics of interchain cysteine-linked antibody-drug conjugates as revealed by hydrogen/deuterium exchange mass spectrometry. *Anal Chem* 86(5):2657-2664.
34. Englander SW, Kallenbach NR 1983. Hydrogen exchange and structural dynamics of proteins and nucleic acids. *Q Rev Biophys* 16(04):521-655.
35. Skinner JJ, Lim WK, Bédard S, Black BE, Englander SW 2012. Protein dynamics viewed by hydrogen exchange. *Protein Sci*:n/a-n/a.
36. Skinner JJ, Lim WK, Bédard S, Black BE, Englander SW 2012. Protein hydrogen exchange: testing current models. *Protein Sci*:n/a-n/a.
37. Woodward C, Carulla N, Barany G. 2004. Native State Hydrogen-Exchange Analysis of Protein Folding and Protein Motional Domains. In Jo M. Holt MLJ, Gary KA, editors. *Methods Enzymol*, ed.: Academic Press. p 379-400.
38. Molday RS, Englander SW, Kallen RG 1972. Primary structure effects on peptide group hydrogen exchange. *Biochemistry* 11(2):150-158.
39. Bai Y, Milne JS, Mayne L, Englander SW 1993. Primary structure effects on peptide group hydrogen exchange. *Proteins: Structure, Function, and Bioinformatics* 17(1):75-86.
40. Berger A, Loewenstein A, Meiboom S 1959. Nuclear Magnetic Resonance Study of the Protolysis and Ionization of N-Methylacetamide¹. *J Am Chem Soc* 81(1):62-67.

41. Englander JJ, Calhoun DB, Englander SW 1979. Measurement and calibration of peptide group hydrogen-deuterium exchange by ultraviolet spectrophotometry. *Anal Biochem* 92(2):517-524.
42. Gregory RB, Crabo L, Percy AJ, Rosenberg A 1983. Water catalysis of peptide hydrogen isotope exchange. *Biochemistry* 22(4):910-917.
43. Englander SW 2006. Hydrogen Exchange and Mass Spectrometry: A Historical Perspective. *J Am Soc Mass Spectrom* 17(11):1481-1489.
44. Henzler-Wildman K, Kern D 2007. Dynamic personalities of proteins. *Nature* 450(7172):964-972.
45. Tokuriki N, Tawfik DS 2009. Protein Dynamism and Evolvability. *Science* 324(5924):203-207.
46. Bryan PN, Orban J 2010. Proteins that switch folds. *Curr Opin Struct Biol* 20(4):482-488.
47. Kim KS, Woodward C 1993. Protein internal flexibility and global stability: effect of urea on hydrogen exchange rates of bovine pancreatic trypsin inhibitor. *Biochemistry* 32(37):9609-9613.
48. Hvidt A, Nielsen SO 1966. Hydrogen exchange in proteins. *Adv Protein Chem* 21:287-386.
49. Engen JR, Wales TE, Chen S, Marzluff EM, Hassell KM, Weis DD, Smithgall TE 2013. Partial cooperative unfolding in proteins as observed by hydrogen exchange mass spectrometry. *Int Rev Phys Chem* 32(1):96-127.
50. Deng Y, Smith DL 1998. Identification of unfolding domains in large proteins by their unfolding rates. *Biochemistry* 37(18):6256-6262.

51. Miranker A, Robinson CV, Radford SE, Aplin RT, Dobson CM 1993. Detection of transient protein folding populations by mass spectrometry. *Science* 262(5135):896-900.
52. Wales TE, Engen JR 2006. Hydrogen exchange mass spectrometry for the analysis of protein dynamics. *Mass Spectrom Rev* 25(1):158-170.
53. Deng Y, Zhang Z, Smith DL 1999. Comparison of continuous and pulsed labeling amide hydrogen exchange/mass spectrometry for studies of protein dynamics. *J Am Soc Mass Spectrom* 10(8):675-684.
54. Glasoe P, Long F 1960. Use of glass electrodes to measure acidities in deuterium oxide. *Journal of Physical Chemistry (US)* 64.
55. Rey M, Mrazek H, Pompach P, Novak P, Pelosi L, Brandolin G, Forest E, Havlicek V, Man P 2010. Effective Removal of Nonionic Detergents in Protein Mass Spectrometry, Hydrogen/Deuterium Exchange, and Proteomics. *Anal Chem* 82(12):5107-5116.
56. Wang L, Pan H, Smith DL 2002. Hydrogen Exchange-Mass Spectrometry: optimization of digestion conditions. *Molecular & Cellular Proteomics* 1(2):132-138.
57. Busby SA, Chalmers MJ, Griffin PR 2007. Improving digestion efficiency under H/D exchange conditions with activated pepsinogen coupled columns. *Int J Mass spectrom* 259(1-3):130-139.
58. Ahn J, Cao M-J, Yu YQ, Engen JR 2013. Accessing the reproducibility and specificity of pepsin and other aspartic proteases. *Biochimica et Biophysica Acta (BBA) - Proteins and Proteomics* 1834(6):1222-1229.
59. Keppel T, Jacques M, Young R, Ratzlaff K, Weis D 2011. An Efficient and Inexpensive Refrigerated LC System for H/D Exchange Mass Spectrometry. *J Am Soc Mass Spectrom* 22(8):1472-1476.

60. Fang J, Rand KD, Beuning PJ, Engen JR 2011. False EX1 signatures caused by sample carryover during HX MS analyses. *Int J Mass Spectrom* 302(1-3):19-25.
61. Majumdar R, Manikwar P, Hickey JM, Arora J, Middaugh CR, Volkin DB, Weis DD 2012. Minimizing Carry-Over in an Online Pepsin Digestion System used for the H/D Exchange Mass Spectrometric Analysis of an IgG1 Monoclonal Antibody. *J Am Soc Mass Spectrom* 23(12):2140-2148.
62. Zhang Z, Zhang A, Xiao G 2012. Improved Protein Hydrogen/Deuterium Exchange Mass Spectrometry Platform with Fully Automated Data Processing. *Anal Chem*.
63. Liu S, Liu L, Uzuner U, Zhou X, Gu M, Shi W, Zhang Y, Dai S, Yuan J 2011. HDX-Analyzer: a novel package for statistical analysis of protein structure dynamics. *BMC Bioinformatics* 12(Suppl 1):S43.
64. Weis DD, Engen JR, Kass IJ 2006. Semi-automated data processing of hydrogen exchange mass spectra using HX-Express. *J Am Soc Mass Spectrom* 17(12):1700-1703.
65. Slys GW, Baker CA, Bozsa BM, Dang A, Percy AJ, Bennett M, Schriemer DC 2009. Hydra: software for tailored processing of H/D exchange data from MS or tandem MS analyses. *BMC Bioinformatics* 10:162.
66. Pascal BD, Willis S, Lauer JL, Landgraf RR, West GM, Marciano D, Novick S, Goswami D, Chalmers MJ, Griffin PR 2012. HDX workbench: software for the analysis of H/D exchange MS data. *J Am Soc Mass Spectrom* 23(9):1512-1521.
67. Houde D, Berkowitz SA, Engen JR 2011. The utility of hydrogen/deuterium exchange mass spectrometry in biopharmaceutical comparability studies. *J Pharm Sci* 100(6):2071-2086.

68. Chalmers MJ, Pascal BD, Willis S, Zhang J, Iturria SJ, Dodge JA, Griffin PR 2011. Methods for the Analysis of High Precision Differential Hydrogen Deuterium Exchange Data. *Int J Mass Spectrom* 302(1-3):59-68.
69. Šali A, Blundell TL 1993. Comparative Protein Modelling by Satisfaction of Spatial Restraints. *J Mol Biol* 234(3):779-815.
70. Wang W, Singh S, Zeng DL, King K, Nema S 2007. Antibody structure, instability, and formulation. *J Pharm Sci* 96(1):1-26.
71. Esfandiary R, Hayes DB, Parupudi A, Casas-Finet J, Bai S, Samra HS, Shah AU, Sathish HA 2013. A systematic multitechnique approach for detection and characterization of reversible self-association during formulation development of therapeutic antibodies. *J Pharm Sci* 102(9):3089-3099.
72. Manning MC, Chou DK, Murphy BM, Payne RW, Katayama DS 2010. Stability of protein pharmaceuticals: an update. *Pharm Res* 27(4):544-575.
73. Torosantucci R, Schoneich C, Jiskoot W 2014. Oxidation of therapeutic proteins and peptides: structural and biological consequences. *Pharm Res* 31(3):541-553.
74. Pan H, Chen K, Chu L, Kinderman F, Apostol I, Huang G 2009. Methionine oxidation in human IgG2 Fc decreases binding affinities to protein A and FcRn. *Protein Sci* 18(2):424-433.
75. Bertolotti-Ciarlet A, Wang W, Lownes R, Pristatsky P, Fang Y, McKelvey T, Li Y, Li Y, Drummond J, Prueksaritanont T, Vlasak J 2009. Impact of methionine oxidation on the binding of human IgG1 to Fc Rn and Fc gamma receptors. *Mol Immunol* 46(8-9):1878-1882.
76. Wang W, Vlasak J, Li Y, Pristatsky P, Fang Y, Pittman T, Roman J, Wang Y, Prueksaritanont T, Ionescu R 2011. Impact of methionine oxidation in human IgG1 Fc on serum half-life of monoclonal antibodies. *Mol Immunol* 48(6-7):860-866.

77. Zhang A, Hu P, Macgregor P, Xue Y, Fan H, Suchecki P, Olszewski L, Liu A 2014. Understanding the conformational impact of chemical modifications on monoclonal antibodies with diverse sequence variation using hydrogen/deuterium exchange mass spectrometry and structural modeling. *Anal Chem* 86(7):3468-3475.
78. Du Y, Walsh A, Ehrick R, Xu W, May K, Liu H 2012. Chromatographic analysis of the acidic and basic species of recombinant monoclonal antibodies. *mAbs* 4(5):578-585.
79. Yan B, Steen S, Hambly D, Valliere-Douglass J, Vanden Bos T, Smallwood S, Yates Z, Arroll T, Han Y, Gadgil H, Latypov RF, Wallace A, Lim A, Kleemann GR, Wang W, Balland A 2009. Succinimide formation at Asn 55 in the complementarity determining region of a recombinant monoclonal antibody IgG1 heavy chain. *J Pharm Sci* 98(10):3509-3521.
80. Harris RJ, Kabakoff B, Macchi FD, Shen FJ, Kwong M, Andya JD, Shire SJ, Bjork N, Totpal K, Chen AB 2001. Identification of multiple sources of charge heterogeneity in a recombinant antibody. *J Chromatogr B Biomed Sci Appl* 752(2):233-245.
81. Khawli LA, Goswami S, Hutchinson R, Kwong ZW, Yang J, Wang X, Yao Z, Sreedhara A, Cano T, Tesar D, Nijem I, Allison DE, Wong PY, Kao YH, Quan C, Joshi A, Harris RJ, Motchnik P 2010. Charge variants in IgG1: Isolation, characterization, in vitro binding properties and pharmacokinetics in rats. *mAbs* 2(6):613-624.
82. Chen S, Lau H, Brodsky Y, Kleemann GR, Latypov RF 2010. The use of native cation-exchange chromatography to study aggregation and phase separation of monoclonal antibodies. *Protein Sci* 19(6):1191-1204.
83. Hawe A, Kasper JC, Friess W, Jiskoot W 2009. Structural properties of monoclonal antibody aggregates induced by freeze-thawing and thermal stress. *Eur J Pharm Sci* 38(2):79-87.

84. Hermeling S, Crommelin DJ, Schellekens H, Jiskoot W 2004. Structure-immunogenicity relationships of therapeutic proteins. *Pharm Res* 21(6):897-903.
85. Garber E, Demarest SJ 2007. A broad range of Fab stabilities within a host of therapeutic IgGs. *Biochem Biophys Res Commun* 355(3):751-757.
86. Kheterpal I, Cook KD, Wetzel R. 2006. Hydrogen/Deuterium Exchange Mass Spectrometry Analysis of Protein Aggregates. In Indu K, Ronald W, editors. *Methods Enzymol*, ed.: Academic Press. p 140-166.
87. Iacob RE, Bou-Assaf GM, Makowski L, Engen JR, Berkowitz SA, Houde D 2013. Investigating Monoclonal Antibody Aggregation Using a Combination of H/DX-MS and Other Biophysical Measurements. *J Pharm Sci* 102(12):4315-4329.
88. Kamerzell TJ, Esfandiary R, Joshi SB, Middaugh CR, Volkin DB 2011. Protein-excipient interactions: mechanisms and biophysical characterization applied to protein formulation development. *Adv Drug Deliv Rev* 63(13):1118-1159.
89. Baldwin RL 1996. How Hofmeister ion interactions affect protein stability. *Biophys J* 71(4):2056-2063.
90. Zhang Y, Cremer PS 2006. Interactions between macromolecules and ions: the Hofmeister series. *Current Opinion in Chemical Biology* 10(6):658-663.
91. Mason BD, Zhang-van Enk J, Zhang L, Remmele RL, Zhang J 2010. Liquid-Liquid Phase Separation of a Monoclonal Antibody and Nonmonotonic Influence of Hofmeister Anions. *Biophys J* 99(11):3792-3800.
92. He F, Woods CE, Becker GW, Narhi LO, Razinkov VI 2011. High-throughput assessment of thermal and colloidal stability parameters for monoclonal antibody formulations. *J Pharm Sci* 100(12):5126-5141.

93. Gibson TJ, McCarty K, McFadyen IJ, Cash E, Dalmonte P, Hinds KD, Dinerman AA, Alvarez JC, Volkin DB 2011. Application of a high-throughput screening procedure with PEG-induced precipitation to compare relative protein solubility during formulation development with IgG1 monoclonal antibodies. *J Pharm Sci* 100(3):1009-1021.
94. Feige MJ, Walter S, Buchner J 2004. Folding mechanism of the CH2 antibody domain. *J Mol Biol* 344(1):107-118.
95. Lee JC, Timasheff SN 1981. The stabilization of proteins by sucrose. *J Biol Chem* 256(14):7193-7201.
96. Arakawa T, Timasheff SN 1982. Stabilization of protein structure by sugars. *Biochemistry* 21(25):6536-6544.
97. Telikepalli SN, Kumru OS, Kalonia C, Esfandiary R, Joshi SB, Middaugh CR, Volkin DB 2014. Structural characterization of IgG1 mAb aggregates and particles generated under various stress conditions. *J Pharm Sci* 103(3):796-809.
98. Roberts CJ, Das TK, Sahin E 2011. Predicting solution aggregation rates for therapeutic proteins: Approaches and challenges. *Int J Pharm* 418(2):318-333.
99. Chennamsetty N, Helk B, Voynov V, Kayser V, Trout BL 2009. Aggregation-Prone Motifs in Human Immunoglobulin G. *J Mol Biol* 391(2):404-413.
100. Li Y, Roberts CJ 2009. Lumry-Eyring nucleated-polymerization model of protein aggregation kinetics. 2. Competing growth via condensation and chain polymerization. *J Phys Chem B* 113(19):7020-7032.
101. Naik S, Kumru OS, Cullom M, Telikepalli SN, Lindboe E, Roop TL, Joshi SB, Amin D, Gao P, Middaugh CR, Volkin DB, Fisher MT 2014. Probing structurally altered and aggregated

states of therapeutically relevant proteins using GroEL coupled to bio-layer Interferometry.

Protein Sci:n/a-n/a.

102. Saphire EO, Parren PW, Pantophlet R, Zwick MB, Morris GM, Rudd PM, Dwek RA, Stanfield RL, Burton DR, Wilson IA 2001. Crystal Structure of a Neutralizing Human IgG Against HIV-1: A Template for Vaccine Design. *Science* 293(5532):1155-1159.

103. Chennamsetty N, Voynov V, Kayser V, Helk B, Trout BL 2009. Design of therapeutic proteins with enhanced stability. *Proc Natl Acad Sci U S A* 106(29):11937-11942.

104. Engen JR 2009. Analysis of Protein Conformation and Dynamics by Hydrogen/Deuterium Exchange MS. *Anal Chem* 81(19):7870-7875.

105. Iacob RE, Engen JR 2012. Hydrogen exchange mass spectrometry: are we out of the quicksand? *J Am Soc Mass Spectrom* 23(6):1003-1010.

106. Yadav S, Laue TM, Kalonia DS, Singh SN, Shire SJ 2012. The influence of charge distribution on self-association and viscosity behavior of monoclonal antibody solutions. *Mol Pharm* 9(4):791-802.

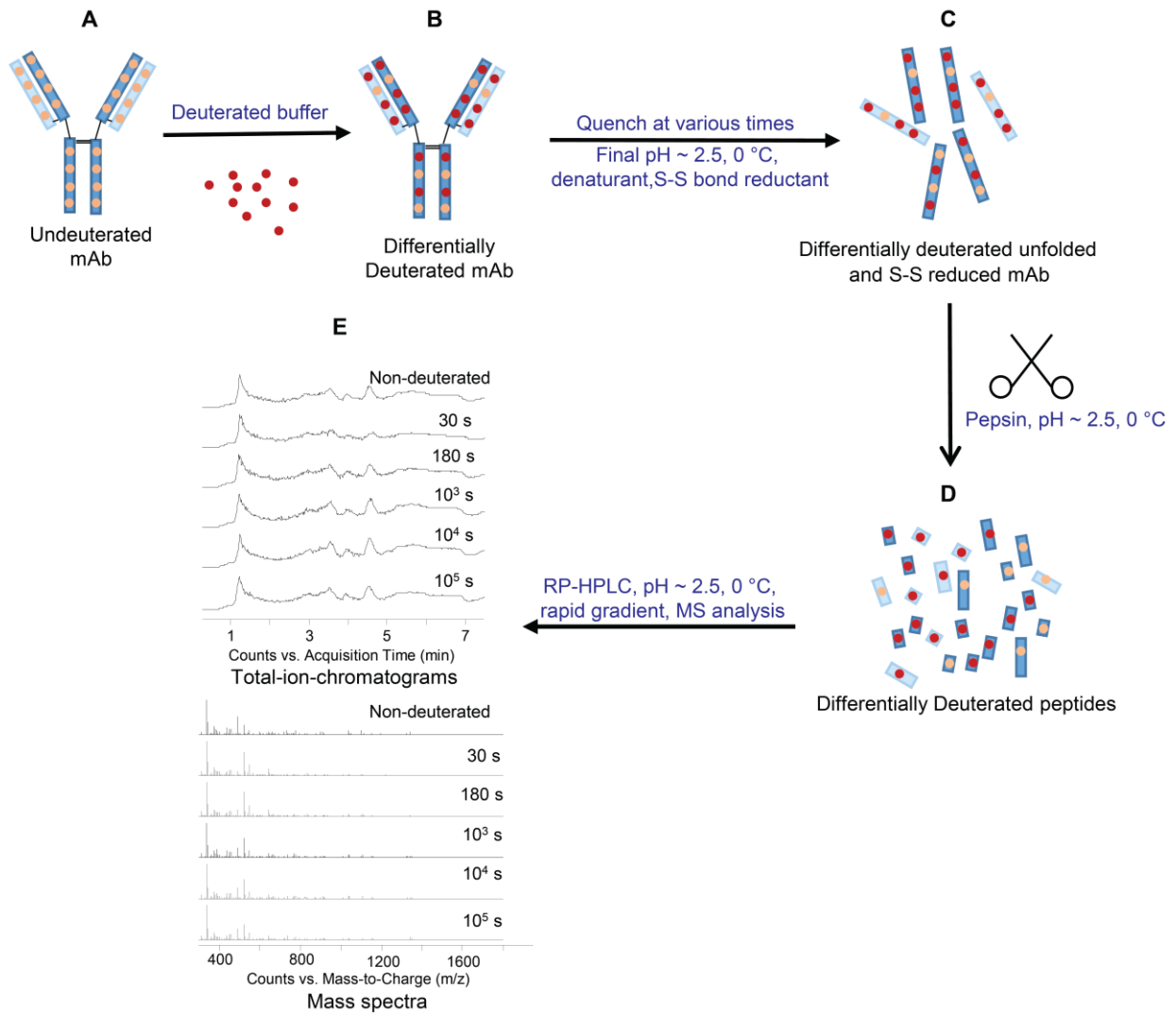
107. Liu J, Nguyen MD, Andya JD, Shire SJ 2005. Reversible self-association increases the viscosity of a concentrated monoclonal antibody in aqueous solution. *J Pharm Sci* 94(9):1928-1940.

108. Yadav S, Liu J, Shire SJ, Kalonia DS 2010. Specific interactions in high concentration antibody solutions resulting in high viscosity. *J Pharm Sci* 99(3):1152-1168.

109. Mason BD, Zhang L, Remmele RL, Jr., Zhang J 2011. Opalescence of an IgG2 monoclonal antibody solution as it relates to liquid-liquid phase separation. *J Pharm Sci* 100(11):4587-4596.

110. Nishi H, Miyajima M, Nakagami H, Noda M, Uchiyama S, Fukui K 2010. Phase separation of an IgG1 antibody solution under a low ionic strength condition. *Pharm Res* 27(7):1348-1360.
111. Shire SJ, Shahrokh Z, Liu J 2004. Challenges in the development of high protein concentration formulations. *J Pharm Sci* 93(6):1390-1402.

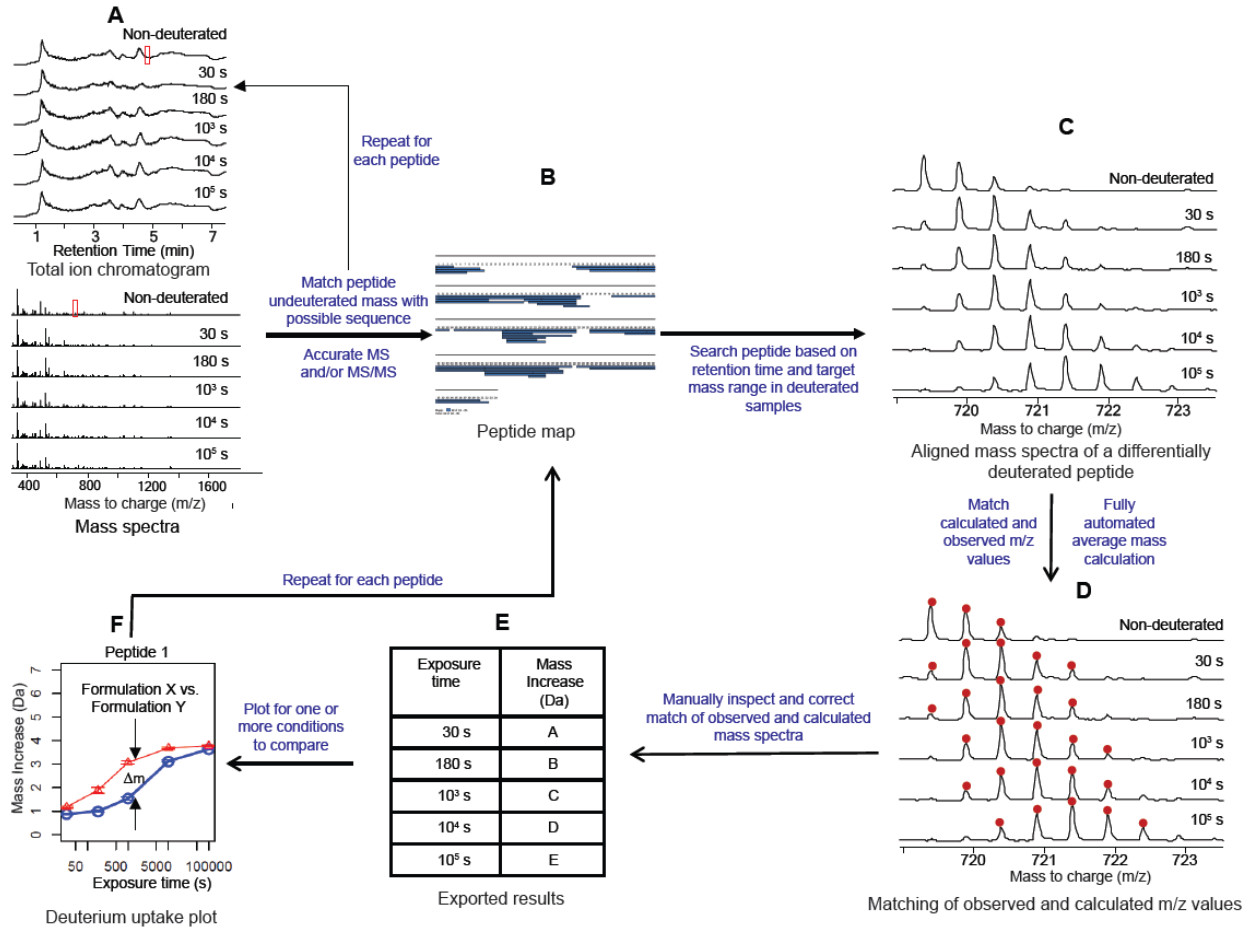
Figure 1.1



Schematic representation of the H/D-MS experimental workflow for a typical IgG mAb. In the first step, the concentrated mAb stock (panel A) is diluted ~ 20-fold with deuterated formulation buffer to initiate deuterium exchange of backbone amide hydrogens (panel B). In the second step, the exchange is quenched after various pre-defined times by mixing with an ice-cold acidic quench buffer to lower the pH to 2.5 and the temperature to 0 °C. The antibody is denatured and

reduced during the quench step as well. In the third step, the quenched antibody solution (panel C) is injected into the sample loop of the LC where a loading pump carries the antibody through an immobilized pepsin column and the resultant peptides (panel D) are trapped by a reversed-phase trap. In the fourth step, the peptides are eluted from the trap by a gradient pump (HPLC or UPLC), separated by a reversed-phase column held at 0 °C, and then analyzed by a mass spectrometer. The data (panel E) obtained from the LC-MS contains the total ion chromatograms and mass spectra for all peptides from each deuterium exchange time point.

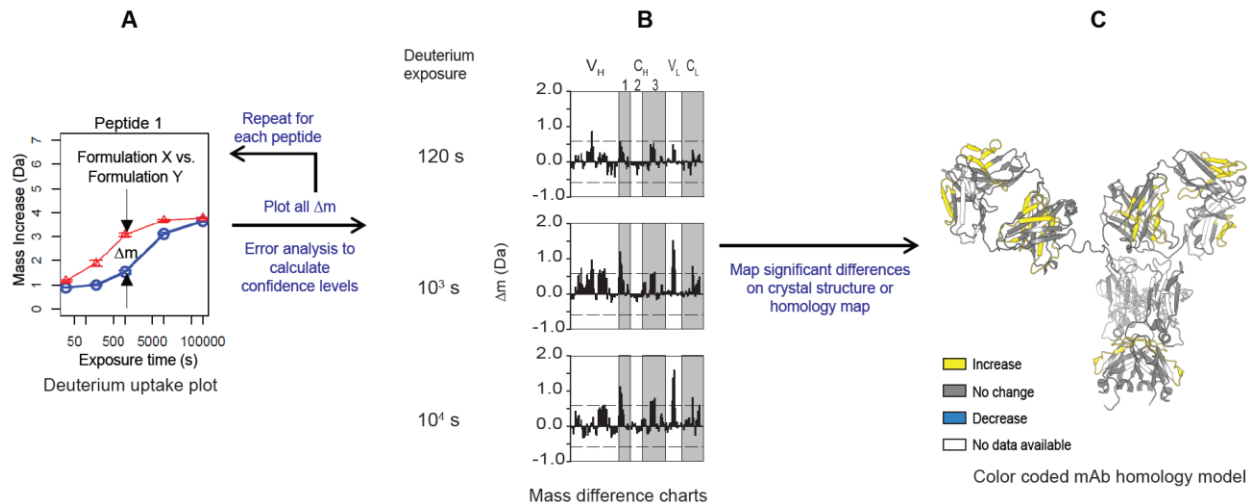
Figure 1.2



Schematic representation of the H/D-MS data processing workflow for a typical IgG mAb. In the first step, the LC-MS data (panel A) are processed to find peptides that match particular sequences of the mAb to obtain an initial peptide map (panel B). All peptides are identified based on accurate mass measurements and/or fragmentation-based tandem mass measurements of undeuterated peptides. In the second step, the sequence and retention time of peptides are fed into the H/D-MS data processing software along with the mAb primary sequence. The H/D-MS data processing software searches for peptides in the deuterated sample (panel C) based on

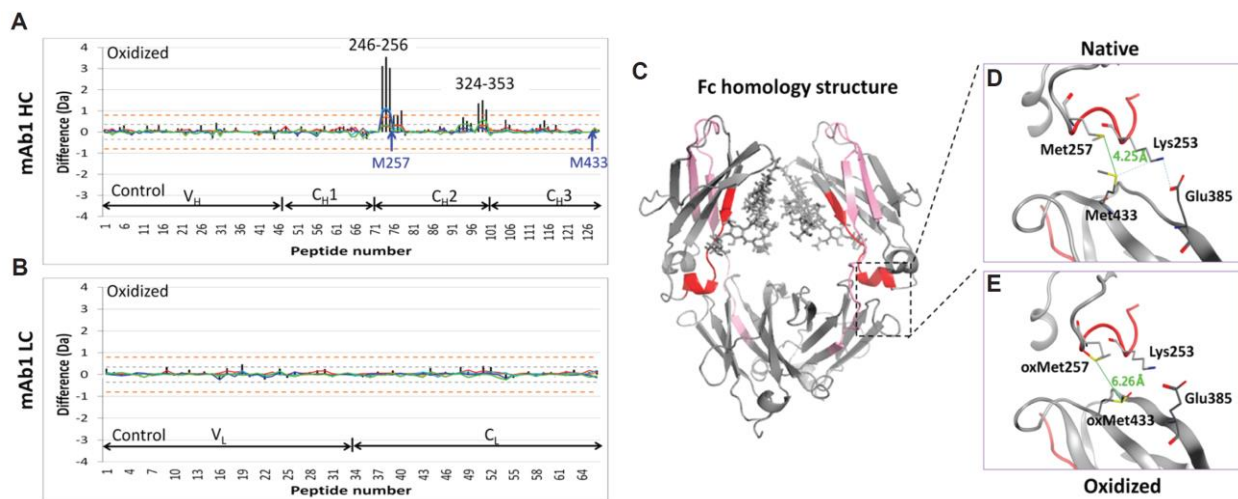
retention time and m/z of the peptides in the non-deuterated sample. In the third step, the software matches observed and calculated m/z values of deuterated peptides in the experiment in fully automated way. When a match is established (as indicated by the red dots in panel D), the centroid m/z value of the peptide isotopic cluster is calculated by the software. In the fourth step, the peptide spectra are manually inspected (and corrected if required) for the accurate matching of observed and calculated mass spectra. The deuterium uptake (in Da or percentage) (panel E) for each peptide segment is calculated from the mass difference values between a deuterated mAb sample and the corresponding undeuterated sample automatically. In the fifth step, the kinetic profile of deuterium uptake for a mAb peptide segment is generally plotted as a graph (panel F) and also used to compare two or more conditions. This analysis is then repeated for each peptide.

Figure 1.3



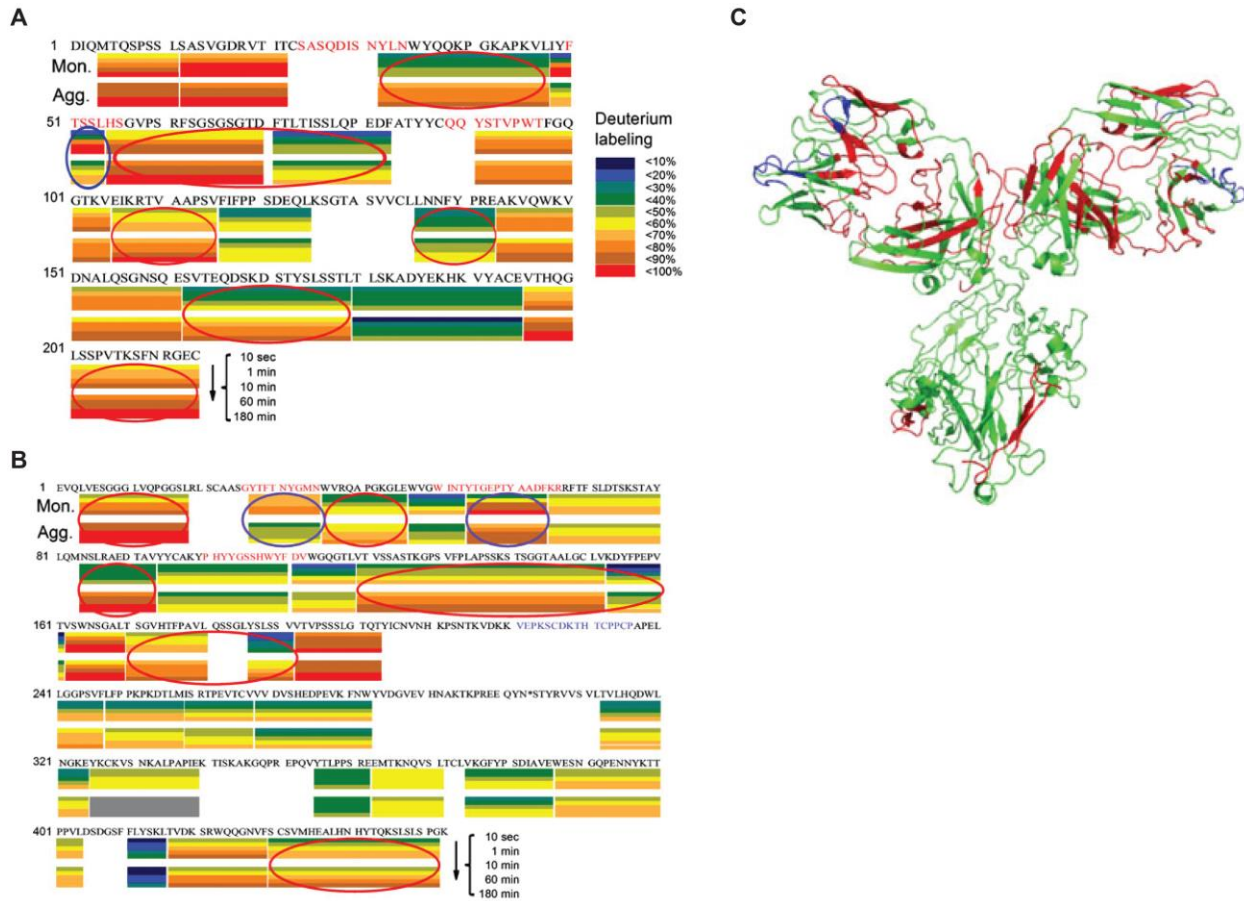
Statistical analysis of H/D-MS data to identify significant changes in local dynamics of a mAb. At the first step, deuterium uptake differences for each peptide segment are calculated for each exchange time point (Δm) (as shown in panel A) and plotted, for example, as bars (panel B). The 99% confidence interval for a significant difference is calculated by pooling variance values of all deuterium uptake measurements and by propagating the error for two measurements. The significant differences are then shown as colored regions in a homology map of the mAb (panel C). The homology model was created from an antibody X-ray crystal structure (PDB 1HZH).¹⁰²

Figure 1.4



H/D exchange differential plots for mAb1 heavy chain (HC, Panel A) and light chain (LC, Panel B). The two protein states compared are Met oxidized and control sample. Deuterium labeling was measured at 10 s (red), 1 min (orange), 5 min (cyan), 30 min (blue), and 180 min (green). Vertical sticks represent the sum total of H/D exchange differences for each peptide from the five labeling times. The gray and orange dotted lines represent the criteria for a significant H/D exchange difference for one single labeling time and for the total exchange difference, respectively. The regions with significant differences are labeled accordingly. Molecular modeling illustrating the effect of Met oxidation on mAb1 conformation (Panel C). Regions 246–256 and 324–353 are highlighted in red and pink, respectively, to represent different levels of conformational changes caused by Met oxidation. Zoomed-in view of the local conformation at the C_{H2}–C_{H3} interface is shown for native (Panel D) and Met oxidized (Panel E) mAb1. The distance between two sulfur atoms of Met257 and Met433 is labeled in green. This figure is reproduced from Zhang and Liu, 2014²⁹ by permission from American Chemical Society.

Figure 1.5

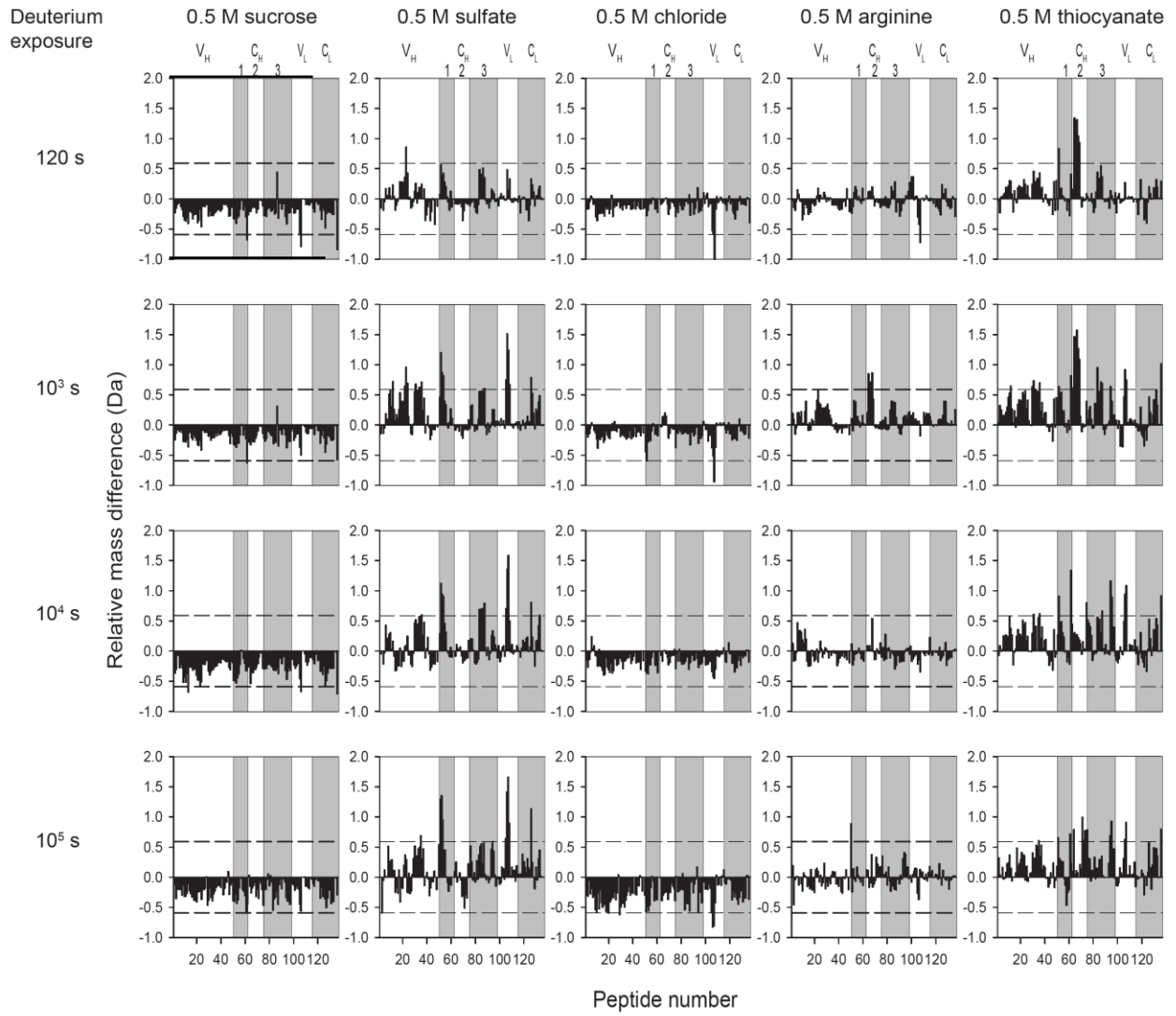


Representation of H/D exchange data mapped onto primary sequence of a mAb. Peptide level H/D exchange labeling patterns of LC (A) and HC (B) of native Bevacizumab and thermally-induced aggregates. The labeling for each peptide is shown by two sets of five colored bars underneath the corresponding portion of the primary sequence. For each peptide, the labeling of native protein is shown by the top five bars, and the labeling of aggregates is shown by the bottom five bars. Each set of bars represents the labeling at five different labeling times (from top to bottom, 10 s, 1 min, 10 min, 60 min and 180 min). The percentage of deuterium labeling in each peptide at each labeling time is color-coded using the scale shown (A). The regions with

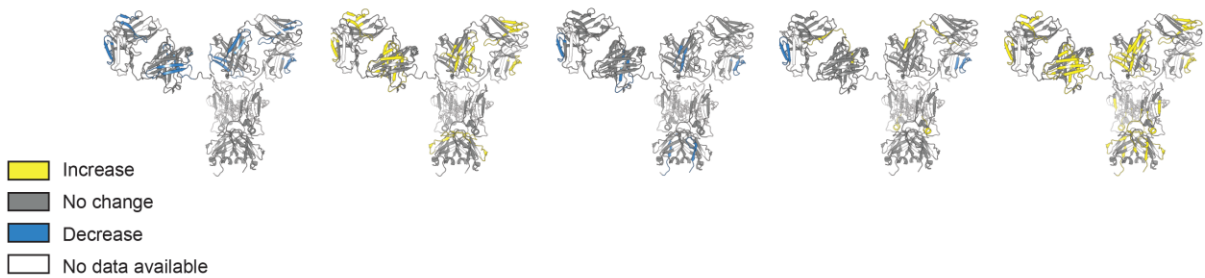
dramatic increases and decreases in deuterium labeling after thermally induced aggregation are circled in red and blue, respectively. The gray block in (B) indicates a peptide that was not detectable in the analysis of the aggregate. (C) Three-dimensional representation of regions of Bevacizumab showing significant increases and decreases in labeling. The peptides from (A) and (B) that showed significant increases (red) and decreases (blue) in deuterium labeling after thermally induced aggregation are indicated. The Bevacizumab structure was created by homology modeling using 1IGY as a template. This figure is reproduced from Zhang and Fernandez, 2012²⁸ with permission from Springer.

Figure 1.6

A

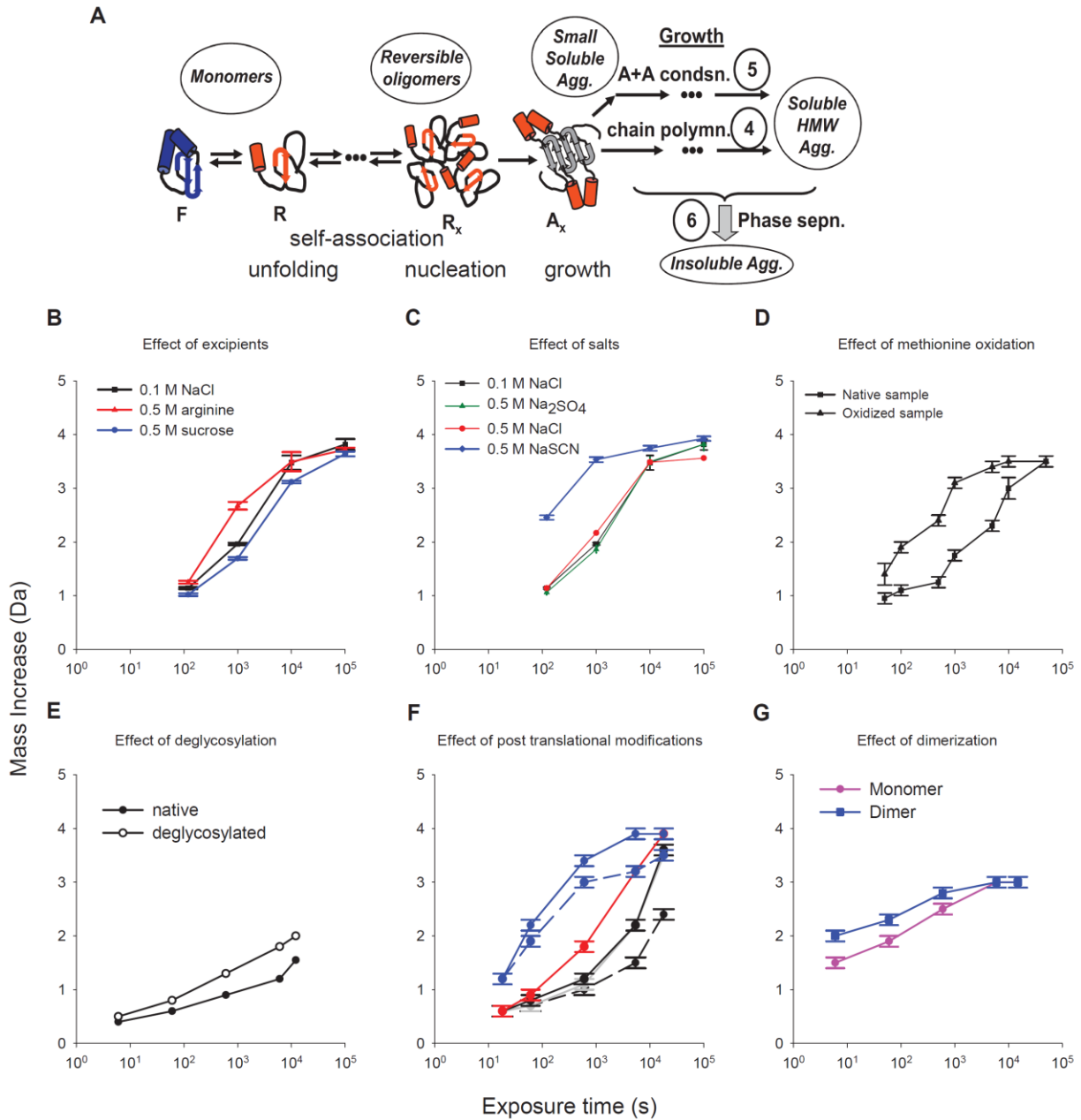


B



(A) Relative deuterium uptake differences for all peptide segments of an IgG1 mAb in the presence of two pharmaceutical excipients and sodium salts from the Hofmeister series as measured by H/D-MS at each deuterium exposure time. Samples contained 0.5 M sucrose, sodium sulfate, sodium chloride, arginine, and sodium thiocyanate in 20 mM citrate-phosphate buffer at pH 6.0 and were compared relative to the control solution (0.1 M sodium chloride in the same buffer). The dashed lines at ± 0.59 Da represent the 99% confidence interval. The horizontal axis denotes the ordinal peptide numbers, sorted in ascending order from the N-terminus of the heavy chain to the C-terminus of the light chain based on the midpoint of their sequences. Positive values in these plots represent increased H/D exchange by a peptide in the presence of the additive relative to the control. Negative values represent decreased H/D exchange. Locations of the mAb domains shown in the figure are approximate since some peptide segments span two different domains. (B) Effects of additives on the H/D exchange of the mAb plotted onto a homology model of the IgG1 mAb. Changes in flexibility are colored according to the legend. These figures have been redrawn and adapted from data presented in Majumdar et al, 2013¹², and Manikwar et al, 2013¹³.

Figure 1.7



Potential aggregation hotspot in the C_{H2} domain of IgG mAbs as identified by H/D-MS. (A) Schematic representation of some of the key steps in protein aggregation pathway (see text for explanation). This figure is reproduced from Roberts and Sahin, 2011⁹⁸ with permission from Elsevier. (B) Arginine increased and sucrose did not affect the deuterium uptake in the C_{H2}

segment HC 241-252.¹³ (C) Thiocyanate increased the deuterium uptake in the C_{H2} segment HC 241-252¹² while chloride and sulfate had no effect. (D) Methionine oxidation increased the deuterium uptake of the C_{H2} segment HC 242-252 (FLFPPKPKDTL).³⁰ (E) Deglycosylation increased the deuterium uptake of the C_{H2} segment 242-253 (FLFPPKPKDTLM).²⁰ The black line represents data from the glycosylated form and the dotted line represent data from deglycosylated form of the mAb. (F) Post-translational modifications alter the deuterium uptake in the C_{H2} segment HC 242-253.²⁷ Solid black, native IgG1; solid gray, degalactosylated IgG1; dotted black, hypergalactosylated IgG1; solid red, deglycosylated IgG1; solid blue, methionine oxidized IgG1; dotted blue, hypergalactosylated-methionine-oxidized IgG1. (G) Dimerization of mAb increased the deuterium uptake of the C_{H2} segment HC 249-259 (FLFPPKPKDTL).⁸⁷ The sequence numbers mentioned here are slightly different for each graph due to slightly different number of residues present in IgG1 mAbs used in these different studies, but they correspond to the same segment in the C_{H2} domain. The deuterium uptake curves marked as (B) to (G) have been redrawn from data presented in Majumdar et al, 2013¹², Manikwar et al, 2013¹³, Burkitt et al, 2010,³⁰ Houde et al. 2009,²⁰ Houde et al. 2010,²⁷ and Iacob et al. 2013.⁸⁷

Chapter 2

Minimizing carry-over in an online pepsin digestion system used for the H/D exchange mass spectrometric analysis of an IgG1 monoclonal antibody

(“Minimizing carry-over in an online pepsin digestion system used for the H/D exchange mass spectrometric analysis of an IgG1 monoclonal antibody.”, Majumdar R., Manikwar P., Hickey J.M., Arora J., Middaugh C.R., Volkin D.B., Weis D.D., J. Am. Soc. Mass Spectrom. 2012 Dec; 23(12): 2140-8.)

2.1 Introduction

Over the past two decades, amide H/D exchange coupled with MS-based detection has matured into a valuable tool in the analysis of protein structure in solution.^{1, 2, 3, 4} When a protein is placed in a large excess of D₂O, the backbone amide hydrogens undergo exchange with deuterium at rates that are characteristic of protein conformation and dynamics. Mass analysis reveals the kinetics of deuterium incorporation, usually expressed in the form of a deuterium uptake curve. The technique is widely used to detect ligand binding⁵ and to understand ligand-induced conformational changes⁶, to define the effects of protein-protein interactions^{7, 8}, to understand the effects of post-translational modifications or other chemical changes⁹, to characterize the dynamics of intrinsically disordered proteins^{10, 11}, to map protein-protein interfaces¹², and to evaluate therapeutic proteins as part of biopharmaceutical comparability studies⁹.

Localized information, at a resolution of ~10 amino acid residues, can be achieved by subjecting deuterated proteins to proteolysis under slow-exchange conditions (so-called quenched conditions, pH ~2, 0 °C)^{1, 13}. Acid-tolerant proteases such as pepsin are required for this digestion step. Even under quenched exchange conditions, the slow deuterium loss during digestion in H₂O-based solutions demands rapid proteolysis. For this reason early H/D-MS work employed high concentrations of solution-phase pepsin. The high protease concentration can interfere with the subsequent LC-MS analysis, and even at high concentrations, digestion is often inadequate. The development of online systems using immobilized pepsin columns for H/D-MS¹⁴ greatly improved digestion efficiency and eliminated pepsin from the downstream analysis.

The abundance of the peptides generated by rapid proteolysis with immobilized protease columns can lead to carry-over artifacts. The problem of carry-over is particularly vexing in H/D

exchange experiments because the retained peptide undergoes extensive back-exchange during the delay between sample injections. Such back-exchanged carry-over will manifest itself in the mass spectral data as isotopic profile doublets consisting of both a deuterated peptide feature and a corresponding undeuterated feature left over from the previous injection (for example, see figure 2.4 in work of the Fang *et al.*¹⁵). Such carry-over can produce a mass spectral profile that can be mistaken for exchange via the EX1 mechanism¹⁵. In this same study, mitigation of carry-over of a collection of so-called sticky peptic peptides in reversed-phase column and trap of a UHPLC was systematically explored¹⁵. The potential for the immobilized pepsin column to also contribute to carry-over artifacts in H/D exchange MS experiments was suggested but not investigated by Fang et al, presumably since the wash protocols identified in their work (for minimizing carry-over in the reversed-phase column and trap) were not expected to be compatible with maintaining pepsin's enzymatic activity.

In the course of recent method development for the H/D-MS analysis of an IgG1 monoclonal antibody in our laboratories, we encountered excessive carry-over of peptic peptides in our online digestion system. Given the recent interest in the potential utility of hydrogen/deuterium exchange mass spectrometry for analysis of IgG monoclonal antibodies (mAbs),^{9, 16, 17, 18} it is important to assess the nature and extent of peptide carry-over issues with each mAb, especially given the large number of peptides generated with these ~150 kDa proteins. In this paper, we show that the primary source for carry-over for our system arose not from the reversed-phase columns, but from the online pepsin digestion process. We further demonstrate that a simple two-step washing procedure can be used to substantially decrease this carry-over and that 100 cycles of the washing process does not adversely affect the activity and specificity of the immobilized pepsin column. Since previous H/D-MS studies with mAbs have not mentioned

this aspect of method development, this work serves as a case study to raise awareness and provide a protocol that minimized carryover during H/D-MS studies with a particular IgG1 mAb.

2.2 Materials and Methods

2.2.1 Reagents and materials

LC mobile phases were prepared from LC/MS grade acetonitrile and water (Fisher Optima) and formic acid (Thermo Scientific, 99+ % LC/MS grade). Phosphoric acid solution and acetic acid (both HPLC grade, > 98.5 %) were obtained from Fluka. Isopropanol (Optima LC/MS grade) was obtained from Fisher Scientific. Guanidine hydrochloride, tris(2-carboxyethyl)phosphine hydrochloride (TCEP), porcine pepsin were obtained from Sigma-Aldrich. The IgG1 monoclonal antibody stock contained 50 mg ml⁻¹ protein containing 0.005 % polysorbate 80 in 10 mM sodium-histidine buffer at pH 6.

2.2.2 Sample preparation

The antibody sample was diluted to 10 mg ml⁻¹ working concentration with 10 mM sodium histidine buffer at pH 6.0. For a typical mAb digest run, 5 µl of antibody sample at working concentration was diluted with 95 µl of 0.1 % formic acid. This solution was mixed with a reducing quench buffer containing 500 mM TCEP, 4 M guanidine hydrochloride and 200 mM sodium phosphate buffer at pH 2.5 in a 1:1 ratio by volume. The antibody sample was incubated at 0 °C for one minute for disulfide bond reduction and then 10 µL of this solution (approximately 16 pmol of antibody) was injected into sample loop of the LC. The short incubation time, low temperature, and low pH mimic typical quenching conditions for H/D exchange.

2.2.3 Chromatography and mass spectrometry

A single-valve, two-pump system for H/D exchange with a refrigerated valve and column compartment was used to maintain 0 °C throughout the online digestion and separation, as described previously (see Fig 2.1)¹⁹. Following sample injection, a loading pump carried the sample through a 50 mm × 2.1 mm immobilized pepsin column, prepared in-house¹⁴, using 0.1 % formic acid at a flow rate of 200 μL min⁻¹. The resultant peptides were captured and desalted on a reversed-phase trap (Peptide Concentration & Desalting microtrap, Bruker-Michrom, Auburn, CA) for 5 minutes at the same flow rate. For gradient elution the mobile phases were 0.1 % formic acid (A) and 90 % acetonitrile/10 % water/0.1 % formic acid (B). The peptides were eluted from the trap and separated on a reversed-phase analytical column (ZORBAX 300SB-C18, 50 mm × 1 mm, 3.5 μm particle diameter, Agilent Technologies, Santa Clara, CA) using a 15-40 %B gradient over 5 min. Following the shallow gradient, the trap and column were cleaned using a 40-90 %B gradient followed by a 5-90 %B gradient in 1 min each with 1 min of equilibration at the highest and lowest organic content. The needle port and sample loop were cleaned between injections by overfilling with mobile phase B followed by mobile phase A. Following positive electrospray ionization (3.5 kV capillary), mass spectra were acquired with a time of flight mass spectrometer (model 6220, Agilent Technologies, Santa Clara, CA) operating in 2 GHz extended dynamic range mode with the fragmentor set to 150 V. The desolvation gas flow was 10 L min⁻¹ at 325 °C with a nebulizer pressure of 20 psig.

Following the completion of a protein digest run, blanks were run to evaluate carry-over. An LC blank was run first to evaluate carry-over in the peptide trap and the reversed phase column. For the LC blank, the valve was kept in the load position (see Fig 2.1); there was no injection of the contents of the loop. One or two digestion blanks followed the LC blank. For the digestion

blanks, 10 μL of 10 mM sodium histidine buffer diluted 1:1 with the reducing quench buffer was injected. The same gradient was used for all blanks and digests.

2.2.4 Peptide identification

Preliminary peptide identities were assigned on the basis of accurate mass (± 20 ppm) using the known antibody sequence. Peptides that could not be unambiguously assigned by mass mapping were assigned in separate MS/MS measurements. The antibody sample was diluted with quench buffer as described in the *Sample Preparation* section. The sample was infused through an immobilized pepsin column at $200 \mu\text{L min}^{-1}$ at 4°C using a syringe pump. The eluate was collected and flash frozen with liquid nitrogen. The resulting peptide mixture was then analyzed by tandem mass spectrometry by a linear quadrupole ion trap mass spectrometer (LTQ-XL, Thermo Scientific). The peptides were separated by HPLC (Shimadzu) through a reversed-phase C18 column (ZORBAX SB300-C18, 2.1×100 mm, Agilent) with a 120 min 0-60% B gradient (A: 99% H_2O , 1% ACN, 0.1% formic acid; B: 99 % ACN, 1% H_2O , 0.1 % formic acid; $200 \mu\text{l min}^{-1}$ flow rate). The capillary temperature and voltage were set to 275°C and 48 V, respectively. The source current was set to 100 μA , the tube lens was set to 115 V, and the sheath gas flow rate was set to 40. Data-dependent MS/MS analysis was performed using the Xcalibur 2.0 software (Thermo Scientific). Survey mass spectra were acquired in the LTQ over an m/z range of 300-2000. The three most intense ions in each spectrum were selected for fragmentation by collision-induced dissociation using normalized collision energy of 35 V. Ion selection threshold was 1,000 counts and the dynamic exclusion duration was 30 s. After the initial MS/MS run, inclusion and exclusion mass lists were included during additional runs to increase the number of confirmed peptides from the consensus list. Raw data was processed

using the *Proteome Discoverer 1.3* software (Thermo Scientific). Only MS/MS spectra with XCorr score of ≥ 2 were used to validate peptide assignments.

2.2.5 Pepsin column washing

The pepsin column wash process consisted of two injections of 100 μL of wash cocktail. Wash cocktail 1 was 5% acetonitrile/5% isopropanol/20% acetic acid in water and wash cocktail 2 was 2 M guanidine hydrochloride / 100 mM sodium phosphate at pH 2.5. Three different washing processes were evaluated: 2 \times wash cocktail 1, 2 \times wash cocktail 2, and wash cocktail 1 + wash cocktail 2. The loading pump was used to carry each injection through the pepsin column and trap at a flow rate of 200 $\mu\text{L min}^{-1}$ for 7.5 min (see Fig 2.1, middle panel). The injection port and sample loop were flushed between injections as described in the previous section.

2.2.6 Pepsin column stress test

To determine if the pepsin column remained stable after extensive washing, an immobilized pepsin column was subjected to 200 wash injections, alternating between wash cocktails 1 and 2, for a total of 100 cycles of the two-step washing process. This test was performed using an HDX PAL robot (LEAP Technologies, Carrboro, NC) with a refrigerated compartment held at 0 $^{\circ}\text{C}$ housing the trap, columns and valves. The HDX PAL system is comprised of two valves and features a back-flush of the pepsin column to waste during the gradient elution step. In other respects, the configuration of the pumps and columns is the same. The pepsin column stress test began with an online antibody digest run. The digest run was followed by 100 wash cycles, as described above. After the 100 wash cycles, the online digestion of the antibody was repeated.

2.2.7 Data processing

Peptide mass spectral features from digestions were extracted using the Find by Molecular Feature algorithm in MassHunter Qualitative Analysis with BioConfirm (Agilent Technologies, Santa Clara, CA). The peptides were quantified using the MS intensity from spectra averaged across the chromatographic band. Peptides were initially assigned by mapping them onto the antibody sequence by mass-matching (± 10 ppm) using Protein Prospector (MS-Product, <http://prospector.ucsf.edu>). An exclusion list, developed from online digest blanks run before antibody digestion, was used to eliminate pepsin autodigestion peptides. The list of extracted antibody peptides was filtered to exclude peptides with low MS response (< 3000 counts) and to remove peptides with fewer than 5 residues or more than 25 residues. To account for variability across the digest runs obtained on different days, a consensus list of 169 peptides found in all digest runs (Figs 2.2, 2.3, and pre-stress digest of Fig 2.4) was constructed. Consensus peptides were those peptides that matched mass within ± 10 ppm across all runs and had a retention time standard deviation of less than 0.2 min. Since the pepsin column stress test was run using a different LC system, only the 10 ppm mass match criterion was imposed for the pre-stress list. For carry-over detection, a signal threshold of 750 counts, the approximate chemical noise level, was imposed. 101 of the 169 consensus peptide assignments were confirmed using MS/MS; 57 of which were not carried-over and 44 of which were carried over in blank digestions. The pI and hydrophobicity for each identified peptide was determined using *ProtParam*^{20, 21} on the ExPASy server (<http://web.expasy.org/protparam/>).

2.3 Results and Discussion

Because carry-over can introduce serious artifacts into H/D exchange measurements, we routinely undertake a carry-over study at the beginning of LC method development for H/D exchange studies of proteins. Recently, method development work in our laboratories with an

IgG1 monoclonal antibody revealed substantial carry-over in blanks following online pepsin digestion of the protein. Some level of carry-over can usually be found in LC/MS data if one looks hard enough. For quantitative analysis, rigorous definitions of carry-over can be derived that can be used to set thresholds for identifying significant carry-over effects^{22, 23}. In the case of qualitative analyses, such as proteomic studies, however, any amount of carry-over can potentially result in false-positives²⁴. In H/D-MS, carry-over can produce a so-called false EX1 MS signature that can skew the average mass determination¹⁵.

2.3.1 Online digestion is the major source of peptide carry-over

The flow path for our online digestion system¹⁹ at different stages in the analysis process is shown in Fig 2.1. The system consists of a two-position twelve port valve. In the A position, the loop was loaded with sample, the immobilized pepsin column was in-line with the loading pump and the reversed-phase trap and separation column are in-line with the gradient pump. Switching to the B position puts the loop and peptide trap in-line with the pepsin column and loading pump (0.1% formic acid). During this stage, the contents of the loop are carried through the pepsin column and then pass through the trap. Following a suitable digestion interval, the valve was switched back to the A position. In this position, the reversed-phase trap and separation columns are in-line with the gradient pump; a water-acetonitrile gradient was then used to elute and separate the peptides.

Representative chromatographic and mass spectral data illustrating the carry-over problem are shown in Figures 2.2(a) and 2.2(b), respectively. The top panels (labeled mAb digest) show a well-defined chromatographic peak in the extracted ion chromatogram for a selected mAb peptide. To isolate sources of the carry-over in the chromatographic system, we used a series of blank runs following an antibody digestion run. First, an LC blank followed each injection of the

antibody for online digestion. The LC blank was simply a second gradient cycle run while the valve was held in the A position (see Fig 2.1); the reversed-phase trap and separation column were not re-exposed to eluate from the immobilized pepsin column. The second set of panels in Figures 2.2(a) and 2.2(b) (labeled LC blank) show a minimal MS response for the peptide (<1% carry-over, quantified by the MS intensity). As the next set of panels show, however, the peptide was readily detected in a subsequent blank digestion (an injection of sample buffer without protein) with a mass spectral response 26% of its original value. Hence, the major source of carry-over for this peptide was the immobilized pepsin column, not the reversed-phase trap and column.

To account for the inherent variability in digestion across the numerous LC/MS runs in this study, a consensus list of 169 peptides found in common across all digests was employed. For this reason, the reported number of peptides detected in the antibody digests is always 169. The number of consensus peptides detected in the antibody digest and in the blanks are shown in Fig 2.2(c). For the LC blank, out of 169 peptides detected in the digestion of the antibody, only 8 ± 5 peptides were carried over. This result shows that only ~5% of the peptides could be detected as carry-over in the trap and the reversed phase column. On average, the peptides carried-over in the LC blank had an MS intensity of 3.4% of their intensities in the digest. In contrast, blank digestions, showed significantly more carry-over (44 ± 12 peptides) that persisted through a second blank digest (21 ± 14 peptides) and the average intensity was 9%. These results show that most of the carry-over from this antibody digestion arose from the immobilized pepsin digestion process, not from peptides retained on the reversed-phase column and trap. Similar results were obtained when these studies were performed using both a different in-house column and a

commercial column (Applied Biosystems) (data not shown). We have also observed that the number of carried-over peptides increased as the mAb load was increased (data not shown).

2.3.2 Pepsin column washing decreases peptide carry-over

Having established that online digestion was the major source of carry-over, we developed a pepsin column wash procedure. A wide variety of washing reagents and washing cocktails to mitigate peptide carry-over have been described in the literature (for example ^{15, 24}) for the reversed-phase column and trap. In the case of the online pepsin column, however, it is essential that the washing reagents do not irreversibly perturb the immobilized enzyme. The manufacturer's literature indicated that immobilized pepsin would tolerate low concentrations of organic co-solvents and moderate concentrations of denaturants. We thus evaluated two different wash solutions: "Wash 1" consisted of acetonitrile (5 vol%) / isopropanol (5 vol%) / acetic acid (20 vol%) in water, and "Wash 2" contained 2 M guanidine hydrochloride and 100 mM sodium phosphate buffer at pH 2.5. Two sequential loop volumes of the wash cocktails were injected onto the pepsin column (see Fig 2.1). Figures 2.2(a) and 2.2(b) (bottom panels) show that there was a significant decrease in MS response for the representative peptide in both the mass spectrum and the corresponding extracted ion chromatogram (~4% carry-over). The effects of different combinations of the two washes on peptide carry-over in digestion blanks are shown in Fig 2.3. For example, Wash1 + Wash2 was equally effective at minimizing carry-over as 2 × Wash2 (9 ± 5 and 12 ± 3 carried-over peptides, respectively). In contrast, injection of two loop volumes of Wash 1 was significantly less effective than the other two combinations (26 ± 3 carried-over peptides), yet still decreased carry-over in the digest blank relative to carry-over observed without washing (44 ± 12 carried-over peptides). These results demonstrate that for this

IgG1 mAb, peptide carry-over can be substantially decreased by post-digest injection of the wash cocktails through the online immobilized pepsin column.

2.3.3 Pepsin column washing does not degrade pepsin column performance

To determine if the washes would have a detrimental effect on the performance of the pepsin column, we subjected a pepsin column to a stress test consisting of 200 alternating injections of Wash 1 and Wash 2. The pepsin column was used to digest the antibody before and after the stress test. After the stress test, 151 of the 169 peptides were detected (Fig 2.4), indicating that the pepsin column retains most of its specificity. To determine if enzymatic activity was lost, we compared the MS response of each of the 151 individual peptides before and after the stress test. Figure 2.5 shows a plot of peptide MS response after the stress test *vs.* MS response before the stress test. The figure shows a near-unity slope (0.97) with an excellent linear correlation ($r^2 = 0.92$) indicating that there was little loss in peptide abundance following the pepsin column stress test. To further examine the effects of wash protocols on pepsin activity, we examined the mass distribution of all abundant peptides that could be mapped onto the mAb sequence (see Table 2.1). The average peptide mass and standard deviations of the distributions were essentially the same before and after the stress test (1697 ± 1250 Da *vs.* 1769 ± 1366 Da), although there was an 18% decrease in the total number of peptides. (This analysis relies on peptide mass rather than length, since not all peptide assignments in this expanded list of peptides were confirmed by MS/MS.) The results indicate that the stress test had little effect on the selectivity of the immobilized pepsin. Taken together these results demonstrate that extensive washing of the pepsin column does not lead to a pronounced decrease in either specificity or activity.

2.3.4 Basis of the carry-over

A variety of hydrodynamic and chemical effects can cause carry-over²⁴. Regions of unswept volume caused by tubing diameter mismatches, scratches in valve components, or inadequate flushing of a needle port are examples of mechanical sources of carry-over. In the experimental setup employed here, the digestion flow-path was flushed continuously by the loading pump (see Fig 2.1) for 12 min during the gradient step and an additional 17 min during the LC blank shown in Fig 2.2. Despite this long washout period, significant carry-over persisted, as shown in Fig 2.2. In addition, the needle port was thoroughly flushed between injections. Finally, only a limited sub-set of the peptic peptides from the antibody digest were found to carry over. Taken together, these observations suggest that the observed carry-over is not attributable to hydrodynamic effects, rather it appears to be chemical in nature. If undigested protein were carried over, then all peptides would exhibit the effect. Thus we conclude that it is carry-over of peptides or partially digested protein, rather than intact protein.

The observed carry-over has been shown to be primarily due to the immobilized pepsin column digestion process (Figs 2.2 and 2.3). Carry-over could potentially arise from the binding to the immobilized pepsin itself, the column stationary phase substrate, or chromatographic system components (frits, tubing, *etc.*). According to the manufacturer's literature, the POROS substrate for pepsin immobilization is a cross-linked poly(styrene-divinylbenzene). Carry-over could therefore arise from slow release of hydrophobic or aromatic peptides from the stationary phase. Carry-over could also potentially arise from specific binding between pepsin and certain amino acid sequences found in the antibody. For example, pepsin inhibitor-3 (PI-3) from *Ascaris suum* is a protein that reversibly inhibits pepsin through the tight binding of short linear segment into the pepsin active site²⁵. Alternatively, carry-over could also arise from non-specific associations with the pepsin.

To determine if there were any chemical characteristics that could distinguish between peptides exhibiting carry-over from peptides that were not carried over, we compared the two sets of peptides with respect to mass, MS response, pI, and hydrophobicity²⁰ (see Fig 2.6). We are unable to distinguish between peptides that were carried-over from peptides that were not carried-over on the basis of mass, pI, or hydrophobicity. This result suggests that there may in fact be several different mechanisms that contribute to carry-over. Our results suggest that carried-over peptides have a greater MS response, but this is attributable to carry-over becoming undetectable in peptides that had low MS response in the digest.

2.4 Conclusions

In this paper we have demonstrated that significant amounts of carry-over can arise from the digestion of an IgG1 monoclonal antibody with an immobilized pepsin column under conditions used in H/D exchange mass spectrometry measurements. Further, we have shown that the online digestion itself was the major source of the observed carry-over. It remains to be determined whether similar carry-over would arise from other proteases^{26, 27, 28} or whether similar results will be observed with different monoclonal antibodies (*e.g.*, IgG2, IgG4). We have developed a two-step washing process for the immobilized pepsin column that greatly diminished the amount of carry-over for the IgG1 mAb being examined in our laboratory. Finally, we have shown with a pepsin column stress test that extensive washing (100 cycles) does not adversely affect either the specificity or activity of the pepsin column. Based on our analysis of chemical properties of the carried-over peptides, there was no single distinctive property of the peptic peptides that can simply explain the basis for the observed carry-over.

The immobilized pepsin column washing procedure described in this work is not easily implemented on single valve systems¹⁹ because injection interrupts the elution step (see Fig 2.1).

This setup requires that the pepsin column wash must be delayed until the end of the gradient run. In contrast, with two-valve in-line systems¹⁴, such as the robotic system we used for the pepsin column stress test, the wash process can be run in parallel with the elution and reversed-phase separation of the peptides.

2.5 References

1. Z. Zhang, D. L. Smith, Determination of amide hydrogen exchange by mass spectrometry: a new tool for protein structure elucidation. *Protein Sci.* **2**, 522-531 (1993).
2. S. W. Englander, Hydrogen Exchange and Mass Spectrometry: A Historical Perspective. *J. Amer. Soc. Mass Spectrom.* **17**, 1481-1489 (2006).
3. L. Konermann, X. Tong, Y. Pan, Protein structure and dynamics studied by mass spectrometry: H/D exchange, hydroxyl radical labeling, and related approaches. *J. Mass Spectrom.* **43**, 1021-1036 (2008).
4. J. R. Engen, Analysis of protein conformation and dynamics by hydrogen/deuterium exchange MS. *Anal. Chem.* **81**, 7870-7875 (2009).
5. S. Ghaemmaghami, M. C. Fitzgerald, T. G. Oas, A quantitative, high-throughput screen for protein stability. *Proc. Natl. Acad. Sci. USA* **97**, 8296-8301 (2000).
6. J. Zhang, M. J. Chalmers, K. R. Stayrook, L. L. Burris, R. D. Garcia-Ordonez, B. D. Pascal, T. P. Burris, J. A. Dodge, P. R. Griffin, Hydrogen/Deuterium Exchange Reveals Distinct Agonist/Partial Agonist Receptor Dynamics within Vitamin D Receptor/Retinoid X Receptor Heterodimer. *Structure* **18**, 1332-1341 (2010).
7. C. R. Morgan, B. V. Miglionico, J. R. Engen, Effects of HIV-1 Nef on human N-myristoyltransferase 1. *Biochemistry* **50**, 3394-3403 (2011).
8. K. Y. Chung, S. G. F. Rasmussen, T. Liu, S. Li, B. T. DeVree, P. S. Chae, D. Calinski, B. K. Kobilka, V. L. Woods, R. K. Sunahara, Conformational changes in the G protein Gs induced by the α_2 adrenergic receptor. *Nature* **477**, 611-615 (2011).

9. D. Houde, J. Arndt, W. Domeier, S. Berkowitz, J. R. Engen, Characterization of IgG1 conformation and conformational dynamics by hydrogen/deuterium exchange mass spectrometry. *Anal. Chem.* **81**, 2644-2651 (2009).
10. T. R. Keppel, B. A. Howard, D. D. Weis, Mapping unstructured regions and synergistic folding in intrinsically disordered proteins with amide H/D exchange mass spectrometry. *Biochemistry* **50**, 8722-8732 (2011).
11. J. Rumi-Masante, F. I. Rusinga, T. E. Lester, T. B. Dunlap, T. D. Williams, A. K. Dunker, D. D. Weis, T. P. Creamer, Structural basis for activation of calcineurin by calmodulin. *J Mol Biol* **415**, 307-317 (2012).
12. M. J. Bennett, K. Barakat, J. T. Huzil, J. Tuszynski, D. C. Schriemer, Discovery and Characterization of the Laulimalide-Microtubule Binding Mode by Mass Shift Perturbation Mapping. *Chemistry & Biology* **17**, 725-734 (2010).
13. J. J. Rosa, F. M. Richards, An experimental procedure for increasing the structural resolution of chemical hydrogen-exchange measurements on proteins: Application to ribonuclease S peptide. *J. Mol. Biol.* **133**, 399-416 (1979).
14. L. Wang, H. Pan, D. L. Smith, Hydrogen exchange-mass spectrometry: optimization of digestion conditions. *Mol. Cell. Proteomics* **1**, 132-138 (2002).
15. J. Fang, K. D. Rand, P. J. Beuning, J. R. Engen, False EX1 signatures caused by sample carryover during HX MS analyses. *Int. J. Mass Spectrom.* **302**, 19-25 (2011).
16. W. Burkitt, P. Domann, G. O'Connor, Conformational changes in oxidatively stressed monoclonal antibodies studied by hydrogen exchange mass spectrometry. *Protein Sci.* **19**, 826-835 (2010).

17. D. Houde, Y. Peng, S. A. Berkowitz, J. R. Engen, Post-translational modifications differentially affect IgG1 conformation and receptor binding. *Mol. Cell. Proteomics* **9**, 1716-1728 (2010).
18. A. Zhang, S. K. Singh, M. R. Shirts, S. Kumar, E. J. Fernandez, Distinct aggregation mechanisms of monoclonal antibody under thermal and freeze-thaw stresses revealed by hydrogen exchange. *Pharm Res* **29**, 236-250 (2012).
19. T. R. Keppel, M. E. Jacques, R. W. Young, K. L. Ratzlaff, D. D. Weis, An efficient and inexpensive refrigerated LC system for H/D exchange mass spectrometry. *J Am Soc Mass Spectrom* **22**, 1472-1476 (2011).
20. J. Kyte, R. F. Doolittle, A simple method for displaying the hydropathic character of a protein. *J. Mol. Biol.* **157**, 105-132 (1982).
21. E. Gasteiger, A. Gattiker, C. Hoogland, I. Ivanyi, R. D. Appel, A. Bairoch, ExPASy: the proteomics server for in-depth protein knowledge and analysis. *Nucleic Acids Res.* **31**, 3784-3788 (2003).
22. R. Haeckel, Recommendations for definition and determination of carry-over effects. *Journal of Automatic Chemistry* **10**, 181-183 (1988).
23. W. Zeng, D. G. Musson, A. L. Fisher, A. Q. Wang, A new approach for evaluating carryover and its influence on quantitation in high-performance liquid chromatography and tandem mass spectrometry assay. *Rapid Commun. Mass Spectrom.* **20**, 635-640 (2006).
24. G. Mitulović, C. Stingl, I. Steinmacher, O. Hudecz, J. R. A. Hutchins, J.-M. Peters, K. Mechtler, Preventing Carryover of Peptides and Proteins in Nano LC-MS Separations. *Anal. Chem.* **81**, 5955-5960 (2009).

25. K. K. S. Ng, J. F. W. Petersen, M. M. Cherney, C. Garen, J. J. Zalatoris, C. Rao-Naik, B. M. Dunn, M. R. Martzen, R. J. Peanasky, M. N. G. James, Structural basis for the inhibition of porcine pepsin by *Ascaris* pepsin inhibitor-3. *Nat. Struct. Mol. Biol.* **7**, 653-657 (2000).
26. S. Brier, G. Maria, V. Carginale, A. Capasso, Y. Wu, R. M. Taylor, N. B. Borotto, C. Capasso, J. R. Engen, Purification and characterization of pepsins-A1 and A2 from the Antarctic rock cod *Trematomus bernacchii*. *FEBS J.* **274**, 6152-6166 (2007).
27. H.-M. Zhang, S. Kazazic, T. M. Schaub, J. D. Tipton, M. R. Emmett, A. G. Marshall, Enhanced Digestion Efficiency, Peptide Ionization Efficiency, and Sequence Resolution for Protein Hydrogen/Deuterium Exchange Monitored by Fourier Transform Ion Cyclotron Resonance Mass Spectrometry. *Anal. Chem.* **80**, 9034-9041 (2008).
28. M. Rey, P. Man, G. Brandolin, E. Forest, L. Pelosi, Recombinant immobilized rhizopuspepsin as a new tool for protein digestion in hydrogen/deuterium exchange mass spectrometry. *Rapid Commun. Mass Spectrom.* **23**, 3431-3438 (2009).

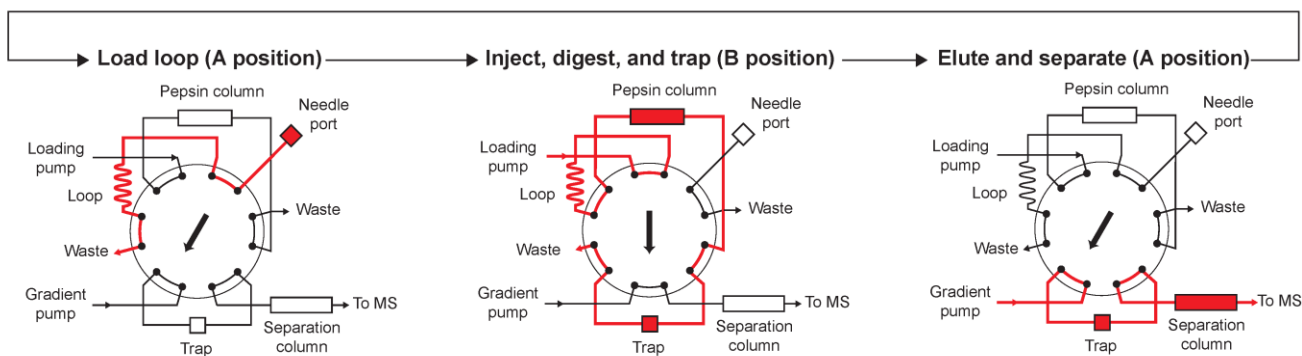
Table 2.1

	before stress test	after stress test
<i>n</i>	565	461
mean mass (Da)	1769	1697
median mass (Da)	1312	1292
standard deviation (Da)	1367	1249

Size distribution and number of IgG1 mAb peptic peptides¹ before and after stress test of immobilized pepsin column. Stress test consisted of 200 alternating injections of Wash 1 and Wash 2; see text).

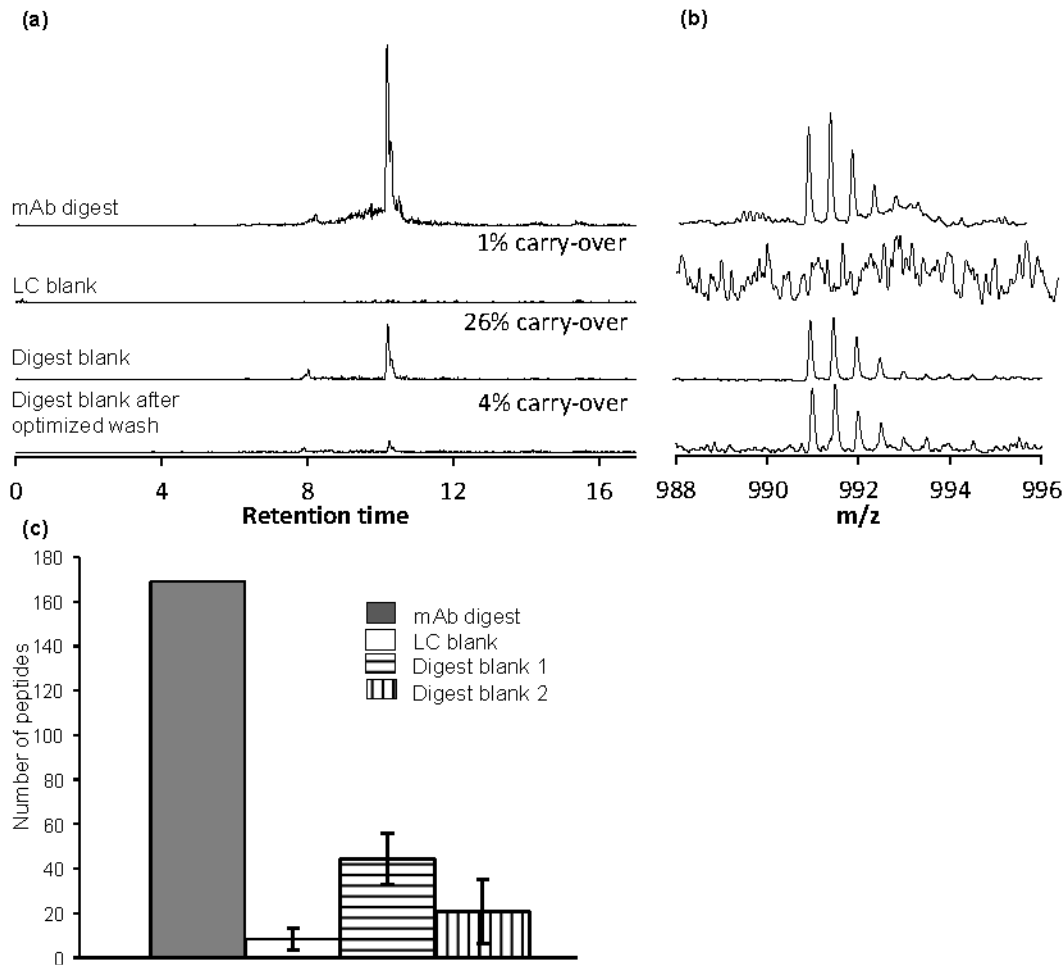
¹MS features that mapped onto the mAb sequence with better than ± 10 ppm mass accuracy and had an MS base-peak response greater than 10^4 cps at the chromatographic peak maximum.

Figure 2.1



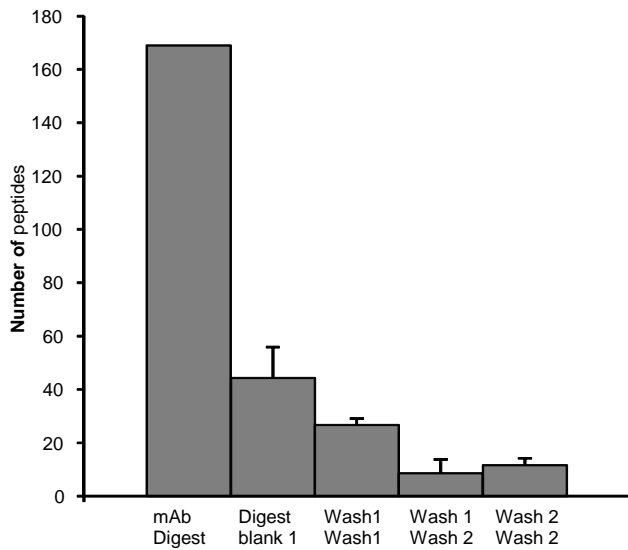
Flow diagram of the LC/MS system for online digestion with an immobilized pepsin column used for carry-over studies. The system is comprised of a two-position, twelve port valve¹⁹. The red regions of the flow path denote the location of sample at the different stages of analysis. In the first step, sample is loaded through the needle port with the valve in the A position. In the second step, the valve is switched to the B position. The loading pump carries sample through the pepsin column where the resulting peptides are captured by the reversed-phase peptide trap. In the third step, the valve is switched back to the A position and a water-acetonitrile gradient elutes the peptides from the trap onto a reversed-phase column for separation and then to the mass spectrometer for analysis.

Figure 2.2



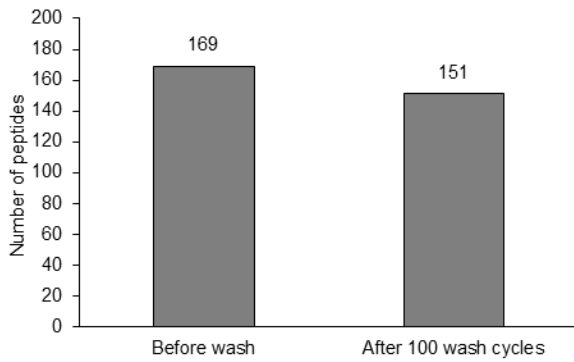
Carry-over from the online digestion of an IgG1 monoclonal antibody with an immobilized pepsin column arises from online digestion. Extracted ion chromatograms (a) and mass spectra (b) of the peptide PEVTCVVVDVSHEDPEVK show that carry-over of this peptide was insignificant in the LC blank compared with the carry-over in the digestion blank. A digest blank following a pepsin column wash (see text for details) shows that washing eliminated the observed carry-over. (c) A list of 169 consensus peptides found in all digestion runs was used to identify carried-over peptides. Only a small number of these consensus peptides were found in the LC blank while a much larger number were detected in two subsequent digestion blanks. Based on flow diagram (see Fig. 2.1), the online pepsin digestion is thus the major source of peptide carry-over. The error bars denote one standard deviation for three independent replicates. (Since all 169 peptides were found in all digestions, no error bars are shown for the digest.)

Figure 2.3



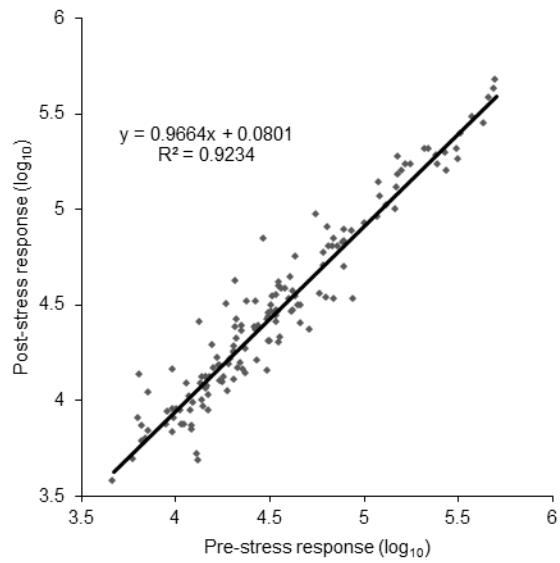
Injections of different combinations of two wash cocktails decreased the number of consensus peptides (see Fig 2.2c) detected as carry-over in the digestion blanks. For comparison, the mAb digest and digest blank 1 values are duplicated from Fig 2.2c. For the composition of the wash cocktails, see the Methods section. The error bars denote one standard deviation for three independent replicates. (Since all 169 peptides were found in all digestions, no error bars are shown for the digest).

Figure 2.4



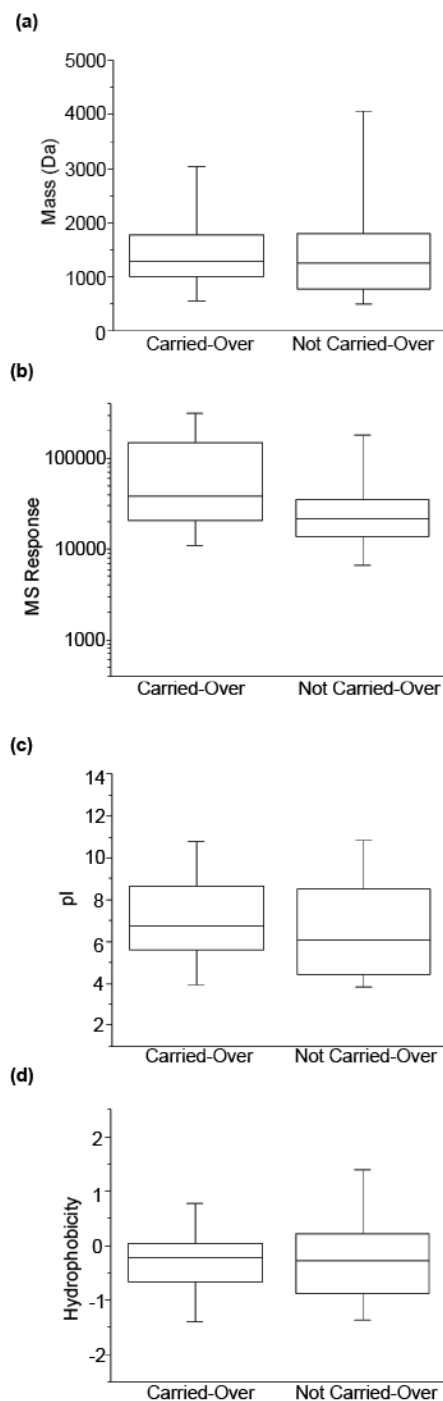
A pepsin column stress test consisting of 200 alternating injections of wash cocktails 1 and 2 did not cause a substantial decrease in the number of detected consensus peptides (see Fig 2.2c) in the online digestion of an IgG1 monoclonal antibody.

Figure 2.5



A pepsin column stress test consisting of 200 alternating injections of wash cocktails 1 and 2 did not cause a substantial decrease in the MS response of the consensus peptides. Each point corresponds to one of the 151 consensus peptides detected after the pepsin column stress test (see Fig 2.4).

Figure 2.6



Carried-over peptides are indistinguishable from peptides that were not carried over on the basis of (a) mass, (b) MS response, (c) pI, and (d) hydrophobicity²⁰. In (d), negative values are hydrophilic and positive values are hydrophobic. For each category, the median value is

designated by the horizontal band in the middle of the box; the box limits indicate the 25th and 75th percentiles. The bars denote the minimum and maximum values.

Chapter 3

Correlating Excipient Effects on Conformational and Storage Stability of an IgG1 Monoclonal Antibody with Local Dynamics as Measured by Hydrogen-Deuterium Exchange Mass Spectrometry

(“Correlating Excipient Effects on Conformational and Storage Stability of an IgG1 Monoclonal Antibody with Local Dynamics as Measured by Hydrogen-Deuterium Exchange Mass Spectrometry.”, Manikwar P., Majumdar R., Hickey J.M., Thakkar S.V., Samra H.S., Hasige A.S, Bishop S.M., Middaugh C.R., Weis D.D., Volkin D.B., J. Pharm. Sci. 2013 Jul;102(7):2136-51.)

3.1 Introduction

Immunoglobulin G1s (IgG1s) are large, complex glycoproteins, belonging to a major class of therapeutic protein drug products approved for treatment of a wide range of human diseases.¹ The IgG1 protein consists of four polypeptide chains that are bridged by disulfide bonds. Each of these polypeptide chains forms distinct globular-like domains (e.g., C_H 1, 2, 3, V_H for the heavy chain; C_L and V_L for the light chain) which in turn form the two antigen binding fragments (F_{ab}) and one crystallizable fragment (F_c) that impart a Y-shaped structure to the molecule. The F_{ab}s are linked to the F_c by a proline-rich hinge region,² which provides flexibility to the molecule.²⁻⁴ Due to these structurally independent fragments, IgG1s are considered to be highly dynamic proteins in solution, with motions ranging from small alterations of side chains and the peptide backbone to larger scale movement of structural domains relative to each other.³⁻⁵ IgG1 molecules are thus not only an excellent model, but also an important therapeutic class of proteins for exploring the inter-relationships between protein stability and dynamics.

A common approach to improve a therapeutic protein's storage stability and protect it from various environmental stresses is adding pharmaceutical excipients to the formulation. Some of the most widely used excipient categories for stabilizing proteins include sugars, polyols, amino acids, salts, and surfactants.⁶ Stabilizing excipients for protein drug candidates, including mAbs, can be identified by high-throughput screening methods that utilize multiple biophysical techniques.⁷⁻¹² For example, a recent study using intrinsic Trp fluorescence spectroscopy examined various stabilizing excipients and identified specific sugars and polyols that increased the thermal unfolding temperature (T_m) of a mAb by ~6 °C. These results correlated well with their effects on aggregation behavior.⁷ Previous studies in our laboratories have shown that excipients such as sucrose and arginine affect both the conformational stability and the global

dynamics of mAbs.¹³ In fact, when two different IgG1 monoclonal antibodies (mAbs) were examined, differential effects of these two excipients on the mAb's conformational stability and global dynamics were observed.^{13,14}

The evaluation of the various physicochemical mechanisms by which excipients interact with and stabilize proteins at the molecular level is an area of active investigation.^{6,15-17} Some excipients stabilize proteins by direct interaction, while others by indirect mechanisms such as preferential hydration.^{6,16} It has been shown that the flexibility of the amide backbone and side-chain interactions can play a significant role in maintaining protein thermal stability.¹⁸⁻²⁰ In addition, solution conditions such as pH and temperature can have profound effects on immunoglobulin dynamics and stability through alteration of solvent fluctuations.^{21,22} These studies suggest a complex relationship between differential flexibility and conformational stability of proteins.²¹⁻²⁵

While several biophysical techniques can provide information about the global dynamics of a protein, localized information is more difficult to obtain, especially for large proteins such as mAbs in solutions containing pharmaceutical excipients. Amide H/D exchange analyzed by mass spectrometry (H/D-MS) has become widely used to measure local backbone dynamics of proteins in solution.²⁶⁻³⁰ H/D-MS in combination with proteolytic fragmentation using pepsin offers peptide-level structural resolution for proteins including mAbs.^{29,31-34} Previously, H/D-MS was successfully applied to study the effect of excipients on protein conformational changes in both the solid state³⁵⁻³⁷ and frozen state.^{29,30} Here, we have adopted H/D-MS to identify regions in an IgG1 mAb with differential flexibility in the presence of stabilizing and destabilizing excipients under solution conditions.

A better mechanistic understanding of protein/excipient interactions as related to their effects on conformational stability, storage stability, and local dynamics may lead to new approaches to improve current protein formulation methodologies. We hypothesize that stabilizing and destabilizing pharmaceutical excipients have differential effects on the local dynamics of certain regions within IgG1 molecules. This, in turn, can be correlated with their effects on the overall conformational and storage stability of mAbs. This work examines the effects of stabilizing (sucrose) and destabilizing (arginine) excipients on the conformational stability as well as the accelerated and long term storage stability of a model IgG1 mAb (mAb-B) at pH 6.0 using differential scanning calorimetry (DSC) and size-exclusion chromatography (SEC), respectively. Concomitantly, H/D-MS analysis was performed with mAb-B in the presence of sucrose and arginine to identify changes in the local flexibility of different regions within mAb-B. Finally, the corresponding local structural flexibility alterations, especially in the C_{H2} domain, were correlated with mAb-B's overall conformational and storage stability.

3.2 Materials and methods

3.2.1 Materials

The IgG1 monoclonal antibody (mAb-B) was obtained at 50 mg/mL containing 0.005 % polysorbate 80 in 10 mM histidine buffer at pH 6.0 from MedImmune (Gaithersburg, MD). Protein concentration was determined with an Agilent 8453 UV-visible spectrophotometer (Palo Alto, CA) using an extinction coefficient $1.45 \text{ M}^{-1} \text{ cm}^{-1}$ after diluting the stock mAb-B solution. Liquid chromatography grade acetic acid and phosphoric acid, tris (2-carboxyethyl) phosphine hydrochloride (TCEP), arginine monohydrochloride, porcine pepsin, guanidine hydrochloride and deuterium oxide (99+%D) were purchased from Fluka/Sigma Aldrich (St Louis, MO). LC/MS grade formic acid (99+ %) was purchased from Thermo Scientific (Rockford, IL).

Sodium chloride and LC-MS grade water, acetonitrile and isopropanol were purchased from Fisher Scientific (Fair Lawn, NJ). Sucrose (ultrapure, RNase free) was purchased from MP Biomedicals LLC. (Solon, OH). Anhydrous forms of sodium phosphate dibasic and citric acid (99.5%) were purchased from Acros Organics (NJ, USA).

3.2.2 Differential scanning calorimetry (DSC)

DSC thermograms were obtained using a Microcal VP-Capillary DSC with autosampler (MicroCal, Northampton, MA). A scan rate of 60 °C/hr. was used over the temperature range 10-100 °C. DSC thermograms of mAb-B in the presence of 0.1 M NaCl (control), and 0.1 M NaCl containing either 0.5 M sucrose, 1 M sucrose, 1.35 M sucrose, 0.5 M arginine, 1 M arginine or 1.35 M arginine in 20 mM citrate-phosphate buffer (pH 6.0) were compared to reference thermograms of buffer alone (sample containing excipients but no mAb-B). Data analysis was performed using the MicroCal LLC DSC plug-in for the Origin 7.0 software package. These results were fit to a multi-state model with three transitions to calculate the midpoint of thermal unfolding (T_m) values. The onset temperature (T_{onset}) was determined by identifying the point where the heat capacity (C_p) value for the first thermal transition reached 500 cal/mol/°C.

3.2.3 Storage stability study

Samples of mAb-B containing 20 mM citrate-phosphate buffer (pH 6.0) with 0.1 M NaCl in the absence of additional excipients (control), or containing either 0.5 M sucrose or 0.5 M arginine were prepared at a concentration of 0.5 mg/mL. Corresponding control solutions were also prepared without mAb-B. All three mAb formulations were sterilized using a 0.22 μ m filter (Millipore, Billerica, MA) in a pre-sterilized laminar flow hood and 0.5 mL aliquots were

dispensed into 1mL borosilicate glass type I vials (West Pharmaceutical Services, Exton, PA) and sealed with rubber stoppers (West Pharmaceutical Services, Exton, PA). Samples were stored in duplicate at -70 , 4 , 25 , and 40 °C and analyzed by SEC at time zero and after storage for approximately 1, 2, 3, 6, 9, and 12 months. For stressed storage, duplicate samples were incubated for 1 month for 55 °C.

3.2.4 Size exclusion high performance liquid chromatography

Samples were analyzed using a Shimadzu HPLC system with photodiode array detector capable of recording 200–400 nm UV absorbance spectra with a 7.8×30 cm Tosoh TSK-Gel BioAssist G3SW_{xL} (TOSOH Biosciences, King of Prussia, PA) and a corresponding guard column. Following preconditioning, the column was calibrated using molecular weight standards (Bio-Rad, Hercules, CA).³⁸ To remove insoluble aggregates, all samples were centrifuged at $14,000 \times g$ for 5 min before injection. To separate soluble mAb-B species based on size, a mobile phase containing 0.2 M sodium phosphate, pH 6.8 and a flow rate of 0.7 mL/min were used. The elution of mAb-B was monitored using the absorbance spectrum from 200-400 nm.

The peak areas for each resolved species (multimer, dimer, monomer, and fragments) were quantified using the dual wavelength quantification method.³⁸ The peak areas for multimers and dimer were combined to obtain the total amount of soluble aggregates. Since this SEC method is primarily used to determine the level of soluble aggregates, monomers and fragments, an indirect method was used to quantify the insoluble aggregates.³⁹ The difference in the total area of mAb-B (sum of all SEC peaks in a chromatogram) at any time point versus time zero was defined as the formation of insoluble aggregates.³⁹ Then, the percentage of each of the species (insoluble

aggregate, soluble aggregate, monomer, and fragment) remaining relative to the total area at time zero was calculated and plotted against incubation time using the equation given below:

$$\% \text{ remaining} = \frac{a_t}{A_0} \times 100$$

where a_t is the area of individual species on any given day (0 or 1 month), A_0 is the total area (combined area) of all the species at time zero. The error bars for soluble aggregate, monomer, and fragment represent standard deviation⁴⁰ of single measurement of duplicate vials, while the error bars for insoluble aggregate were obtained by calculating propagation of uncertainty resulting from the errors in three different measurements (soluble aggregate, monomer, and fragment).

3.2.5 Preparation of deuterated formulation buffers

Deuterated formulation buffers containing 0.5, 1.0, and 1.35 M excipients (arginine or sucrose), 0.1 M sodium chloride and 20 mM citrate-phosphate at pH 6.0 were prepared for deuterium labeling mAb-B. The molar percentage of exchangeable deuterium was fixed at 90 by accounting for exchangeable hydrogens in the excipients. The procedures for preparing a fixed percent of deuterated excipient buffers are discussed below.

The desired mole fraction of exchangeable deuterium in the buffer, F , is given by

$$F = \frac{2n_{D_2O}}{2n_{D_2O} + 2n_{H_2O} + \lambda n_{ex}} \quad (1)$$

where n represents the number of moles of the subscripted substance, the subscript ex denotes the excipient, and λ is the number of exchangeable hydrogens in an excipient molecule. (Equation (1) is accurate to $\pm 0.01\%$ for a typical 20 mM buffer, such as citrate-phosphate. For strongly-buffered solutions, the equation would need to be modified to incorporate the contribution of buffer agents to the pool of total exchangeable hydrogens.)

This equation can be re-arranged into a linear form:

$$2Fn_{\text{H}_2\text{O}} + \lambda Fn_{\text{ex}} = 2(1 - F)n_{\text{D}_2\text{O}} \quad (2)$$

The first step is to fix the number of moles of D2O by choosing a convenient nominal buffer volume (V_{nom}). This volume is arbitrary, but reduces the number of free parameters:

$$n_{\text{D}_2\text{O}} = \frac{V_{\text{nom}}\rho_{\text{D}_2\text{O}}}{M_{\text{D}_2\text{O}}} \quad (3)$$

where ρ is the density of D2O and M is the molar mass of D2O in kg mol⁻¹. Because of changes in solution volume upon addition of solutes, this nominal buffer volume will not be achieved. V_{nom} is used to ensure that sufficient buffer is prepared to within perhaps 20%. Fixing the number of moles of D2O leaves two unknowns in equation (2).

The molal concentration of the excipient (mol kg⁻¹):

$$C_{\text{ex}} = \frac{n_{\text{ex}}}{M_{\text{D}_2\text{O}}n_{\text{D}_2\text{O}} + M_{\text{H}_2\text{O}}n_{\text{H}_2\text{O}}} \quad (4)$$

can be fixed at the desired value. Rearranging into a linear form:

$$C_{\text{ex}}M_{\text{D}_2\text{O}}N_{\text{D}_2\text{O}} = -C_{\text{ex}}M_{\text{H}_2\text{O}}N_{\text{H}_2\text{O}} + n_{\text{ex}} \quad (5)$$

leaves a system of two linear equations, (2) and (5), with two unknowns, n_{ex} and $N_{\text{H}_2\text{O}}$.

Solving these equations provides the general recipe for the deuterated buffer:

$$\begin{aligned} \begin{bmatrix} 2(1-F)n_{\text{D}_2\text{O}} \\ C_{\text{ex}}M_{\text{D}_2\text{O}}N_{\text{D}_2\text{O}} \end{bmatrix} &= \begin{bmatrix} 2F & \lambda F \\ -C_{\text{ex}}M_{\text{H}_2\text{O}} & 1 \end{bmatrix} \begin{bmatrix} n_{\text{H}_2\text{O}} \\ n_{\text{ex}} \end{bmatrix} \\ n_{\text{H}_2\text{O}} &= \frac{\begin{vmatrix} 2(1-F)n_{\text{D}_2\text{O}} & \lambda F \\ C_{\text{ex}}M_{\text{D}_2\text{O}}N_{\text{D}_2\text{O}} & 1 \end{vmatrix}}{\begin{vmatrix} 2F & \lambda F \\ -C_{\text{ex}}M_{\text{H}_2\text{O}} & 1 \end{vmatrix}} = \frac{2(1-F)n_{\text{D}_2\text{O}} + \lambda FC_{\text{ex}}M_{\text{H}_2\text{O}}}{2F + \lambda FC_{\text{ex}}M_{\text{H}_2\text{O}}} \\ n_{\text{ex}} &= \frac{\begin{vmatrix} 2(1-F)n_{\text{D}_2\text{O}} & 2F \\ C_{\text{ex}}M_{\text{D}_2\text{O}}N_{\text{D}_2\text{O}} & -C_{\text{ex}}M_{\text{H}_2\text{O}} \end{vmatrix}}{\begin{vmatrix} 2F & \lambda F \\ -C_{\text{ex}}M_{\text{H}_2\text{O}} & 1 \end{vmatrix}} = \frac{-2(1-F)n_{\text{D}_2\text{O}}C_{\text{ex}}M_{\text{H}_2\text{O}} + 2FC_{\text{ex}}M_{\text{D}_2\text{O}}N_{\text{D}_2\text{O}}}{2F + \lambda FC_{\text{ex}}M_{\text{H}_2\text{O}}} \end{aligned} \quad (6)$$

We confirmed that $\lambda = 8$ for both arginine and sucrose by mass spectrometry as follows. About 1 mg of each excipient was separately incubated in 1 mL of D2O for 24 hours at 25 °C. The solution was then diluted 103 fold in 80% acetonitrile/20% D2O/0.1% formic acid and directly

infused into the electrospray ionization source of a time of flight mass spectrometer (Agilent 6220). The mass spectrometer was operated in positive ion mode for arginine and negative ion mode for sucrose. The number of exchangeable hydrogens was obtained by calculating the mass increase of arginine or the sucrose-formate adduct in the deuterated forms compared to their protonated forms.

The buffers were prepared directly in a graduated cylinder so that the final volume of the solution could be measured. The excipient, D₂O, and H₂O were added according to their calculated weights from equation (6). Once the total solution volume was determined, sodium chloride was added to 0.10 M. Then solid anhydrous citric acid and anhydrous dibasic sodium phosphate (Na₂HPO₄) were added directly at 4.0 mM and 16.0 mM, respectively. The small amounts of buffering agents, < 2 g L⁻¹, did not significantly change the total volume of the solution. The pH was then adjusted to 6.0 without any further correction for the isotope effect.

The final molar concentrations of the excipients were within 4% of their targeted concentrations.

3.2.6 Hydrogen/deuterium exchange mass spectrometry (H/D-MS)

Sample handling for H/D exchange experiments was done using an H/DX PAL (LEAP Technologies, Carrboro, NC) robot. 2 µL of mAb-B (10mg/ml), held at 1 °C, was deuterium labeled with 38 µL of 90 atom% labeling buffer at 25 °C for 120, 10³, 10⁴ and 10⁵ s. The exchange was quenched by 1:1 dilution in a quench buffer (0.5 M TCEP, 4 M guanidine HCl and 0.2 M phosphate at pH 2.5) at 1 °C. 10 µL of the quenched solution (approximately 16 pmoles of mAb-B) was injected into the sample loop of a refrigerated compartment (attached to the H/D exchange PAL and the LC) housing the two valves, the immobilized pepsin column, the reversed phase trap and column. The refrigerated compartment was maintained at 0 °C for our experiments. The LC-MS analysis of the mAb-B peptides were performed as described

previously.⁴¹

3.2.7 MS data processing and analysis

The peptides were identified using a combination of accurate mass data from the TOF and tandem mass spectrometry data from a linear ion-trap mass spectrometer (LTQ-XL; Thermo Scientific).⁴¹ A peptide map covering 85% of the primary sequence of mAb-B with a total of 137 segments was created. H/D exchange data was processed and analyzed in the same manner as described elsewhere.⁴² Briefly, HDExaminer (Sierra Analytics, CA) was used to process the H/D exchange data. All peptide mass spectra from three independent replicate experiments were processed by three different analysts to eliminate any potential bias in data processing. The 99th percentile for a deuterium uptake difference for a peptide segment was ± 0.59 Da in our experimental setup⁴². H/D exchange data were mapped onto a homology model of mAb-B based on human IgG1 b12 (PDB ID: 1HZH)⁴³ as described in the Supporting Information.

3.2.8 Construction of the homology map of mAb-B

mAb-B and IgG1 B12 (PDB ID 1HZH)¹ shared approximately 90% sequence homology with most differences located in the CDR region. Discovery Studio 3.0 (Accelrys, San Diego CA) was used to thread the primary sequence of mAb-B onto the 1HZH structure. Manual reassignment of secondary structures for mAb-B was done after correcting for gaps in the secondary structure assignment and renumbering the residues. Models were displayed using Pymol (Schrödinger, LLC, Portland, OR).

3.3 Results

3.3.1 Sucrose increases whereas arginine decreases the T_{onset} and T_m temperatures of mAb-B

The conformational stability of mAb-B was examined in the presence and absence of excipients. Sucrose and arginine were selected based on their previous recognition as stabilizers and destabilizers of immunoglobulins. Figure 3.1A shows a representative DSC thermogram of mAb-B at pH 6.0 at 0.5 mg/mL which displays three thermal unfolding events with transition temperatures T_{m1} , T_{m2} , and T_{m3} . The first transition (T_{m1}) is associated with the unfolding of the C_{H2} domain,^{44,45} and is more prominent in samples containing arginine than NaCl (control) and sucrose (see Figures 3.1B and 3.1C). The second (T_{m2}) and third (T_{m3}) transitions are associated with the unfolding of the F_{ab} and C_{H3} domains.⁴⁴⁻⁴⁸ A decrease in T_{m1} , T_{m2} , was observed, while T_{m3} increased slightly, with increasing concentrations of arginine compared to control (Figure 3.1B and Table 3.1). In contrast, an increase in all three unfolding temperatures was observed with sucrose in a concentration dependent manner (Figure 3.1C and Table 3.1). The observed changes in conformational stability of mAb-B at pH 6.0, indicated by either increased or decreased T_m values, were consistent with previous results obtained at pH 4.5.¹³ To better understand the effects of arginine and sucrose on the thermal stability of mAb-B, the onset temperatures for unfolding (T_{onset}) were also determined from the same DSC thermograms. As shown in Table 3.1, in the presence of arginine, the T_{onset} values decreased with increasing excipient concentrations. In contrast, the T_{onset} values were delayed in a concentration dependent manner in the presence of sucrose.

3.3.2 Arginine decreases whereas sucrose increases the accelerated storage stability of mAb-B

To better understand the effects of arginine and sucrose on the accelerated and long-term storage stability of mAb-B, protein samples were stored in stoppered glass vials at different temperatures (-70, 4, 25, 40, and 55 °C) for up to 12 months. First, the total area, monomer,

aggregate, and fragment content of SEC chromatograms were compared at day 0; chromatograms of mAb-B at time zero in formulation buffer (20 mM citrate-phosphate buffer at pH 6.0 containing 0.1 M NaCl) without additional excipients (control) and in the presence of 0.5 M arginine or 0.5 M sucrose are shown in Figure 3.2A (dotted lines). These three mAb-B samples contain primarily monomer with low levels of dimer and fragments, and the SEC chromatograms of mAb-B in the three buffers superimpose well with no notable differences (Figure 3.2A; dotted lines). Figure 3.2A (solid lines) also shows an overlay of SEC chromatograms of mAb-B in the same formulation buffers after storage for 4 weeks at 55 °C. It can be seen that these stressed mAb-B samples show an additional, earlier eluting peak (multimeric species), a decrease in monomer, and elevated levels of fragments (peak assignments are based on molecular weight). The loss of monomer was more pronounced in mAb-B samples containing arginine than in NaCl and sucrose.

To better evaluate the effects of arginine and sucrose on formation of different degradants (fragments, soluble, and insoluble aggregates) of mAb-B, SEC results are summarized in a bar chart format at time zero and compared to the same samples incubated for 1 month at 55 °C (Figure 3.2B and 3.2C). At time zero, there are no initial differences between the different forms of mAb-B formulated with either arginine or sucrose compared to control (Figure 3.2B). Samples of mAb-B incubated at 55 °C for 4 weeks showed significant differences in the type and extent of aggregates formed (Fig. 3.2C). For mAb-B samples containing NaCl only (control), both soluble aggregates (i.e., dimers and multimers, 7%) and insoluble aggregates (i.e., derived from total area of chromatograms, 23%) were formed. In comparison, the addition of arginine induced formation of more soluble aggregates (42%) but less insoluble material (12%). In contrast, sucrose essentially completely suppresses formation of insoluble aggregates (i.e., none

detected) with lower levels of soluble aggregates (10%) compared to the control. Although sucrose containing mAb-B samples showed somewhat higher levels of fragmentation (17%) compared to control (13%) and arginine containing formulations (6%), this effect is probably due improved mAb-B solubility (i.e., less insoluble protein) in the presence of sucrose when stored at 55 °C for 4 weeks (Fig 2A).

Figure 3.3 shows the accelerated and long-term storage stability of mAb-B, as quantified by monomer relative to time zero, in different formulations at different temperatures. No significant difference in the rate of loss of monomer was observed in mAb-B samples containing different excipients stored at 4 °C and 25 °C over 12 months (Fig. 3). In addition, no change in loss was observed for the same samples stored over 12 months at -70 °C (data not shown). Samples of mAb-B incubated at 40 °C showed a more rapid rate of loss of monomer compared to 25 and 4 °C (Fig. 3). At 40 °C, mAb-B samples formulated with arginine showed a faster monomer loss after 8 months than NaCl (control), whereas, samples formulated with sucrose manifested slower disappearance of monomer than control throughout the time course studied.

3.3.3 Effect of excipients on the local flexibility of mAb-B in solution

3.3.3.1 mAb-B in control sample (0.1 M NaCl)

For H/D-MS analysis, mAb-B was incubated in 90% deuterated solutions containing 20 mM citrate-phosphate buffer (pH 6.0) and 0.1 M NaCl in the absence (control) and presence of 0.5 M excipients (arginine or sucrose). The exchange reaction was quenched at various times over ~28 hours at room temperature, and the mAb was then subjected to rapid proteolysis using pepsin, and the resulting peptides were separated and mass analyzed using LC-MS. Deuterium uptake plots were generated by plotting the mass increase for each peptide as a function of incubation time. Deuterium uptake plots for six out of 137 mAb-B peptides observed are shown in Figure

3.4. Plots for all 137 mAb-B peptides from mAb-B incubated in the three deuterated formulations are provided in the supporting information Figure 3.S1. For the 0.1M NaCl control, the exchange processes in the various peptides can be classified as relatively fast or slow. For example, the heavy chain 300-306 segment (peptide number 71) in the C_{H2} domain exchanges slowly while the HC 156-174 segment (peptide number 53) in the C_{H1} domain exchanges relatively rapidly (Fig. 3.4). To assess the relative polypeptide backbone flexibility of the entire mAb-B molecule in the control formulation (0.1M NaCl), we reported in a separate study the percentage deuteration at 120 s relative to maximum theoretical deuteration possible (in a companion paper on the inherent flexibility of mAb-B and effects of salts from the Hofmeister series, Majumdar et al, manuscript submitted⁴², backbone dynamics of mAb-B formulated in 0.1 M NaCl are also described; these data serve as a control in this work). The results showed that the C_{H3} and C_{H1} domains of mAb-B are relatively more dynamic, while the C_{H2} domain is relatively rigid, under these solution conditions.⁴²

3.3.3.2 Identifying the effects of excipients on local backbone flexibility of mAb-B

Changes in deuterium uptake for a peptide segment compared to the control (0.1 M sodium chloride in 20 mM citrate-phosphate buffer at pH 6.0) were also used to infer changes in local flexibility due to presence of excipients. These effects are shown in the representative deuterium uptake plots from different regions of mAb-B in Figure 3.4. In the presence of excipients, there can be either an increase or decrease in the rate of H/D exchange at one or more time points compared to the control. For example, in the presence of arginine, the heavy chain 241-252 segment (peptide number 66) in the C_{H2} domain exchanged more quickly with the largest difference, relative to the control, evident at 10³ s. In contrast, samples containing sucrose showed slower exchange in the same region at two different time points, 10³ and 10⁴ s compared

to control. As perhaps expected, the extent of exchange levels-off at later time points (e.g., after 27.8 hr.). As shown in Fig. 3.4, only minor differences in the H/D exchange rates were observed in the five other representative peptide segments of mAb-B across the three formulations. The statistical significance of these observations is addressed below.

To better quantify the effects of excipients on H/D exchange across the 137 peptide segments from mAb-B, we calculated the differential uptake of deuterium, $\Delta D(t) = m_{\text{excipient}}(t) - m_{\text{control}}(t)$, i.e., the difference in the average mass of a given peptide (in the presence of an excipient compared to the 0.1 M sodium chloride control). The relative deuterium uptake differences for each peptide at each labeling time are plotted on the y-axis of Fig. 5 against the corresponding peptide number on the x-axis. Peptide numbers were assigned to each peptide based on ascending order of the sequence midpoint from the N-terminus. In cases where the mid points of two sequences were the same, the peptide sequence with a starting amino acid closer to the N-terminus of the chain was given priority for a smaller peptide number, similar to plots described earlier.³¹ The peptide locations are listed in Table 3.S1.

Following the procedure described by Houde et al.,³² a statistical analysis of the H/D exchange data set for mAb-B peptide segments was performed (Majumdar et al., submitted manuscript)⁴² which showed that the 99% confidence interval for relative uptake differences was ± 0.59 Da. Hence, results in which $|\Delta D(t)| > 0.59$ Da are statistically significant (Figure 3.5, dotted lines). Significant differences were either classified as an increase or decrease based on their corresponding deuterium uptake. This classification was used to identify regions of mAb-B with significant changes in local backbone flexibility due to the presence of excipients. The results are mapped onto a homology model of mAb-B in Figure 3.6. Regions showing increases and decreases are colored red and blue, respectively and unaffected regions are shown in grey.

Regions not covered by H/D exchange measurements are colored yellow. Based on this classification, the effects of 0.5 M excipient (arginine or sucrose) on the local flexibility of mAb-B are discussed below relative to the control (0.1 M NaCl).

3.3.3.3 Arginine alters the local flexibility of certain regions of mAb-B

The effect of arginine on two peptides, HC 241-252 (peptide number 66) in the C_H2 domain and HC 105-126 (peptide number 50) connecting the V_H and C_H1 domains, are classified as a significant increase in local flexibility at 10³ s and 10⁵ s, respectively (Fig. 5), and thus are colored in red in the homology model (Figure 3.6A). The segment LC 47-70 (peptide number 106) in the V_L domain is classified as a significant decrease in local flexibility (colored in blue in Figure 3.6A) at 120 s. The differences in the other four representative segments shown in Figure 3.4 were not significant. As shown in Figure 3.5, only a few significant changes were observed in mAb-B local flexibility (across the 137 peptides) in the presence of arginine compared to the control. Interestingly, the effect of arginine was localized to a few regions of mAb-B (Fig. 3.6A); there were both significant increases, and in some cases decreases, in local flexibility of mAb-B due to the presence of arginine.

3.3.3.4 Sucrose causes small global changes in the flexibility of the mAb-B

As shown in Figure 3.5, the presence of sucrose caused a clear trend of slower rates of deuterium exchange for almost all of the 137 peptides of mAb-B compared to the control; however, many of these small differences were not statistically significant. For example, although the HC 241-252 segment located in the C_H2 domain experienced slower deuterium uptake compared to the control (Fig. 3.4), the relative mass differences for this segment (peptide number 66 in Figure 3.5) do not exceed the 0.59 Da threshold (Fig 3.5). For the other peptide segments shown in Figure 3.4, no significant difference in deuterium uptake were noted except

the segment LC 47-70 (peptide number 106) located in the V_L domain showed a significant negative relative mass difference at 120 and 10^4 s (Fig. 5). Although most of the differences for the remaining 131 peptides across mAb-B were not significant, the segments 36-65 (peptide number 12), 198-220 (peptide number 61), 47-70 (peptide number 106) and 186-212 (peptide number 137) located in V_H , C_{H1} , V_L , and C_L domains, respectively, showed significant decreases in deuterium uptake compared to the control (Fig. 3.5). The regions of significant differences in local flexibility in the presence of sucrose are mapped onto the homology model of the mAb-B in Figure 3.6B.

3.3.4 H/D exchange experiments in the presence of higher concentration of excipients

To explore the effect of increasing concentrations of excipients on local flexibility measurements of mAb-B, H/D exchange experiments were performed in the presence of 1.0 and 1.35 M arginine and sucrose at the 10^3 s time point. A total of 43 mAb-B segments, representing all of the domains of the mAb-B, were analyzed. The mass increase of the 43 segments in the presence of the control, and the control containing either 1.0 or 1.35 M excipients are plotted against excipient concentration as shown in the Supporting Information Figure 3.S2. Although there was generally an increase in deuterium uptake with concentration for arginine and sucrose, the differences, relative to 0.5 M, were not statistically significant. In other words, relative mass differences that were insignificant at 0.5 M did not become significant changes at higher concentrations of arginine or sucrose. These results not only suggest that the effect is fully saturated at a concentration less than 0.5 M, but also suggest sucrose and arginine have no notable effect on intrinsic H/D exchange kinetics (see discussion). Similar studies performed at high concentrations of chloride, sulfate and thiocyanate (1.0 to 1.5 M) also showed no significant differences in the deuterium uptake compared to 0.5 M salts for the same 43 peptides of mAb-

B.⁴²

3.4 Discussion

3.4.1 Physical stability of mAb-B in the presence of arginine and sucrose

Differential scanning calorimetry (DSC) is a powerful and robust technique often used in formulation development for determining thermodynamic properties of macromolecules⁴⁶. DSC has been extensively used to probe the conformational stability of individual mAb domains as a result of environmental stress such as pH and temperature.^{7,13,21,40,45,47} Temperature-induced unfolding of mAbs has displayed either two or three distinct DSC transitions depending on the solution conditions and F_{ab} sequence.^{3,44,45,48} In the case of a 2-peak distribution, each of these transitions corresponds to either C_{H2}/F_{ab} and C_{H3} or C_{H2} and F_{ab}/C_{H3}, respectively. Typically the unfolding of the C_{H2} domain takes place at a lower temperature than the C_{H3} domain while the unfolding of the F_{ab} region can occur at similar temperature comparable to that of the C_{H2} or C_{H3} domain depending on the stability of F_{ab}. In the case of a 3-peak distribution, the unfolding of the F_{ab} takes place at an intermediate temperature between that of the C_{H2} and C_{H3} domains.

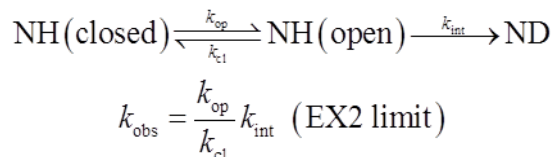
Based on these studies, the DSC thermograms of mAb-B in the presence of NaCl (control), sucrose and arginine at pH 6.0 were evaluated and showed a three-peak distribution (Figure 3.1A) including a major, large peak (T_{m2}) between 65 °C and 85 °C presumably arising from the unfolding of the F_{ab}; a smaller shoulder (T_{m1}) between 57 °C and 80 °C associated with the unfolding of the C_{H2} domain; and a second, minor peak (T_{m3}) between 80 °C and 90 °C which can be assigned to the C_{H3} domain. In the presence of sucrose (Fig 3.1B) and arginine (Fig. 3.1C), the T_{m1} peak moves to higher (between 60 and 80 °C) and lower temperatures (between 50 °C and 80 °C), respectively, probably primarily due to a structural changes in the C_{H2} region, followed by effects on the second and third transitions (T_{m2} and T_{m3}) corresponding to the

thermal unfolding of the F_{ab} and C_{H3} domains, respectively. In the presence of sucrose and arginine, the T_{onset} values increased and decreased, respectively, in a concentration dependent manner (Table 3.1). To further examine the effects of sucrose and arginine on the physical stability of mAb-B, accelerated and long term storage stability studies were then performed with mAb-B in the formulations containing sucrose or arginine at different temperatures to monitor the extent and type of protein aggregation occurring over time.

Size-exclusion chromatography is commonly used to quantify monomer loss and, indirectly, the formation of insoluble aggregates.^{38,39,49} Aggregation is a major concern because it not only decreases product purity but also due to its link to immunogenicity.⁵⁰⁻⁵² Aggregation of mAbs can arise from different environmental stresses such as temperature,⁵³ agitation^{8,54} and freeze-thaw^{8,53} and has recently been shown to involve, under certain conditions, decreases in solvent accessibility of the CDR region due to new intermolecular contacts.³⁰ In this work, under accelerated temperature conditions (40 °C over 12 months and 55 °C over 1 month), sucrose slowed the rate of monomer loss and the rate of formation of soluble and insoluble aggregates (Figure 3.2 and 3.3). Arginine had the opposite effect leading to increased loss of monomer and higher levels of soluble and insoluble aggregates. At lower temperatures (4 and 25 °C over 12 months), no notable differences were observed in the rate of monomer loss in the presence or absence of sucrose and arginine compared to the control (citrate-phosphate buffer pH 6.0 with 0.1 M NaCl). Additional stability data over the next 12-24 month time period will be required to better determine the extent to which sucrose and arginine affect the long term storage stability of mAb-B, compared to storage at higher temperatures, as measured by SEC.

3.4.2 Effects of excipients on intrinsic exchange

Changes in the rate of H/D exchange in the presence of an excipient can be caused either by the effect of the excipient on the protein or by the effect of the excipient on the chemical exchange process. In the usual EX2 limit of the Linderstrøm-Lang mechanism,^{55,56} the rate of H/D exchange depends on both flexibility (k_{cl}/k_{op}) and intrinsic chemical exchange (k_{int}).



If the rate of intrinsic exchange was excipient-dependent, then the observed rate of H/D exchange could be altered even if the flexibility of mAb-B was not affected.

Changes in intrinsic exchange by sucrose and arginine could potentially arise through different mechanisms. For example, in the case of sucrose, solution viscosity and water activity could potentially affect intrinsic exchange. Experimental data however, argue the presence of sucrose has no significant effect. Exchange by poly-DL-alanine was unaltered in presence of 1 M sucrose.⁵⁷ Moreover, two independent studies have shown that the intrinsic exchange rates are unaffected by decreasing the water activity⁵⁸ or by increasing the solution viscosity induced by osmolytes (such as sorbitol).⁵⁹ It was proposed that viscosity has little influence on intrinsic exchange because of the anomalous migration mechanism of protons in liquid water.⁵⁹ On this basis, we conclude that the changes in H/D exchange kinetics induced by sucrose are attributable to changes in the backbone flexibility of mAb-B, k_{cl}/k_{op} . In this work, no significant differences in the magnitude of change in local flexibility with increasing sucrose concentration were noted across 43 peptides, covering all of the domains of mAb-B. The absence of concentration

dependence further supports the conclusion that sucrose has no significant effect on the intrinsic H/D exchange rates.

Arginine could alter an intrinsic exchange either by changes in ionic strength or through interactions of arginine or its chloride counter-ion with mAb-B. In a separate study with mAb-B, we found that increasing the NaCl concentration from 0.1 M to 0.5 M induced subtle decreases in the rate of H/D exchange across many regions of mAb-B (Majumdar et al, submitted manuscript).⁴² The pattern of altered H/D exchange of mAb-B in presence of 0.5M NaCl is not, however, consistent with the arginine-induced changes observed here. On this basis, we conclude that it is the influence of arginine, not chloride, which dominates this effect. While base-catalyzed intrinsic exchange by poly-DL-arginine shows a strong ionic strength dependence,⁶⁰ in more realistic peptide models, these effects are much smaller.⁶¹ Exchange by alanine model peptides also has little dependence on ionic strength.⁶² If k_{int} were sensitive to arginine, we would expect that altered exchange kinetics in mAb-B would be widespread and show concentration-dependence. Instead, we have found that 0.5 M arginine significantly altered exchange for only a few regions of mAb-B (see Figs 5 and 6A) relative to a 0.1 M NaCl control. Furthermore, the level of differential exchange was not significantly altered when the arginine concentration was increased to 1.0 M and 1.35 M. Hence, we conclude that changes in the kinetics of amide H/D exchange in mAb-B under our experimental conditions are due to the effects of arginine on mAb-B internal mobility and not due to alterations in the intrinsic kinetics of exchange.

3.4.3 Sucrose effects on mAb-B physical stability and local flexibility

As monitored by DSC at pH 6.0, sucrose (0.5 M) increased the onset temperature and three thermal unfolding temperatures for mAb-B (Figure 3.1B and Table 3.1). In addition, 0.5 M

sucrose at pH 6 resulted in slowed monomer loss and slowed soluble and insoluble aggregate formation compared to control when incubated at 55 °C for 1 month and 40 °C for 12 months (Fig. 3.2C and Figure 3.3). These observations are consistent with earlier reports that sucrose prevented formation of soluble aggregates and slowed the rate of monomer loss in two different mAbs^{63,64} and a recombinant human interferon- γ .⁶⁵ Increases in the thermal stability of the native state were also associated with an increase in the free energy of unfolding in the presence of different sugars⁶⁶ and in proportion to sucrose concentration⁶⁷ in several different proteins.

The stabilizing effects of sucrose in aqueous solution were first explained by Lee and Timasheff, more than three decades ago, by a mechanism known as “preferential exclusion”.⁶⁸ Based on this mechanism, sucrose is preferentially excluded from the surface of proteins, and as a result, there is an increase in solution chemical potential. According to the Le Chatelier’s principle, to counteract the imposed changes in the chemical potential, a new equilibrium is established to minimize thermodynamically unfavorable states. In such conditions, proteins adopt to a smaller surface area with more compact and rigid structure to overcome the thermodynamically unfavorable condition.^{68,69} Furthermore, addition of sugars results in an increase in free energy of unfolding and hence the native state is thermodynamically favored.⁷⁰

Bolen et al. studied the internal dynamics of ribonuclease A by following the hydrogen-deuterium exchange rates of individual amide protons using NMR.⁵⁷ They reported a shift in equilibrium to the smallest surface area in the presence of 1 M sucrose. This effect was also associated with a decrease in hydrogen-deuterium exchange rates of amide protons because of preferential exclusion of sucrose from the protein. Similarly, a decrease in H/D exchange rates, along with concomitant decreases cysteine reactivity, were observed for recombinant interleukin-

1 receptor antagonist in the presence of 1 M sucrose as a result of restricted conformational fluctuations and solvent accessibility.⁶⁹

In the current study, a decrease in the local conformational fluctuations throughout mAb-B can be visualized in the differential plots shown in Figure 3.5. Sucrose caused significant decreases in local flexibility in four separate segments of mAb-B, all located in the F_{ab} region (V_H, C_{H1}, V_L, and C_L domains). These changes in local flexibility were associated with improved thermal stability as measured by DSC and slowed aggregation as monitored by SEC. Flexibility changes in these regions of the F_{ab} could be important for mAb stability since it was found recently that site specific mutations in the variable domains (V_H and V_L) of a human antibody resulted in an aggregation resistant protein.⁷¹ Although the significant changes in mAb-B local flexibility defined in this work are based on 99% confidence limits, our H/D-MS studies clearly indicate a global trend in which sucrose causes an overall decrease in deuterium uptake across essentially all regions of mAb-B (Fig. 5). These H/D-MS exchange results across the 137 peptides of mAb-B are consistent with previous observations for H/D exchange in various intact proteins in presence of sucrose (1 M) and trehalose (0.5 and 1 M) monitored by NMR,⁵⁷ FT-IR,^{67,69,72} and H/D-MS.^{73,74} Each of these studies report similar effects of sugars in the form of a global decrease in deuterium uptake in the presence of sucrose and trehalose.

3.4.4 Arginine effects on mAb-B physical stability and local flexibility

In contrast to sucrose-induced stabilization, arginine causes conformational destabilization of mAb-B. This effect is evident in DSC measurements where the appearance of the T_{m1} peak (corresponding to the unfolding of C_{H2} domain) at lower temperatures, along with a significant decrease in the T_{onset} temperature, proportional to arginine concentration is present (Fig. 1C and Table 3.1). Interestingly, decreases in thermal stability correlate well with faster monomer loss

(at 40 °C and 55 °C), and faster aggregation in the presence of 0.5 M arginine at pH 6.0 during storage as measured by SEC (Fig. 3.2C and 3.3B). Similar decreases in thermal stability due to arginine have been reported with the same mAb-B at pH 4.5,¹³ in a different mAb (IgG2)⁷ and in other proteins.^{75,76} The destabilization of RNase A with increasing concentrations of arginine (up to 1.5 M) was proposed to be due to extensive binding of arginine to the protein.⁷⁵ A similar decrease in the thermal stability of cytochrome c was observed in the presence of arginine.⁷⁶

Arginine caused a significant increase in local flexibility in two particular regions of mAb-B: in the C_{H2} domain (HC 241-252) and in the region connecting the C_{H1} and V_H domain (105-126) of mAb-B (Fig 3.4, 3.5, and 3.6A). In addition, a significant decrease in local flexibility was also observed in the region LC 47-70 corresponding to the V_L domain (Fig. 3.5 and 3.6A). The effect of arginine was more prominent on the conformational stability of the C_{H2} domain of mAb-B as is evident from DSC results that show a decrease in T_{m1} values as a function of arginine concentration (Table 3.1). A relatively small decrease in the conformational stability of the F_{ab} (T_{m2}), and no effect on C_{H3} (T_{m3}) is seen as measured by DSC under the same conditions. These conformational stability changes correlate reasonably well with the extent of changes in local flexibility of the F_{ab} (C_{H1}-V_H and V_L domains) and lack of notable changes in the local flexibility of the C_{H3} domain.

In the solution state, arginine is known to interact with a number of functional groups of proteins. This can occur through interaction with charged residues via hydrogen bonding and electrostatic interactions (such as salt-bridge formation), and with aromatic residues through cation- π interactions.⁷⁷⁻⁷⁹ The guanidinium group and methylene groups of arginine can interact directly with a protein's backbone as well as apolar regions.^{78,80} Interactions of arginine with a protein's surface can vary with concentration. At lower concentrations (<0.5 M), arginine is

expected to be directly bound to protein's surface. At higher concentrations (0.5-1.5 M), arginine favors self-interaction forming clusters resulting in reduced interaction with a protein's surface.^{78,81} In this study, we investigated the effect of arginine on thermal stability and local flexibility of mAb-B at three different concentrations of arginine (0.5 M, 1 M and 1.35 M). The H/D-MS results with 43 peptides representing all regions of mAb-B do not show a significant titration effect on deuterium uptake; this result could potentially be due to the self-interaction of arginine at higher concentrations. At such concentrations, even though self-interaction of arginine predominates, it is still possible that weak interactions of arginine with the protein surface may exist. Recently, small angle X-ray scattering (SAXS) analysis of two IgG1s in the presence of arginine (0.1–0.6 M) revealed an increase in structural relaxation and size of two antibodies in a concentration dependent manner, and such changes were not observed in the presence of sulfate and thiocyanate.⁸² With arginine present, structural relaxation of the molecule may result in local conformation changes within mAb-B, resulting in either an increase or decrease in the backbone amide hydrogen bonding network in specific regions leading to altered deuterium uptake. As described above, several studies report the possibility of such specific interactions of arginine with both aromatic side chain residues and the peptide backbone.⁷⁷⁻⁸⁰

3.4.5 mAb-B physical stability and local flexibility of segments within the C_{H2} domain

Arginine-induced physical destabilization of mAb-B correlates with an increase in local flexibility of HC 241-252 within the C_{H2} domain and a segment connecting C_{H1} and V_H domain (105-126) of the F_{ab} region. When compared to the DSC results, a more notable decrease in thermal stability of the C_{H2} domain (T_{m1}) was observed compared to the F_{ab} region (T_{m2}) (Table 3.1) in the presence of varying amounts of arginine. Furthermore, a companion study conducted

in our laboratories (Majumdar et al., submitted manuscript)⁴² showed a substantial increase in flexibility of two different regions in the C_{H2} domain (HC 241-252 and HC 300-306) in the presence of the destabilizing salt (chaotrope) NaSCN. The increase in local flexibility was associated with conformational destabilization as measured by DSC and increased aggregation determined by SEC.⁴² Consistent with these results, two studies from different labs have reported similar regions within the C_{H2} domain to be least stable⁸³ and more prone to aggregation.^{83,84} For example, the binding of protein A to residues in the from C_{H2} and C_{H3} domain of an intact IgG resulted in inhibition of aggregation.⁸⁴ In a separate study, this region (HC 243-247) of the C_{H2} domain in both oxidized and deglycosylated IgG1s was found to be associated with increased deuterium uptake.⁸³ In addition, the oxidized IgG1 was found to be the least stable form of the antibody. Moreover, the thermal stability of an engineered C_{H2} domain was increased by about 20 °C by incorporating an additional non-native disulfide bond.^{85,86} One of the two Cys mutations (L242C) was performed within the 241-252 region of the C_{H2} domain and the other Cys (K334C) was inserted in a neighboring β -sheet. Often the introduction of a disulfide bond decreases the flexibility of the molecule.^{87,88} Together, these results further support the hypothesis that decreasing flexibility of key regions within the C_{H2} domain results in increasing the overall physical stability of an IgG molecule.

Based on results from this work, combined with previous literature results with IgGs as described above, key regions within the C_{H2} domain may dictate the overall physical stability of the mAb-B. The physical stability of mAb-B itself may therefore be further improved by either mutation,⁸⁶ truncation,⁸⁹ or masking the hydrophobic segments⁸⁴ of these key regions of the C_{H2} domain. There are two phenylalanine residues in this region (Phe241 and Phe243) that pack against the glycans as observed in the crystal structure.⁴³ It is possible that destabilizers like

arginine increase conformational fluctuations in this region which expose these aromatic side-chains allowing them to interact with other apolar side-chains. Arginine is often added to protein solutions to improve refolding efficiency and suppress aggregation.⁹⁰⁻⁹² With mAb-B, however, the addition of arginine results in lowering of the T_{onset} temperature (Table 3.1) and an increase in both soluble and insoluble aggregate formation during storage at elevated temperatures (Fig 3.2C and Figure 3.3). This result may be due to increased local flexibility of the C_{H2} domain of mAb-B in the presence of arginine. Finally, these data demonstrate the potential utility of H/D-MS as a new analytical tool to identify stabilizing excipients as part of protein formulation development. To further explore the utility of this approach, ongoing experiments are evaluating the effect of a variety of excipients on local flexibility changes in certain key regions of IgGs using H/D-MS along with their effects on mAb physical stability.

3.5 References

1. Wang W, Singh S, Zeng DL, King K, Nema S 2007. Antibody structure, instability, and formulation. *J Pharm Sci* 96(1):1-26.
2. Kessler H, Mronga S, Muller G, Moroder L, Huber R 1991. Conformational analysis of a IgG1 hinge peptide derivative in solution determined by NMR spectroscopy and refined by restrained molecular dynamics simulations. *Biopolymers* 31(10):1189-1204.
3. Hanson DC, Yguerabide J, Schumaker VN 1981. Segmental flexibility of immunoglobulin G antibody molecules in solution: a new interpretation. *Biochemistry* 20(24):6842-6852.
4. Kim H, Matsunaga C, Yoshino A, Kato K, Arata Y 1994. Dynamical Structure of the Hinge Region of Immunoglobulin G as Studied by ¹³C Nuclear Magnetic Resonance Spectroscopy. *J Mol Biol* 236(1):300-309.
5. Boehm MK, Woof JM, Kerr MA, Perkins SJ 1999. The Fab and Fc fragments of IgA1 exhibit a different arrangement from that in IgG: a study by X-ray and neutron solution scattering and homology modelling. *J Mol Biol* 286(5):1421-1447.
6. Kamerzell TJ, Esfandiary R, Joshi SB, Middaugh CR, Volkin DB 2011. Protein-excipient interactions: mechanisms and biophysical characterization applied to protein formulation development. *Adv Drug Deliv Rev* 63(13):1118-1159.
7. Cheng W, Joshi SB, He F, Brems DN, He B, Kerwin BA, Volkin DB, Middaugh CR 2012. Comparison of high-throughput biophysical methods to identify stabilizing excipients for a model IgG2 monoclonal antibody: conformational stability and kinetic aggregation measurements. *J Pharm Sci* 101(5):1701-1720.

8. Cordes AA, Carpenter JF, Randolph TW 2012. Accelerated stability studies of abatacept formulations: comparison of freeze-thawing- and agitation-induced stresses. *J Pharm Sci* 101(7):2307-2315.
9. Gibson TJ, McCarty K, McFadyen IJ, Cash E, Dalmonte P, Hinds KD, Dinerman AA, Alvarez JC, Volkin DB 2011. Application of a high-throughput screening procedure with PEG-induced precipitation to compare relative protein solubility during formulation development with IgG1 monoclonal antibodies. *J Pharm Sci* 100(3):1009-1021.
10. Goldberg DS, Bishop SM, Shah AU, Sathish HA 2010. Formulation development of therapeutic monoclonal antibodies using high-throughput fluorescence and static light scattering techniques: Role of conformational and colloidal stability. *J Pharm Sci* 100(4):1306-1315.
11. He F, Hogan S, Latypov RF, Narhi LO, Razinkov VI 2010. High throughput thermostability screening of monoclonal antibody formulations. *J Pharm Sci* 99(4):1707-1720.
12. He F, Phan DH, Hogan S, Bailey R, Becker GW, Narhi LO, Razinkov VI 2010. Detection of IgG aggregation by a high throughput method based on extrinsic fluorescence. *J Pharm Sci* 99(6):2598-2608.
13. Thakkar SV, Joshi SB, Jones ME, Sathish HA, Bishop SM, Volkin DB, Middaugh CR 2012. Excipients differentially influence the conformational stability and pretransition dynamics of two IgG1 monoclonal antibodies. *J Pharm Sci* 101(9):3062-3077.
14. Thakkar SV, Kim JH, Samra HS, Sathish HA, Bishop SM, Joshi SB, Volkin DB, Middaugh CR 2012. Local dynamics and their alteration by excipients modulate the global conformational stability of an IgG1 monoclonal antibody. *J Pharm Sci* 101(12):4444-4457.
15. Akers MJ 2002. Excipient-drug interactions in parenteral formulations. *J Pharm Sci* 91(11):2283-2300.

16. Ohtake S, Kita Y, Arakawa T 2011. Interactions of formulation excipients with proteins in solution and in the dried state. *Adv Drug Deliv Rev* 63(13):1053-1073.
17. Parkins DA, Lashmar UT 2000. The formulation of biopharmaceutical products. *Pharm Sci Technolo Today* 3(4):129-137.
18. Cuneo MJ, Tian Y, Allert M, Hellinga HW 2008. The backbone structure of the thermophilic *Thermoanaerobacter tengcongensis* ribose binding protein is essentially identical to its mesophilic *E. coli* homolog. *BMC Struct Biol* 8(20).
19. Feng X-l, Zhao X, Yu H, Sun T-d, Huang X-r 2012. Molecular dynamics simulations of the thermal stability of tteRBP and ecRBP. *J Biomol Struct Dyn*:1-15.
20. Leone M, Di Lello P, Ohlenschlager O, Pedone EM, Bartolucci S, Rossi M, Di Blasio B, Pedone C, Saviano M, Isernia C, Fattorusso R 2004. Solution structure and backbone dynamics of the K18G/R82E *Alicyclobacillus acidocaldarius* thioredoxin mutant: a molecular analysis of its reduced thermal stability. *Biochemistry* 43(20):6043-6058.
21. Kamerzell TJ, Ramsey JD, Middaugh CR 2008. Immunoglobulin dynamics, conformational fluctuations, and nonlinear elasticity and their effects on stability. *J Phys Chem B* 112(10):3240-3250.
22. Kamerzell TJ, Middaugh CR 2008. The complex inter-relationships between protein flexibility and stability. *J Pharm Sci* 97(9):3494-3517.
23. Kamerzell TJ, Middaugh CR 2007. Two-dimensional correlation spectroscopy reveals coupled immunoglobulin regions of differential flexibility that influence stability. *Biochemistry* 46(34):9762-9773.

24. Kamerzell TJ, Unruh JR, Johnson CK, Middaugh CR 2006. Conformational flexibility, hydration and state parameter fluctuations of fibroblast growth factor-10: effects of ligand binding. *Biochemistry* 45(51):15288-15300.
25. Ramsey JD, Gill ML, Kamerzell TJ, Price ES, Joshi SB, Bishop SM, Oliver CN, Middaugh CR 2009. Using empirical phase diagrams to understand the role of intramolecular dynamics in immunoglobulin G stability. *J Pharm Sci* 98(7):2432-2447.
26. Engen JR 2009. Analysis of protein conformation and dynamics by hydrogen/deuterium exchange MS. *Anal Chem* 81(19):7870-7875.
27. Kaltashov IA, Bobst CE, Abzalimov RR, Wang G, Baykal B, Wang S 2011. Advances and challenges in analytical characterization of biotechnology products: Mass spectrometry-based approaches to study properties and behavior of protein therapeutics. *Biotechnol Adv* 30(1):210-222.
28. Konermann L, Tong X, Pan Y 2008. Protein structure and dynamics studied by mass spectrometry: H/D exchange, hydroxyl radical labeling, and related approaches. *J Mass Spectrom* 43(8):1021-1036.
29. Zhang A, Qi W, Singh SK, Fernandez EJ 2011. A new approach to explore the impact of freeze-thaw cycling on protein structure: hydrogen/deuterium exchange mass spectrometry (HX-MS). *Pharm Res* 28(5):1179-1193.
30. Zhang A, Singh SK, Shirts MR, Kumar S, Fernandez EJ 2012. Distinct aggregation mechanisms of monoclonal antibody under thermal and freeze-thaw stresses revealed by hydrogen exchange. *Pharm Res* 29(1):236-250.

31. Houde D, Arndt J, Domeier W, Berkowitz S, Engen JR 2009. Characterization of IgG1 conformation and conformational dynamics by hydrogen/deuterium exchange mass spectrometry. *Anal Chem* 81(7):2644-2651.
32. Houde D, Berkowitz SA, Engen JR 2011. The utility of hydrogen/deuterium exchange mass spectrometry in biopharmaceutical comparability studies. *J Pharm Sci* 100(6):2071-2086.
33. Burkitt W, Domann P, O'Connor G 2010. Conformational changes in oxidatively stressed monoclonal antibodies studied by hydrogen exchange mass spectrometry. *Protein Sci* 19(4):826-835.
34. Tang L, Sundaram S, Zhang J, Carlson P, Matathia A, Parekh B, Zhou Q, Hsieh MC 2013. Conformational characterization of the charge variants of a human IgG1 monoclonal antibody using H/D exchange mass spectrometry. *mAbs* 5(1):114-125.
35. Li Y, Williams TD, Schowen RL, Topp EM 2007. Characterizing protein structure in amorphous solids using hydrogen/deuterium exchange with mass spectrometry. *Anal Biochem* 366(1):18-28.
36. Li Y, Williams TD, Topp EM 2008. Effects of excipients on protein conformation in lyophilized solids by hydrogen/deuterium exchange mass spectrometry. *Pharm Res* 25(2):259-267.
37. Sinha S, Li Y, Williams TD, Topp EM 2008. Protein conformation in amorphous solids by FTIR and by hydrogen/deuterium exchange with mass spectrometry. *Biophys J* 95(12):5951-5961.
38. Bond MD, Panek ME, Zhang Z, Wang D, Mehndiratta P, Zhao H, Gunton K, Ni A, Nedved ML, Burman S, Volkin DB 2010. Evaluation of a dual-wavelength size exclusion HPLC

method with improved sensitivity to detect protein aggregates and its use to better characterize degradation pathways of an IgG1 monoclonal antibody. *J Pharm Sci* 99(6):2582-2597.

39. Barnard JG, Singh S, Randolph TW, Carpenter JF 2011. Subvisible particle counting provides a sensitive method of detecting and quantifying aggregation of monoclonal antibody caused by freeze-thawing: insights into the roles of particles in the protein aggregation pathway. *J Pharm Sci* 100(2):492-503.

40. Welfle K, Misselwitz R, Hausdorf G, Hohne W, Welfle H 1999. Conformation, pH-induced conformational changes, and thermal unfolding of anti-p24 (HIV-1) monoclonal antibody CB4-1 and its Fab and Fc fragments. *Biochim Biophys Acta* 1431(1):120-131.

41. Majumdar R, Manikwar P, Hickey JM, Arora J, Middaugh CR, Volkin DB, Weis DD 2012. Minimizing Carry-Over in an Online Pepsin Digestion System used for the H/D Exchange Mass Spectrometric Analysis of an IgG1 Monoclonal Antibody. *J Am Soc Mass Spectrom* 23(12):2140-2148.

42. Majumdar R, Manikwar P, Hickey JM, Samra HS, Sathish HA, Bishop SM, Middaugh CR, Volkin DB, Weis DD 2013. Effect of Salts from Hofmeister Series on Conformational Stability, Aggregation Propensity and Local Flexibility of an IgG1 Monoclonal Antibody. Submitted manuscript.

43. Saphire EO, Parren PW, Pantophlet R, Zwick MB, Morris GM, Rudd PM, Dwek RA, Stanfield RL, Burton DR, Wilson IA 2001. Crystal structure of a neutralizing human IGG against HIV-1: a template for vaccine design. *Science* 293(5532):1155-1159.

44. Chennamsetty N, Voynov V, Kayser V, Helk B, Trout BL 2009. Design of therapeutic proteins with enhanced stability. *Proc Natl Acad Sci U S A* 106(29):11937-11942.

45. Ionescu RM, Vlasak J, Price C, Kirchmeier M 2008. Contribution of variable domains to the stability of humanized IgG1 monoclonal antibodies. *J Pharm Sci* 97(4):1414-1426.
46. Freire E 1995. Differential scanning calorimetry. *Methods Mol Biol* 40:191-218.
47. Li CH, Narhi LO, Wen J, Dimitrova M, Wen ZQ, Li J, Pollastrini J, Nguyen XC, Tsuruda T, Jiang Y 2012. The Effect of pH, temperature and salt on the stability of E. coli and CHO derived IgG1 Fc. *Biochemistry* 51(50):10056-10065.
48. Vermeer AW, Norde W 2000. The thermal stability of immunoglobulin: unfolding and aggregation of a multi-domain protein. *Biophys J* 78(1):394-404.
49. Gabrielson JP, Brader ML, Pekar AH, Mathis KB, Winter G, Carpenter JF, Randolph TW 2007. Quantitation of aggregate levels in a recombinant humanized monoclonal antibody formulation by size-exclusion chromatography, asymmetrical flow field flow fractionation, and sedimentation velocity. *J Pharm Sci* 96(2):268-279.
50. Rosenberg AS 2006. Effects of protein aggregates: an immunologic perspective. *AAPS J* 8(3):E501-507.
51. Wang W, Singh SK, Li N, Toler MR, King KR, Nema S 2012. Immunogenicity of protein aggregates--concerns and realities. *Int J Pharm* 431(1-2):1-11.
52. Chirmule N, Jawa V, Meibohm B 2012. Immunogenicity to therapeutic proteins: impact on PK/PD and efficacy. *AAPS J* 14(2):296-302.
53. Hawe A, Kasper JC, Friess W, Jiskoot W 2009. Structural properties of monoclonal antibody aggregates induced by freeze-thawing and thermal stress. *Eur J Pharm Sci* 38(2):79-87.
54. Kumru OS, Liu J, Ji JA, Cheng W, Wang YJ, Wang T, Joshi SB, Middaugh CR, Volkin DB 2012. Compatibility, physical stability, and characterization of an IgG4 monoclonal antibody after dilution into different intravenous administration bags. *J Pharm Sci* 101(10):3636-3650.

55. Hvidt A, Linderstrom-Lang K 1954. Exchange of hydrogen atoms in insulin with deuterium atoms in aqueous solutions. *Biochim Biophys Acta* 14(4):574-575.
56. Hvidt A, Nielsen SO 1966. Hydrogen exchange in proteins. *Adv Protein Chem* 21:287-386.
57. Wang A, Robertson AD, Bolen DW 1995. Effects of a naturally occurring compatible osmolyte on the internal dynamics of ribonuclease A. *Biochemistry* 34(46):15096-15104.
58. Hutcheon GA, Parker MC, Moore BD 2000. Measuring enzyme motility in organic media using novel H-D exchange methodology. *Biotechnol Bioeng* 70(3):262-269.
59. Lim WK, Rosgen J, Englander SW 2009. Urea, but not guanidinium, destabilizes proteins by forming hydrogen bonds to the peptide group. *Proc Natl Acad Sci U S A* 106(8):2595-2600.
60. Kim PS, Baldwin RL 1982. Influence of charge on the rate of amide proton exchange. *Biochemistry* 21(1):1-5.
61. Rohl CA, Baldwin RL 1997. Comparison of NH exchange and circular dichroism as techniques for measuring the parameters of the helix-coil transition in peptides. *Biochemistry* 36(28):8435-8442.
62. Bai Y, Milne JS, Mayne L, Englander SW 1993. Primary structure effects on peptide group hydrogen exchange. *Proteins* 17(1):75-86.
63. Abbas SA, Sharma VK, Patapoff TW, Kalonia DS 2012. Opposite effects of polyols on antibody aggregation: thermal versus mechanical stresses. *Pharm Res* 29(3):683-694.
64. Banks DD, Latypov RF, Ketchem RR, Woodard J, Scavezze JL, Siska CC, Razinkov VI 2012. Native-state solubility and transfer free energy as predictive tools for selecting excipients to include in protein formulation development studies. *J Pharm Sci* 101(8):2720-2732.

65. Kendrick BS, Carpenter JF, Cleland JL, Randolph TW 1998. A transient expansion of the native state precedes aggregation of recombinant human interferon-gamma. *Proc Natl Acad Sci U S A* 95(24):14142-14146.
66. Khan RH, Shabnum MS 2001. Effect of sugars on rabbit serum albumin stability and induction of secondary structure. *Biochemistry (Mosc)* 66(9):1042-1046.
67. Kim YS, Jones LS, Dong A, Kendrick BS, Chang BS, Manning MC, Randolph TW, Carpenter JF 2003. Effects of sucrose on conformational equilibria and fluctuations within the native-state ensemble of proteins. *Protein Sci* 12(6):1252-1261.
68. Lee JC, Timasheff SN 1981. The stabilization of proteins by sucrose. *J Biol Chem* 256(14):7193-7201.
69. Kendrick BS, Chang BS, Arakawa T, Peterson B, Randolph TW, Manning MC, Carpenter JF 1997. Preferential exclusion of sucrose from recombinant interleukin-1 receptor antagonist: role in restricted conformational mobility and compaction of native state. *Proc Natl Acad Sci U S A* 94(22):11917-11922.
70. Arakawa T, Timasheff SN 1982. Stabilization of protein structure by sugars. *Biochemistry* 21(25):6536-6544.
71. Dudgeon K, Rouet R, Kokmeijer I, Schofield P, Stolp J, Langley D, Stock D, Christ D 2012. General strategy for the generation of human antibody variable domains with increased aggregation resistance. *Proc Natl Acad Sci U S A* 109(27):10879-10884.
72. DePaz RA, Barnett CC, Dale DA, Carpenter JF, Gaertner AL, Randolph TW 2000. The excluding effects of sucrose on a protein chemical degradation pathway: methionine oxidation in subtilisin. *Arch Biochem Biophys* 384(1):123-132.

73. Barreca D, Laganà G, Ficarra S, Gattuso G, Magazù S, Torre R, Tellone E, Bellocco E 2012. Spectroscopic Determination of Lysozyme Conformational Changes in the Presence of Trehalose and Guanidine. *Cell Biochem Biophys*:1-11.
74. Hodkinson JP, Radford SE, Ashcroft AE 2012. The role of conformational flexibility in beta2-microglobulin amyloid fibril formation at neutral pH. *Rapid Commun Mass Spectrom* 26(16):1783-1792.
75. Lin TY, Timasheff SN 1996. On the role of surface tension in the stabilization of globular proteins. *Protein Sci* 5(2):372-381.
76. Taneja S, Ahmad F 1994. Increased thermal stability of proteins in the presence of amino acids. *Biochem J* 303 (Pt 1):147-153.
77. Ito L, Shiraki K, Matsuura T, Okumura M, Hasegawa K, Baba S, Yamaguchi H, Kumasaka T 2011. High-resolution X-ray analysis reveals binding of arginine to aromatic residues of lysozyme surface: implication of suppression of protein aggregation by arginine. *Protein Eng Des Sel* 24(3):269-274.
78. Schneider CP, Trout BL 2009. Investigation of cosolute-protein preferential interaction coefficients: new insight into the mechanism by which arginine inhibits aggregation. *J Phys Chem B* 113(7):2050-2058.
79. Shukla D, Trout BL 2010. Interaction of arginine with proteins and the mechanism by which it inhibits aggregation. *J Phys Chem B* 114(42):13426-13438.
80. Arakawa T, Ejima D, Tsumoto K, Obeyama N, Tanaka Y, Kita Y, Timasheff SN 2007. Suppression of protein interactions by arginine: a proposed mechanism of the arginine effects. *Biophys Chem* 127(1-2):1-8.

81. Shukla D, Trout BL 2011. Preferential interaction coefficients of proteins in aqueous arginine solutions and their molecular origins. *J Phys Chem B* 115(5):1243-1253.
82. Lilyestrom WG, Shire SJ, Scherer TM 2012. Influence of the cosolute environment on IgG solution structure analyzed by small-angle X-ray scattering. *J Phys Chem B* 116(32):9611-9618.
83. Houde D, Peng Y, Berkowitz SA, Engen JR 2010. Post-translational modifications differentially affect IgG1 conformation and receptor binding. *Mol Cell Proteomics* 9(8):1716-1728.
84. Zhang J, Topp EM 2012. Protein G, protein A and protein A-derived peptides inhibit the agitation induced aggregation of IgG. *Mol Pharm* 9(3):622-628.
85. Dimitrov DS 2009. Engineered CH2 domains (nanoantibodies). *mAbs* 1(1):26-28.
86. Gong R, Vu BK, Feng Y, Prieto DA, Dyba MA, Walsh JD, Prabakaran P, Veenstra TD, Tarasov SG, Ishima R, Dimitrov DS 2009. Engineered human antibody constant domains with increased stability. *J Biol Chem* 284(21):14203-14210.
87. Gasymov OK, Abduragimov AR, Glasgow BJ 2011. The conserved disulfide bond of human tear lipocalin modulates conformation and lipid binding in a ligand selective manner. *Biochim Biophys Acta* 1814(5):671-683.
88. Yu XW, Tan NJ, Xiao R, Xu Y 2012. Engineering a Disulfide Bond in the Lid Hinge Region of *Rhizopus chinensis* Lipase: Increased Thermostability and Altered Acyl Chain Length Specificity. *PloS one* 7(10):e46388.
89. Gong R, Wang Y, Feng Y, Zhao Q, Dimitrov DS 2011. Shortened engineered human antibody CH2 domains: increased stability and binding to the human neonatal Fc receptor. *J Biol Chem* 286(31):27288-27293.

90. Arakawa T, Tsumoto K 2003. The effects of arginine on refolding of aggregated proteins: not facilitate refolding, but suppress aggregation. *Biochem Biophys Res Commun* 304(1):148-152.
91. Lange C, Rudolph R 2009. Suppression of protein aggregation by L-arginine. *Curr Pharm Biotechnol* 10(4):408-414.
92. Shiraki K, Kudou M, Fujiwara S, Imanaka T, Takagi M 2002. Biophysical effect of amino acids on the prevention of protein aggregation. *J Biochem* 132(4):591-595.

Table 3.1

Excipient concentration	T _{onset} (°C)	T _{m 1} (°C)	T _{m 2} (°C)	T _{m 3} (°C)
	Mean SD ΔT _{onset}	Mean SD ΔT _{m 1}	Mean SD ΔT _{m 2}	Mean SD ΔT _{m 3}
Control	57.7 0.2 -	69.3 0.1 -	73.6 <0.1 -	82.4 <0.1 -
0.5 M arginine	50.3 0.3 -7.4	67.4 0.1 -1.9	72.4 <0.1 -1.2	81.8 <0.1 -0.6
1.0 M arginine	47.0 0.8 -10.7	65.7 0.2 -3.6	72.3 <0.1 -1.3	81.8 <0.1 -0.6
1.35 M arginine	46.7 0.5 -11.0	64.9 0.1 -4.4	72.8 <0.1 -0.8	82.4 <0.1 0.0
0.5 M sucrose	60.2 0.4 2.5	70.8 0.1 1.5	75.3 <0.1 1.7	84.6 <0.1 2.2
1.0 M sucrose	63.9 0.1 6.2	73.4 <0.1 4.1	77.6 <0.1 4.0	87.3 <0.1 4.9
1.35 M sucrose	66.2 0.2 8.5	75.3 <0.1 6.0	79.5 <0.1 5.9	89.7 <0.1 7.3
Formulations contained 0.5 mg/mL protein in 20 mM citrate-phosphate buffer, 0.1 M NaCl, pH 6.0 and the indicated level of excipients. The difference in melting temperature (ΔT _m) was obtained from T _{m,excipient} – T _{m,control} . The mean and standard deviation ⁴⁰ are based on three separate measurements.				

Effect of excipient concentration on thermal onset temperature (T_{onset}) and thermal melting temperatures (T_{m1}, T_{m2}, and T_{m3}) for mAb-B as measured by DSC.

Table 3.S1

Peptide number	Peptide_ID
1	mAbB Heavy 4-17 (VH)
2	mAbB Heavy 5-22 (VH)
3	mAbB Heavy 30-35 (VH)
4	mAbB Heavy 33-36 (VH)
5	mAbB Heavy 36-47 (VH)
6	mAbB Heavy 37-46 (VH)
7	mAbB Heavy 36-49 (VH)
8	mAbB Heavy 36-58 (VH)
9	mAbB Heavy 36-59 (VH)
10	mAbB Heavy 37-58 (VH)
11	mAbB Heavy 37-59 (VH)
12	mAbB Heavy 36-65 (VH)
13	mAbB Heavy 47-58 (VH)
14	mAbB Heavy 47-59 (VH)
15	mAbB Heavy 47-60 (VH)
16	mAbB Heavy 47-61 (VH)
17	mAbB Heavy 47-62 (VH)
18	mAbB Heavy 48-61 (VH)
19	mAbB Heavy 47-63 (VH)
20	mAbB Heavy 47-65 (VH)
21	mAbB Heavy 47-68 (VH)
22	mAbB Heavy 48-68 (VH)
23	mAbB Heavy 50-68 (VH)
24	mAbB Heavy 59-68 (VH)
25	mAbB Heavy 60-68 (VH)
26	mAbB Heavy 61-68 (VH)
27	mAbB Heavy 62-68 (VH)
28	mAbB Heavy 64-68 (VH)
29	mAbB Heavy 61-79 (VH)
30	mAbB Heavy 61-80 (VH)
31	mAbB Heavy 62-79 (VH)
32	mAbB Heavy 63-79 (VH)
33	mAbB Heavy 63-80 (VH)
34	mAbB Heavy 64-79 (VH)
35	mAbB Heavy 64-80 (VH)
36	mAbB Heavy 66-79 (VH)
37	mAbB Heavy 66-80 (VH)
38	mAbB Heavy 69-79 (VH)
39	mAbB Heavy 69-80 (VH)

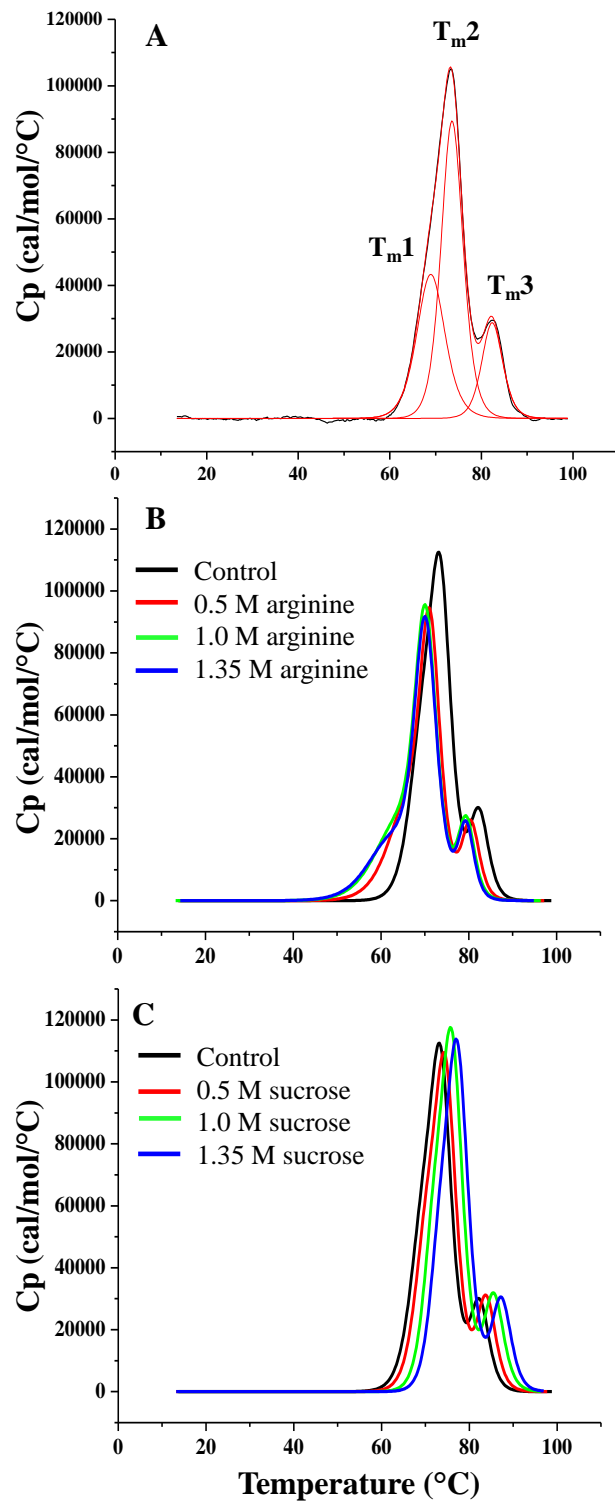
40	mAbB Heavy 69-83 (VH)
41	mAbB Heavy 80-83 (VH)
42	mAbB Heavy 80-86 (VH)
43	mAbB Heavy 81-86 (VH)
44	mAbB Heavy 84-90 (VH)
45	mAbB Heavy 84-93 (VH)
46	mAbB Heavy 85-93 (VH)
47	mAbB Heavy 87-104 (VH)
48	mAbB Heavy 105-114 (VH)
49	mAbB Heavy 105-118
50	mAbB Heavy 105-126
51	mAbB Heavy 124-147 (CH1)
52	mAbB Heavy 146-174 (CH1)
53	mAbB Heavy 156-174 (CH1)
54	mAbB Heavy 159-174 (CH1)
55	mAbB Heavy 163-174 (CH1)
56	mAbB Heavy 171-183 (CH1)
57	mAbB Heavy 180-185 (CH1)
58	mAbB Heavy 185-193 (CH1)
59	mAbB Heavy 185-197 (CH1)
60	mAbB Heavy 186-197 (CH1)
61	mAbB Heavy 198-220 (CH1)
62	mAbB Heavy 208-229
63	mAbB Heavy 235-240
64	mAbB Heavy 235-252 (CH2)
65	mAbB Heavy 241-251 (CH2)
66	mAbB Heavy 241-252 (CH2)
67	mAbB Heavy 243-252 (CH2)
68	mAbB Heavy 244-251 (CH2)
69	mAbB Heavy 263-277 (CH2)
70	mAbB Heavy 266-277 (CH2)
71	mAbB Heavy 300-306 (CH2)
72	mAbB Heavy 301-305 (CH2)
73	mAbB Heavy 301-306 (CH2)
74	mAbB Heavy 307-318 (CH2)
75	mAbB Heavy 334-348
76	mAbB Heavy 349-364 (CH3)
77	mAbB Heavy 349-365 (CH3)
78	mAbB Heavy 355-365 (CH3)
79	mAbB Heavy 369-376 (CH3)
80	mAbB Heavy 369-379 (CH3)

81	mAbB Heavy 369-380 (CH3)
82	mAbB Heavy 381-390 (CH3)
83	mAbB Heavy 379-398 (CH3)
84	mAbB Heavy 380-398 (CH3)
85	mAbB Heavy 381-398 (CH3)
86	mAbB Heavy 382-398 (CH3)
87	mAbB Heavy 381-404 (CH3)
88	mAbB Heavy 391-398 (CH3)
89	mAbB Heavy 392-398 (CH3)
90	mAbB Heavy 391-404 (CH3)
91	mAbB Heavy 399-404 (CH3)
92	mAbB Heavy 406-410 (CH3)
93	mAbB Heavy 411-423 (CH3)
94	mAbB Heavy 424-446 (CH3)
95	mAbB Heavy 429-446 (CH3)
96	mAbB Heavy 431-446 (CH3)
97	mAbB Heavy 433-446 (CH3)
98	mAbB Light 1-4 (VL)
99	mAbB Light 1-7 (VL)
100	mAbB Light 1-10 (VL)
101	mAbB Light 1-11 (VL)
102	mAbB Light 32-46 (VL)
103	mAbB Light 33-46 (VL)
104	mAbB Light 36-46 (VL)
105	mAbB Light 47-62 (VL)
106	mAbB Light 47-70 (VL)
107	mAbB Light 47-74 (VL)
108	mAbB Light 51-70 (VL)
109	mAbB Light 71-74 (VL)
110	mAbB Light 71-83 (VL)
111	mAbB Light 72-82 (VL)
112	mAbB Light 74-82 (VL)
113	mAbB Light 75-82 (VL)
114	mAbB Light 75-83 (VL)
115	mAbB Light 80-85 (VL)
116	mAbB Light 91-103 (VL)
117	mAbB Light 105-116
118	mAbB Light 116-122 (CL)
119	mAbB Light 117-123 (CL)
120	mAbB Light 116-125 (CL)
121	mAbB Light 117-125 (CL)

122	mAbB Light 116-131 (CL)
123	mAbB Light 116-132 (CL)
124	mAbB Light 117-132 (CL)
125	mAbB Light 136-148 (CL)
126	mAbB Light 136-161 (CL)
127	mAbB Light 144-161 (CL)
128	mAbB Light 149-161 (CL)
129	mAbB Light 162-172 (CL)
130	mAbB Light 162-175 (CL)
131	mAbB Light 162-178 (CL)
132	mAbB Light 162-179 (CL)
133	mAbB Light 162-181 (CL)
134	mAbB Light 172-175 (CL)
135	mAbB Light 173-179 (CL)
136	mAbB Light 183-210 (CL)
137	mAbB Light 186-212 (CL)

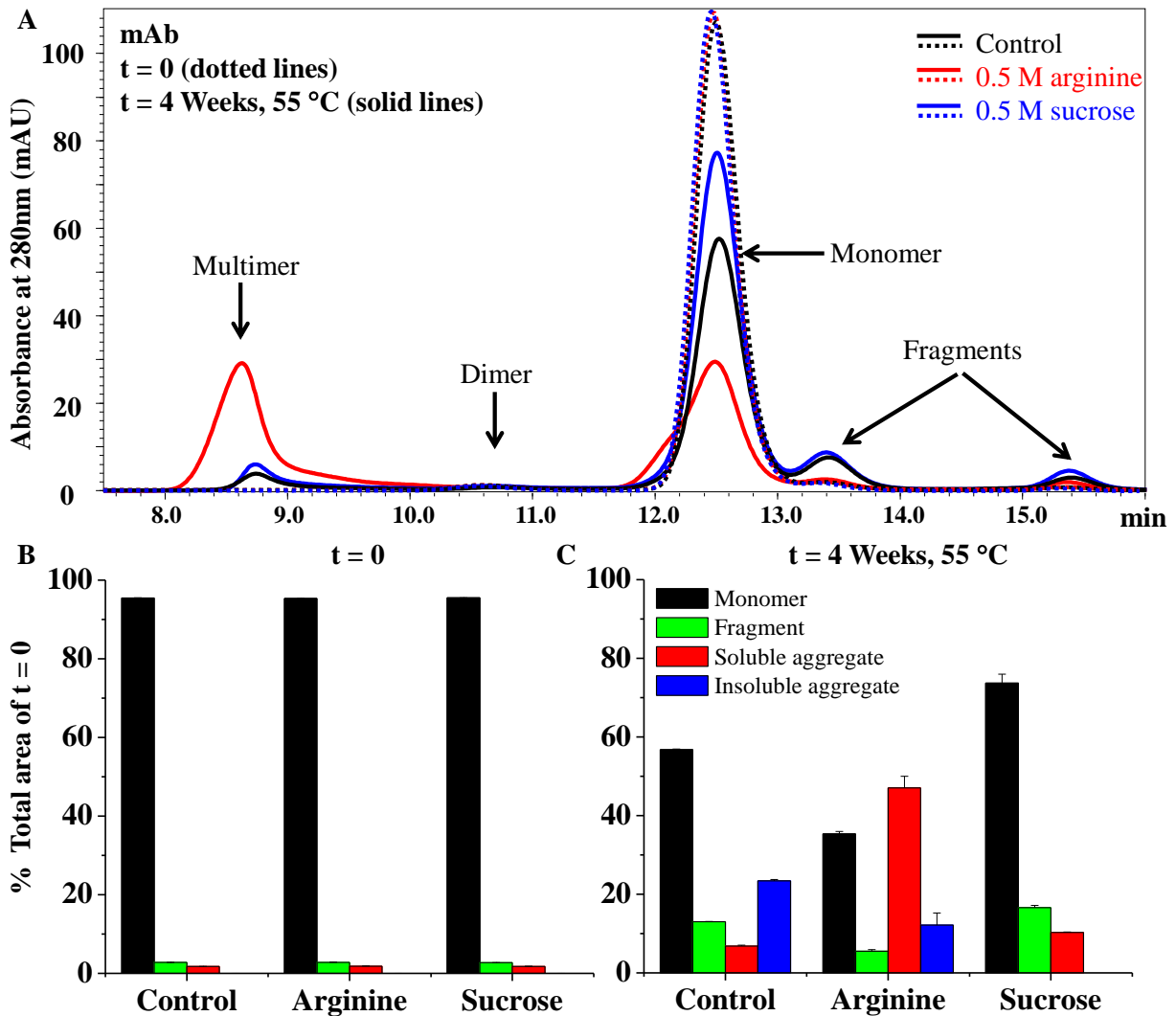
Ordinal peptide numbers matched to their location identities.

Figure 3.1



Representative DSC thermograms of mAb-B in different formulations (20 mM citrate-phosphate buffer, 0.1 M NaCl, pH 6.0) containing the indicated level of excipients. (A) Representative curve-fitted DSC thermogram for mAb-B with T_{m1} , T_{m2} , and T_{m3} . (B) Effect of arginine on mAb-B conformational stability. (C) Effect of sucrose on mAb-B conformational stability.

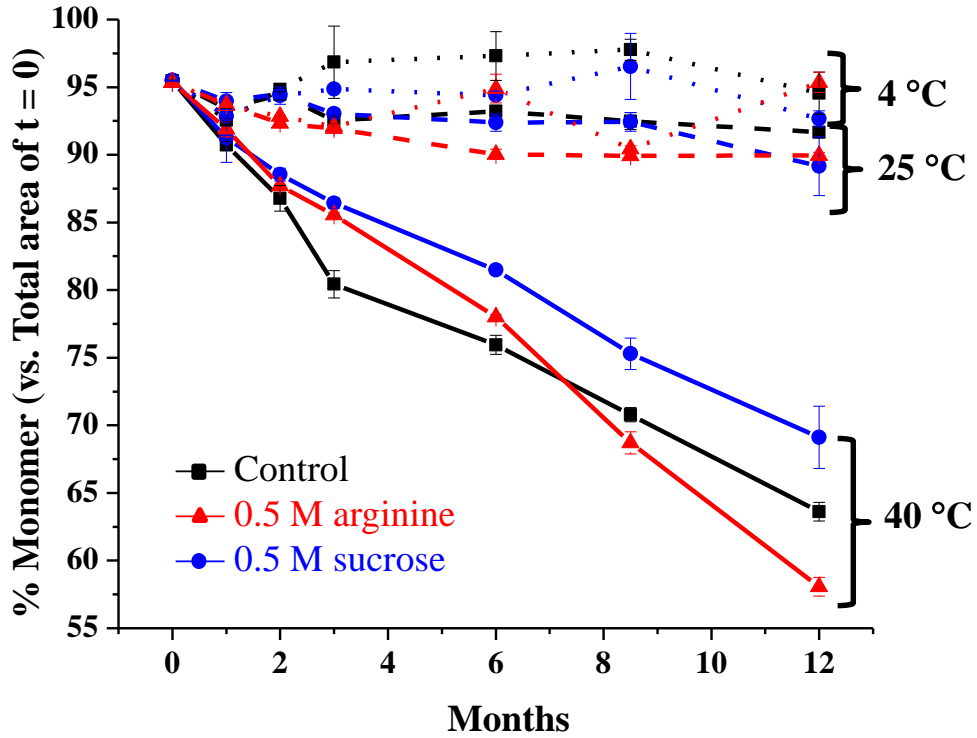
Figure 3.2



SEC analysis of mAb-B samples in different formulations before and after storage at 55 °C for 4 weeks. (A) Overlay of SEC chromatograms of mAb-B before and after thermal stress: dotted lines correspond to mAb-B samples at time zero (no stress) and solid lines correspond to mAb-B samples incubated at 55 °C for four weeks. Samples of mAb-B were prepared in 20 mM citrate-phosphate buffer, 0.1 M NaCl, pH 6.0 without additional additives (control) (black trace) and with 0.5 M sucrose (blue trace) or 0.5 M arginine (red trace). The bar chart represents the effect

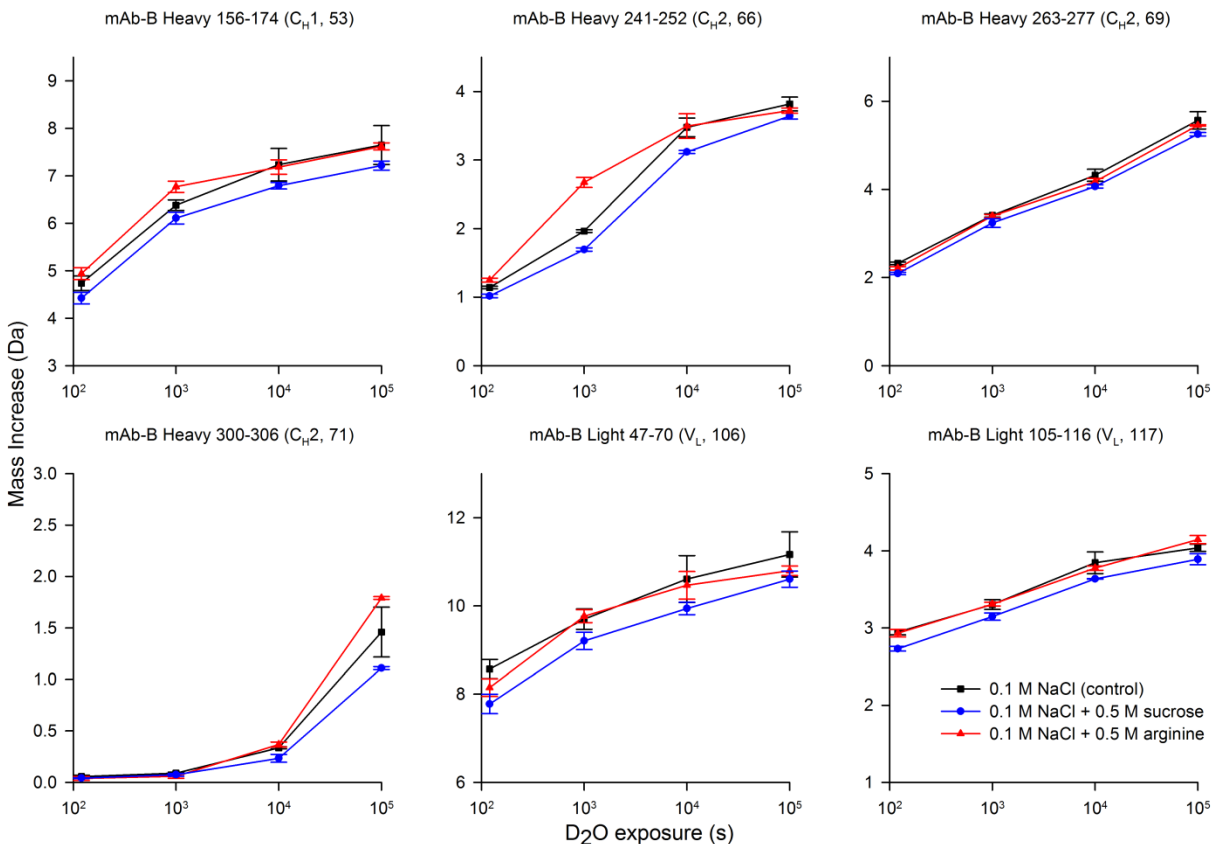
of excipients on different forms (monomer, fragment, soluble, and insoluble aggregates) of mAb-B as measured on (B) day zero and (C) after 4 weeks at 55 °C.

Figure 3.3



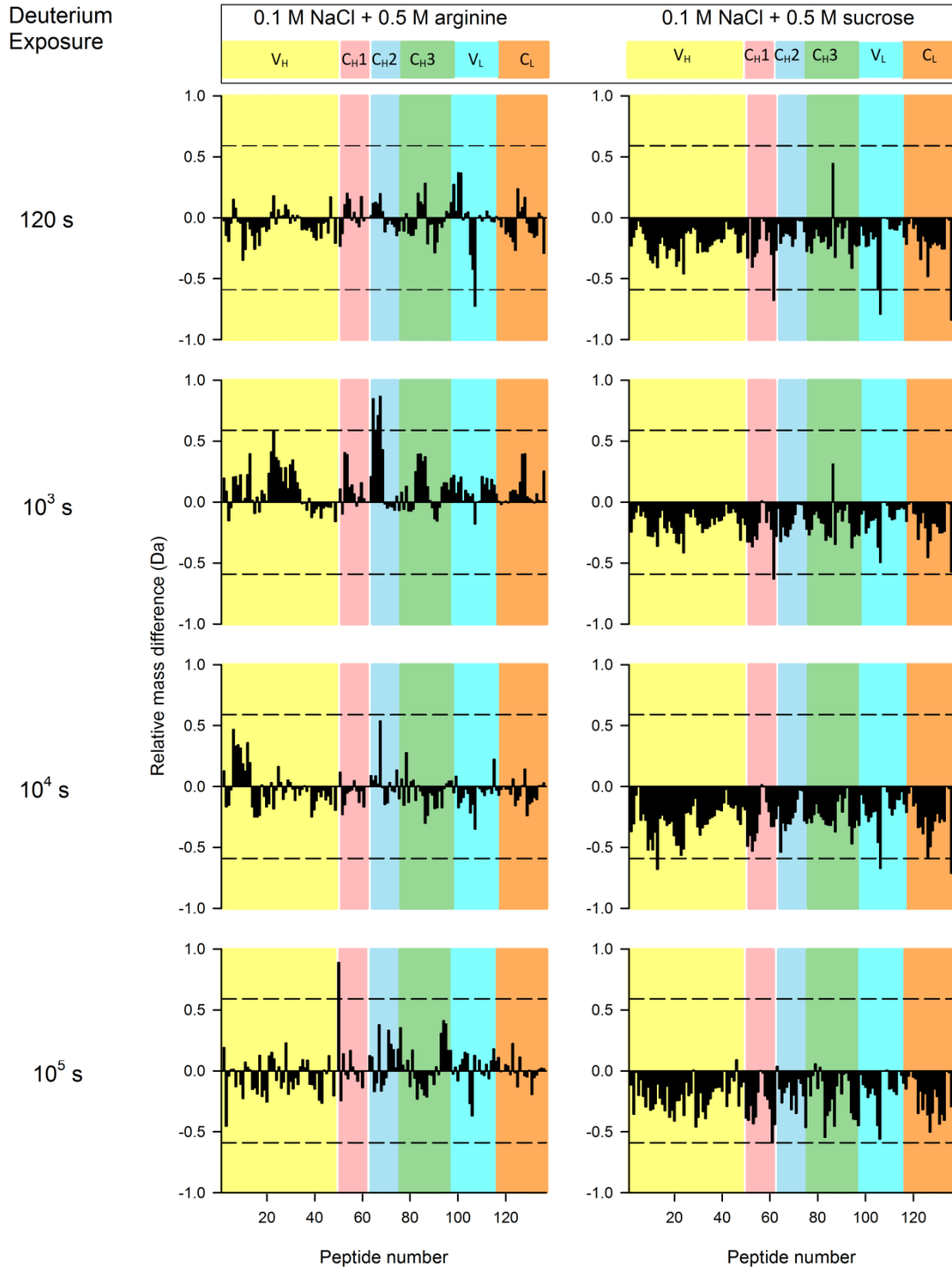
Effect of sucrose and arginine on accelerated and long term storage stability of mAb-B. The percentage of monomer remaining was measured by SEC. Samples of mAb-B were prepared in 20 mM citrate-phosphate buffer, 0.1 M NaCl, pH 6.0 without additional additives (control) (black trace) or with 0.5 M sucrose (blue trace) or 0.5 M arginine (red trace). Error bars represent one standard deviation with duplicate vials.

Figure 3.4



Effect of presence and absence of arginine and sucrose on the deuterium uptake of six peptides from different regions of mAb-B as measured by H/D-MS. The domain location and peptide identity are provided on each graph. Samples of mAb-B (in a 90% deuterium solution) contain 20 mM citrate-phosphate buffer at pH 6.0 and 0.1 M sodium chloride without additional additives (control) or with 0.5 M arginine or 0.5 M sucrose. The error bars denote one standard deviation for three independent replicates.

Figure 3.5

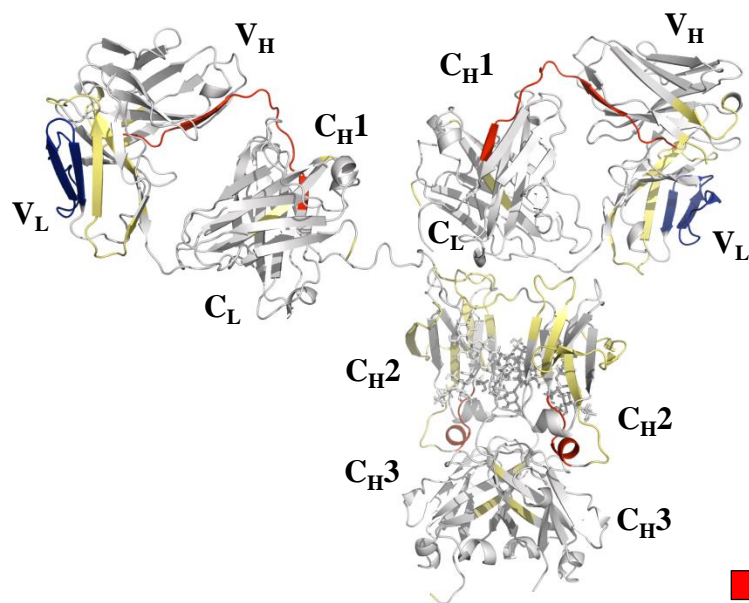


Mass difference plots of mAb-B in the presence of 0.5 M arginine and 0.5 M sucrose compared to the control as measured by H/D-MS. Mass differences of the average deuterium update were

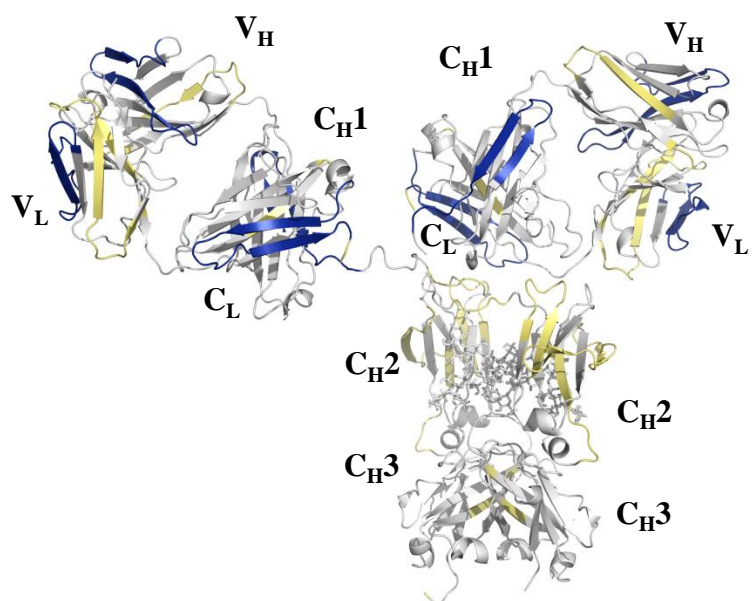
calculated for each of the 137 peptide of mAb-B for four different exchange times (120, 10^3 , 10^4 and 10^5 s) in 90% deuterium solution. Each mass difference data point is an average of three independent H/D exchange experiments with mAb-B in 20 mM citrate-phosphate buffer at pH 6.0 and 0.1 M NaCl without additional additives (control) or with either 0.5 M arginine or 0.5 M sucrose added. The y-axis denotes $\Delta D(t) = m_{\text{excipient}}(t) - m(t)_{\text{control}}$ where m denotes the mass of the peptide as a function of deuterium exposure time, t. The x-axis denotes the ordinal peptide number, a sequential arrangement of 137 peptides of mAb-B by the midpoints in the sequence. The black dotted lines at $|\Delta D(t)| > 0.59$ Da represent the 99% confidence limit for significant mass differences. The background is colored to represent and differentiate the individual domains of mAb-B. Table 3.S1 contains the mAb-B peptide locations and domain information.

Figure 3.6

A Effect of 0.5 M arginine



B Effect of 0.5 M sucrose



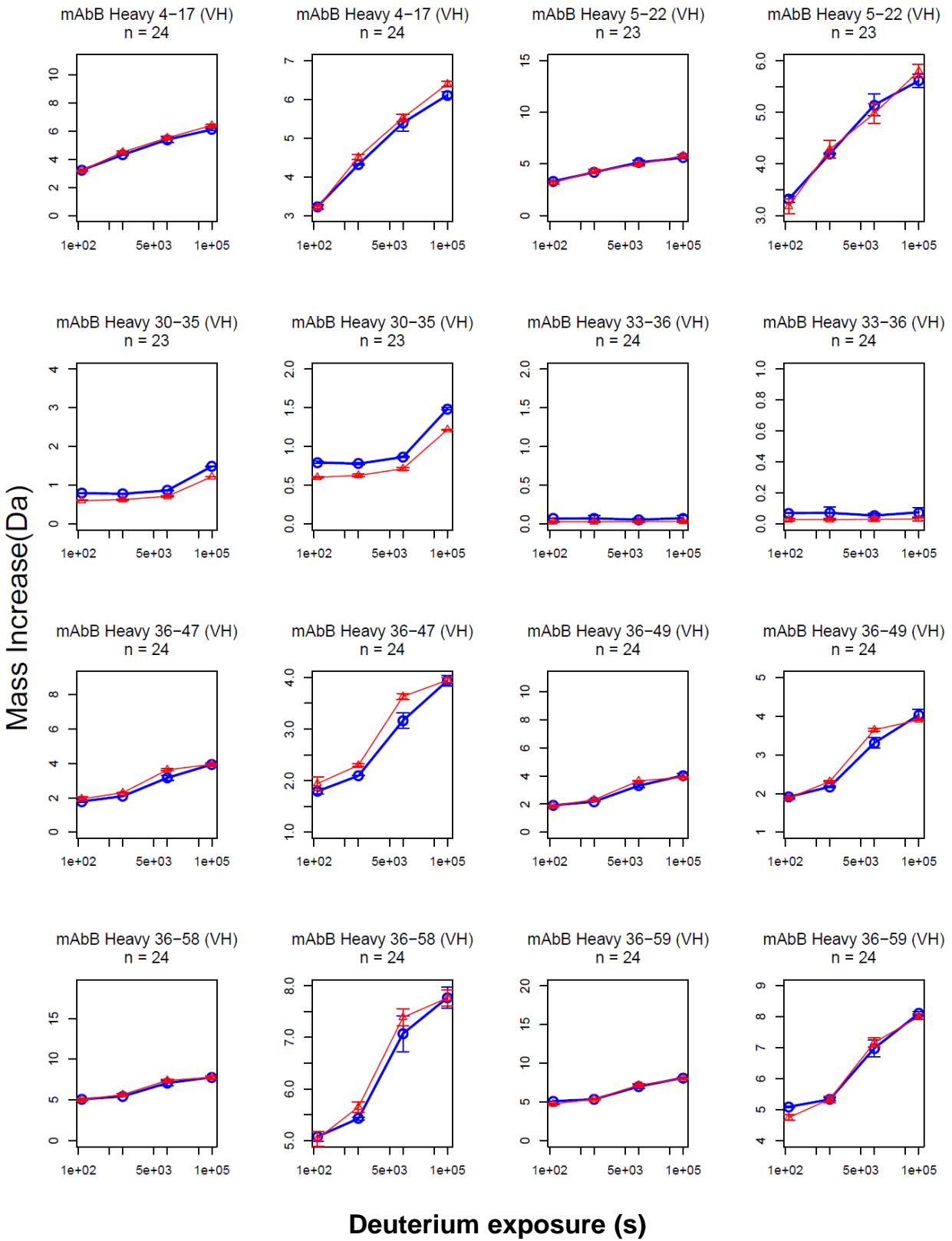
- Increase
- No change
- Decrease
- No data available

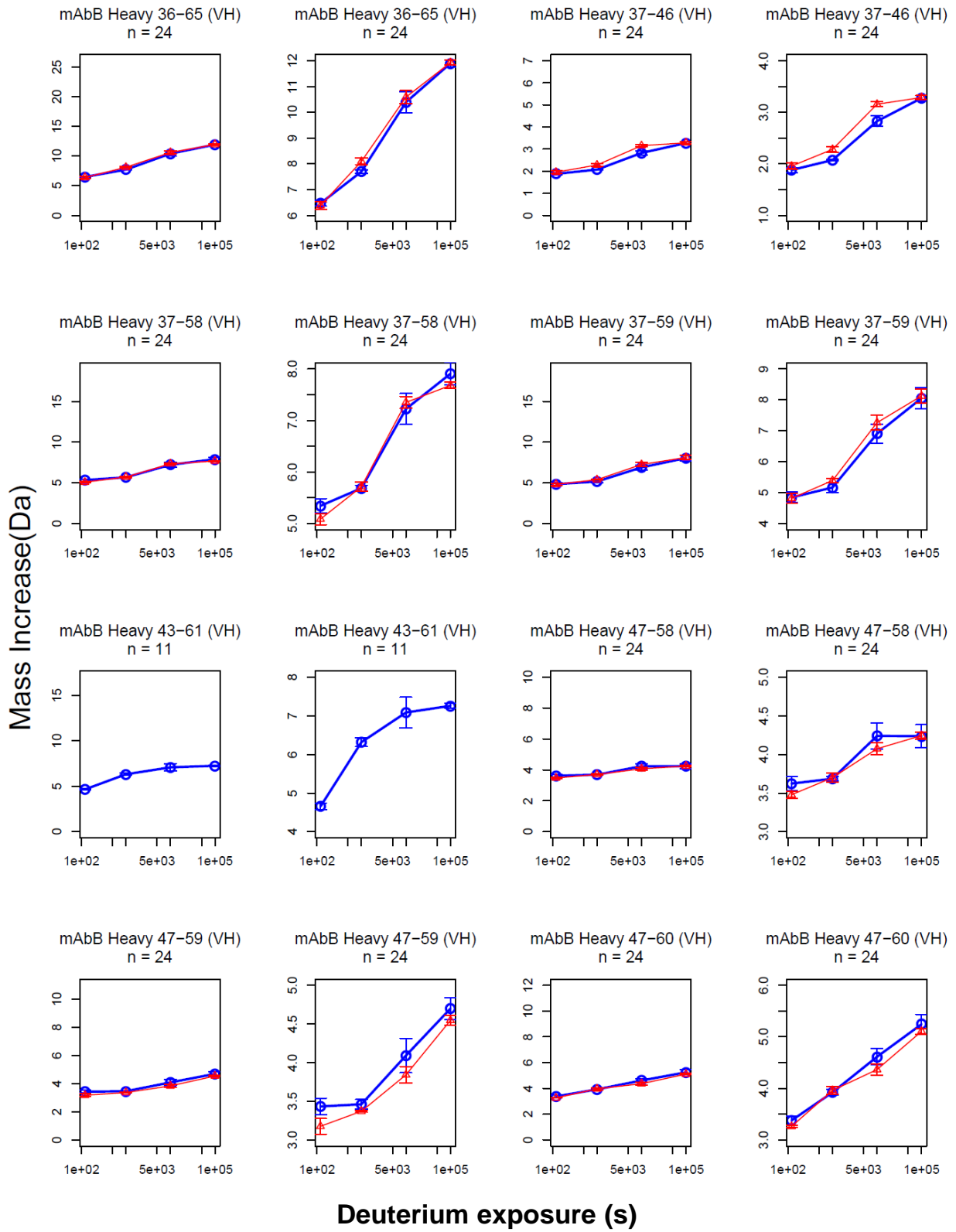
Effect of arginine and sucrose on the local flexibility of mAb-B as measured by H/D-MS. The color code is derived from comparison of mass differences of the average deuterium uptake data

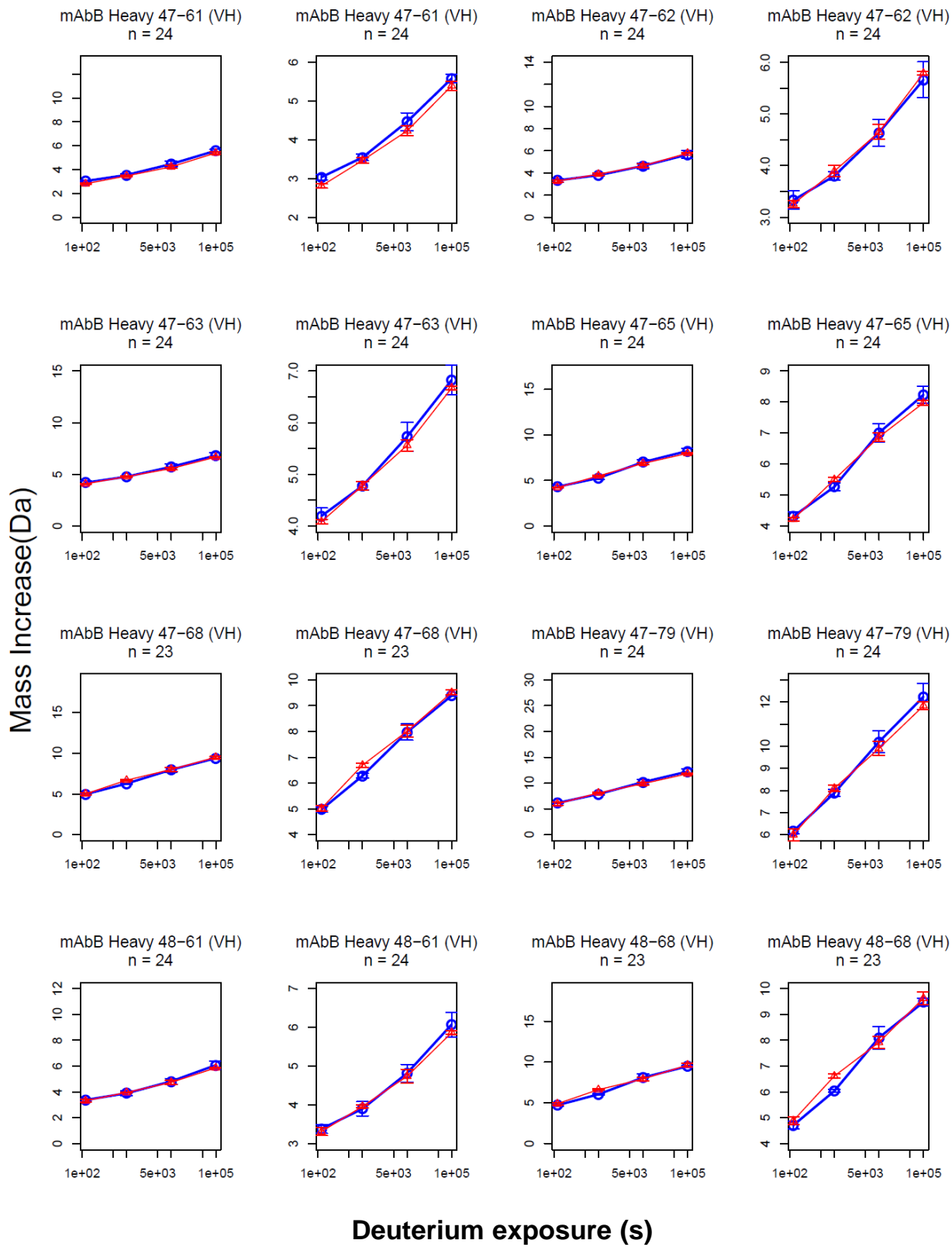
(Figure 3.5) in the presence of 0.5 M arginine (A) and 0.5 M sucrose (B) compared to the control (20 mM citrate-phosphate buffer, pH 6.0, 0.1 M sodium chloride). (A) Arginine caused an increase in flexibility in the region of the C_{H2} and C_{H1} domain and a decrease in flexibility in the V_L domain. (B) Sucrose caused decreases in local flexibility across several domains of mAb-B. The data are an average of three independent H/D-MS experiments performed on three different days. Regions colored in yellow indicate non availability of H/D exchange data (~85% sequence coverage in mAb-B). The homology map of mAb-B was constructed from PDB ID 1HZH⁴³ (see Methods section for more details).

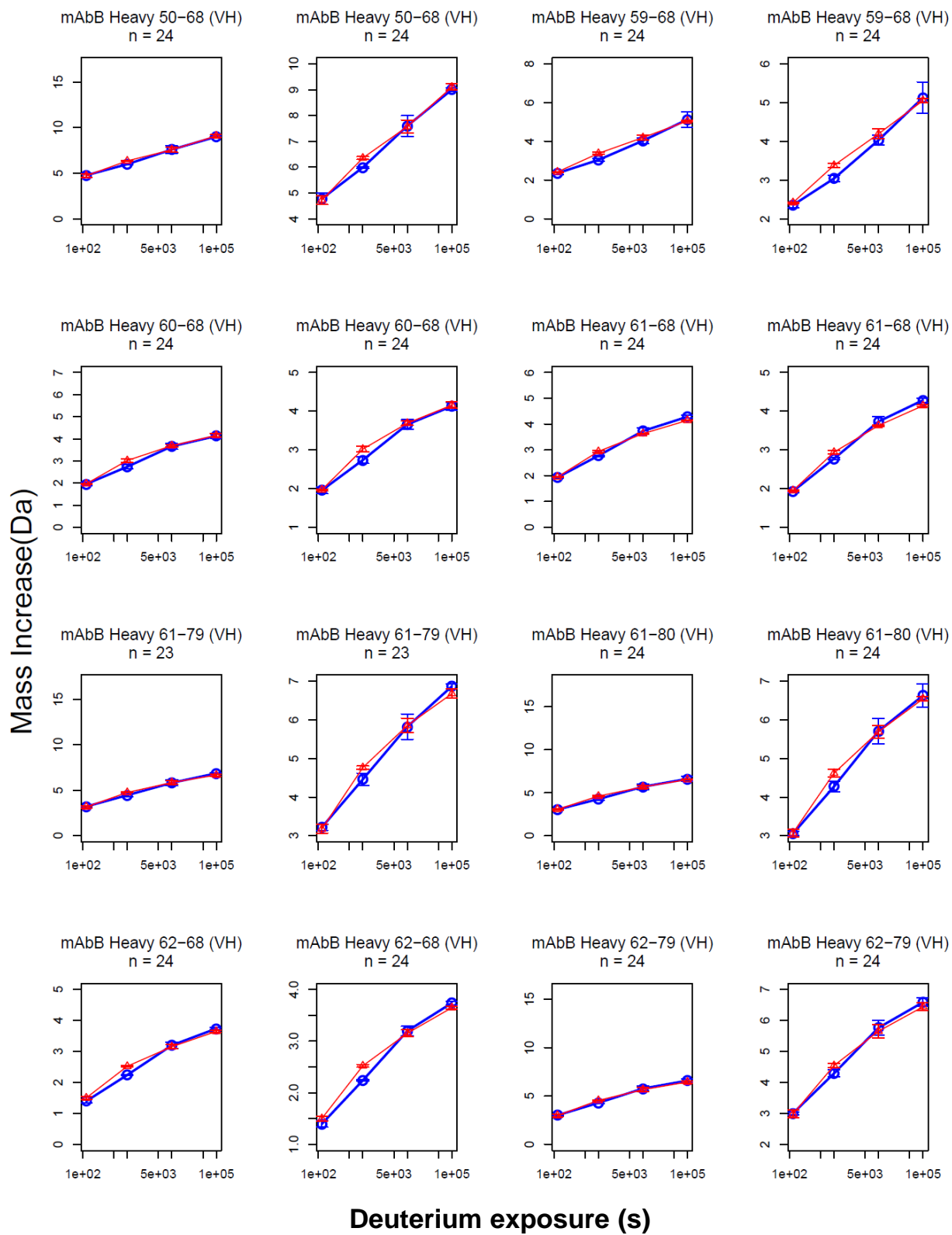
Figure 3.S1

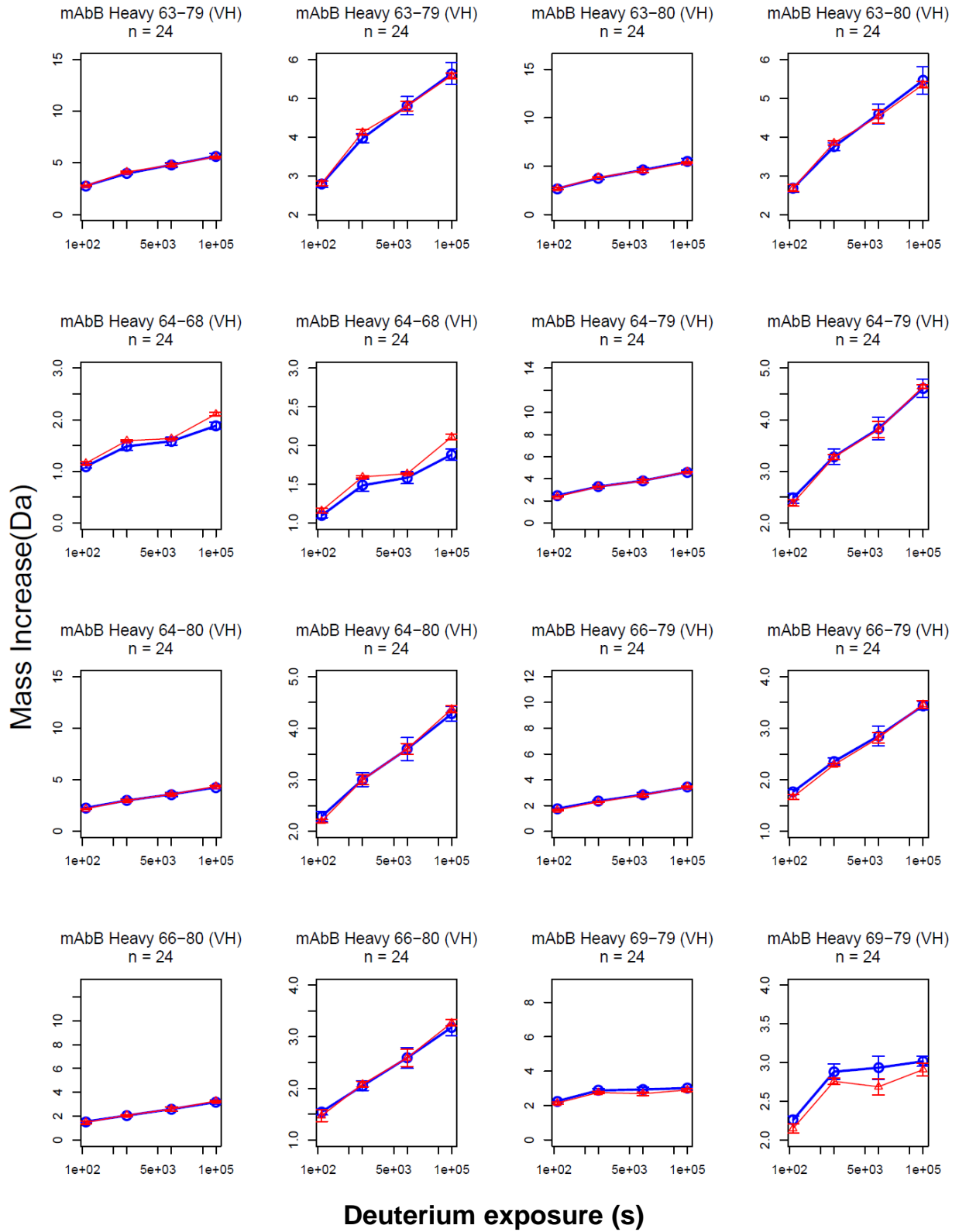
- 0.1 M NaCl
- △— 0.1 M NaCl + 0.5 M arginine

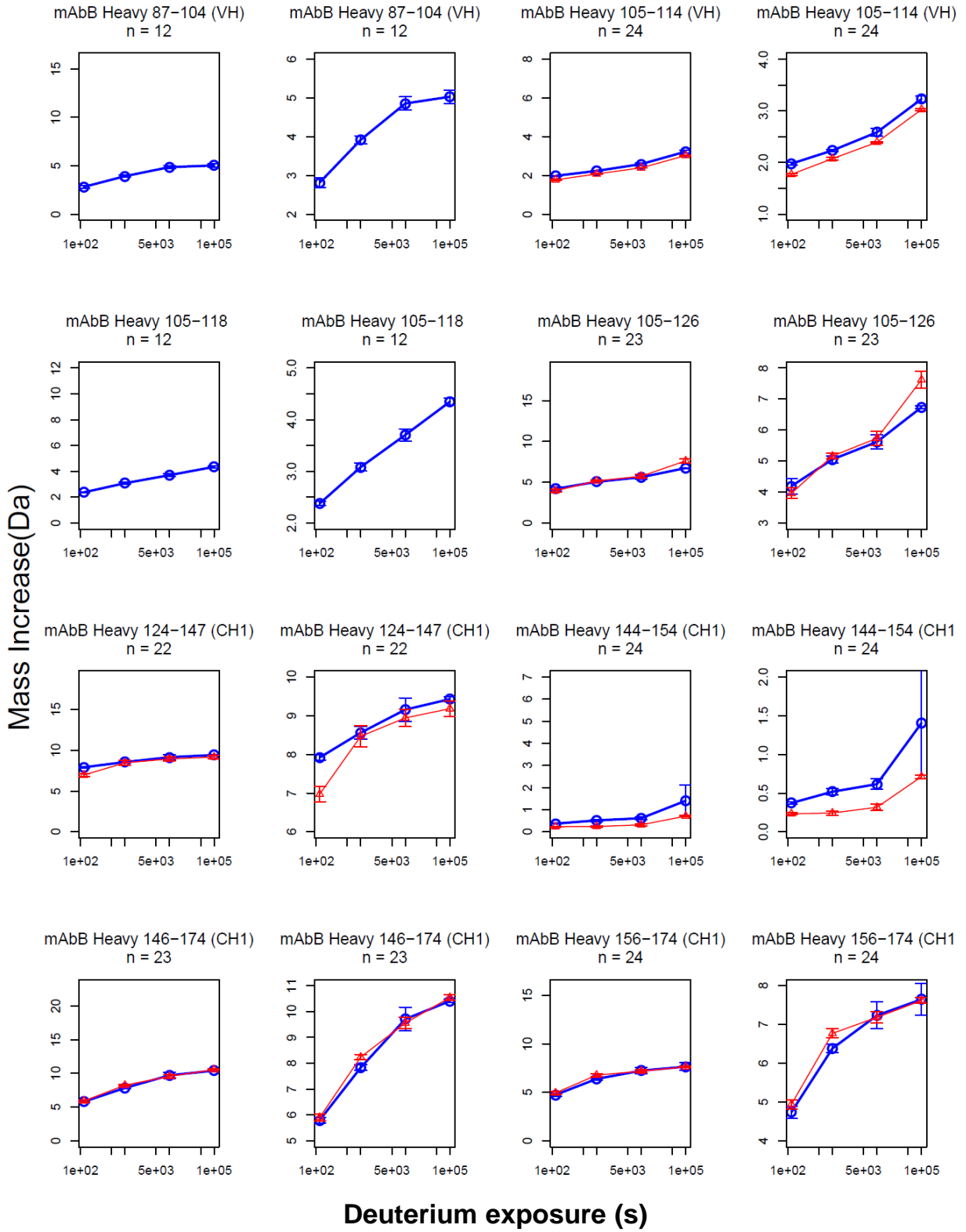


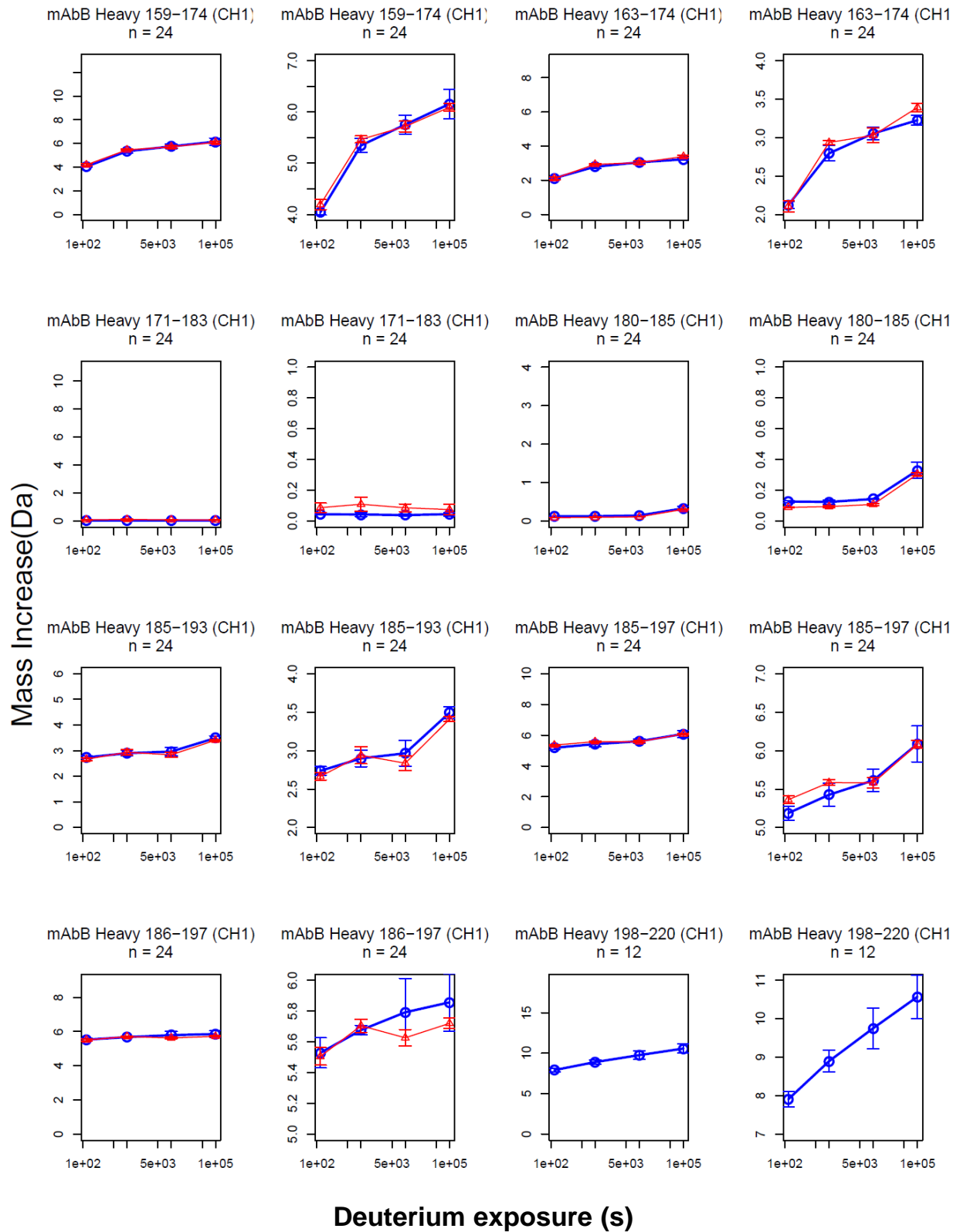


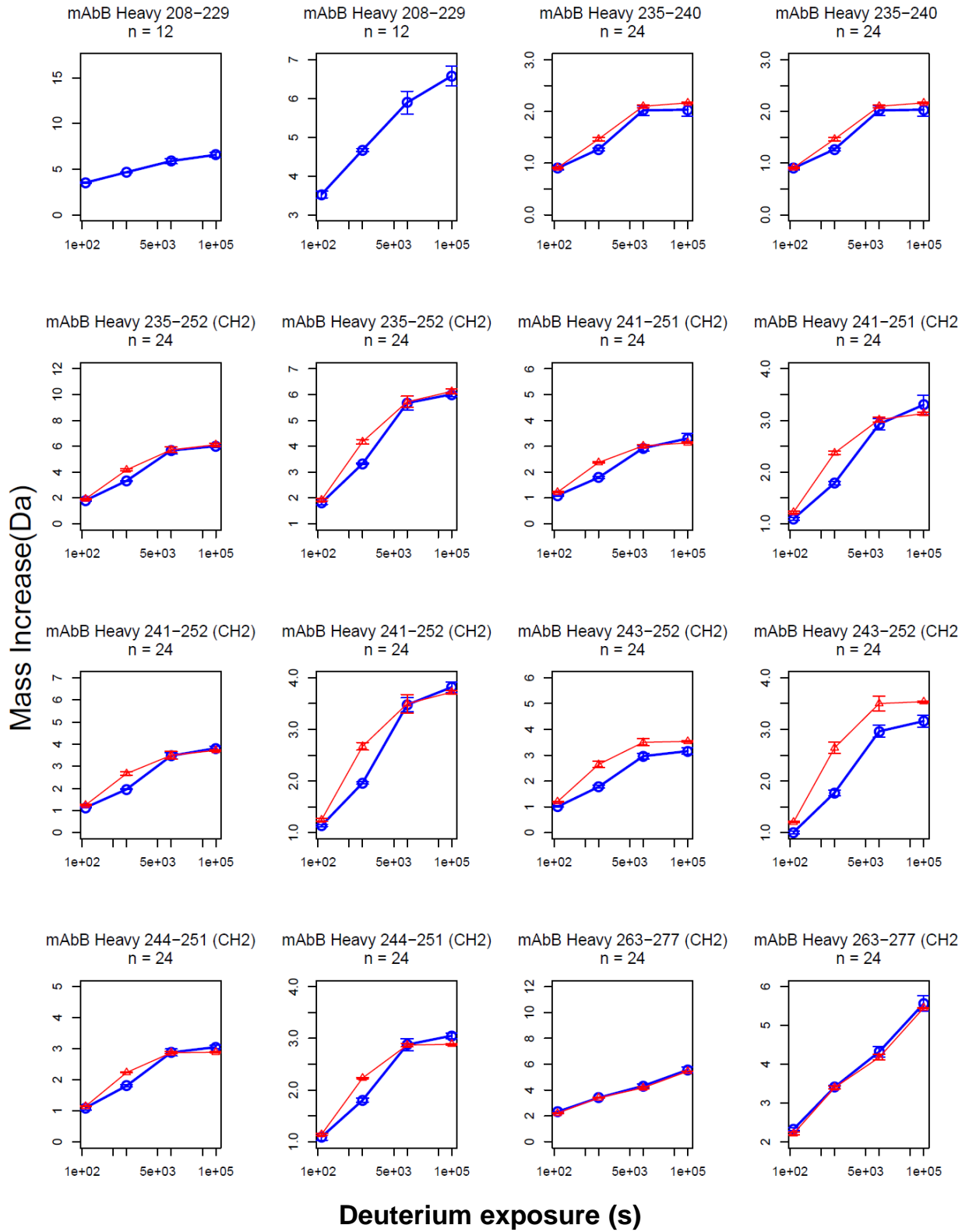


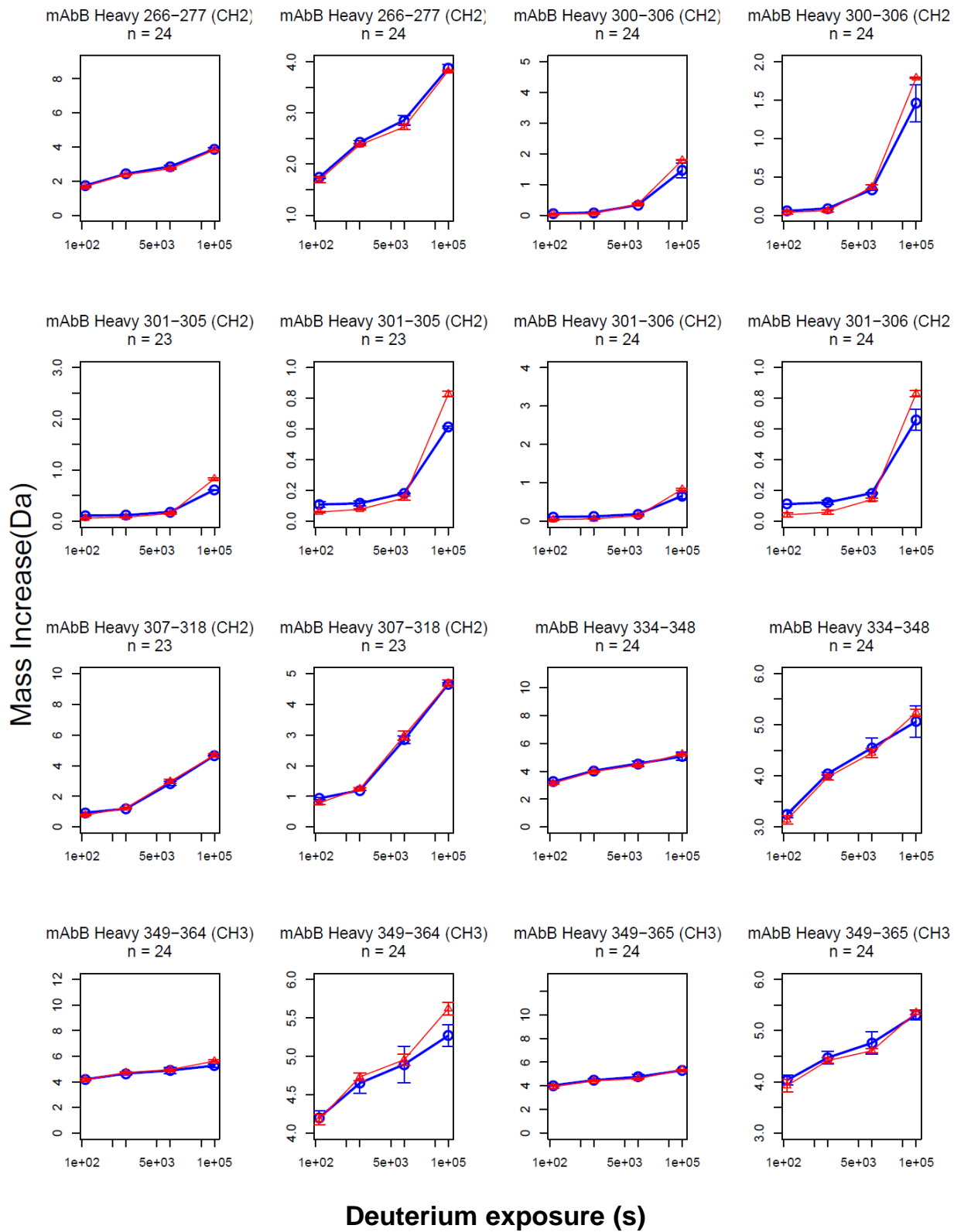


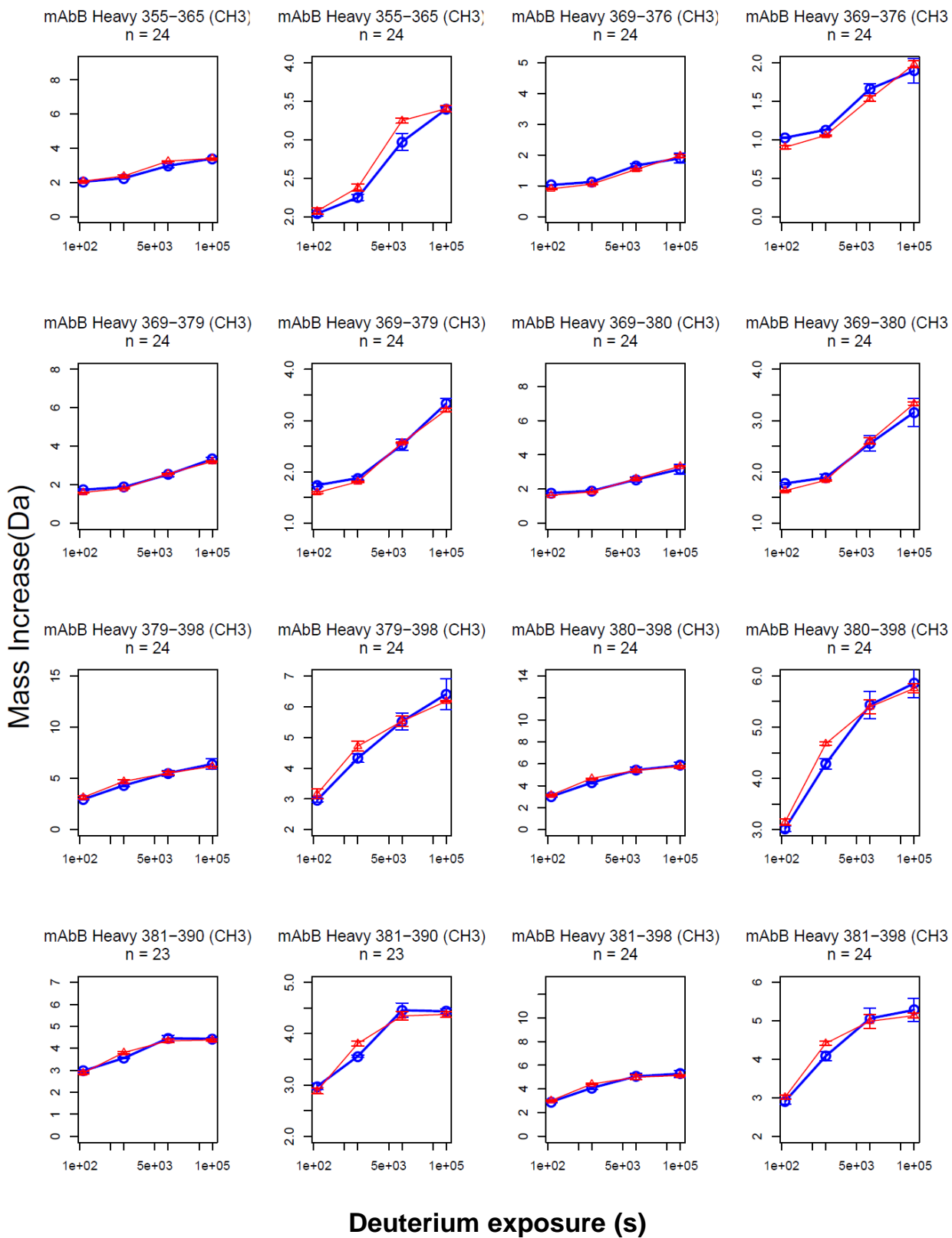


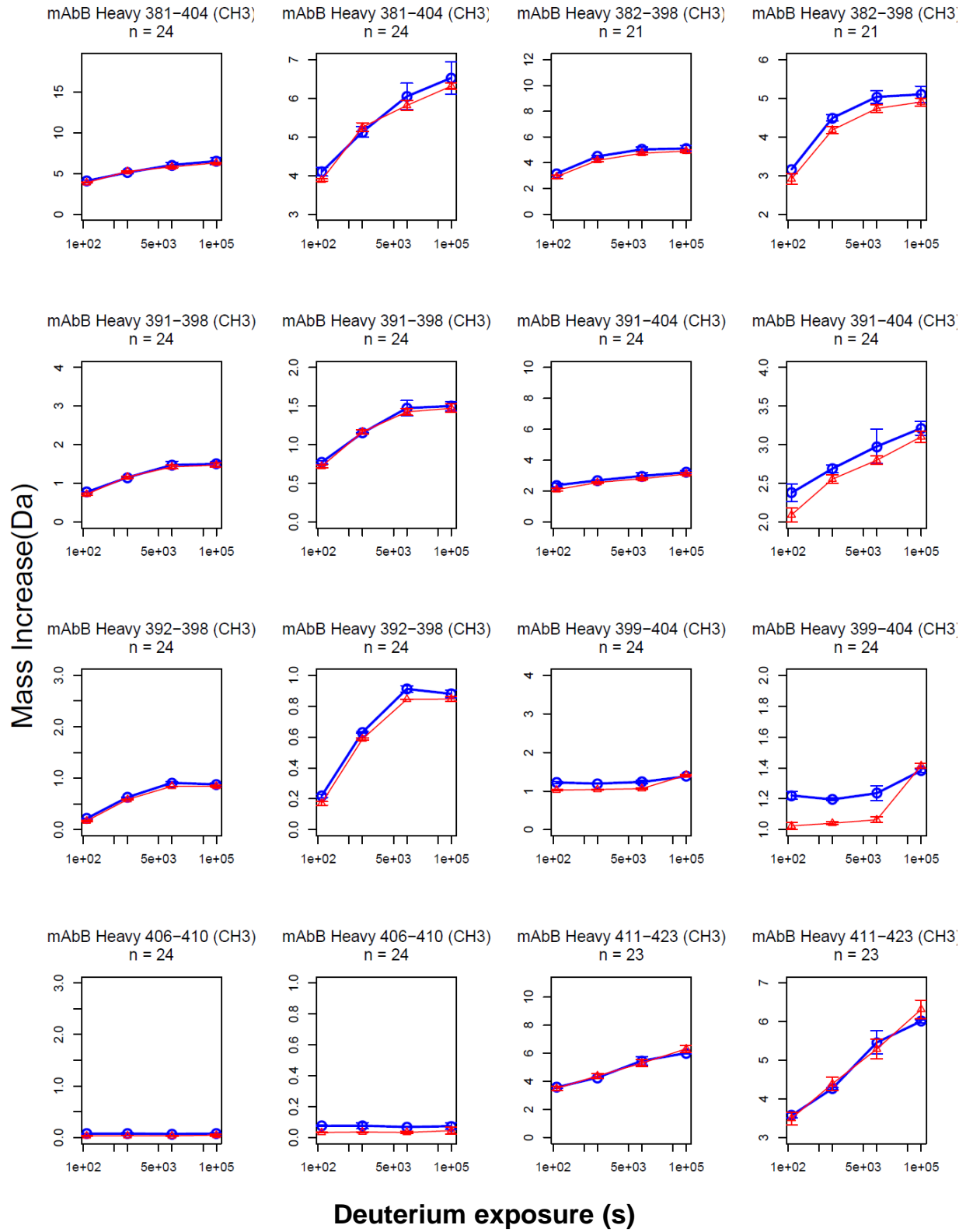


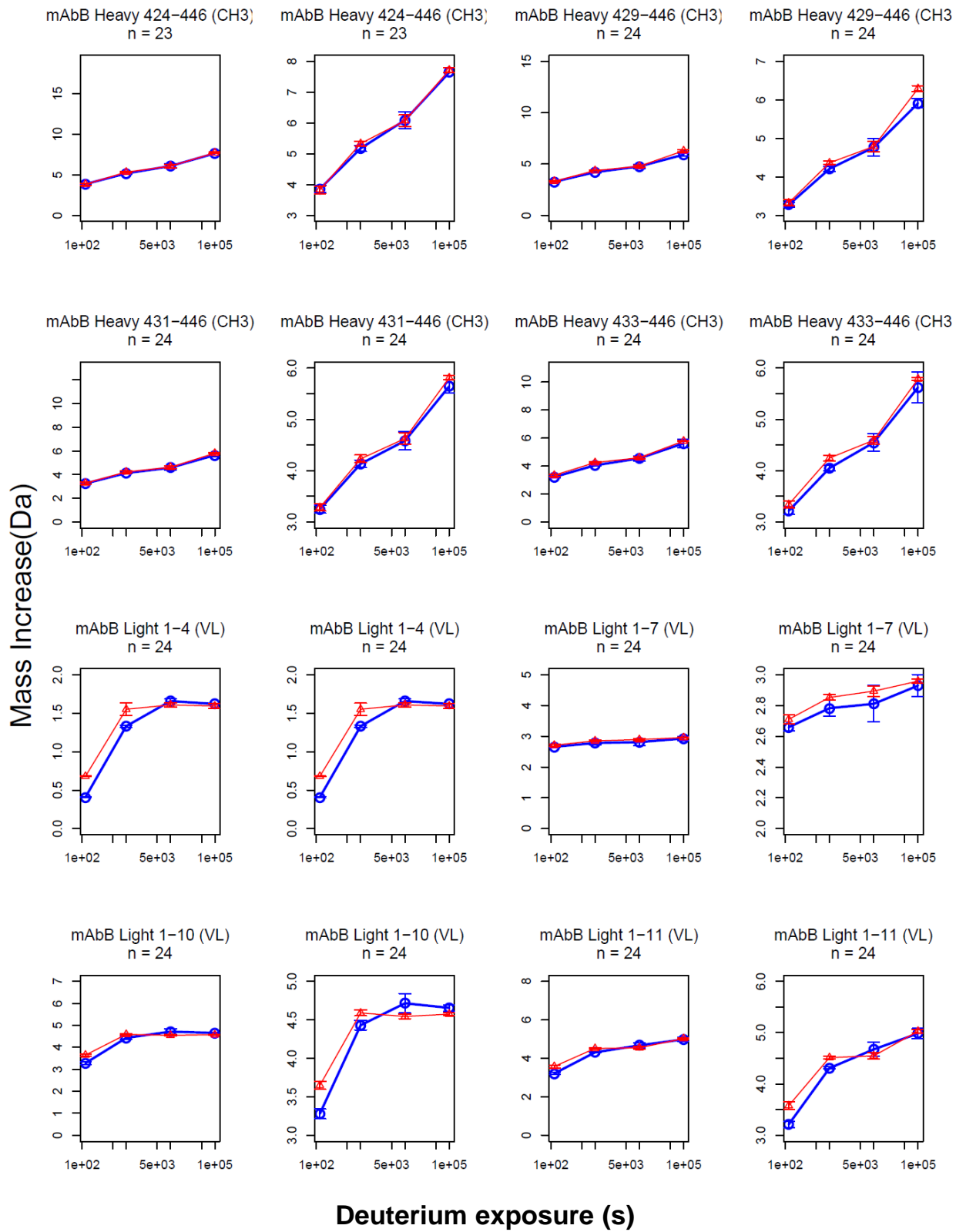


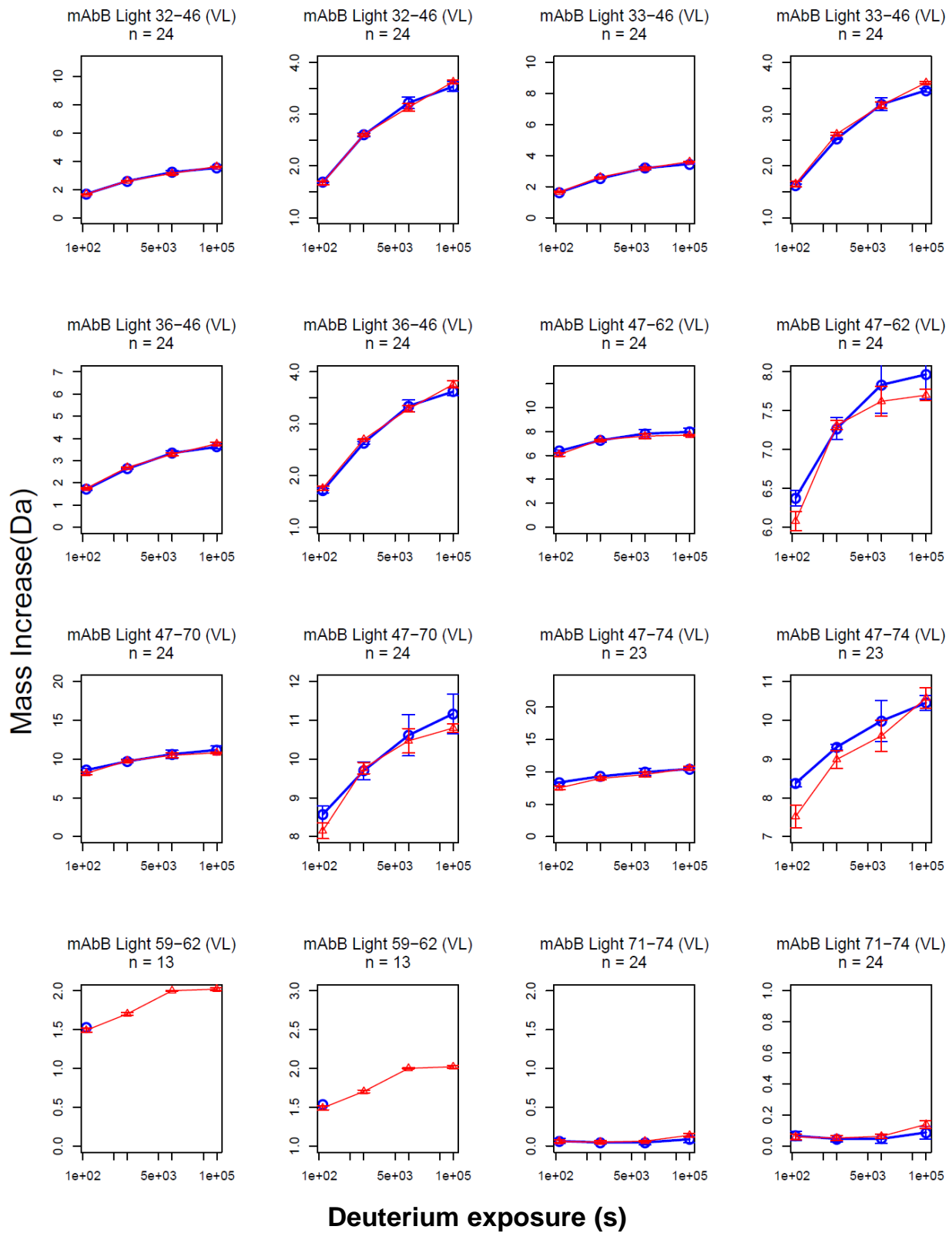


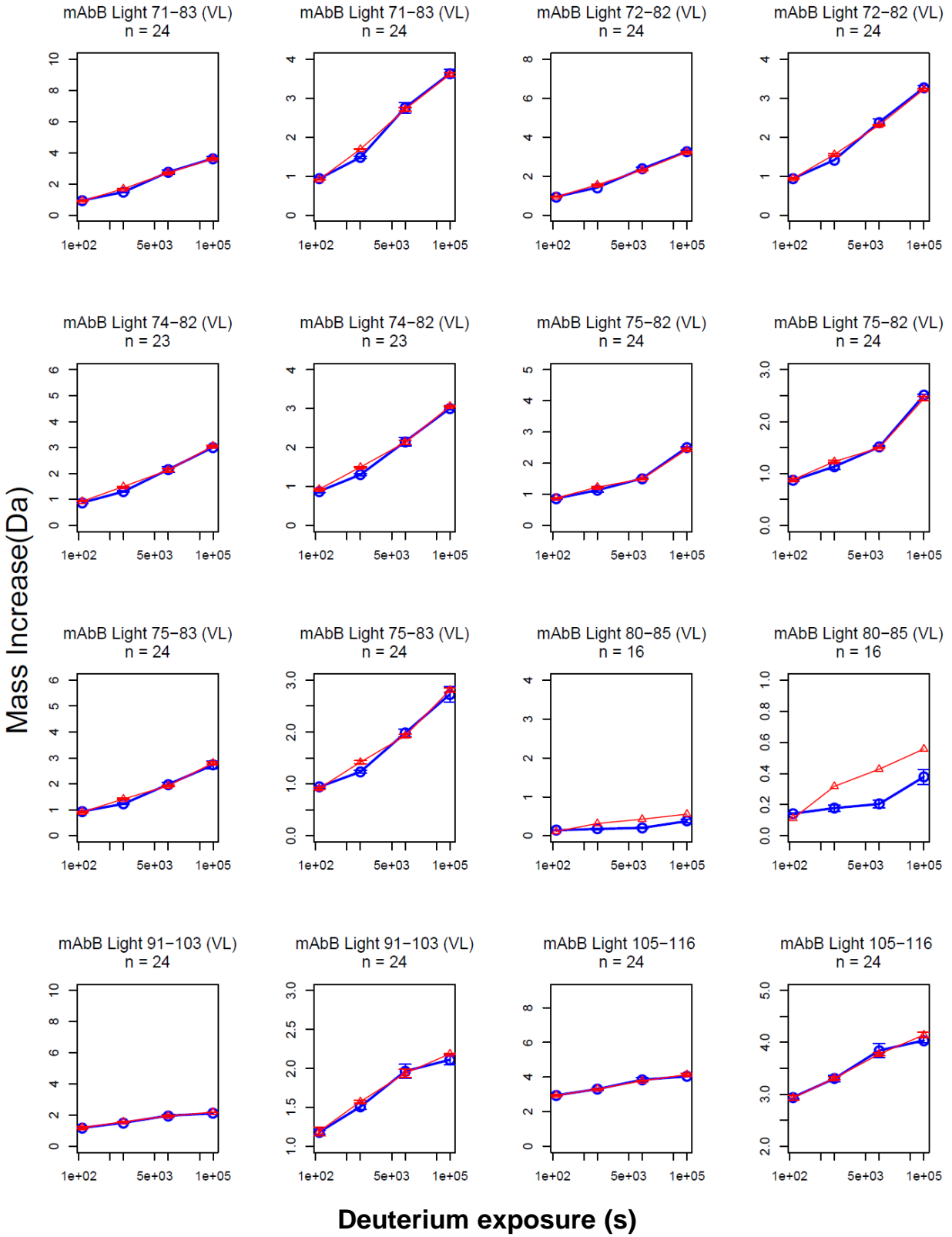


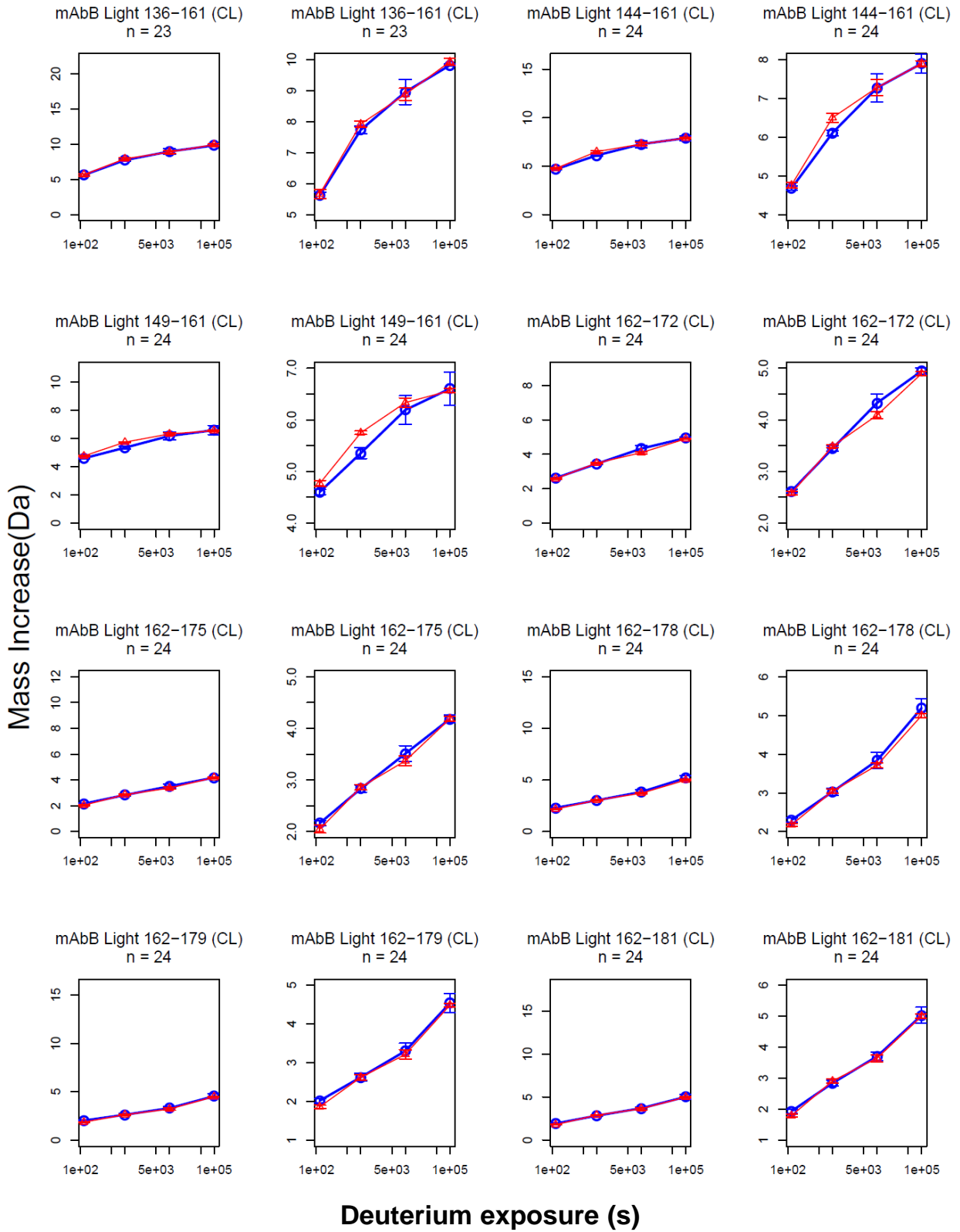


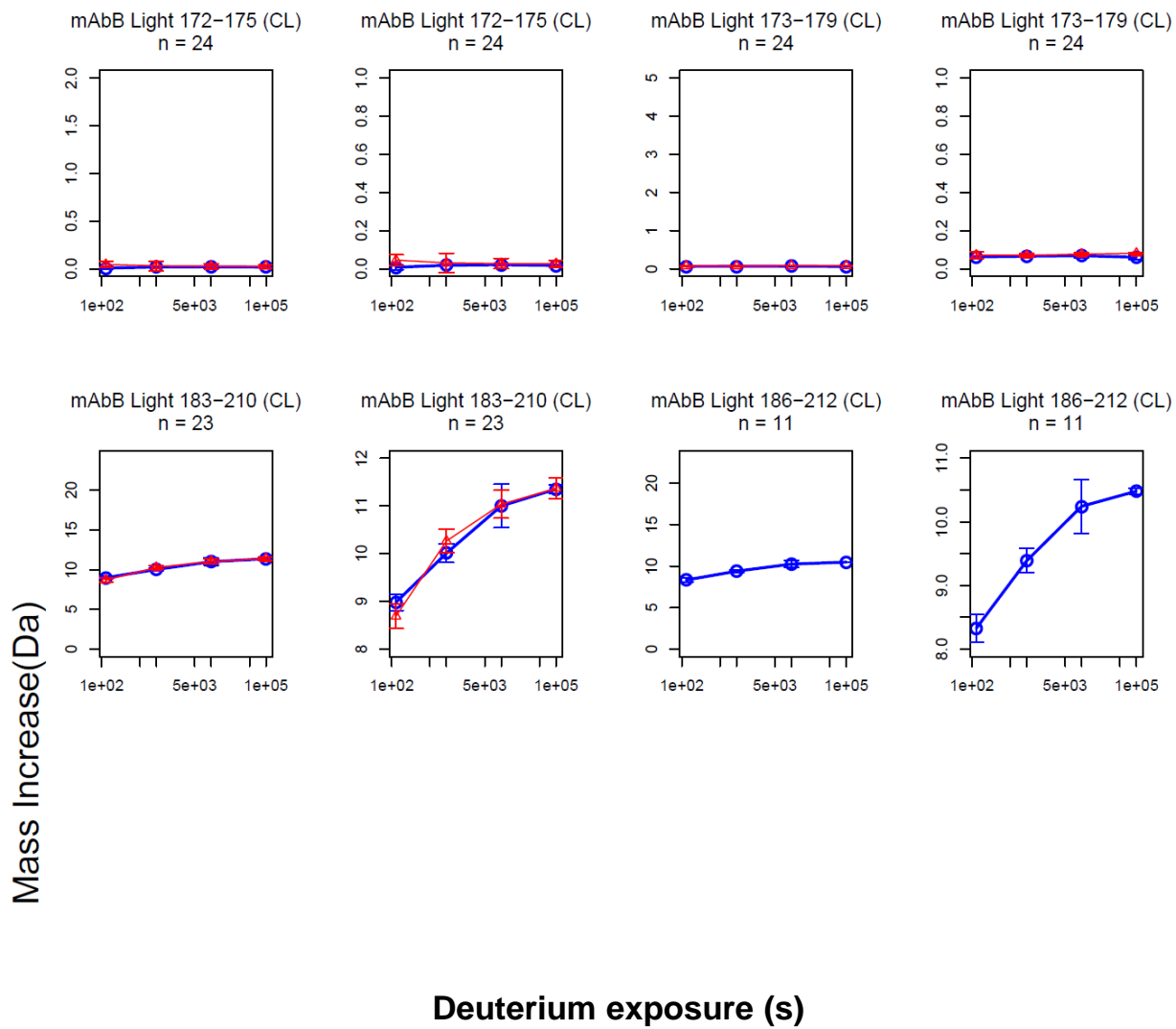




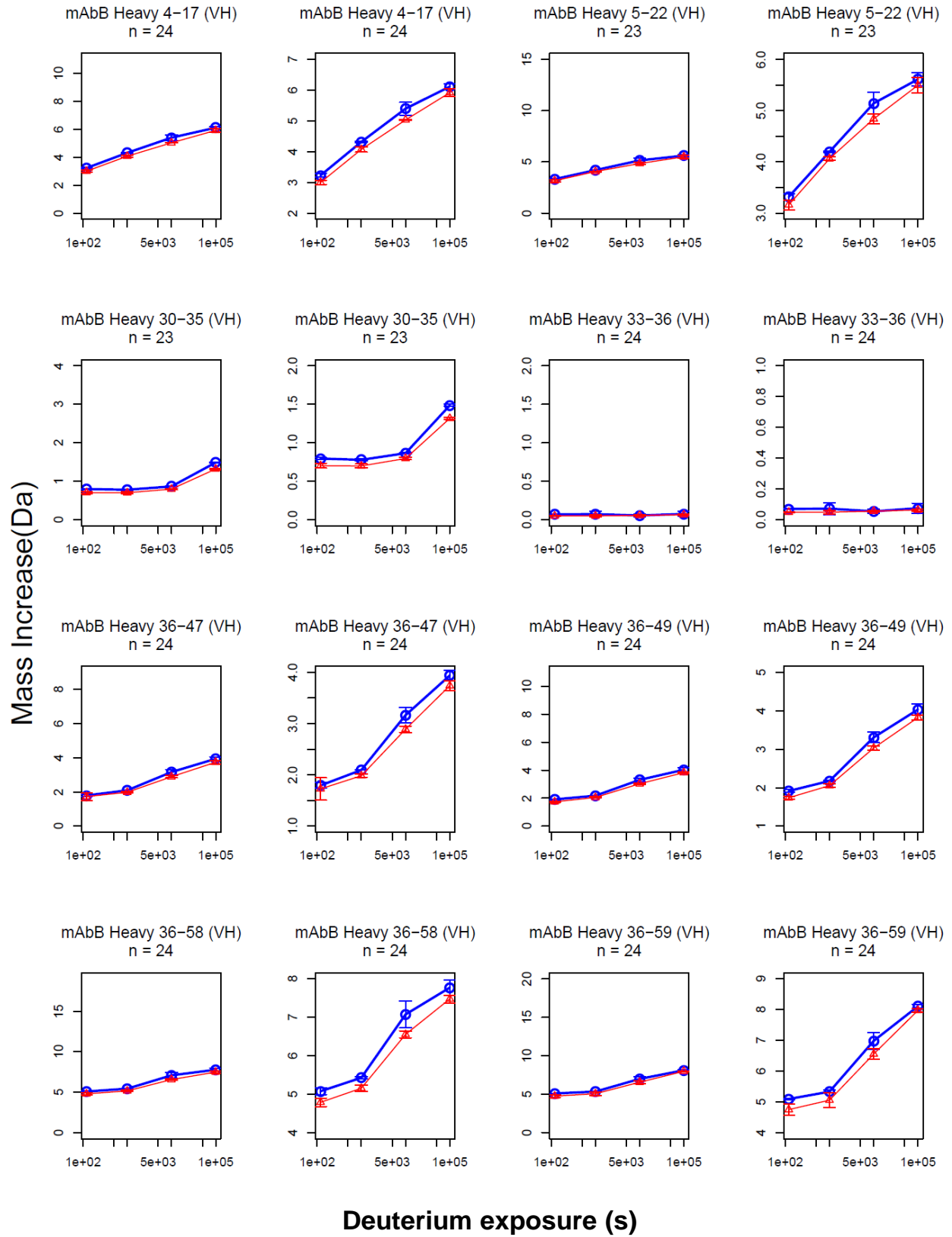


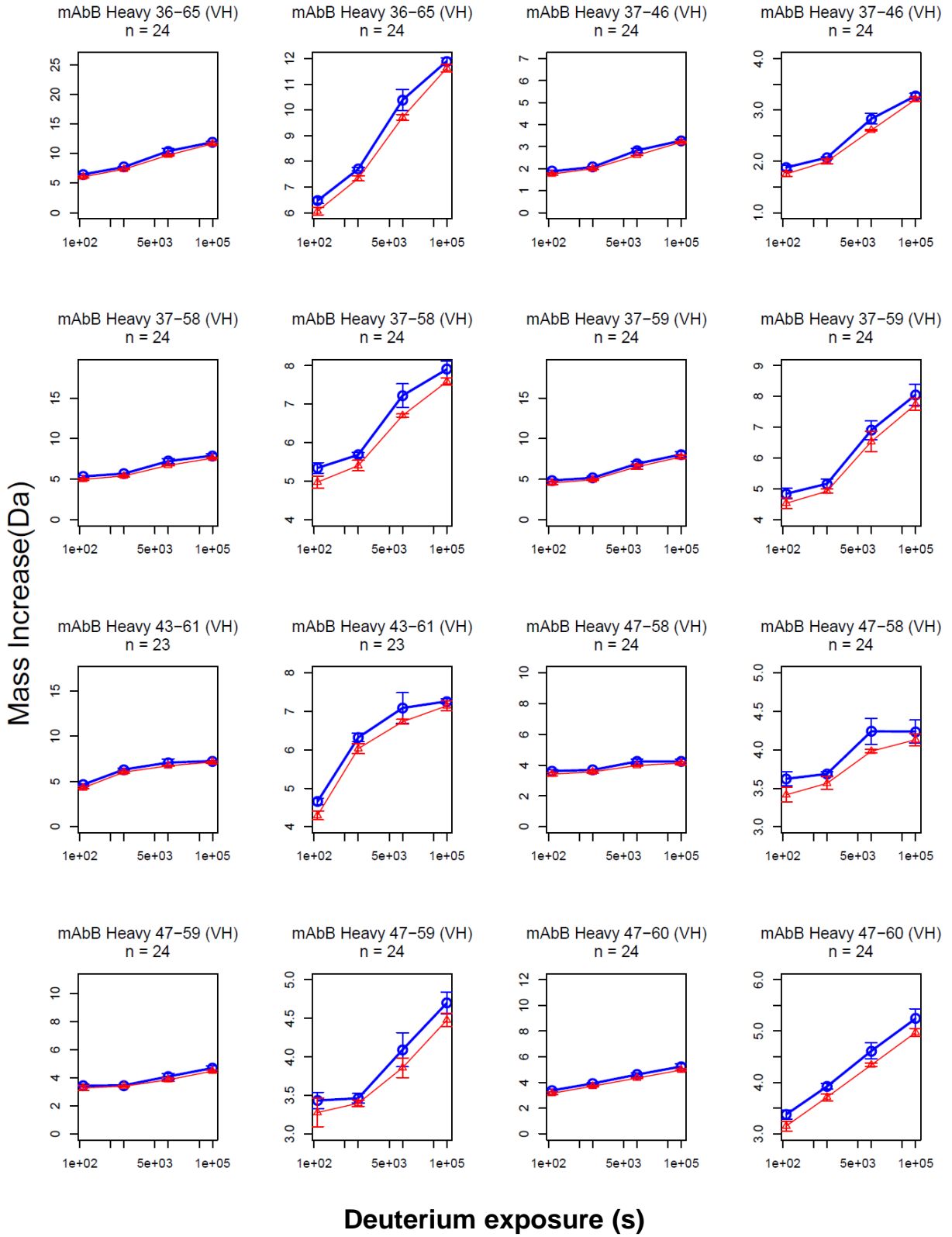


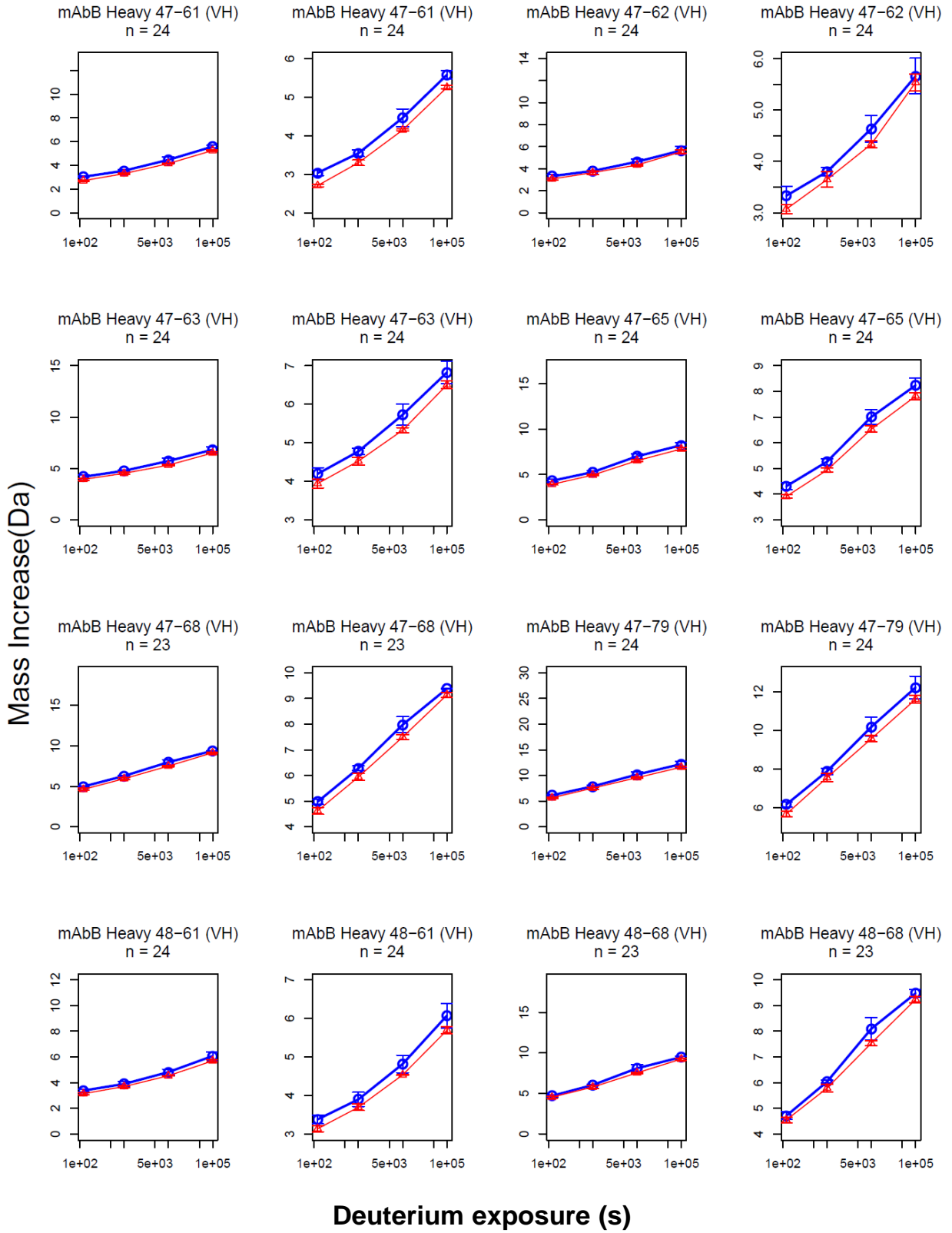


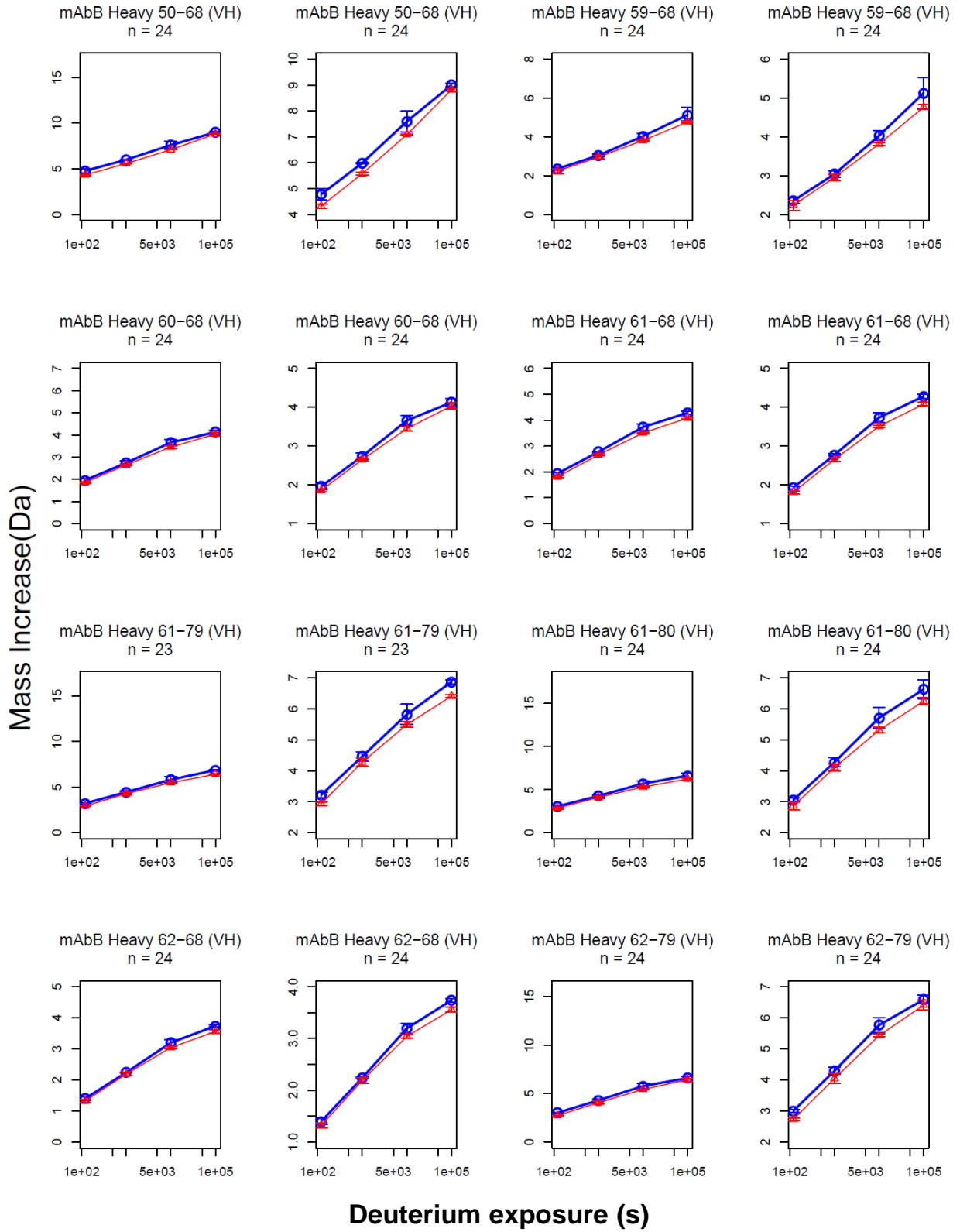


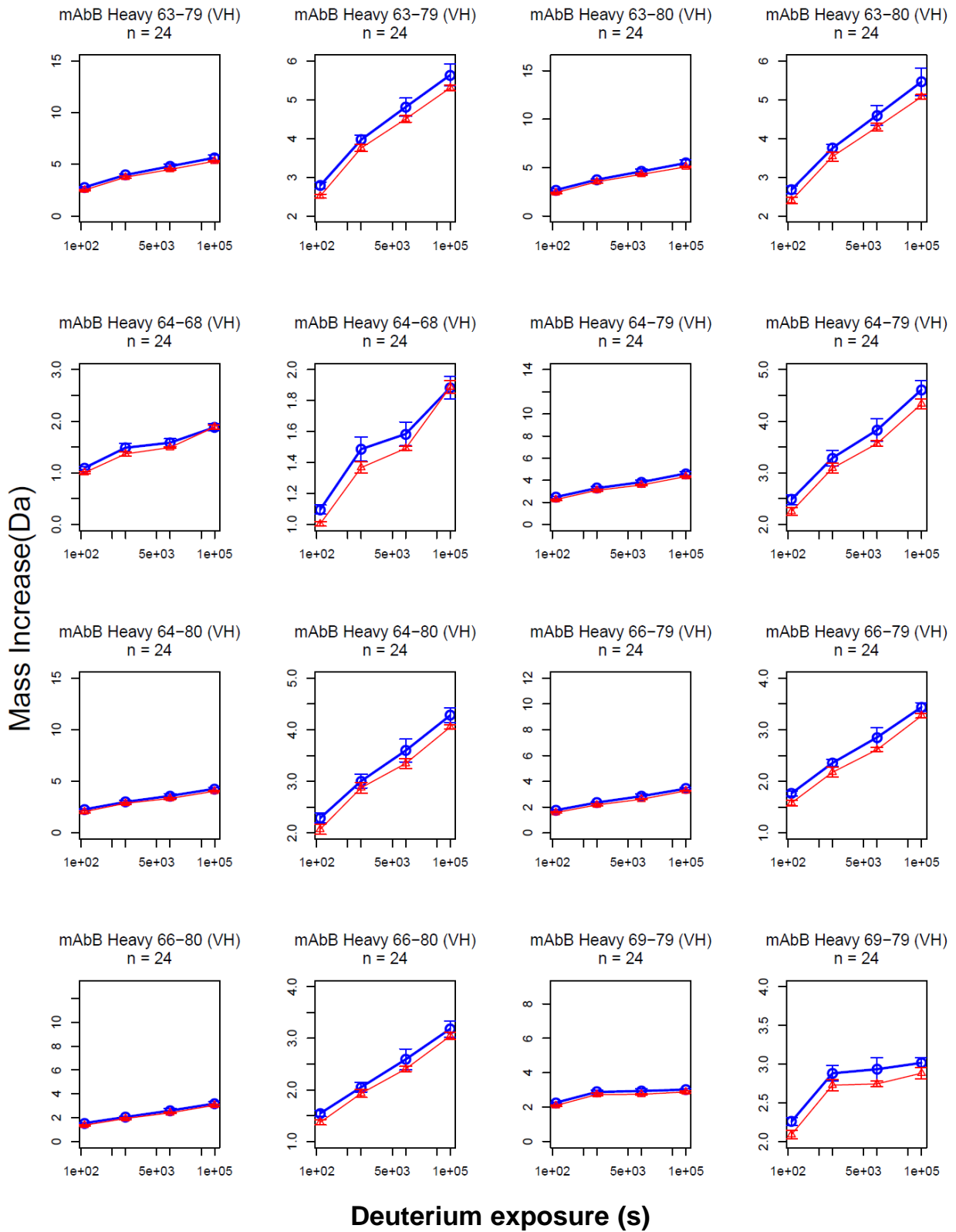
- 0.1 M NaCl
- △— 0.1 M NaCl + 0.5 M sucrose

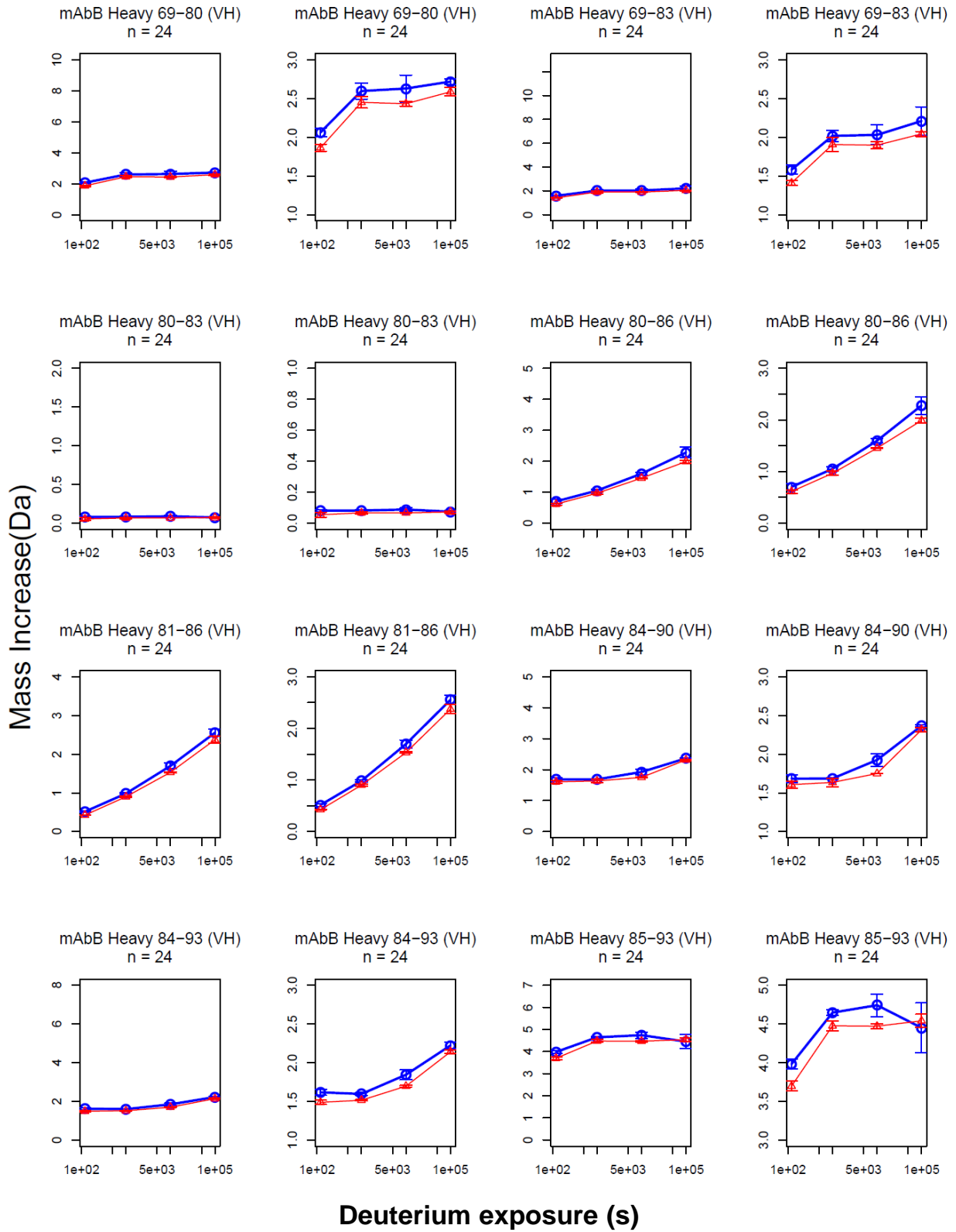


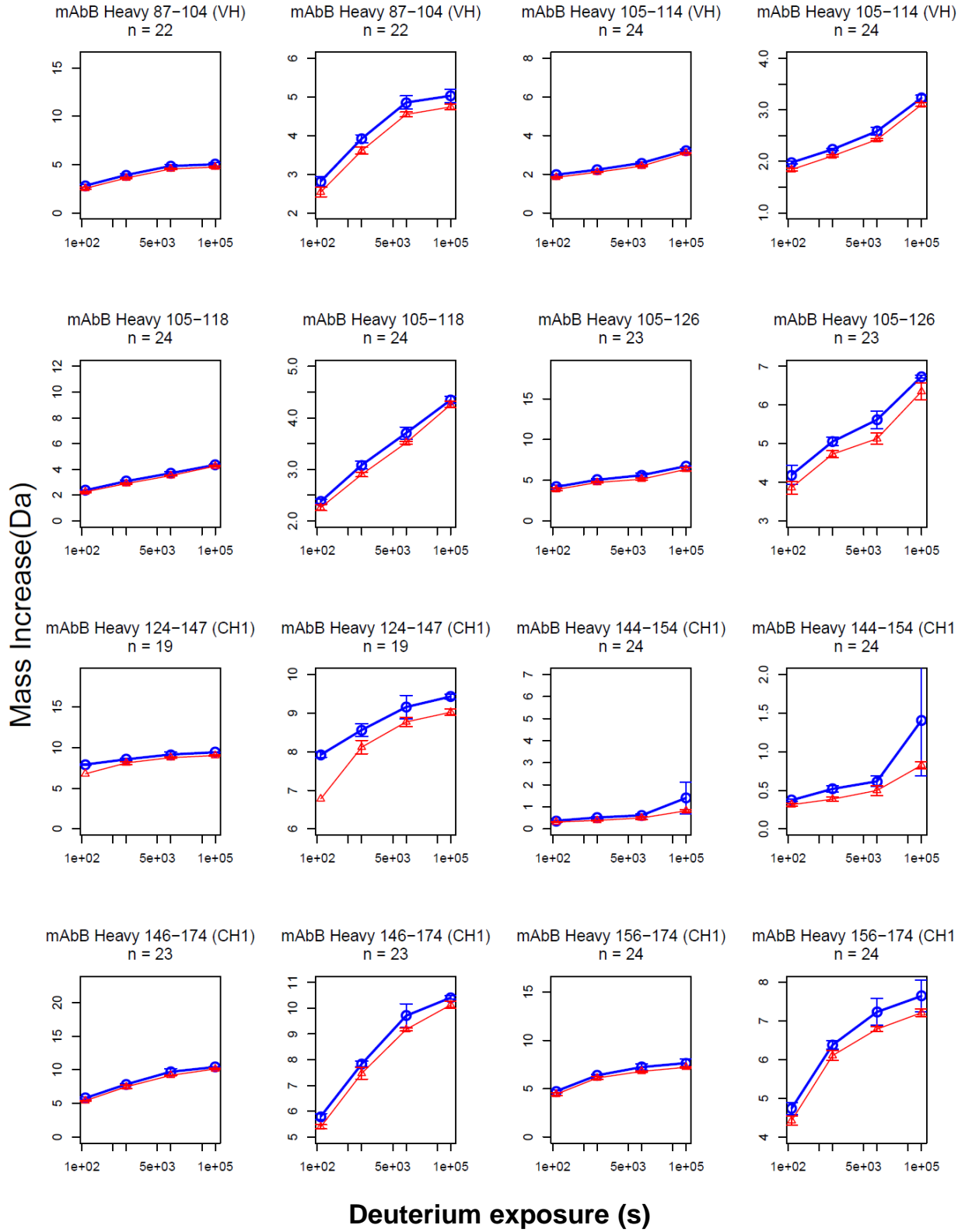


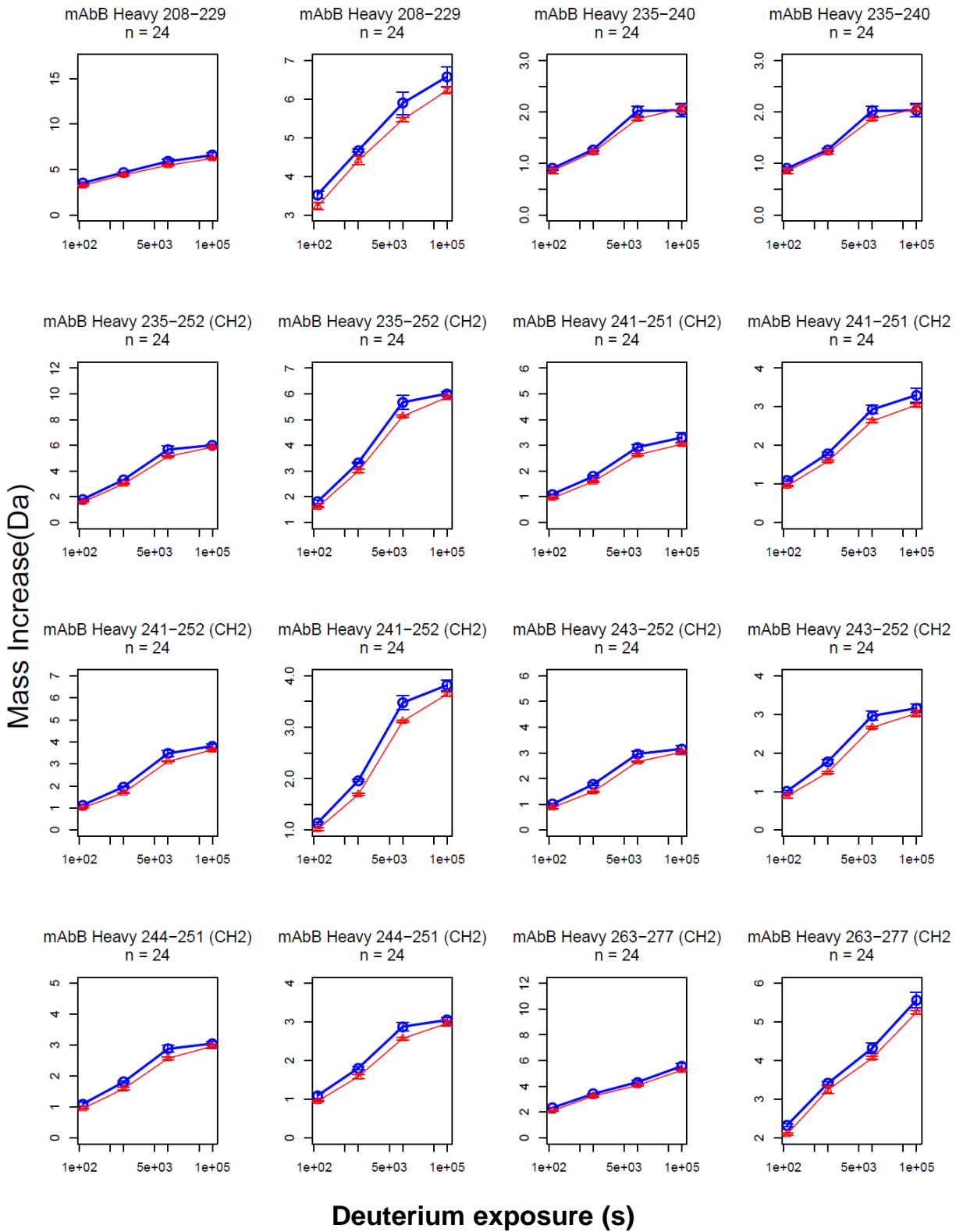


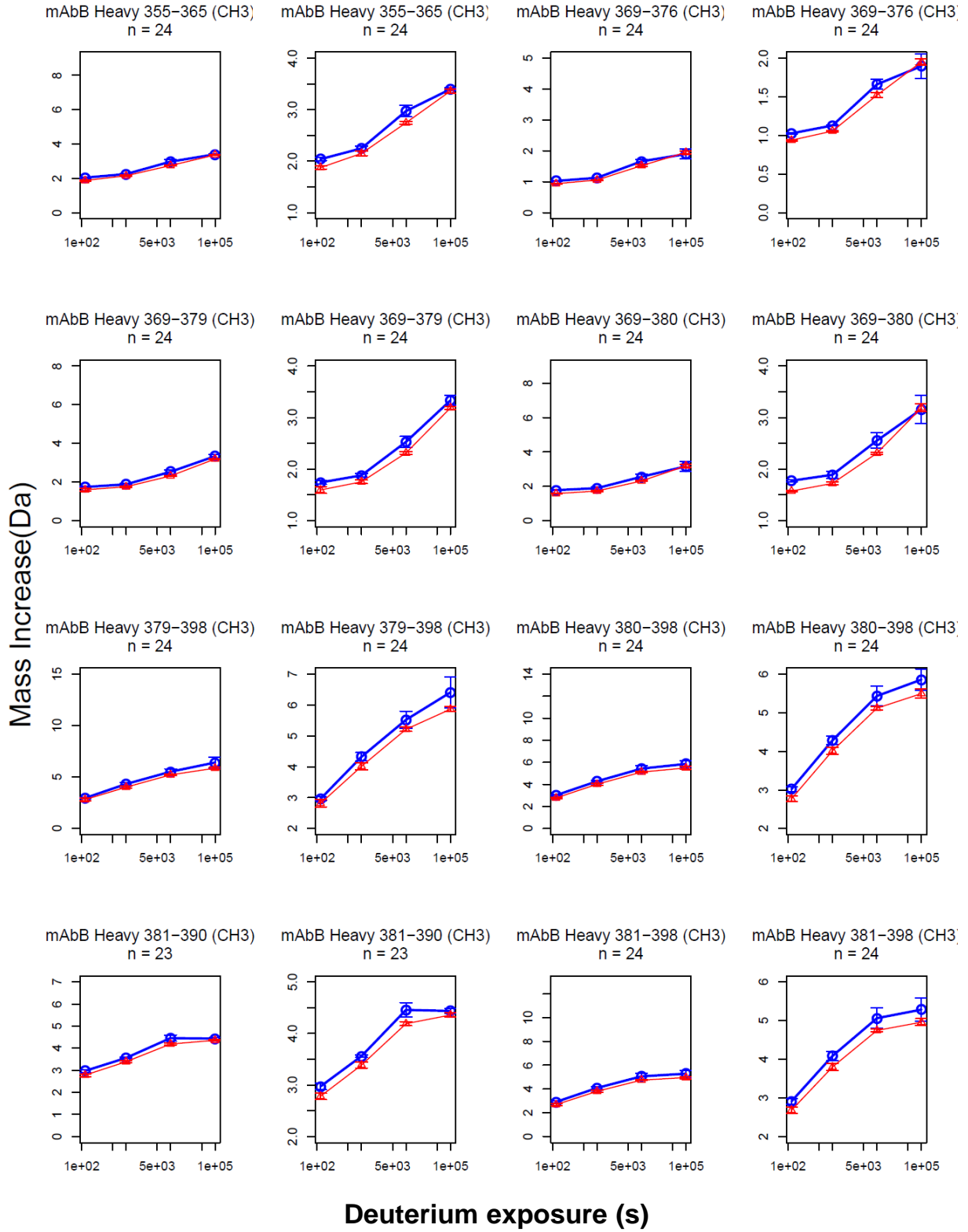


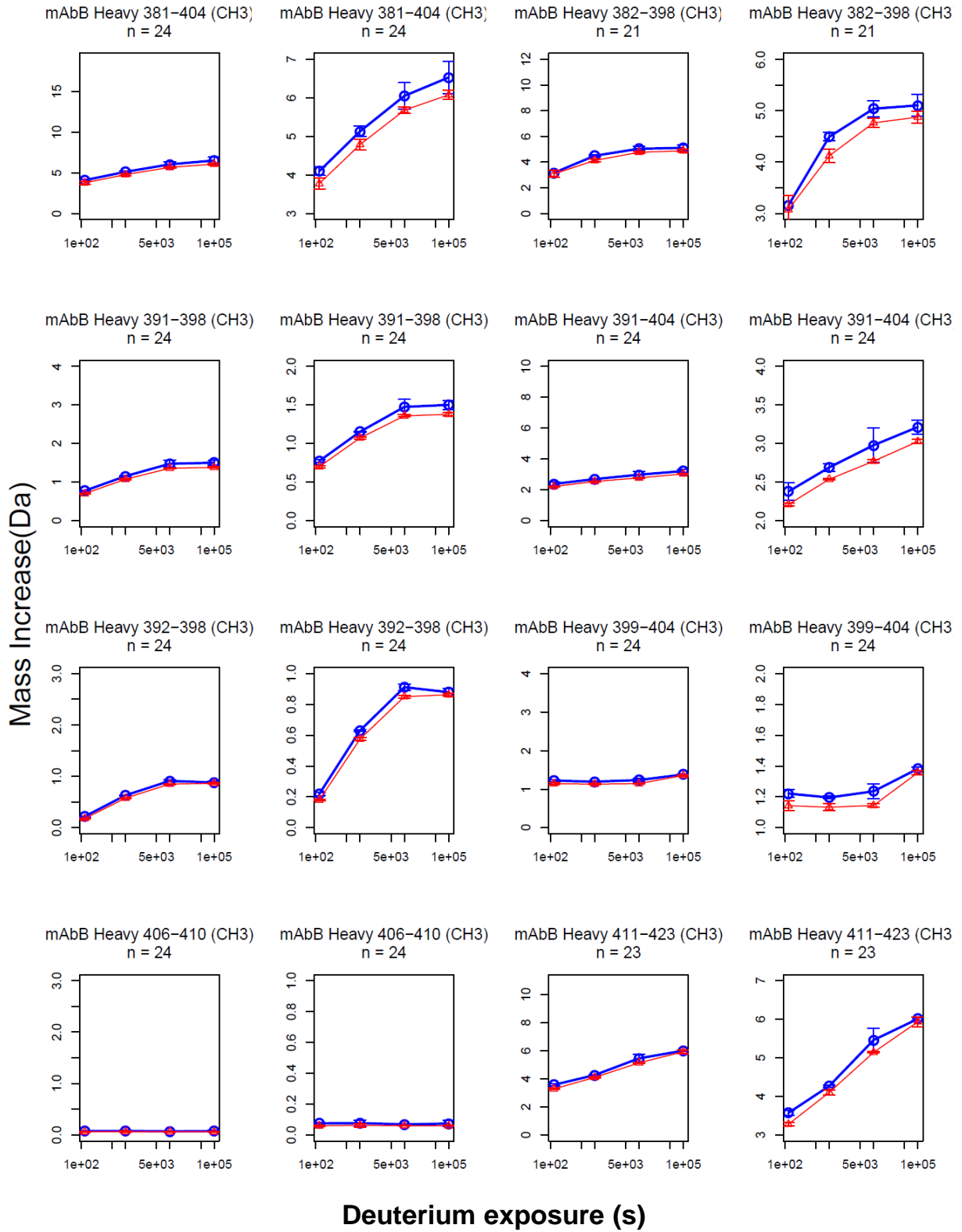


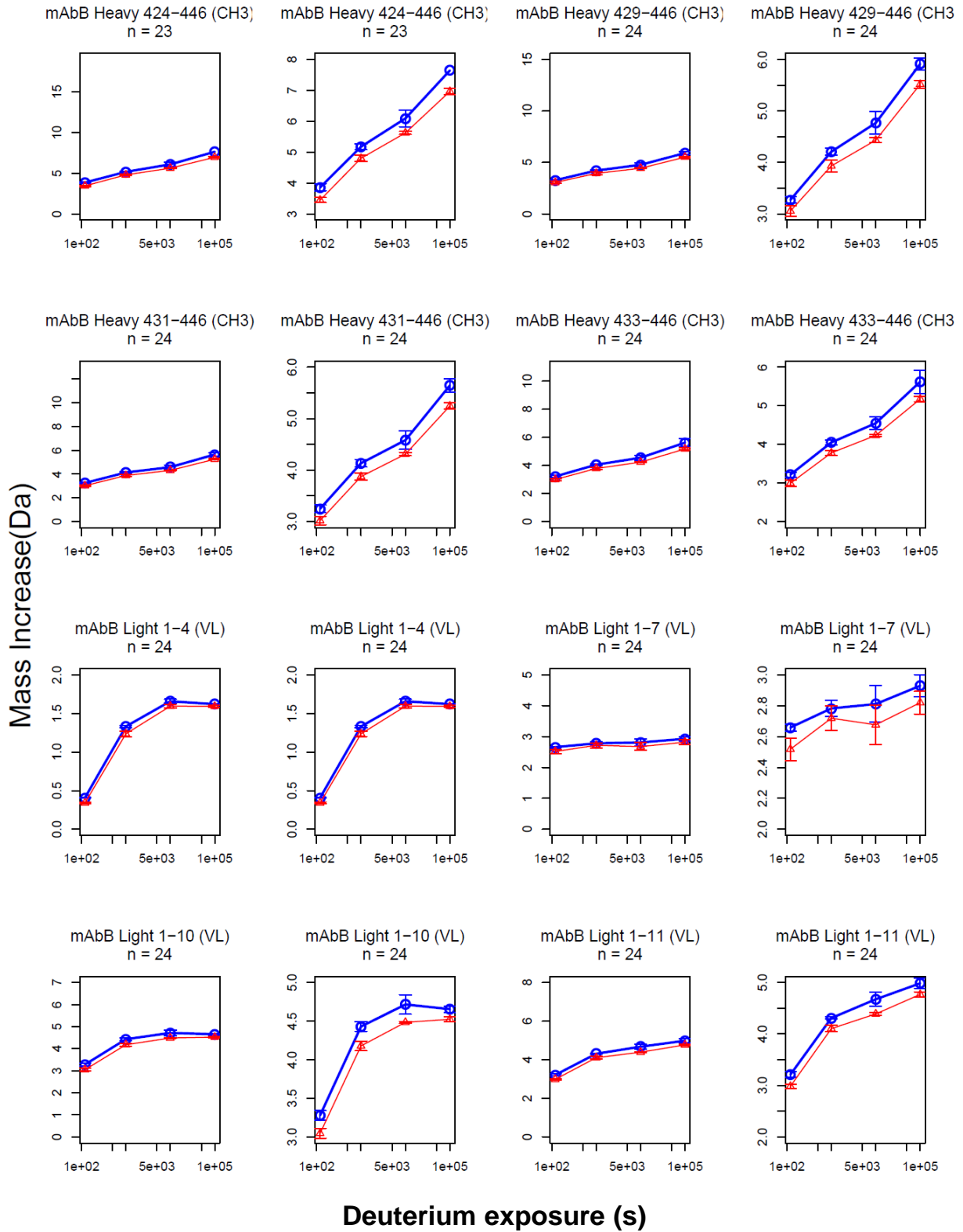


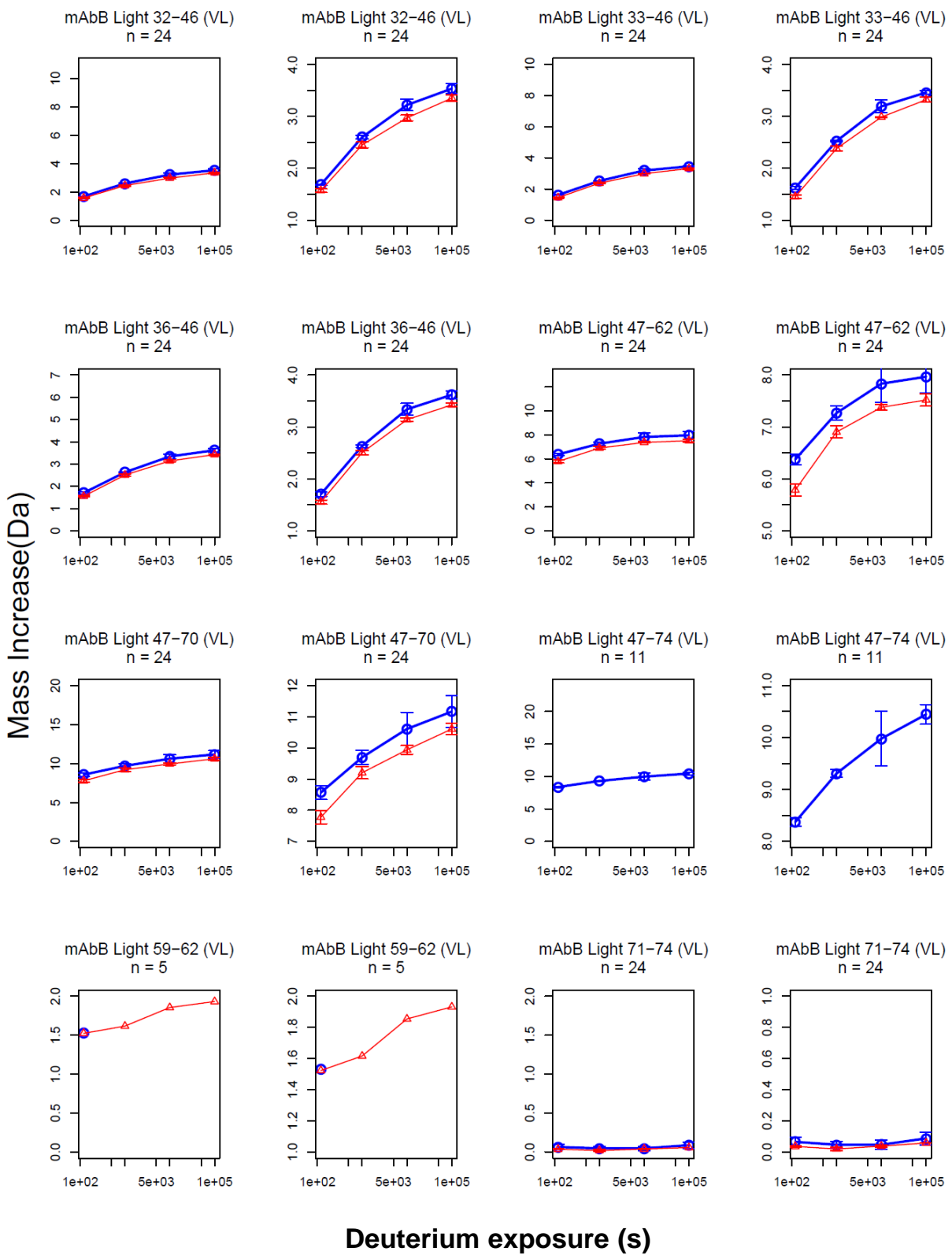


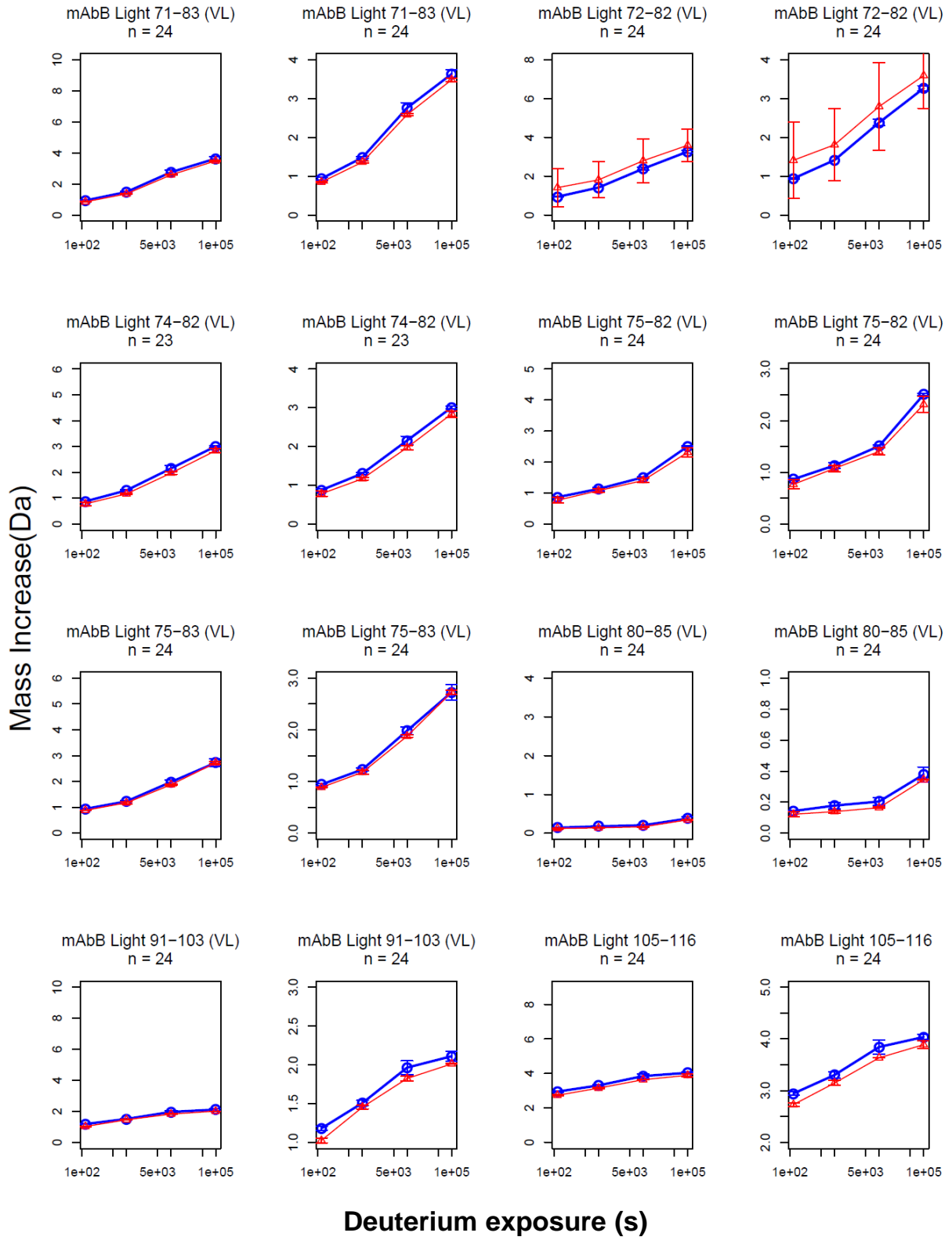


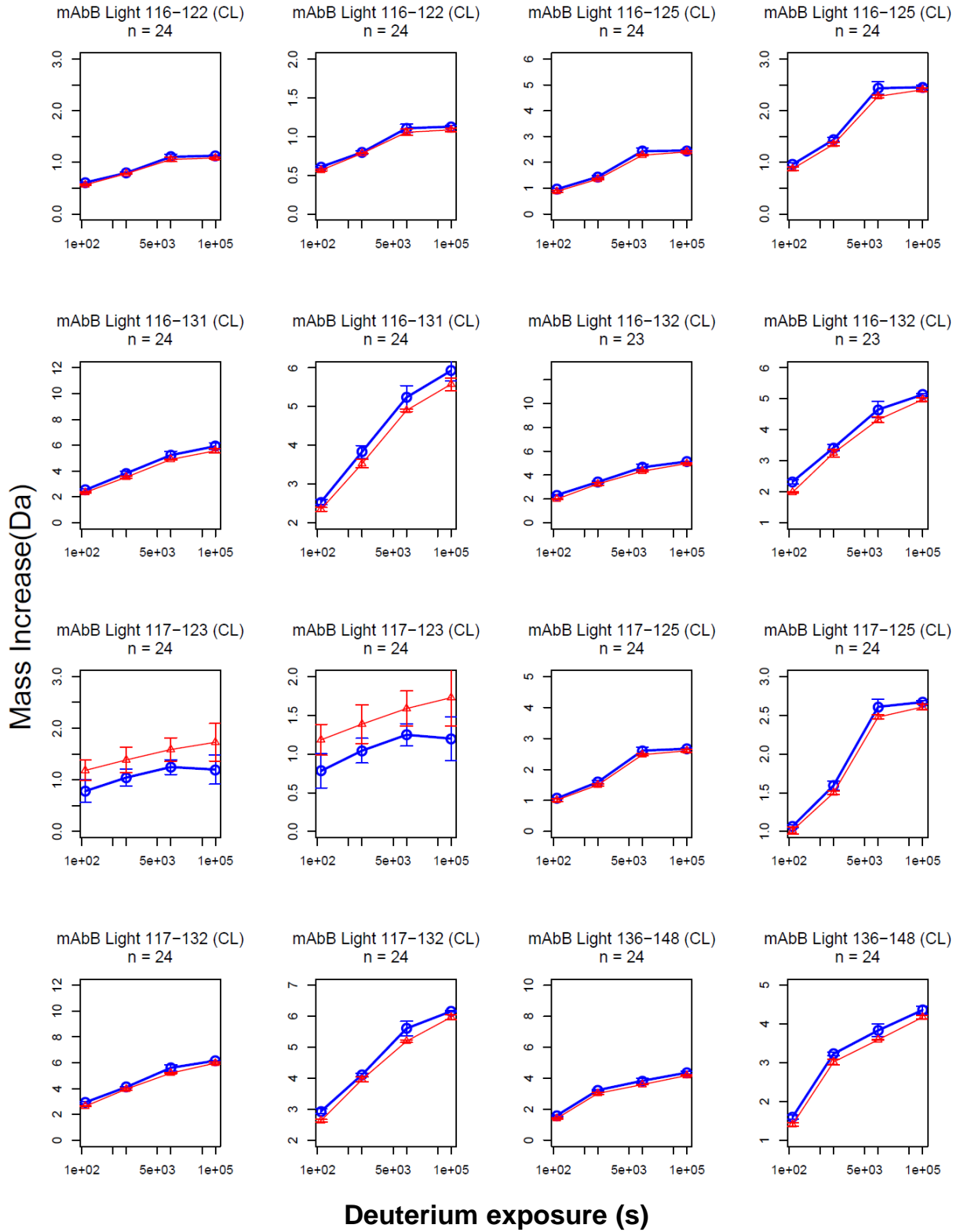


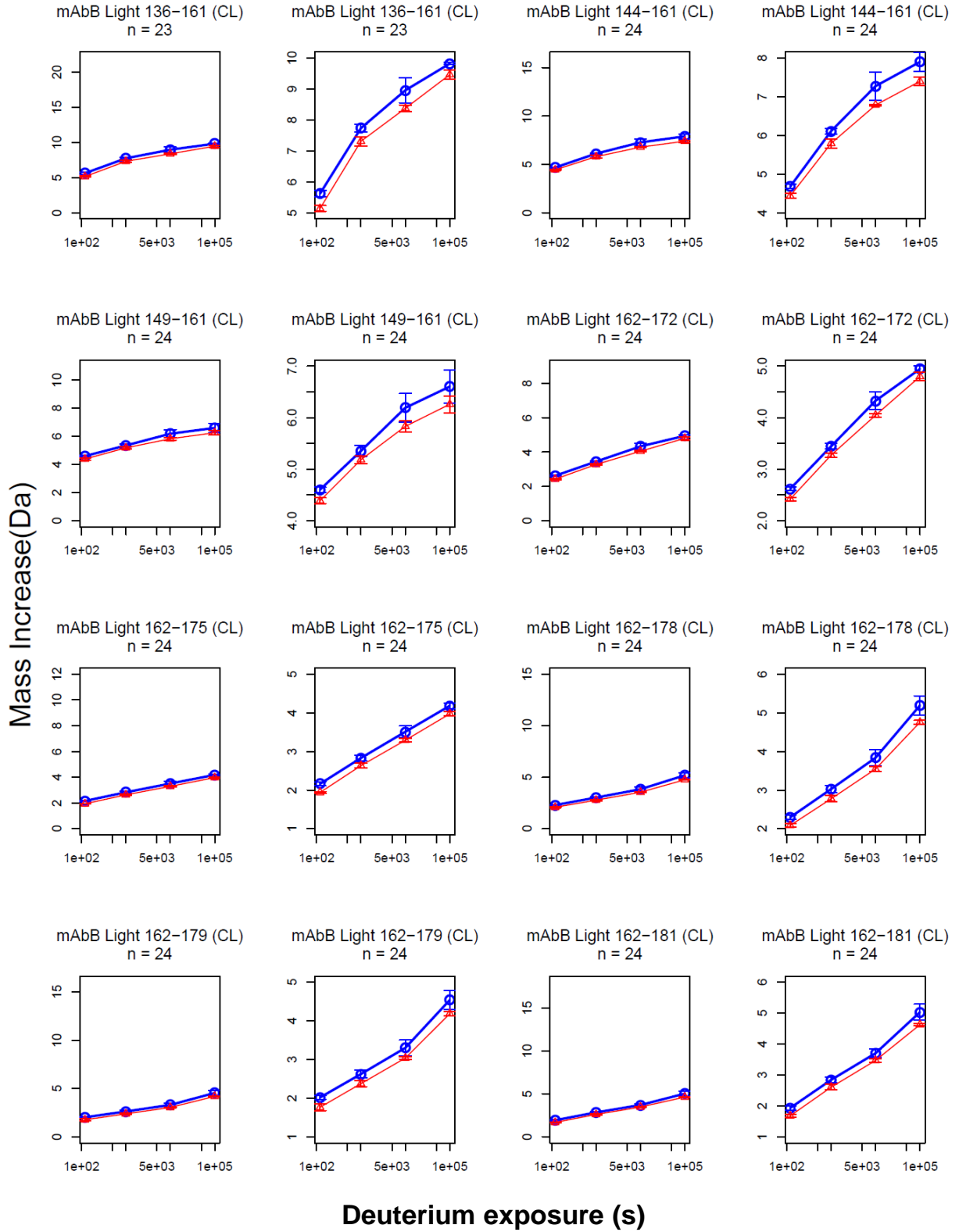


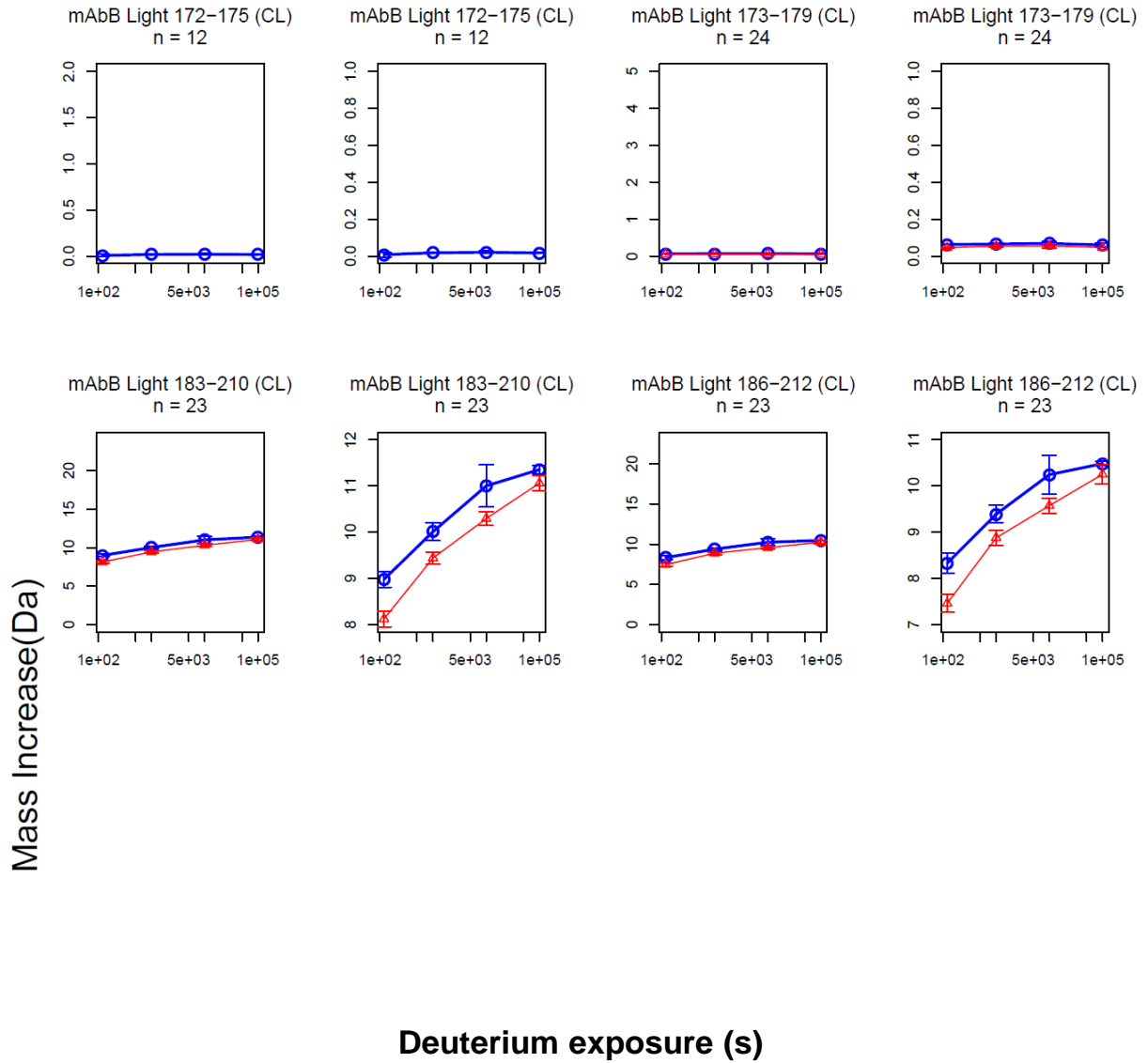






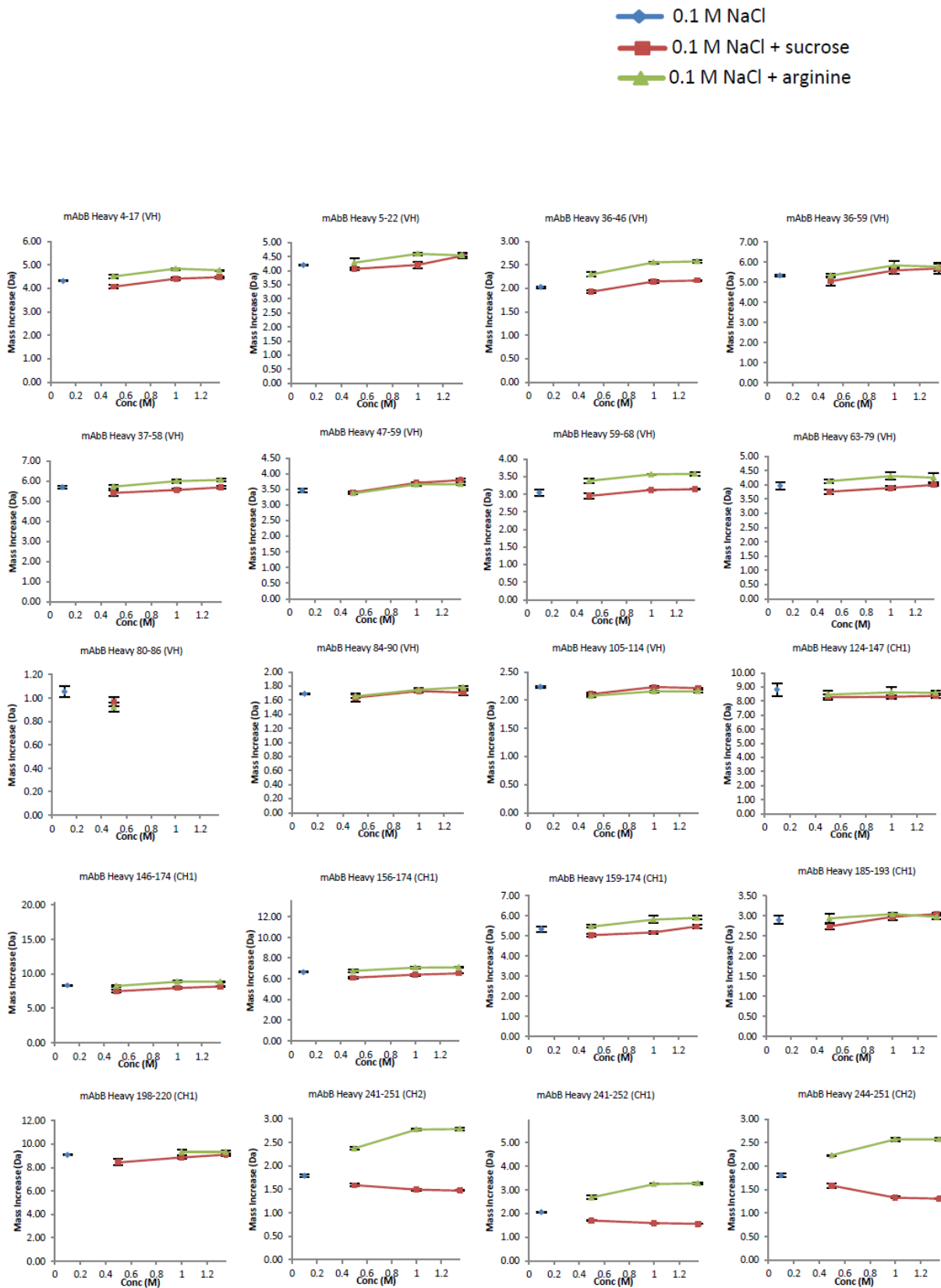


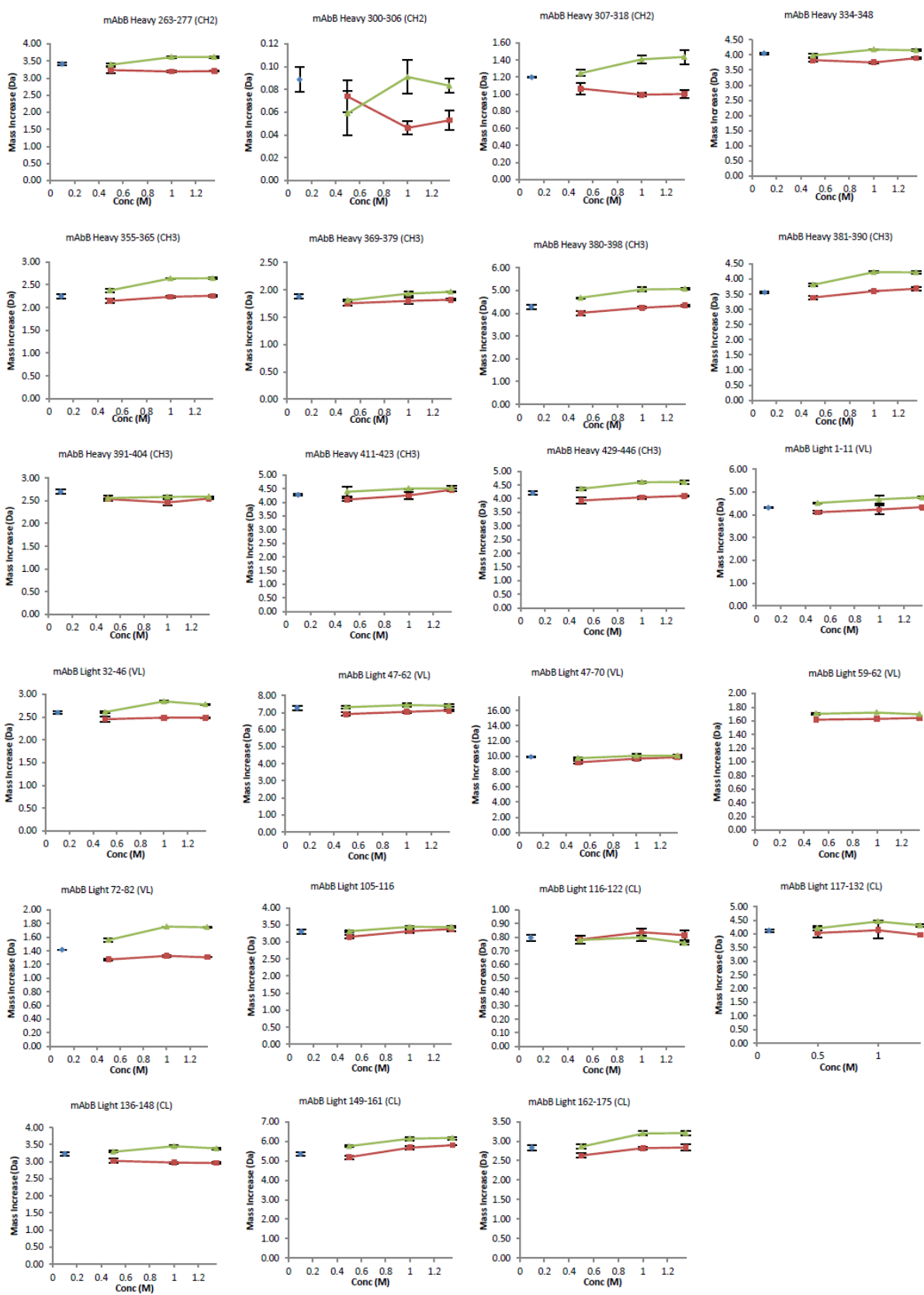




Deuterium update curves for 137 peptides of mAb-B. The first set of curves is for mAb-B labeled in presence of arginine and the second set of curves is for mAb-B labeled in presence of sucrose.

Figure 3.S2





Scatter plots of the mass increase for the 43 peptides of mAb-B with increasing concentration of either sucrose or arginine (0.5, 1.0, and 1.35 M) containing 0.1 M NaCl along with the control (0.1 M NaCl).

Chapter 4

Effects of Salts from the Hofmeister Series on Conformational Stability, Aggregation Propensity, and Local Flexibility of an IgG1 Monoclonal Antibody

(“Effects of Salts from the Hofmeister Series on Conformational Stability, Aggregation Propensity, and Local Flexibility of an IgG1 Monoclonal Antibody.”, Majumdar R., Manikwar P., Hickey J.M., Samra H.S., Hasige A.S, Bishop S.M., Middaugh C.R., Volkin D.B., Weis D.D., *Biochemistry*. 2013 May 14;52(19):3376-89.)

4.1 Introduction

Monoclonal antibodies (mAbs) have become successful therapeutic agents due to their high binding specificities to biological targets implicated in a wide range of human diseases. The presence of protein aggregates in therapeutic mAb preparations are of particular concern due to their potential to cause immune responses that may affect the safety or limit the efficacy of therapeutic mAb treatments.¹⁻³ Antibodies are multi-domain, homodimeric proteins with a molecular weight of ~150 kDa, in which the precise value fluctuates due to post-translational modifications such as glycosylation. Their Y-shaped structure can be classified into the antigen binding fragment (F_{ab}) and the crystallizable fragment (F_c) consisting of two heavy (H) and two light (L) chains held together by inter- and intra-chain disulfide bonds. The F_{ab} and F_c regions consist of multiple domains. These include the variable (V_L and V_H) and constant (C_L , C_{H1}) domains within the F_{ab} and the constant domains (C_{H2} , and C_{H3}) within the F_c . Antibody structures are further defined into different classes (IgA, IgG, IgM, IgE and IgD) and subclasses (IgG1, IgG2, IgG3 and IgG4) based on the composition of the constant regions and the number of disulfide bonds.⁴ Antibodies exhibit an array of intrinsic internal motions⁵ and can exist as a number of conformers with asymmetric structures⁶⁻⁸ that exhibit inter-domain flexibility.⁶⁻⁸ These motions play an important role in their functional activity and biological responses.⁹⁻¹¹ The effect of protein flexibility on overall mAb conformational stability, however, is a more complex relationship and an active area of research.^{12, 13} Examining the inter-relationships between flexibility and stability is especially important not only to help design more stable antibodies, but also to better understand how different excipients and salts predispose, initiate, or delay the cascade of events leading to conformational destabilization and aggregation during manufacturing, long-term storage, and administration.¹⁴

Aggregation of mAbs in solution can occur as a result of covalent or non-covalent protein-protein interactions initiated by changes in pH, temperature, agitation, or interaction with solution impurities.¹⁵⁻¹⁸ These interactions occur due to either conformational changes within individual molecules that lead to exposure of nonpolar residues, colloidal effects in solution that alter charge-charge repulsion between molecules, or a combination of both conformational and colloidal effects.¹⁹ In other words, different salts may affect aggregation behavior of mAbs in solution by decreasing conformational stability and/or charge-charge repulsion between two IgG molecules. Protein aggregation has been shown to occur through the formation of partially unfolded monomeric states whose population is minimal under stable solution conditions.¹⁹ With increasing stress, the partially unfolded population increases, leading to subsequent multi-order aggregation that results in irreversible loss of protein. For a multi-domain protein like an IgG, aggregation-prone segments may also play a key role in the initiation of aggregation^{20, 21} and in overall antibody instability.²² The flexibility of the aggregation-prone motifs may change in response to solution conditions or temperature, which may in turn facilitate conformational instability and/or aggregate formation.

Identification of solution conditions that maintain IgG stability and solubility during long-term storage, especially at high protein concentrations, remains a significant challenge in the development of mAbs as biotherapeutics. Salts are generally included in antibody formulations as buffering agents, tonicity modifiers, or viscosity enhancers.²³ Salts can also affect the solubility and stability of proteins according to their relative position in the Hofmeister series. The Hofmeister series of anions, which have more pronounced effects on protein stability than cations, is: $\text{SCN}^- > \text{ClO}_4^- > \text{I}^- > \text{ClO}_3^- > \text{Br}^- > \text{NO}_3^- > \text{Cl}^- > \text{CH}_3\text{CO}_2^- > \text{HPO}_4^{2-} > \text{SO}_4^{2-}$.²⁴ The members on the left of the series (e.g., thiocyanate, perchlorate, and iodide) are chaotropes that

unfold and solubilize proteins. The members on right (e.g., sulfate and phosphate) are kosmotropes that preserve the native structure and decrease solubility, causing proteins to salt-out of solution.²⁵ Chloride is an intermediate member dividing the two groups. The influences of salts on the physical properties of proteins in solution including melting temperature coefficients,²⁶ salting-out coefficients,²⁷ and B-viscosity coefficients^{28, 29} can be ranked according to the positions of the salts in the Hofmeister series, but other properties such as surface tension²⁹ do not follow the prescribed order. Anions have been found to affect protein conformational stability^{30, 31} and rates of aggregation^{32, 33} in order of their position in the Hofmeister series. Mechanistic explanation of ion effects on protein stability remains an active area of research.^{34, 35} For example, their influence on protein stability can vary by protein and ion type, as well as by ion concentration and solution pH, by affecting factors such as the water affinity of ions, water structure around proteins, and/or by ions interacting directly with protein surfaces.³⁶⁻³⁹

Flexibility is also a crucial consideration for understanding the physicochemical stability of a protein including its aggregation propensity.⁴⁰ Previous work using global measures of dynamics, such as red edge excitation shift fluorescence and high resolution ultrasonic spectroscopy, has shown that there is a complex relationship between mAb dynamics and aggregation.^{14, 41, 42} However, global approaches cannot be used to assign changes in dynamics to specific regions that contribute to aggregation. Hydrogen/deuterium exchange coupled to mass spectrometry (H/D-MS) can measure backbone flexibility at a resolution of 5-20 residues^{43, 44} and has been used with mAbs for biopharmaceutical analysis and comparability studies^{45, 46}. The effects, on monoclonal antibodies, of methionine oxidation, glycan modification or

deglycosylation,⁴⁷⁻⁴⁹ deamidation and other chemical modifications,⁵⁰ and freeze-thaw cycles⁵¹ have all been examined using H/D-MS.

The purpose of this study was to develop a better understanding of the influence of three different anions from the Hofmeister series (sulfate, chloride, and thiocyanate) on the conformational stability, aggregation rate, and polypeptide backbone flexibility of an IgG1 mAb (mAb-B). We have correlated the physical stability changes (measured by DSC and SEC) induced by the anions with changes observed in local backbone flexibility (measured by H/D-MS). In particular, we have identified a potential key role for the local flexibility of two specific segments within the C_{H2} domain in modulating the physical stability of mAb-B.

4.2 Materials and Methods

4.2.1 Materials

Sodium chloride, LC-MS-grade water, acetonitrile, and isopropanol were obtained from Fisher Scientific (Fair Lawn, NJ). LC-grade acetic acid and phosphoric acid were obtained from Fluka (St Louis, MO). Formic acid (99+% LC/MS-grade) was obtained from Thermo Scientific (Rockford, IL). Porcine pepsin, tris(2-carboxyethyl)phosphine hydrochloride (TCEP), deuterium oxide (99+%D), and guanidine hydrochloride were purchased from Sigma Aldrich (St Louis, MO). Citric acid anhydrous (99.5%), sodium phosphate dibasic anhydrous, sodium sulfate anhydrous (99%), and sodium thiocyanate (>98%) were purchased from Acros Organics (Fair Lawn, NJ). The IgG1 monoclonal antibody, referred to here as mAb-B, was formulated at 50 mg mL⁻¹ in 10 mM histidine buffer, pH 6.0 containing 0.005% polysorbate 80.

4.2.2 Differential Scanning Calorimetry (DSC)

Prior to analysis, mAb-B was diluted to 0.5 mg mL^{-1} with 20 mM citrate-phosphate (4 mM citrate and 16 mM dibasic sodium phosphate) buffer at pH 6.0 containing NaCl, Na_2SO_4 , or NaSCN at concentrations ranging from 0.1 to 1.5 M. DSC was performed using a VP-Capillary differential scanning calorimeter (MicroCal, Northampton, MA). mAb-B samples were analyzed in triplicate over a temperature range of 10-100 °C with a scan rate of 60 °C/hr. The data were processed using MicroCal and Origin software (OriginLab Ltd.). The data were fitted using a multi-state model with three transitions. The onset temperature (T_{onset}) of the first transition was taken as the temperature at which the heat capacity exceeded $500 \text{ cal mol}^{-1} \text{ }^\circ\text{C}^{-1}$.

4.2.3 Storage Stability and Analysis by Size Exclusion Chromatography (SEC)

mAb-B was diluted to 0.5 mg mL^{-1} with 20 mM citrate-phosphate (4 mM citrate and 16 mM dibasic sodium phosphate) buffer at pH 6.0 containing either 0.1 M NaCl (control), 0.5 M NaCl, 0.5 M Na_2SO_4 , or 0.5 M NaSCN. Aliquots of 0.5 mL of mAb-B were sterilized by passing through 0.22 μm filters (Millipore, Billerica, MA), dispensed into type I glass vials (West Pharmaceutical Services, Exton, PA) in a pre-sterilized laminar flow hood, stoppered, and stored at four different temperatures (-70 , 4, 25, and 40 °C) for a period of up to twelve months. To remove insoluble aggregates, each sample was centrifuged at $14,000 \times g$ for 5 min prior to analysis. SEC was carried out using a $7.8 \times 30 \text{ cm}$ TSK-Gel BioAssist G3SW_{xL} column (TOSOH Biosciences, King of Prussia, PA) at 0.7 mL/min using a Shimadzu HPLC system equipped with a photodiode array detector. Gel filtration standards (Bio-Rad, Hercules, CA) were used for column calibration. The mobile phase was 200 mM sodium phosphate buffer (pH 6.8). The resulting chromatograms were analyzed by integrating the area of the monomer peak detected at 280 nm. The percentage of monomer was measured relative to the total area of all peaks on day zero.

4.2.4 Deuterated labeling buffer preparation

The deuterated labeling buffers contained 0.5, 1.0, or 1.5 M salt (sodium chloride, sodium sulfate or sodium thiocyanate) and 20 mM citrate-phosphate (4 mM citric acid and 16 mM dibasic sodium phosphate) buffer at pH 6.0 in 90 atom% D₂O. The pH values are reported directly from the pH meter reading without any further correction for the deuterium isotope effect. Based on the total volume of H₂O and D₂O, the salts, citric acid, and dibasic sodium phosphate were added. The final volume was noted after adjusting the pH to 6.0. The final concentrations of the salts were within 3% of their target molarities. The use of 90 atom% D₂O was adopted here to enable direct comparison with H/D exchange work in a companion study (manuscript in preparation) in which some of the buffer components (sucrose and arginine) contributed a non-negligible amount of exchangeable hydrogen to the labeling buffer.

4.2.5 H/D-MS

The antibody was diluted to 10 mg mL⁻¹ in 20 mM citrate-phosphate buffer (4 mM citric acid, 16 mM dibasic sodium phosphate, and 64 mM sodium chloride) at pH 6.0. An H/D-X PAL robot (LEAP Technologies, Carrboro, NC) was used for sample preparation and injection. The protein (2 μL) was mixed with labeling buffer (38 μL) in 1:20 ratio by volume and incubated at 25 °C for four exchange times (120, 10³, 10⁴ and 10⁵ s). Three independent replicates of each labeling condition were prepared. Following deuterium labeling, the exchange reaction solution (40 μL) was quenched at 1 °C with 40 μL of 0.5 M TCEP/ 4 M guanidine hydrochloride / 0.2 M sodium phosphate at pH 2.5. 10 μL of the solution (approximately 16 pmol of mAb-B) was analyzed. Protein stocks and quench buffers were maintained at 1 °C and the labeling buffers were held at 25 °C using the two temperature controlled drawers of the H/D-X PAL. LC-MS analysis of the deuterated samples were conducted as described previously⁵² with the following differences. The

refrigerated compartment of the H/D-X PAL was used to house the columns, traps and valves at 1 °C during the course of the experiments. Secondly, the immobilized pepsin column was back-flushed during the gradient elution step. To minimize carry-over, the pepsin column was also washed first with acetonitrile (5 %)/ isopropanol (5 %)/ acetic acid (20 %) in water and then with 2 M guanidine hydrochloride in 100 mM phosphate buffer pH 2.5 and after each injection.⁵² The typical deuterium recovery achieved with our experimental set-up was 60-90% as determined from the deuterium content of fully-deuterated model peptides. Data are reported as relative deuterium content levels without correction for back-exchange.

4.2.6 MS Data Analysis

A total of 137 peptides covering 85% of the primary sequence of mAb-B were identified using a combination of accurate mass measurement using time-of-flight mass spectrometry and collision-induced dissociation-tandem mass spectrometry on a linear quadrupole ion-trap mass spectrometer (LTQ-XL; Thermo-Scientific) as described previously.⁵² A coverage map and a listing of all mapped peptides can be found in the supporting information (see Fig 4.S1 and Table 4.S1). H/D exchange data were processed using HDExaminer (Sierra Analytics, Modesto, CA). All mass spectra were manually curated after initial processing. To help ensure consistency, the charge state for each peptide was kept constant from run to run. To minimize potential biases in data interpretation, each replicate was curated by a different analyst. Most peptide segments were detected in all three replicates, but a smaller number were found in only one or two of the replicates (see Fig S2). An R script, written in-house, was used to calculate average deuterium uptake and standard deviations and generate deuterium uptake plots from the exported data. All data with standard deviations exceeding the 95th percentile in the dataset were inspected and corrected for data processing errors, if any were found. A statistical analysis of our replicate

data, following Houde et. al⁴⁵ (see Fig S3 and Fig S4) established the 99% confidence limit for a deuterium uptake difference as ± 0.59 Da.

4.2.7 Homology modeling of mAb-B

The primary sequence of the heavy and light chains of mAb-B and human IgG1 b12 (PDB ID: 1HZH)⁵³ were aligned using CLUSTAL W.⁵⁴ The two sequences are approximately 90% homologous with the most sequence differences in the complementarity determining region. The primary sequence of mAb-B was threaded onto the 1HZH structure using Discovery Studio 3.0 (Accelrys, San Diego CA) and re-numbered to correct for gaps. The secondary structure of mAb-B was manually reassigned based on the sequence alignment. Models were displayed using Pymol (Schrödinger, LLC, Portland, OR).

4.3 Results

4.3.1 Effect of salts on the conformational stability of mAb-B

Representative DSC thermograms showing the thermal transitions of mAb-B in presence of each of the three salts, are shown in Figure 4.1. The thermal transitions in the DSC thermograms of mAbs have been shown previously to be independent,^{55, 56} sensitive to changes in pH and ionic strength, and reflect the multistep unfolding of the C_{H2},⁵⁷ F_{ab},⁵⁸ and F_c⁵⁹ domains. For mAb-B formulated in sodium chloride and sodium sulfate, a low temperature shoulder and two distinct peaks can be seen (Fig 1A and 1B). DSC analysis of mAb-B in sodium thiocyanate (see Figure 4.1C) revealed three distinct peaks. The temperatures of the three conformational transitions (T_{m1}, T_{m2}, and T_{m3}) at pH 6.0 are listed in Table 4.1. Thiocyanate (at 0.5 M and 1.0 M) had large destabilizing effects on mAb-B as indicated by decreases in the T_{m1}, T_{m2}, and T_{m3} values compared to control (0.1 M NaCl). In contrast, 0.5 M and 1.0 M sulfate increased the three T_m

values of mAb-B. Increasing concentrations of chloride (0.1 M to 0.5 M, 1.0 M, and 1.5 M) had no notable effect on T_{m1} but a small increase in T_{m2} and T_{m3} .

The onset temperature, T_{onset} , was also measured to determine the temperature at which the first observed structural transition within mAb-B began (see Table 4.1). Chloride, sulfate, and thiocyanate lowered T_{onset} values compared to the control (0.1 M chloride). The effect of 0.5 M and 1.0 M thiocyanate on the T_{onset} ($\Delta T_{onset} = -14.9$ °C and -23.8 °C, respectively) was notably more pronounced than 0.5 M and 1.0 M sulfate ($\Delta T_{onset} = -2.1$ °C and -1.8 °C, respectively) and 0.5 M, 1.0 M and 1.5 M chloride ($\Delta T_{onset} = -3.7$ °C, -5.7 °C, and -7.0 °C, respectively). In summary, at pH 6.0, sulfate and thiocyanate showed opposite effects on the thermal transition temperatures of mAb-B: sulfate stabilized whereas thiocyanate destabilized mAb-B. In addition, all three anions (sulfate, chloride and thiocyanate) showed titratable effects on the conformational stability of mAb-B.

4.3.2 Effect of salts on aggregation during storage of mAb-B

MAb-B samples formulated in a citrate-phosphate buffer containing either 0.1 M sodium chloride, 0.5 M sodium chloride, 0.5 M sodium sulfate, or 0.5 M sodium thiocyanate at pH 6.0 were incubated at various temperatures (-70 , 4 , 25 , and 40 °C) in stoppered glass vials. Individual vials were analyzed by SEC over a period of twelve months. An overlay of representative chromatograms is shown in Figure 4.2A. The SEC peaks were assigned as described previously.⁶⁰ Initially, there were no differences in the composition of mAb-B in the different formulations compared to the control (Figure 4.2A, dotted chromatograms). After incubation at 40 °C for 60 days, the amount of soluble monomer decreased, the amount of dimer remained unchanged, and there was an increase in the abundance of fragments (Figure 4.2A,

solid chromatograms). In addition, multimeric aggregates formed in samples of mAb-B containing thiocyanate. Figure 4.2B shows a plot of the fraction of soluble monomer (relative to the total peak area at time zero) over 12 months storage at different temperatures. It can be seen that mAb-B degraded more rapidly in the presence of thiocyanate, and slightly more slowly in the presence of sulfate (up to 9 months), relative to the control at 40 °C. At 4 °C and 25 °C, the rate of loss of monomer was slower and essentially independent of salt type. Additional time would be required to ascertain if salts cause differences in aggregation rate at lower temperatures. Interestingly, when frozen (−70 °C), mAb-B samples containing thiocyanate precipitated out of solution, while no differences in the rate of loss of monomer were observed in samples formulated with sulfate and chloride, especially during multiple freeze-thaws (data not shown).

4.3.3 Backbone flexibility of mAb-B in 0.1 M NaCl

Figure 4.3 shows representative deuterium uptake curves for six segments from mAb-B, across different IgG1 domains, in 0.1 M sodium chloride (control) and 0.5 M concentration of the three different salts. These six uptake curves are representative of the diverse range of H/D exchange kinetics for mAb-B. (Additional deuterium uptake curves for 137 mAb-B segments covering 85% of the total sequence are provided in Fig S5 of the Supporting Information.). The differences can be used to assess relative local backbone flexibility. For example, in the C_{H2} domain (heavy chain 300-306, peptide 71) deuterium uptake is only apparent after 10³ s of labeling. This high level of protection against deuterium exchange indicates that this part of the C_{H2} is relatively rigid. In contrast, a region between the V_L and V_H domains in the light chain (LC 105-116, peptide 117) was ~75% deuterated within 120 s (relative to the deuterium uptake after 27 hours of incubation), indicating that this is a relatively flexible region of mAb-B.

To better define a relative backbone flexibility scale, we used the extent of deuteration at 120 s relative to the theoretical maximum exchange without correction for back-exchange:

$$\text{flexibility (\%)} = \frac{\Delta m_{120\text{ s}}}{Nf} \times 100\% \quad (1)$$

where $\Delta m_{120\text{ s}}$ denotes the measured mass increase, N is the number of exchangeable amides, and f is mole fraction of deuterium under labeling conditions, here 0.86. The number of exchangeable amides is determined by counting all non-proline residues starting at position three. (After proteolysis, the first amide becomes a rapidly-exchanging amine and the second amide also undergoes rapid back-exchange.⁶¹) Figure 4.4A shows the distribution of local flexibility of segments within mAb-B based on this scale. The segments of mAb-B in the lowest quartile on this scale are classified as rigid, segments in the top quartile as flexible, and segments in the middle 50% as intermediate. Figure 4.4B shows the locations of rigid and flexible segments projected onto a homology model of mAb-B. The H/D exchange measurements show that several loops and β -strands on the surface of the F_{ab} region and C_{H3} domain are relatively flexible (yellow segments). Most regions within the C_{H2} domain as well as some buried β -strands and loops in other domains of mAb-B are relatively rigid (blue segments). Similar to other studies,⁶²⁻⁶⁴ we found no strong correlation between the mAb-B flexibilities, measured in solution, and segment-averaged B-factor values from the crystal structure of 1HZH⁵³ for 22 peptides with identical sequences from the constant domains of the two IgG1s (data not shown).

4.3.4 Identifying the effects of salts on local backbone flexibility of mAb-B

In addition to providing information on relative local flexibility of mAb-B in 0.1 M NaCl, we can identify regions that undergo changes in H/D exchange kinetics in response to changes in salt type or concentration. The representative H/D exchange data in Figure 4.3 show some of the effects of the three different salts, at 0.5 M, on the local flexibility of mAb-B. For each region, there was an increase or decrease in deuterium uptake at one or more of the exchange times, however, not all of these differences exceed the 99% confidence limit of ± 0.59 Da. These individual curves provided a visual representation of salt effects on deuterium uptake for the individual segments. To obtain a more quantitative and global view of salt-induced changes in deuterium uptake, individual differences in deuterium uptake, i.e., $\Delta\Delta m(t) = \Delta m_{\text{salt}}(t) - \Delta m_{\text{control}}(t)$, for every peptide at every labeling time are plotted in Figure 4.5. This figure shows both the magnitudes and signs of the differences and whether the differences exceeded the 99% confidence level for significance. Positive values indicate segments where flexibility increased relative to the 0.1 M NaCl control while negative values indicate a decrease in flexibility. In Figure 4.5, the x-axis arranges the peptides in order from the N-terminal end of the heavy chain to the C-terminal end of the light chain, similar to the plots described by Houde et al.⁴⁷ The domain location for each peptide is denoted by the shading. Mass difference exceeding statistical significance at the 99% confidence level, $|\Delta\Delta m| \geq 0.59$ Da (see Experimental section and Supporting Information Figures 4.S2, 4.S3 and 4.S4), are indicated by the dashed horizontal lines. mAb-B regions that experienced significant changes in deuterium uptake in the presence of 0.5 M chloride, sulfate, and thiocyanate at one or more deuterium exchange times compared to the 0.1 M NaCl control are mapped onto a homology model of mAb-B in Figure 4.6. Regions that showed increases in flexibility (positive values in Fig 5) are colored yellow; decreases in

flexibility (negative values in Fig 5) are blue. Unaffected regions are grey and regions without H/D exchange data are colored white.

4.3.5 The effects of 0.5 M chloride

For the six representative peptide segments shown in Figure 4.3, the only significant effect of chloride at 0.5 M was in the light chain 47-70 segment, located in the V_L domain of mAb-B (peptides 106-108 in Figure 4.5), which experienced an increased protection against H/D exchange. For the other five segments shown in Figure 4.3, chloride had no significant effect on deuterium uptake relative to the control. Figures 4.5 and 4.6 show the effect of 0.5 M chloride across the entire mAb molecule. The addition of 0.5 M chloride caused only a few significant changes in mAb-B local flexibility compared to the 0.1 M chloride control. In addition to the V_L segment (47-70), there were also decreases in flexibility in the HC 124-147 segment (peptide 51) in the C_{H1} domain and HC 424-446 segment (peptide 94) in the C_{H3} domain. Interestingly, there was an overall trend of decreased flexibility across mAb-B (defined by slower deuterium uptake for most segments in Figure 4.5) in the presence of 0.5 M chloride, but most of the individual differences were not significant at the 99% confidence level.

4.3.6 The effects of 0.5 M sulfate

Sulfate caused localized changes in the flexibility of mAb-B as summarized in Figure 4.6. For example, data in Figures 4.3 and 4.5 show that 0.5 M sulfate caused substantial increases in deuterium uptake in the C_{H1} domain (HC 156-174 in Figure 4.3; peptides 51-53 in Figure 4.5) and in the V_L domain (LC 47-70 in Figure 4.3; peptides 106-108 in Figure 4.5). In addition to these increases, several other segments (HC 37-80 corresponding to peptides 11, 22, 23, 30 and

35; HC 380-404 corresponding to peptides 83-85, 87; and LC 136-161 corresponding to peptide 126) exchanged slightly faster than the control.

4.3.7 The effects of 0.5 M thiocyanate

Thiocyanate caused substantial increases in deuterium uptake in two different segments of the C_{H2} domain, as summarized in Figure 4.6. Exchange was faster in the HC 241-252 region (120 s and 10³ s in Figure 4.3; also see peptides 64-68 in Figure 4.5). In addition, the HC 300-306 region also exchanged more quickly, but this increase in deuterium uptake was only evident at the longest exchange time, 10⁵ s, (see Figure 4.3; see also peptides 71-73 in Figure 4.5). Figure 4.5 shows that several additional regions in the heavy chain (peptides HC 37-59, 61-80, 124-147, 198-220, 334-348, 382-398, 429-446) and light chain (peptides LC 47-70, 136-161, 186-212) in mAb-B, corresponding to peptides 11, 29-30, 51, 61, 75, 86, 95, 106-107, 126, 136-137 exchanged faster compared to the control.

4.3.8 Overlapping effects of anions

For a few of the peptide segments of mAb-B, the three anions had more complex effects on the deuterium exchange kinetics. For example, in the C_{H1} domain, HC 124-147 (peptide 51) and in the V_L domain, LC 47-70 (peptide 106), both sulfate and thiocyanate accelerated, while chloride slowed H/D exchange (see Figure 4.5). Similarly, both sulfate and thiocyanate accelerated exchange in HC 37-59 in the V_H domain (peptide 11) and HC 382-398 in the C_{H3} domain (peptide 86). Finally, 0.5 M chloride and thiocyanate caused opposite effects on deuterium uptake in the HC 429-446 segment of the C_{H3} domain corresponding to peptide 95 (see Figure 4.5 and Table 4.S1).

4.3.9 The effects of salt concentration on mAb-B local flexibility

The H/D exchange experiments at 25 °C show that the three salts at 0.5 M concentration have localized effects on the flexibility of mAb-B. To determine if the magnitudes of these local effects were concentration-dependent, we measured H/D exchange at 10^3 s of labeling for mAb-B in 1.0 M and 1.5 M sodium chloride as well as in 1.0 M sodium sulfate and 1.0 M sodium thiocyanate. A minimized set of 43 mAb-B segments was selected for analysis. This set represented all domains of mAb-B and consisted of both regions that were and were not affected by 0.5 M salts. No significant differences in H/D exchange were noted for any of these 43 segments in 1.0 M salts compared to 0.5 M salts (plots of deuterium uptake vs. salt concentration for each segment are in the Supporting Information Figure 4.S6). These results show that changes in local flexibility of mAb-B do not titrate to any appreciable extent beyond 0.5 M salt concentration, at least in the citrate-phosphate, pH 6.0 buffer employed in these experiments. Since increased ionic strength with 1.0 M or 1.5 M chloride did not have any further significant effect on the local flexibility of the mAb, the changes observed with sulfate were not due to changes in ionic strength differences but rather are due to the anion. Moreover, since the majority of mAb-B segments do not show any perturbation of flexibility in the presence of the different salts (see Figure 4.S6 in Supporting Information), intrinsic exchange rates of various mAb-B segments were not substantially altered by changes in salt types or ionic strength conditions.

4.3.10 Reproducibility of H/D-MS data

Figure 4.S3 shows the distribution of standard deviations in measured deuterium uptake for a set of H/D exchange experiments performed on mAb-B. This set includes both results presented in this work and in a companion study using different labeling buffers (manuscript in preparation). With a total of 6473 data points, 74% of the data had a standard deviation less than or equal to

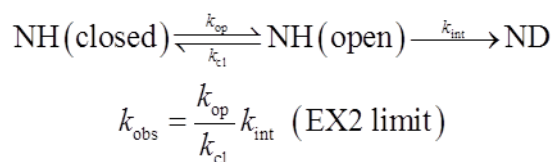
± 0.1 Da and 90% of the data had a standard deviation of less than ± 0.2 Da. 5054 data points were obtained in triplicate, 1120 data points were obtained in duplicate and 299 data points were obtained as single measurements (Figure 4.S2). The 99th percentile for the standard deviations was ± 0.42 Da. Propagation of this confidence interval to deuterium uptake differences sets the 99 percent confidence limit for deuterium uptake differences to ± 0.59 Da. We further observed that there was no specific trend of standard deviation for different peptide sizes (represented as number of exchangeable hydrogens in Figure 4.S4).

4.4 Discussion

The purpose of this work was to probe the effects of anions from the extremes of the Hofmeister series on the local flexibility of various domains of an IgG1 mAb and examine these results in the context of conformational stability and aggregation propensity. Thiocyanate, an extreme chaotrope, decreased mAb-B's thermal stability, as indicated by DSC, and accelerated aggregation, as measured by SEC. Sulfate, an extreme kosmotrope, had the opposite effects. Chloride, positioned in the middle of the Hofmeister series, had minor effects on both thermal and physical stability of mAb-B. In contrast, the effects of the anions on local flexibility, as revealed by H/D exchange, were more complex (see Figures 4.5 and 4.6). Sodium chloride induced a small, but nearly-global decrease in flexibility, although most changes in individual peptide segments were not statistically significant. While thiocyanate and sulfate had opposing effects on physical stability, both anions increased local flexibility in mAb-B. The increases in flexibility were not global; many regions of mAb-B were unaffected by either anion. While thiocyanate and sulfate had similar effects on many regions of mAb-B, notably in the C_{H1} and V_L domains, there were notable differences in C_{H2} domain, where thiocyanate increased flexibility, but sulfate had no effect. We will return to the significance of these findings to the

mechanisms by which anions alter physical stability later in the discussion. First, we address the issue of how these anions might directly alter the kinetics of H/D exchange.

Salts might alter the kinetics of H/D exchange by changing the protein or by changing the chemical exchange process. According to the Linderstrøm-Lang mechanism in the usual EX2 limit, the rate of H/D exchange depends on both flexibility (k_{cl}/k_{op}) and intrinsic chemical exchange (k_{int}).^{65, 66}



Changes in intrinsic exchange would lead to altered H/D exchange kinetics even if the flexibility of mAb-B was not affected. While base-catalyzed exchange in poly-DL-arginine is highly sensitive to changes in ionic strength,⁶⁷ charged side-chains exhibit only moderate ionic strength dependence in more realistic peptide models⁶⁸. Similarly, changes in ionic strength have only very modest effects on intrinsic exchange by amides in alanine model peptides.⁶¹ Increasing the concentration of NaCl from 0.1 M up to 1.5 M and Na₂SO₄ and NaSCN from 0.5 to 1.0 M in our work with mAb-B did not result in any significant changes in H/D exchange kinetics (see Fig S6 in Supporting Information). Although sulfate was shown to slow and thiocyanate to increase intrinsic exchange in N-acetyl-alanine at pH 4,⁶⁹ in our work we found that H/D exchange was not significantly affected by salts in the large majority of peptide segments at pH 6.0. On the whole, we conclude that these anions do not have substantial effects on intrinsic exchange in mAb-B. Thus we attribute the observed effects, instead, to the influence of the anions on the backbone flexibility of mAb-B.

The pattern of backbone flexibility of mAb-B at pH 6.0, as reported by H/D exchange at 120 s (see Figure 4.4), is consistent with several other H/D exchange studies of IgG1 monoclonal antibodies.⁴⁷⁻⁵¹ We note in particular, the HC 241-252 (peptide 65, FLFPPKPKDTL) and HC 300-306 (peptide 71, YRVVSVL) segments, both found in the C_{H2} domain, which we have found to be thiocyanate-sensitive. H/D exchange kinetic data are available for both of these segments in two previous studies^{47, 49} and for HC 241-252 in two others^{50, 70} (the sequence numberings are offset slightly). In all of these other works HC 241-252 exchanges with an approximate mid-point of $\sim 10^3$ sec. All of uptake data, when plotted on a logarithmic scale, have the same sigmoidal profile. In the case of HC 300-306, no deuterium uptake was observed because the maximum labeling in previous work was only 3×10^4 s; in our study, we were able to detect H/D exchange by extending D₂O exposure to 10^5 s. The consistency in these results in the C_{H2} domain is a testament to the intra-laboratory repeatability of H/D exchange measurements on mAbs.

Although direct, quantitative comparisons are impeded by slight differences in peptide coverage and labeling conditions, domain-scale qualitative comparisons can still be drawn. On a domain-by-domain basis, our H/D exchange data for mAb-B, are in good agreement with previous work. What emerges is a general picture of backbone flexibility in the conserved regions of IgG1 mAbs, validated across several different IgG1s examined in different labs. We find that the C_{H1} and C_{H3} domains are relatively more dynamic while the C_{H2} domain is the most rigid domain. (In one of these works,⁴⁷ exchange in the C_{H2} appears to be more protected, but this is probably because maximum exchange was limited to 240 min.)

In comparison to the 0.1 M NaCl control, 0.5 M NaCl caused only small changes in the thermal melting (Figure 4.1). Aggregation kinetics, as measured by loss of monomer, were similar in 0.1

M and 0.5 M NaCl at 4, 25, and 40 °C over 12 months (Figure 4.2). 0.5 M NaCl caused only a few significant decreases in local flexibility in the C_{H1}, V_L and C_{H3} domains of mAb-B, along with an overall trend toward reduced flexibility across the molecule (Figure 4.5). This overall trend is interesting, although it must be noted that most of these effects are not greater than the statistically significant cutoff of 99% confidence (Figure 4.5). Chloride anions decreased the local flexibility of EnvZ, an osmolality-sensing inner membrane histidine kinase, but the effect was attributed to a change in solution osmolality.⁷¹ Chloride-protein interactions can occur via weak binding of chloride to protein surface residues either through electrostatic or non-specific interactions.⁷² For example, the aggregation propensity of three different monoclonal antibodies correlated directly with decreases in their net charge (reduced valence) and the apparent T_{m1} at low salt chloride concentrations (0-160 mM).⁷³

Sulfate anions increased the T_m values of all the three thermal transitions of mAb-B with the largest increase observed for T_{m2}, corresponding to melting of the Fab region⁷⁴ (Figure 4.1). In the accelerated storage stability studies, 0.5 M Na₂SO₄ protected mAb-B against aggregation to a small extent at 40 °C over 12 months of storage (Figure 4.2), with less differences noted at 12 months. Concomitantly, substantial increases in flexibility were observed in two segments of the C_{H1} and V_L domains along with more subtle increases in flexibility in certain regions of the V_H, C_{H1} and C_{H3} domains (Figures 4.5 and 4.6). Stabilizing effects of sulfate on other proteins⁷⁵ have been proposed to occur by stabilization of the native folded state,^{76, 77} by the binding of sulfate to positively charged residues,^{72, 76, 78, 79} or by increased hydration arising from a higher number of dipoles on protein surfaces⁸⁰. Sulfate anions, however, also increase the surface tension of aqueous solutions^{29, 81-83} with increasing concentration leading to higher protein surface energy (salting-out activity) that may accelerate protein aggregation^{37, 84}. Sulfate can also

over-charge proteins leading to the increased local flexibility of the C_{H1} and V_L domains via charge repulsion between bound sulfate anions.³⁸ The interplay of these competing phenomena gives rise to the intriguing effects of sulfate anions on the stability and solubility of different proteins.^{76, 81, 85, 86} The effect of sulfate anions on stabilizing mAb-B in terms of conformational stability, and to a lesser extent against aggregation over time, combined with increases in local flexibility in two segments of the C_{H1} and V_L domains, highlight the complex inter-relationships between protein stability and flexibility⁴⁰.

Thiocyanate anions substantially destabilized mAb-B. The largest effect of thiocyanate was on T_{m1} (Figure 4.1), corresponding to the unfolding of the C_{H2} domain⁷⁴. Thiocyanate also dramatically increased aggregation, as measured by monomer loss, at 40 °C over 12 months of storage (Figure 4.2). In contrast to sulfate or chloride, only thiocyanate caused substantial increases in local flexibility in two separate segments of the C_{H2} domain (Figure 4.3 and 4.6). The mechanism of thiocyanate-induced protein destabilization is thought to involve its interaction with both positively charged residues and apolar hydrophobic regions on the surface of either native proteins or partially unfolded intermediates,⁸⁷⁻⁹⁰ thereby decreasing the overall charge on the protein and weakening the electrostatic repulsion^{91, 92} leading to enhanced protein-protein interactions⁹³⁻⁹⁵ resulting in aggregation. The destabilizing effects of thiocyanate on protein flexibility are not necessarily observed with all proteins. In the case of recombinant γ -interferon, no notable differences in H/D exchange kinetics were observed in 0.3 M KSCN vs. KCl, although the two salts had different effects on this protein's solubility and aggregation.⁹⁶ In addition to effects on the C_{H2} domain of mAb-B, additional subtle increases in local flexibility were observed across mAb-B (Figure 4.5), indicating thiocyanate may have specific weaker interactions with several other segments throughout the mAb. These results also correlate with

the decrease in conformational stability of mAb-B as observed for T_{m2} (F_{ab} region) and T_{m3} (C_{H3} domain) caused by thiocyanate.

The increase in local flexibility (HC 241-252 and 300-306) of the C_{H2} domain of mAb-B in presence of thiocyanate correlates with conformational destabilization of the C_{H2} domain (T_{m1}) and accelerated aggregation during storage. Similar effects were observed in a separate study in our laboratories where arginine hydrochloride also destabilized mAb-B and increased the flexibility of the HC 241-252 segment in the C_{H2} domain.⁹⁷ At the same time, stabilizing additives had no effect on these two regions within the C_{H2} domain (NaCl and Na_2SO_4 in the present work and sucrose in our companion study). These observations lead to the conclusion that the flexibility of HC 241-252 and 300-306 regions in the C_{H2} domain is an important factor in maintaining the overall physical stability of mAb-B. We also observed increases in flexibility in the N-terminal region of the C_{H3} domain (HC 379-398, peptide 83). All of these observations are consistent with increases in the flexibility in the C_{H2} and C_{H3} domains of other IgG1 mAbs caused by glycan modifications,^{47, 48} and methionine oxidation^{48, 49}. Whether these changes merely correlate with loss of stability or actually cause the destabilization cannot be determined simply on the basis of the H/D exchange measurements. However, several additional pieces of evidence suggest that the C_{H2} domain plays a causal role in aggregation. Agitation-induced aggregation of an F_c was inhibited by the binding of protein A and protein A-derived peptides.⁹⁸ Since Protein A binds to several residues from the C_{H2} and C_{H3} domains of an IgG protein, these results further support the idea that the C_{H2} region is important in mediating IgG aggregation. In a separate study, an isolated C_{H2} domain was stabilized by engineering a L242C and K334C double mutant that introduced a stabilizing disulfide bond.⁹⁹ This disulfide bond presumably decreased the flexibility of the HC 241-251 region. Hence our results, with an intact IgG1 mAb,

further highlights the importance of HC 241-251 segment of the C_H2 domain in the physical stability of IgG1 mAbs.

On the other hand, both sulfate and thiocyanate increased the local flexibility in small regions of both the F_{ab} and C_H3 domains while chloride decreased flexibility in these same regions (see Figure 4.6). These changes in local flexibility in mAb-B do not correlate with conformational stability or the aggregation propensity of mAb-B. These results highlight once again the complex interrelationships between protein flexibility and stability⁴⁰ as well as the need for local measurements of dynamics. Global measurements of dynamics of a mAb may be less informative than local measurements because not all increases in flexibility result in decreases in stability. Here, the overall change in dynamics would depend on the balance of effects between the relatively flexible F_{ab} and C_H3 domains and the comparatively rigid C_H2 domain (Figure 4.4).

Identification of backbone flexibility changes in specific regions within an IgG1 mAb that respond to changes in solution conditions (e.g., the presence of various additives) and correlation of these changes with conformational stability and physical stability during long term storage should provide better mechanistic insight into stabilization and formulation development of antibody-based drugs. H/D-MS measurements could complement high-resolution theoretical approaches for predicting stability of proteins based on salt-protein interactions.^{31, 100} For example, the salt induced effects observed in this work were localized to short segments of the mAb-B backbone. Hence H/D-MS experiments could be designed to screen specific regions of a mAb for the effects of different additives to better predict their effects on physical stability. It remains to be seen whether the correlations between flexibility and stability persist across different subclasses (e.g., IgG1, IgG2, IgG4) or different classes of mAbs (IgG, IgM, IgA). Finally, computational studies mapping electrostatic potentials on the surface of the antibody at a

specific pH and in presence of various salts may help to further explain the molecular mechanism of anion induced changes in local flexibility observed in this study.¹⁰¹⁻¹⁰³

4.5 References

1. Rosenberg, A. S. (2006) Effects of protein aggregates: an immunologic perspective, *AAPS J* 8, E501-507.
2. Wang, W., Singh, S. K., Li, N., Toler, M. R., King, K. R., and Nema, S. (2012) Immunogenicity of protein aggregates—Concerns and realities, *Int. J. Pharm.* 431, 1-11.
3. Filipe, V., Jiskoot, W., Basmeh, A. H., Halim, A., and Schellekens, H. (2012) Immunogenicity of different stressed IgG monoclonal antibody formulations in immune tolerant transgenic mice, *mAbs* 4, 740-752.
4. Janeway CA, T. P., Walport M, Shlomchik MJ. (2001) *Immunobiology*, 5th ed., Garland Publishing, New York.
5. Roux, K. H., Strelets, L., and Michaelsen, T. E. (1997) Flexibility of human IgG subclasses, *J. Immunol.* 159, 3372-3382.
6. Saphire, E. O., Stanfield, R. L., Max Crispin, M. D., Parren, P. W. H. I., Rudd, P. M., Dwek, R. A., Burton, D. R., and Wilson, I. A. (2002) Contrasting IgG Structures Reveal Extreme Asymmetry and Flexibility, *J. Mol. Biol.* 319, 9-18.
7. Marquart, M., Deisenhofer, J., Huber, R., and Palm, W. (1980) Crystallographic refinement and atomic models of the intact immunoglobulin molecule Kol and its antigen-binding fragment at 3.0 Å and 1.9 Å resolution, *J. Mol. Biol.* 141, 369-391.
8. Sandin, S., Öfverstedt, L.-G., Wikström, A.-C., Wrangé, Ö., and Skoglund, U. (2004) Structure and Flexibility of Individual Immunoglobulin G Molecules in Solution, *Structure* 12, 409-415.

9. Teilum, K., Olsen, J. G., and Kragelund, B. B. (2009) Functional aspects of protein flexibility, *Cell. Mol. Life Sci.* 66, 2231-2247.
10. Závodszky, P., Kardos, J., Svingor, Á., and Petsko, G. A. (1998) Adjustment of conformational flexibility is a key event in the thermal adaptation of proteins, *Proc. Natl. Acad. Sci. USA* 95, 7406-7411.
11. Eisenmesser, E. Z., Millet, O., Labeikovsky, W., Korzhnev, D. M., Wolf-Watz, M., Bosco, D. A., Skalicky, J. J., Kay, L. E., and Kern, D. (2005) Intrinsic dynamics of an enzyme underlies catalysis, *Nature* 438, 117-121.
12. Tang, K. E., and Dill, K. A. (1998) Native protein fluctuations: the conformational-motion temperature and the inverse correlation of protein flexibility with protein stability, *J. Biomol. Struct. Dyn.* 16, 397-411.
13. Vihinen, M. (1987) Relationship of protein flexibility to thermostability, *Protein Eng.* 1, 477-480.
14. Thakkar, S. V., Kim, J. H., Samra, H. S., Sathish, H. A., Bishop, S. M., Joshi, S. B., Volkin, D. B., and Middaugh, C. R. (2012) Local dynamics and their alteration by excipients modulate the global conformational stability of an IgG1 monoclonal antibody, *J. Pharm. Sci.* 101, 4444-4457.
15. Mahler, H.-C., Friess, W., Grauschopf, U., and Kiese, S. (2009) Protein aggregation: Pathways, induction factors and analysis, *J. Pharm. Sci.* 98, 2909-2934.
16. Tyagi, A. K., Randolph, T. W., Dong, A., Maloney, K. M., Hitscherich, C., and Carpenter, J. F. (2009) IgG particle formation during filling pump operation: A case

- study of heterogeneous nucleation on stainless steel nanoparticles, *J. Pharm. Sci.* 98, 94-104.
17. Harris, R. J., Shire, S. J., and Winter, C. (2004) Commercial manufacturing scale formulation and analytical characterization of therapeutic recombinant antibodies, *Drug Dev. Res.* 61, 137-154.
 18. Mahler, H. C., Muller, R., Friess, W., Delille, A., and Matheus, S. (2005) Induction and analysis of aggregates in a liquid IgG1-antibody formulation, *Eur. J. Pharm. Biopharm.* 59, 407-417.
 19. Roberts, C. J., Das, T. K., and Sahin, E. (2011) Predicting solution aggregation rates for therapeutic proteins: Approaches and challenges, *Int. J. Pharm.* 418, 318-333.
 20. Wang, X., Das, T. K., Singh, S. K., and Kumar, S. (2009) Potential aggregation prone regions in biotherapeutics: A survey of commercial monoclonal antibodies, *mAbs* 1, 254-267.
 21. Chennamsetty, N., Helk, B., Voynov, V., Kayser, V., and Trout, B. L. (2009) Aggregation-Prone Motifs in Human Immunoglobulin G, *J. Mol. Biol.* 391, 404-413.
 22. Wang, W., Singh, S., Zeng, D. L., King, K., and Nema, S. (2007) Antibody structure, instability, and formulation, *J. Pharm. Sci.* 96, 1-26.
 23. Kamerzell, T. J., Esfandiary, R., Joshi, S. B., Middaugh, C. R., and Volkin, D. B. (2011) Protein-excipient interactions: mechanisms and biophysical characterization applied to protein formulation development, *Adv Drug Deliv Rev* 63, 1118-1159.

24. Hofmeister, F. (1888) Zur Lehre von der Wirkung der Salze, Naunyn-Schmiedeberg's Arch. Pharmacol. 24, 247-260.
25. Baldwin, R. L. (1996) How Hofmeister ion interactions affect protein stability, Biophys. J. 71, 2056-2063.
26. Vonhippel, P. H., and Wong, K. Y. (1964) Neutral salts: the generality of their effects on the stability of macromolecular conformations, Science 145, 577-580.
27. Cohn, E. J. E., J.T. (1943) Proteins, amino acids, and peptides as ions and dipolar ions, Reinhold Publishing Corporation, New York.
28. Nakagawa, T. (1995) Is viscosity B coefficient characteristic for solute-solvent interaction?, J. Mol. Liq. 63, 303-316.
29. Broering, J. M., and Bommarius, A. S. (2005) Evaluation of Hofmeister Effects on the Kinetic Stability of Proteins, J. Phys. Chem. B 109, 20612-20619.
30. Von Hippel, P. H., and Schleich, T. (1969) Ion effects on the solution structure of biological macromolecules, Acc. Chem. Res. 2, 257-265.
31. Shukla, D., Schneider, C. P., and Trout, B. L. (2011) Complex Interactions between Molecular Ions in Solution and Their Effect on Protein Stability, J. Am. Chem. Soc. 133, 18713-18718.
32. Rubin, J., San Miguel, A., Bommarius, A. S., and Behrens, S. H. (2010) Correlating Aggregation Kinetics and Stationary Diffusion in Protein–Sodium Salt Systems Observed with Dynamic Light Scattering, J. Phys. Chem. B 114, 4383-4387.

33. Zhang-van Enk, J., Mason, B. D., Yu, L., Zhang, L., Hamouda, W., Huang, G., Liu, D., Remmele, R. L., and Zhang, J. (2012) Perturbation of Thermal Unfolding and Aggregation of Human IgG1 Fc Fragment by Hofmeister Anions, *Mol. Pharm.* 10, 619-630.
34. Zhang, Y., and Cremer, P. S. (2006) Interactions between macromolecules and ions: the Hofmeister series, *Curr. Opin. Chem. Biol.* 10, 658-663.
35. Parsons, D. F., Bostrom, M., Nostro, P. L., and Ninham, B. W. (2011) Hofmeister effects: interplay of hydration, nonelectrostatic potentials, and ion size, *Phys. Chem. Chem. Phys.* 13, 12352-12367.
36. Gokarn, Y. R., Fesinmeyer, R. M., Saluja, A., Razinkov, V., Chase, S. F., Laue, T. M., and Brems, D. N. (2011) Effective charge measurements reveal selective and preferential accumulation of anions, but not cations, at the protein surface in dilute salt solutions, *Protein Sci.* 20, 580-587.
37. Arakawa, T., and Timasheff, S. N. (1982) Preferential interactions of proteins with salts in concentrated solutions, *Biochemistry* 21, 6545-6552.
38. Collins, K. D. (2012) Why continuum electrostatics theories cannot explain biological structure, polyelectrolytes or ionic strength effects in ion-protein interactions, *Biophys. Chem.* 167, 43-59.
39. Collins, K. D., and Washabaugh, M. W. (1985) The Hofmeister effect and the behaviour of water at interfaces, *Q. Rev. Biophys.* 18, 323-422.

40. Kamerzell, T. J., and Middaugh, C. R. (2008) The complex inter-relationships between protein flexibility and stability, *J. Pharm. Sci.* 97, 3494-3517.
41. Thakkar, S. V., Joshi, S. B., Jones, M. E., Sathish, H. A., Bishop, S. M., Volkin, D. B., and Middaugh, C. R. (2012) Excipients differentially influence the conformational stability and pretransition dynamics of two IgG1 monoclonal antibodies, *J. Pharm. Sci.* 101, 3062-3077.
42. Lilyestrom, W. G., Shire, S. J., and Scherer, T. M. (2012) Influence of the Cosolute Environment on IgG Solution Structure Analyzed by Small-Angle X-ray Scattering, *J. Phys. Chem. B* 116, 9611-9618.
43. Zhang, Z., and Smith, D. L. (1993) Determination of amide hydrogen exchange by mass spectrometry: A new tool for protein structure elucidation, *Protein Sci.* 2, 522-531.
44. Englander, S. W. (2006) Hydrogen Exchange and Mass Spectrometry: A Historical Perspective, *J. Amer. Soc. Mass Spectrom.* 17, 1481-1489.
45. Houde, D., Berkowitz, S. A., and Engen, J. R. (2011) The utility of hydrogen/deuterium exchange mass spectrometry in biopharmaceutical comparability studies, *J. Pharm. Sci.* 100, 2071-2086.
46. Federici, M., Lubiniecki, A., Manikwar, P., and Volkin, D. B. (2012) Analytical lessons learned from selected therapeutic protein drug comparability studies, *Biologicals*.
47. Houde, D., Arndt, J., Domeier, W., Berkowitz, S., and Engen, J. R. (2009) Characterization of IgG1 Conformation and Conformational Dynamics by Hydrogen/Deuterium Exchange Mass Spectrometry, *Anal. Chem.* 81, 2644-2651.

48. Houde, D., Peng, Y., Berkowitz, S. A., and Engen, J. R. (2010) Post-translational Modifications Differentially Affect IgG1 Conformation and Receptor Binding, *Mol. Cell. Proteomics* 9, 1716-1728.
49. Burkitt, W., Domann, P., and O'Connor, G. (2010) Conformational changes in oxidatively stressed monoclonal antibodies studied by hydrogen exchange mass spectrometry, *Protein Sci.* 19, 826-835.
50. Tang, L., Sundaram, S., Zhang, J., Carlson, P., Matathia, A., Parekh, B., Zhou, Q., and Hsieh, M. C. (2013) Conformational characterization of the charge variants of a human IgG1 monoclonal antibody using H/D exchange mass spectrometry, *mAbs* 5, 114-125.
51. Zhang, A., Singh, S., Shirts, M., Kumar, S., and Fernandez, E. (2012) Distinct Aggregation Mechanisms of Monoclonal Antibody Under Thermal and Freeze-Thaw Stresses Revealed by Hydrogen Exchange, *Pharm. Res.* 29, 236-250.
52. Majumdar, R., Manikwar, P., Hickey, J. M., Arora, J., Middaugh, C. R., Volkin, D. B., and Weis, D. D. (2012) Minimizing Carry-Over in an Online Pepsin Digestion System used for the H/D Exchange Mass Spectrometric Analysis of an IgG1 Monoclonal Antibody, *J. Am. Soc. Mass Spectrom.* 23, 2140-2148.
53. Saphire, E. O., Parren, P. W. H. I., Pantophlet, R., Zwick, M. B., Morris, G. M., Rudd, P. M., Dwek, R. A., Stanfield, R. L., Burton, D. R., and Wilson, I. A. (2001) Crystal Structure of a Neutralizing Human IgG Against HIV-1: A Template for Vaccine Design, *Science* 293, 1155-1159.
54. Larkin, M. A., Blackshields, G., Brown, N. P., Chenna, R., McGettigan, P. A., McWilliam, H., Valentin, F., Wallace, I. M., Wilm, A., Lopez, R., Thompson, J. D.,

- Gibson, T. J., and Higgins, D. G. (2007) Clustal W and Clustal X version 2.0, *Bioinformatics* 23, 2947-2948.
55. Vermeer, A. W., and Norde, W. (2000) The thermal stability of immunoglobulin: unfolding and aggregation of a multi-domain protein, *Biophys. J.* 78, 394-404.
56. Vermeer, A. W., Norde, W., and van Amerongen, A. (2000) The unfolding/denaturation of immunoglobulin of isotype 2b and its F(ab) and F(c) fragments, *Biophys. J.* 79, 2150-2154.
57. Feige, M. J., Walter, S., and Buchner, J. (2004) Folding mechanism of the CH2 antibody domain, *J. Mol. Biol.* 344, 107-118.
58. Lilie, H., Jaenicke, R., and Buchner, J. (1995) Characterization of a quaternary-structured folding intermediate of an antibody Fab-fragment, *Protein Sci.* 4, 917-924.
59. Li, C. H., Narhi, L. O., Wen, J., Dimitrova, M., Wen, Z. Q., Li, J., Pollastrini, J., Nguyen, X., Tsuruda, T., and Jiang, Y. (2012) Effect of pH, Temperature, and Salt on the Stability of Escherichia coli- and Chinese Hamster Ovary Cell-Derived IgG1 Fc, *Biochemistry* 51, 10056-10065.
60. Bond, M. D., Panek, M. E., Zhang, Z., Wang, D., Mehndiratta, P., Zhao, H., Gunton, K., Ni, A., Nedved, M. L., Burman, S., and Volkin, D. B. (2010) Evaluation of a dual-wavelength size exclusion HPLC method with improved sensitivity to detect protein aggregates and its use to better characterize degradation pathways of an IgG1 monoclonal antibody, *J. Pharm. Sci.* 99, 2582-2597.

61. Bai, Y., Milne, J. S., Mayne, L., and Englander, S. W. (1993) Primary structure effects on peptide group hydrogen exchange, *Proteins: Struct. Funct. Bioinform.* 17, 75-86.
62. Milne, J. S., Mayne, L., Roder, H., Wand, A. J., and Englander, S. W. (1998) Determinants of protein hydrogen exchange studied in equine cytochrome c, *Protein Sci.* 7, 739-745.
63. Wang, F., Shi, W., Nieves, E., Angeletti, R. H., Schramm, V. L., and Grubmeyer, C. (2001) A transition-state analogue reduces protein dynamics in hypoxanthine-guanine phosphoribosyltransferase, *Biochemistry* 40, 8043-8054.
64. Bennett, B. C., Gardberg, A. S., Blair, M. D., and Dealwis, C. G. (2008) On the determinants of amide backbone exchange in proteins: a neutron crystallographic comparative study, *Acta crystallographica. Section D, Biological crystallography* D64, 764-783.
65. Hvidt, A., and Linderstrom-Lang, K. (1954) Exchange of hydrogen atoms in insulin with deuterium atoms in aqueous solutions, *Biochim. Biophys. Acta* 14, 574-575.
66. Hvidt, A., and Nielsen, S. O. (1966) Hydrogen exchange in proteins, *Adv. Protein Chem* 21, 287-386.
67. Kim, P. S., and Baldwin, R. L. (1982) Influence of charge on the rate of amide proton exchange, *Biochemistry* 21, 1-5.
68. Rohl, C. A., and Baldwin, R. L. (1997) Comparison of NH exchange and circular dichroism as techniques for measuring the parameters of the helix-coil transition in peptides, *Biochemistry* 36, 8435-8442.

69. Tadeo, X., Castano, D., and Millet, O. (2007) Anion modulation of the 1H/2H exchange rates in backbone amide protons monitored by NMR spectroscopy, *Protein Sci.* 16, 2733-2740.
70. Zhang, A., Qi, W., Singh, S., and Fernandez, E. (2011) A New Approach to Explore the Impact of Freeze-Thaw Cycling on Protein Structure: Hydrogen/Deuterium Exchange Mass Spectrometry (HX-MS), *Pharm. Res.*, 1-15.
71. Wang, L. C., Morgan, L. K., Godakumbura, P., Kenney, L. J., and Anand, G. S. (2012) The inner membrane histidine kinase EnvZ senses osmolality via helix-coil transitions in the cytoplasm, *EMBO J.* 31, 2648-2659.
72. Vrbka, L., Jungwirth, P., Bauduin, P., Touraud, D., and Kunz, W. (2006) Specific ion effects at protein surfaces: a molecular dynamics study of bovine pancreatic trypsin inhibitor and horseradish peroxidase in selected salt solutions, *J. Phys. Chem. B* 110, 7036-7043.
73. Fesinmeyer, R. M., Hogan, S., Saluja, A., Brych, S. R., Kras, E., Narhi, L. O., Brems, D. N., and Gokarn, Y. R. (2009) Effect of ions on agitation- and temperature-induced aggregation reactions of antibodies, *Pharm. Res.* 26, 903-913.
74. Ionescu, R. M., Vlasak, J., Price, C., and Kirchmeier, M. (2008) Contribution of variable domains to the stability of humanized IgG1 monoclonal antibodies, *J. Pharm. Sci.* 97, 1414-1426.
75. Faria, T. Q., Mingote, A., Siopa, F., Ventura, R., Maycock, C., and Santos, H. (2008) Design of new enzyme stabilizers inspired by glycosides of hyperthermophilic microorganisms, *Carbohydr. Res.* 343, 3025-3033.

76. Ramos, C. H. I., and Baldwin, R. L. (2002) Sulfate anion stabilization of native ribonuclease A both by anion binding and by the Hofmeister effect, *Protein Sci.* 11, 1771-1778.
77. Nishimura, C., Uversky, V. N., and Fink, A. L. (2001) Effect of salts on the stability and folding of staphylococcal nuclease, *Biochemistry* 40, 2113-2128.
78. Mason, P. E., Dempsey, C. E., Vrbka, L., Heyda, J., Brady, J. W., and Jungwirth, P. (2009) Specificity of Ion-Protein Interactions: Complementary and Competitive Effects of Tetrapropylammonium, Guanidinium, Sulfate, and Chloride Ions, *J. Phys. Chem. B* 113, 3227-3234.
79. Wernersson, E., Heyda, J., Kubickova, A., Krizek, T., Coufal, P., and Jungwirth, P. (2010) Effect of association with sulfate on the electrophoretic mobility of polyarginine and polylysine, *J. Phys. Chem. B* 114, 11934-11941.
80. Broide, M. L., Tominc, T. M., and Saxowsky, M. D. (1996) Using phase transitions to investigate the effect of salts on protein interactions, *Phys. Rev. E* 53, 6325-6335.
81. Arosio, P., Jaquet, B., Wu, H., and Morbidelli, M. (2012) On the role of salt type and concentration on the stability behavior of a monoclonal antibody solution, *Biophys. Chem.* 168-169, 19-27.
82. Weissenborn, P. K., and Pugh, R. J. (1996) Surface Tension of Aqueous Solutions of Electrolytes: Relationship with Ion Hydration, Oxygen Solubility, and Bubble Coalescence, *J. Colloid Interface Sci.* 184, 550-563.

83. Melander, W., and Horváth, C. (1977) Salt effects on hydrophobic interactions in precipitation and chromatography of proteins: An interpretation of the lyotropic series, *Arch. Biochem. Biophys.* 183, 200-215.
84. Foster, P. R., Dunnill, P., and Lilly, M. D. (1976) The kinetics of protein salting-out: precipitation of yeast enzymes by ammonium sulfate, *Biotechnol. Bioeng.* 18, 545-580.
85. Pedersen, J. S., Flink, J. M., Dikov, D., and Otzen, D. E. (2006) Sulfates Dramatically Stabilize a Salt-Dependent Type of Glucagon Fibrils, *Biophys. J.* 90, 4181-4194.
86. Arakawa, T., and Timasheff, S. N. (1984) Mechanism of protein salting in and salting out by divalent cation salts: balance between hydration and salt binding, *Biochemistry* 23, 5912-5923.
87. Washabaugh, M. W., and Collins, K. D. (1986) The systematic characterization by aqueous column chromatography of solutes which affect protein stability, *J. Biol. Chem.* 261, 12477-12485.
88. Ries-Kautt, M. M., and Ducruix, A. F. (1989) Relative effectiveness of various ions on the solubility and crystal growth of lysozyme, *J. Biol. Chem.* 264, 745-748.
89. Huang, H., Manciu, M., and Ruckenstein, E. (2004) On the Restabilization of Protein-Covered Latex Colloids at High Ionic Strengths, *Langmuir* 21, 94-99.
90. Gibb, C. L. D., and Gibb, B. C. (2011) Anion Binding to Hydrophobic Concavity Is Central to the Salting-in Effects of Hofmeister Chaotropes, *J. Am. Chem. Soc.* 133, 7344-7347.

91. Collins, K. D. (2004) Ions from the Hofmeister series and osmolytes: effects on proteins in solution and in the crystallization process, *Methods* 34, 300-311.
92. Collins, K. D., Neilson, G. W., and Enderby, J. E. (2007) Ions in water: Characterizing the forces that control chemical processes and biological structure, *Biophys. Chem.* 128, 95-104.
93. Mason, B. D., Zhang-van Enk, J., Zhang, L., Remmele, R. L., and Zhang, J. (2010) Liquid-Liquid Phase Separation of a Monoclonal Antibody and Nonmonotonic Influence of Hofmeister Anions, *Biophys. J.* 99, 3792-3800.
94. Zhang, L., and Zhang, J. (2012) Specific ion-protein interactions dictate solubility behavior of a monoclonal antibody at low salt concentrations, *Mol. Pharm.* 9, 2582-2590.
95. Zhang, L., Tan, H., Fesinmeyer, R. M., Li, C., Catrone, D., Le, D., Remmele, R. L., and Zhang, J. (2012) Antibody solubility behavior in monovalent salt solutions reveals specific anion effects at low ionic strength, *J. Pharm. Sci.* 101, 965-977.
96. Tobler, S. A., and Fernandez, E. J. (2002) Structural features of interferon- γ aggregation revealed by hydrogen exchange, *Protein Sci.* 11, 1340-1352.
97. Manikwar P, M. R., Hickey J.M., Santosh V.T., Samra H.S., Sathish H.A., Bishop S.M., Middaugh C.R., Volkin D.B., Weis D.D. (2013) Pharmaceutical Excipient Effects on IgG1 Local Dynamics as Measured by Hydrogen-Deuterium Exchange Mass Spectrometry and Correlations with Physical and Storage Stability, *J. Pharm. Sci.* In Press.

98. Zhang, J., and Topp, E. M. (2012) Protein G, Protein A and Protein A-Derived Peptides Inhibit the Agitation Induced Aggregation of IgG, *Mol. Pharm.* 9, 622-628.
99. Gong, R., Vu, B. K., Feng, Y., Prieto, D. A., Dyba, M. A., Walsh, J. D., Prabakaran, P., Veenstra, T. D., Tarasov, S. G., Ishima, R., and Dimitrov, D. S. (2009) Engineered Human Antibody Constant Domains with Increased Stability, *J. Biol. Chem.* 284, 14203-14210.
100. Tomé, L. I. N., Jorge, M., Gomes, J. R. B., and Coutinho, J. o. A. P. (2010) Toward an Understanding of the Aqueous Solubility of Amino Acids in the Presence of Salts: A Molecular Dynamics Simulation Study, *J. Phys. Chem. B* 114, 16450-16459.
101. Shukla, D., and Trout, B. L. (2011) Preferential interaction coefficients of proteins in aqueous arginine solutions and their molecular origins, *J. Phys. Chem. B* 115, 1243-1253.
102. Shukla, D., Shinde, C., and Trout, B. L. (2009) Molecular computations of preferential interaction coefficients of proteins, *J. Phys. Chem. B* 113, 12546-12554.
103. Shukla, D., Schneider, C. P., and Trout, B. L. (2011) Molecular level insight into intra-solvent interaction effects on protein stability and aggregation, *Adv. Drug Del. Rev.* 63, 1074-1085.

Table 4.1

Salt Concentration*	T _{onset} (°C)			T _m 1 (°C)			T _m 2 (°C)			T _m 3 (°C)		
	Mean	SD	ΔT _{onset}	Mean	SD	ΔT _m 1	Mean	SD	ΔT _m 2	Mean	SD	ΔT _m 3
0.1 M NaCl (control)	57.7	0.2	-	69.3	0.1	-	73.6	<0.1	-	82.4	<0.1	-
0.5 M NaCl	54.0	0.2	-3.7	69.5	<0.1	0.3	73.8	<0.1	0.2	82.7	<0.1	0.3
1.0 M NaCl	52.1	0.2	-5.7	69.1	0.2	-0.1	74.7	<0.1	1.1	83.6	<0.1	1.2
1.5 M NaCl	50.7	0.1	-7.0	68.7	0.1	-0.5	75.8	<0.1	2.2	84.7	<0.1	2.3
0.5 M Na ₂ SO ₄	55.6	0.7	-2.1	71.1	0.2	1.8	77.7	<0.1	4.1	84.7	<0.1	2.3
1.0 M Na ₂ SO ₄	55.9	0.8	-1.8	70.8	0.4	1.5	80.7	<0.1	7.1	87.8	<0.1	5.4
0.5 M NaSCN	42.8	0.5	-14.9	60.3	0.2	-9.0	67.0	<0.1	-6.6	75.8	<0.1	-6.6
1.0 M NaSCN	33.9	0.6	-23.8	51.6	0.5	-17.7	62.2	<0.1	-11.4	70.7	<0.1	-11.7

Effect of salt type and concentration on thermal unfolding transitions (T_m) and onset of thermal unfolding (T_{onset}) for mAb-B as measured by DSC.

*Samples contained 0.5 mg/ml protein in 20 mM citrate-phosphate buffer at pH 6 with salt as indicated. The mean and SD are from three separate measurements.

Table 4.S1

Peptide Number	Location
1	mAbB Heavy 4-17 (VH)
2	mAbB Heavy 5-22 (VH)
3	mAbB Heavy 30-35 (VH)
4	mAbB Heavy 33-36 (VH)
5	mAbB Heavy 36-47 (VH)
6	mAbB Heavy 37-46 (VH)
7	mAbB Heavy 36-49 (VH)
8	mAbB Heavy 36-58 (VH)
9	mAbB Heavy 36-59 (VH)
10	mAbB Heavy 37-58 (VH)
11	mAbB Heavy 37-59 (VH)
12	mAbB Heavy 36-65 (VH)
13	mAbB Heavy 47-58 (VH)
14	mAbB Heavy 47-59 (VH)
15	mAbB Heavy 47-60 (VH)
16	mAbB Heavy 47-61 (VH)
17	mAbB Heavy 47-62 (VH)
18	mAbB Heavy 48-61 (VH)
19	mAbB Heavy 47-63 (VH)
20	mAbB Heavy 47-65 (VH)
21	mAbB Heavy 47-68 (VH)
22	mAbB Heavy 48-68 (VH)
23	mAbB Heavy 50-68 (VH)
24	mAbB Heavy 59-68 (VH)
25	mAbB Heavy 60-68 (VH)
26	mAbB Heavy 61-68 (VH)
27	mAbB Heavy 62-68 (VH)
28	mAbB Heavy 64-68 (VH)
29	mAbB Heavy 61-79 (VH)
30	mAbB Heavy 61-80 (VH)
31	mAbB Heavy 62-79 (VH)
32	mAbB Heavy 63-79 (VH)
33	mAbB Heavy 63-80 (VH)
34	mAbB Heavy 64-79 (VH)
35	mAbB Heavy 64-80 (VH)
36	mAbB Heavy 66-79 (VH)
37	mAbB Heavy 66-80 (VH)
38	mAbB Heavy 69-79 (VH)

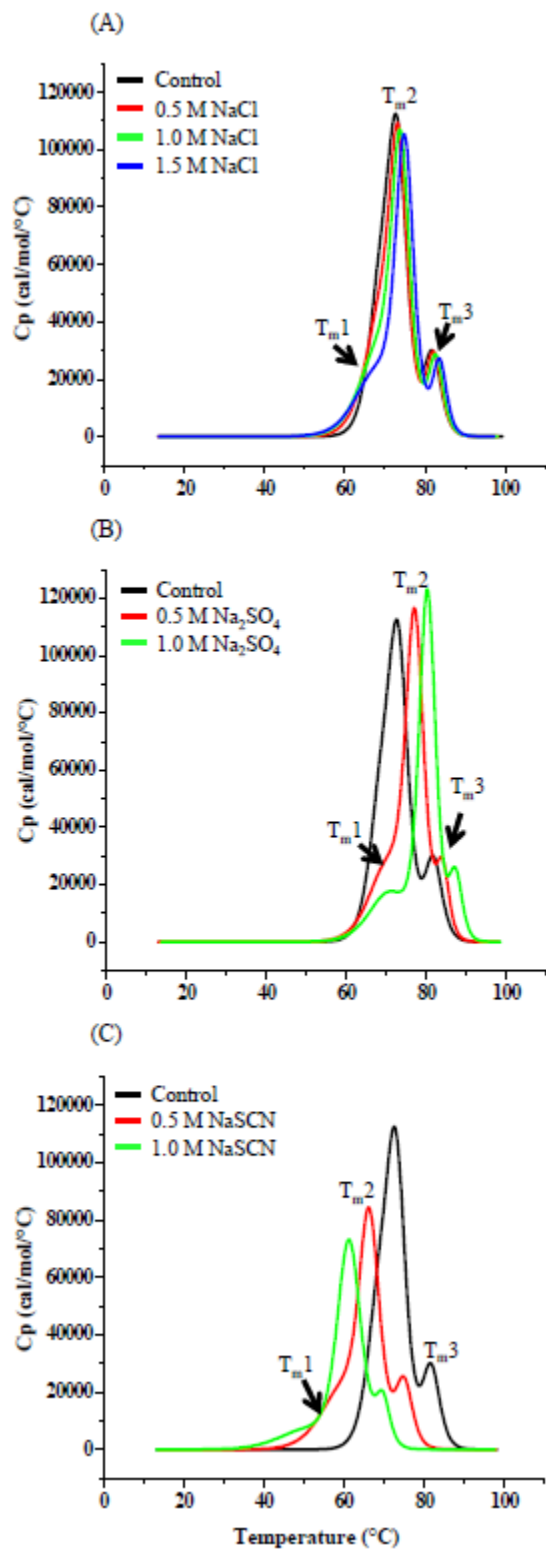
39	mAbB Heavy 69-80 (VH)
40	mAbB Heavy 69-83 (VH)
41	mAbB Heavy 80-83 (VH)
42	mAbB Heavy 80-86 (VH)
43	mAbB Heavy 81-86 (VH)
44	mAbB Heavy 84-90 (VH)
45	mAbB Heavy 84-93 (VH)
46	mAbB Heavy 85-93 (VH)
47	mAbB Heavy 87-104 (VH)
48	mAbB Heavy 105-114 (VH)
49	mAbB Heavy 105-118
50	mAbB Heavy 105-126
51	mAbB Heavy 124-147 (CH1)
52	mAbB Heavy 146-174 (CH1)
53	mAbB Heavy 156-174 (CH1)
54	mAbB Heavy 159-174 (CH1)
55	mAbB Heavy 163-174 (CH1)
56	mAbB Heavy 171-183 (CH1)
57	mAbB Heavy 180-185 (CH1)
58	mAbB Heavy 185-193 (CH1)
59	mAbB Heavy 185-197 (CH1)
60	mAbB Heavy 186-197 (CH1)
61	mAbB Heavy 198-220 (CH1)
62	mAbB Heavy 208-229
63	mAbB Heavy 235-240
64	mAbB Heavy 235-252 (CH2)
65	mAbB Heavy 241-251 (CH2)
66	mAbB Heavy 241-252 (CH2)
67	mAbB Heavy 243-252 (CH2)
68	mAbB Heavy 244-251 (CH2)
69	mAbB Heavy 263-277 (CH2)
70	mAbB Heavy 266-277 (CH2)
71	mAbB Heavy 300-306 (CH2)
72	mAbB Heavy 301-305 (CH2)
73	mAbB Heavy 301-306 (CH2)
74	mAbB Heavy 307-318 (CH2)
75	mAbB Heavy 334-348
76	mAbB Heavy 349-364 (CH3)
77	mAbB Heavy 349-365 (CH3)
78	mAbB Heavy 355-365 (CH3)
79	mAbB Heavy 369-376 (CH3)

80	mAbB Heavy 369-379 (CH3)
81	mAbB Heavy 369-380 (CH3)
82	mAbB Heavy 381-390 (CH3)
83	mAbB Heavy 379-398 (CH3)
84	mAbB Heavy 380-398 (CH3)
85	mAbB Heavy 381-398 (CH3)
86	mAbB Heavy 382-398 (CH3)
87	mAbB Heavy 381-404 (CH3)
88	mAbB Heavy 391-398 (CH3)
89	mAbB Heavy 392-398 (CH3)
90	mAbB Heavy 391-404 (CH3)
91	mAbB Heavy 399-404 (CH3)
92	mAbB Heavy 406-410 (CH3)
93	mAbB Heavy 411-423 (CH3)
94	mAbB Heavy 424-446 (CH3)
95	mAbB Heavy 429-446 (CH3)
96	mAbB Heavy 431-446 (CH3)
97	mAbB Heavy 433-446 (CH3)
98	mAbB Light 1-4 (VL)
99	mAbB Light 1-7 (VL)
100	mAbB Light 1-10 (VL)
101	mAbB Light 1-11 (VL)
102	mAbB Light 32-46 (VL)
103	mAbB Light 33-46 (VL)
104	mAbB Light 36-46 (VL)
105	mAbB Light 47-62 (VL)
106	mAbB Light 47-70 (VL)
107	mAbB Light 47-74 (VL)
108	mAbB Light 51-70 (VL)
109	mAbB Light 71-74 (VL)
110	mAbB Light 71-83 (VL)
111	mAbB Light 72-82 (VL)
112	mAbB Light 74-82 (VL)
113	mAbB Light 75-82 (VL)
114	mAbB Light 75-83 (VL)
115	mAbB Light 80-85 (VL)
116	mAbB Light 91-103 (VL)
117	mAbB Light 105-116
118	mAbB Light 116-122 (CL)
119	mAbB Light 117-123 (CL)
120	mAbB Light 116-125 (CL)

121	mAbB Light 117-125 (CL)
122	mAbB Light 116-131 (CL)
123	mAbB Light 116-132 (CL)
124	mAbB Light 117-132 (CL)
125	mAbB Light 136-148 (CL)
126	mAbB Light 136-161 (CL)
127	mAbB Light 144-161 (CL)
128	mAbB Light 149-161 (CL)
129	mAbB Light 162-172 (CL)
130	mAbB Light 162-175 (CL)
131	mAbB Light 162-178 (CL)
132	mAbB Light 162-179 (CL)
133	mAbB Light 162-181 (CL)
134	mAbB Light 172-175 (CL)
135	mAbB Light 173-179 (CL)
136	mAbB Light 183-210 (CL)
137	mAbB Light 186-212 (CL)

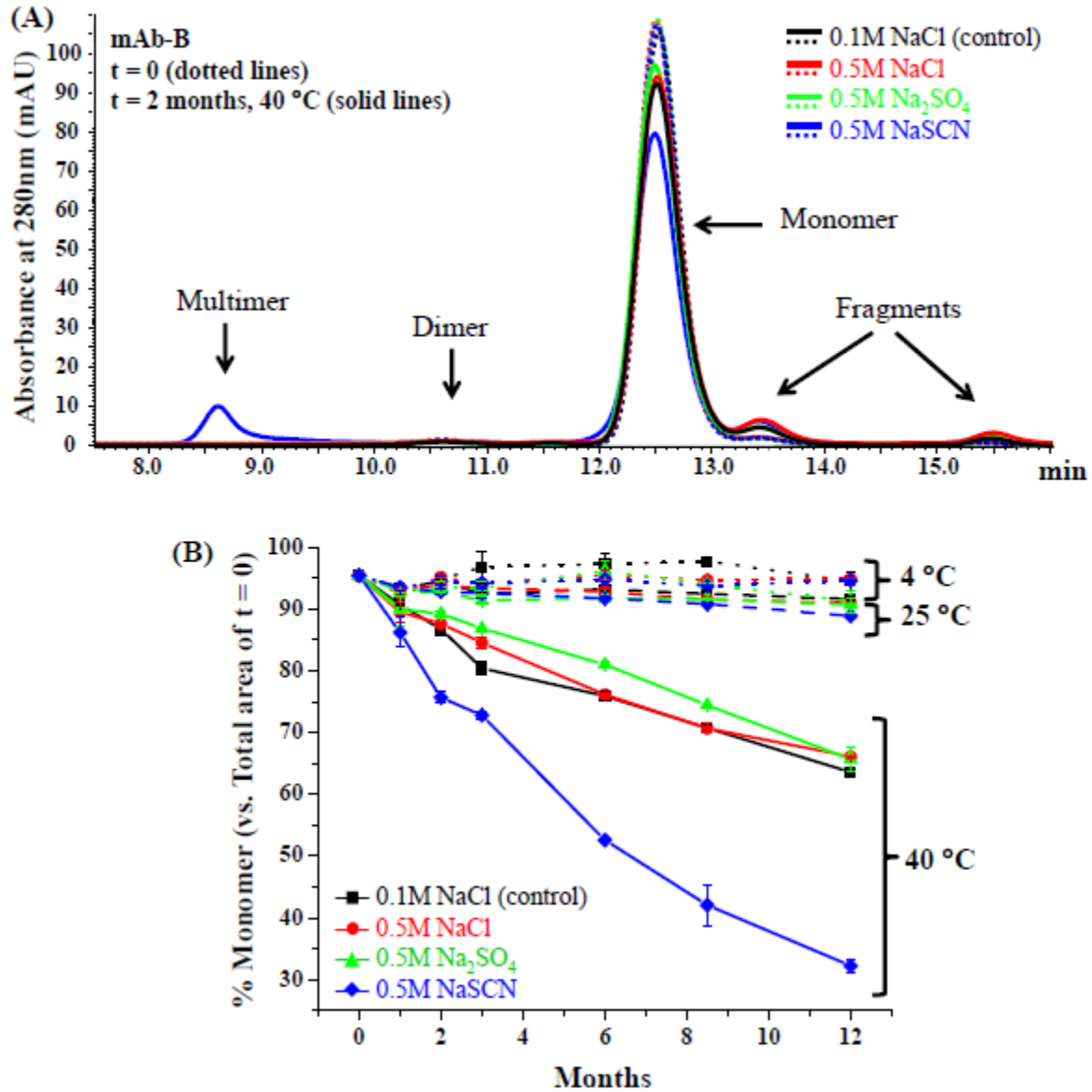
Locations of peptides based on their ordinal numbers.

Figure 4.1



Representative DSC thermograms of mAb-B in 20 mM citrate-phosphate buffer pH 6.0 containing indicated concentrations of different salts. Effect of (A) NaCl, (B) Na₂SO₄, and (C) NaSCN on mAb-B conformational stability along with T_{m1}, T_{m2}, and T_{m3} are shown.

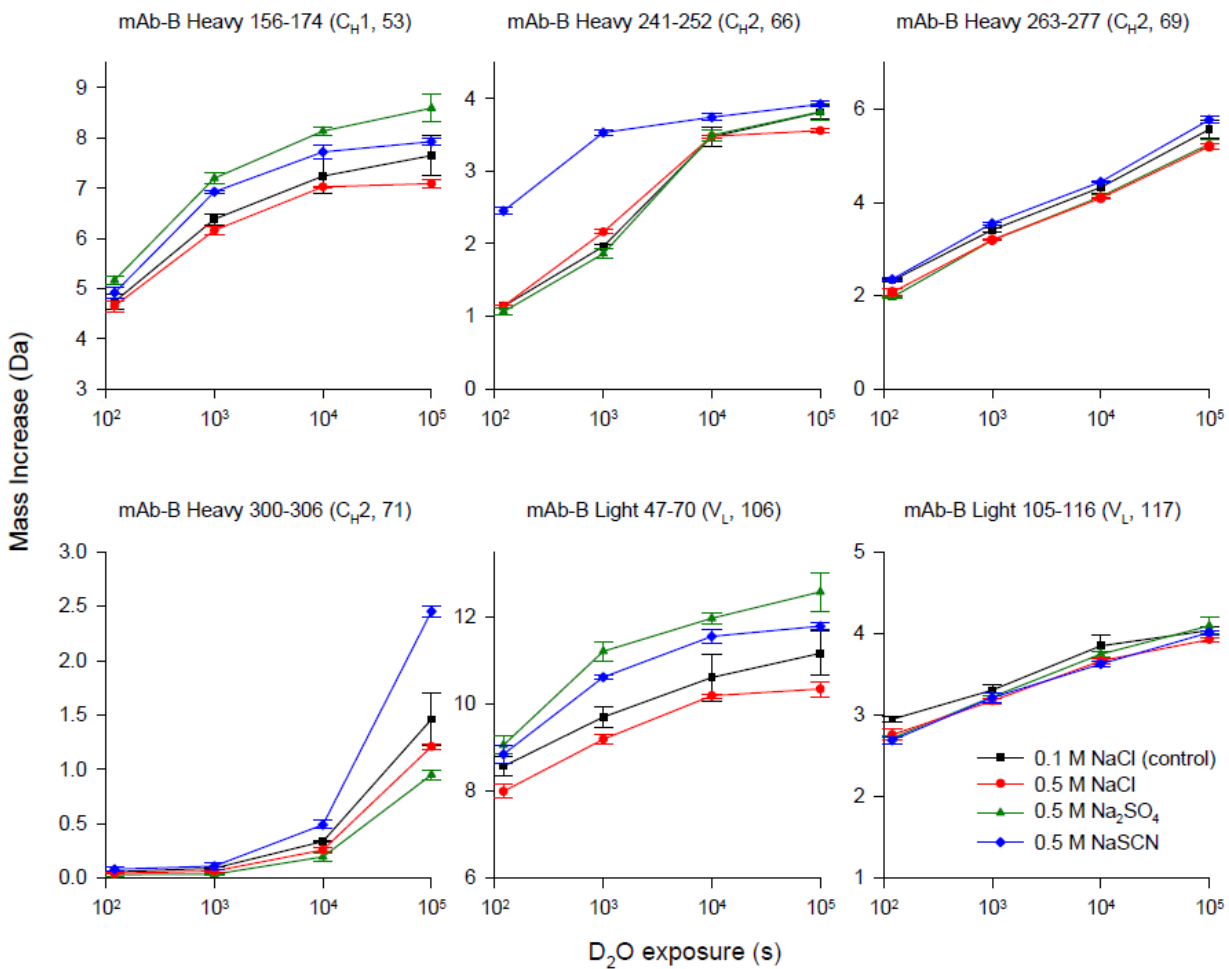
Figure 4.2



MAb-B aggregation during storage at different temperatures as monitored by SE-HPLC. (A) Overlay of SEC chromatograms of mAb-B before and after thermal stress: dotted lines correspond to mAb-B samples at time zero (no stress) and solid lines correspond to mAb-B samples incubated at 40 °C for 2 months. (B) Effect of salts (NaCl, Na₂SO₄, and NaSCN) and thermal stress (4, 25, and 40 °C) on mAb-B monomer loss. Data were collected in duplicate on

days 0, 28, 60, 90, 180, 260, and 360. Samples of mAb-B were prepared in 20 mM citrate-phosphate buffer, pH 6.0 with either 0.1 M NaCl (control, black trace), 0.5 M NaCl (red trace), 0.5 M Na₂SO₄ (green trace), or 0.5 M NaSCN (blue trace).

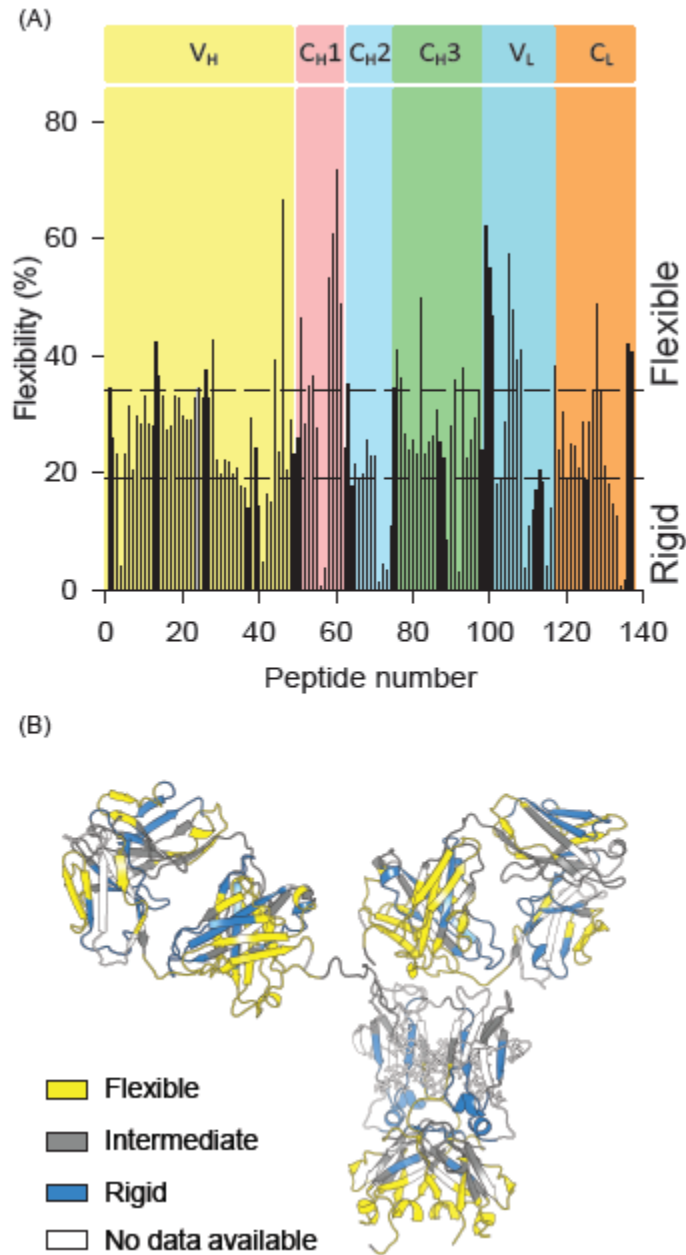
Figure 4.3



Effect of different salts on the deuterium uptake in six segments from different domains of mAb-

B. The error bars denote one standard deviation.

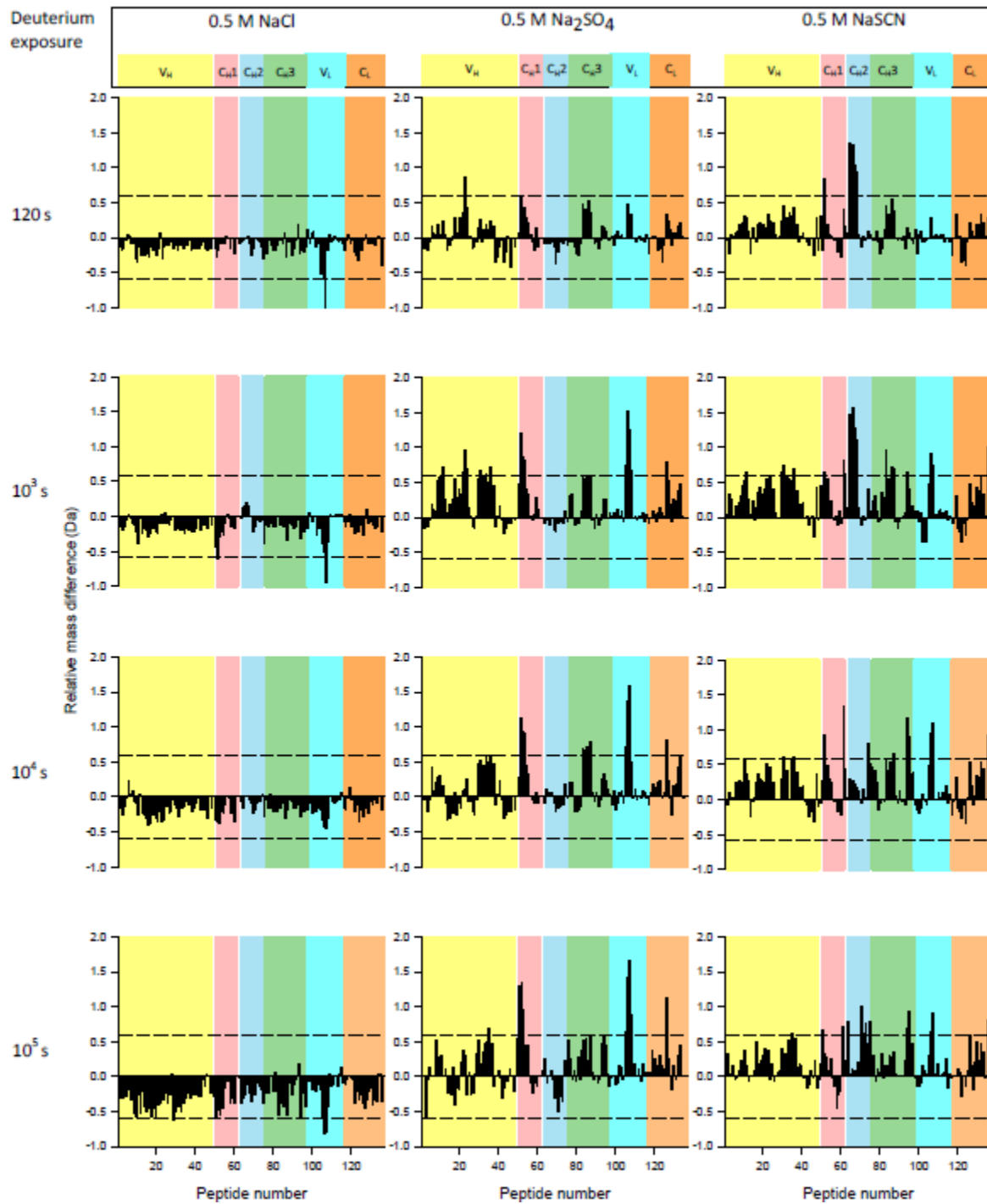
Figure 4.4



Local flexibility of mAb-B, as measured by H/D exchange in 0.1 M NaCl at pH 6.0. (A) Flexibility, as obtained from the ratio of the extent of deuteration at 120 s relative to the theoretical maximum exchange without correction for back-exchange (equation 1). Colors

denote the different domain boundaries. The broken lines denote the top and bottom quartiles. The maximum flexibility is 85.5%. (B) Flexibility data plotted on a homology model of mAb-B. Peptides representing the bottom quartile are classified as rigid (blue), the middle 50% as intermediate (gray), and the top quartile as flexible (yellow). Regions without H/D exchange data are colored white. In cases where overlapping segments had different flexibility categories, flexible and rigid categories took priority over the intermediate category, and rigid category took priority over flexible category (5 amino acids only).

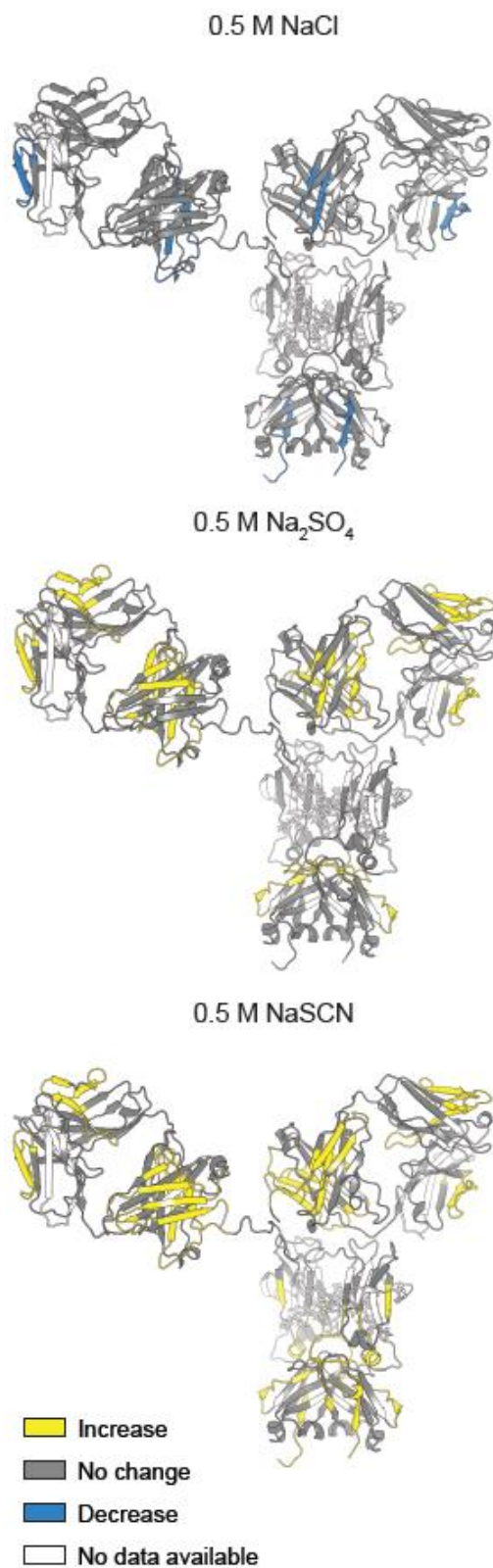
Figure 4.5



Relative deuterium uptake differences for all 137 segments of mAb-B in the presence of 0.5 M concentration of the salts relative to the control solution (0.1 M sodium chloride) as measured by

H/D-MS at each deuterium exposure time. The dashed lines at ± 0.59 Da represent the 99% confidence limit for the mass difference values. The x-axis denotes the ordinal peptide numbers, which are sorted in ascending order based on the midpoint of their sequences. Colors denote the different domain boundaries. Positive y-values in these plots denote increased flexibility in the particular segment in presence of the particular salt compared to the control (0.1 M sodium chloride) and negative y-values denote decreased flexibility. Locations of the mAb domains shown in the figure are only approximate because some peptide segments span two different domains. See Table 4.S1 for the locations of the peptides in the mAb-B sequence.

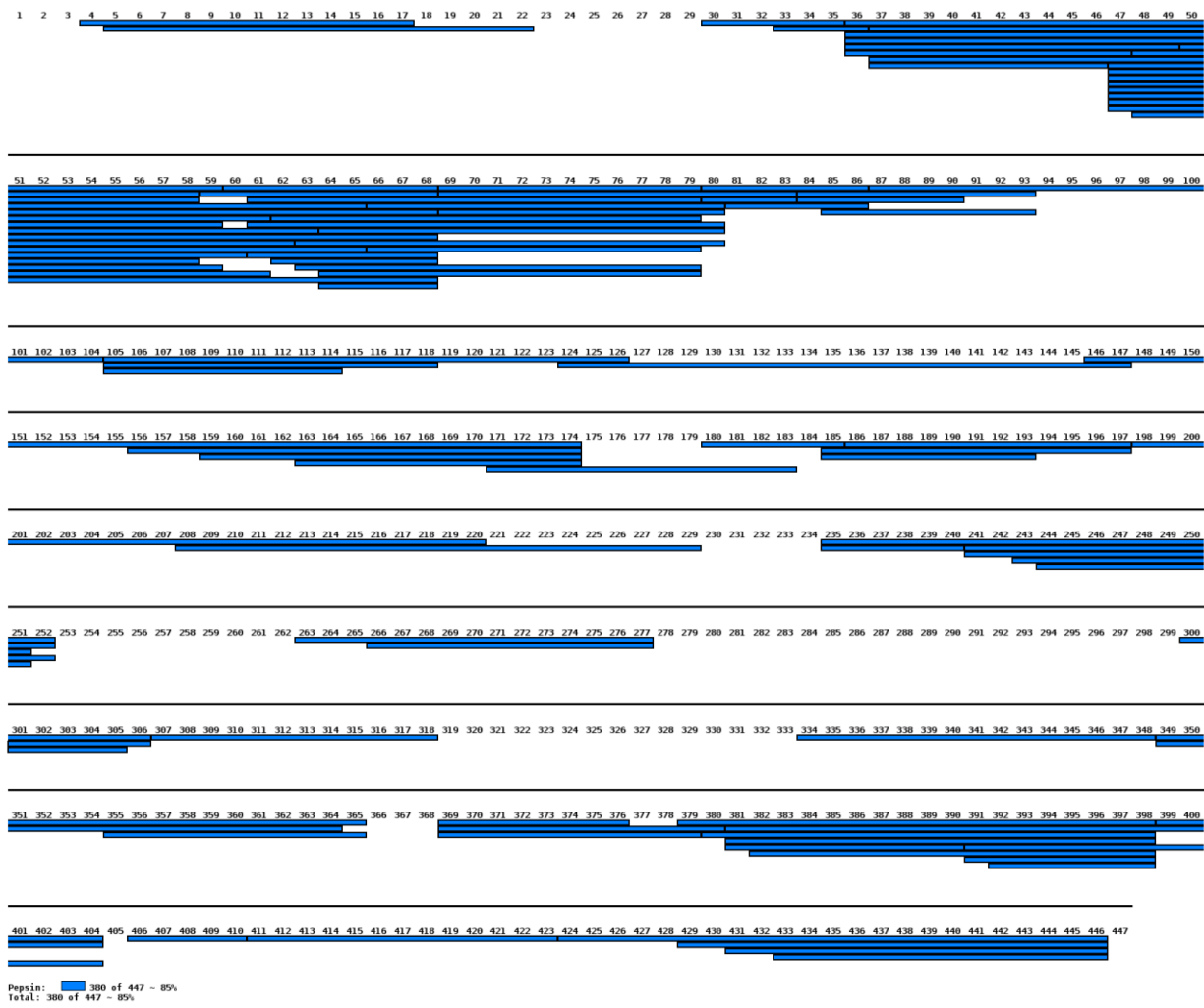
Figure 4.6



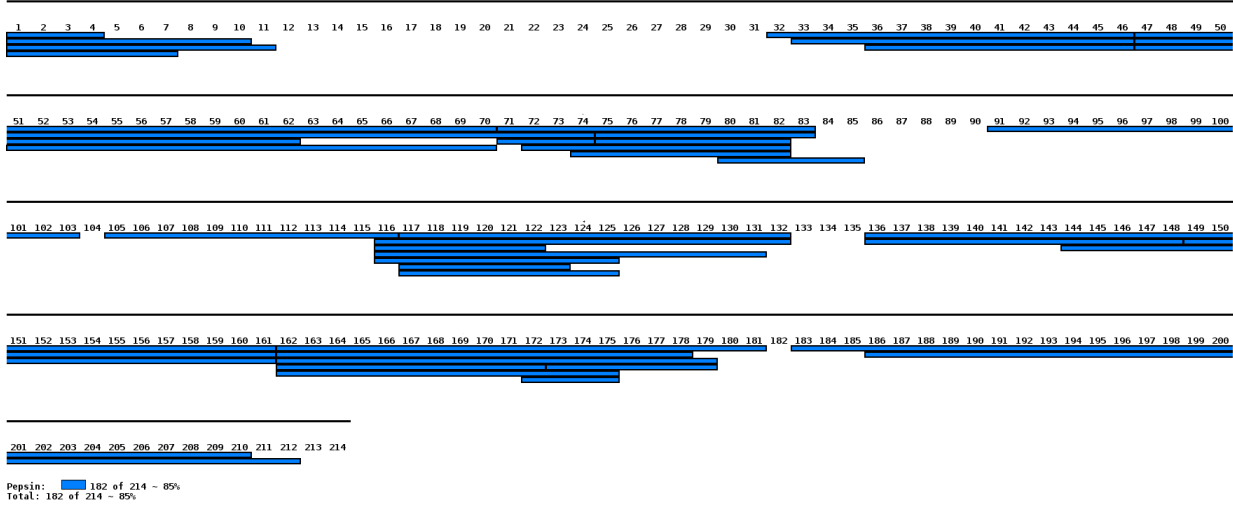
Effects of salts on the flexibility of mAb-B relative to the control (0.1 M sodium chloride), as measured by H/D-MS plotted onto a homology model of mAb-B. Changes in flexibility are colored according to the legend.

Figure 4.S1

(A)

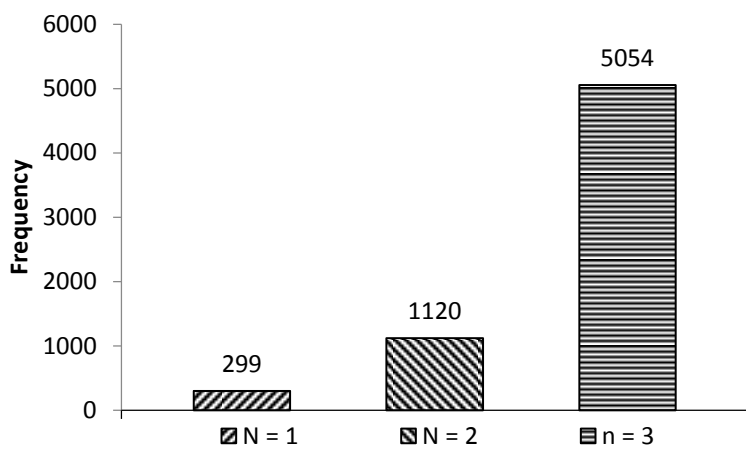


(B)



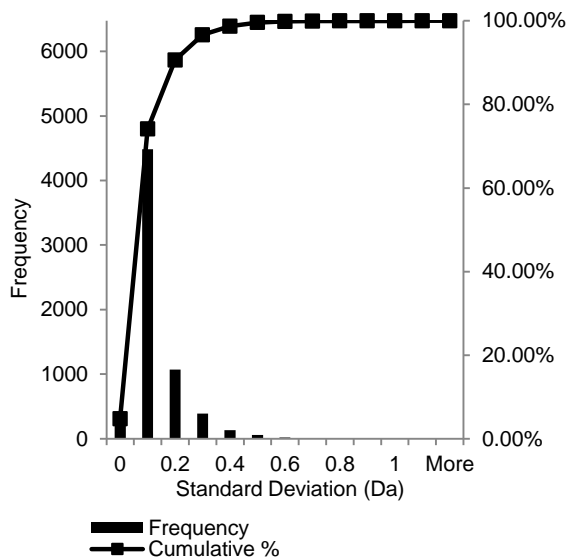
Primary sequence coverage map for (A) Heavy chain and (B) Light chain of mAb-B based on 137 identified peptides. The total coverage was 85% in the heavy chain and 85% in the light chain giving a total coverage of 85%.

Figure 4.S2



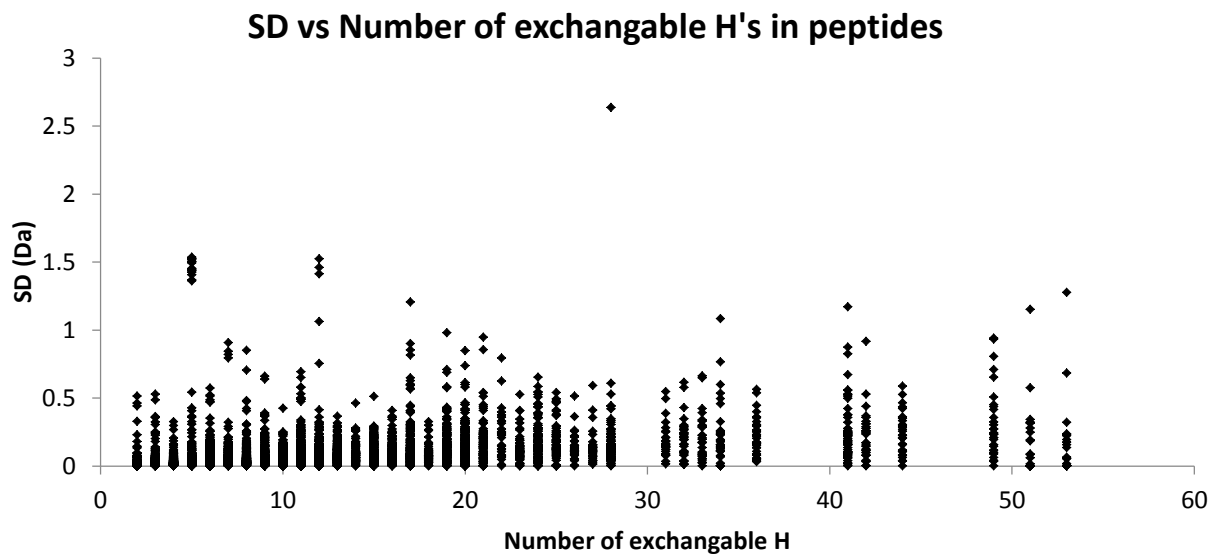
Distribution of number of replicates available across all data points. Here 'N' represents the number of replicates and the y-axis denoted the number of data points in the experiment.

Figure 4.S3



Reproducibility of H/D-MS data from our experimental setup represented by the distribution of standard deviations for the mass increase across all time points and peptides of mAb-B from triplicate experiments (run on different days, N = 6473). The 99th percentile for standard deviations was 0.42 Da.

Figure 4.S4

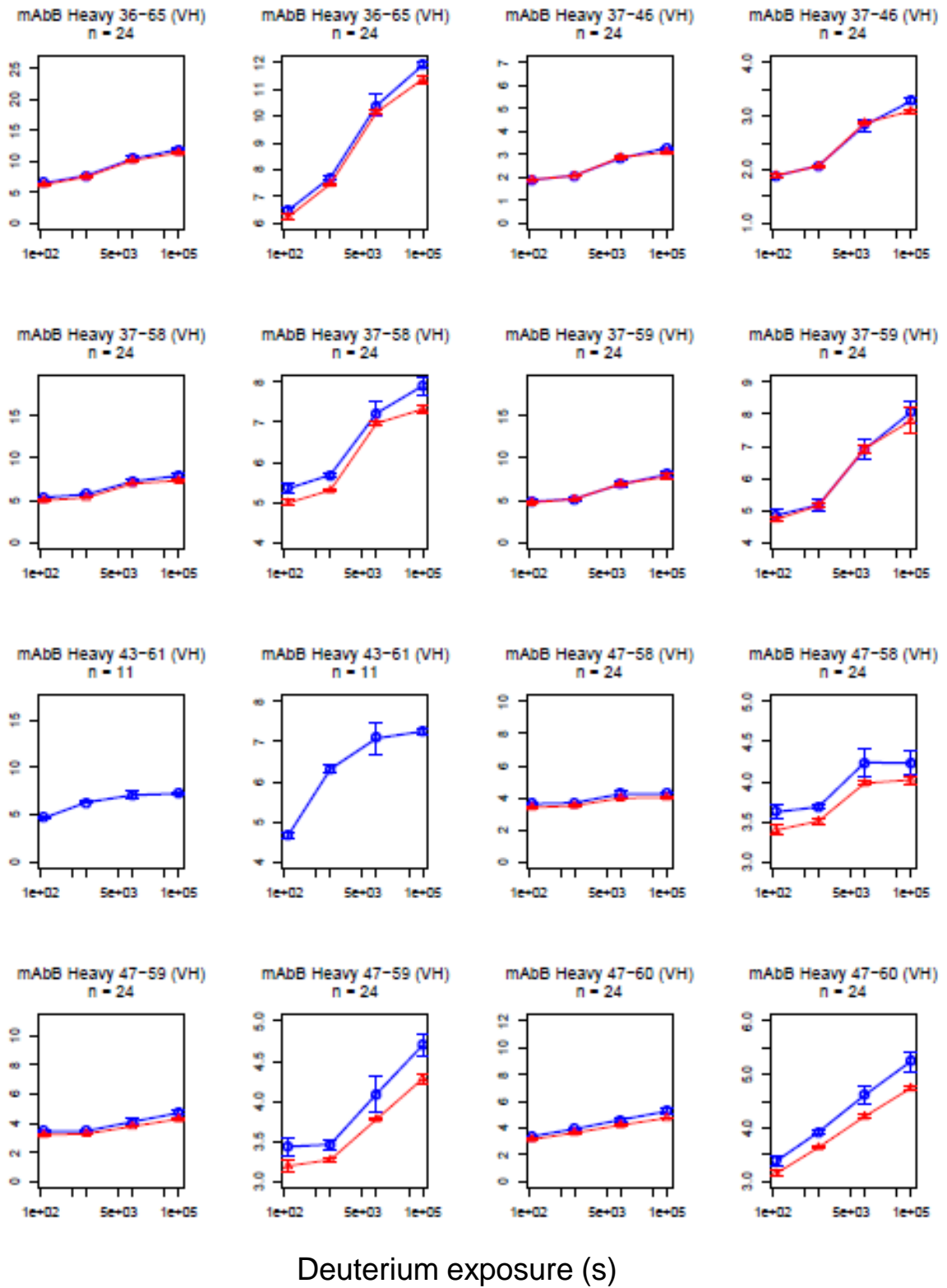


Standard deviation of deuterium uptake measurements does not depend on peptide size. Distribution of standard deviations (SD) for all data points vs. the number of exchangeable hydrogens (representative of peptide size) in all the peptides analyzed for mAb-B.

Figure 4.S5

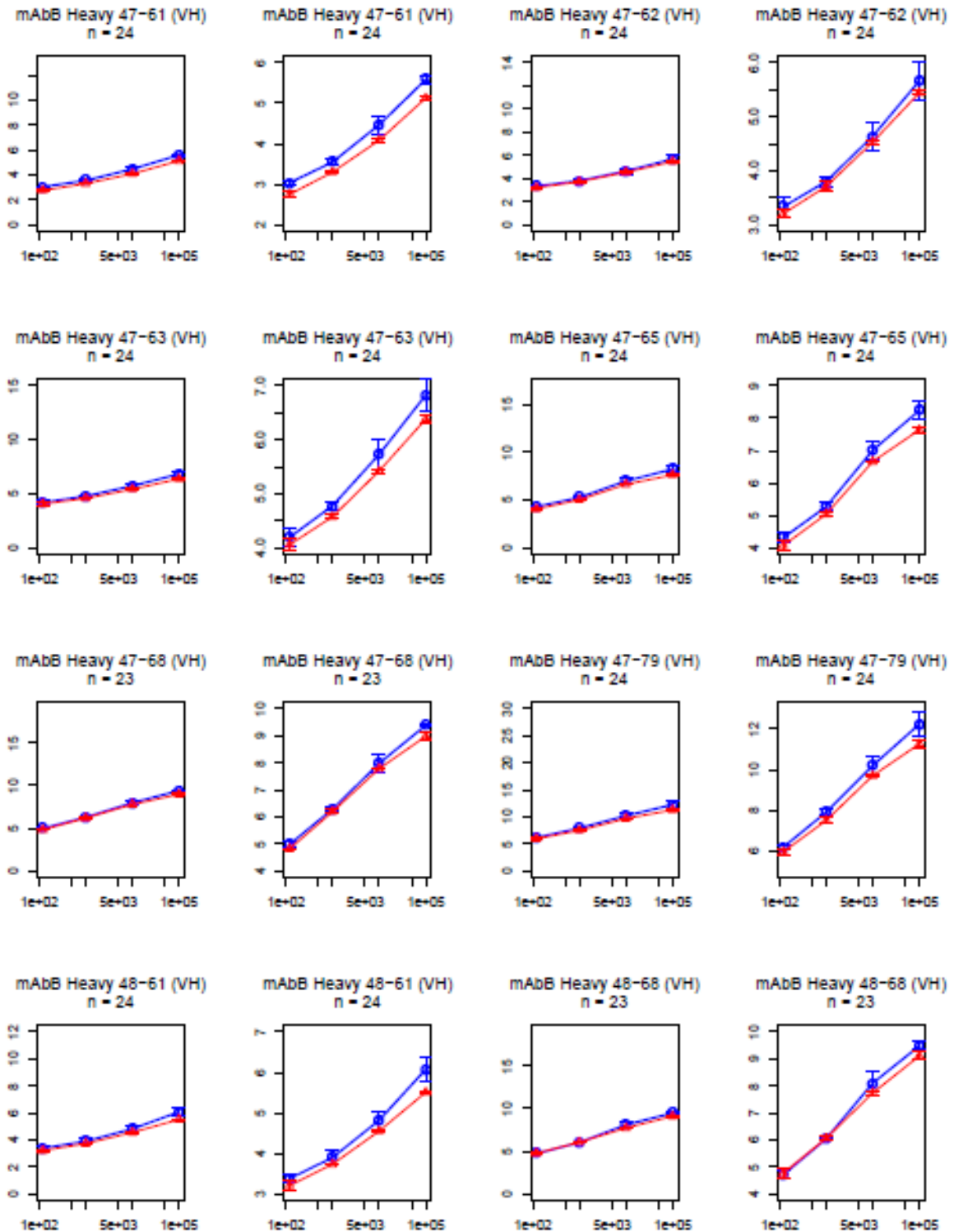
—○— 100 mM NaCl
—△— 500 mM NaCl

Mass Increase(Da)



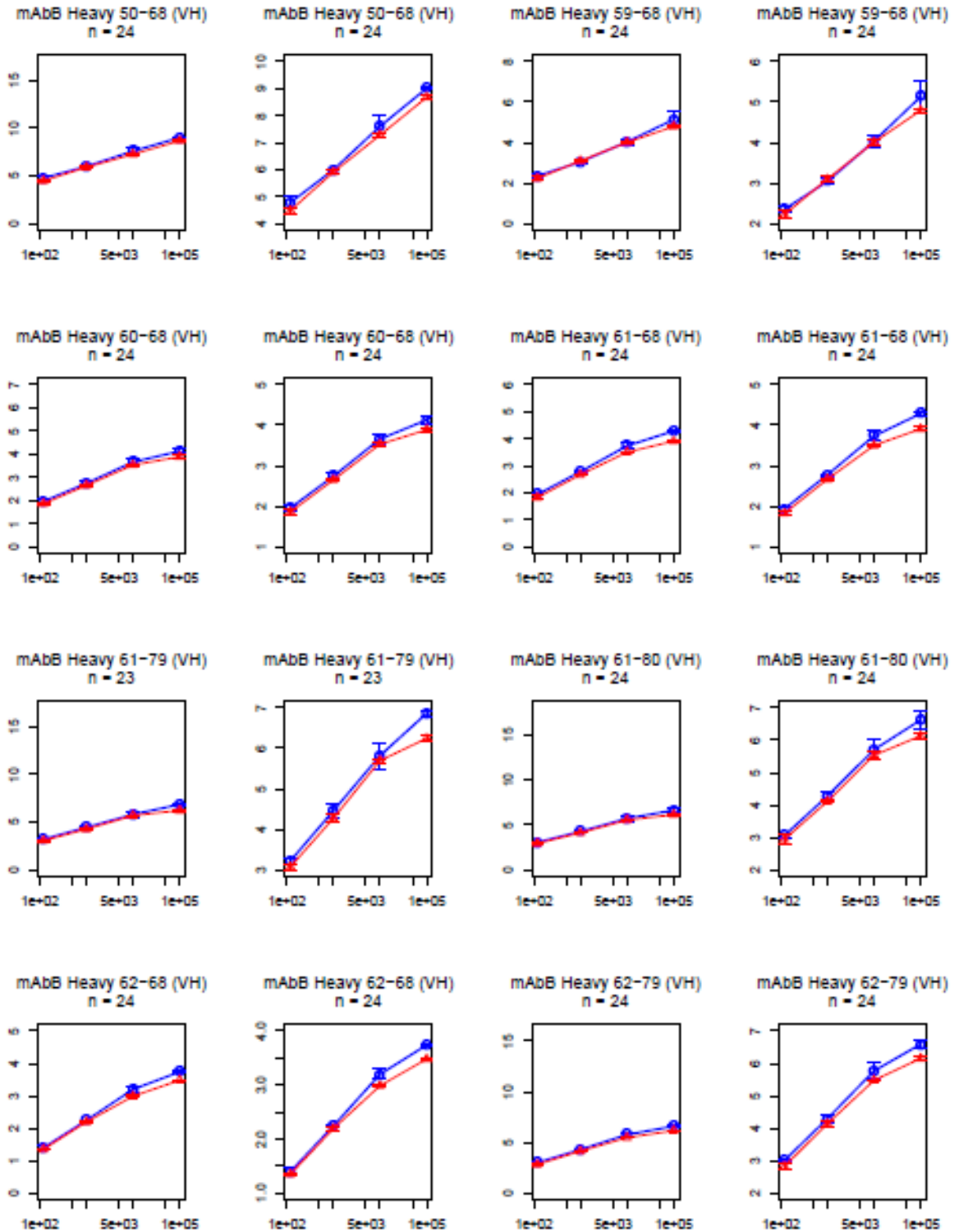
Deuterium exposure (s)

Mass Increase(Da)



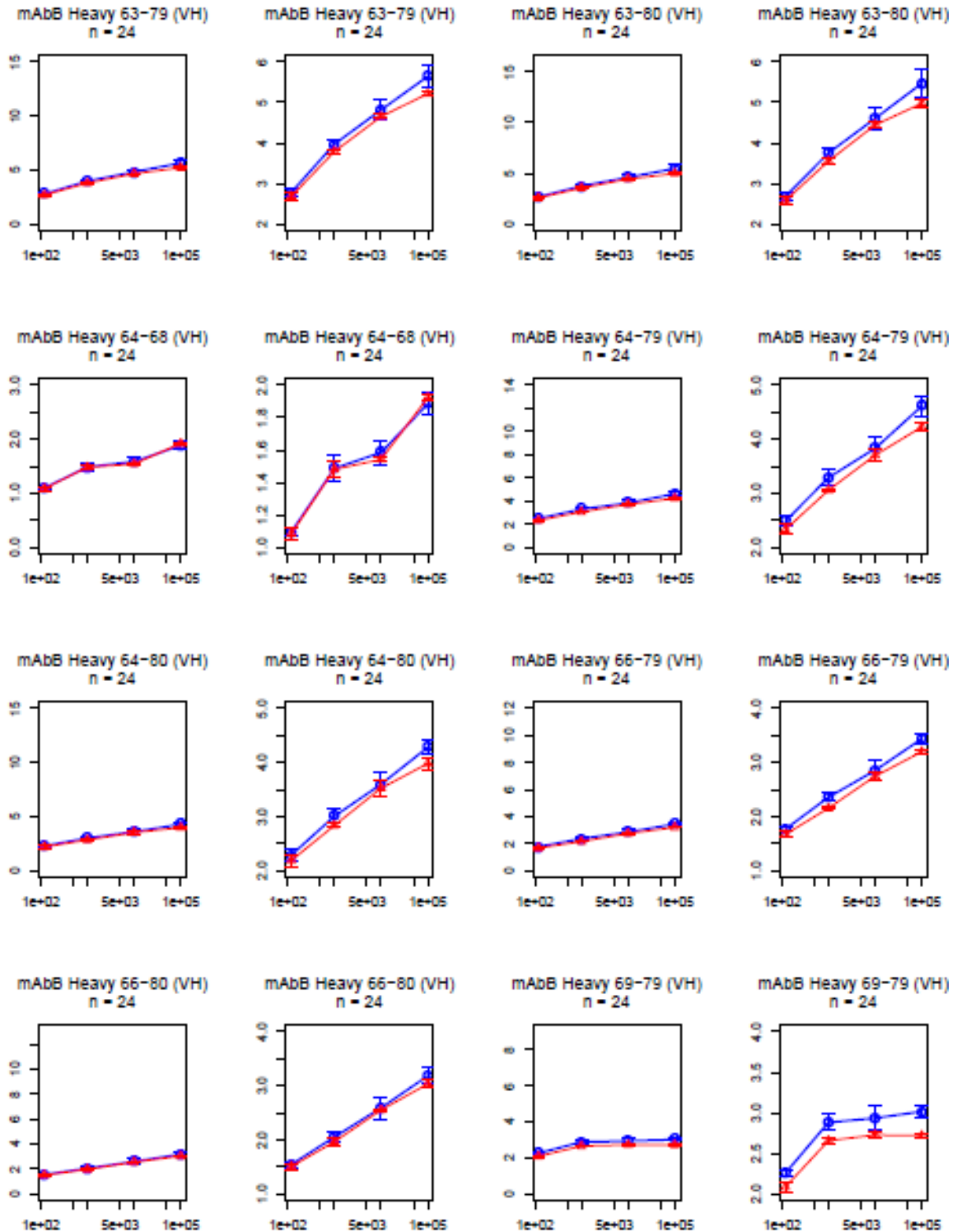
Deuterium exposure (s)

Mass Increase(Da)



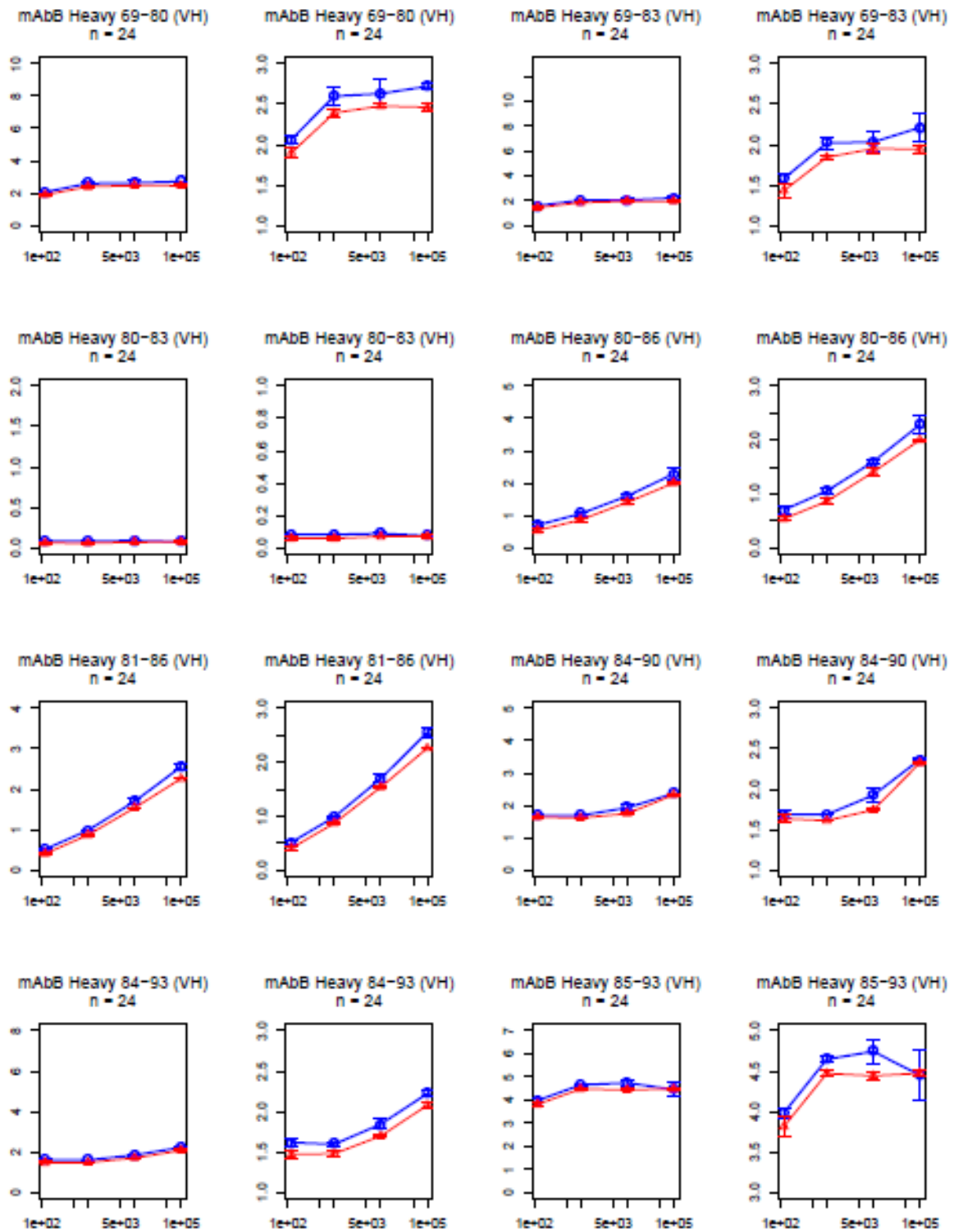
Deuterium exposure (s)

Mass Increase(Da)



Deuterium exposure (s)

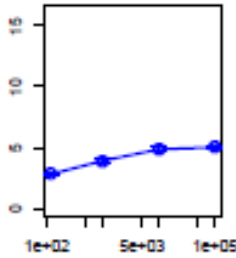
Mass Increase(Da)



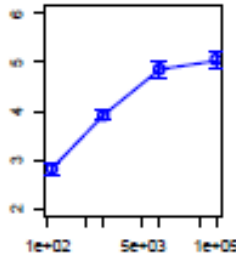
Deuterium exposure (s)

Mass Increase(Da)

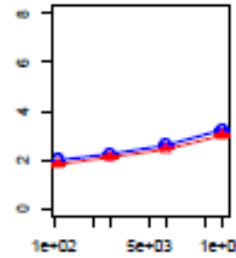
mAbB Heavy 87-104 (VH)
n = 12



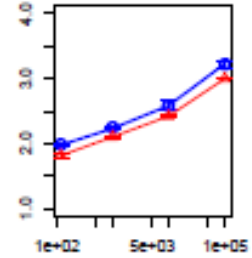
mAbB Heavy 87-104 (VH)
n = 12



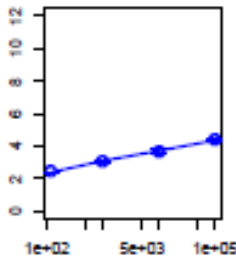
mAbB Heavy 105-114 (VH)
n = 24



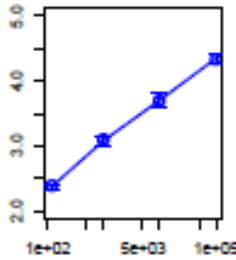
mAbB Heavy 105-114 (VH)
n = 24



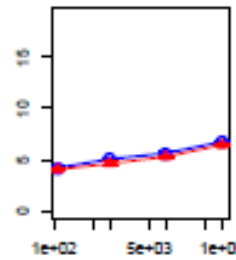
mAbB Heavy 105-118
n = 12



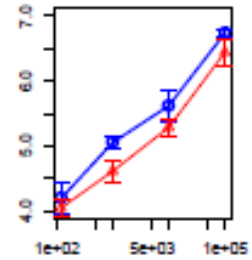
mAbB Heavy 105-118
n = 12



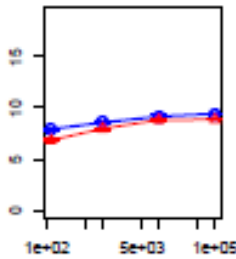
mAbB Heavy 105-126
n = 23



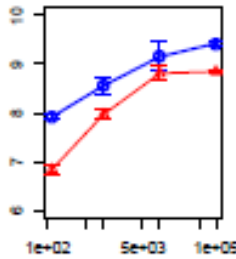
mAbB Heavy 105-126
n = 23



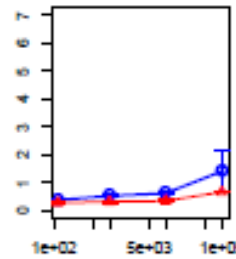
mAbB Heavy 124-147 (CH1)
n = 22



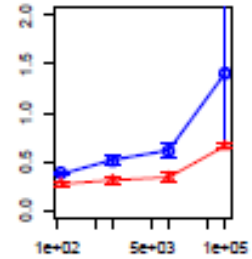
mAbB Heavy 124-147 (CH1)
n = 22



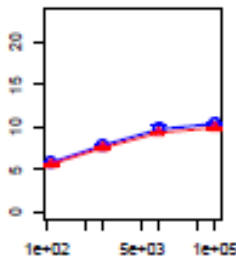
mAbB Heavy 144-154 (CH1)
n = 24



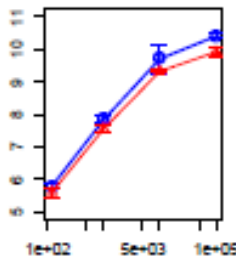
mAbB Heavy 144-154 (CH1)
n = 24



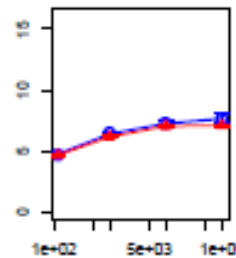
mAbB Heavy 146-174 (CH1)
n = 23



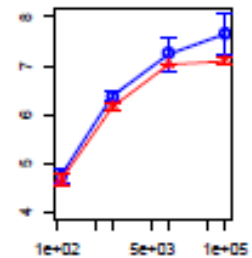
mAbB Heavy 146-174 (CH1)
n = 23



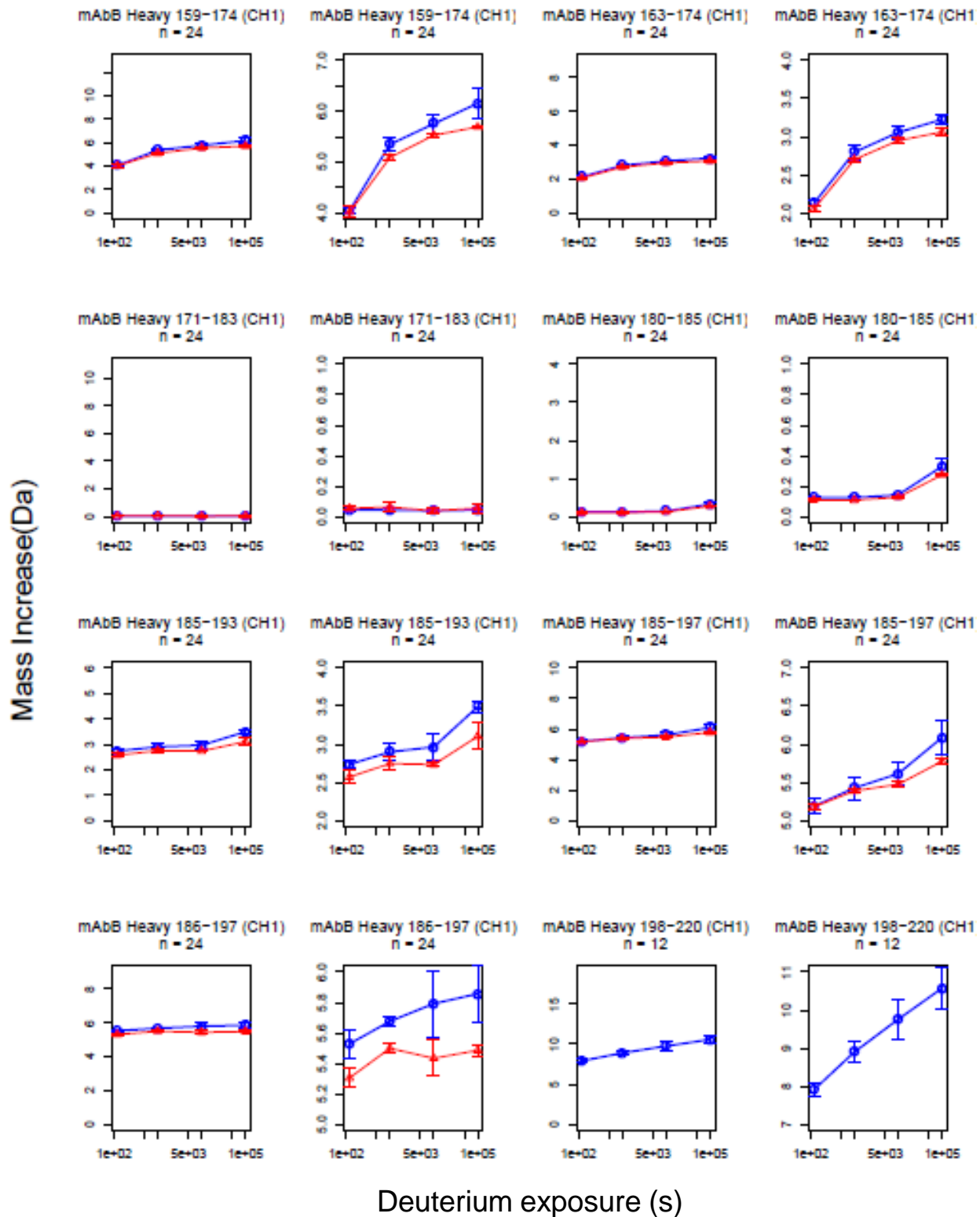
mAbB Heavy 156-174 (CH1)
n = 24



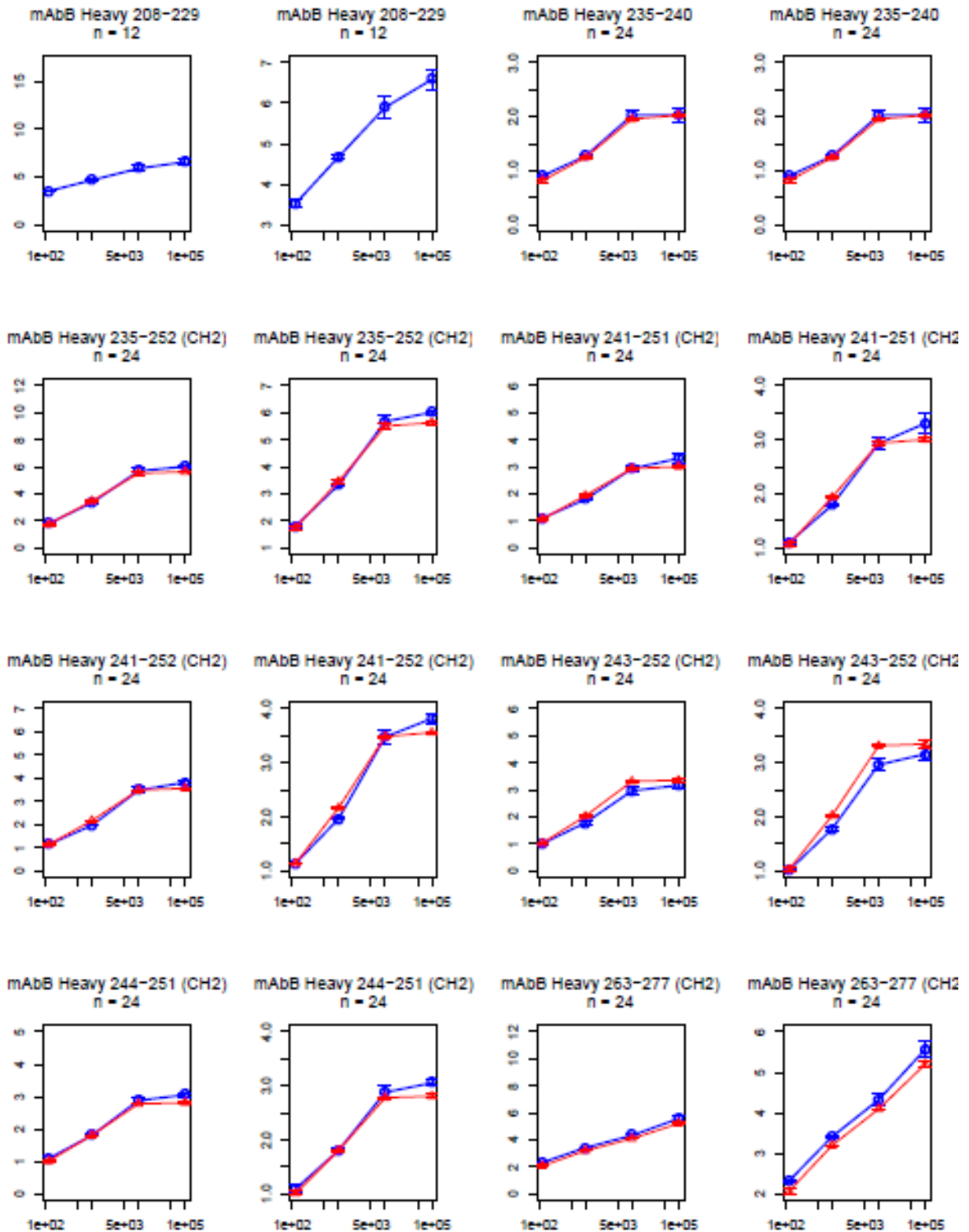
mAbB Heavy 156-174 (CH1)
n = 24



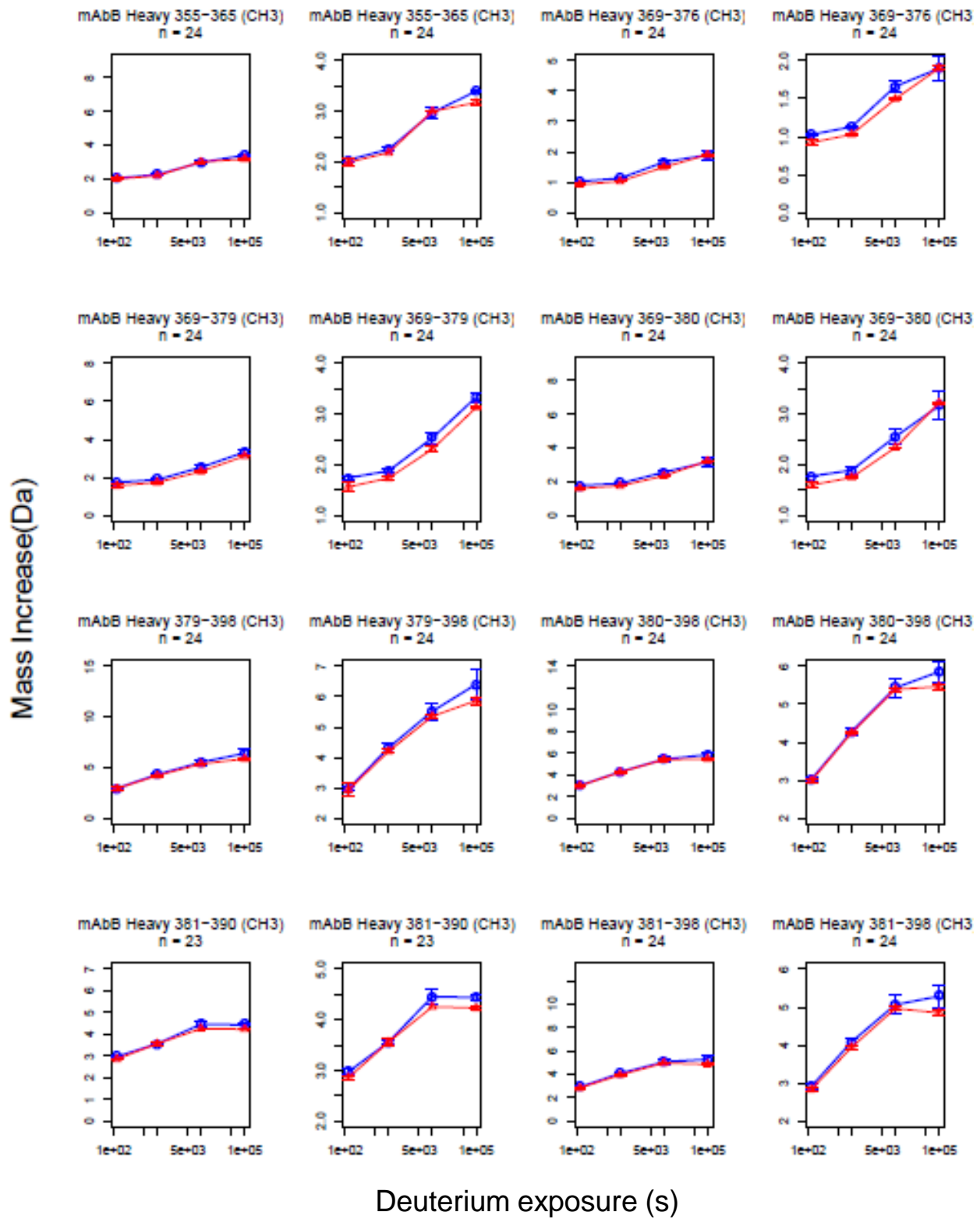
Deuterium exposure (s)

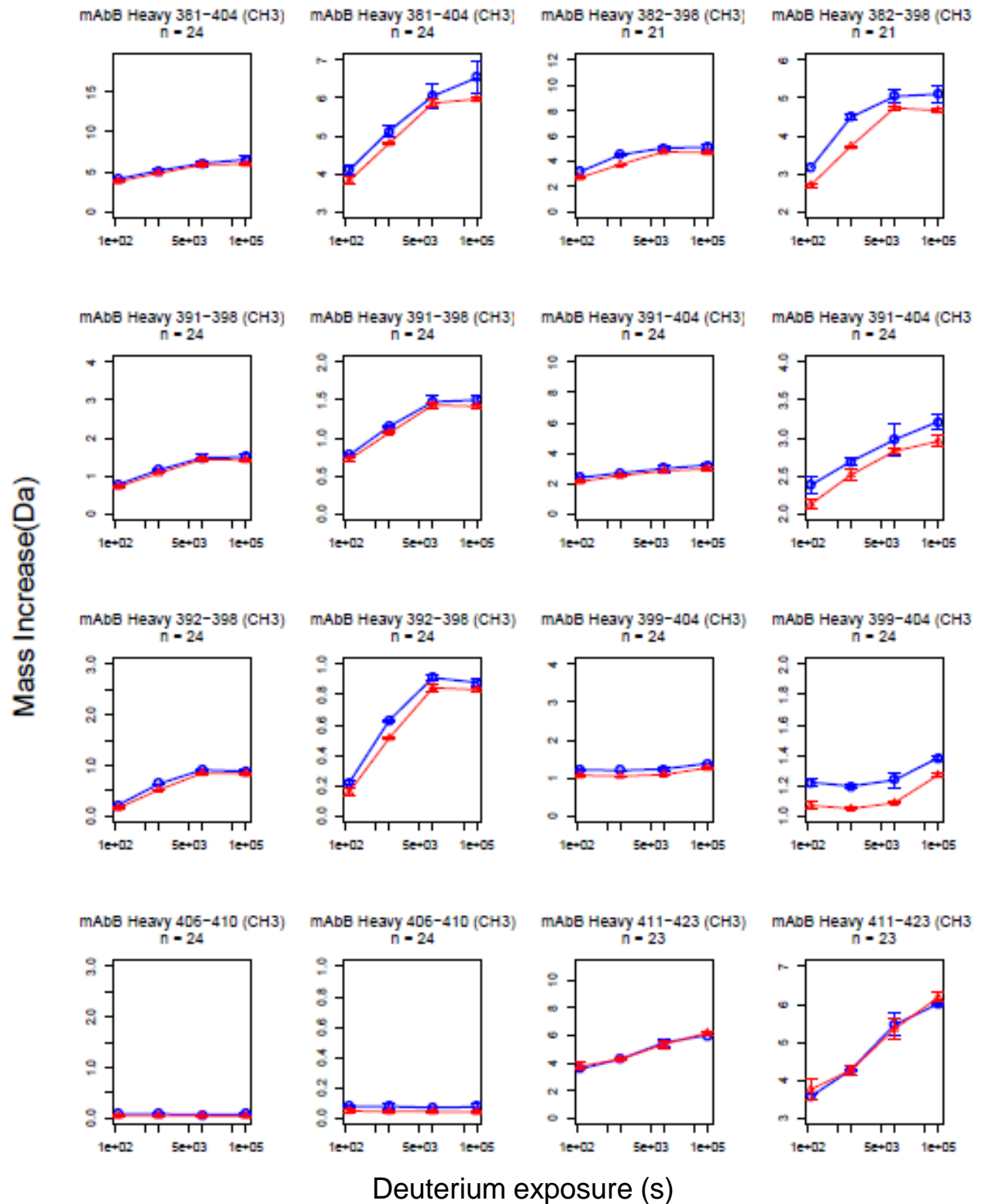


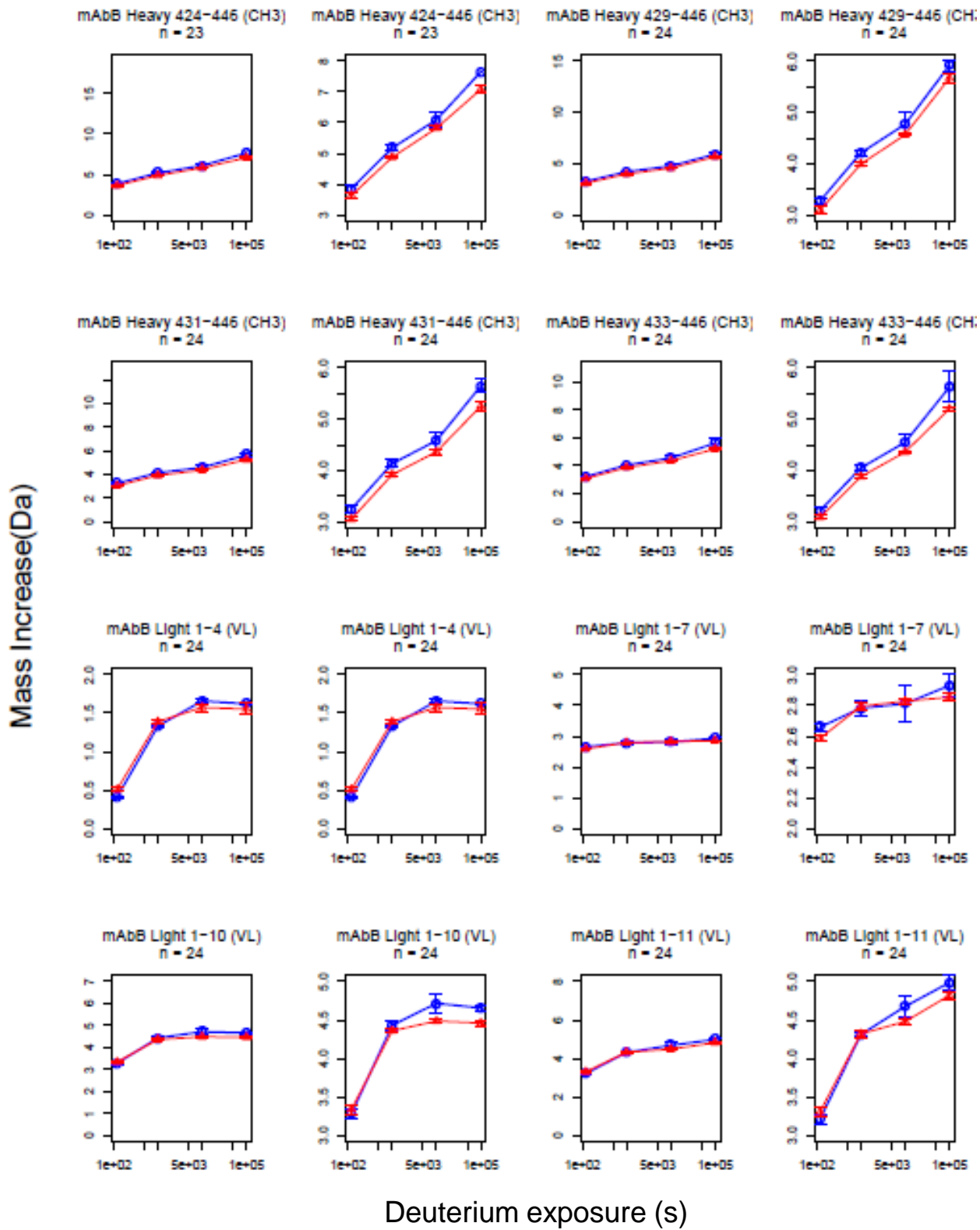
Mass Increase(Da)



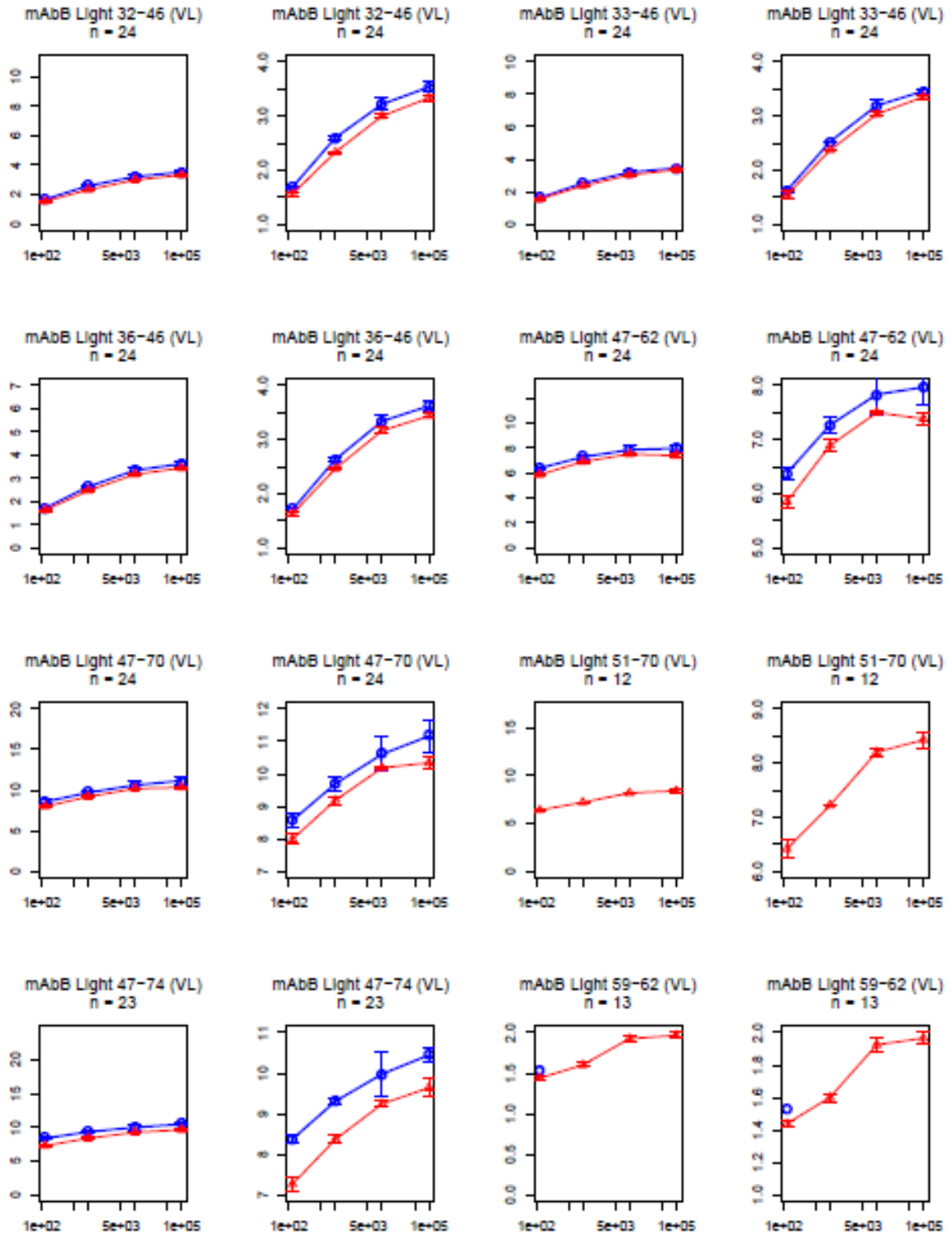
Deuterium exposure (s)





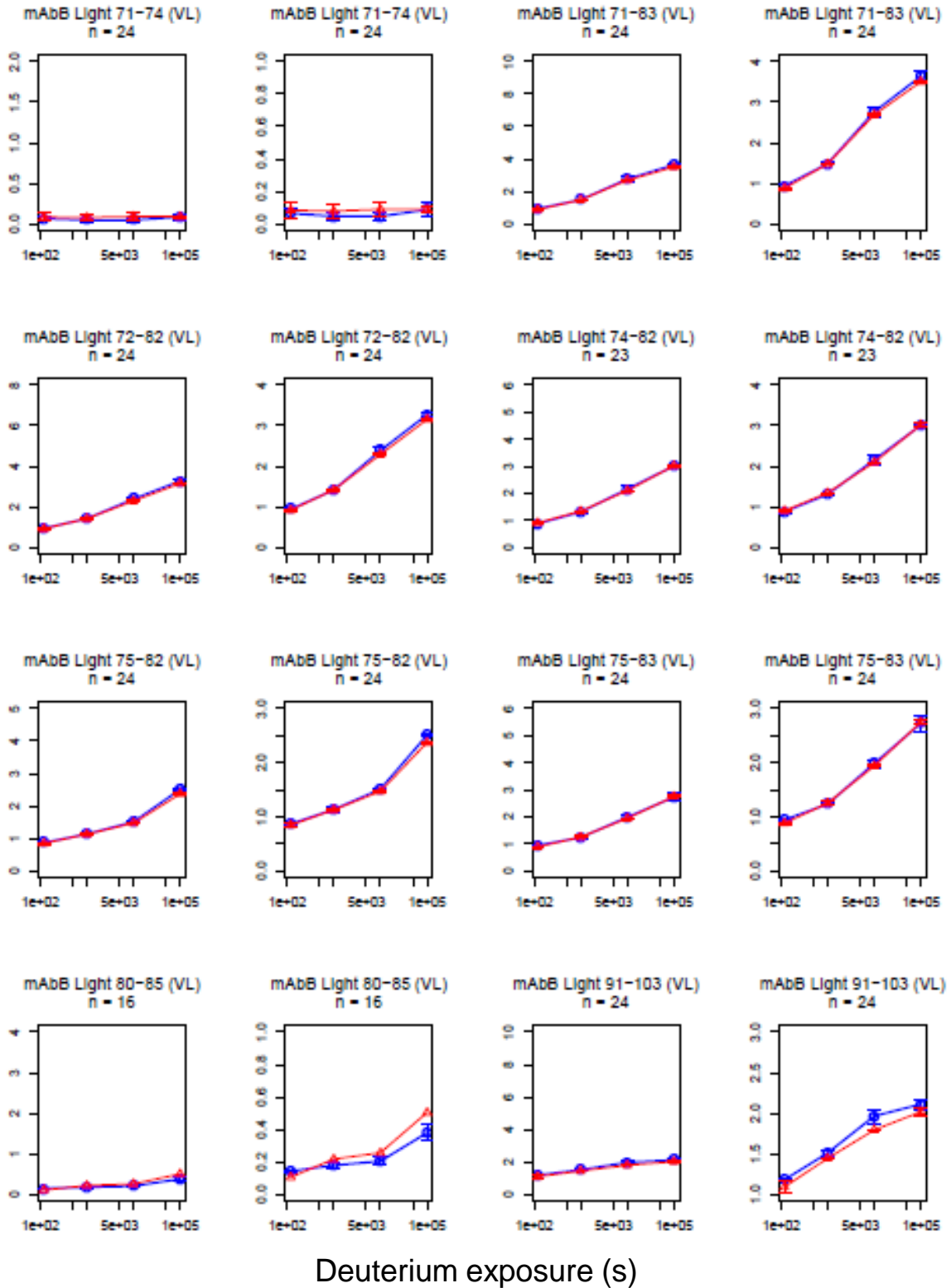


Mass Increase(Da)

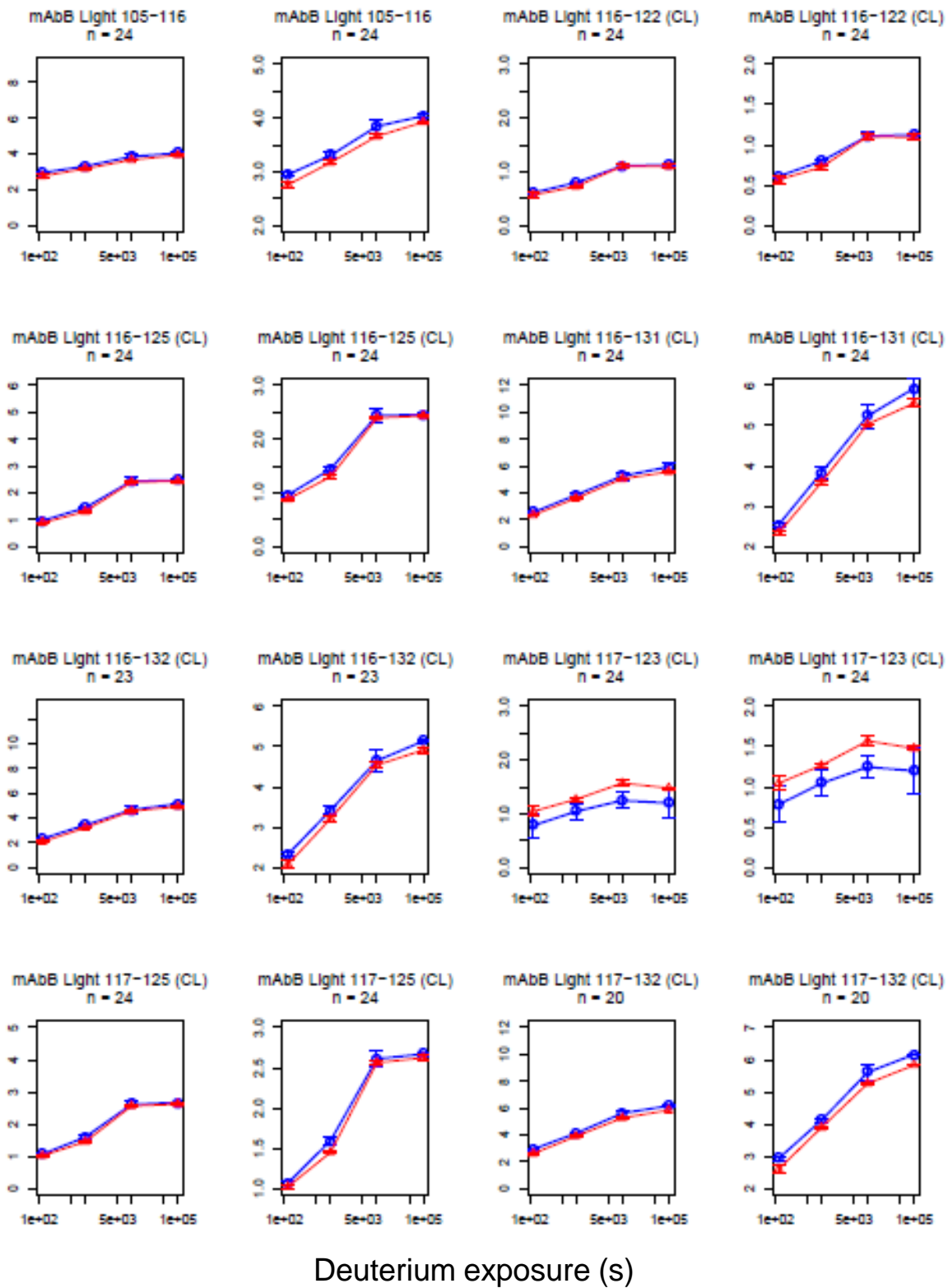


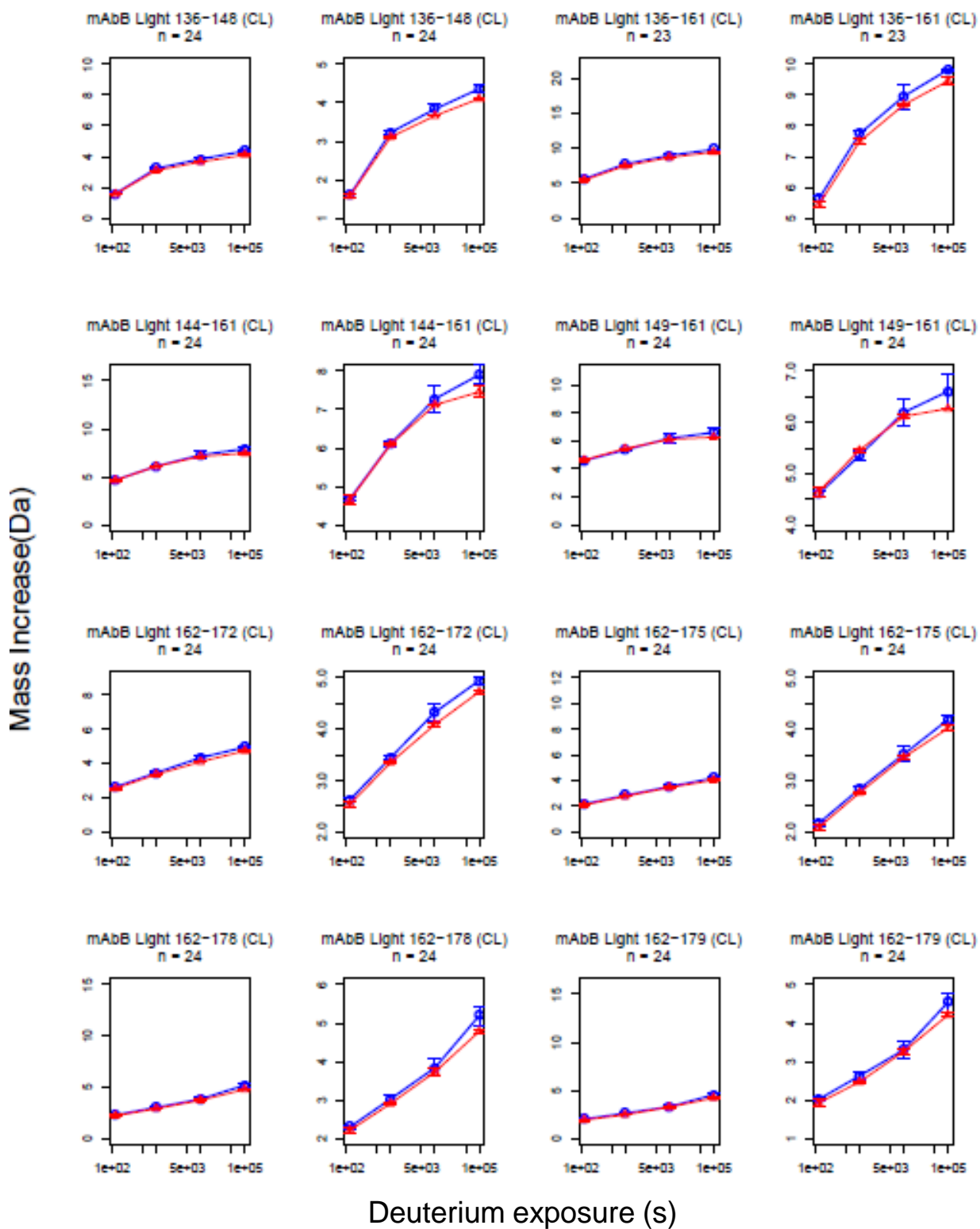
Deuterium exposure (s)

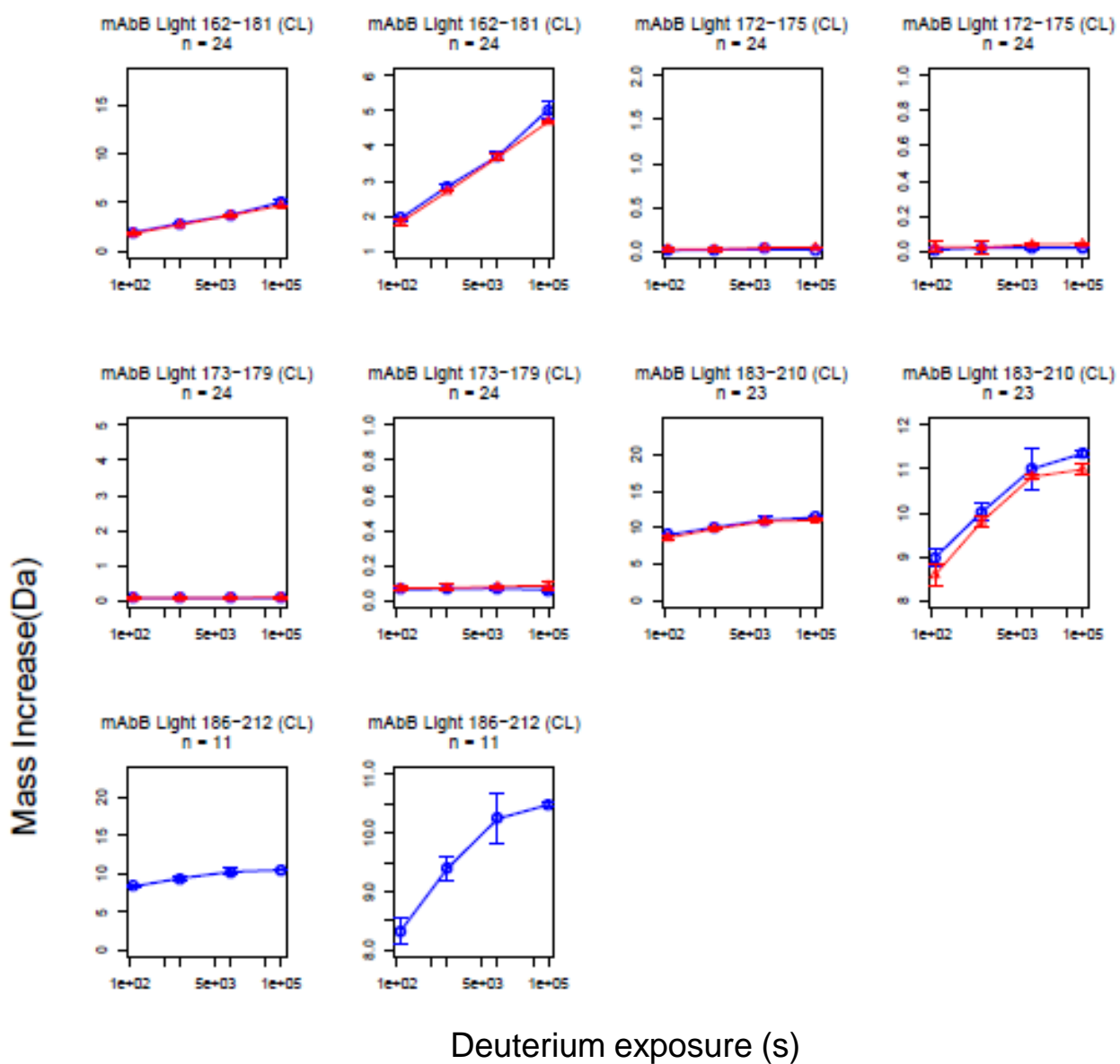
Mass Increase(Da)



Mass Increase(Da)

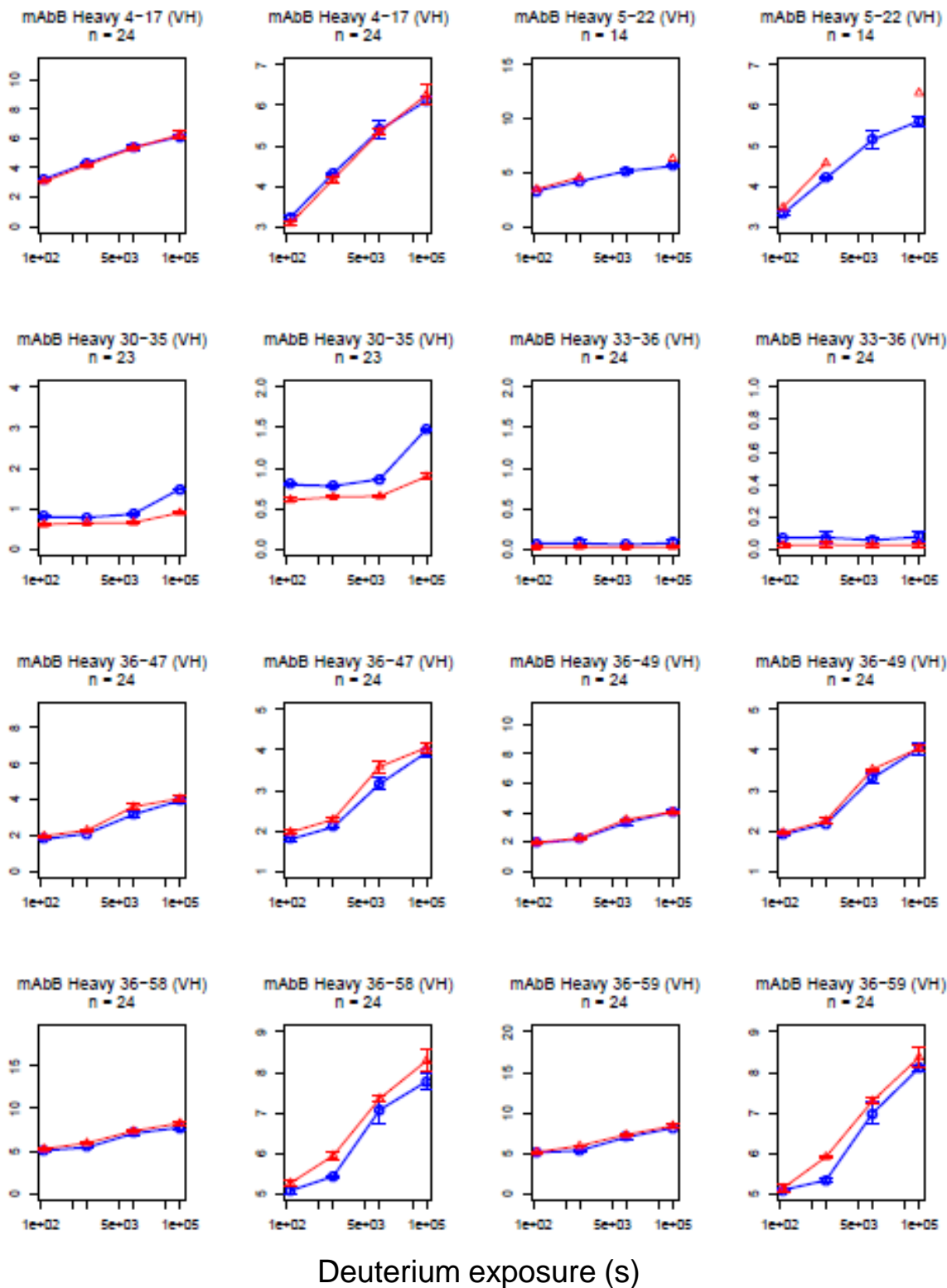




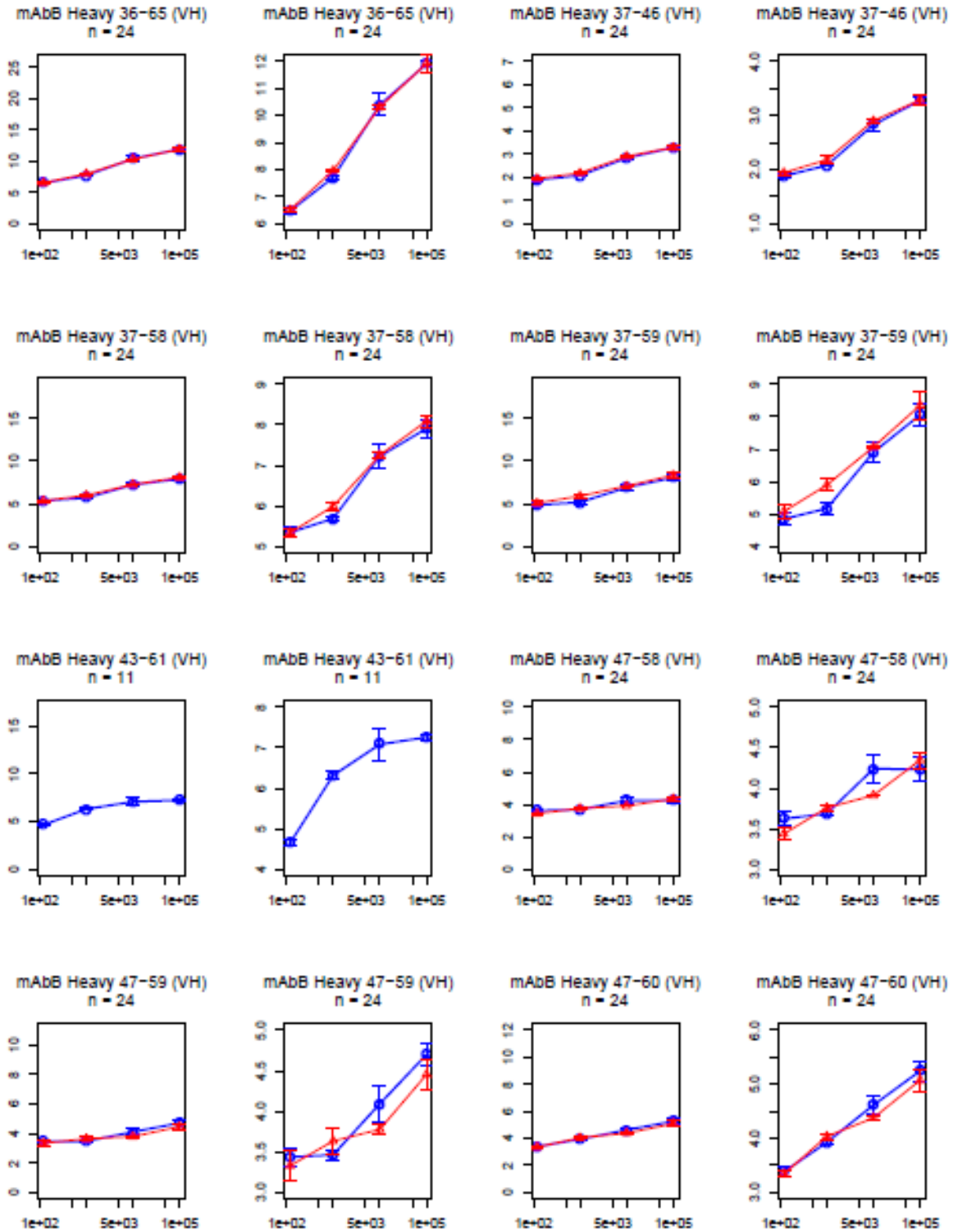


- 100 mM NaCl
- △— 500 mM Na₂SO₄

Mass Increase(Da)

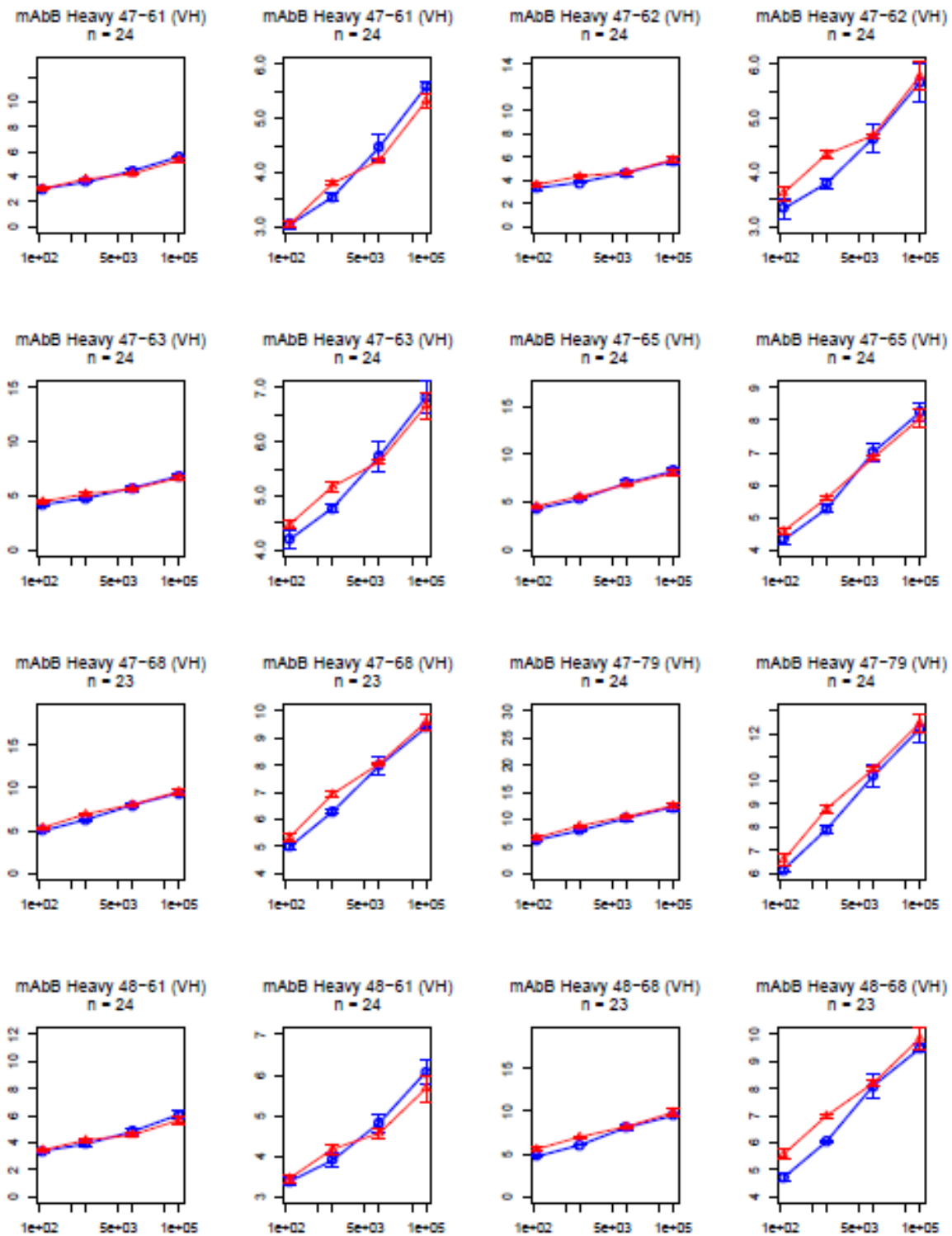


Mass Increase(Da)



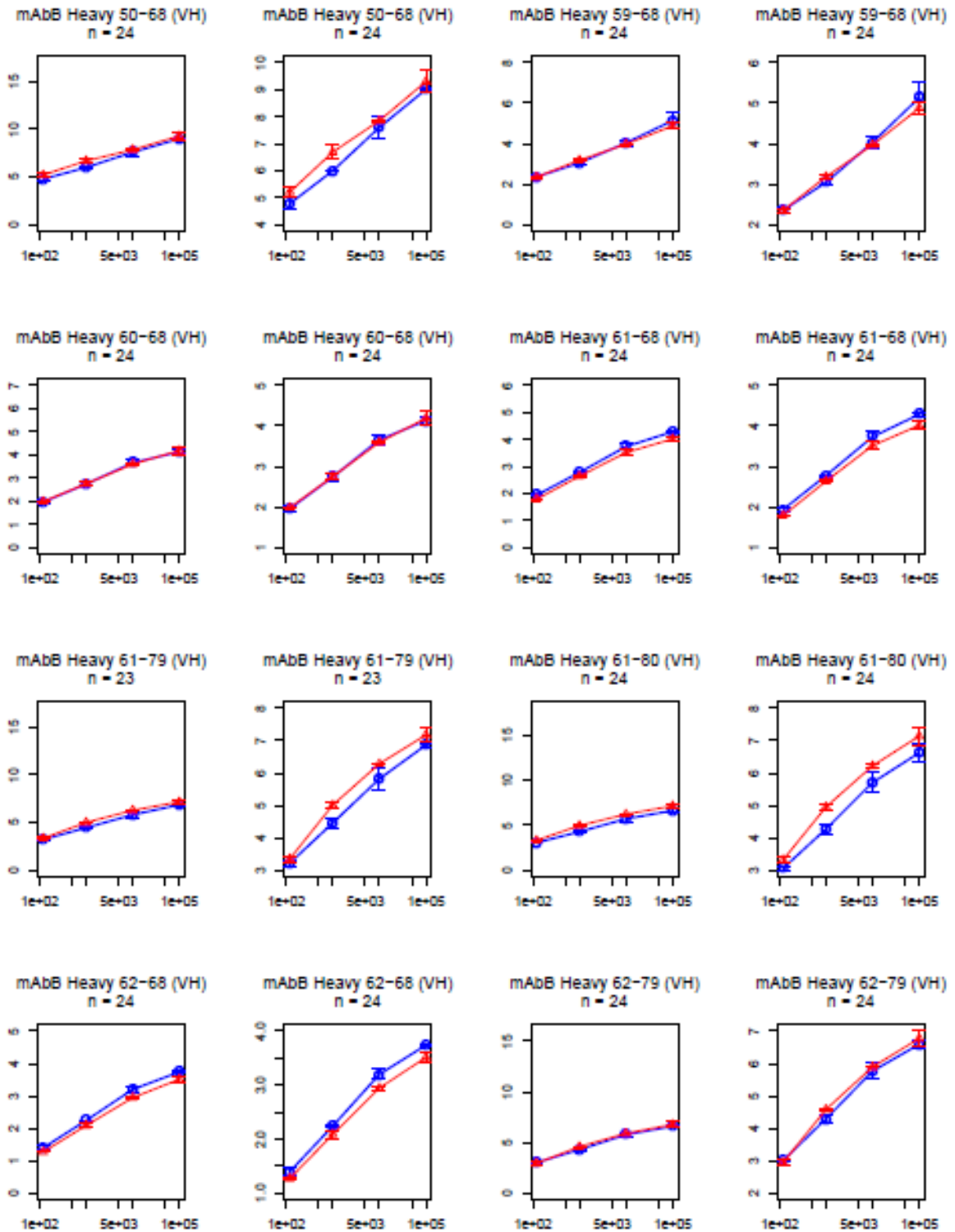
Deuterium exposure (s)

Mass Increase(Da)



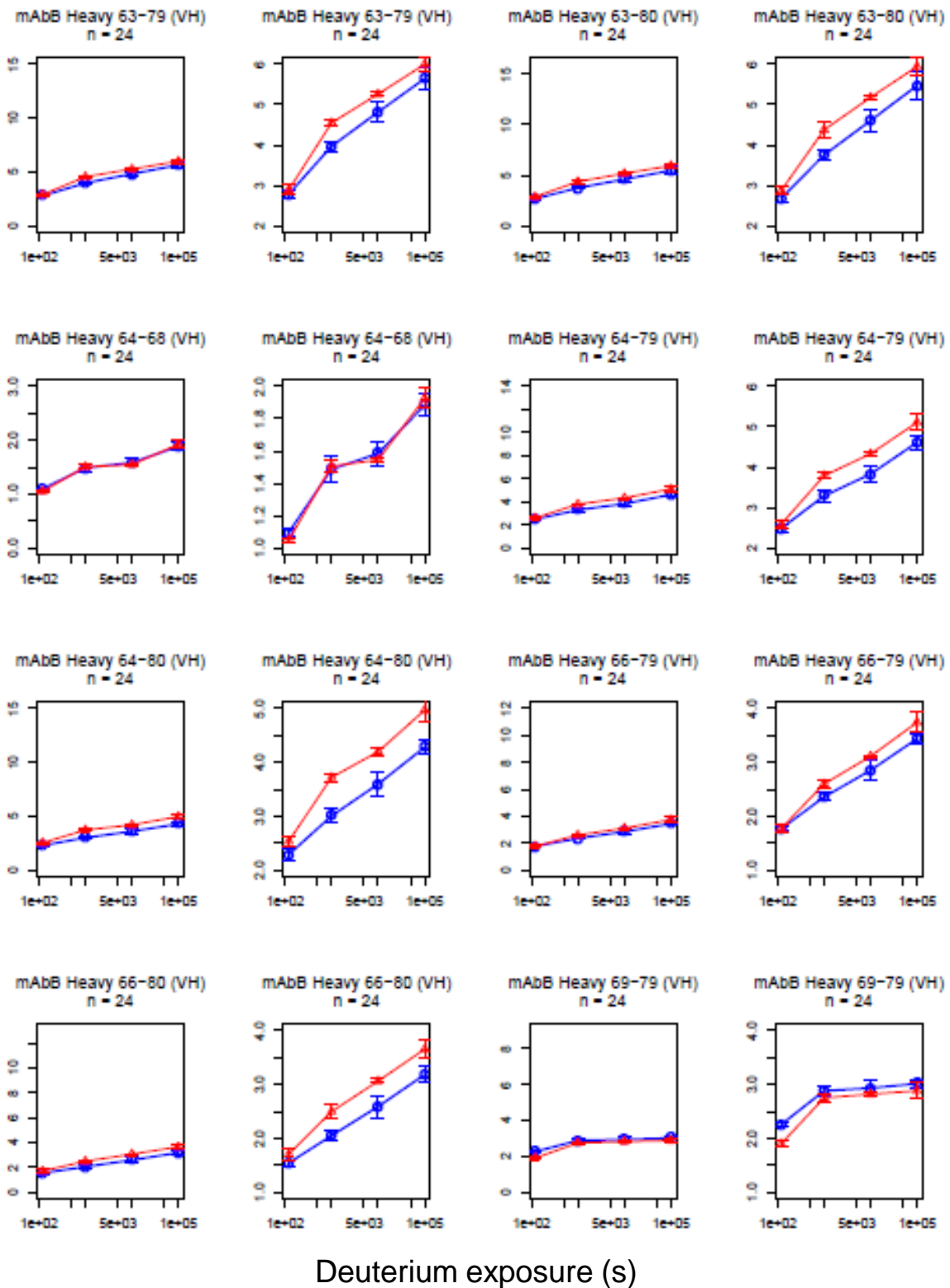
Deuterium exposure (s)

Mass Increase(Da)

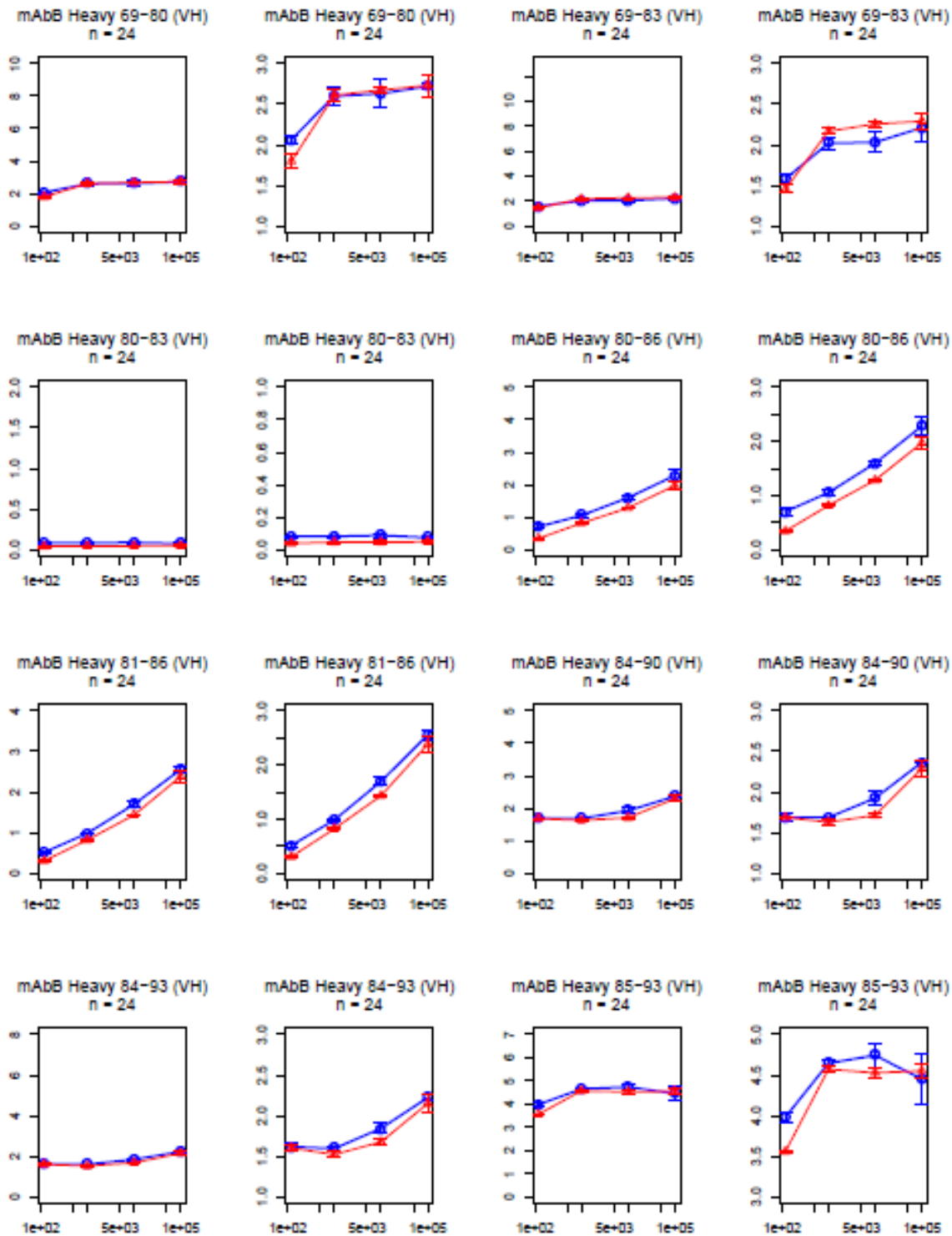


Deuterium exposure (s)

Mass Increase(Da)

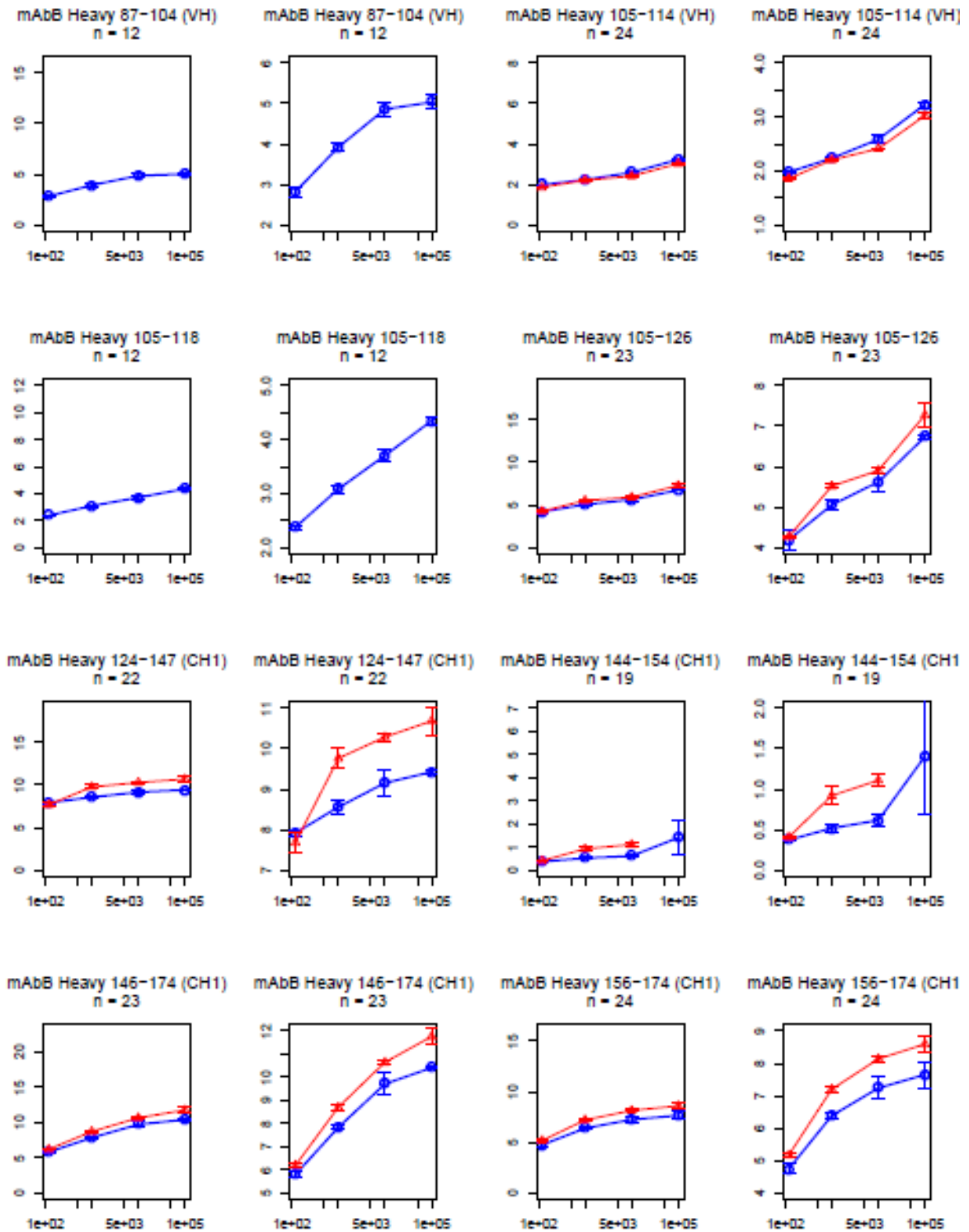


Mass Increase(Da)

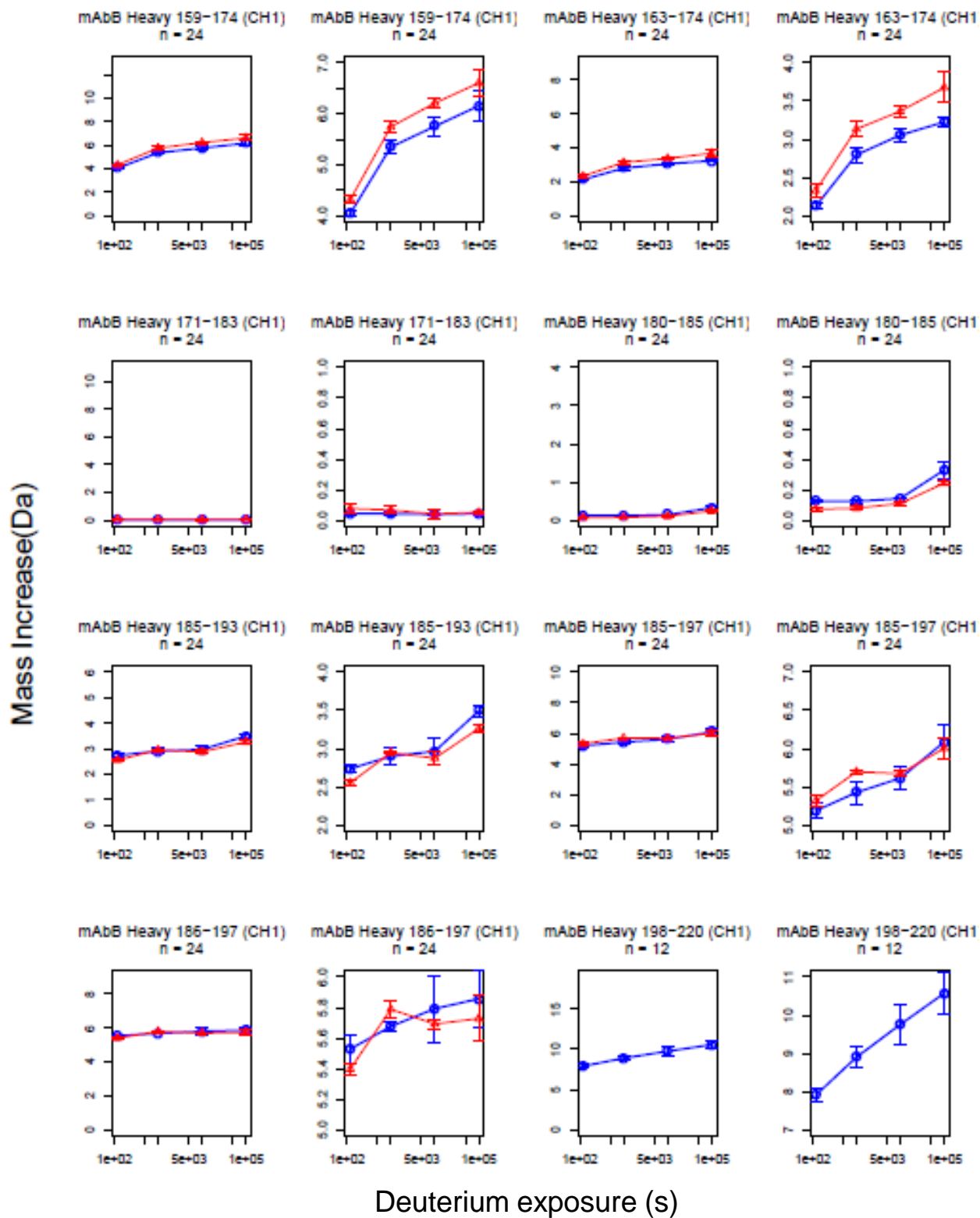


Deuterium exposure (s)

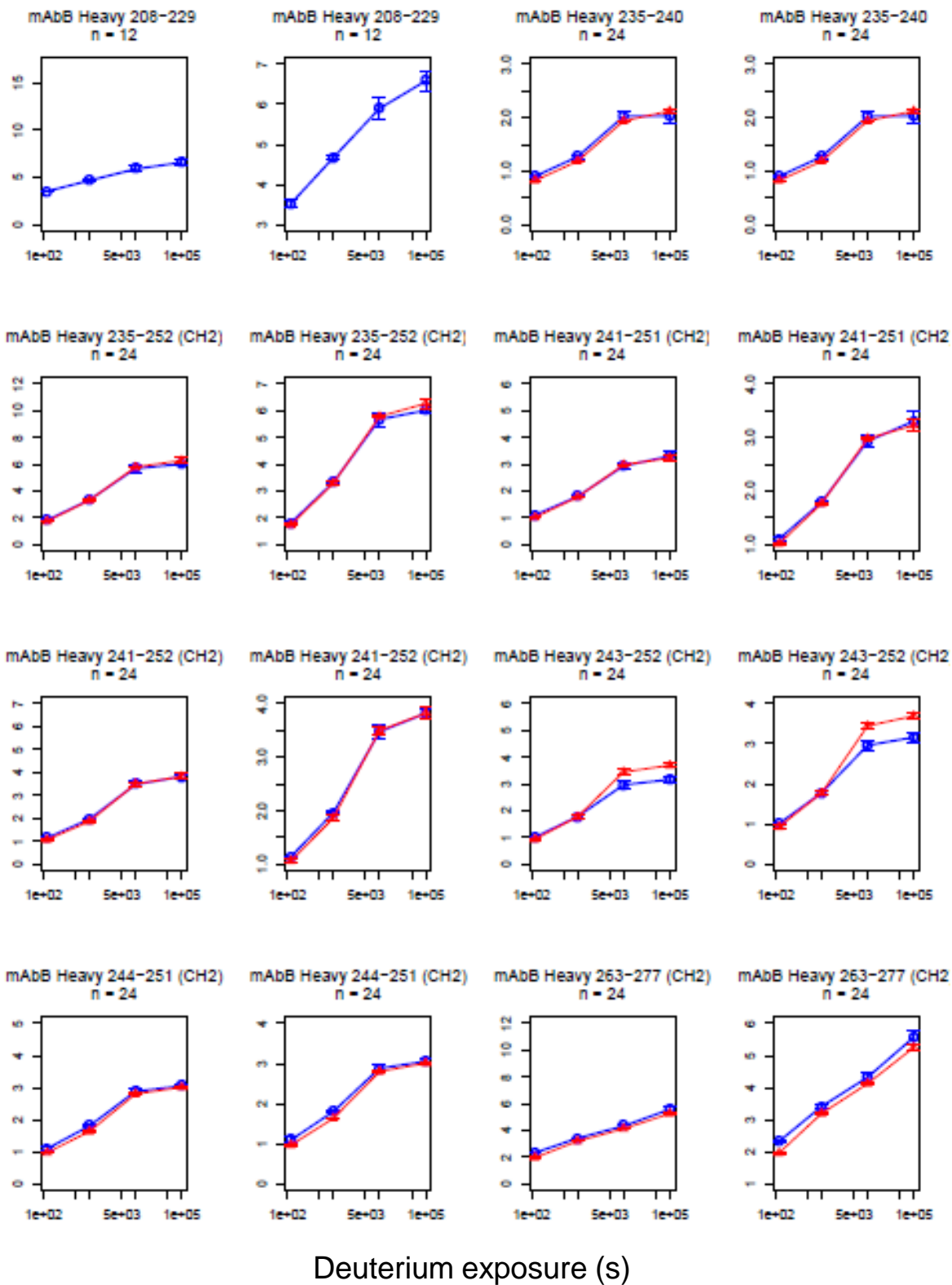
Mass Increase(Da)



Deuterium exposure (s)

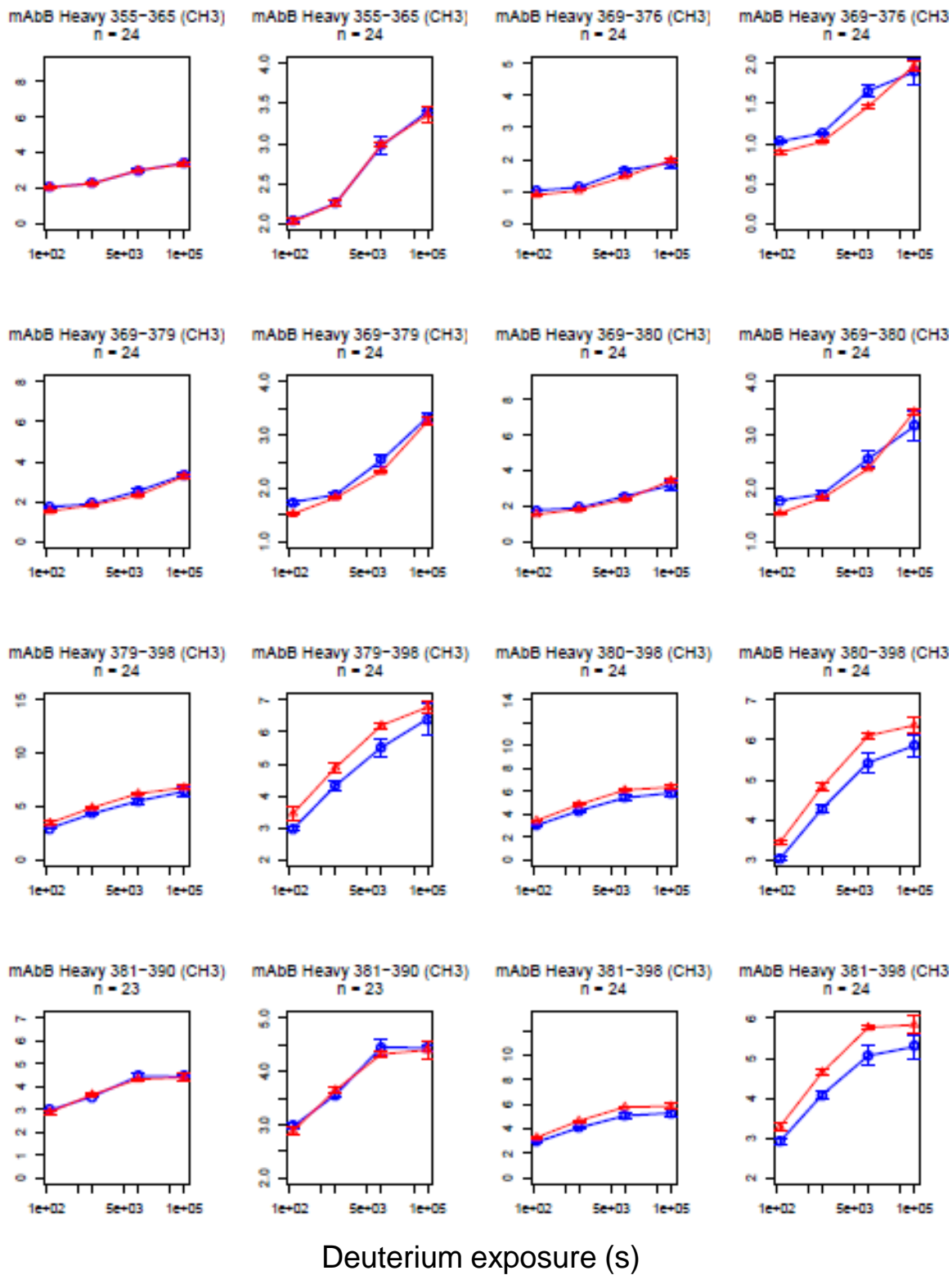


Mass Increase(Da)

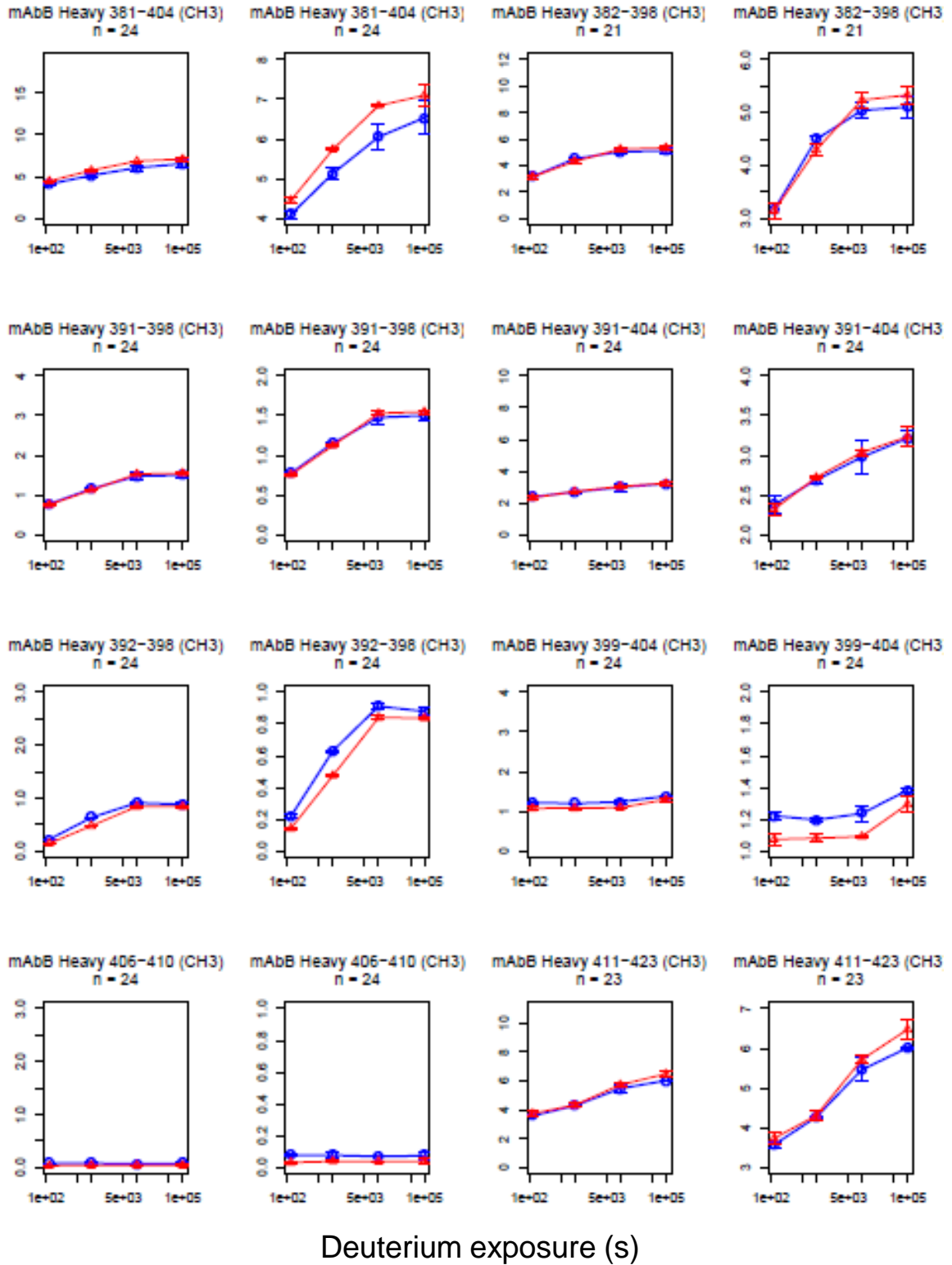


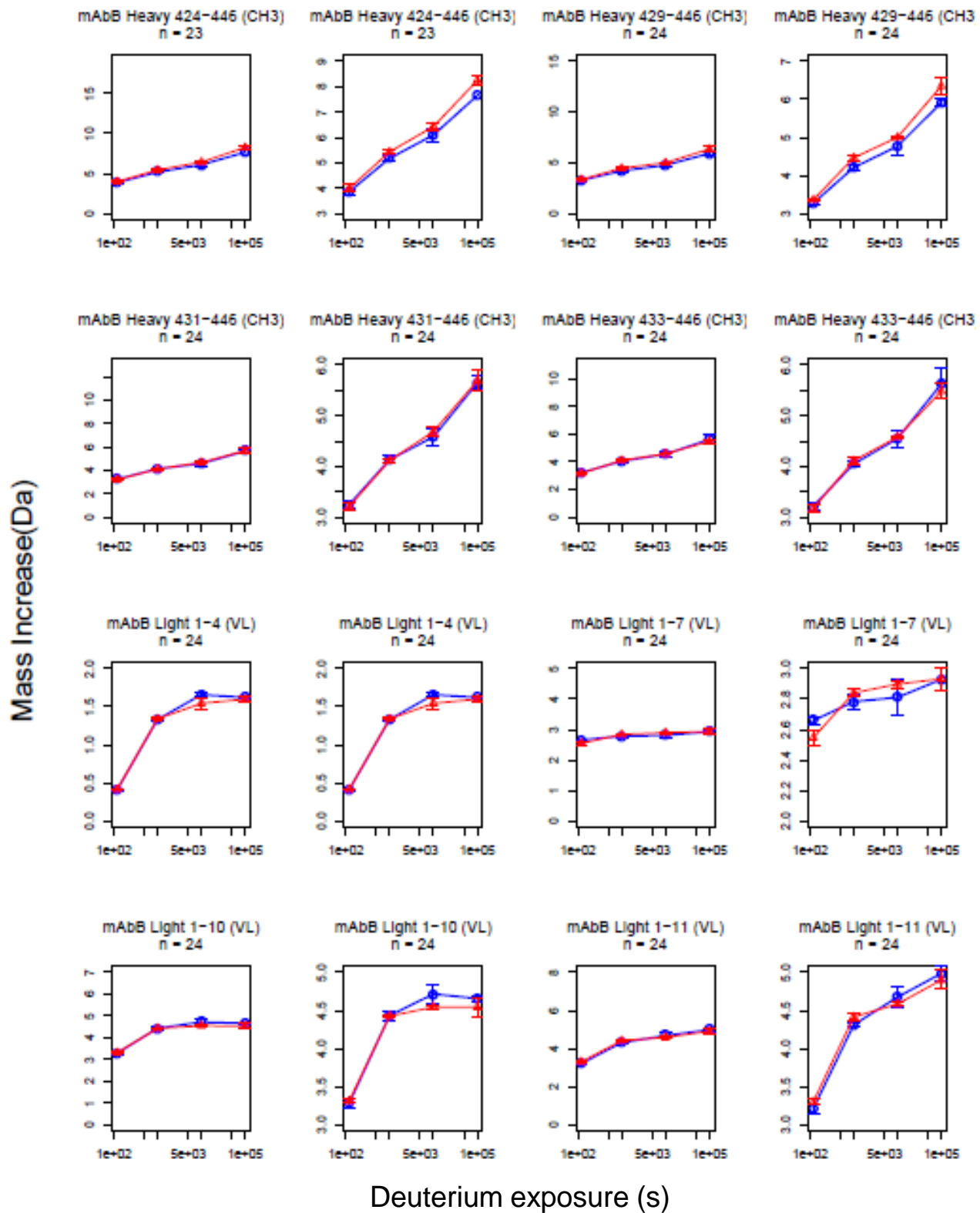
Deuterium exposure (s)

Mass Increase(Da)

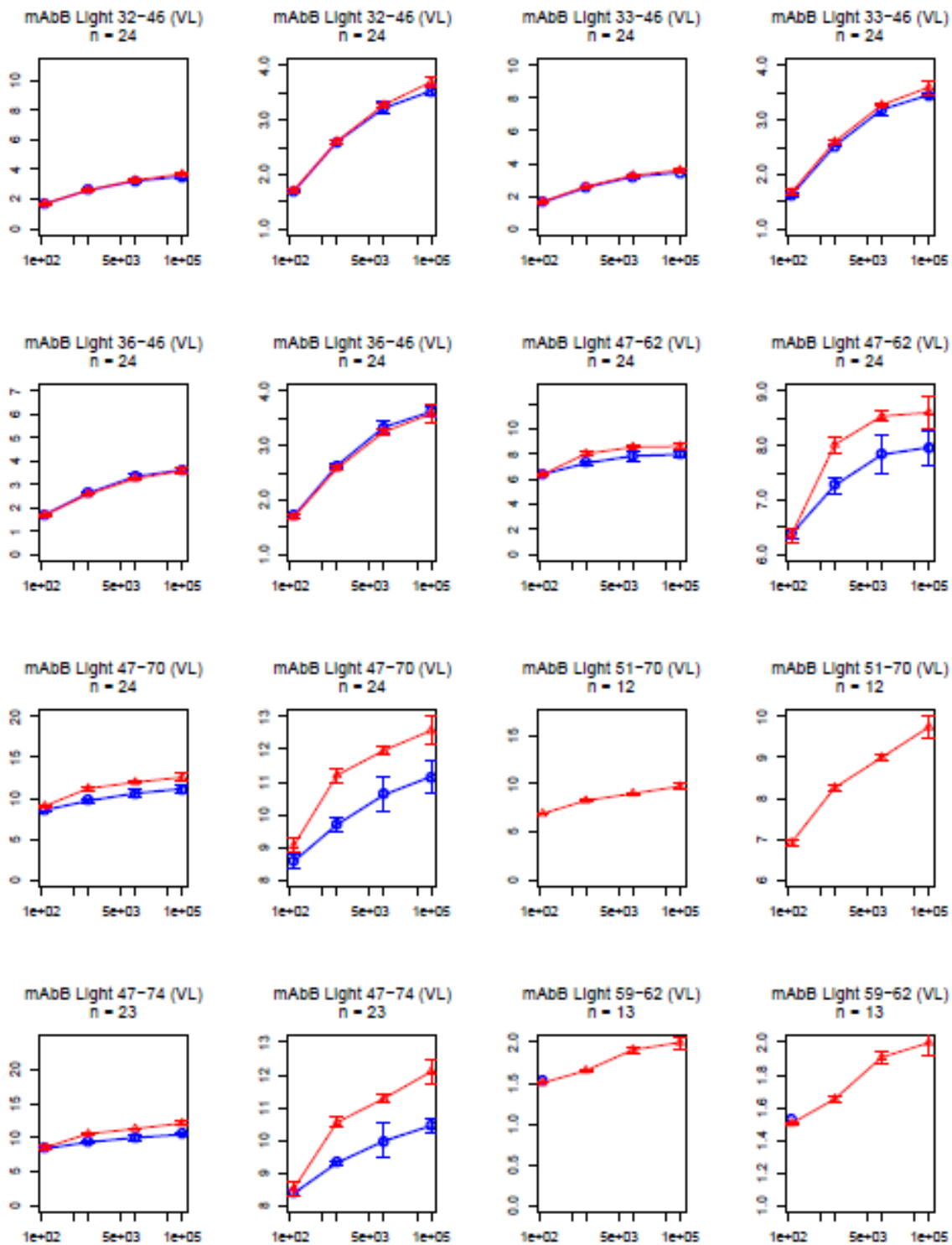


Mass Increase(Da)



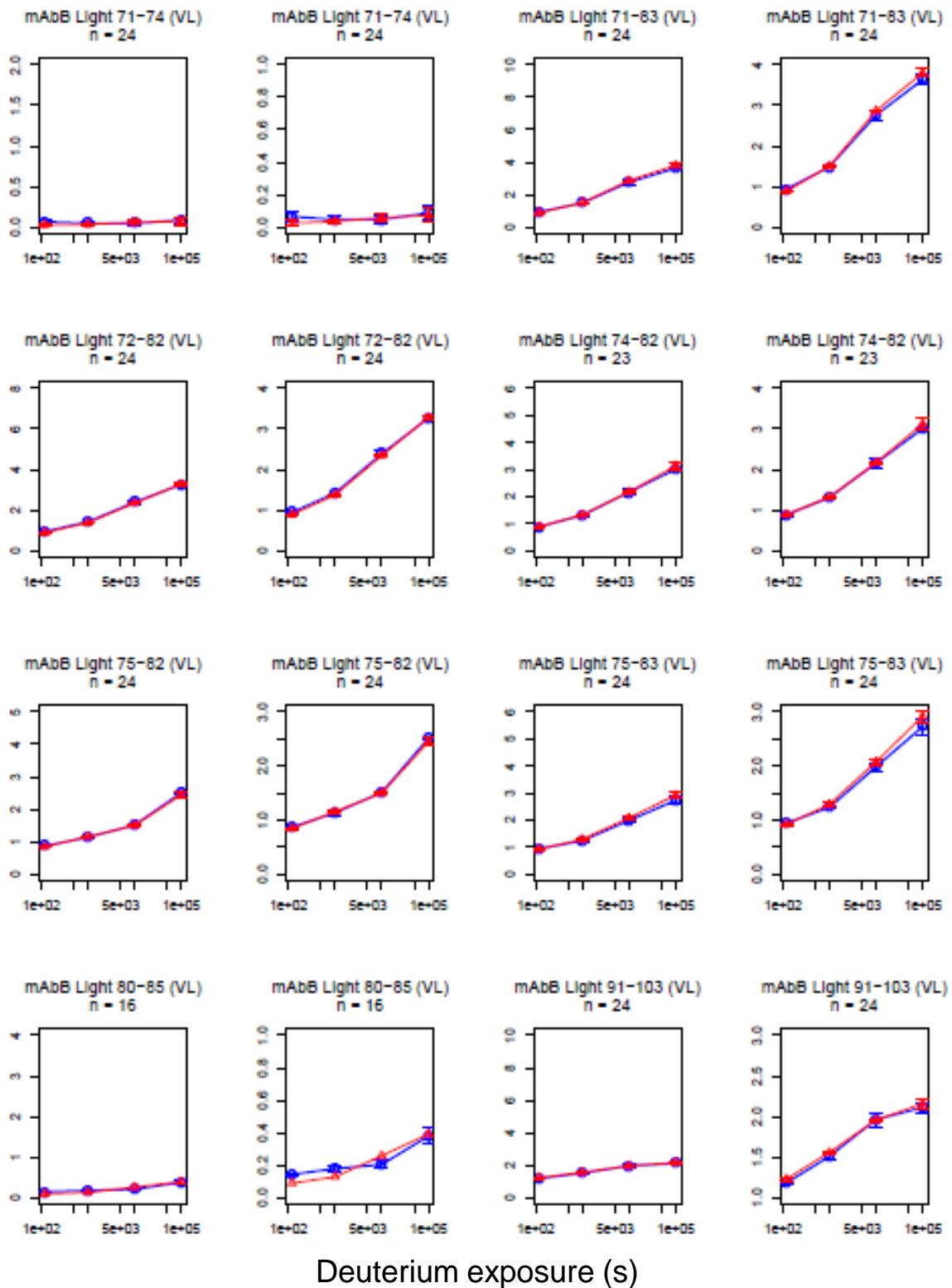


Mass Increase(Da)

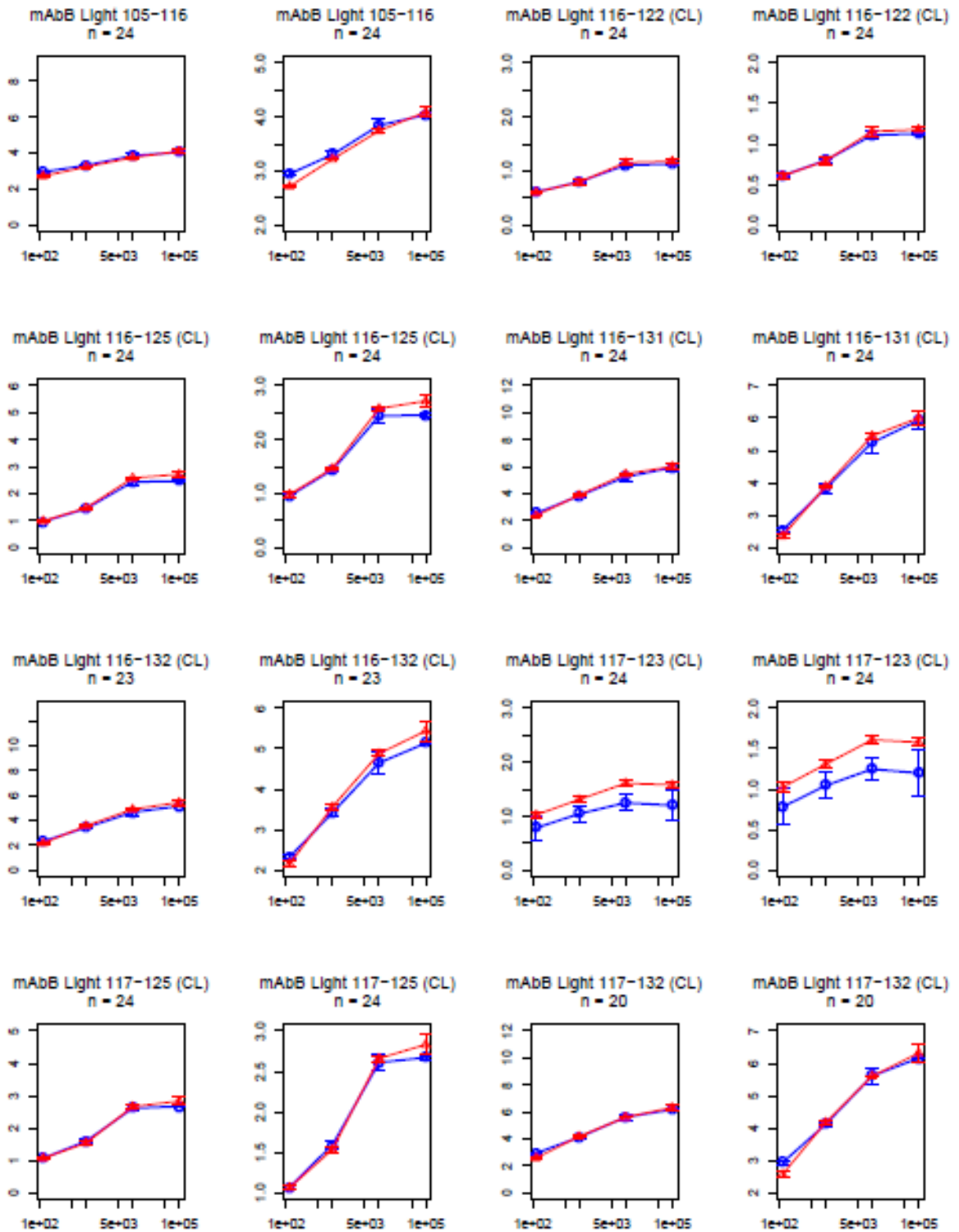


Deuterium exposure (s)

Mass Increase(Da)

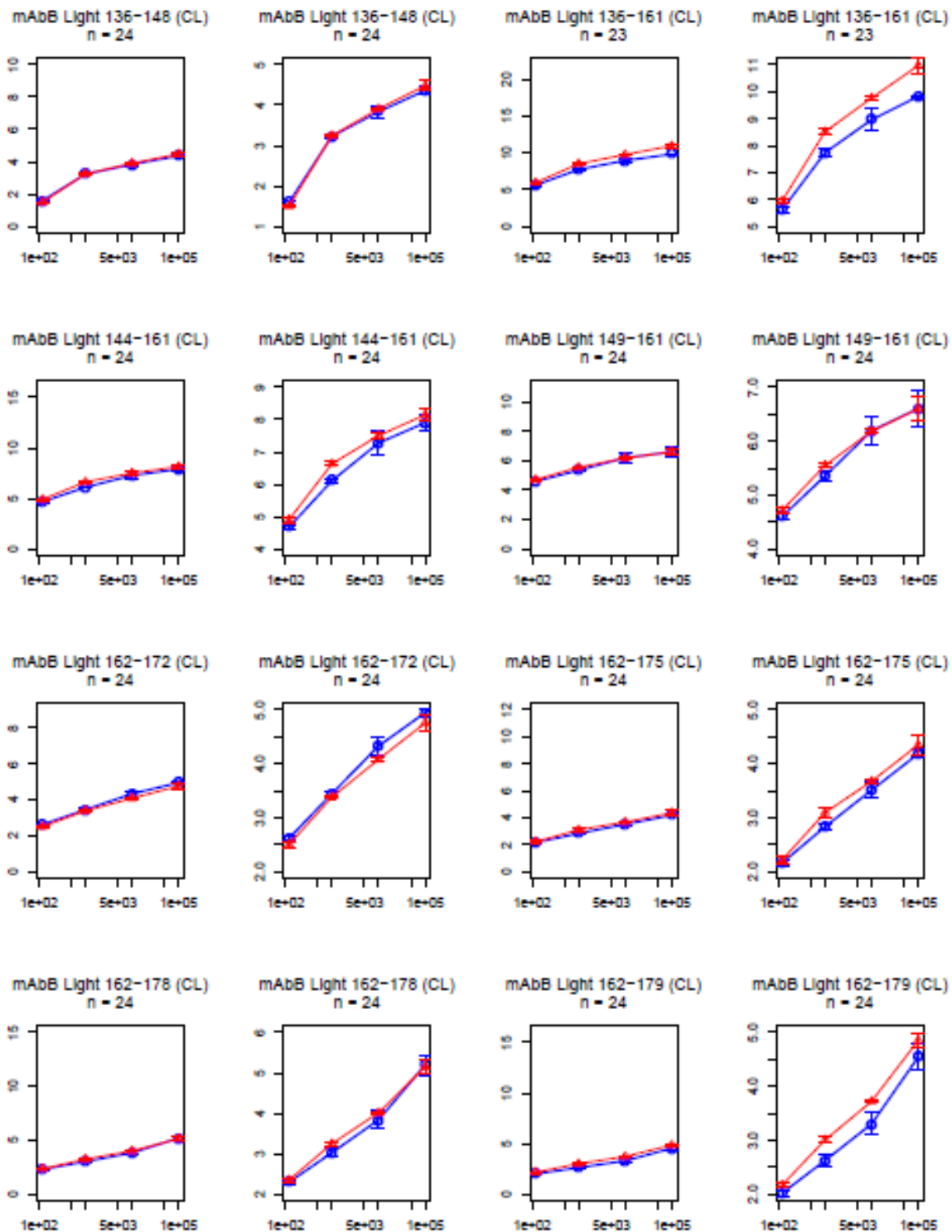


Mass Increase(Da)

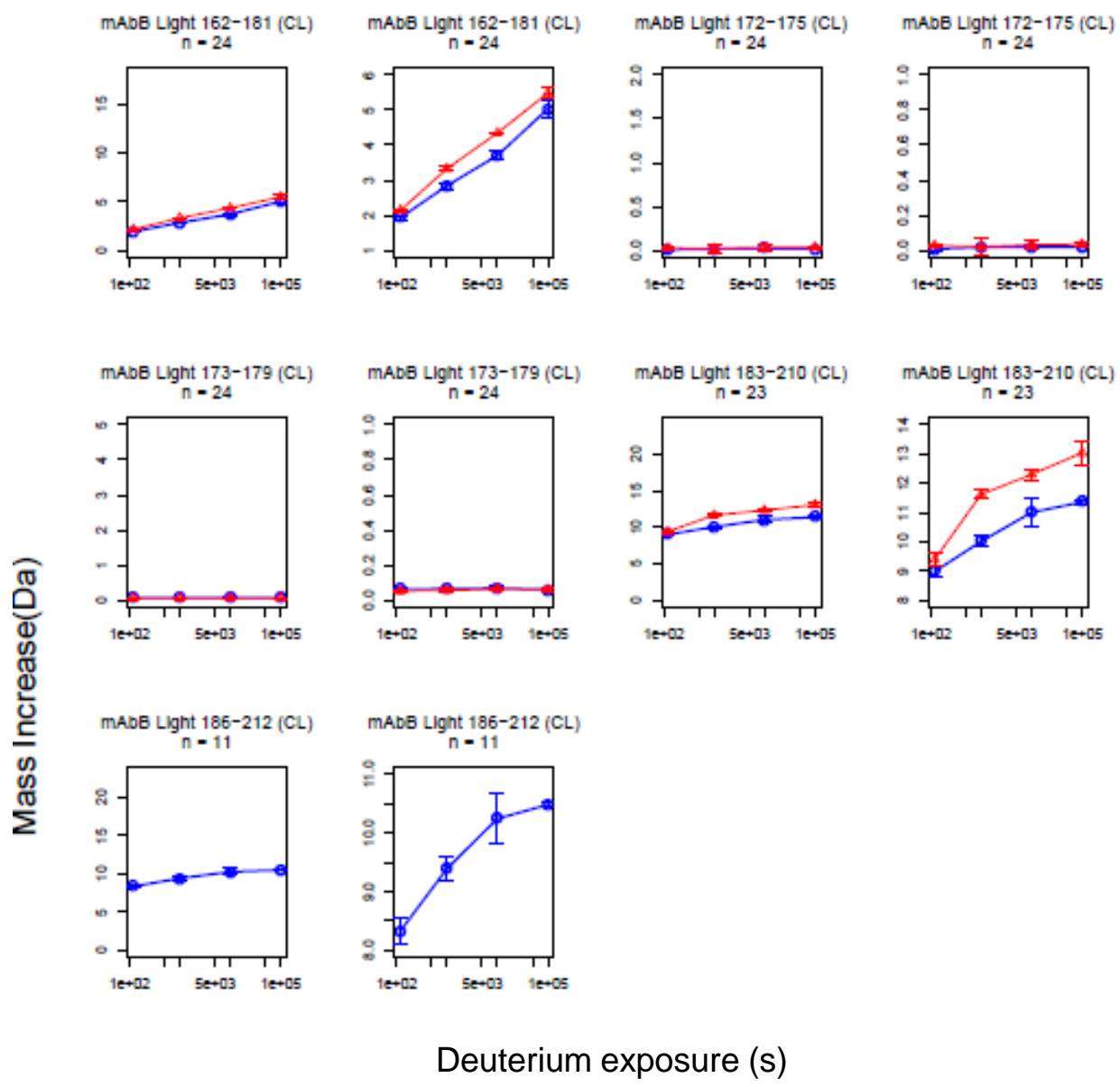


Deuterium exposure (s)

Mass Increase(Da)

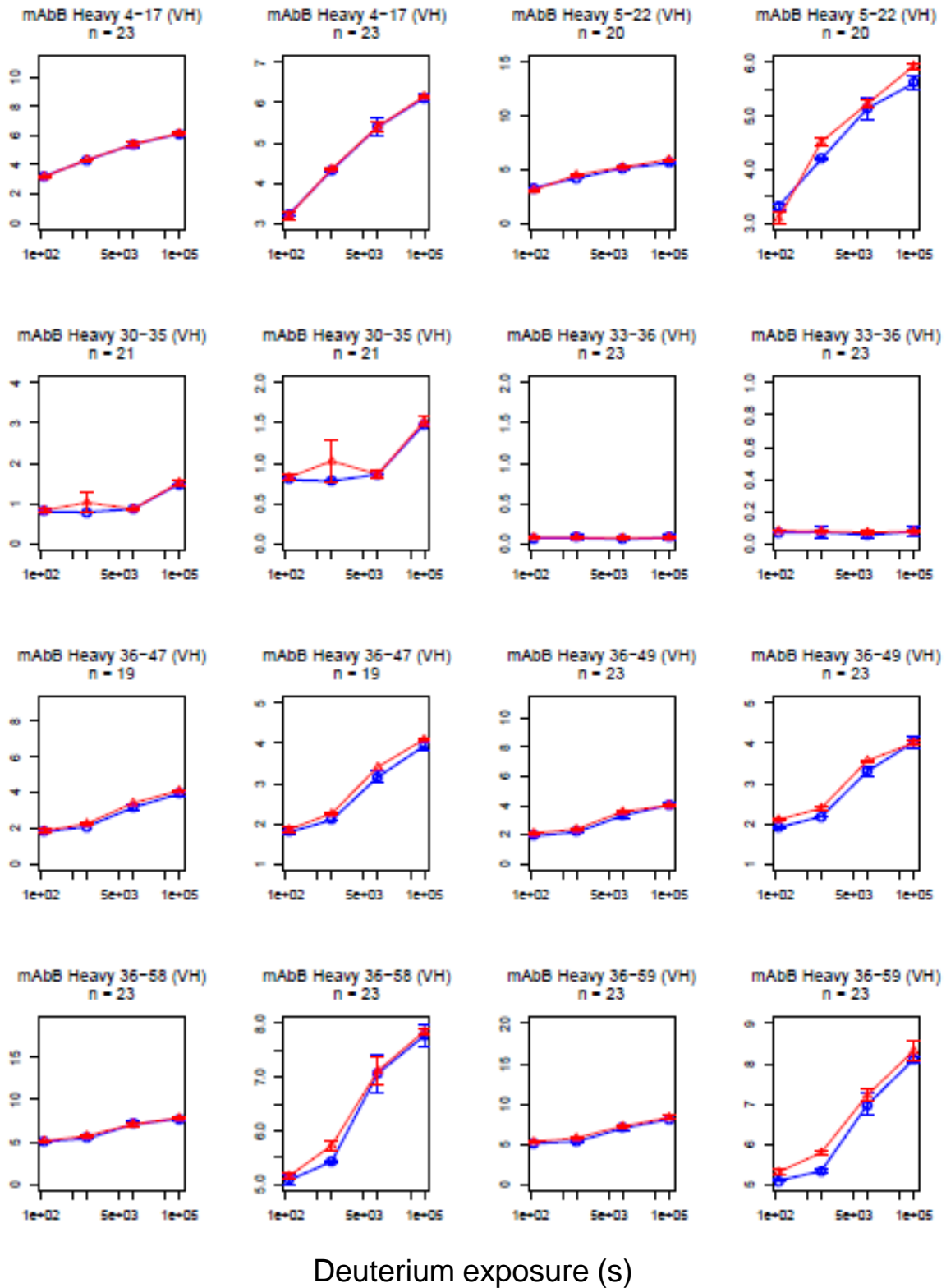


Deuterium exposure (s)

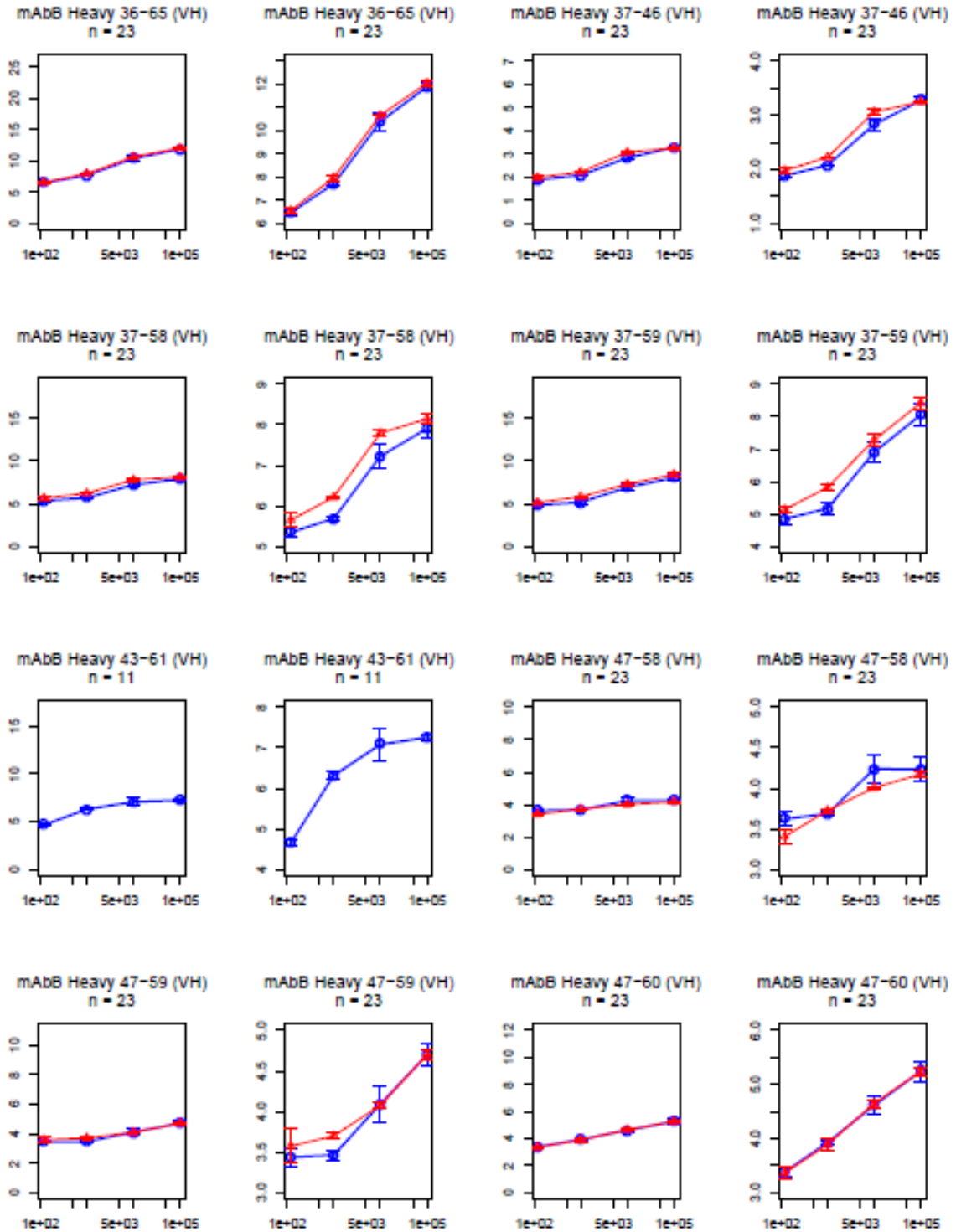


—○— 100 mM NaCl
—△— 500 mM NaSCN

Mass Increase(Da)

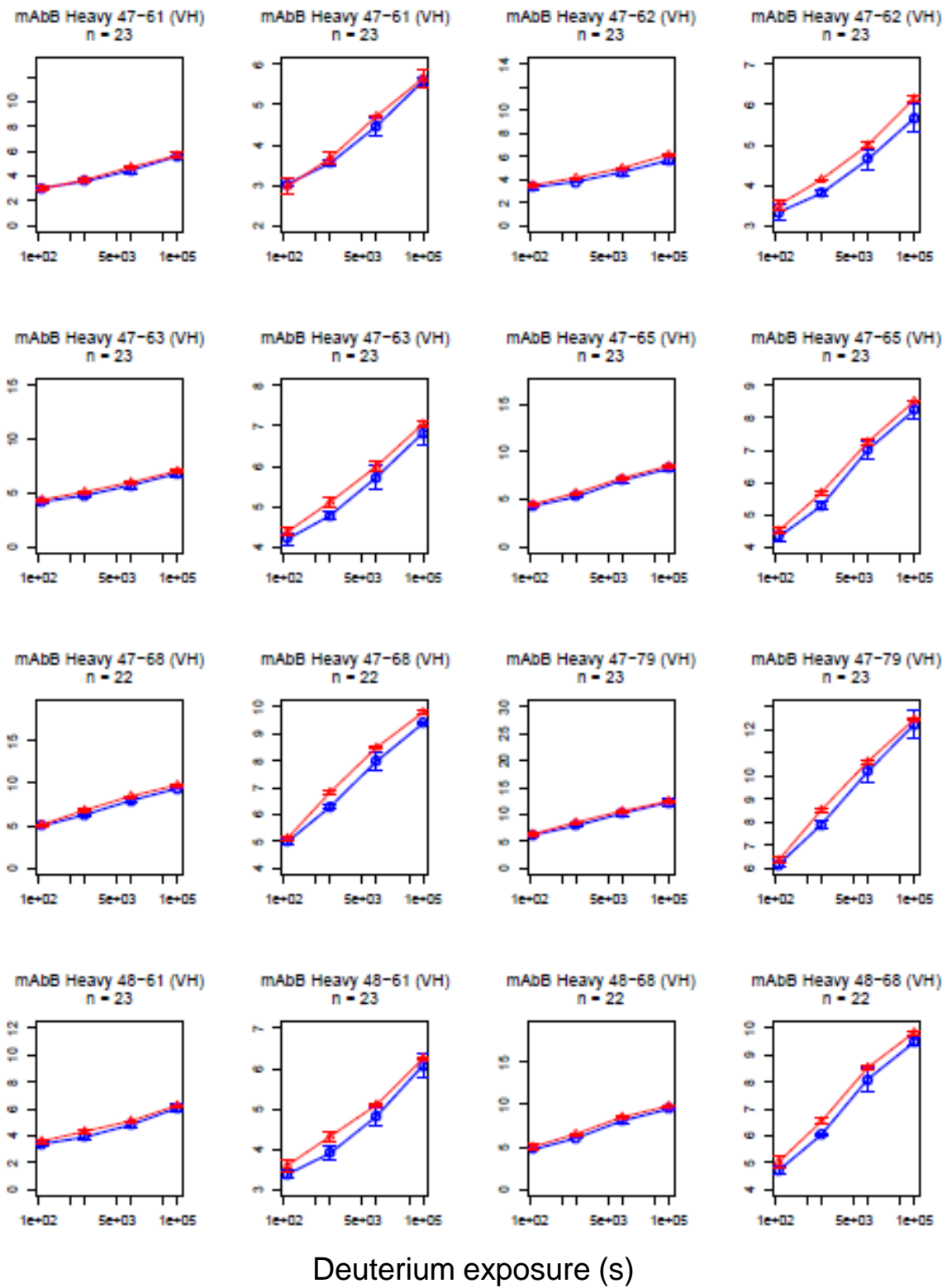


Mass Increase(Da)

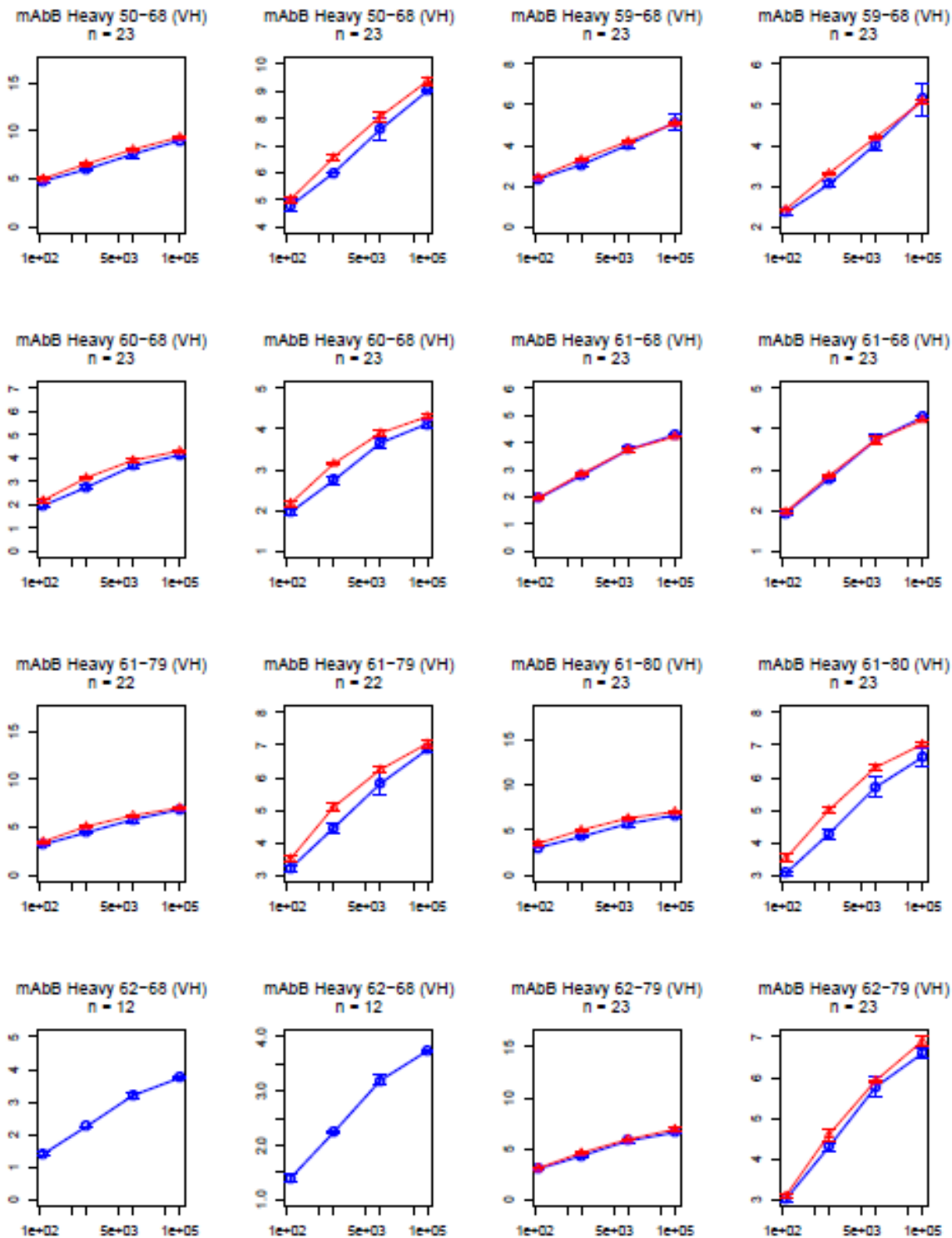


Deuterium exposure (s)

Mass Increase(Da)

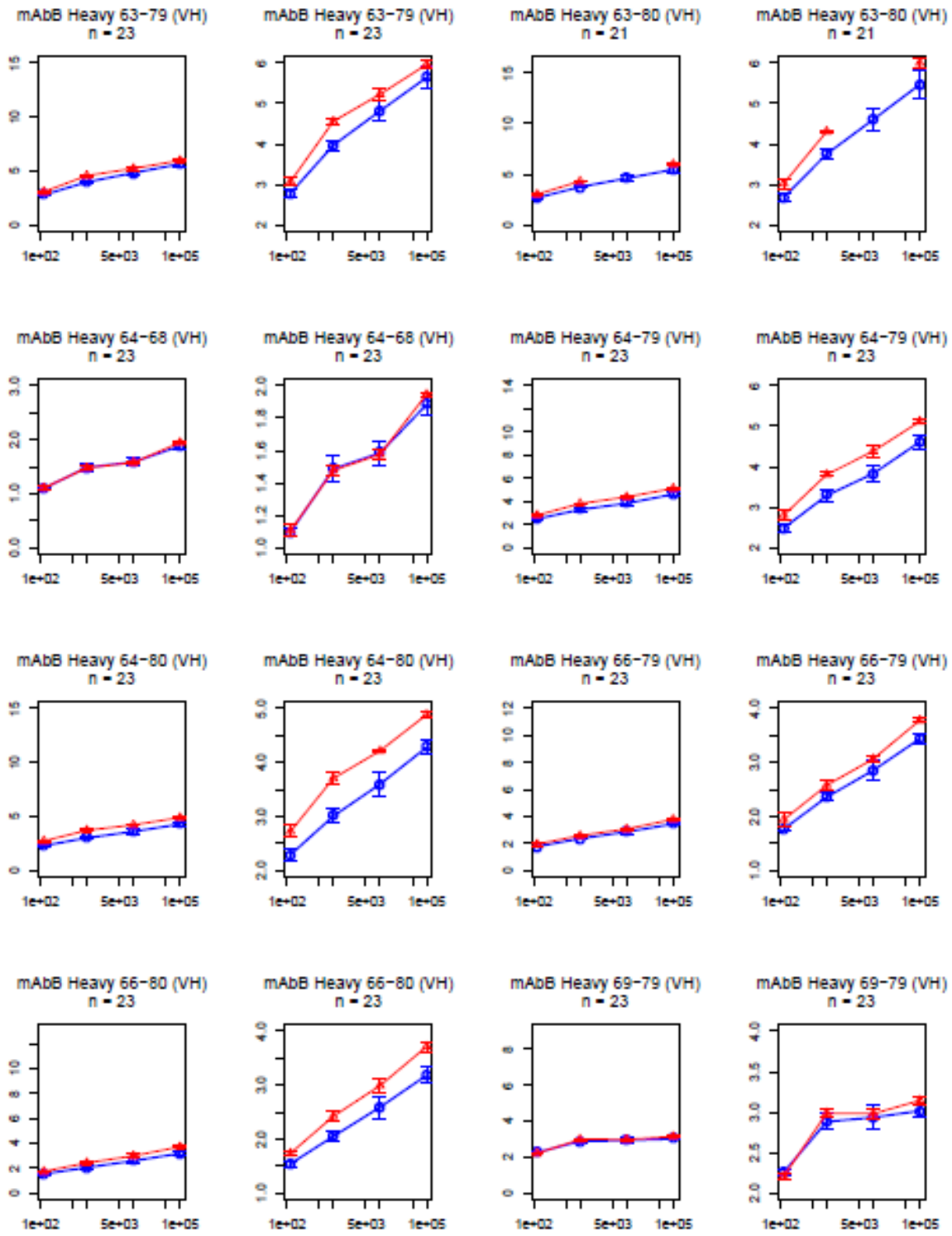


Mass Increase(Da)



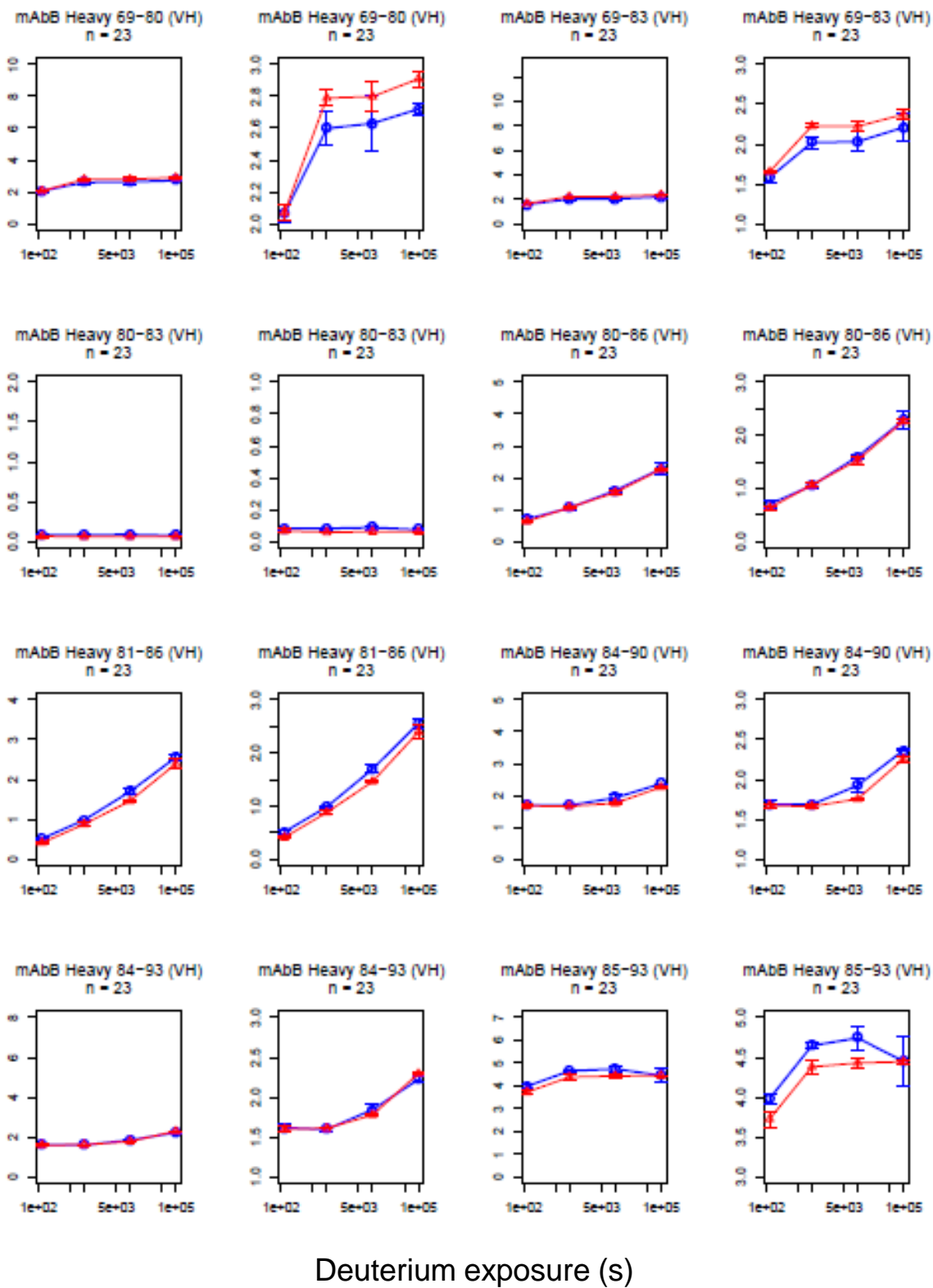
Deuterium exposure (s)

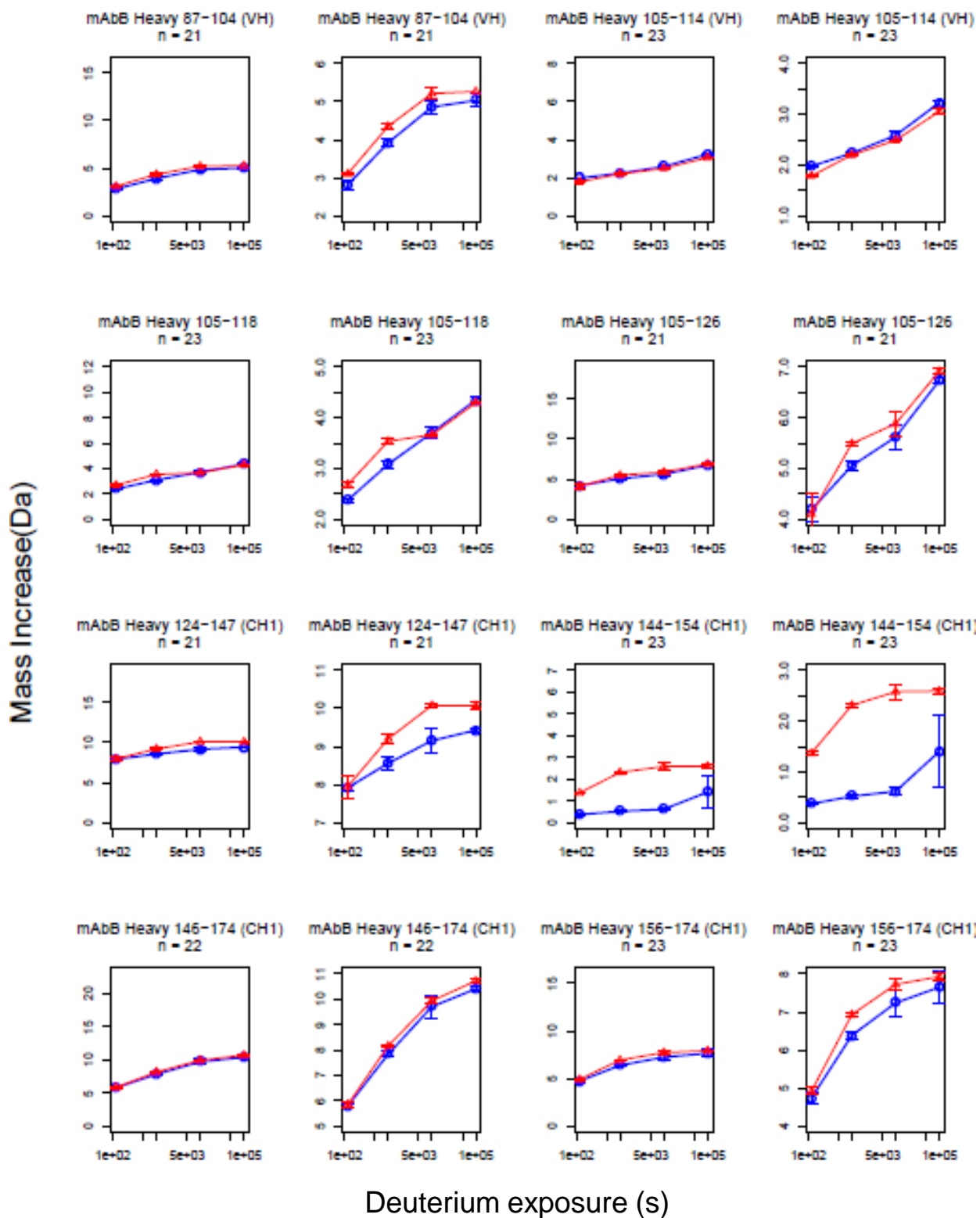
Mass Increase(Da)



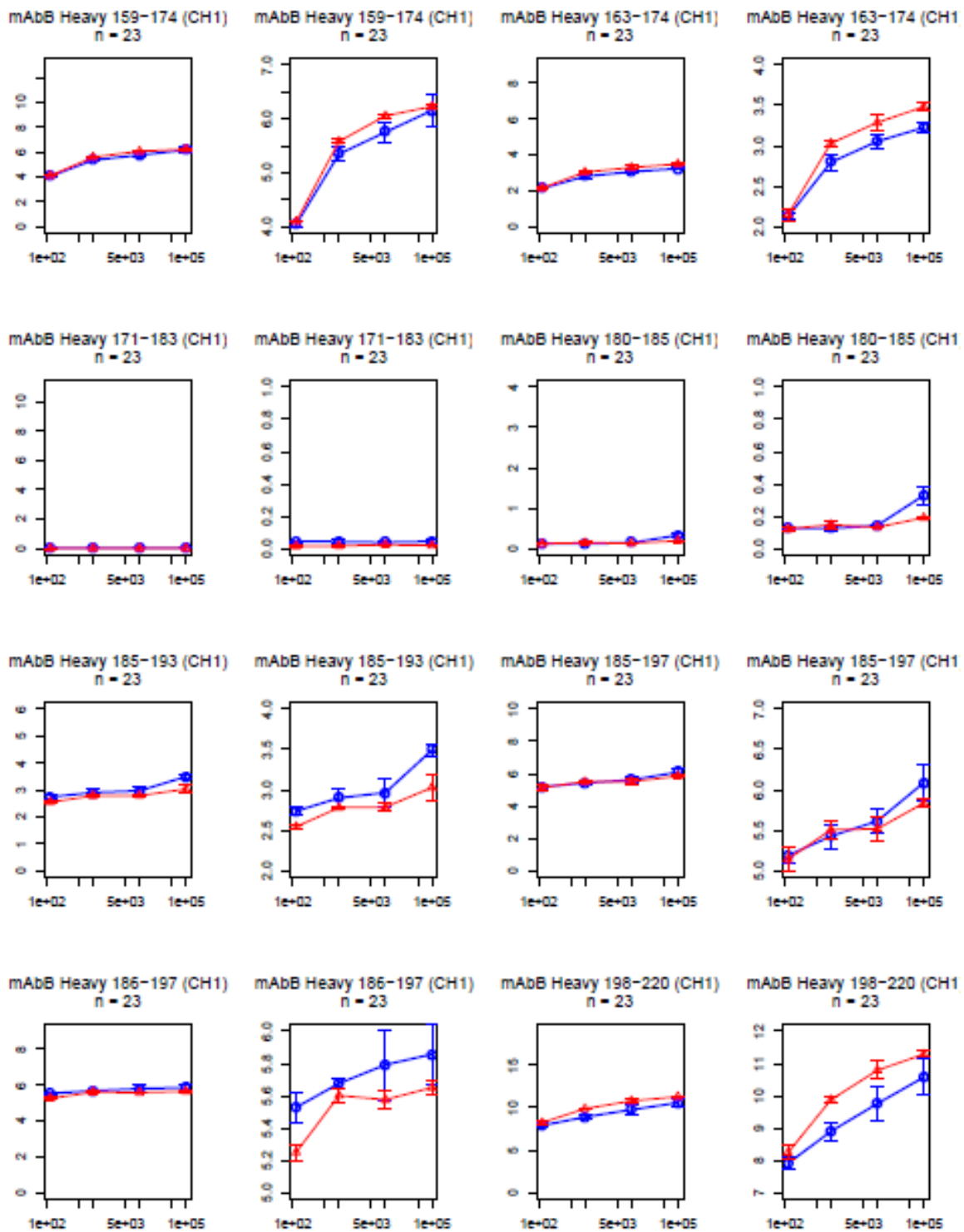
Deuterium exposure (s)

Mass Increase(Da)

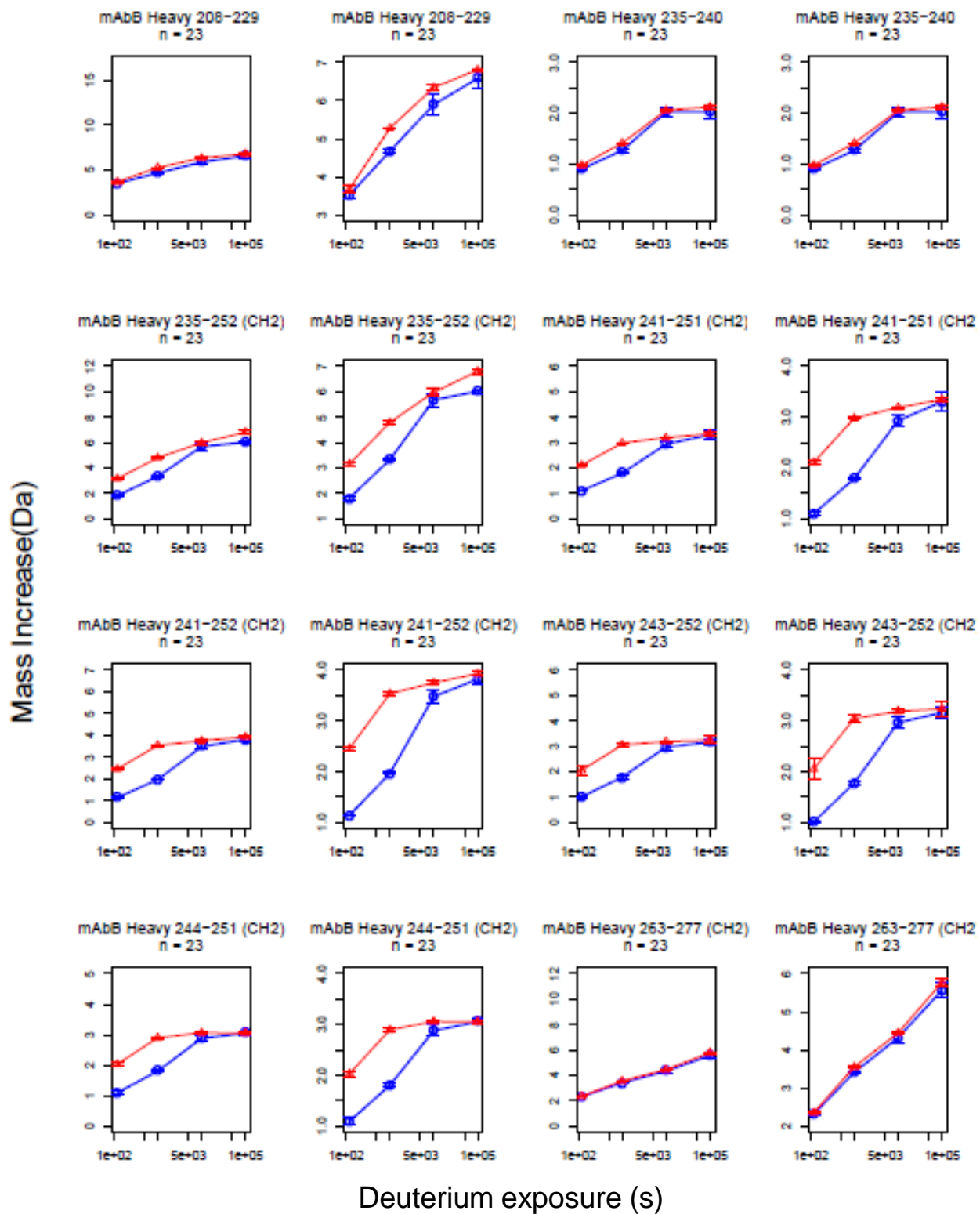


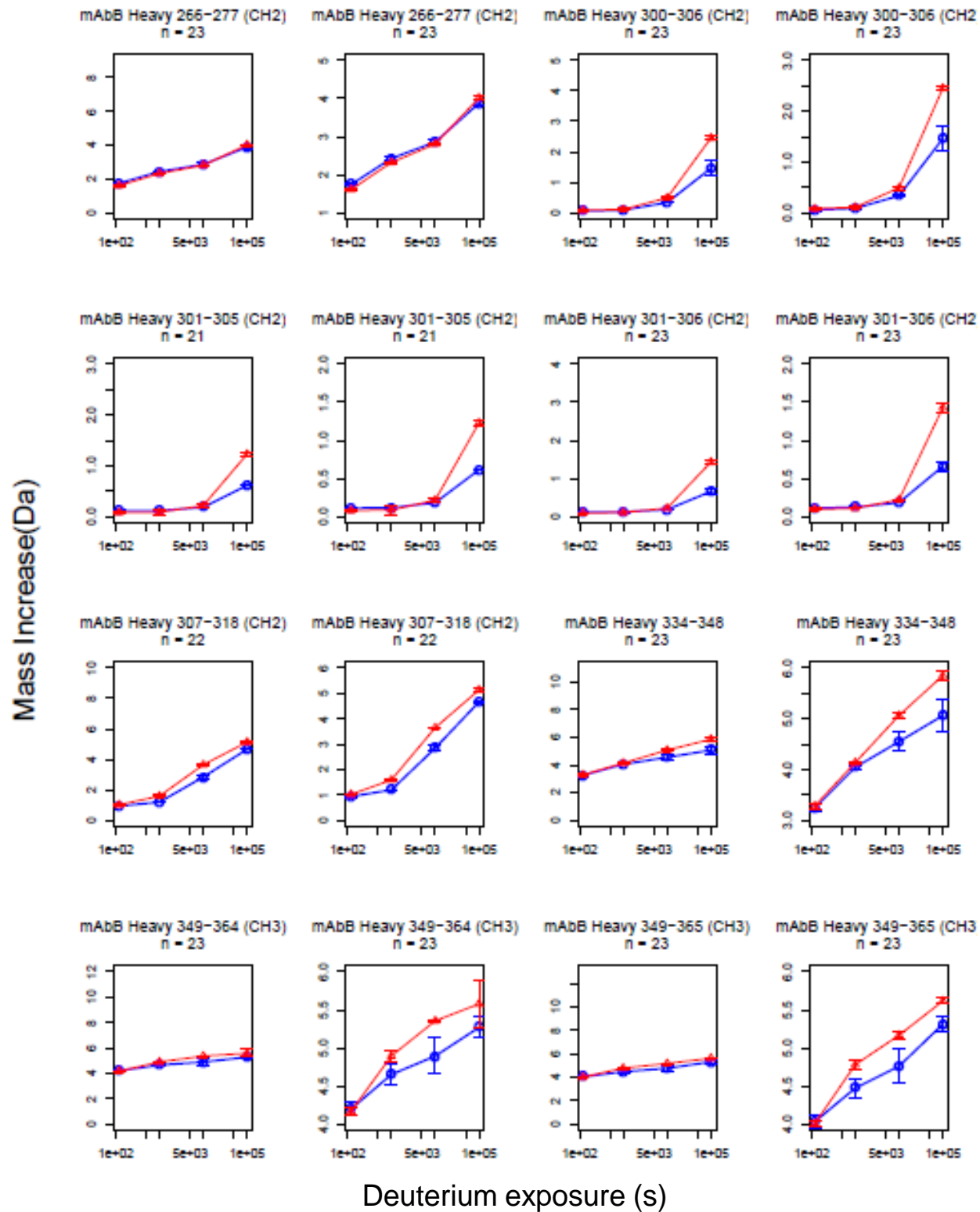


Mass Increase(Da)

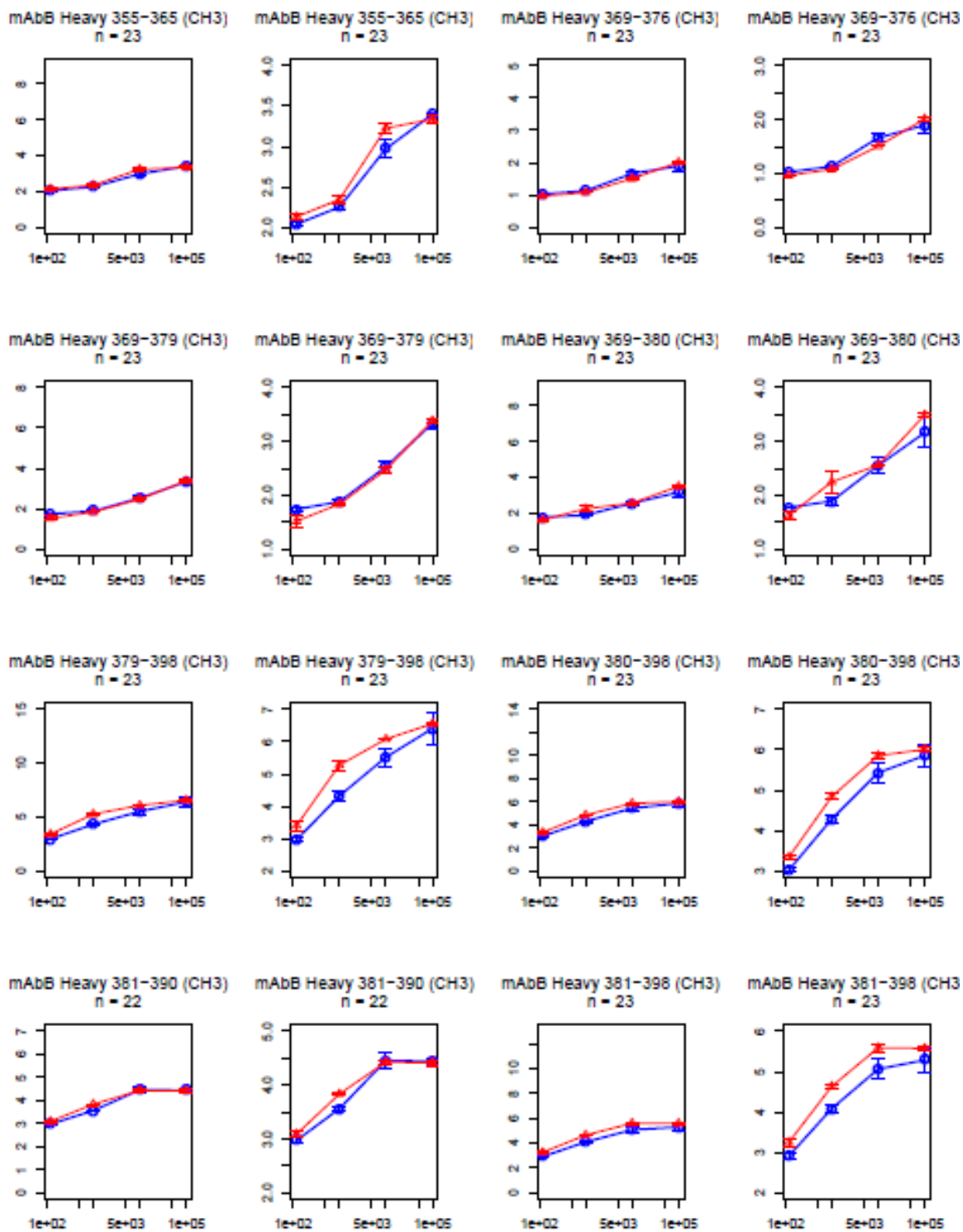


Deuterium exposure (s)



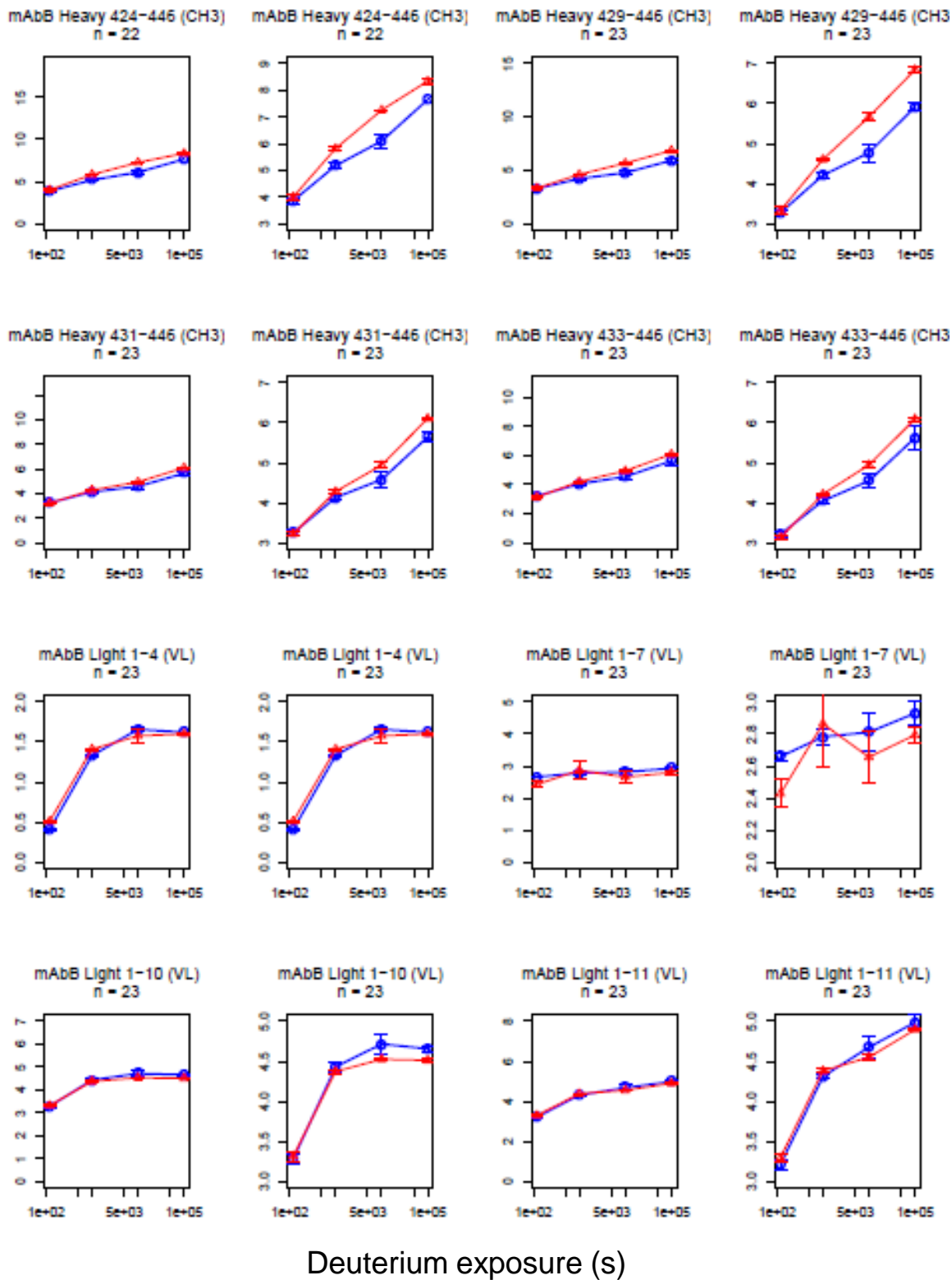


Mass Increase(Da)

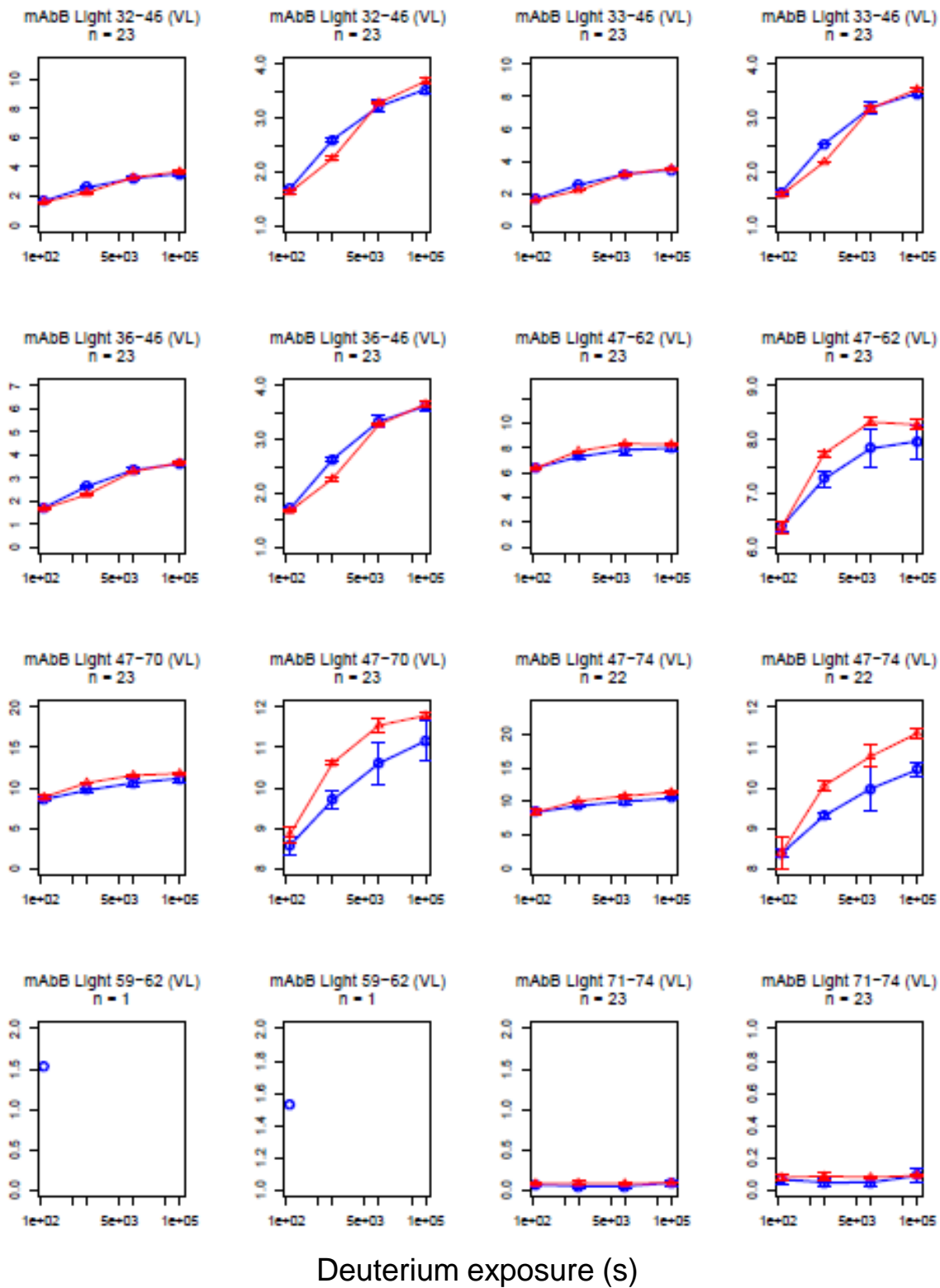


Deuterium exposure (s)

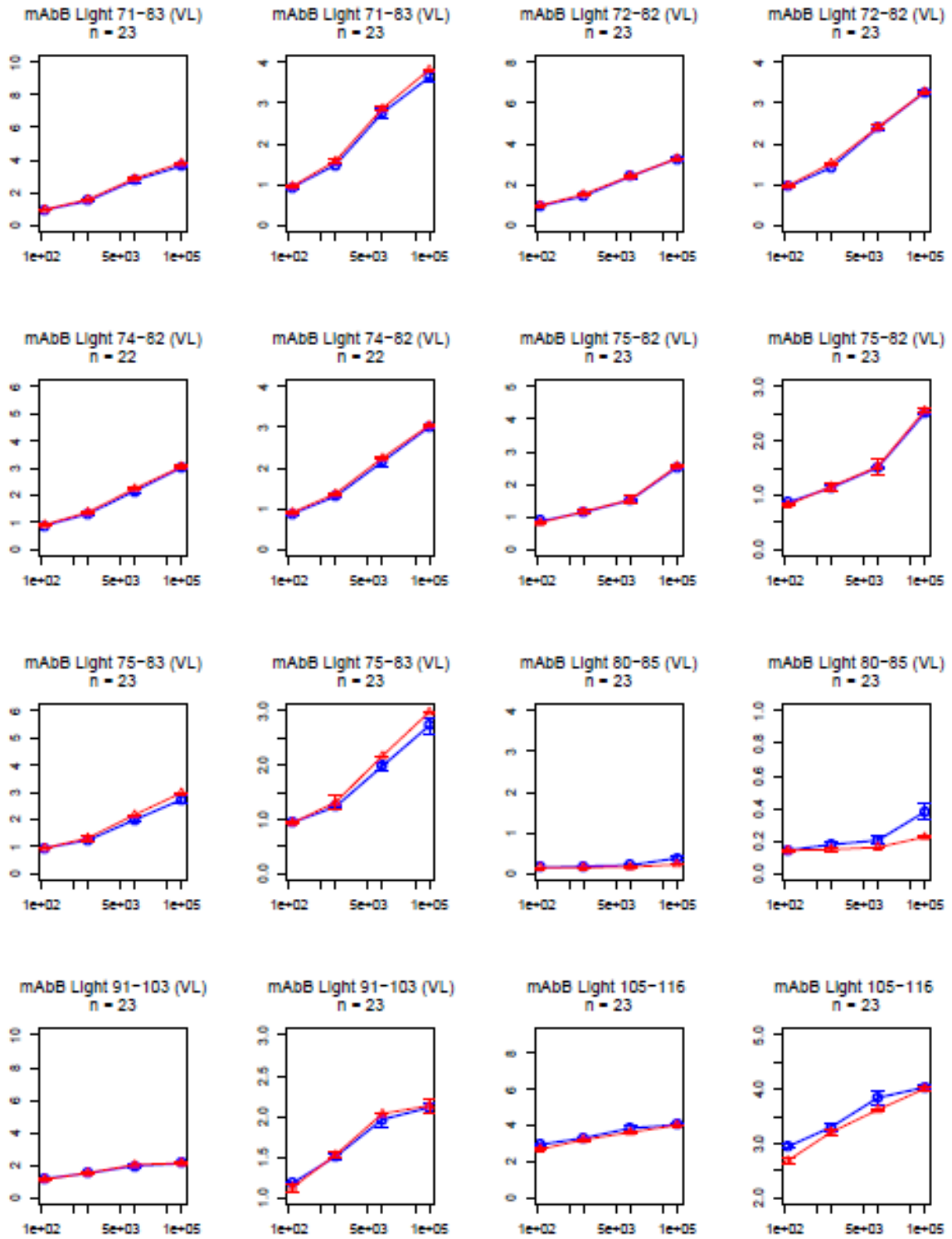
Mass Increase(Da)



Mass Increase(Da)

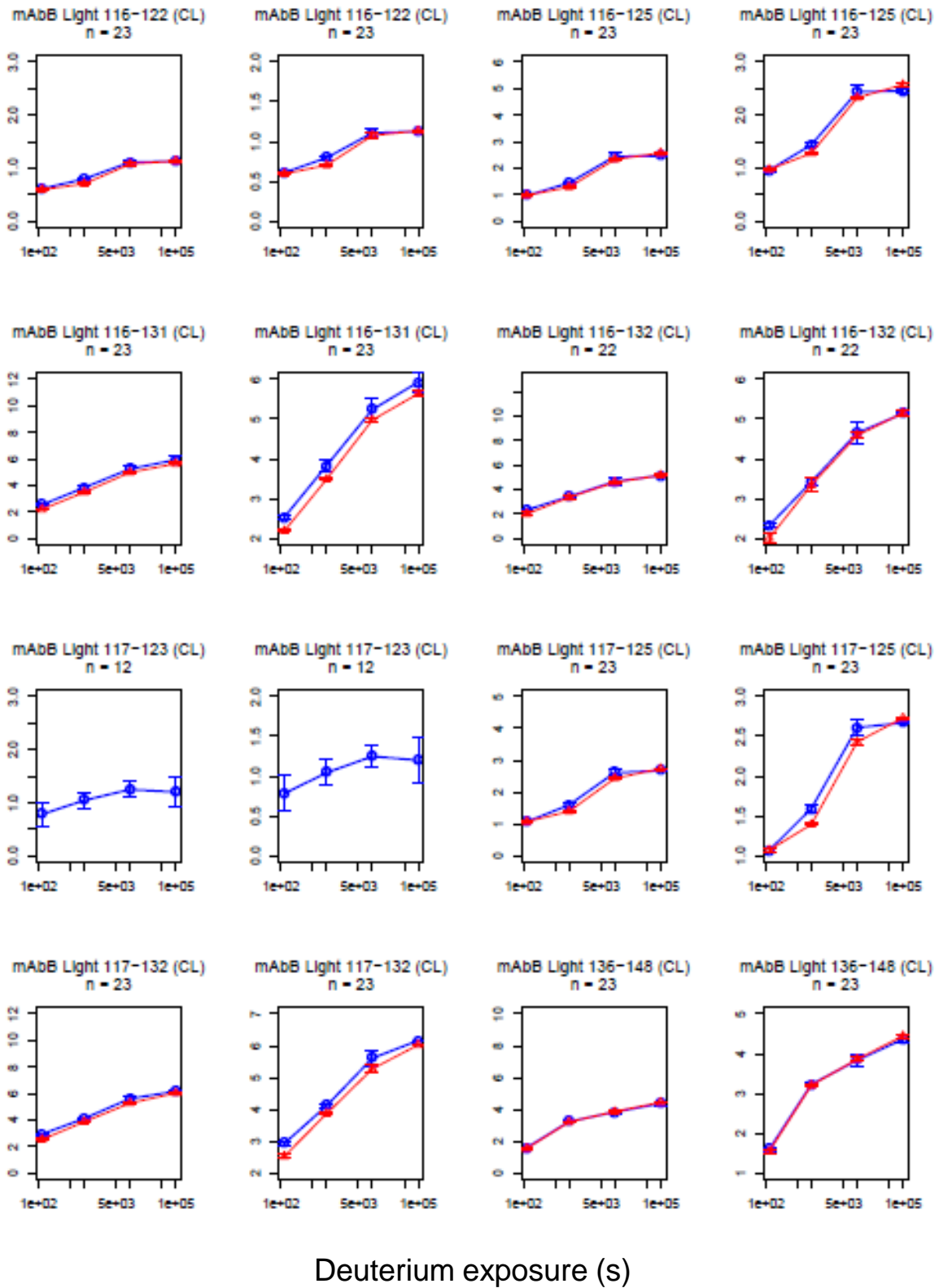


Mass Increase(Da)

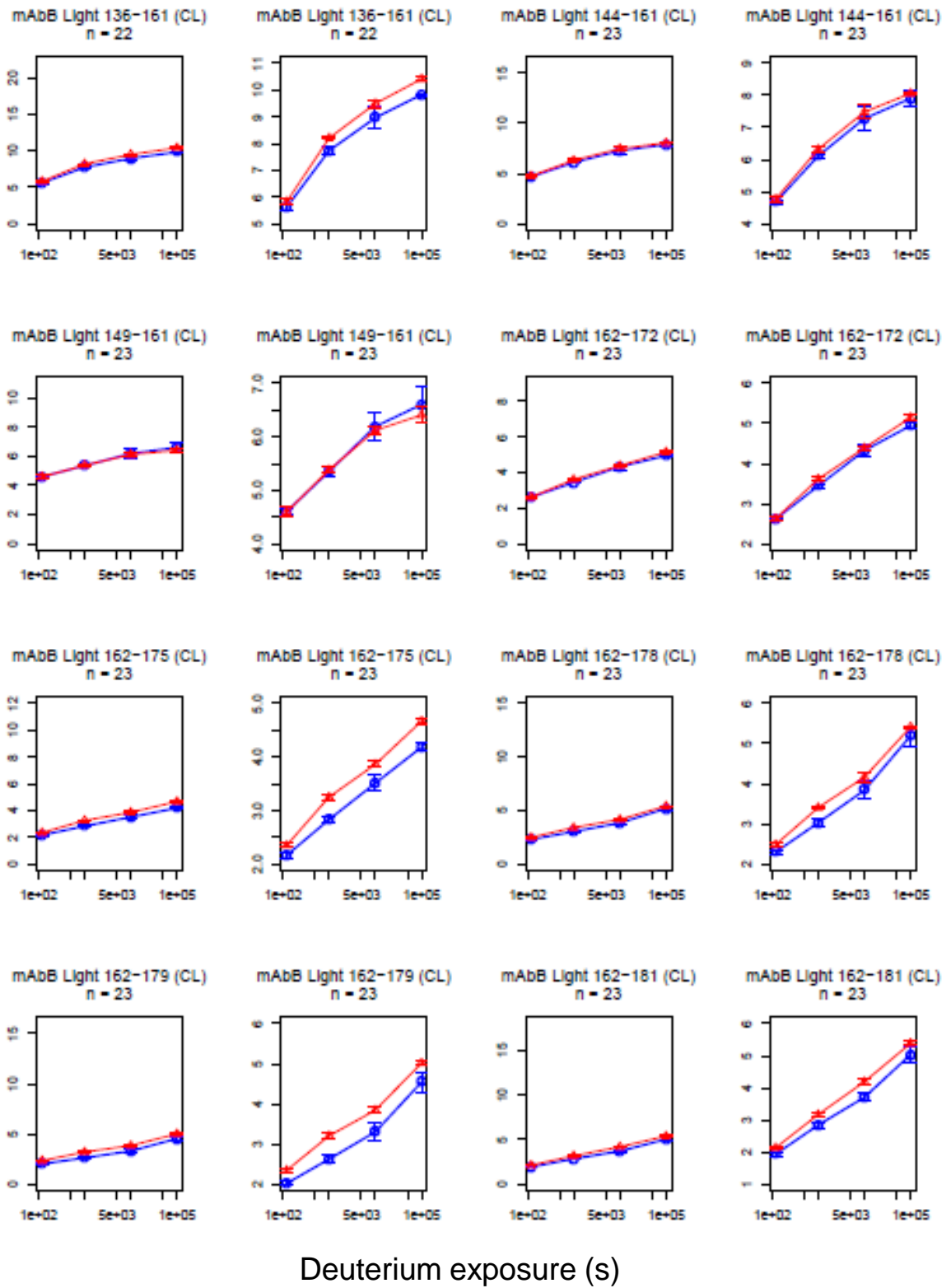


Deuterium exposure (s)

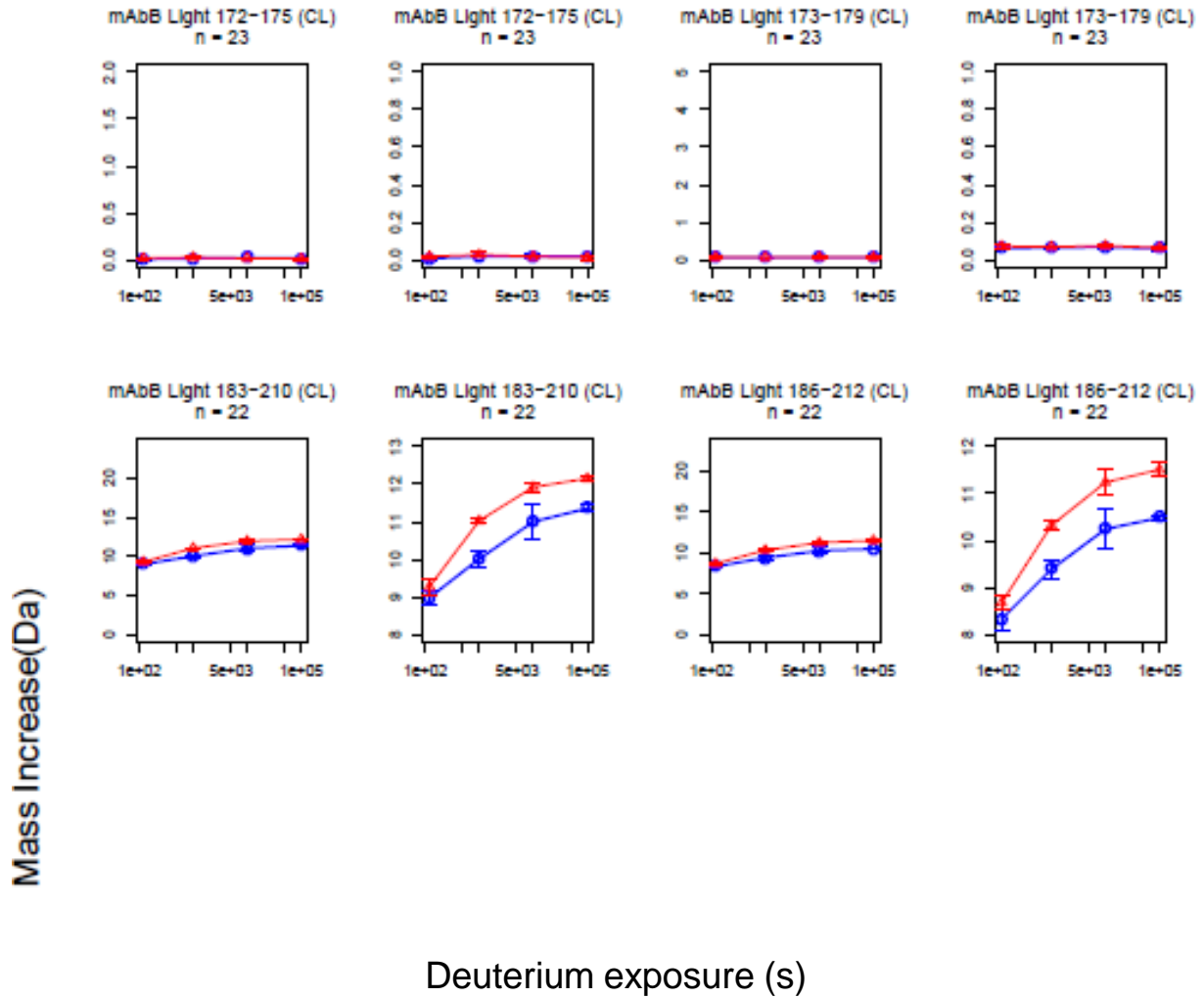
Mass Increase(Da)



Mass Increase(Da)



Deuterium exposure (s)



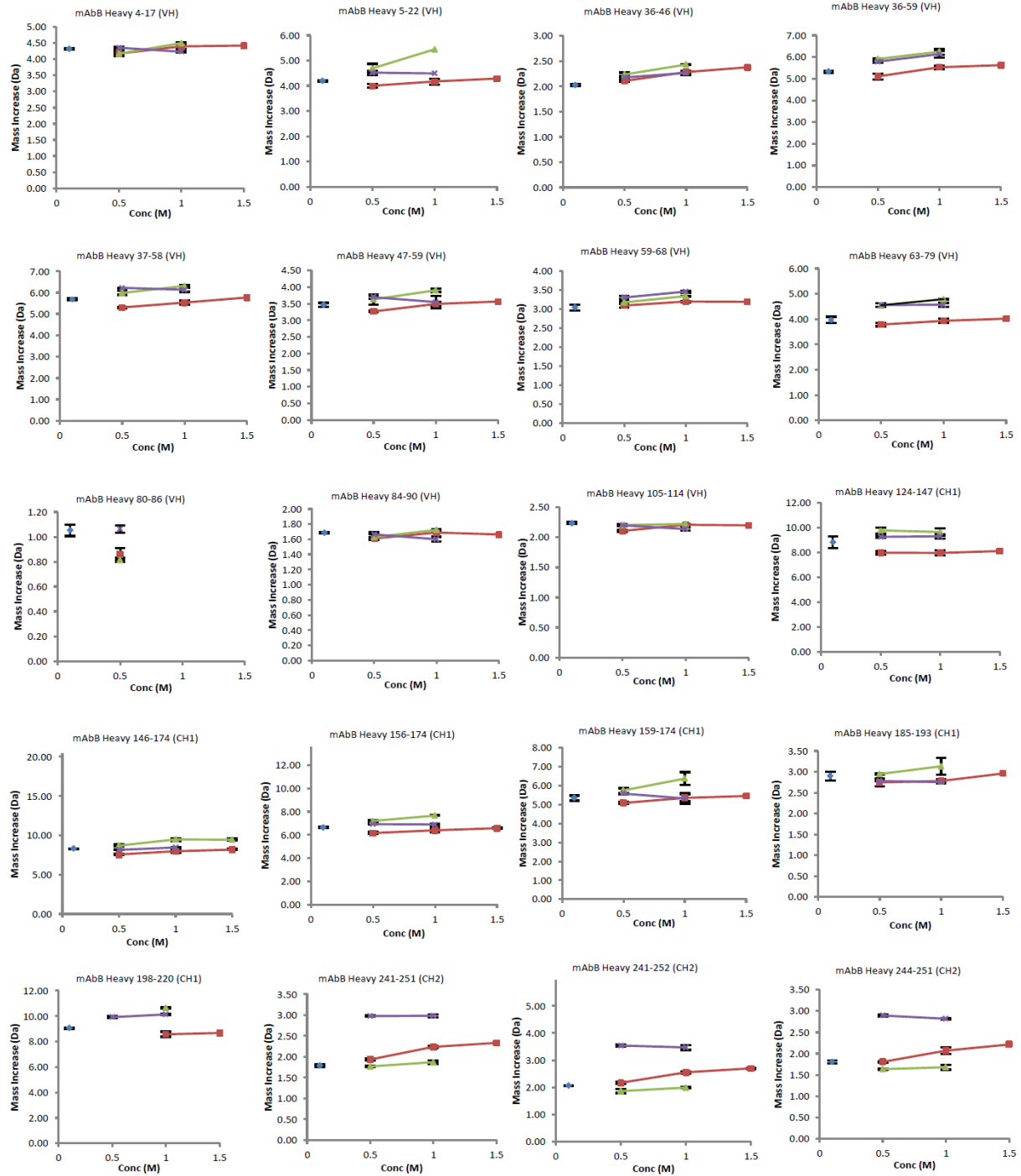
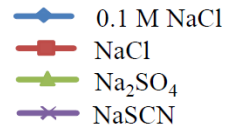
Deuterium uptake curves for the 137 segments from mAb-B in formulations containing 0.5 M chloride, sulfate or thiocyanate compared to the control (0.1 M chloride).

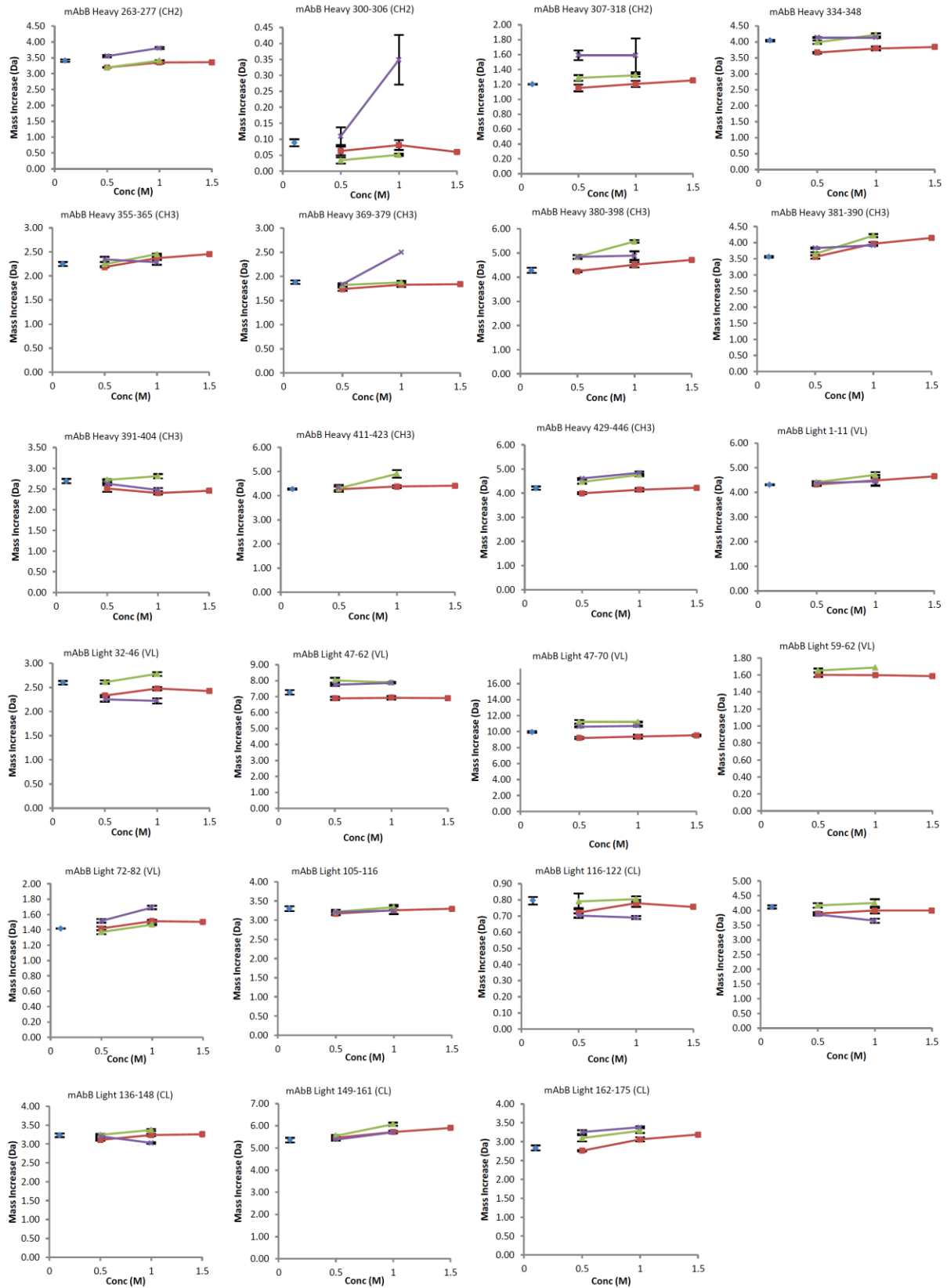
Figure 4.S6

NaCl (0.1, 0.5, 1 and 1.5 M)

Na₂SO₄ (0.5 and 1 M)

NaSCN (0.5 and 1 M)





Plots of deuterium uptake vs. salt concentration for 43 segments of mAb-B.

Chapter 5

Correlations between changes in conformational dynamics and physical stability in a mutant IgG1 mAb engineered for extended serum half-life

5.1 Introduction

The IgG1 framework is the most widely used platform for designing and developing therapeutic monoclonal antibodies (mAbs) targeted for treatment of cancer, autoimmune and infectious diseases.^{1, 2} The F_c region of IgG1 mAbs, whose sequence is primarily dictated by antibody subtype and host, serves a variety of biological functions, the most important of which include binding to specific Fcγ receptors to trigger various immunological events (e.g., complement activation, ADCC, opsonization),³⁻⁵ and determining pharmacokinetic properties of the mAb through interaction with FcRn receptors.⁶ Recent work has also implicated the F_c region in reducing mobility of infectious viruses in the mucosa after antibody binding.⁷ These biological properties are often mediated by the glycosylation profile of the N-linked Asn 297 residue within the C_H2 domain of the IgG1-Fc region.⁸ Thus, engineering specific sequences to improve the therapeutic utility of IgG1 mAbs is not limited to the amino acid residues of the complementarity determining regions (CDRs) in the F_{ab} to enhance antigen binding specificity and affinity.⁹ The constant regions in the F_c can also be engineered to improve mAb-based therapeutics including better engagement of the immune system^{10, 11} as well as extension of the circulation half-life.¹²⁻¹⁴

Increasing the serum half-life of mAbs is an attractive proposition since it potentially results in changes in their pK/pD profiles as well as decreased dosing frequency leading to higher patient compliance.¹⁵ The serum half-life of IgG1 antibodies is known to be regulated by the neonatal Fc receptor (FcRn) located primarily in the acidic endosomes of endothelial and hematopoietic cells.^{16, 17} Free or antigen-bound antibodies enter these cells through pinocytosis or endocytosis, respectively, and are then transported to the endosomes. FcRn interaction then marks the antibodies for either recycling or lysosomal degradation. The recycling mechanism is based on selective binding of IgG to the FcRn receptor in the relatively more acidic (pH <6.5)

environment of endosomes, followed by release from the receptor upon exposure to the more basic (pH ~ 7.4) milieu of the bloodstream.¹⁸ The binding sites of the F_c region of an antibody to the FcRn receptor, as well as the amino acid residues responsible for the pH-dependent recycling, have been identified and are well documented for human IgGs.¹⁹⁻²¹ The pH-dependence of this binding within acidic endosomes is driven by positively charged histidine residues in human IgG1 antibodies, specifically His 310 and His 436 at pH 6.5 or below, that form salt bridges with negatively charged Glu 117 and Asp 137 residues of FcRn.^{18, 19, 21} Under the more physiological conditions (pH ~ 7.4) of the bloodstream, however, these histidine residues are no longer charged and hence there is little histidine-mediated binding between the IgG-Fc region and the FcRn receptor.

The recycling machinery has been widely targeted through random and specific mutations of the IgG primary sequence to increase or decrease the affinity for binding to FcRn and thereby extend or reduce the circulation half-life of IgG based therapeutics.^{14, 22-28} For example, the increased FcRn binding at pH 6.0 by a YTE triple mutant mAb is mediated by the creation of one additional salt bridge between Glu 256 (E) of Fc YTE and Gln 2 (Q) of the β 2-microglobulin chain of FcRn compared to the original IgG1 Fc structure.²⁹ The YTE-mutations (M252Y/S254T/T256E) in the C_H2 domain of an IgG1 mAb resulted in a nearly four-fold higher in vivo half-life in cynomolgus monkeys, the largest increase in IgG mAb half-life reported to-date for non-human primates.²³ The YTE triple mutation also resulted in ten-fold higher FcRn binding, four-fold higher tissue bioavailability, and modulated antibody-dependent cell cytotoxicity in non-human primates.²³ In a recent human clinical trial, the YTE mutant of an IgG1 mAb targeted towards RSV (Motavizumab) had two- to four-fold longer in vivo half-life compared to the original mAb.¹⁵

The X-ray crystal structures of the original human IgG1 Fc (PDB ID 3AVE) and the Fc-YTE (PDB ID 3FJT) mutant reveal no apparent structural differences between the two molecules.^{14, 30} A recent study, however, suggested that the YTE mutant has relatively lower physical stability in solution than the same mAb without the mutations.³¹ One possibility is that these stability differences are mediated by changes in structural dynamics of specific sequences in the mAbs due to the YTE mutations. Although the interrelationships between dynamics and stability of proteins are complex,³² growing evidence suggests that physical destabilization of mAbs can, in at least some cases, be mediated by changes in local dynamics of specific sequences.^{33, 34} Hydrogen/deuterium exchange coupled to mass spectrometry (H/D-MS) is now a well-established technique to explore the local dynamics of the amide backbone of monoclonal antibodies (mAbs) with peptide-level resolution.^{35, 36} H/D-MS has been used to study changes in mAb conformational dynamics imparted by stabilizing and destabilizing excipients³⁴ and salts³³, mutation in the IgG1 C_H3 domain,³⁷ deglycosylation,³⁵ chemical and post-translational modifications,^{38, 39} thermal and freeze-thaw stress,⁴⁰ and cytotoxic drug conjugation⁴¹ in IgG1 mAbs.

This work investigates the nature of the relative differences in physical stability between an IgG1 mAb (mAb-A) and its corresponding YTE-mutant (mAb-E) by examining effects of the YTE-mutations on amide backbone local dynamics measured by amide H/D exchange, conformational stability measured by differential scanning calorimetry (DSC), and aggregation propensity measured by size exclusion chromatography (SEC). Since solution pH plays a very important role in the interaction of antibodies with FcRn receptors (i.e., binding at pH 6.0 and release at pH 7.4), we explored differences in flexibility and stability between the two mAbs at

both pH values. We then correlate the observed changes in physical stability to changes observed in the amide backbone dynamics due to the YTE mutations.

5.2 Materials and Methods

5.2.1 Materials

Two highly purified IgG1 mAbs were supplied by MedImmune, Gaithersburg, MD: mAb-A and the corresponding YTE (M255Y/S257T/T259E) mutant of the same IgG1 designated as mAb-E. The residue number is slightly different from numbering reported elsewhere^{14, 23} due to the presence of three extra amino acids in the sequence of mAb-A/mAb-E. Residue numbers of other IgG1 mAbs mentioned in the Discussion section of this report are adjusted according to the sequence numbering scheme for mAb-A/mAb-E by adding +3 to the residue numbers. Both mAbs were produced in the same cell line and had overall similar N-linked glycosylation patterns in the C_H2 domain containing primarily G0f and G1f oligosaccharides (see Supplemental Figure 5.S4 and Supplemental Table 5.S2). In addition, mAb-E had ~ 50% C-terminal lysine heterogeneity while mAb-A had little to no C-terminal lysine. The relatively elevated levels of C-terminal lysine heterogeneity of mAb-E was not considered while interpreting our results, as it has been shown previously to have no effect on the pharmacokinetics, stability or conformational dynamics of mAbs.^{60, 61} Both mAb-A and mAb-E showed ~99% purity as measured by SDS-PAGE analysis (data not shown), and greater than 99% monomer content as measured by size exclusion chromatography (see results). The mAbs were provided at 100 mg/mL and were buffer exchanged into 50 mM sodium phosphate, 150 mM sodium chloride at pH 6.0 or 7.4. The protein concentration was adjusted to 10 mg/mL based on absorbance at 280 nm measured with an Agilent 8453 UV-visible spectrophotometer. Extinction coefficient values of 1.47 (mg/mL)⁻¹ cm⁻¹ and 1.42 (mg/mL)⁻¹ cm⁻¹ were used for

calculation of concentrations of mAb-A and mAb-E, respectively. Anhydrous sodium phosphate dibasic (code number 42437), and monobasic (code number 389870010) were purchased from Acros Organics. Sodium chloride (product number M-11628), LC-MS grade water, acetonitrile, and isopropanol were purchased from Fisher Scientific. TCEP (Catalogue # C4706), guanidine hydrochloride (Catalog # 50933), porcine pepsin, acetic acid, deuterium oxide (99+%D; catalogue number 151882) were purchased from Fluka/Sigma Aldrich. All chemicals used were of the highest purity grade commercially available from these vendors.

5.2.2 Differential scanning calorimetry (DSC)

DSC experiments and corresponding data analysis were performed as described previously.³⁴ The mAb-A and mAb-E samples were diluted to 0.5 mg/mL in buffers containing 50 mM sodium phosphate and 150 mM sodium chloride, either at pH 6.0 or 7.4, using the appropriate dilution buffer and filtered by 0.22 μ m filter before analysis. All analyses were done in triplicate.

5.2.3 Accelerated storage stability study and analysis by size exclusion chromatography (SEC)

Both mAb-A and mAb-E were prepared at 0.5 mg/mL in 50 mM sodium phosphate, 150 mM sodium chloride at both pH 6.0 and 7.4. The stock mAb formulations were filtered by passing through 0.22 μ m filters (Millipore, Billerica, Massachusetts), aliquoted, 0.5 mL each, into separate 3 mL type 1 glass vials (West Pharmaceutical Services, Exton, Pennsylvania), stoppered with rubber stoppers (West Pharmaceutical Services, Exton, Pennsylvania), crimped and then stored in a 50 °C incubator. Sample filtration, aliquoting, and vial sealing were performed in a pre-sanitized laminar flow hood. Samples were taken out of the incubator and analyzed by SEC

at days 0, 2, 4, 7, 14, and 28. SEC was performed and data were analyzed in the same manner as described in our earlier work³⁴ with the following exception. Duplicate vials were analyzed two times each by SEC for each incubation time and condition. Hence the error values for the amounts of mAb monomer, soluble aggregates and fragments measured by SEC were derived from four different measurements. The error values for insoluble aggregate content were calculated by propagating the variances in the measurements of monomers, soluble aggregates and fragments.

5.2.4 Preparation of deuterated labeling buffers

Calculated weights of anhydrous sodium phosphate monobasic, dibasic and sodium chloride were added to 90 atom % D₂O to prepare 50 mM sodium phosphate, 150 mM sodium chloride at pH 6.0 and 7.4. (90 atom % D was used for consistency with our previous work^{33, 34}). Addition of the chemicals did not result in any appreciable change in volume and hence concentrations of buffer components are accurate to 1% of their reported molarities. The pH values reported are directly from pH meter readings without correction for the deuterium isotope effect on pH measurement⁶².

5.2.5 Hydrogen/deuterium-exchange mass spectrometry

Sample preparation for hydrogen/deuterium exchange experiments followed by LC-MS analyses were performed as described in detail elsewhere.³³ H/D exchange sample preparations were performed using the H/DX PAL robot (LEAP Technologies, Carrboro, NC) equipped with temperature-controlled sample drawers. The mAb samples at 10 mg/mL in 50 mM sodium phosphate and 150 mM sodium chloride at either pH 6.0 or 7.4 were diluted 20-fold in 90% deuterated buffer at the same pH at 25 °C to initiate deuterium exchange. Exchange reactions

were quenched after 30, 180, 10^3 , 10^4 and 10^5 s using quench buffer (0.5 M TCEP, 4 M guanidine hydrochloride, and 0.2 M phosphate, pH = 2.4) held at 1 °C resulting in a final pH of ~ 2.5. Immediately following quench, samples were digested by passing through an immobilized pepsin column prepared in-house,^{63, 64} desalted and concentrated on a reversed phase trap (Peptide Concentration and Desalting Microtrap; Bruker-Michrom, Auburn, CA, USA), separated on a C-18 reversed phase column and mass analyzed (Agilent 6220 time-of-flight LC-MS system). All the columns and tubing were housed inside a refrigerated compartment maintained at 0 °C to minimize back-exchange. Deuterium recovery measured separately using fully deuterated peptides ranged from 64-85 %.

5.2.6 Mass spectrometry data analysis

A peptic peptide map shown in Supplemental Figure 5.S1 covering 96 % of the heavy chain and 92 % of the light chain was constructed from common peptic peptides generated by digestion of both mAb-A and mAb-E. Peptide identities were confirmed using a combination of accurate mass measurement (± 10 ppm) and tandem mass spectrometry data from a time-of-flight mass spectrometer and a linear ion trap mass spectrometer respectively.⁶⁵ Three replicate sets of H/D-exchange data were processed using HDExaminer (Sierra Analytics, California). Each set of data was manually curated independently to minimize bias by the analyst. Deuterium uptake data averaging and plotting were achieved using an R script. The 99% confidence interval was calculated by combining all of the standard deviations from earlier studies in our laboratories with another IgG1 mAb^{33, 34} and from this study with mAb-A and mAb-E. The newly calculated value for the 99% confidence levels based on 9580 triplicate measurements, with error propagation for the differential measurement, is the same as our previously-established value of

± 0.59 Da. (Supplemental Figure 5.S5) All significant differences in deuterium content between the two mAbs were mapped onto the homology model of mAb-A.

5.2.7 Construction of the homology model

The homology model for the F_{ab} and hinge regions of mAb-A were produced with the in silico KOL-Padlan structure⁶⁶ as a template, using Modeller version 9.12⁶⁷. The F_c domain was derived from PDBID: 3AVE³⁰, which has the same amino acid sequence as mAb-A. Mutations were introduced into this model to represent the YTE residues. Very few changes were observed in the structure after the mutations. Hence the same homology model was used to represent both mAb-A and mAb-E. Of note, the F_c domain of YTE has been crystallized (3FJT), and the secondary and tertiary structure folds of 3FJT are highly homologous with 3AVE¹⁴. However, the 3FJT structure contains two extra residues, not present in mAb-A or mAb-E. Therefore, it was not used as a starting structure. The glycan structures in 3AVE were maintained, containing homodimeric G0F sequences, which represent a high population of carbohydrate species found in mAb-A and mAb-E by intact mass spectrometry measurements (see Figure 5.S4).

5.3 Results

5.3.1 YTE mutation decreased the conformational stability of only the C_H2 domain

DSC was used to examine the conformational stability of mAb-A and mAb-E (YTE-mutant of mAb-A). Representative DSC thermograms comparing the two mAbs are shown in Figure 5.1. Both the mAbs display three thermal melting (T_m) transitions at both pH 6.0 and 7.4. The T_{m1} value (Figure 5.1) has been shown previously to represent the thermal unfolding of the C_H2 domain.⁴² The T_{m2} and T_{m3} values (Figure 5.1) have been shown to represent the unfolding of either the F_{ab} or the C_H3 domain depending on the antibody and solution conditions.^{42, 43} In

addition, the T_{onset} values, marking the temperature at which the first structural transition initiates (an important value for formulation stability considerations),⁴⁴ were also determined. A summary of the three T_{m} and T_{onset} values are listed in Table 5.1. The YTE mutation decreased $T_{\text{m}1}$ values by 6.5 °C and 6.7 °C, at pH 6 and 7.4 respectively, and decreased T_{onset} values by ~7 °C at both pH values. The $T_{\text{m}2}$ and $T_{\text{m}3}$ values were not affected by the YTE mutation. Comparing the effect of pH 6.0 to 7.4 on protein conformational stability as measured by DSC, both mAbs had similar values for $T_{\text{m}1}$ and $T_{\text{m}2}$ at the two pH values. However, both mAb-A and mAb-E had ~4.7 °C higher values for $T_{\text{m}3}$ and ~ 1.4 °C lower T_{onset} values at pH 6.0 compared to 7.4. In summary, the YTE mutation decreased conformational stability in the $C_{\text{H}2}$ domain while the other domains in the two mAbs were similar in terms of their thermal stability.

5.3.2 YTE mutation increased the aggregation propensity of mAb-E under accelerated storage conditions

The aggregation propensities of the two mAbs at pH 6.0 and 7.4 under accelerated storage conditions were measured by SEC at 50 °C over 28 days. Figure 5.2A shows the loss of IgG monomer and formation of fragments, soluble, and insoluble aggregates for the mAb samples. Peaks in the SEC chromatograms were assigned based on molecular weight as described previously.³⁴ Both mAbs had greater than 99% monomer content at time zero and small amounts of fragments and soluble aggregates. Quantitation of the various mAb species after storage was determined relative to the respective peak areas at time 0. Loss in total integrated area of the chromatogram was attributed to formation of insoluble aggregates. The YTE mutation caused faster monomer loss at 50 °C at both pH 6.0 and 7.4, but had no effect on the rate of fragment formation. In addition, the YTE mutant produced higher amounts of soluble aggregates at either pH value which became evident after 14 days at 50 °C. Although minimal

amounts were observed until 14 days, the YTE mutant (mAb-E) also produced significantly higher amounts of insoluble aggregates (~9-11%) compared to mAb-A (~4-5%) after storage for 28 days at 50 °C. To better display these differences in soluble, insoluble, and total aggregate content after incubation for 28 days, the data are shown as bar charts in Figure 5.2B and 5.2C, respectively. Both mAbs produced higher amounts of insoluble aggregates than soluble aggregates after 28 days storage. At both pH 6.0 and 7.4, the YTE mutant produced higher amounts of soluble and insoluble aggregates. The total aggregate content for the YTE mutant after 28 days of storage is roughly 2 fold higher than the original mAb at both pH values.

5.3.3 Identifying the effects of YTE mutation on the backbone flexibility

Amide H/D exchange with mass spectrometric detection was used to measure the effects of the YTE mutation on protein amide backbone flexibility. As an initial step in the analysis of both mAbs by H/D-exchange mass spectrometry, a peptic peptide map was developed. A total of 167 common peptides were reproducibly obtained by pepsin digestion of both mAb-A and mAb-E resulting in 92% and 96% sequence coverage in the light chain and heavy chain, respectively, as shown in Supplemental Figure 5.S1. The two mAbs were incubated in deuterium-containing solutions, quenched at various time points and passed through a pepsin column. The deuterium content of the peptides was determined by LC-MS (see Methods section). Examples of deuterium uptake plots for six different segments from mAb-A and mAb-E at pH 6.0 and 7.4 are shown in Figure 5.3A and 5.3B, respectively. The shapes of the different deuterium uptake profiles illustrate the different degrees of flexibility in different regions of the mAb. Similar deuterium uptake profiles for all 167 common peptides found in both mAb-A and mAb-E at pH 6.0 and 7.4 are presented in Supplemental Figures 5.S2 and 5.S3. Differences in deuterium uptake between mAb-A and mAb-E at various exchange times were found in four of the six

peptides shown in Figure 5.3 (HC 244-254, HC 255-264, HC 320-332, and LC 179-194) at both pH 6.0 and 7.4. However, not all of these differences exceed the 99% confidence interval for significance (see below). The segment locations in the primary sequence of mAb-A or mAb-E corresponding to peptide numbers are tabulated in Supplemental Table 5.S1.

To more clearly display the effects of the YTE mutation on deuterium uptake for all peptide segments, the data are presented as differential deuterium uptake as described previously.³³ The differential deuterium uptake i.e. $\Delta\Delta m(t) = \Delta m_{\text{mAb-E}}(t) - \Delta m_{\text{mAb-A}}(t)$ where Δm represents the measured mass increase upon deuteration for each peptide is plotted as a vertical bar (Figure 5.4 for pH 6.0 and Figure 5.5 for pH 7.4) and t denotes the labeling time. A positive value for $\Delta\Delta m$ indicates that the YTE mutation caused faster exchange, corresponding to increased flexibility, while a negative value indicates slower exchange, corresponding to decreased flexibility. The dotted lines denote the 99% confidence interval (± 0.59 Da) for a statistically significant difference in exchange. The 99% confidence interval was determined by pooling all standard deviation values for triplicate measurements in our earlier studies with another IgG1 mAb^{33, 34} and this study. Differential exchange that exceeds the 99% confidence interval is mapped onto a homology model for the mAb in Figure 5.6A, and in more detail for the F_c portion only in Figure 5.6B. The YTE mutation-induced increases in local flexibility are colored in yellow, decreases in blue, and no changes in grey. The absence of H/D exchange data is shown in white. The H/D exchange results are discussed in detail in the next section.

5.3.4 The YTE mutation caused localized increases in backbone flexibility at pH 6.0

At pH 6.0, nearly all of the significant differences in exchange were positive and localized to narrow regions indicating that the YTE mutation increases flexibility in only a limited number of segments (see Figure 5.4). The highest positive deuterium uptake differences

were observed in the HC 244-255 region of the C_{H2} domain at 10³ s followed by 180 s, a region covered by the overlapping peptides HC 238-254, HC 244-254, HC 244-255, HC 245-254, HC 247-254 and HC 247-255 (corresponding to peptide numbers 52, 54-58 in Figure 5.4). The mutation also caused two other segments in the C_{H1} domain (HC 174-188 corresponding to peptide 42 in Figure 5.4) and the C_{H2}-C_{H3} interface (HC 320-332 corresponding to peptide 81 in Figure 5.4) to exchange significantly faster. In addition, the YTE mutation caused several other segments (HC 28-46, HC 144-168, HC 159-177, and LC 147-174 corresponding to peptides 12, 36, 40, and 159 in Figure 5.4) to exchange faster than mAb-A. Only one segment LC 179-194 (corresponding to peptide 165 in Figure 5.4), exchanged more slowly in the YTE-mutant.

5.3.5 Mutation-induced differences in local flexibility at pH 7.4 were similar to differences at pH 6.0

Deuterium uptake by the representative peptides was faster at pH 7.4 than at pH 6.0 (see Figure 5.3A vs. 5.3B), as expected from the known pH dependence of intrinsic deuterium exchange.⁴⁵ Looking across all of the peptides in Figure 5.5, it can be seen that most of the differences in deuterium uptake were at early exchange times (30s and 180s) at pH 7.4 rather than later times (180s and 10³s) at pH 6.0. The shift arises from faster intrinsic exchange at pH 7.4.^{45, 46} Essentially all of the peptide segments that had significant differences in deuterium uptake at pH 6.0 also had significant differences at pH 7.4 (Figures 5.4 and 5.5), with only two exceptions noted. One segment in the C_L domain (LC 147-174 corresponding to peptide 159 in Figures 5.4 and 5.5) had increased deuteration at 10⁵ s in the mutant mAb-E at pH 6.0, but not at pH 7.4. Another segment in the C_{H2} domain (HC 269-280 corresponding to peptide 68 in Figures 5.4 and 5.5) had increased deuteration at 10³ s at pH 7.4, but not at pH 6.0.

5.3.6 Backbone flexibility of the peptide segments containing the YTE mutation

Three overlapping peptide segments covering the YTE mutation sites were detected in the peptic peptide maps of both mAb-A and mAb-E. The H/D exchange kinetics of one of the three segments (HC 255-264) is shown in Figure 5.3 while the two others are shown in Supplemental Figures 5.S2 and 5.S3. The point mutations resulted in trends showing slightly faster deuterium exchange in these three segments in mAb-E, but observed differences in deuterium uptake at every exchange time were less than the 99% confidence interval for a significant difference. Under typical exchange conditions (i.e., the EX2 kinetic limit), the kinetics of exchange depend on both backbone dynamics and on intrinsic exchange.^{47, 48} When comparing homologous backbone segments with different amino acid sequences, the rate of intrinsic exchange must be considered. We used tabulated values for intrinsic exchange^{40, 41} to calculate the intrinsic exchange by these segments at pD 6, as shown in Figure 5.7. All three segments in mAb-A have slightly faster intrinsic exchange compared to mAb-E. The differences in the calculated intrinsic exchange rates oppose the trend observed experimentally in the two mAbs. Therefore, the differences in backbone flexibility in the mutation region are likely somewhat larger than they appear in Figure 5.3. Given the complex, multi-exponential nature of H/D exchange kinetics, no suitable method has yet been developed to directly correct the experimental results for these differences. It remains possible that the small differences in backbone flexibility induced by the YTE mutation at the mutation sites would be statistically significant if they could be corrected for intrinsic exchange effects.

5.4 Discussion

Previous work has shown that the YTE mutations in the C_H2 domain of IgG1 mAbs resulted in ten-fold higher FcRn binding and four-fold longer serum half-life in animal models.²³ In-house formulation work (data not shown) and characterization studies,³¹ however, have shown

a relative decrease in physical stability of various mAbs containing the YTE mutations. The purpose of this study was to probe the potential mechanisms of this destabilization by examining the YTE mutation induced changes in backbone flexibility of an IgG1 mAb and correlating results to DSC and SEC analysis of physical stability. To accomplish this purpose, two IgG1 mAbs were generated with identical primary sequences in the F_{ab} domains, one molecule containing the YTE triple mutations in the F_c domain (mAb-E), while the other molecule had the native IgG1 sequence for the F_c domain (mAb-A). The N-linked glycosylation patterns in the F_c region of mAb-A and mAb-E were overall similar containing primarily G0f and G1f oligosaccharides (see Supplemental Figure 5.S4 and Supplemental Table 5.S2).

DSC is a robust and widely utilized technique to assess the thermal stability of mAbs.⁴⁹ The endothermic unfolding transitions have been found to be independent of each other and generally irreversible for mAbs.⁵⁰ In the case of three distinct transitions, the peaks can be attributed to unfolding of the C_H2 domain followed by the F_{ab} and then the C_H3 domain in order of increasing melting temperatures.⁴² Although both mAbs displayed high thermal stability as measured by DSC, typical for IgG molecules, the mutant mAb-E had relatively lower T_{m1} values at both pH 6.0 and 7.4 (Figure 5.1 and Table 5.1). The YTE mutant had ~ 7 °C lower T_{onset} value and ~ 6.7 °C lower T_{m1} value compared to mAb-A. There were no differences in the other thermal melting transition temperatures (T_{m2} and T_{m3}) between mAb-A and mAb-E. In addition, accelerated stability studies monitoring mAb dimer and multimer formation by SEC analysis showed that the YTE mutant has a higher aggregation propensity (Figure 5.2). Despite these observed relative differences in physical stability, the YTE molecules can be formulated as biopharmaceuticals to be sufficiently stable during manufacturing and long-term storage by

appropriate design of formulation conditions including solution pH, excipients, and dosage form selection.

An examination of the X-ray crystal structures of Fc-YTE of mAb-E (PDB ID 3FJT) and the Fc of mAb-A (PDB ID 3AVE) indicated that there is little structural difference between the two.^{14, 30} However several adjacent as well as distant segments from the mutation site in the C_{H2} domain were shown in the current work to have increased flexibility due to the YTE mutations. Earlier reports indicated that single as well as concerted mutations far from the F_c binding epitopes in the F_c region enhanced the IgG1/FcRn binding.^{25, 27} Using the residue numbering scheme of mAb-A or mAb-E, these mutations are P233S/T, F244L, T253Q, V267A/E, N318D, A333V, N364D, A381V/T, M431L).^{25, 27} Several of these previously reported mutations (e.g., F244L, T253Q, V267A/E, N318D, and A333V) are in the peptide segments (HC 244-255, HC 269-280, HC 320-332) that showed increased local flexibility due to the YTE-mutations in our work. Hence, it can be inferred that residue/s in the segments with increased flexibility in the C_{H2} domain and the C_{H2}-C_{H3} interface may have indirect interactions with the conformation of the 255-259 segment which is the location for YTE-mutations as well as one of the FcRn binding epitopes of Fc.

Additional segments in the F_{ab} region (HC 28-46, HC 144-168, HC 159-177, HC 174-188, and LC 147-174 corresponding to peptide 9, 36, 40, 42 and 158 in Figures 5.4 and 5.5) had increased flexibility in the YTE mutant and the LC 179-194 had decreased flexibility. It is surprising that the YTE mutations in the C_{H2} domain caused flexibility changes at distant sites in different domains. Molecular dynamics simulations have shown that the two arms of the F_{ab} can have polar and non-specific interactions with regions of the F_c not far from the FcRn binding sites.⁵¹ Furthermore, recent studies have shown that mAbs with identical F_c but differing F_{ab}

sequences,⁵² as well as mAbs and F_c fusion proteins with the same F_c sequences,⁵³ can bind FcRn differentially with varying pharmacokinetic properties. The H/D exchange data in our study further support the notion that certain segments of the F_{ab} sequence may have some yet-to-be-defined indirect interactions with the 255-259 region in the C_{H2} domain of the F_c, one of the FcRn binding epitopes. At the same time, the YTE mutation did not cause any changes in the thermal unfolding temperatures of the F_{ab} region measured by DSC (Figure 5.1 and Table 5.1). These results further highlight the complex interrelationships between protein flexibility and conformational stability.³²

The YTE mutation increased the flexibility of the 244-255 region of the C_{H2} domain at both pH 6.0 and 7.4. This region, covered by six overlapping segments (peptide numbers 52, 54-58 in Figures 5.4 and 5.5), had the largest magnitude of increase among all differences detected by H/D-MS. This segment is adjacent to the 255-259 segment containing the YTE mutations. A visual comparison of the deuterium uptake kinetic profiles of segments covering the 244-255 region at pH 6.0 show very similar overall shapes across three different IgG1 mAbs (mAbs A and E in this study and mAb-B in previous studies) examined in our laboratories with the midpoint of deuterium uptake at $\sim 10^3$ s.^{33, 34} Moreover, similar kinetic profiles are evident in H/D-MS studies at pH ~ 6 with other IgG1 mAbs in other laboratories.^{35, 38, 54} Hence it can be concluded that this region has similar dynamic behavior across all of these distinct IgG1 mAbs.

Increased flexibility of the 244-255 sequence caused by the YTE mutation (mAb-E vs. mAb-A) correlates with decreased thermal stability of the C_{H2} domain and increased aggregation propensity. Significant increases in flexibility of this same segment have been correlated previously in our labs in another IgG1 mAb with arginine and sodium thiocyanate-induced decreases in conformational stability, and concomitant increases in the aggregation propensity.^{33,}

³⁴ Furthermore, several reports by others have correlated increased flexibility of this same primary sequence segment in the C_H2 domain with methionine oxidation,^{38, 39, 54} destabilization by deglycosylation,³⁵ changes in glycosylation³⁸ and even decreased stability due to drug conjugation to free cysteine residues⁴¹. The 244-255 segment in the C_H2 domain is relatively apolar in nature with two valine residues and two phenylalanine residues and whose phenyl rings pack closely with the glycans in crystal structures.³⁰ It is possible that the increased flexibility of the peptide backbone disrupts the packing interactions between the peptide backbone and the glycan chains leading to unfolding of this hydrophobic segment. This unfolded apolar segment, in turn, may act as a hotspot for subsequent structural alterations that could lead to irreversible aggregation in IgG1 mAbs,⁵⁵⁻⁵⁷ for example, as observed by SEC analysis.

Limiting the flexibility of this particular segment may therefore serve as a good indicator for designing mAbs (and mAb-related products such as IgG-Fc, fusion proteins, or antibody drug conjugates) with higher thermostability and resistance to aggregation. In fact, it has been reported that engineering an additional disulfide bond at the Leu (L) 245 residue between two Phe (F) residues in this segment (L245C mutation), and the Lys (K) 337 residue to Cys (C) residues (K337C mutation) in an isolated IgG1 C_H2 domain results in an ~ 20 °C increase in thermal stability possibly by limiting the flexibility of the segment.⁵⁸ Furthermore soluble IgG1 C_H2 and C_H3 domains with engineered disulfides have been shown to have increased thermostability and binding to FcRn.⁵⁹ Therefore it appears that this particular segment in the C_H2 domain, whose sequence is conserved across all human IgG1 mAbs, can act as a destabilizing motif or aggregation hotspot and thus can play a crucial role in modulating the overall physical stability in many IgG1 mAbs.

5.5 References

1. Beck A, Wurch T, Bailly C, Corvaia N. Strategies and challenges for the next generation of therapeutic antibodies. *Nat Rev Immunol* 2010; 10:345-52.
2. Nelson AL, Dhimolea E, Reichert JM. Development trends for human monoclonal antibody therapeutics. *Nat Rev Drug Discov* 2010; 9:767-74.
3. Cohen-Solal JFG, Cassard L, Fridman W-H, Sautès-Fridman C. Fc γ receptors. *Immunol Lett* 2004; 92:199-205.
4. Raghavan M, Bjorkman PJ. Fc receptors and their interactions with immunoglobulins. *Annu Rev Cell Dev Biol* 1996; 12:181-220.
5. Ravetch JV, Bolland S. IgG Fc receptors. *Annu Rev Immunol* 2001; 19:275-90.
6. Albanesi M, Daron M. The interactions of therapeutic antibodies with Fc receptors. *Immunol Lett* 2012; 143:20-7.
7. Chen A, McKinley Scott A, Wang S, Shi F, Mucha Peter J, Forest MG, Lai Samuel K. Transient Antibody-Mucin Interactions Produce a Dynamic Molecular Shield against Viral Invasion. *Biophys J* 2014; 106:2028-36.
8. Jiang XR, Song A, Bergelson S, Arroll T, Parekh B, May K, Chung S, Strouse R, Mire-Sluis A, Schenerman M. Advances in the assessment and control of the effector functions of therapeutic antibodies. *Nat Rev Drug Discov* 2011; 10:101-11.
9. Igawa T, Tsunoda H, Kuramochi T, Sampei Z, Ishii S, Hattori K. Engineering the variable region of therapeutic IgG antibodies. *mAbs* 2011; 3:243-52.
10. Nimmerjahn F, Ravetch JV. Translating basic mechanisms of IgG effector activity into next generation cancer therapies. *Cancer immunity* 2012; 12:13.

11. Strohl WR. Optimization of Fc-mediated effector functions of monoclonal antibodies. *Curr Opin Biotechnol* 2009; 20:685-91.
12. Kuo TT, Aveson VG. Neonatal Fc receptor and IgG-based therapeutics. *mAbs* 2011; 3:422-30.
13. Roopenian DC, Akilesh S. FcRn: the neonatal Fc receptor comes of age. *Nat Rev Immunol* 2007; 7:715-25.
14. Oganessian V, Damschroder MM, Woods RM, Cook KE, Wu H, Dall'Acqua WF. Structural characterization of a human Fc fragment engineered for extended serum half-life. *Mol Immunol* 2009; 46:1750-5.
15. Robbie GJ, Criste R, Dall'acqua WF, Jensen K, Patel NK, Losonsky GA, Griffin MP. A novel investigational Fc-modified humanized monoclonal antibody, motavizumab-YTE, has an extended half-life in healthy adults. *Antimicrob Agents Chemother* 2013; 57:6147-53.
16. Ghetie V, Ward ES. Multiple roles for the major histocompatibility complex class I-related receptor FcRn. *Annu Rev Immunol* 2000; 18:739-66.
17. Zhu X, Meng G, Dickinson BL, Li X, Mizoguchi E, Miao L, Wang Y, Robert C, Wu B, Smith PD, et al. MHC class I-related neonatal Fc receptor for IgG is functionally expressed in monocytes, intestinal macrophages, and dendritic cells. *J Immunol* 2001; 166:3266-76.
18. Raghavan M, Bonagura VR, Morrison SL, Bjorkman PJ. Analysis of the pH dependence of the neonatal Fc receptor/immunoglobulin G interaction using antibody and receptor variants. *Biochemistry* 1995; 34:14649-57.
19. Kim J-K, Firan M, Radu CG, Kim C-H, Ghetie V, Ward ES. Mapping the site on human IgG for binding of the MHC class I-related receptor, FcRn. *Eur J Immunol* 1999; 29:2819-25.

20. Martin WL, West AP, Gan L, Bjorkman PJ. Crystal Structure at 2.8 Å of an FcRn/Heterodimeric Fc Complex: Mechanism of pH-Dependent Binding. *Mol Cell* 2001; 7:867-77.
21. Vaughn DE, Milburn CM, Penny DM, Martin WL, Johnson JL, Bjorkman PJ. Identification of critical IgG binding epitopes on the neonatal Fc receptor. *J Mol Biol* 1997; 274:597-607.
22. Hinton PR, Johlfs MG, Xiong JM, Hanestad K, Ong KC, Bullock C, Keller S, Tang MT, Tso JY, Vasquez M, et al. Engineered human IgG antibodies with longer serum half-lives in primates. *J Biol Chem* 2004; 279:6213-6.
23. Dall'Acqua WF, Kiener PA, Wu H. Properties of human IgG1s engineered for enhanced binding to the neonatal Fc receptor (FcRn). *J Biol Chem* 2006; 281:23514-24.
24. Shields RL, Namenuk AK, Hong K, Meng YG, Rae J, Briggs J, Xie D, Lai J, Stadlen A, Li B, et al. High resolution mapping of the binding site on human IgG1 for Fc gamma RI, Fc gamma RII, Fc gamma RIII, and FcRn and design of IgG1 variants with improved binding to the Fc gamma R. *J Biol Chem* 2001; 276:6591-604.
25. Monnet C, Jorieux S, Souyris N, Zaki O, Jacquet A, Fournier N, Crozet F, de Romeuf C, Bouayadi K, Urbain R, et al. Combined glyco- and protein-Fc engineering simultaneously enhance cytotoxicity and half-life of a therapeutic antibody. *mAbs* 2014; 6:422-36.
26. Petkova SB, Akilesh S, Sproule TJ, Christianson GJ, Al Khabbaz H, Brown AC, Presta LG, Meng YG, Roopenian DC. Enhanced half-life of genetically engineered human IgG1 antibodies in a humanized FcRn mouse model: potential application in humorally mediated autoimmune disease. *Int Immunol* 2006; 18:1759-69.

27. Hinton PR, Xiong JM, Johlfs MG, Tang MT, Keller S, Tsurushita N. An engineered human IgG1 antibody with longer serum half-life. *J Immunol* 2006; 176:346-56.
28. Kenanova V, Olafsen T, Crow DM, Sundaresan G, Subbarayan M, Carter NH, Ikle DN, Yazaki PJ, Chatziioannou AF, Gambhir SS, et al. Tailoring the pharmacokinetics and positron emission tomography imaging properties of anti-carcinoembryonic antigen single-chain Fv-Fc antibody fragments. *Cancer Res* 2005; 65:622-31.
29. Oganessian V, Damschroder MM, Cook KE, Li Q, Gao C, Wu H, Dall'Acqua WF. Structural insights into neonatal Fc receptor-based recycling mechanisms. *J Biol Chem* 2014; 289:7812-24.
30. Matsumiya S, Yamaguchi Y, Saito J-i, Nagano M, Sasakawa H, Otaki S, Satoh M, Shitara K, Kato K. Structural Comparison of Fucosylated and Nonfucosylated Fc Fragments of Human Immunoglobulin G1. *J Mol Biol* 2007; 368:767-79.
31. Tavakoli-Keshe R, Phillips JJ, Turner R, Bracewell DG. Understanding the relationship between biotherapeutic protein stability and solid-liquid interfacial shear in constant region mutants of IgG1 and IgG4. *J Pharm Sci* 2014; 103:437-44.
32. Kamerzell TJ, Middaugh CR. The complex inter-relationships between protein flexibility and stability. *J Pharm Sci* 2008; 97:3494-517.
33. Majumdar R, Manikwar P, Hickey JM, Samra HS, Sathish HA, Bishop SM, Middaugh CR, Volkin DB, Weis DD. Effects of salts from the Hofmeister series on the conformational stability, aggregation propensity, and local flexibility of an IgG1 monoclonal antibody. *Biochemistry* 2013; 52:3376-89.
34. Manikwar P, Majumdar R, Hickey JM, Thakkar SV, Samra HS, Sathish HA, Bishop SM, Middaugh CR, Weis DD, Volkin DB. Correlating excipient effects on conformational and

storage stability of an IgG1 monoclonal antibody with local dynamics as measured by hydrogen/deuterium-exchange mass spectrometry. *J Pharm Sci* 2013; 102:2136-51.

35. Houde D, Arndt J, Domeier W, Berkowitz S, Engen JR. Characterization of IgG1 Conformation and Conformational Dynamics by Hydrogen/Deuterium Exchange Mass Spectrometry. *Anal Chem* 2009; 81:2644-51.

36. Chen G, Warrack BM, Goodenough AK, Wei H, Wang-Iverson DB, Tymiak AA. Characterization of protein therapeutics by mass spectrometry: recent developments and future directions. *Drug Discov Today* 2011; 16:58-64.

37. Rose RJ, van Berkel PHC, van den Bremer ETJ, Labrijn AF, Vink T, Schuurman J, Heck AJR, Paren PWHI. Mutation of Y407 in the CH3 domain dramatically alters glycosylation and structure of human IgG. *mAbs* 2013; 5:0-1.

38. Houde D, Peng Y, Berkowitz SA, Engen JR. Post-translational Modifications Differentially Affect IgG1 Conformation and Receptor Binding. *Mol Cell Proteomics* 2010; 9:1716-28.

39. Zhang A, Hu P, Macgregor P, Xue Y, Fan H, Suchecki P, Olszewski L, Liu A. Understanding the conformational impact of chemical modifications on monoclonal antibodies with diverse sequence variation using hydrogen/deuterium exchange mass spectrometry and structural modeling. *Anal Chem* 2014; 86:3468-75.

40. Zhang A, Singh S, Shirts M, Kumar S, Fernandez E. Distinct Aggregation Mechanisms of Monoclonal Antibody Under Thermal and Freeze-Thaw Stresses Revealed by Hydrogen Exchange. *Pharm Res* 2012; 29:236-50.

41. Pan LY, Salas-Solano O, Valliere-Douglass JF. Conformation and dynamics of interchain cysteine-linked antibody-drug conjugates as revealed by hydrogen/deuterium exchange mass spectrometry. *Anal Chem* 2014; 86:2657-64.
42. Ionescu RM, Vlasak J, Price C, Kirchmeier M. Contribution of variable domains to the stability of humanized IgG1 monoclonal antibodies. *J Pharm Sci* 2008; 97:1414-26.
43. Iacob RE, Bou-Assaf GM, Makowski L, Engen JR, Berkowitz SA, Houde D. Investigating Monoclonal Antibody Aggregation Using a Combination of H/DX-MS and Other Biophysical Measurements. *J Pharm Sci* 2013; 102:4315-29.
44. Hawe A, Wiggendorff M, van de Weert M, Garbe JHO, Mahler H-c, Jiskoot W. Forced degradation of therapeutic proteins. *J Pharm Sci* 2012; 101:895-913.
45. Bai Y, Milne JS, Mayne L, Englander SW. Primary structure effects on peptide group hydrogen exchange. *Proteins: Struct Funct Bioinform* 1993; 17:75-86.
46. Connelly GP, Bai Y, Jeng MF, Englander SW. Isotope effects in peptide group hydrogen exchange. *Proteins: Struct Funct Bioinform* 1993; 17:87-92.
47. Hvidt A, Nielsen SO. Hydrogen exchange in proteins. *Adv Protein Chem* 1966; 21:287-386.
48. Englander SW, Kallenbach NR. Hydrogen exchange and structural dynamics of proteins and nucleic acids. *Q Rev Biophys* 1983; 16:521-655.
49. Vermeer AW, Norde W. The thermal stability of immunoglobulin: unfolding and aggregation of a multi-domain protein. *Biophys J* 2000; 78:394-404.
50. Vermeer AW, Norde W, van Amerongen A. The unfolding/denaturation of immunoglobulin of isotype 2b and its F(ab) and F(c) fragments. *Biophys J* 2000; 79:2150-4.

51. Kortkhonjia E, Brandman R, Zhou JZ, Voelz VA, Chorny I, Kabakoff B, Patapoff TW, Dill KA, Swartz TE. Probing antibody internal dynamics with fluorescence anisotropy and molecular dynamics simulations. *mAbs* 2013; 5:306-22.
52. Wang W, Lu P, Fang Y, Hamuro L, Pittman T, Carr B, Hochman J, Prueksaritanont T. Monoclonal Antibodies with Identical Fc Sequences Can Bind to FcRn Differentially with Pharmacokinetic Consequences. *Drug Metab Disposition* 2011; 39:1469-77.
53. Suzuki T, Ishii-Watabe A, Tada M, Kobayashi T, Kanayasu-Toyoda T, Kawanishi T, Yamaguchi T. Importance of neonatal FcR in regulating the serum half-life of therapeutic proteins containing the Fc domain of human IgG1: a comparative study of the affinity of monoclonal antibodies and Fc-fusion proteins to human neonatal FcR. *J Immunol* 2010; 184:1968-76.
54. Burkitt W, Domann P, O'Connor G. Conformational changes in oxidatively stressed monoclonal antibodies studied by hydrogen exchange mass spectrometry. *Protein Sci* 2010; 19:826-35.
55. Alsenaidy MA, Kim JH, Majumdar R, Weis DD, Joshi SB, Tolbert TJ, Middaugh CR, Volkin DB. High-throughput biophysical analysis and data visualization of conformational stability of an IgG1 monoclonal antibody after deglycosylation. *J Pharm Sci* 2013; 102:3942-56.
56. Kayser V, Chennamsetty N, Voynov V, Forrer K, Helk B, Trout BL. Glycosylation influences on the aggregation propensity of therapeutic monoclonal antibodies. *Biotechnol J* 2011; 6:38-44.
57. Alsenaidy MA, Okbazghi SZ, Kim JH, Joshi SB, Middaugh CR, Tolbert TJ, Volkin DB. Physical Stability Comparisons of IgG1-Fc Variants: Effects of N-Glycosylation Site Occupancy and Asp/Gln Residues at Site Asn 297. *J Pharm Sci* 2014.

58. Gong R, Vu BK, Feng Y, Prieto DA, Dyba MA, Walsh JD, Prabakaran P, Veenstra TD, Tarasov SG, Ishima R, et al. Engineered Human Antibody Constant Domains with Increased Stability. *J Biol Chem* 2009; 284:14203-10.
59. Ying T, Chen W, Feng Y, Wang Y, Gong R, Dimitrov DS. Engineered soluble monomeric IgG1 CH3 domain: generation, mechanisms of function, and implications for design of biological therapeutics. *J Biol Chem* 2013; 288:25154-64.
60. Tang L, Sundaram S, Zhang J, Carlson P, Matathia A, Parekh B, Zhou Q, Hsieh MC. Conformational characterization of the charge variants of a human IgG1 monoclonal antibody using H/D exchange mass spectrometry. *mAbs* 2013; 5:114-25.
61. Khawli LA, Goswami S, Hutchinson R, Kwong ZW, Yang J, Wang X, Yao Z, Sreedhara A, Cano T, Tesar D, et al. Charge variants in IgG1: Isolation, characterization, in vitro binding properties and pharmacokinetics in rats. *mAbs* 2010; 2:613-24.
62. Glasoe P, Long F. Use of glass electrodes to measure acidities in deuterium oxide. *J Phys Chem* 1960; 64.
63. Wang L, Pan H, Smith DL. Hydrogen Exchange-Mass Spectrometry: optimization of digestion conditions. *Mol Cell Proteomics* 2002; 1:132-8.
64. Busby SA, Chalmers MJ, Griffin PR. Improving digestion efficiency under H/D exchange conditions with activated pepsinogen coupled columns. *Int J Mass spectrom* 2007; 259:130-9.
65. Majumdar R, Manikwar P, Hickey JM, Arora J, Middaugh CR, Volkin DB, Weis DD. Minimizing Carry-Over in an Online Pepsin Digestion System used for the H/D Exchange Mass Spectrometric Analysis of an IgG1 Monoclonal Antibody. *J Am Soc Mass Spectrom* 2012; 23:2140-8.

66. Padlan EA. Anatomy of the antibody molecule. *Mol Immunol* 1994; 31:169-217.
67. Šali A, Blundell TL. Comparative Protein Modelling by Satisfaction of Spatial Restraints. *J Mol Biol* 1993; 234:779-815.

Table 5.1

Proteins	pH	T _{onset} (°C)		T _{m1} (°C)		T _{m2} (°C)		T _{m3} (°C)	
		Mean	SD	Mean	SD	Mean	SD	Mean	SD
mAb-A	6.0	62.1	0.9	69.6	<0.1	82.9	<0.1	91.9	<0.1
mAb-E		55.2	0.4	63.1	<0.1	83.1	<0.1	91.8	<0.1
Δ (mAb-A – mAb-E)		6.9		6.5		- 0.2		0.1	
mAb-A	7.4	63.5	0.2	70.3	<0.1	83.1	<0.1	87.2	<0.1
mAb-E		56.5	0.2	63.6	<0.1	83.0	<0.1	87.2	<0.1
Δ (mAb-A – mAb-E)		7.0		6.7		0.1		0.0	

Thermal stability of mAb-A and mAb-E at pH 6.0 and pH 7.4 indicated by the melting onset temperature (T_{onset}) and the melting transitions (T_{m1}, T_{m2}, and T_{m3}) as measured by DSC. Formulations contained 50 mM sodium phosphate, 150 mM sodium chloride with 0.5 mg ml⁻¹ of mAb-A or mAb-E. The mean and standard deviations are based on three independent measurements.

Table 5.S1

Peptide Number	Location
1	Heavy 4-19 (VH)
2	Heavy 5-19 (VH)
3	Heavy 5-20 (VH)
4	Heavy 18-22 (VH)
5	Heavy 9-32 (VH)
6	Heavy 16-39 (VH)
7	Heavy 27-30 (VH)
8	Heavy 27-45 (VH)
9	Heavy 28-46 (VH)
10	Heavy 28-47 (VH)
11	Heavy 27-50 (VH)
12	Heavy 28-50 (VH)
13	Heavy 35-44 (VH)
14	Heavy 35-50 (VH)
15	Heavy 35-52 (VH)
16	Heavy 37-52 (VH)
17	Heavy 41-52 (VH)
18	Heavy 51-62 (VH)
19	Heavy 51-69 (VH)
20	Heavy 53-82 (VH)
21	Heavy 63-73 (VH)
22	Heavy 63-77 (VH)
23	Heavy 66-82 (VH)
24	Heavy 70-82 (VH)
25	Heavy 78-81 (VH)
26	Heavy 83-94 (VH)
27	Heavy 79-103 (VH)
28	Heavy 91-112 (VH)
29	Heavy 106-119 (VH)
30	Heavy 112-119 (VH)
31	Heavy 108-124 (VH)
32	Heavy 113-125 (VH)
33	Heavy 115-130
34	Heavy 136-143 (CH1)
35	Heavy 147-154 (CH1)
36	Heavy 144-168 (CH1)
37	Heavy 151-168 (CH1)

38	Heavy 158-163 (CH1)
39	Heavy 149-177 (CH1)
40	Heavy 159-177 (CH1)
41	Heavy 166-172 (CH1)
42	Heavy 174-188 (CH1)
43	Heavy 183-188 (CH1)
44	Heavy 183-200 (CH1)
45	Heavy 188-200 (CH1)
46	Heavy 189-200 (CH1)
47	Heavy 195-205 (CH1)
48	Heavy 201-212 (CH1)
49	Heavy 214-219 (CH1)
50	Heavy 220-238
51	Heavy 238-243 (CH2)
52	Heavy 238-254 (CH2)
53	Heavy 245-251 (CH2)
54	Heavy 244-254 (CH2)
55	Heavy 244-255 (CH2)
56	Heavy 245-254 (CH2)
57	Heavy 247-254 (CH2)
58	Heavy 247-255 (CH2)
59	Heavy 255-263 (CH2)
60	Heavy 255-264 (CH2)
61	Heavy 256-263 (CH2)
62	Heavy 261-269 (CH2)
63	Heavy 266-271 (CH2)
64	Heavy 267-271 (CH2)
65	Heavy 264-280 (CH2)
66	Heavy 265-280 (CH2)
67	Heavy 266-280 (CH2)
68	Heavy 269-280 (CH2)
69	Heavy 272-290 (CH2)
70	Heavy 273-290 (CH2)
71	Heavy 279-294 (CH2)
72	Heavy 303-309 (CH2)
73	Heavy 304-309 (CH2)
74	Heavy 309-312 (CH2)
75	Heavy 312-318 (CH2)
76	Heavy 310-321 (CH2)
77	Heavy 311-327 (CH2)
78	Heavy 314-327

79	Heavy 320-327
80	Heavy 315-337
81	Heavy 320-332
82	Heavy 328-336
83	Heavy 337-351 (CH3)
84	Heavy 346-349 (CH3)
85	Heavy 337-359 (CH3)
86	Heavy 338-362 (CH3)
87	Heavy 352-358 (CH3)
88	Heavy 352-359 (CH3)
89	Heavy 352-361 (CH3)
90	Heavy 352-367 (CH3)
91	Heavy 352-370 (CH3)
92	Heavy 360-367 (CH3)
93	Heavy 360-369 (CH3)
94	Heavy 371-379 (CH3)
95	Heavy 372-379 (CH3)
96	Heavy 369-383 (CH3)
97	Heavy 371-382 (CH3)
98	Heavy 372-381 (CH3)
99	Heavy 372-382 (CH3)
100	Heavy 372-383 (CH3)
101	Heavy 372-401 (CH3)
102	Heavy 380-393 (CH3)
103	Heavy 384-393 (CH3)
104	Heavy 380-401 (CH3)
105	Heavy 382-401 (CH3)
106	Heavy 383-401 (CH3)
107	Heavy 384-401 (CH3)
108	Heavy 380-407 (CH3)
109	Heavy 383-407 (CH3)
110	Heavy 384-407 (CH3)
111	Heavy 394-401 (CH3)
112	Heavy 392-409 (CH3)
113	Heavy 394-407 (CH3)
114	Heavy 402-407 (CH3)
115	Heavy 394-416 (CH3)
116	Heavy 402-408 (CH3)
117	Heavy 408-413 (CH3)
118	Heavy 409-413 (CH3)
119	Heavy 408-425 (CH3)

120	Heavy 408-426 (CH3)
121	Heavy 409-426 (CH3)
122	Heavy 410-426 (CH3)
123	Heavy 408-429 (CH3)
124	Heavy 414-425 (CH3)
125	Heavy 414-426 (CH3)
126	Heavy 428-433 (CH3)
127	Heavy 427-449 (CH3)
128	Heavy 429-449 (CH3)
129	Heavy 430-449 (CH3)
130	Heavy 432-449 (CH3)
131	Heavy 434-449 (CH3)
132	Heavy 436-449 (CH3)
133	Light 21-25 (VL)
134	Light 17-34 (VL)
135	Light 20-37 (VL)
136	Light 35-45 (VL)
137	Light 46-53 (VL)
138	Light 43-60 (VL)
139	Light 46-71 (VL)
140	Light 60-81 (VL)
141	Light 73-79 (VL)
142	Light 67-90 (VL)
143	Light 95-102 (VL)
144	Light 90-108 (VL)
145	Light 106-118 (CL)
146	Light 115-124 (CL)
147	Light 115-130 (CL)
148	Light 116-129 (CL)
149	Light 115-131 (CL)
150	Light 116-130 (CL)
151	Light 116-131 (CL)
152	Light 125-142 (CL)
153	Light 128-147 (CL)
154	Light 135-160 (CL)
155	Light 143-160 (CL)
156	Light 148-160 (CL)
157	Light 152-163 (CL)
158	Light 147-174 (CL)
159	Light 151-171 (CL)
160	Light 161-177 (CL)

161	Light 161-178 (CL)
162	Light 172-178 (CL)
163	Light 178-194 (CL)
164	Light 179-194 (CL)
165	Light 185-195 (CL)
166	Light 195-213 (CL)
167	Light 203-209 (CL)

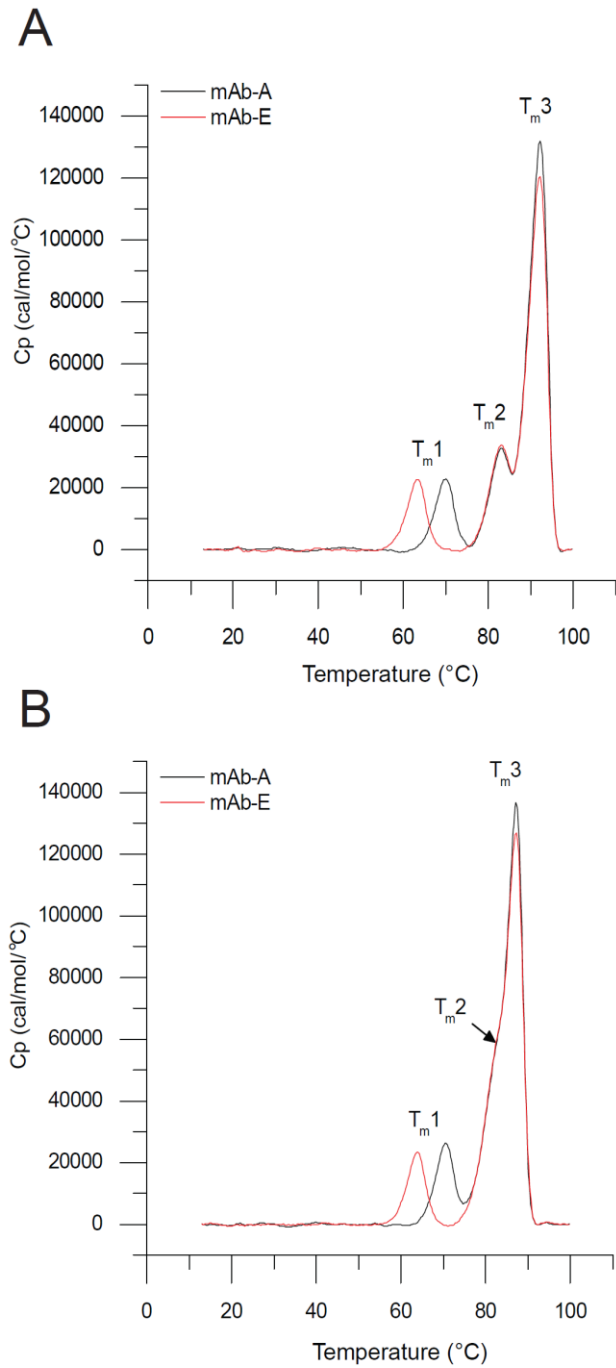
Segment location in the primary sequence of mAb-A or mAb-E corresponding to peptide numbers assigned based on segment midpoint calculated in ascending order from N-to-C termini of the heavy followed by the light chain of mAb-A/mAb-E.

Table 5.S2

Protein	Observed MS peaks	Theoretical mass (Da)	Possible glycans	Error (Da)
mAb-A	148040.50	148038.20	G0f/G0f	2.30
	148202.12	148200.36	G0f/G1f	1.76
	148364.04	148362.51	G1f/G1f	1.53
mAb-E	148188.55	148186.30	G0f/G0f	2.25
	148350.82	148348.40	G0f/G1f	2.42
	148513.43	148510.50	G1f/G1f	2.93

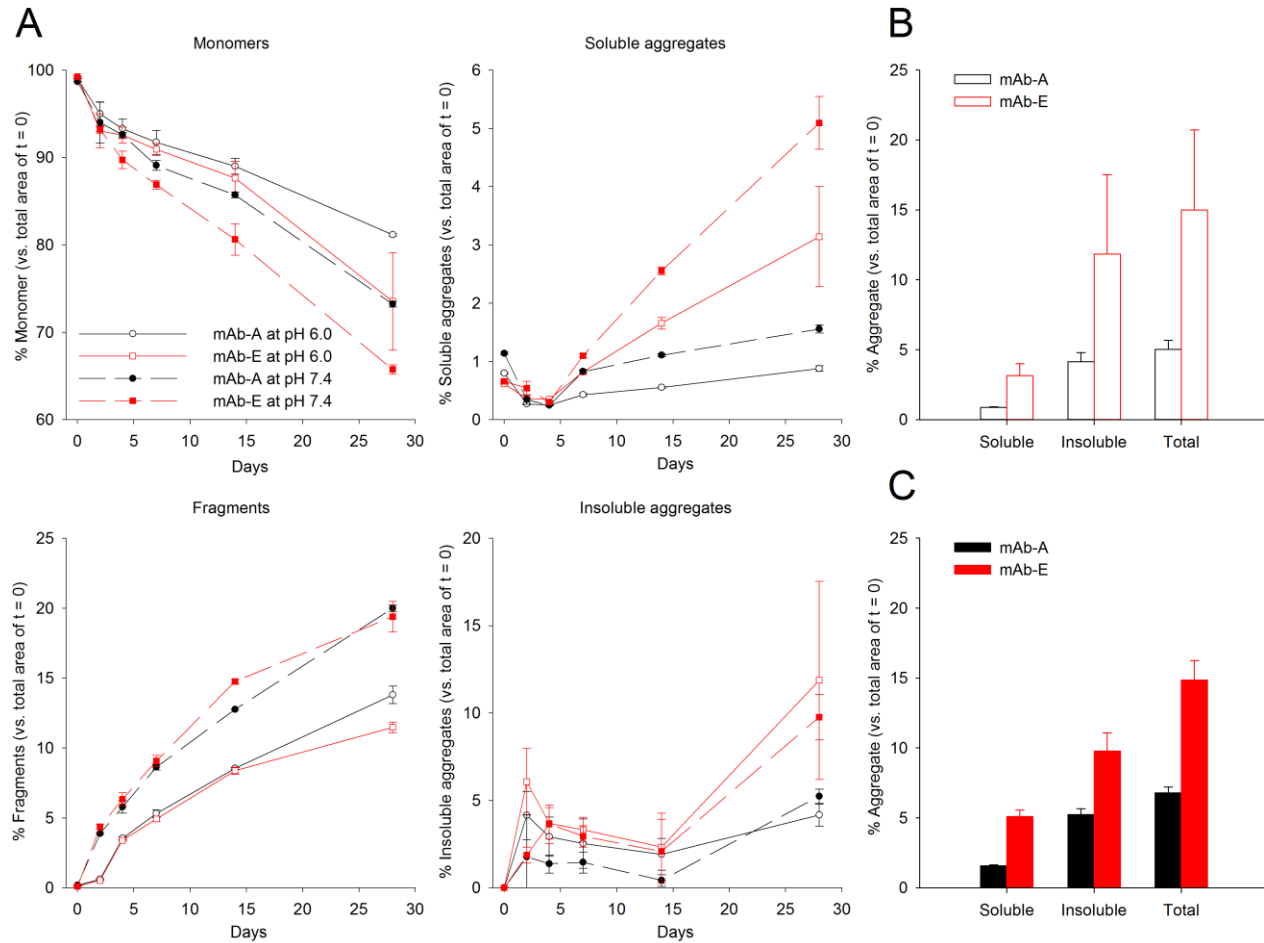
Possible glycoforms of mAb-A and mAb-E are shown according to the intact mass spectra of both the mAbs. The mass difference between the two mAbs is due to the YTE mutations. These results were further confirmed using FabRICATOR protease digestion and accurate mass measurement of the glycosylated fragments (results not shown).

Figure 5.1



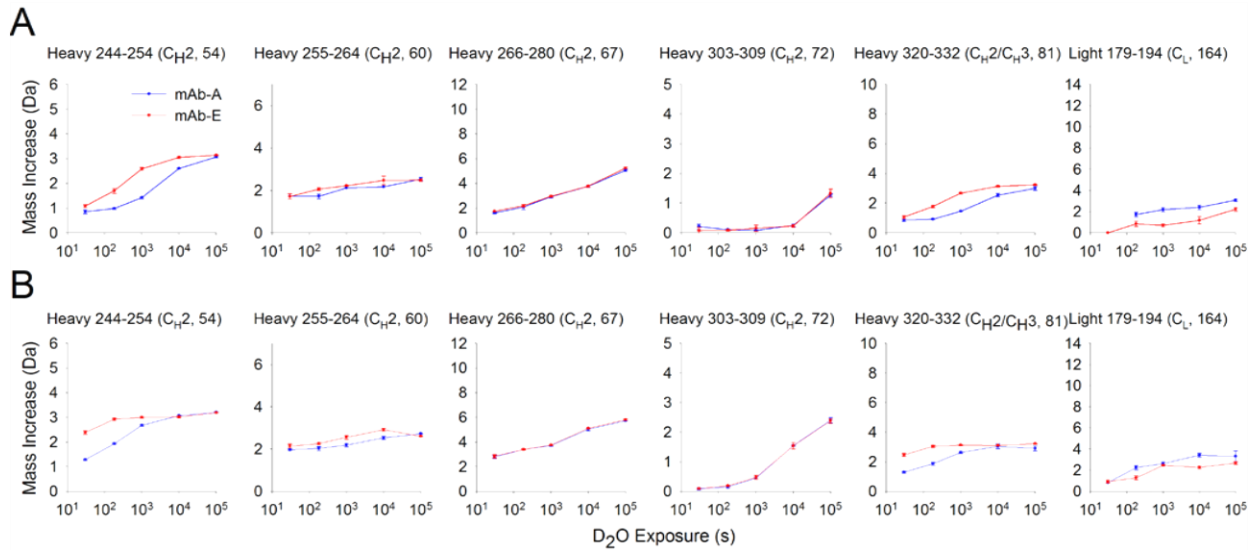
Representative overlay of DSC thermograms of mAb-A and mAb-E at (A) pH 6.0 and (B) pH 7.4. The T_{m1}, T_{m2}, and T_{m3} values indicate the first, second, and third thermal melting transitions for the two mAbs.

Figure 5.2



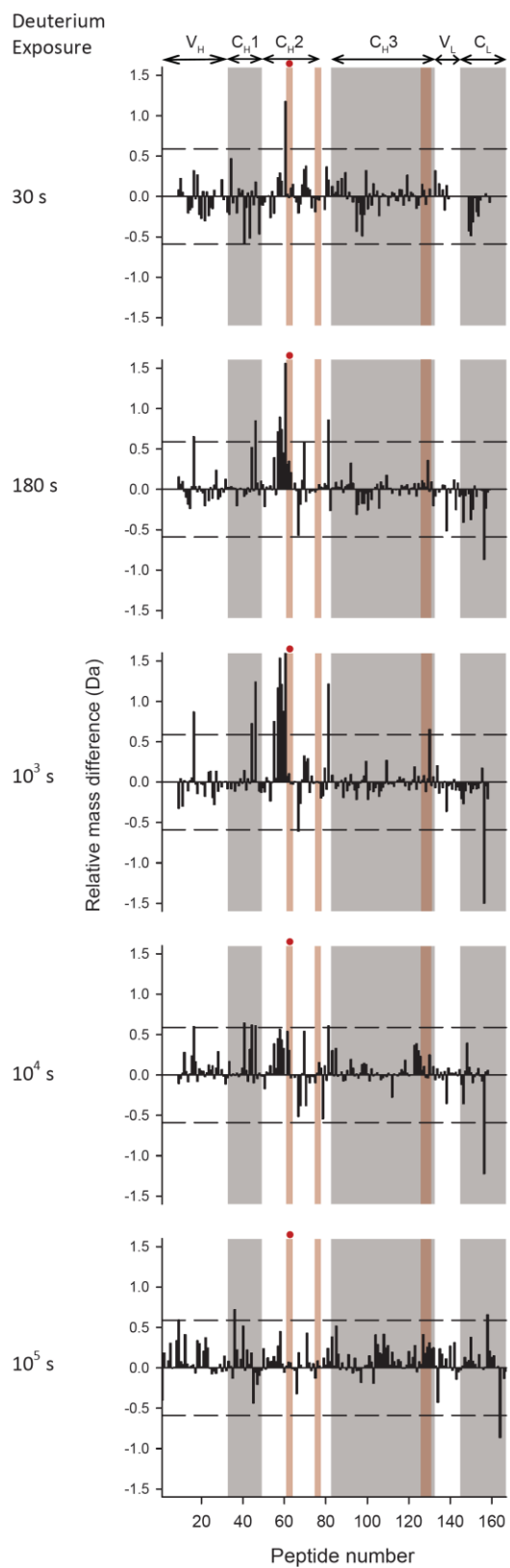
Accelerated storage stability of mAb-A and mAb-E after incubation at 50 °C for up to 28 days as measured by SEC. The mAbs were formulated in 50 mM sodium phosphate and 150 mM sodium chloride at pH 6.0 and 7.4. (A) The percentage of monomer, fragments, soluble aggregates, and insoluble aggregates of mAb-A and mAb-E analyzed by SEC after incubation at 50 °C for 0, 2, 4, 7, 14, and 28 days relative to day zero. Error bars represent one standard deviation for duplicate analyses of duplicate vials. Bar charts representing the percentage of soluble, insoluble, and total aggregate content in mAb-A and mAb-E after incubation for 28 days at 50 °C are shown at (B) pH 6.0 and at (C) pH 7.4.

Figure 5.3



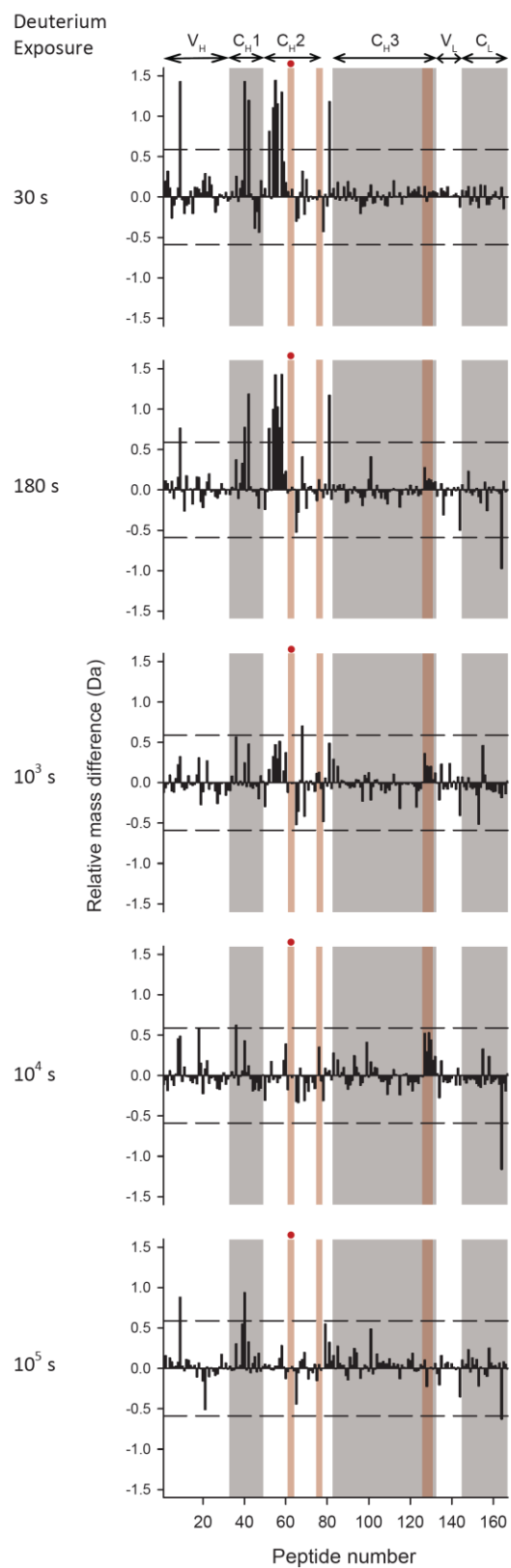
Effect of the YTE triple mutation on deuterium uptake of six peptide segments from mAb-A and mAb-E at (A) pH 6.0, and (B) pH 7.4. Domain location and peptide number of the segment are shown in parentheses. The error bars represent one standard deviation from three independent experiments.

Figure 5.4



Differential deuterium uptake at five exposure times for 167 common peptide segments of mAb-E relative to mAb-A at pH 6.0. Average mass corresponding to each exposure time for each segment is calculated based on three independent measurements. The horizontal axes denote the ordinal peptide numbers assigned based on peptide midpoints spread in ascending order from the N-to-C termini of the heavy chain followed by the light chain of mAb-A or mAb-E. Positive and negative vertical bars imply increased or decreased deuterium uptake respectively for a segment in mAb-E compared to mAb-A. The dashed lines at ± 0.59 Da indicate the 99% confidence limits for significant differences. Domain locations shown on the top of the figure are approximate as some segments span two neighboring domains. Alternate shades of white and grey in the background demarcate domain boundaries. Shades in pink demarcate segments with residues of Fc epitopes of Fc-FcRn binding interfaces. The red circles denote segments that contain the YTE mutations. Segment locations in the mAb-A/mAb-E sequence corresponding to peptide numbers can be found in the Table S1 in the supporting information.

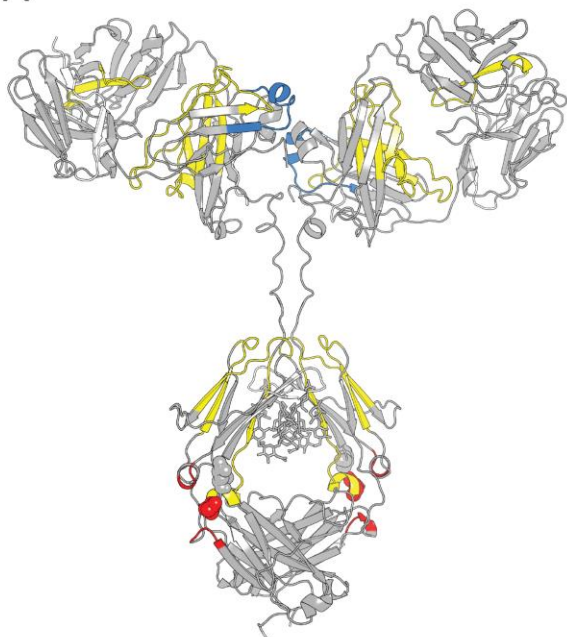
Figure 5.5



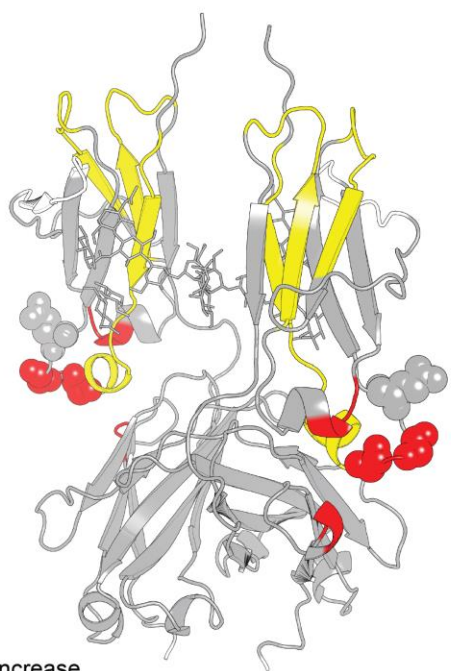
Differential deuterium uptake at five exposure times for 167 common peptide segments of mAb-E relative to mAb-A at pH 7.4. Refer to the legend for Figure 5.4 for description of the figure.

Figure 5.6

A



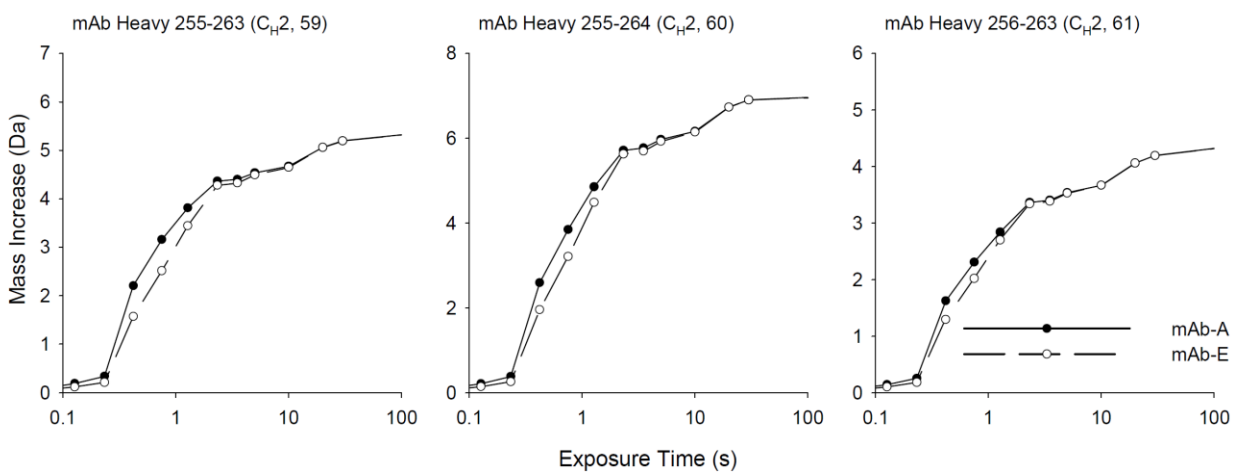
B



- Increase
- No change
- Decrease
- No data available
- Fc-FcRn binding interface
- Mutated residues

Effect of the YTE mutation (mAb-E) on the local flexibility of the native mAb (mAb-A) at pH 6.0 as measured by H/D-MS plotted on the homology models of (A) intact mAb-A and (B) Fc domain of mAb-A. Changes in flexibility of particular peptide segments are colored as shown in the legend and are derived from the differential exchange data shown in Figure 5.4.

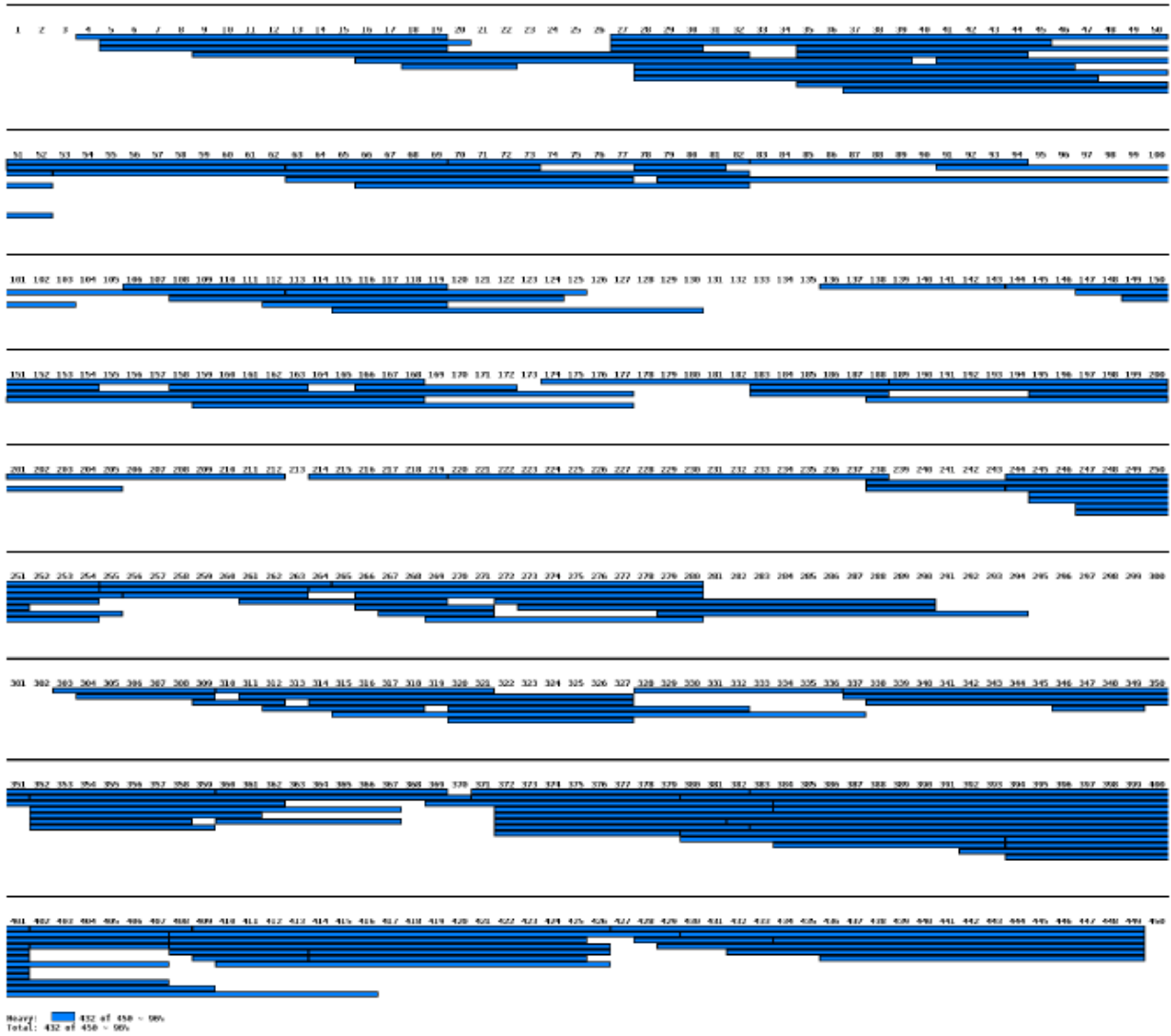
Figure 5.7



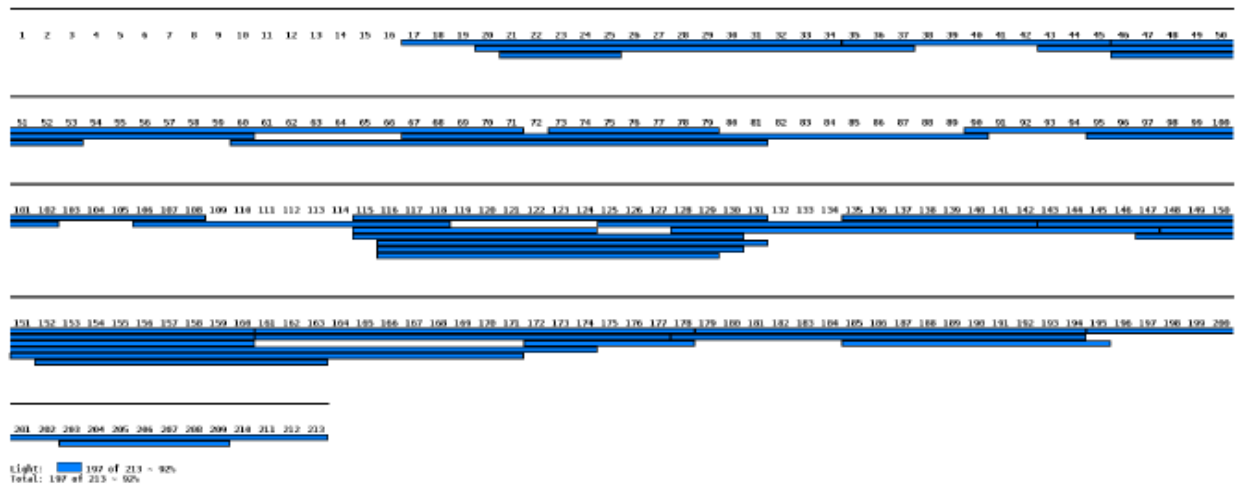
Calculated intrinsic deuterium exchange rates of three peptide segments of mAb-A and mAb-E at pD 6.0 at 25 °C. The segment identity and domain location are shown on top of each graph.

Figure 5.S1

A



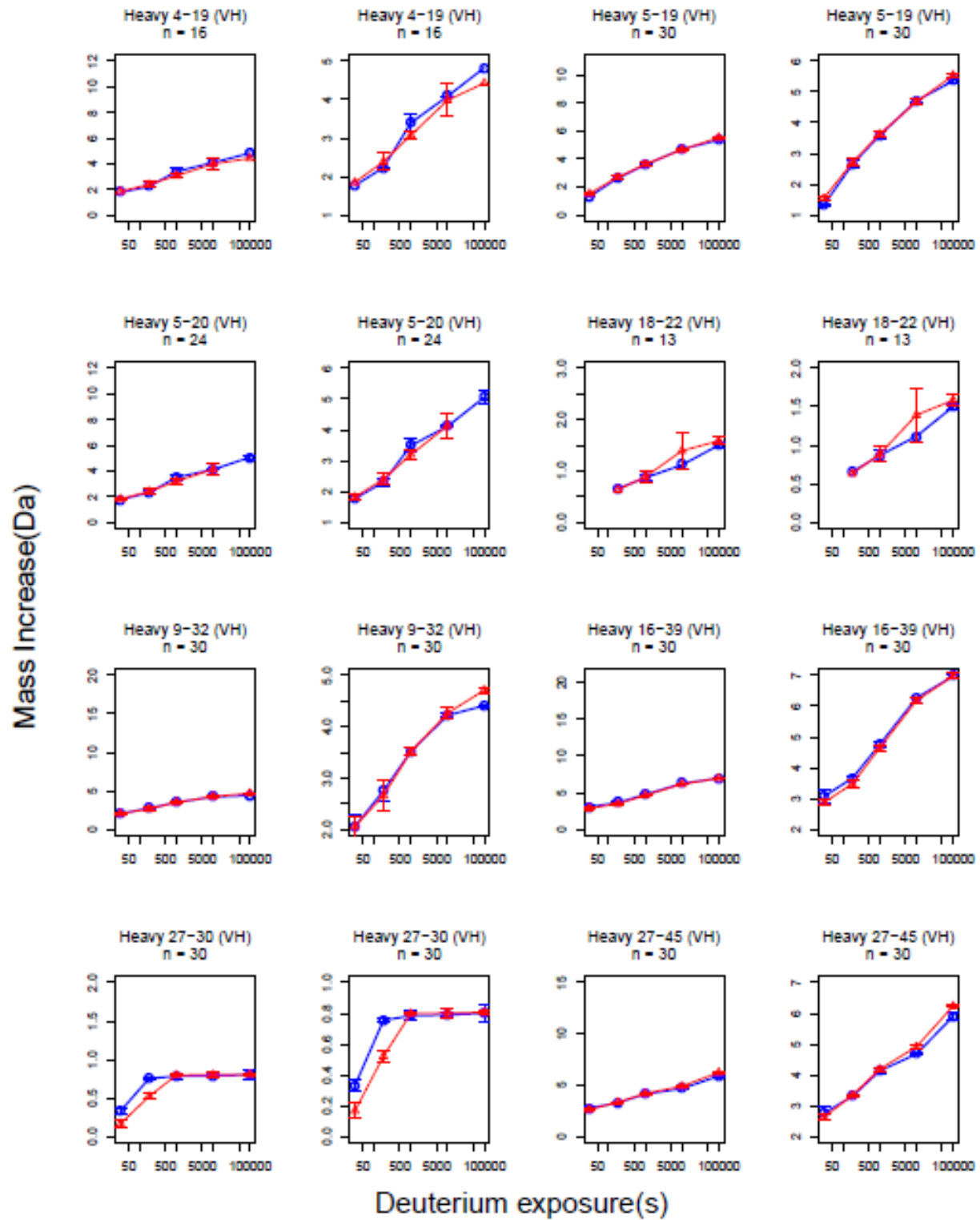
B

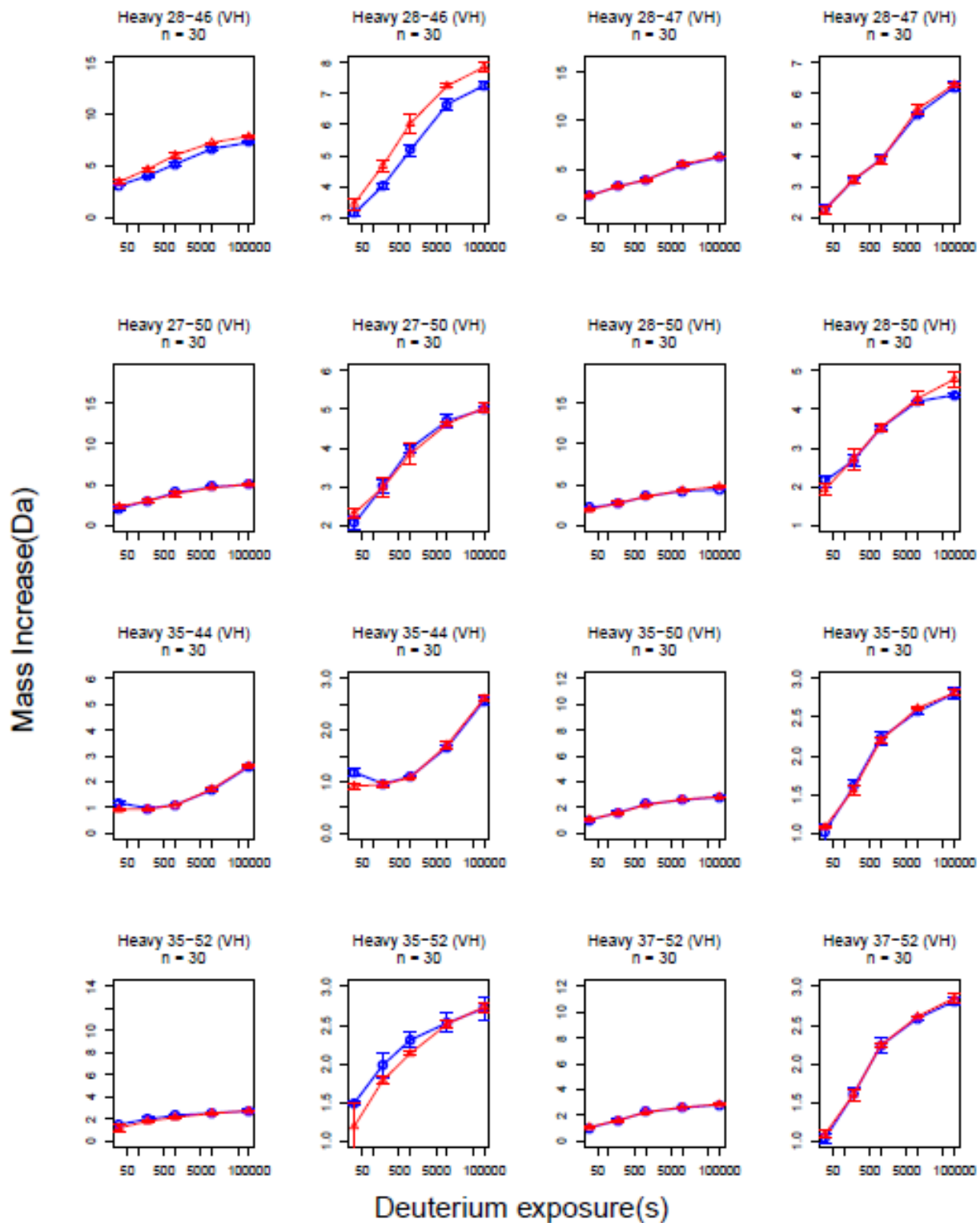


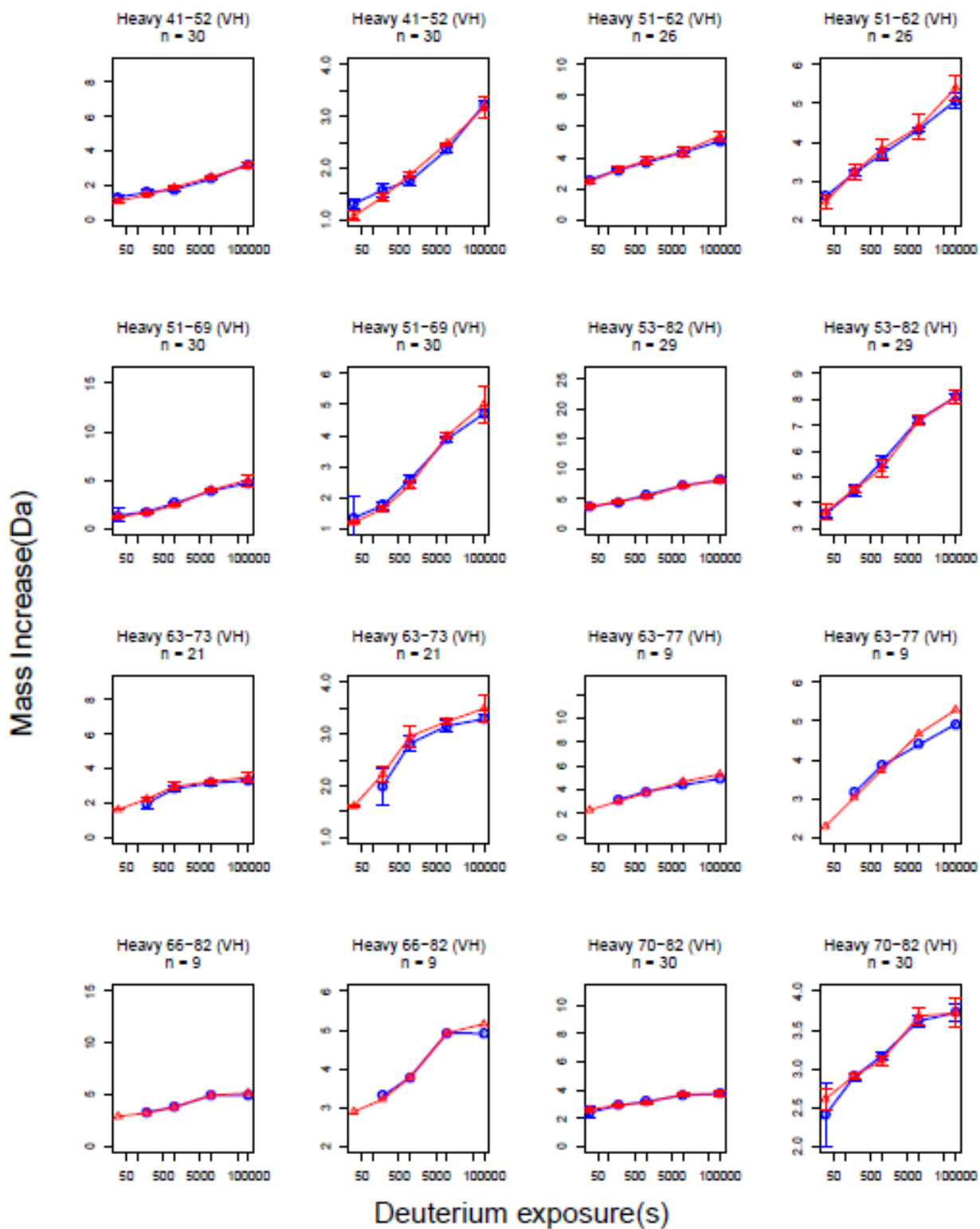
Peptide map of the (A) Heavy chain and (B) Light chain of mAb-A/mAb-E composed of 167 common segments covering the primary sequence of 96% of the HC and 92% of the LC.

Figure 5.S2

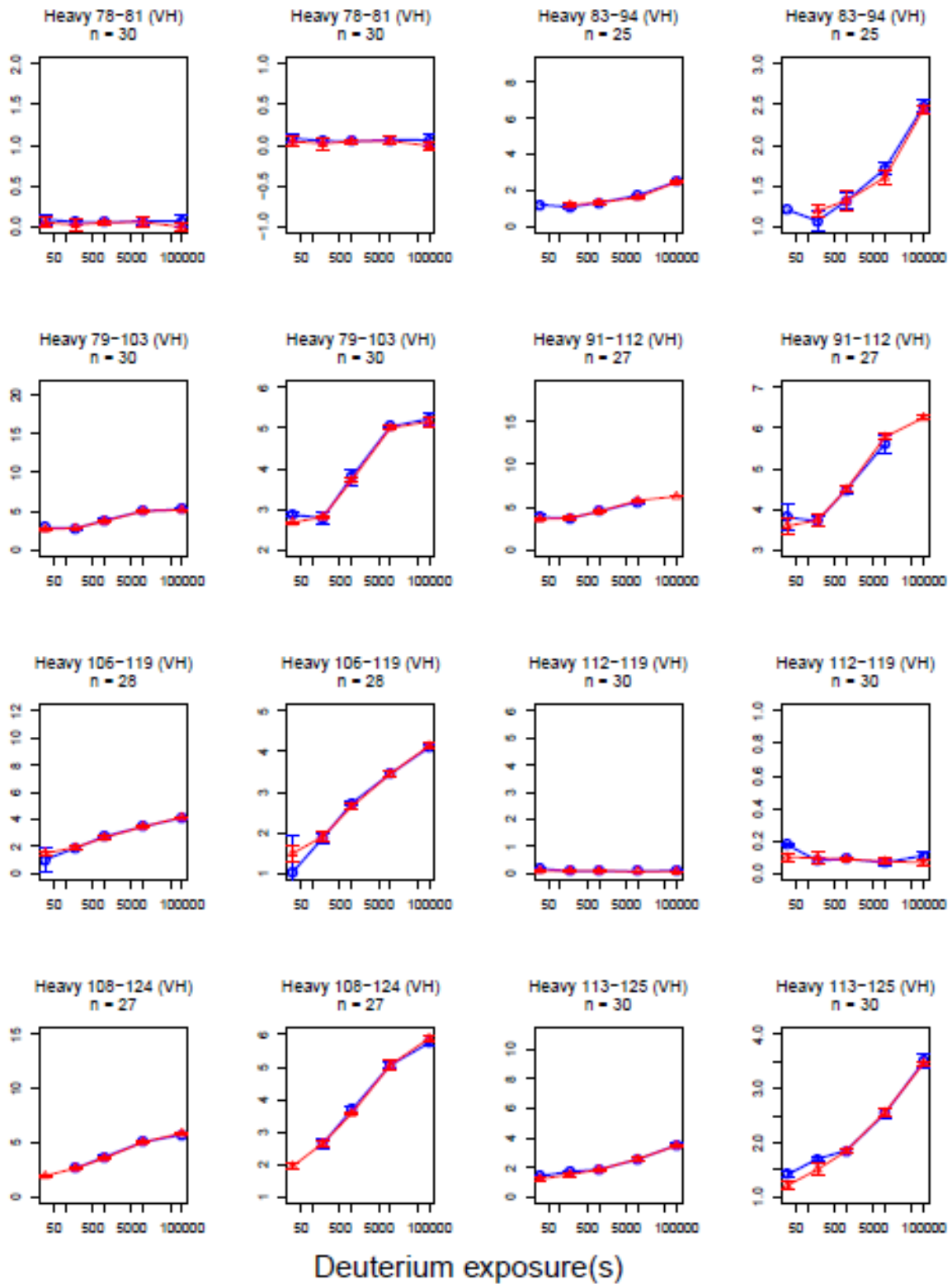
—○— mAb-A
—△— mAb-E



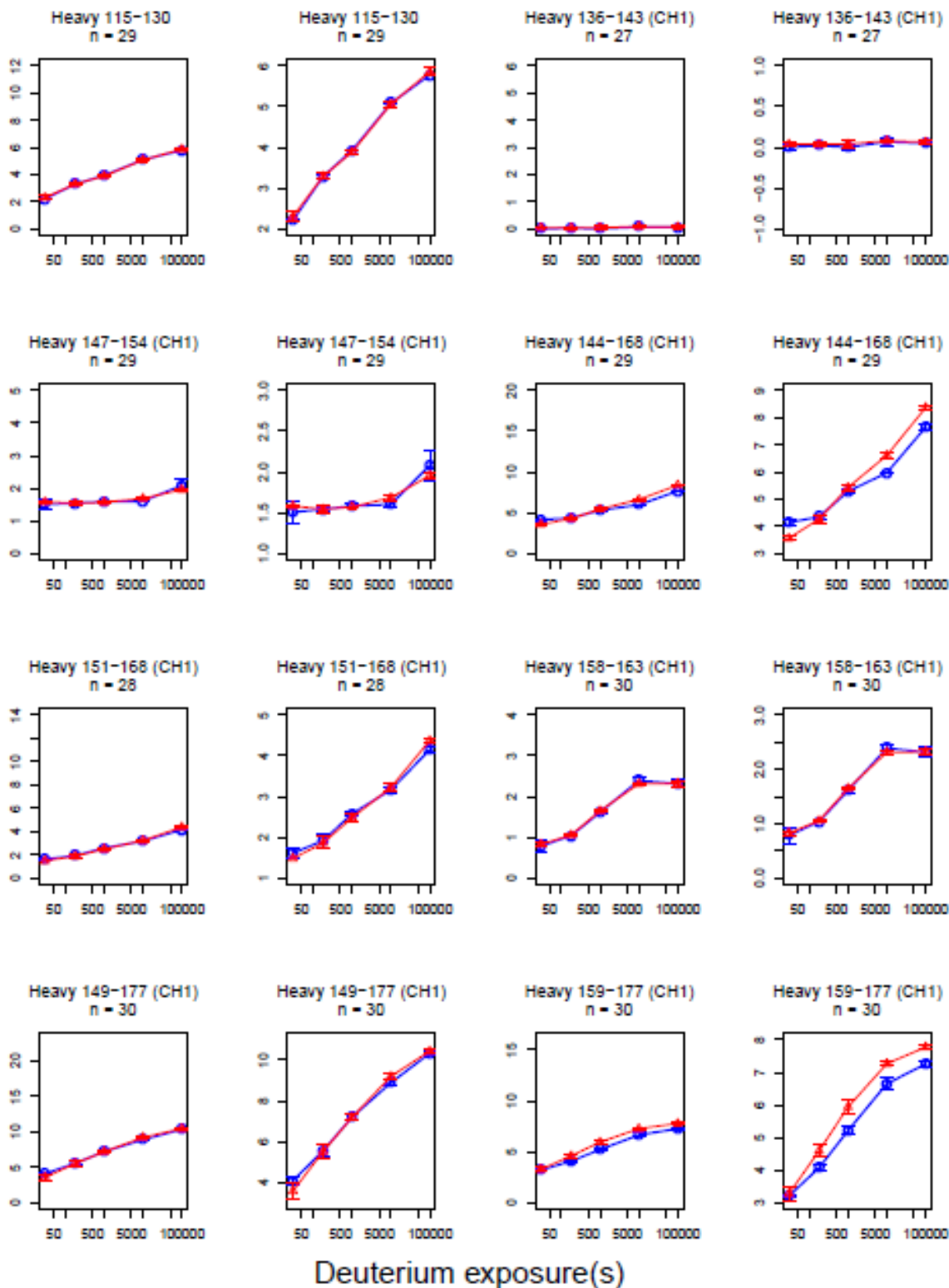


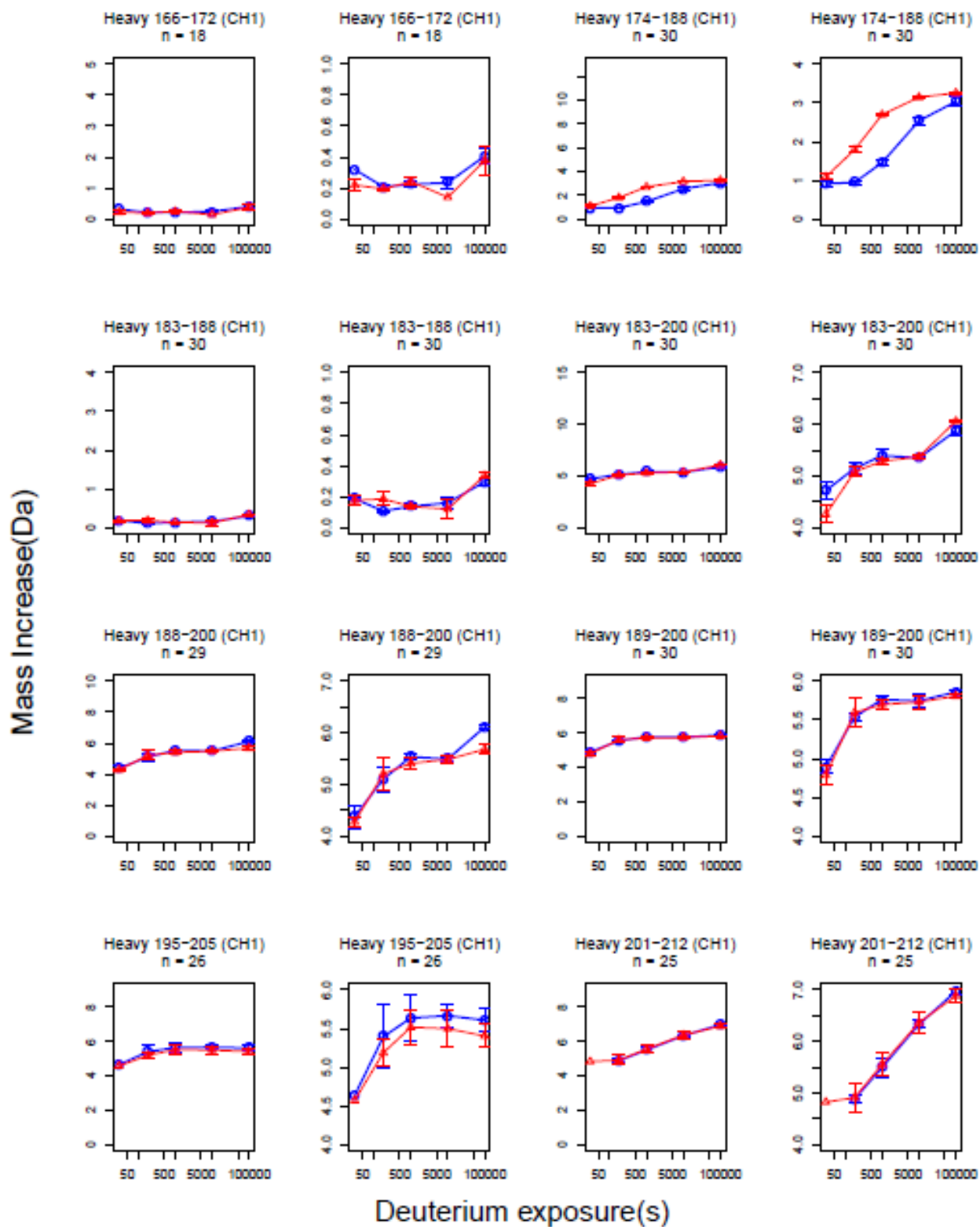


Mass Increase(Da)

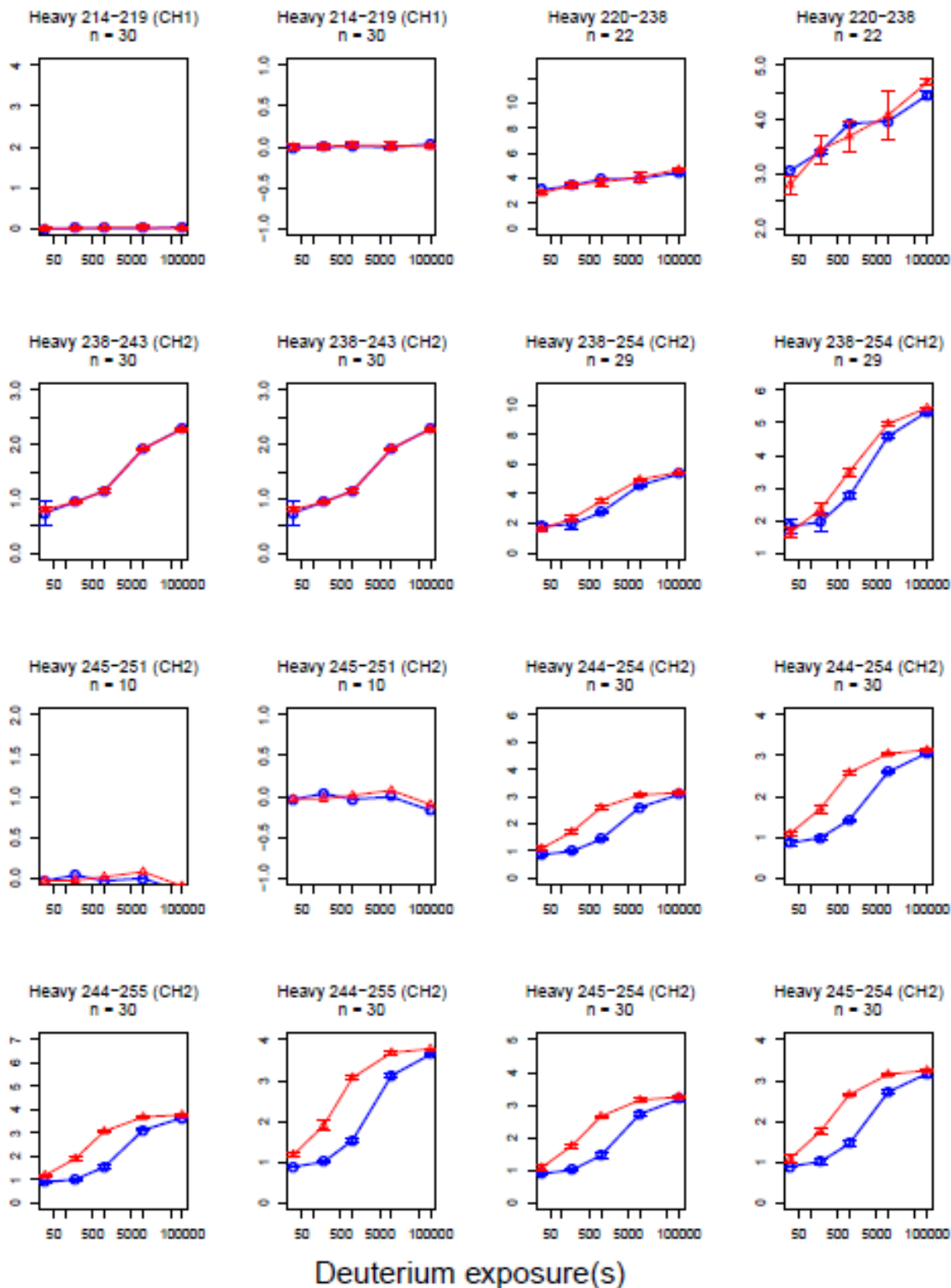


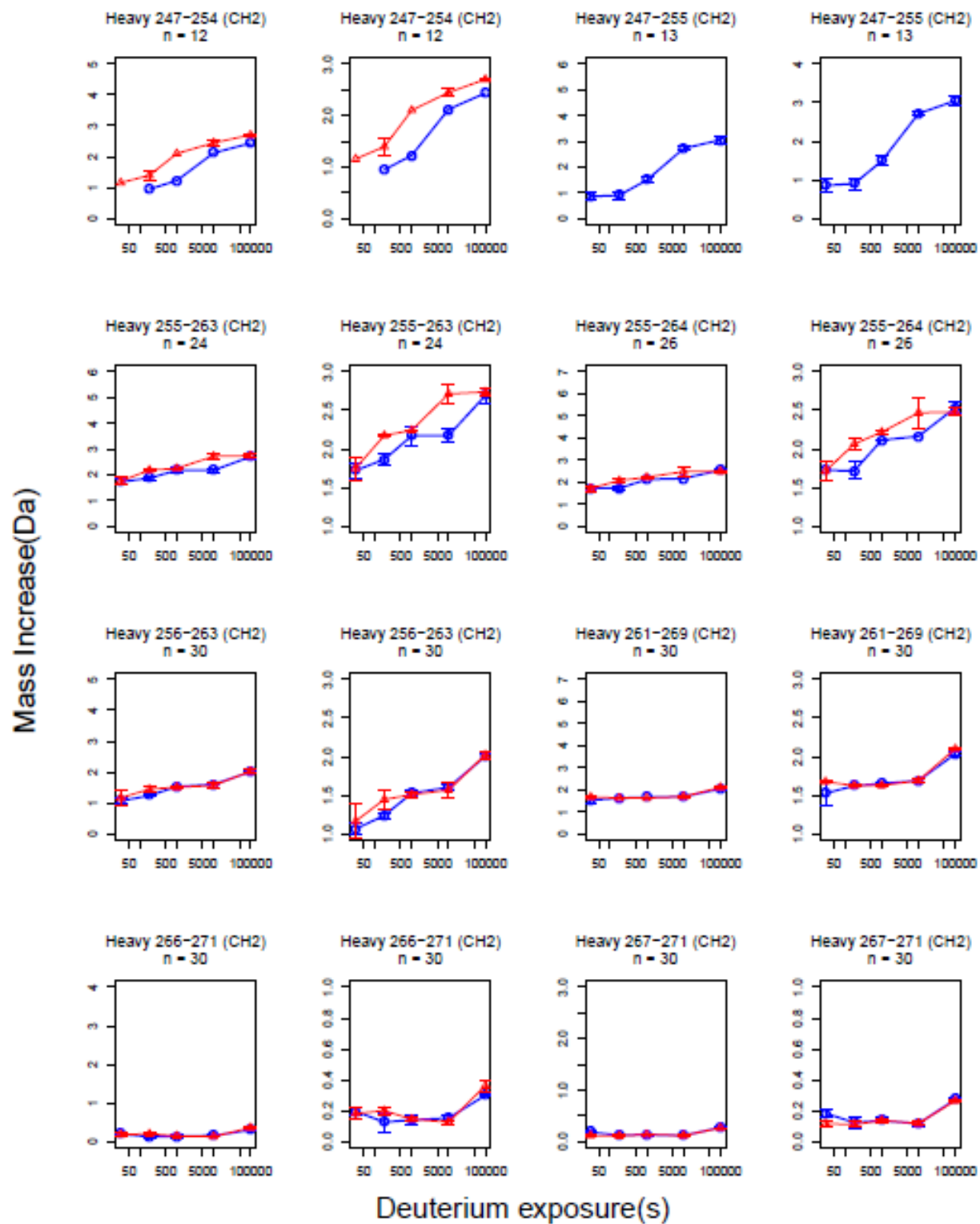
Mass Increase(Da)

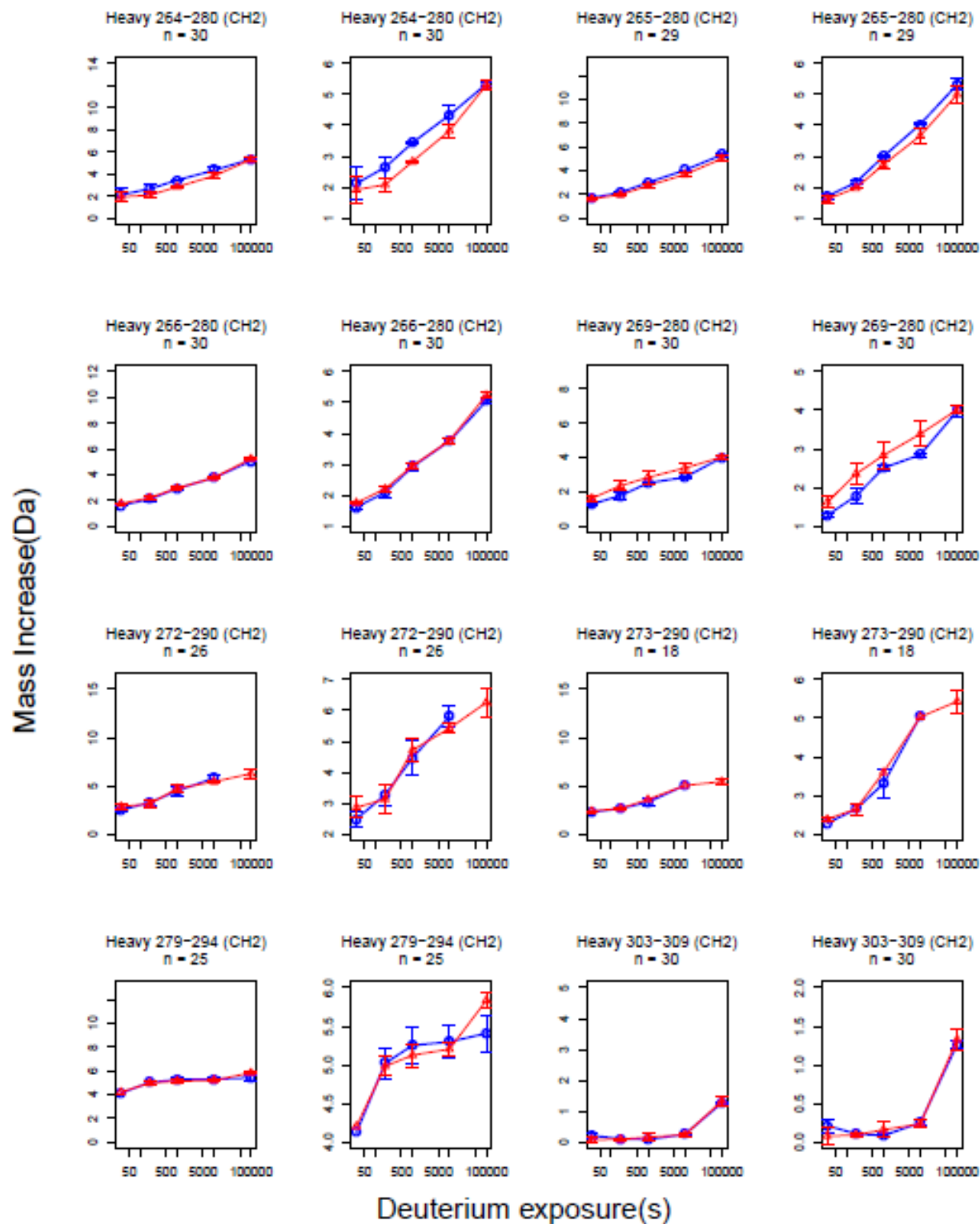


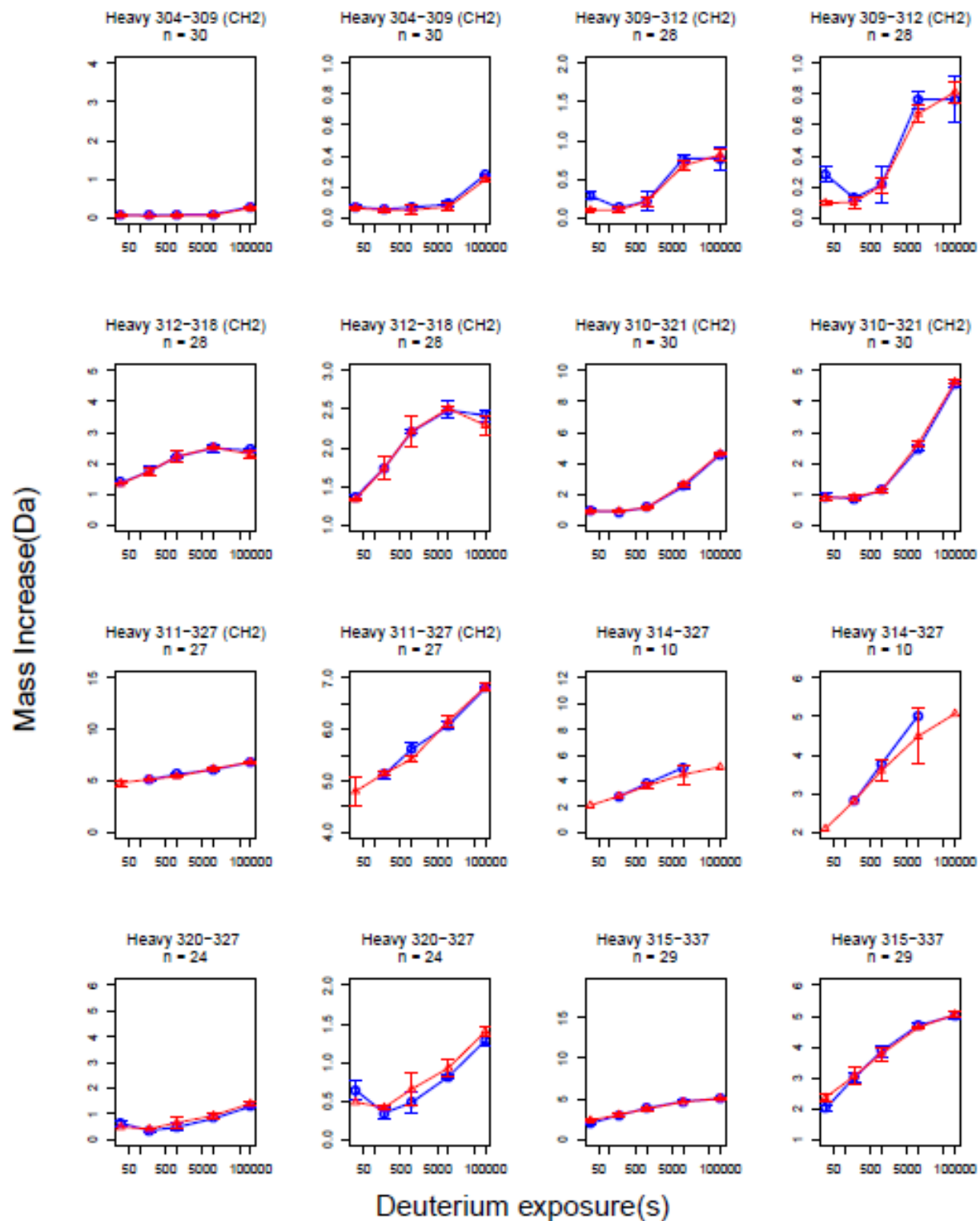


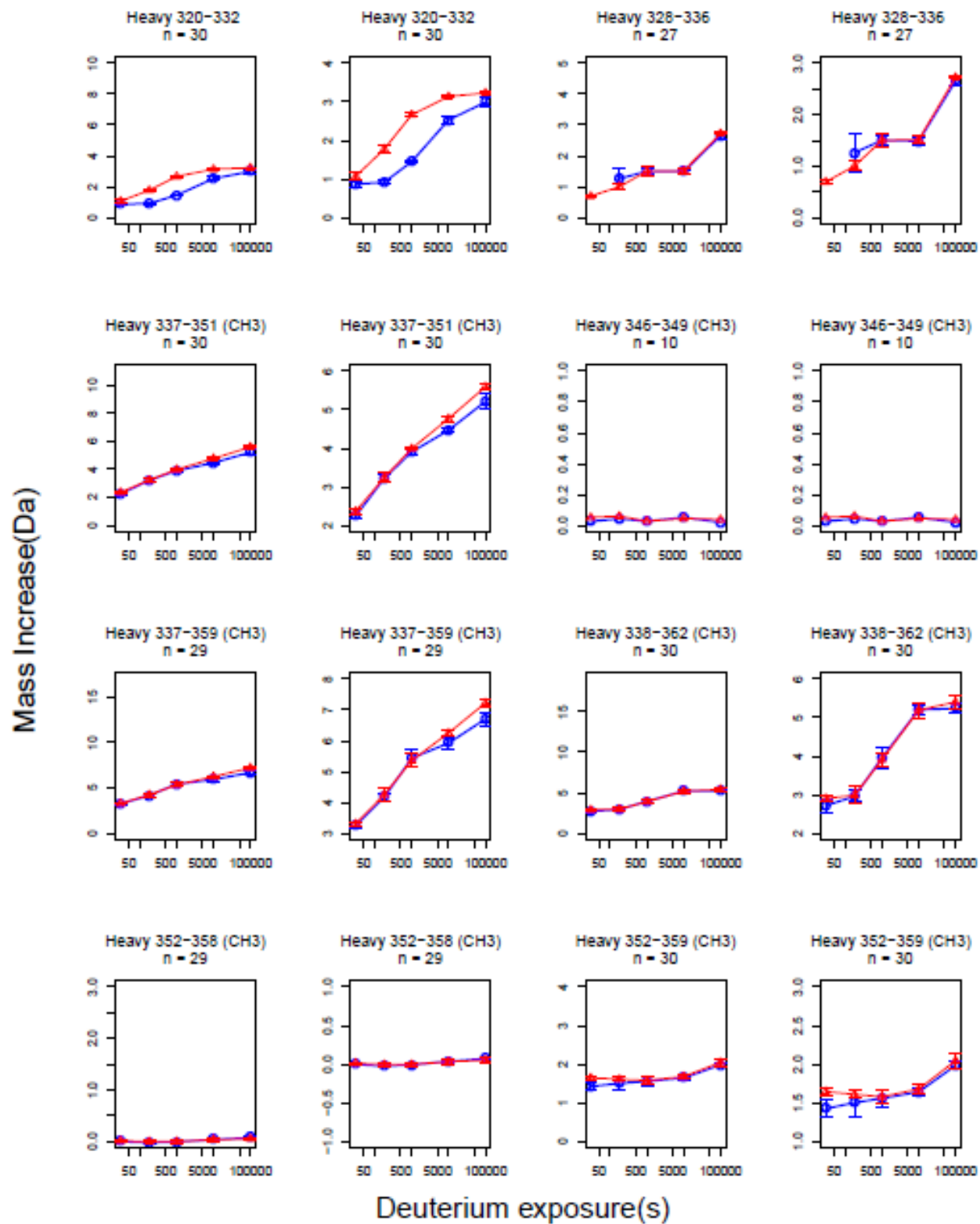
Mass Increase(Da)



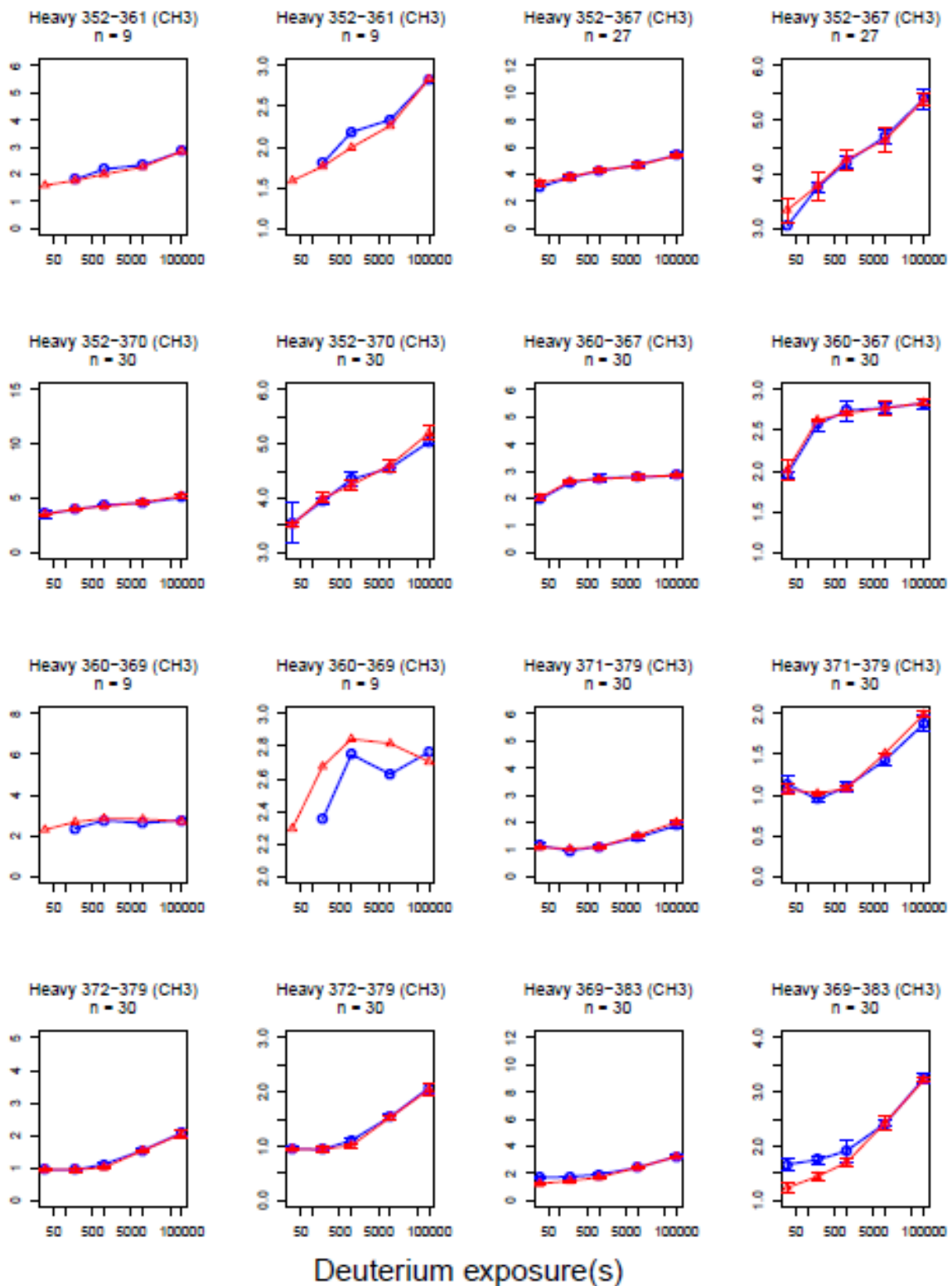


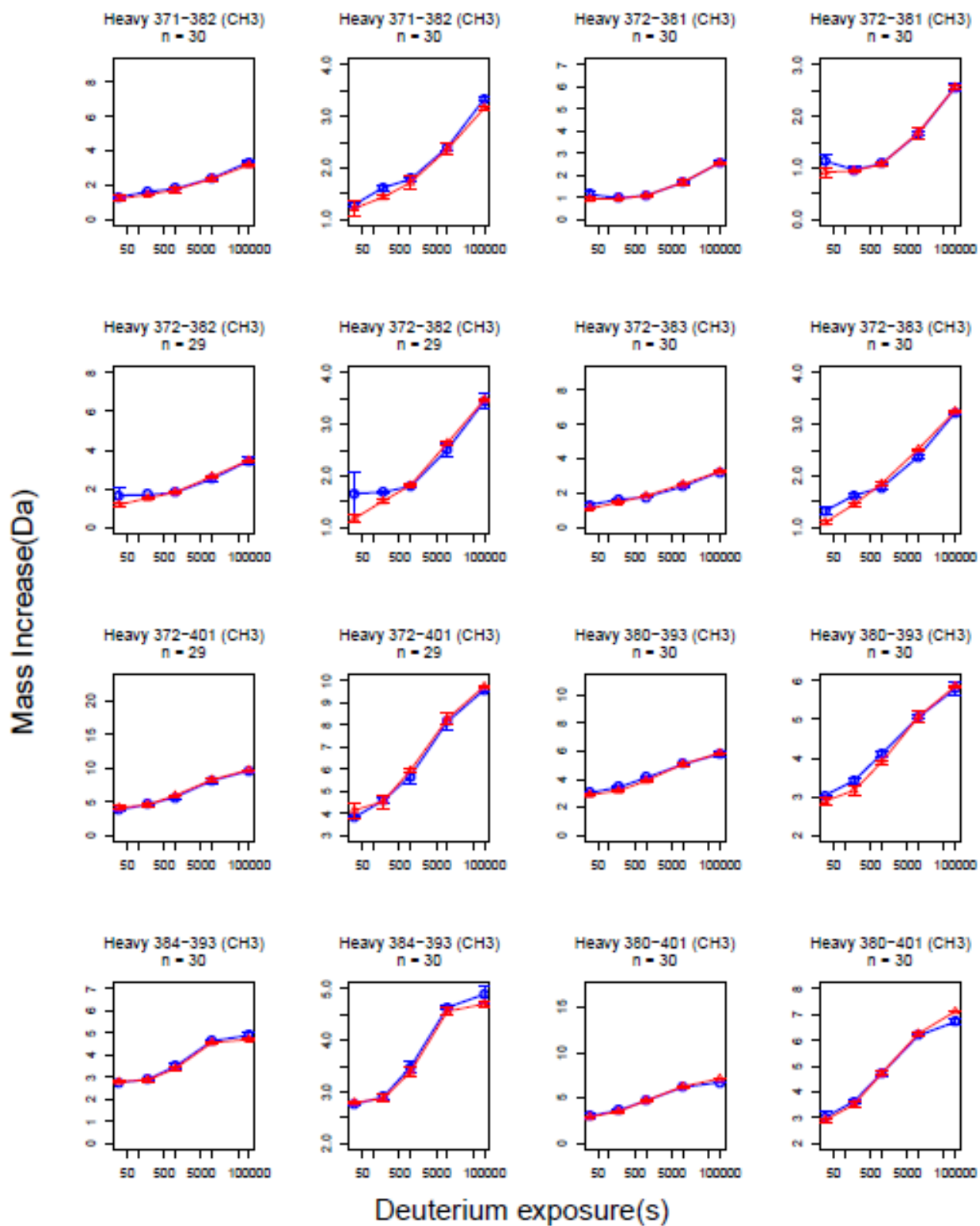


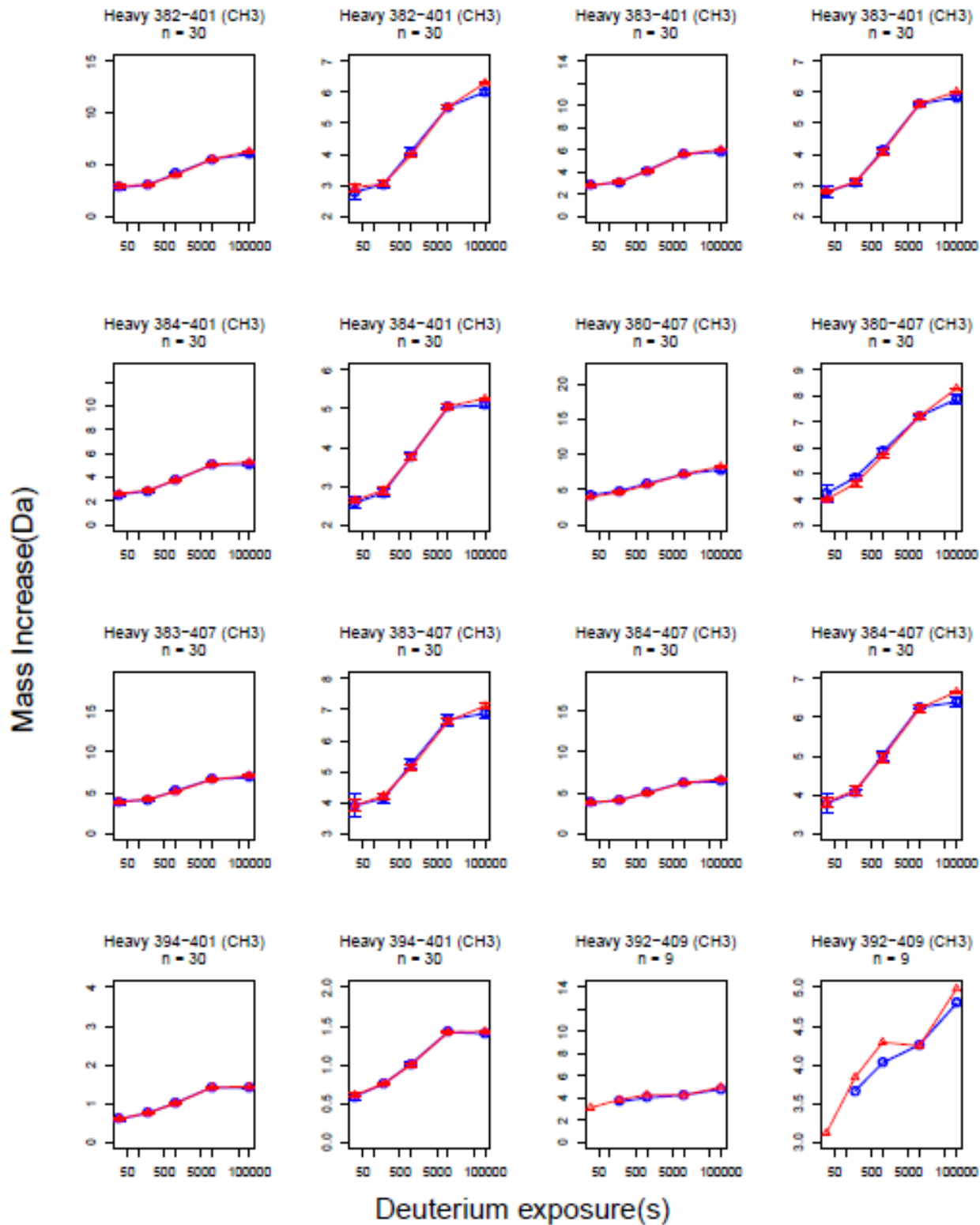




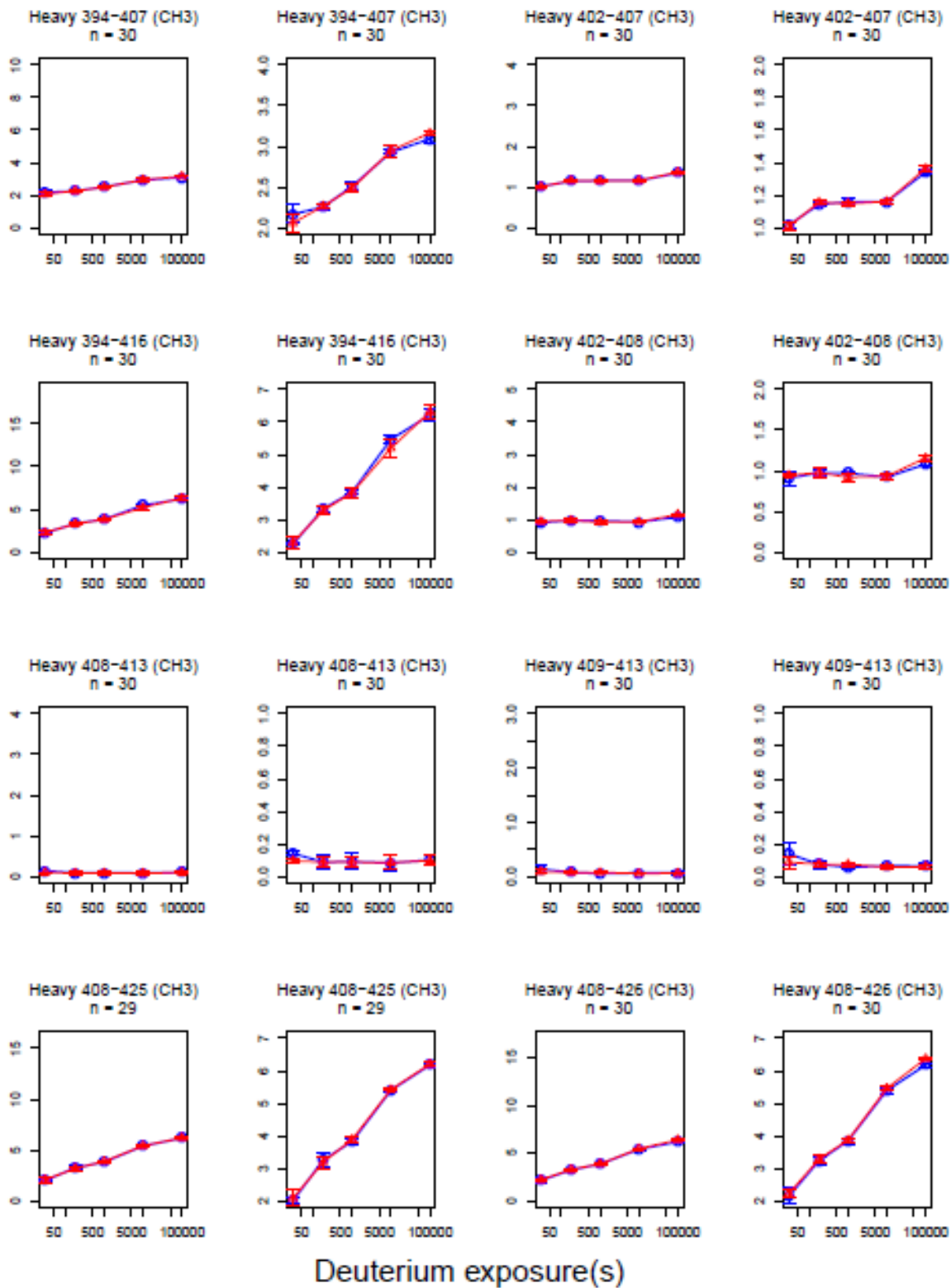
Mass Increase(Da)



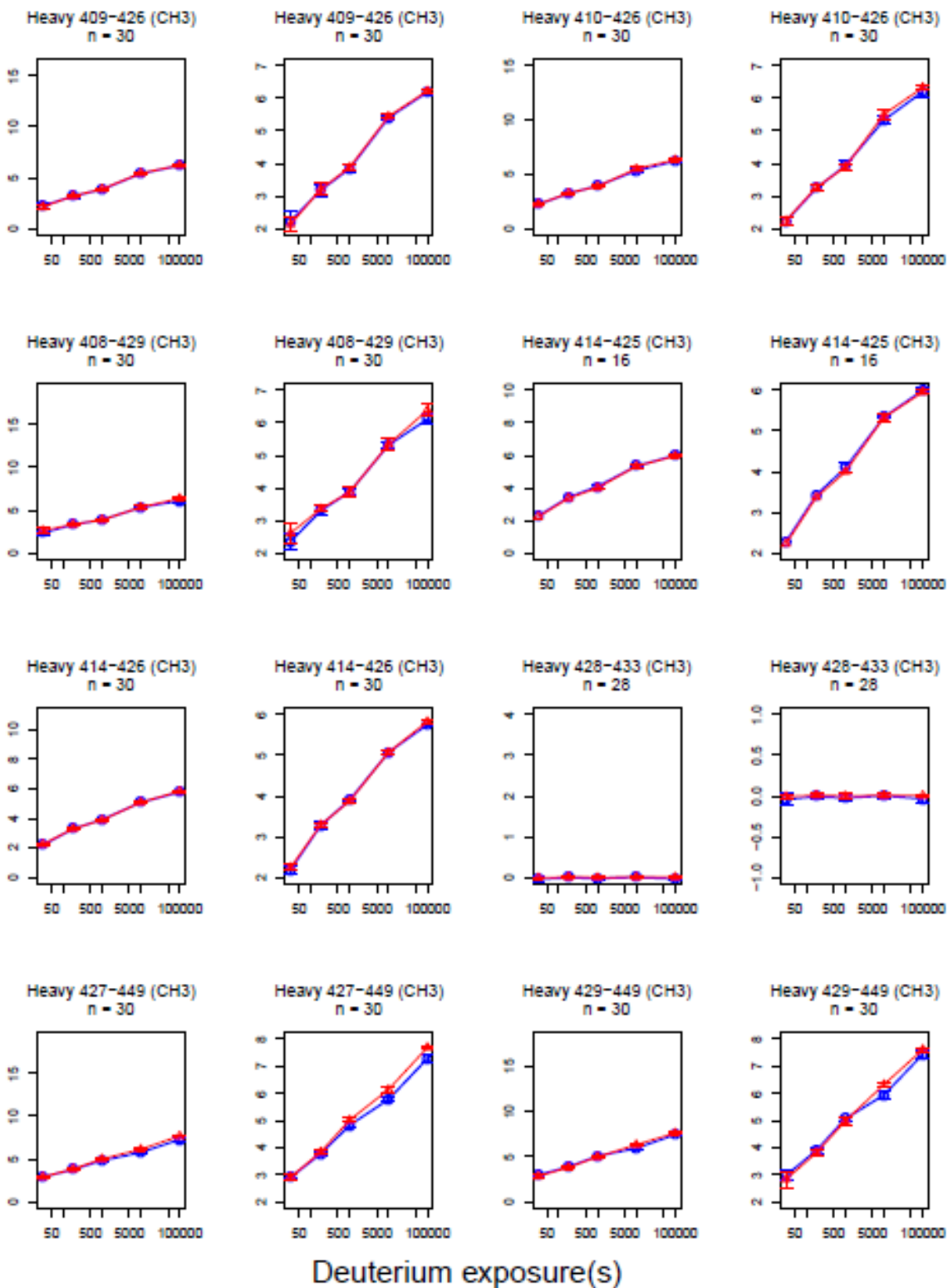




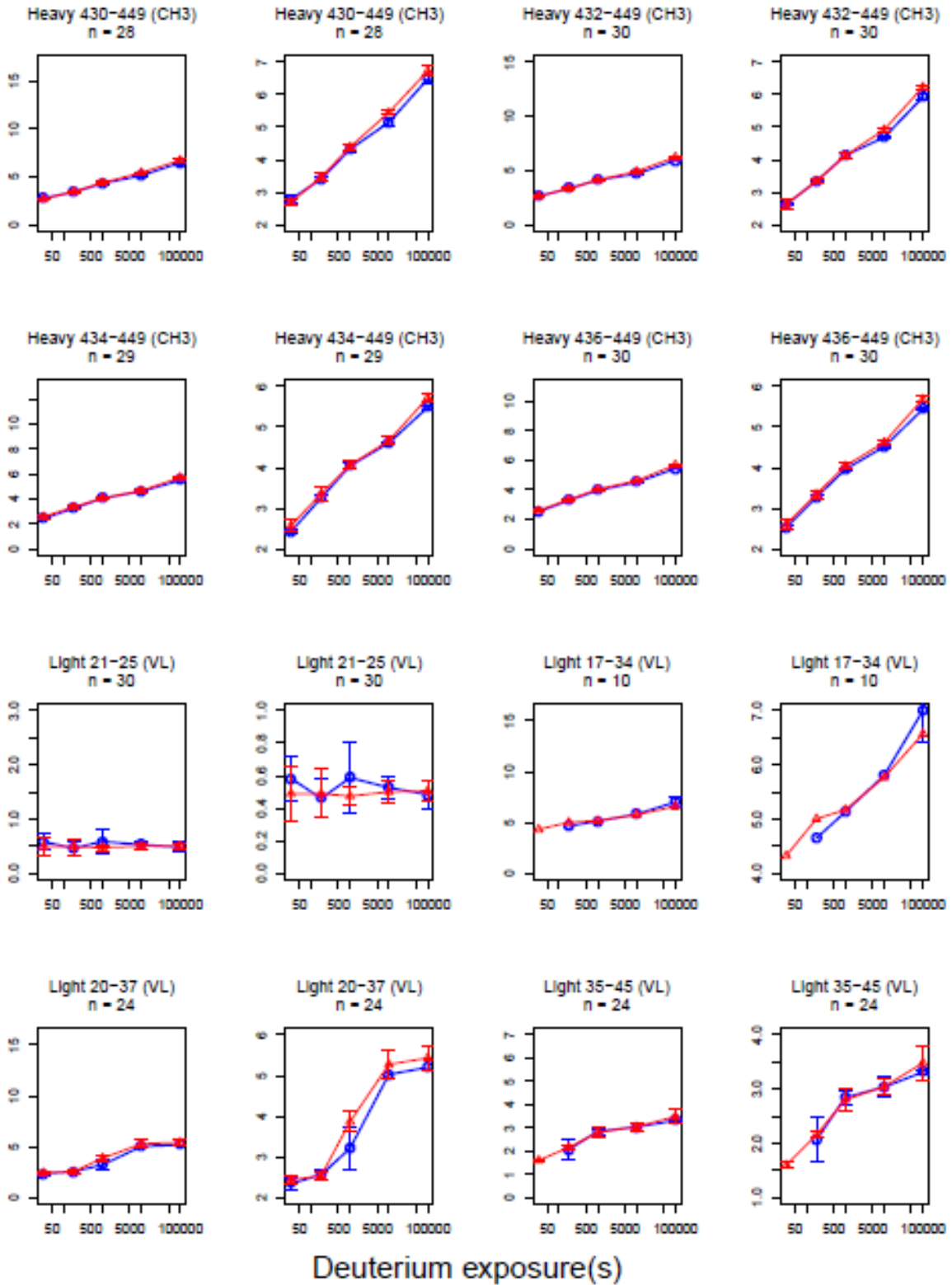
Mass Increase(Da)



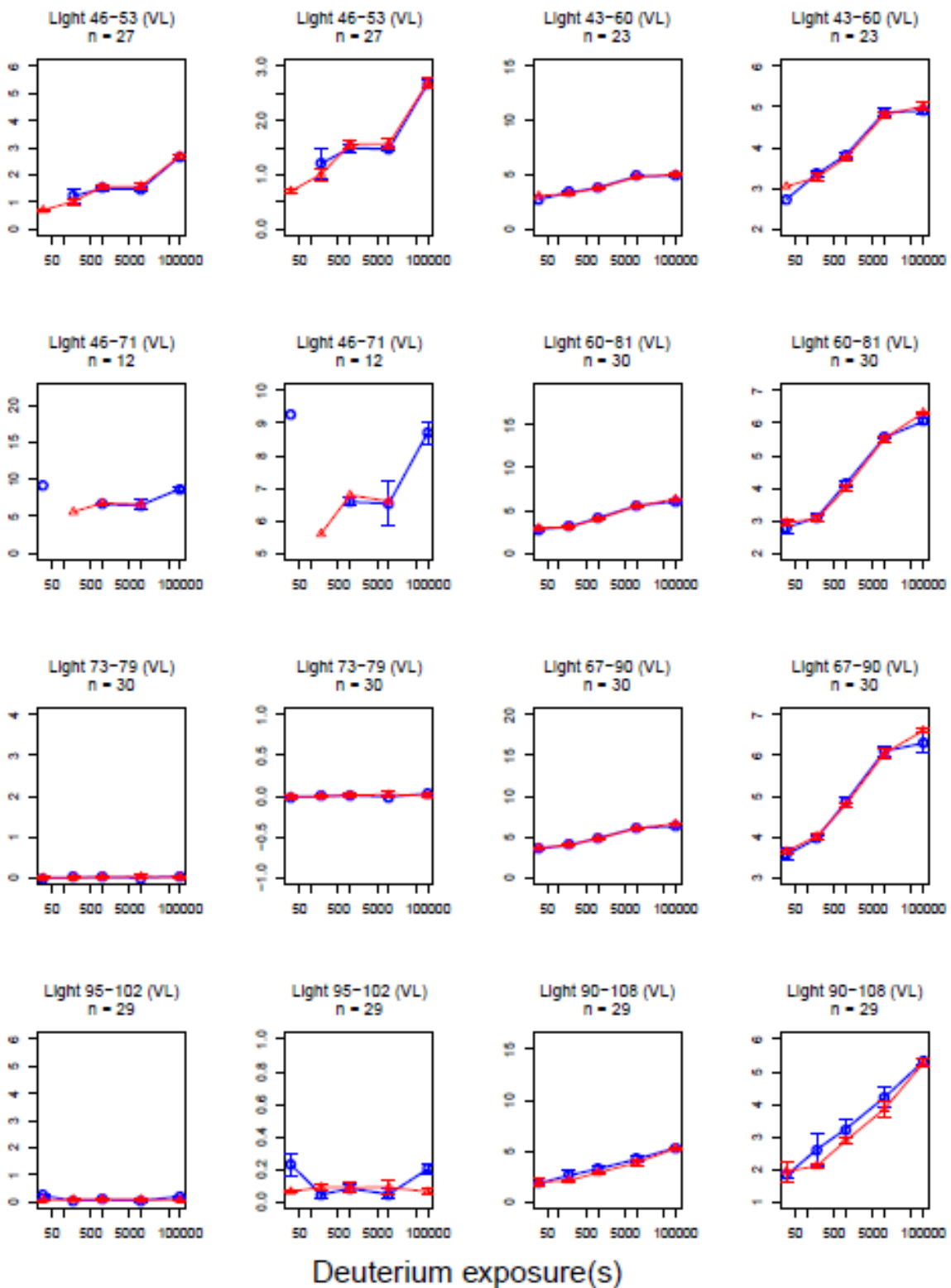
Mass Increase(Da)

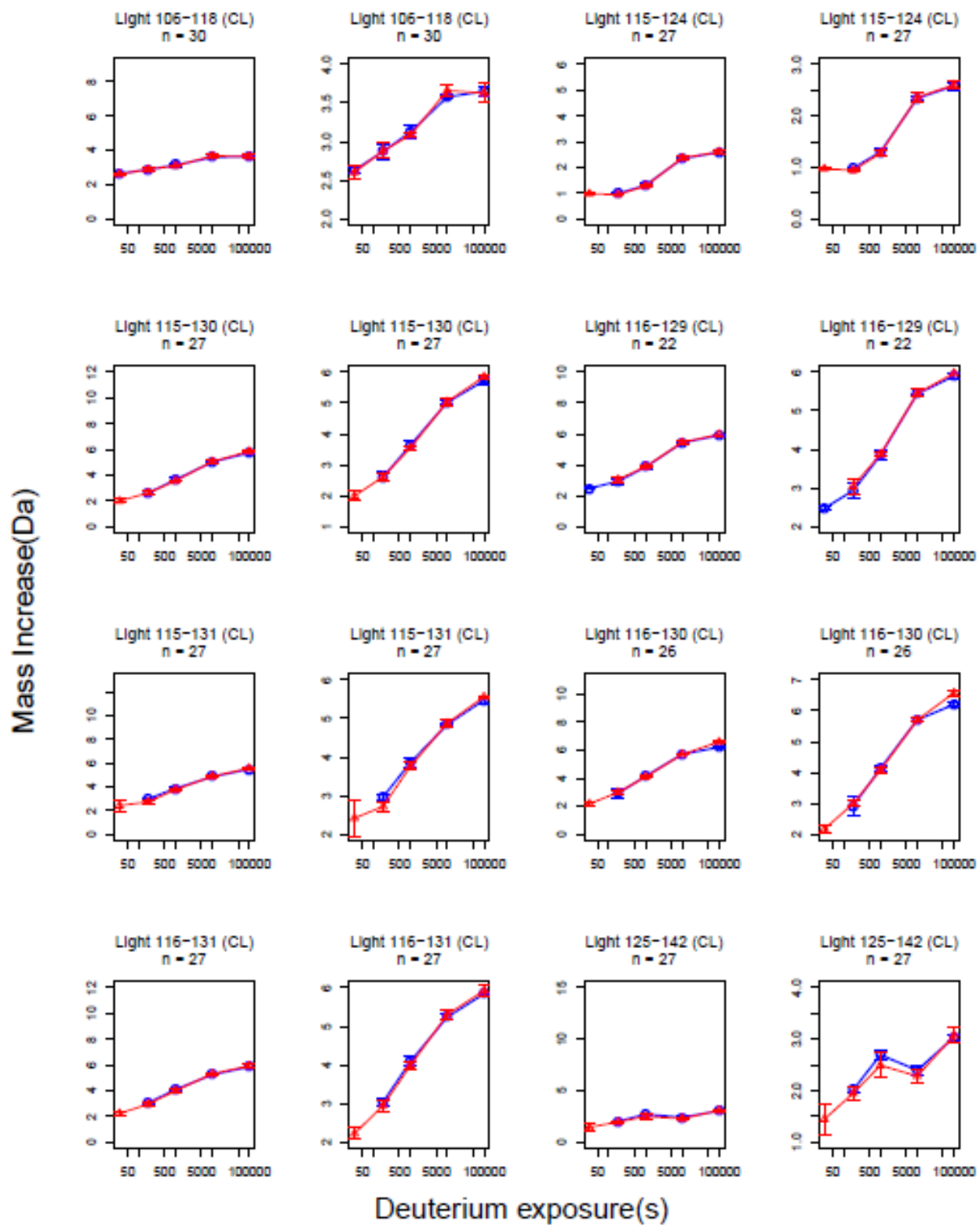


Mass Increase(Da)

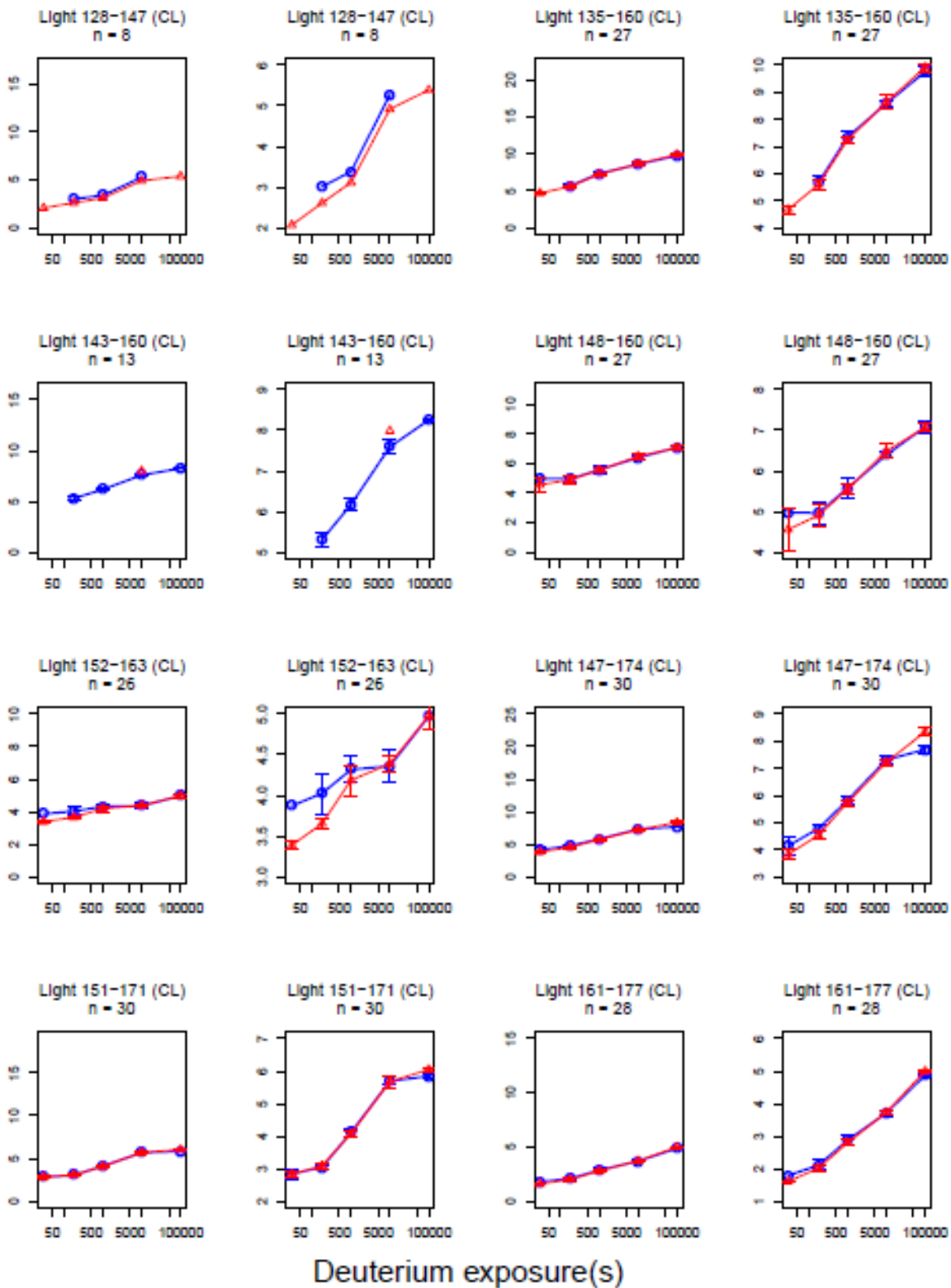


Mass Increase(Da)

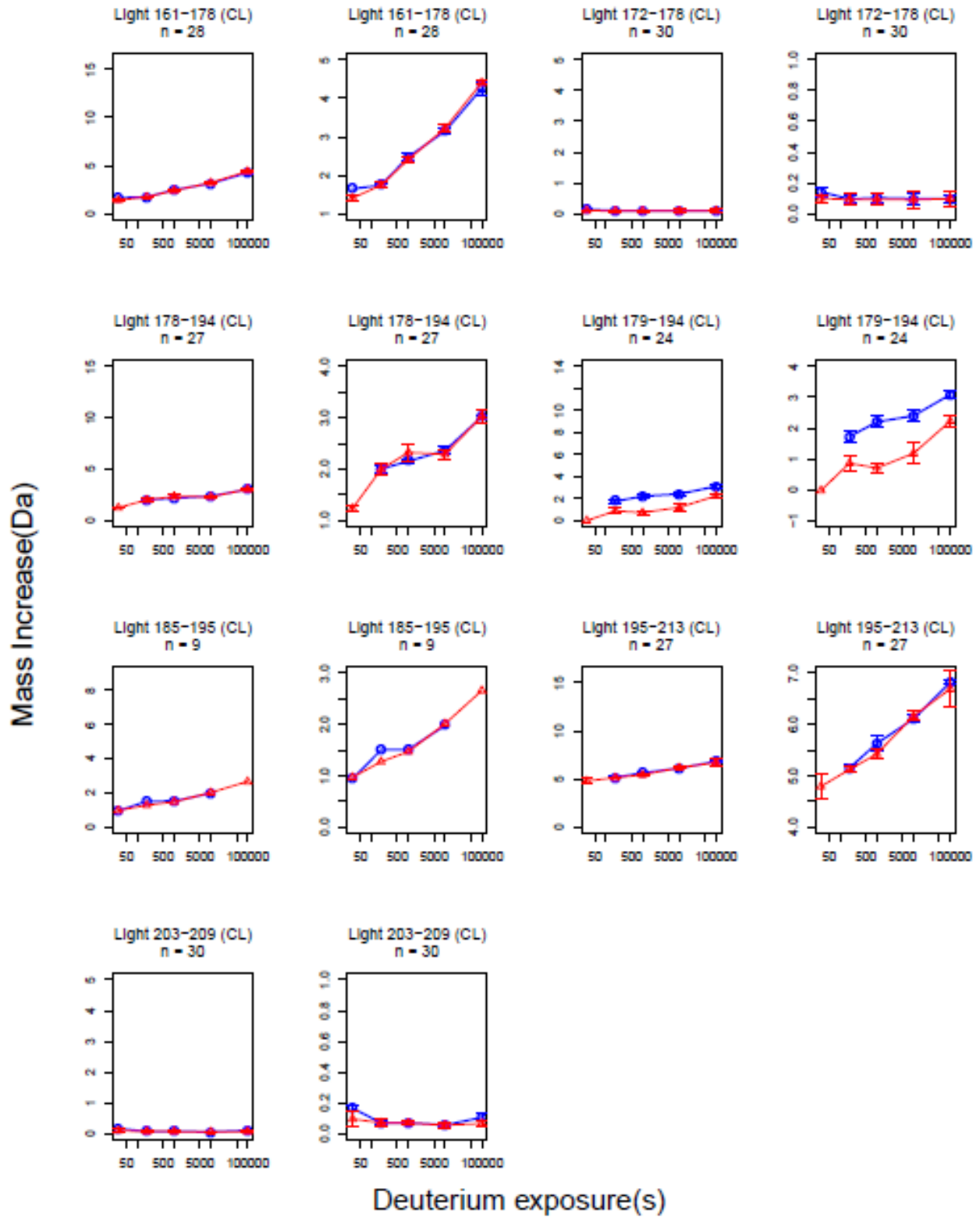




Mass Increase(Da)



Deuterium exposure(s)

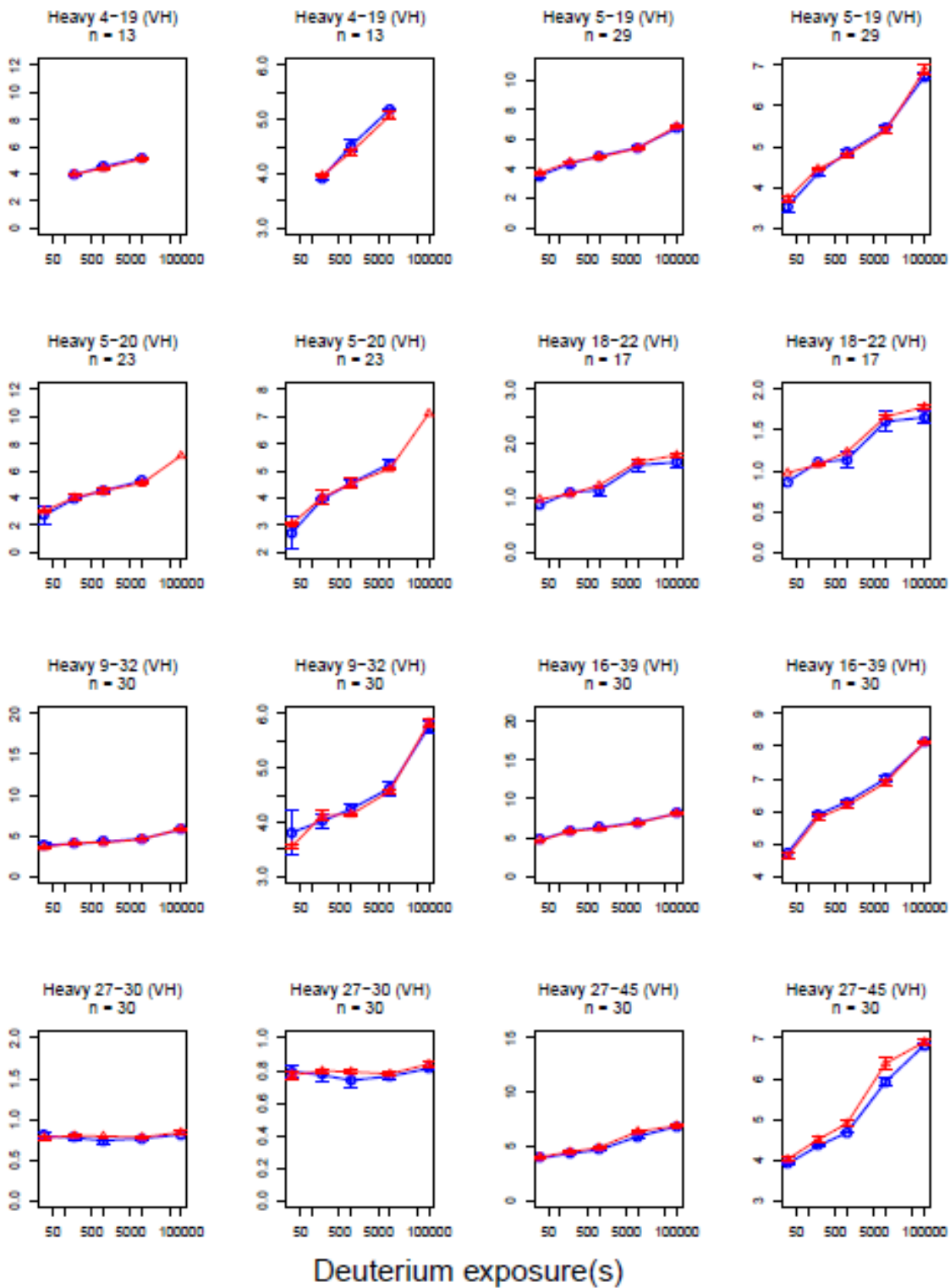


Deuterium uptake plots of 167 common segments between mAb-A and mAb-E at pH 6.0.

Figure 5.S3

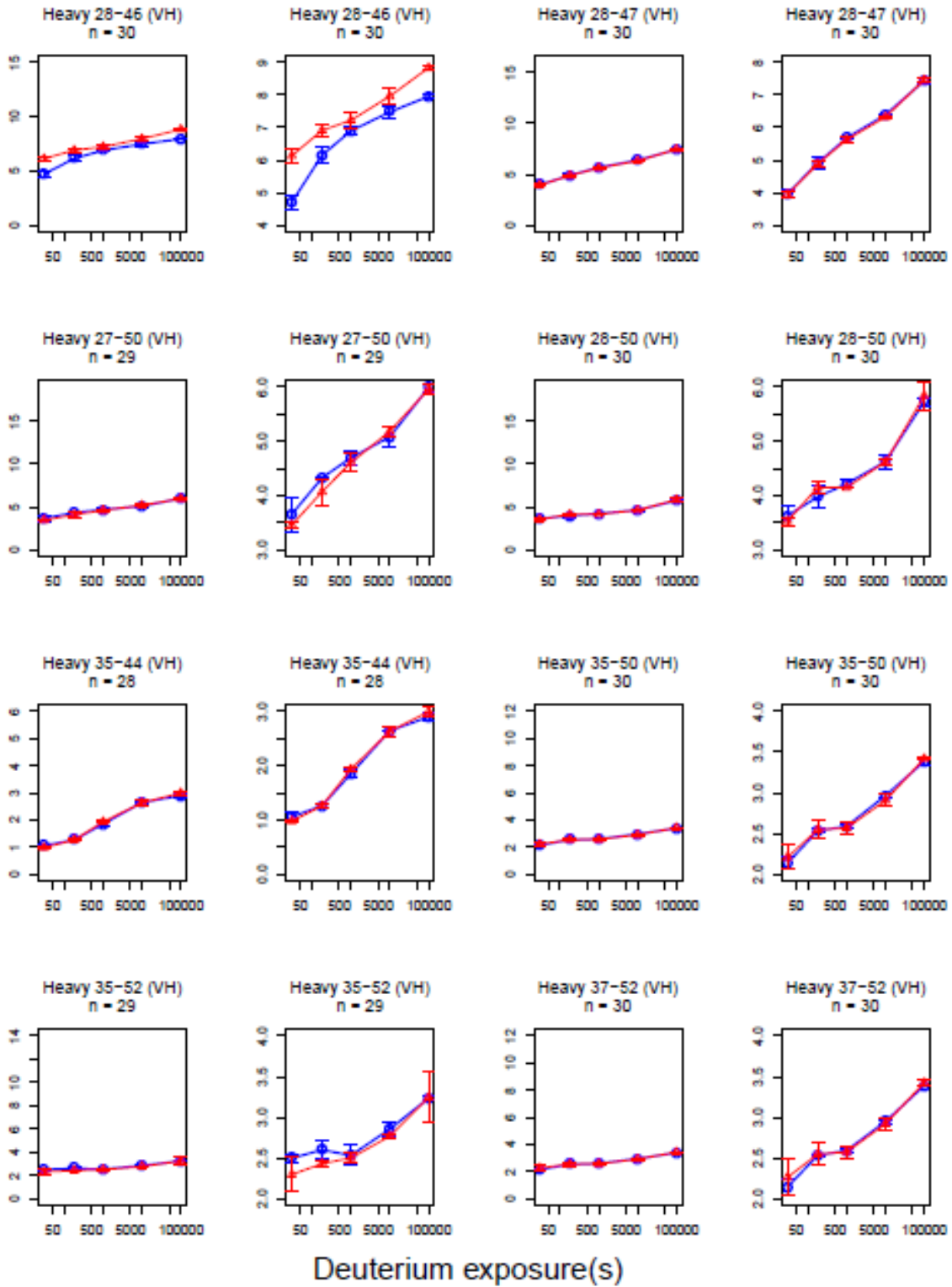
—○— mAb-A
—△— mAb-E

Mass Increase(Da)

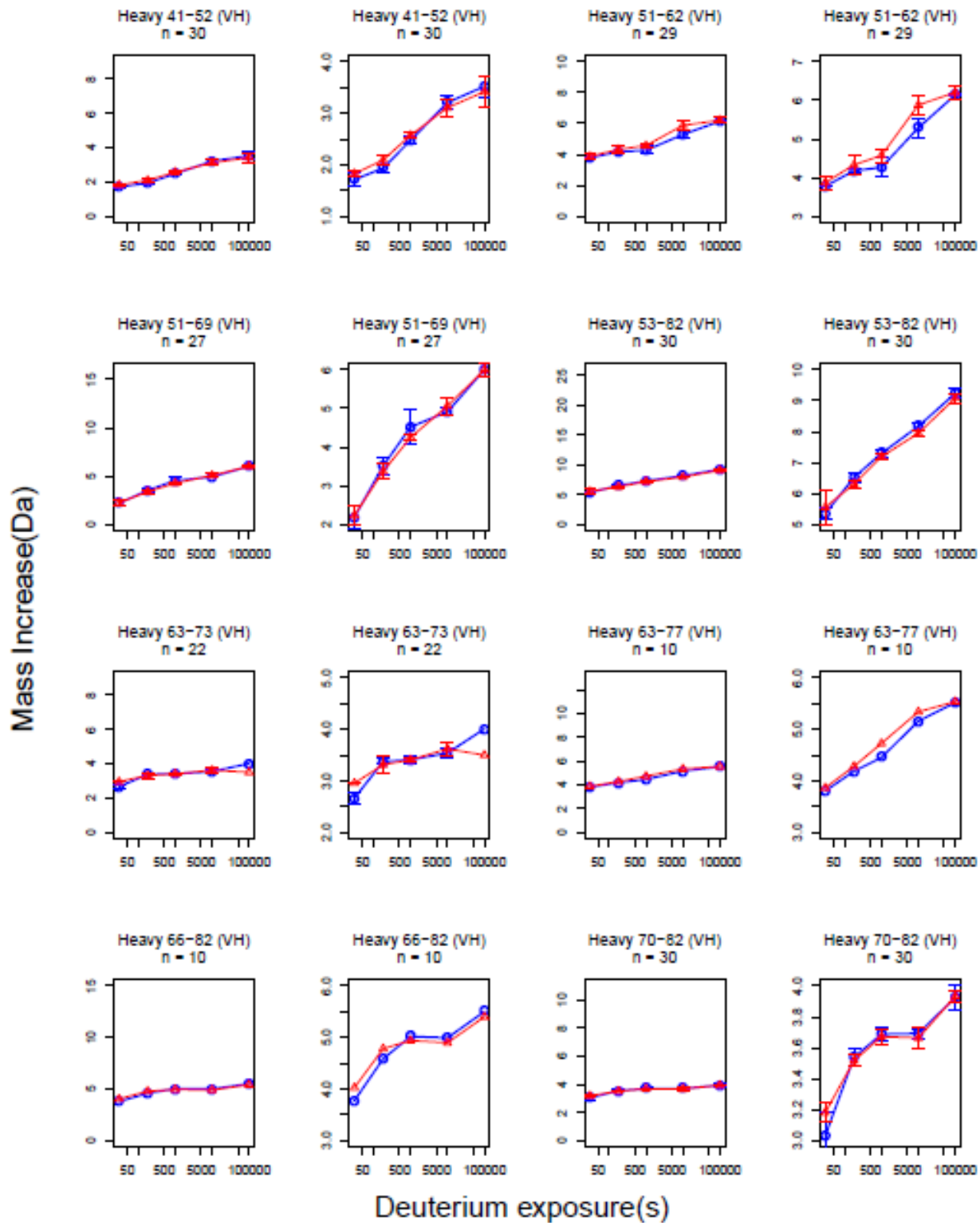


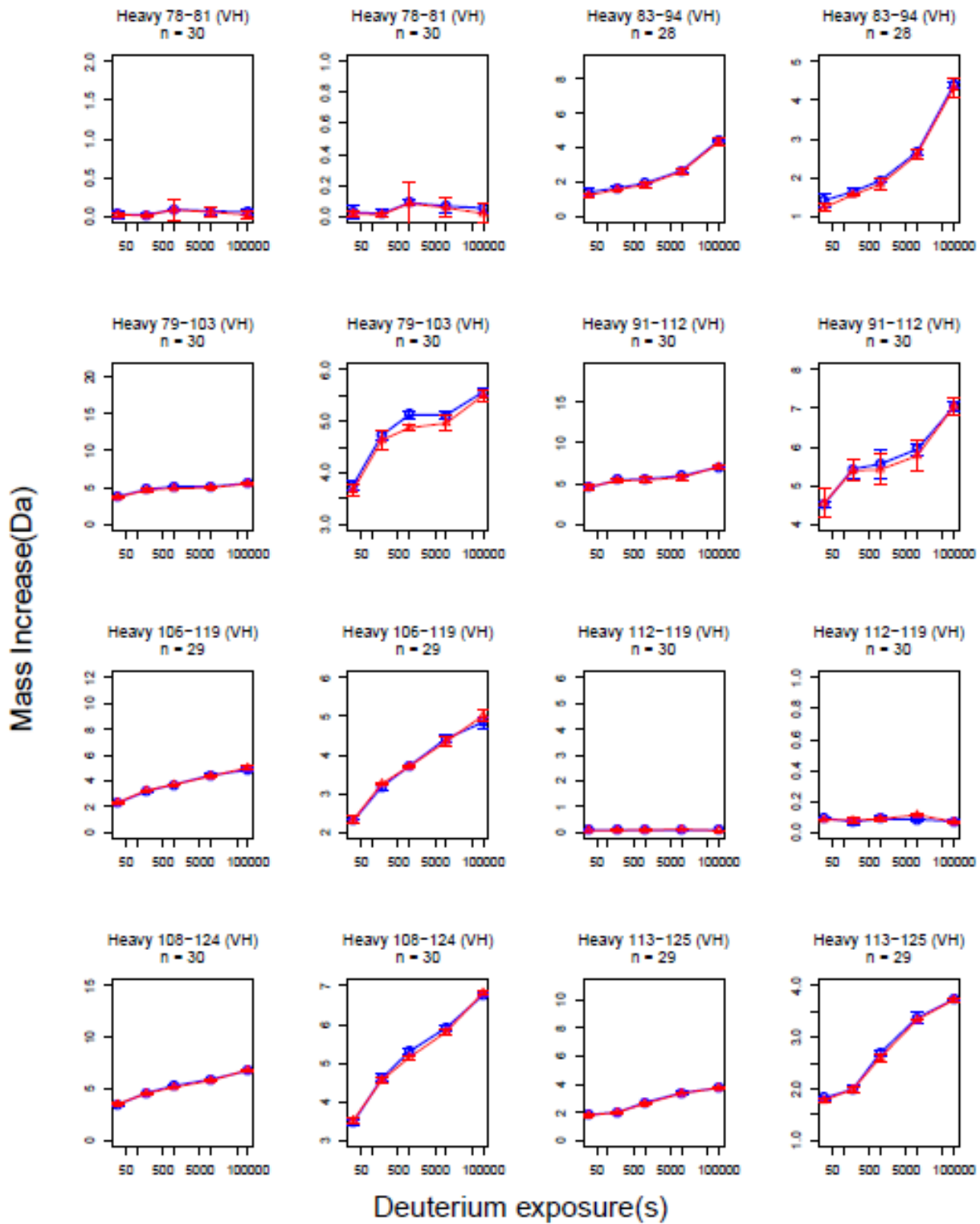
Deuterium exposure(s)

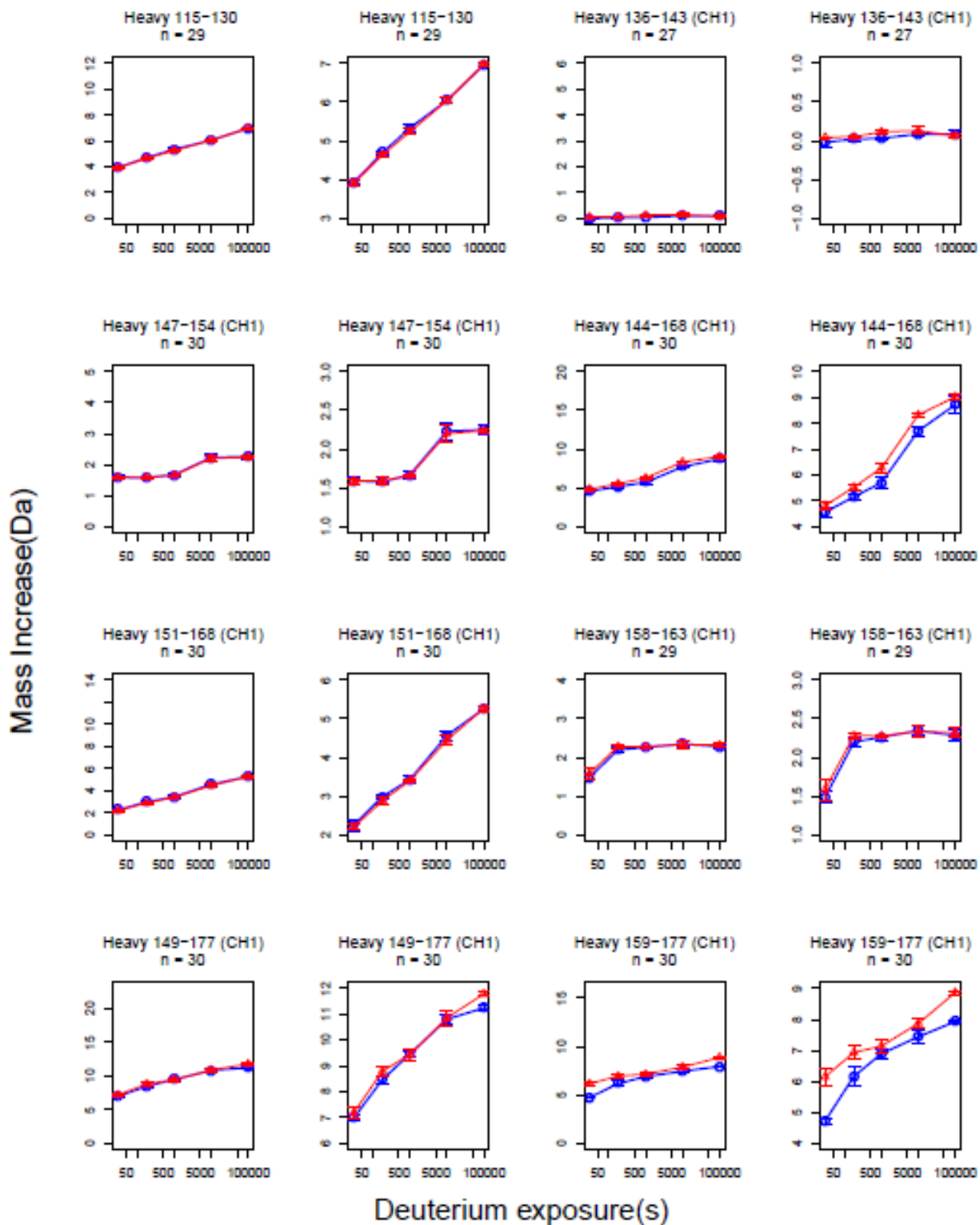
Mass Increase(Da)

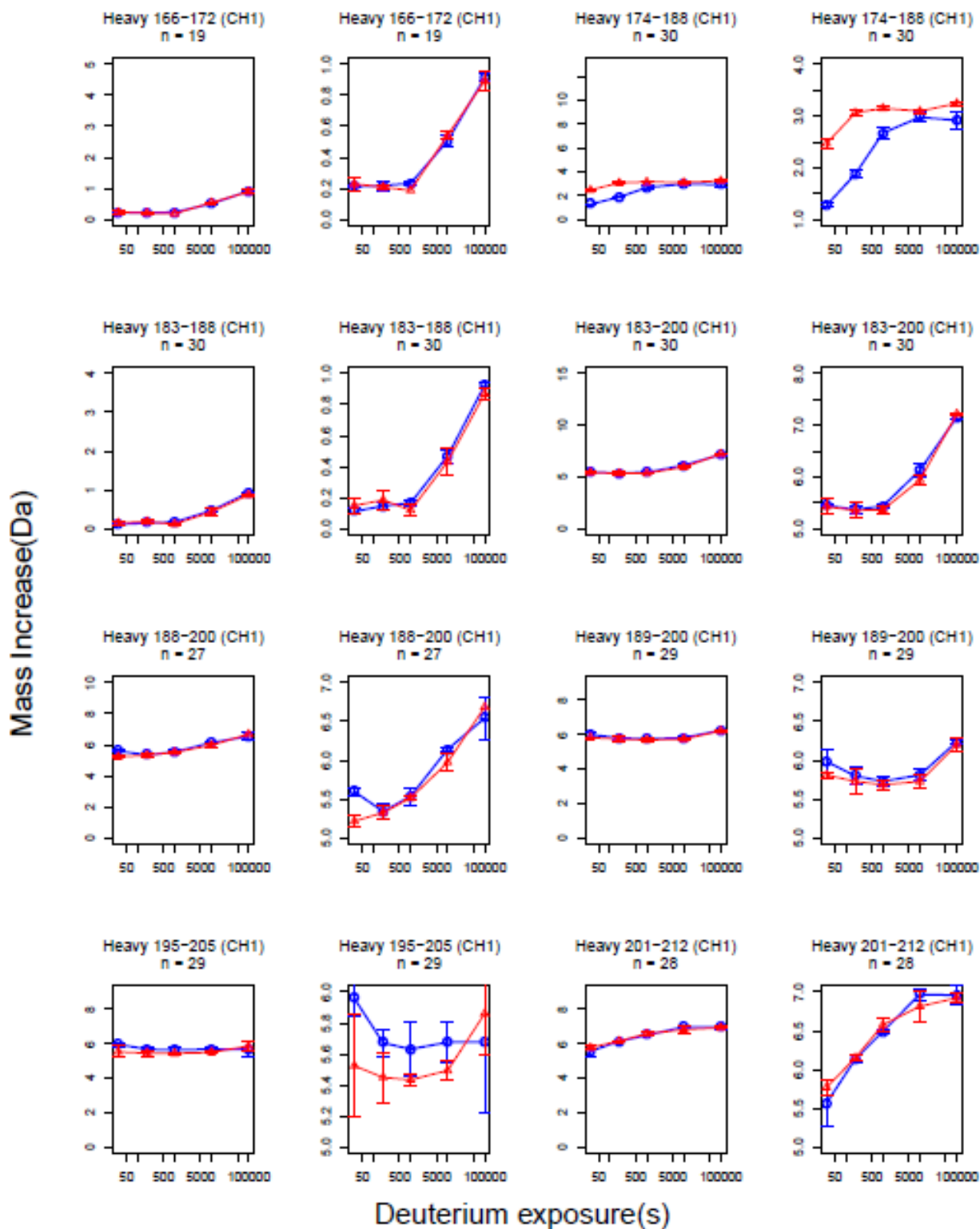


Deuterium exposure(s)

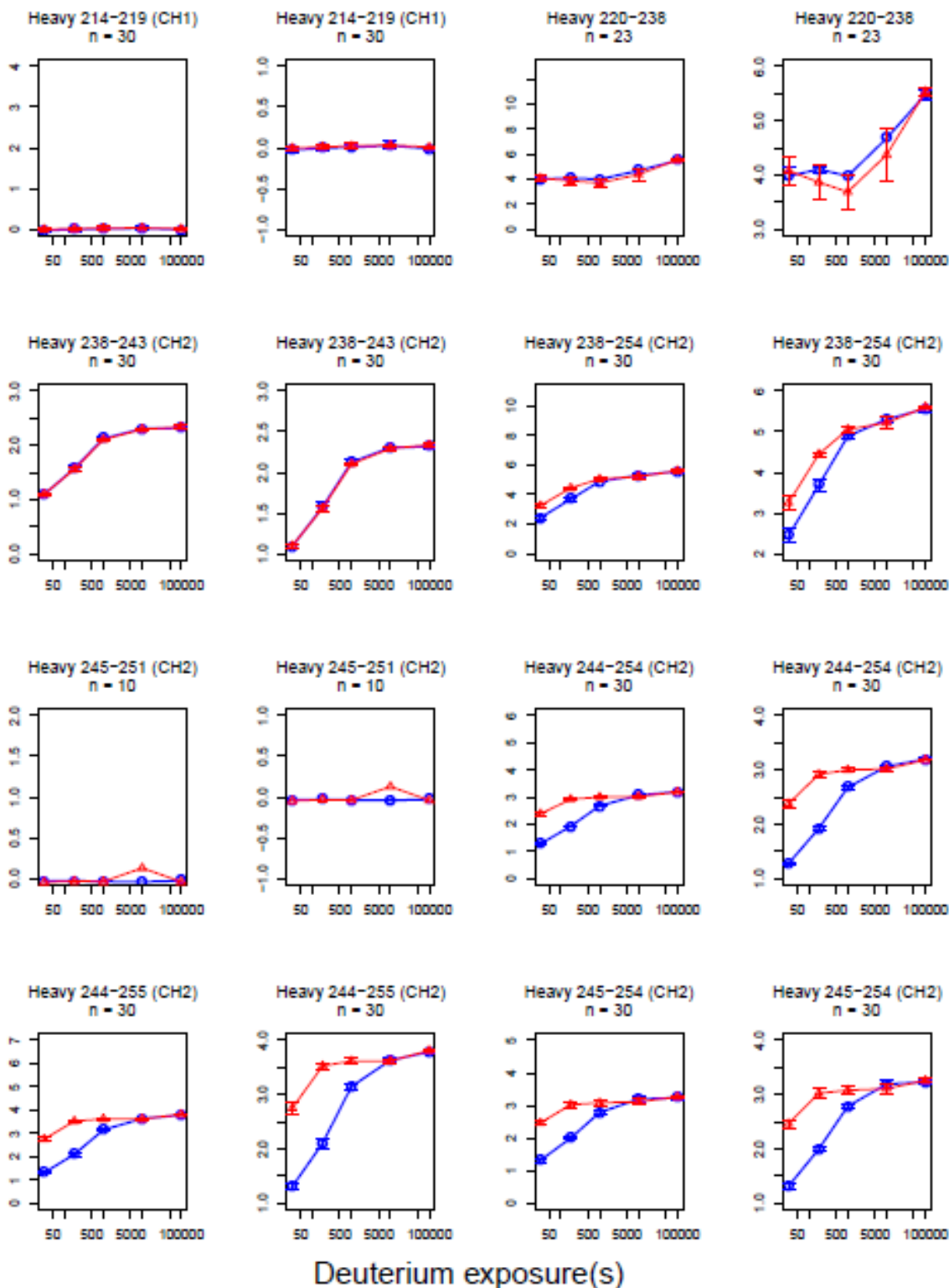




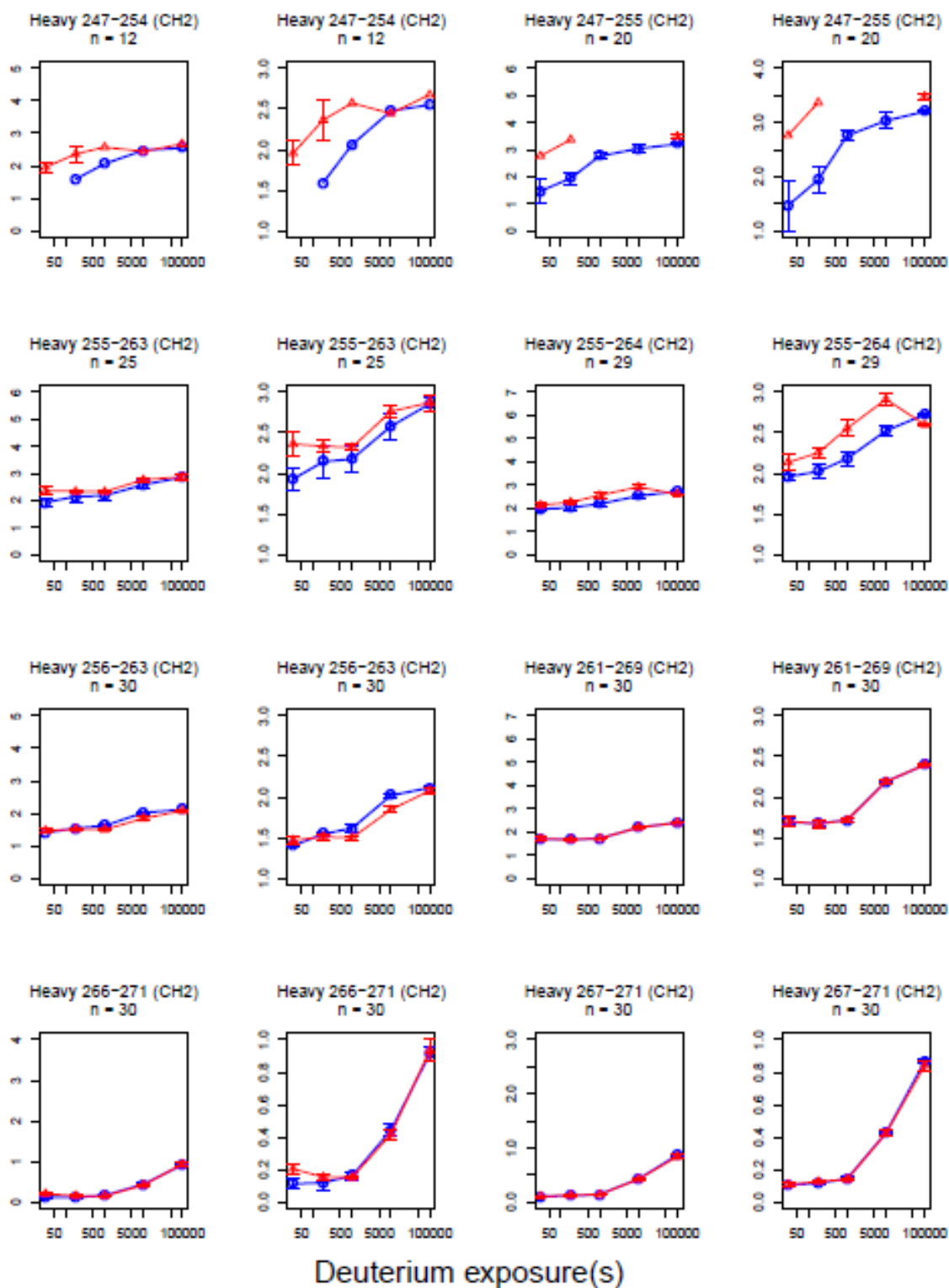


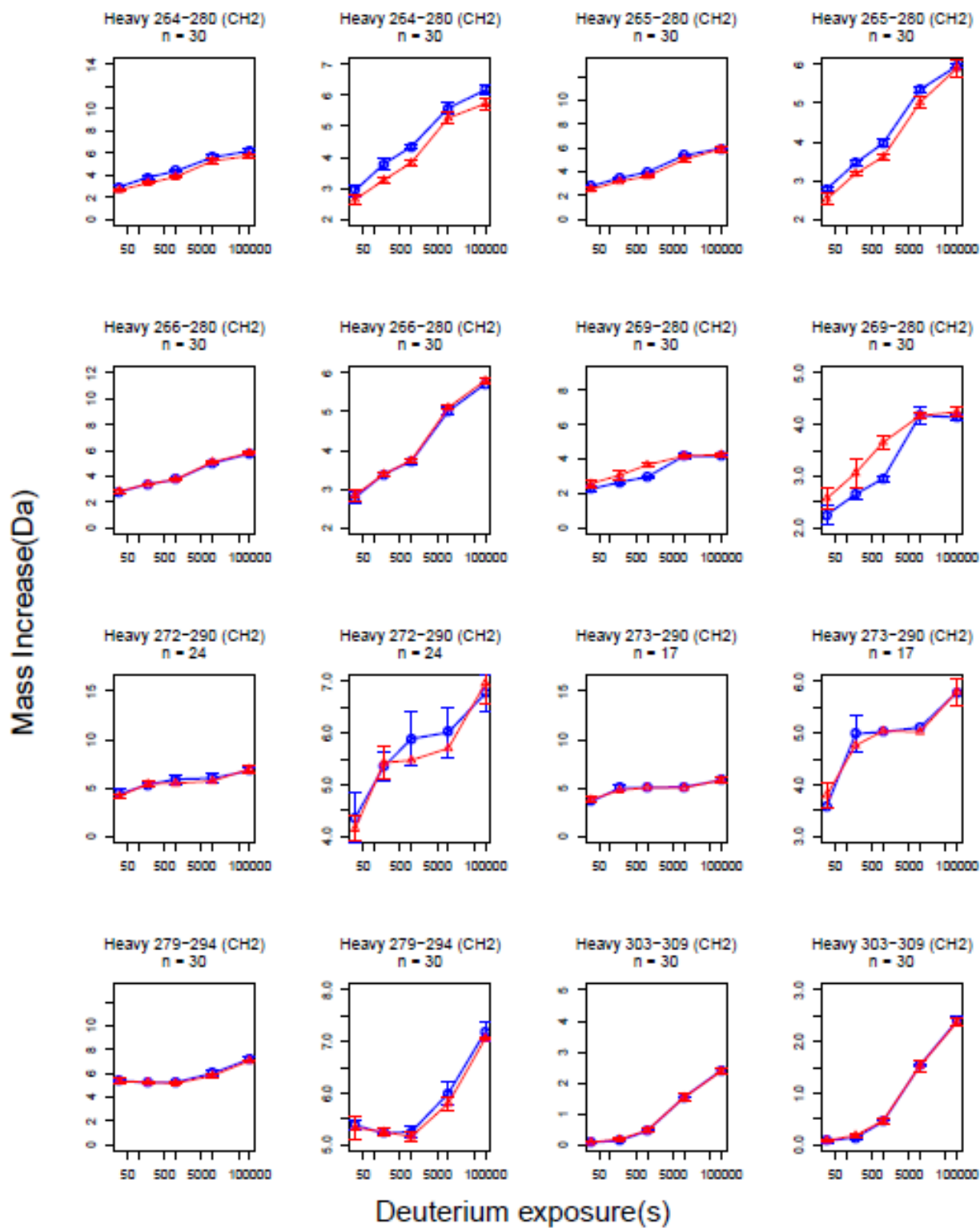


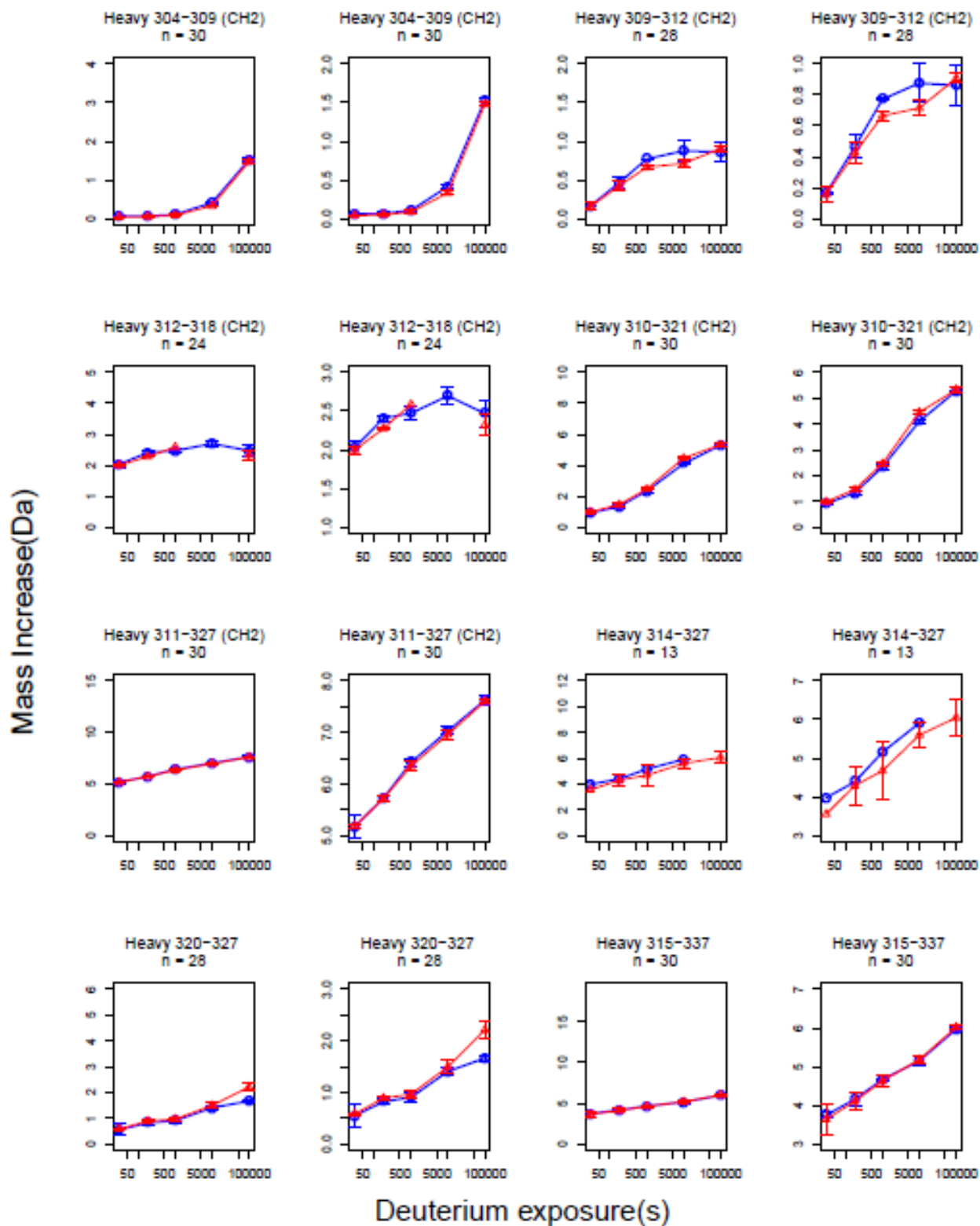
Mass Increase(Da)

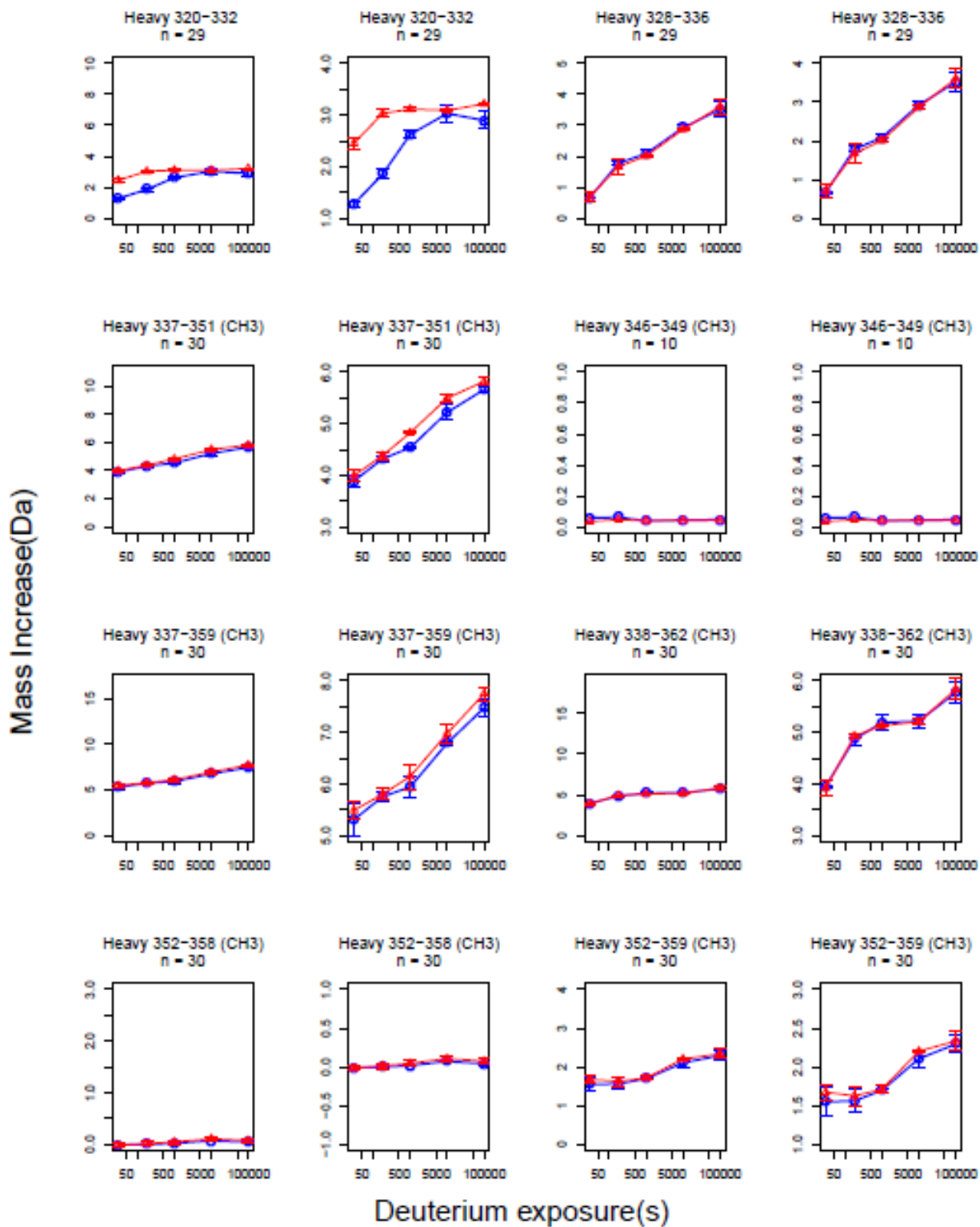


Mass Increase(Da)

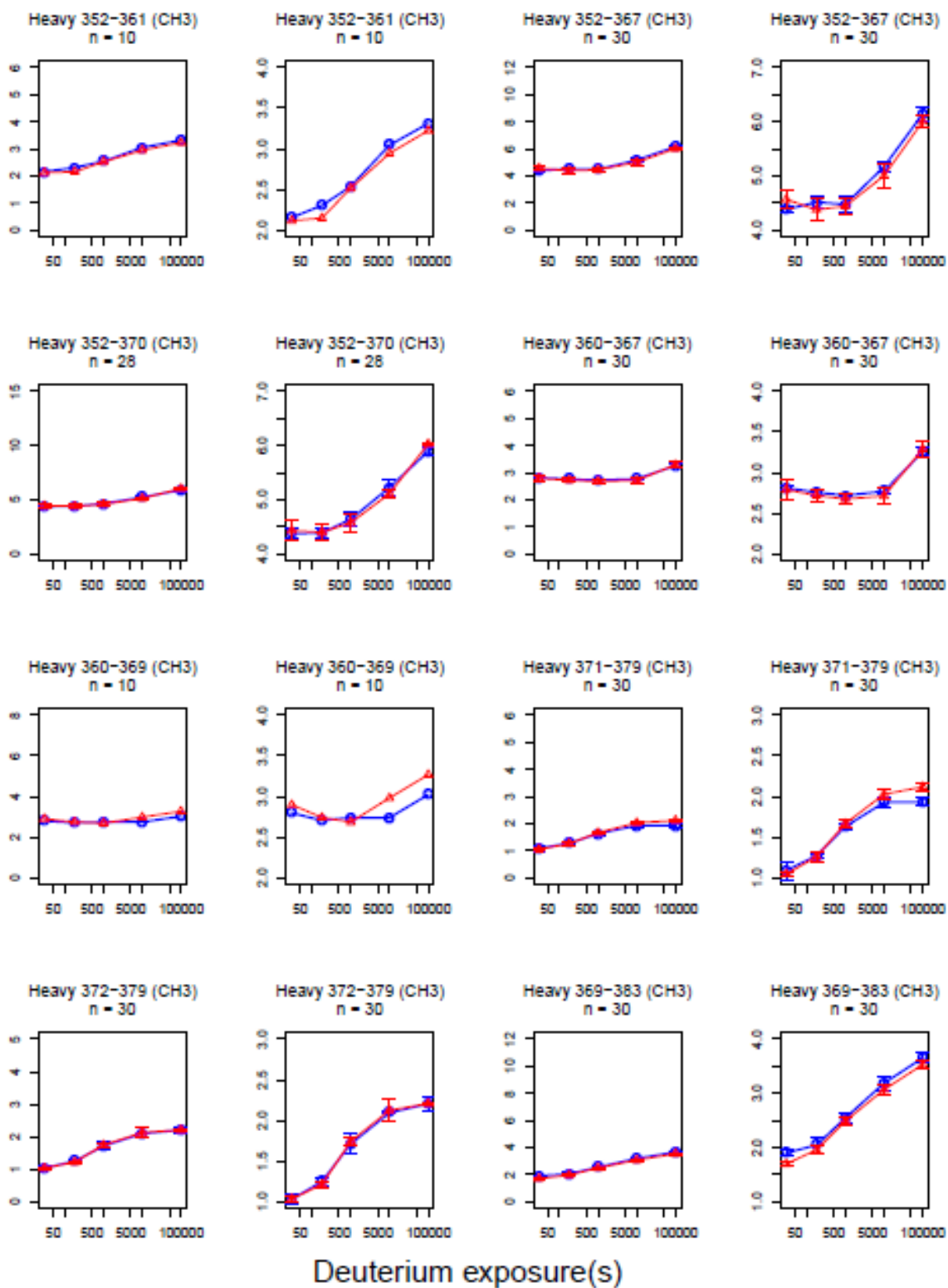


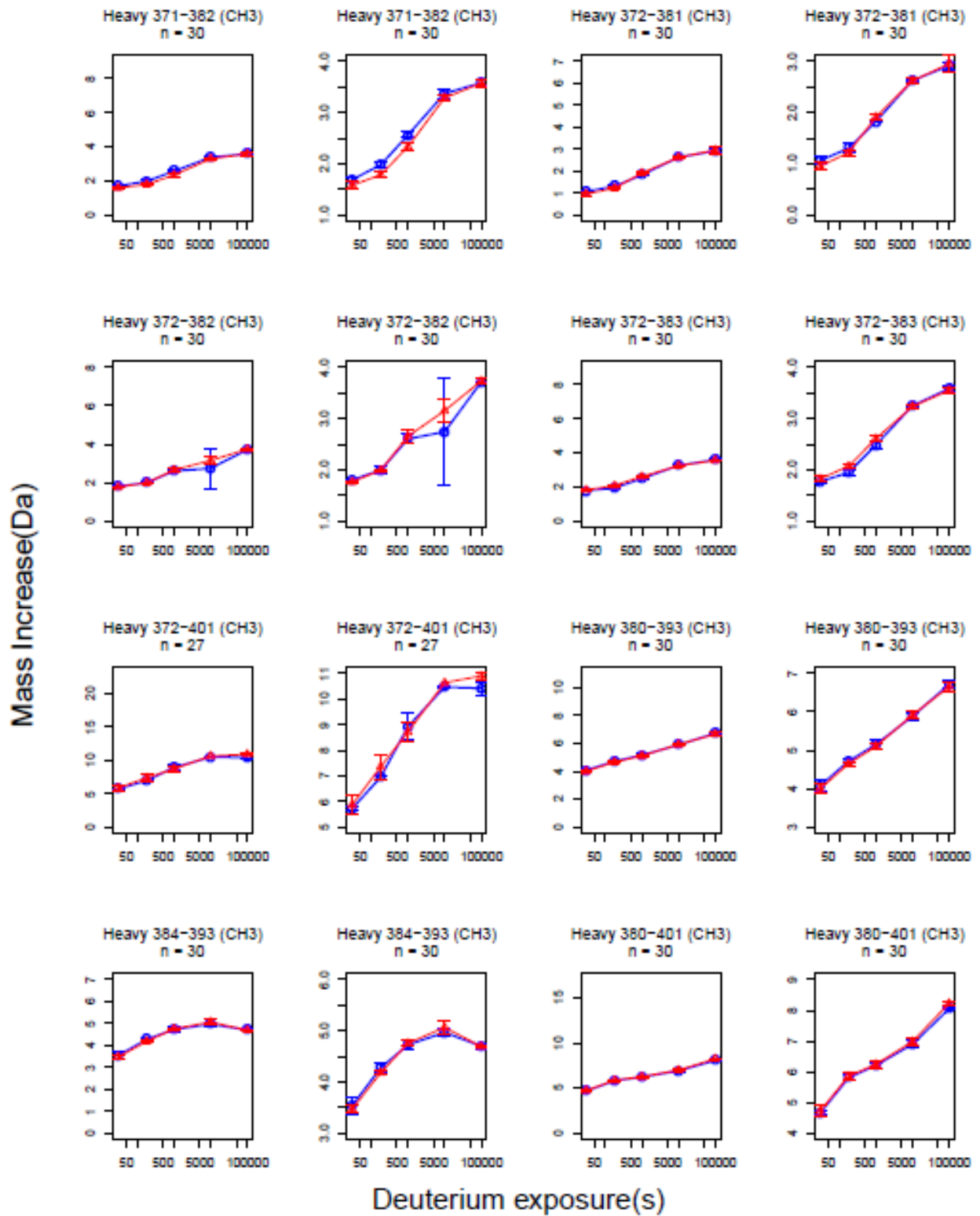


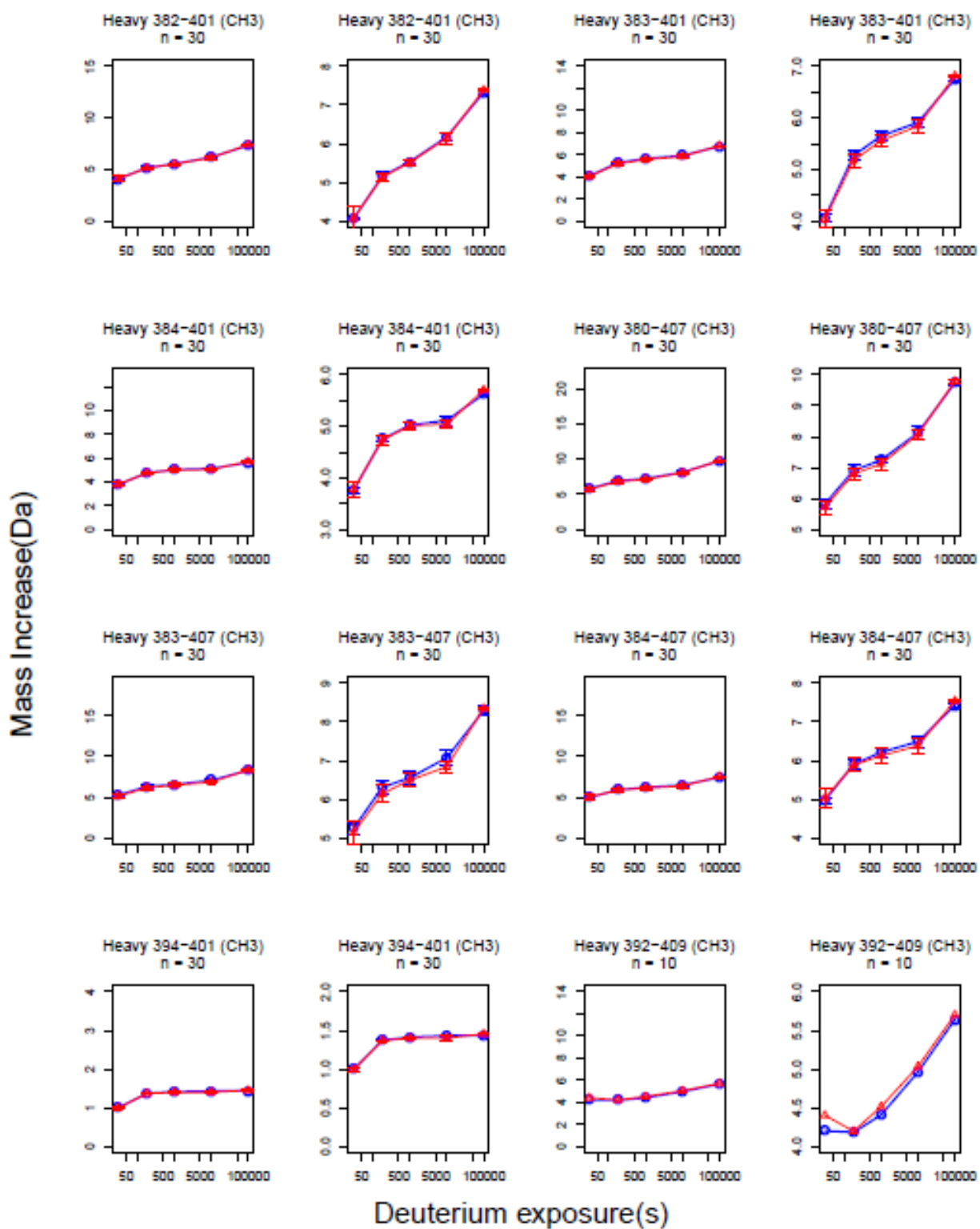


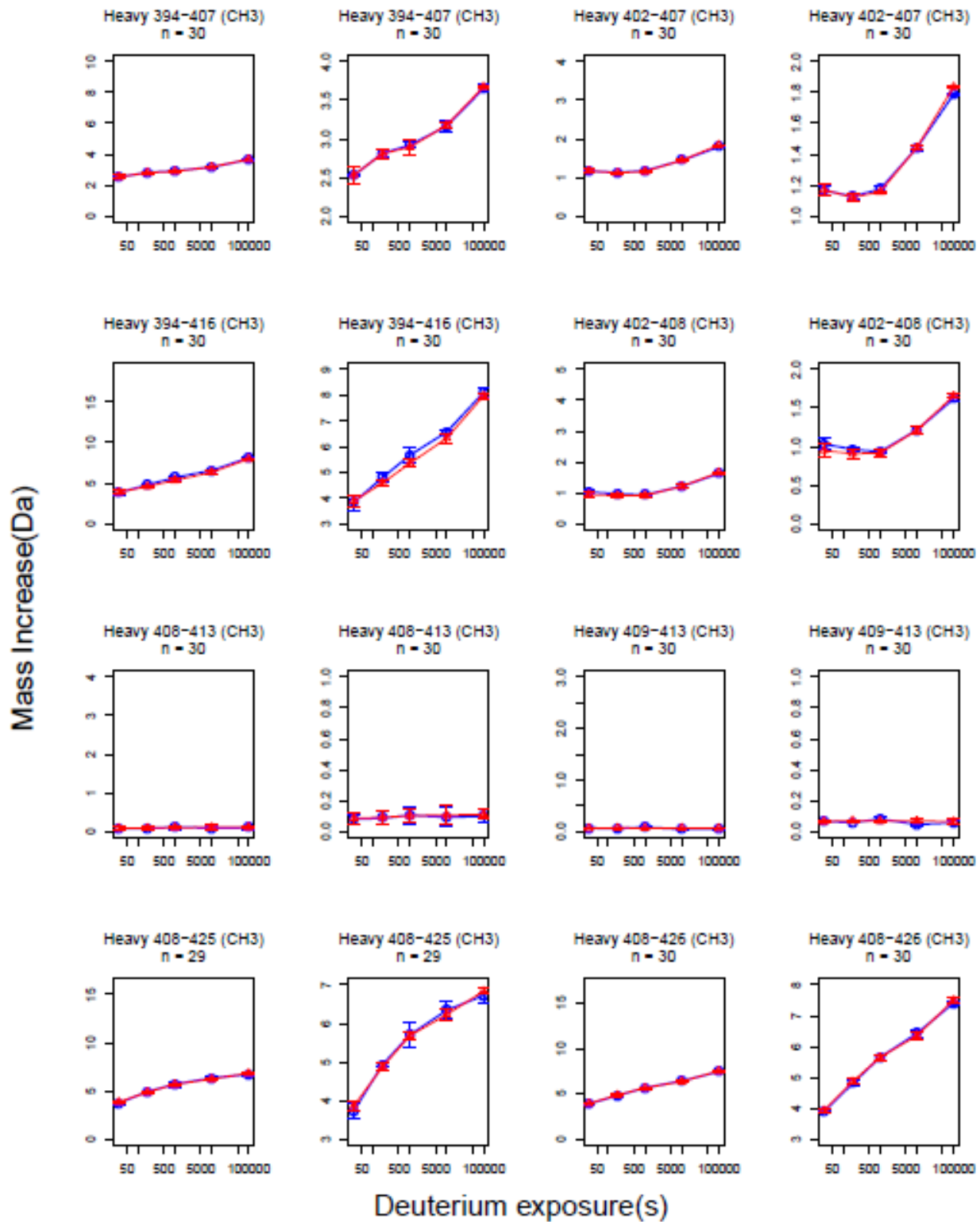


Mass Increase(Da)

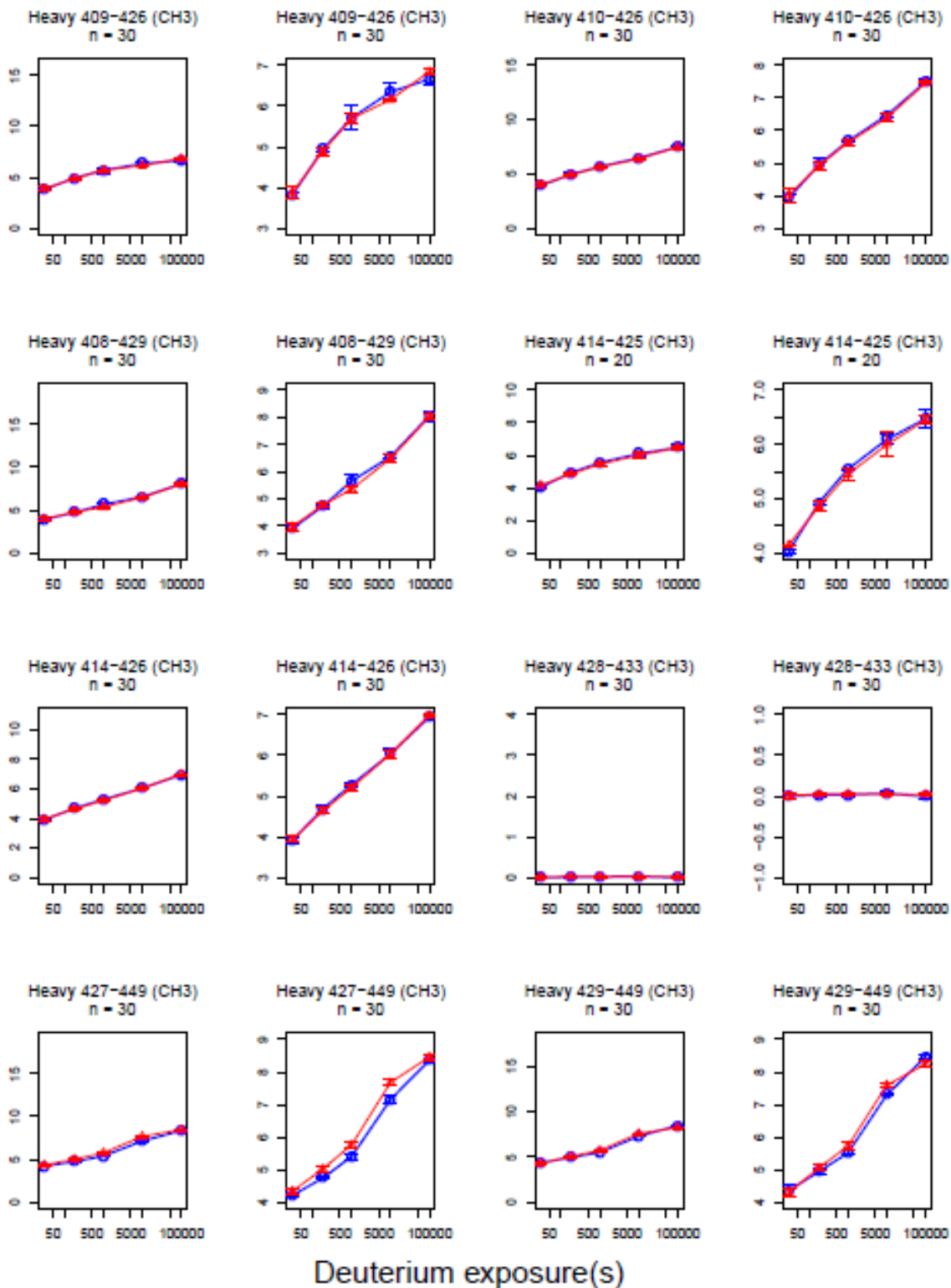




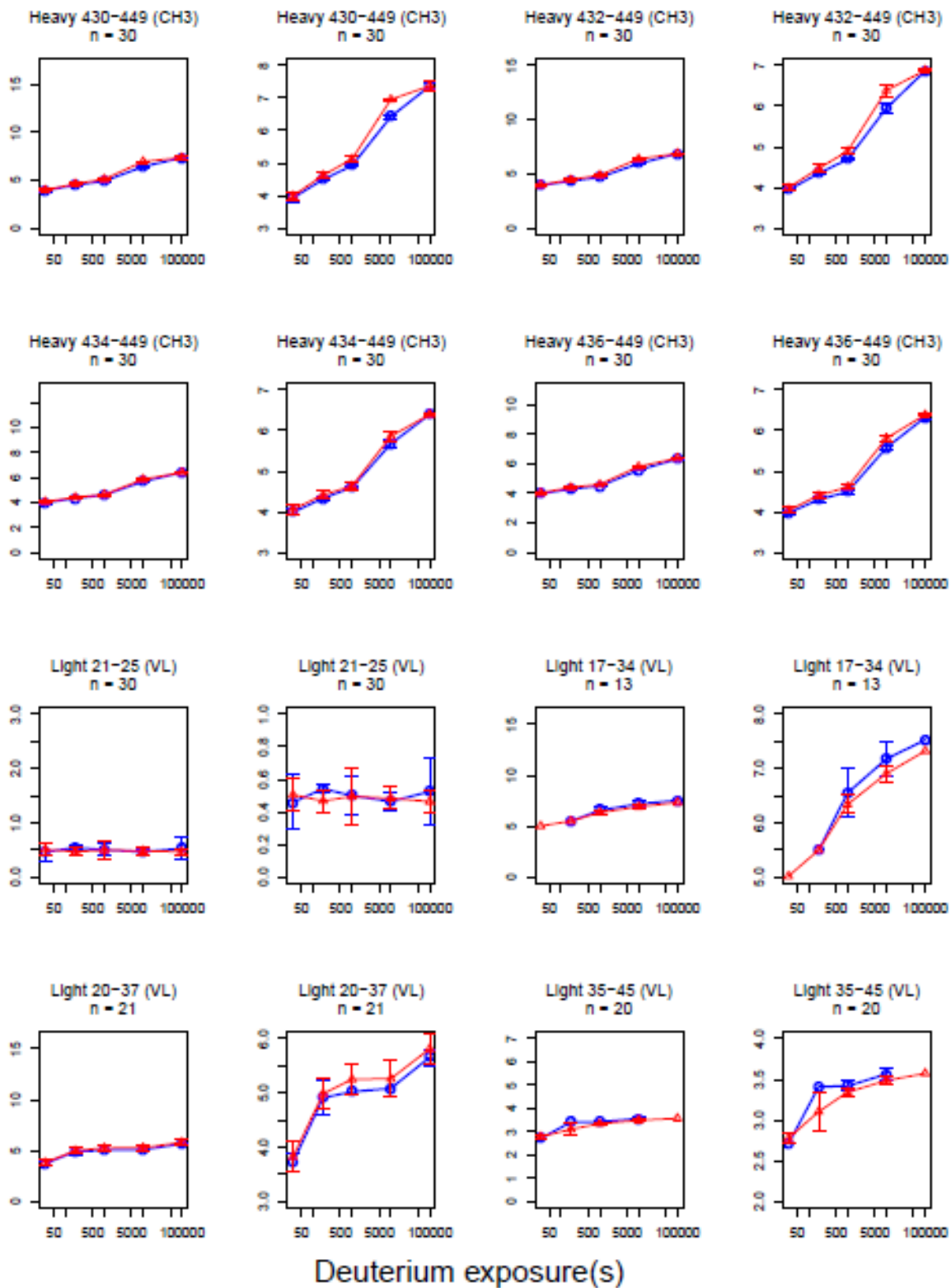




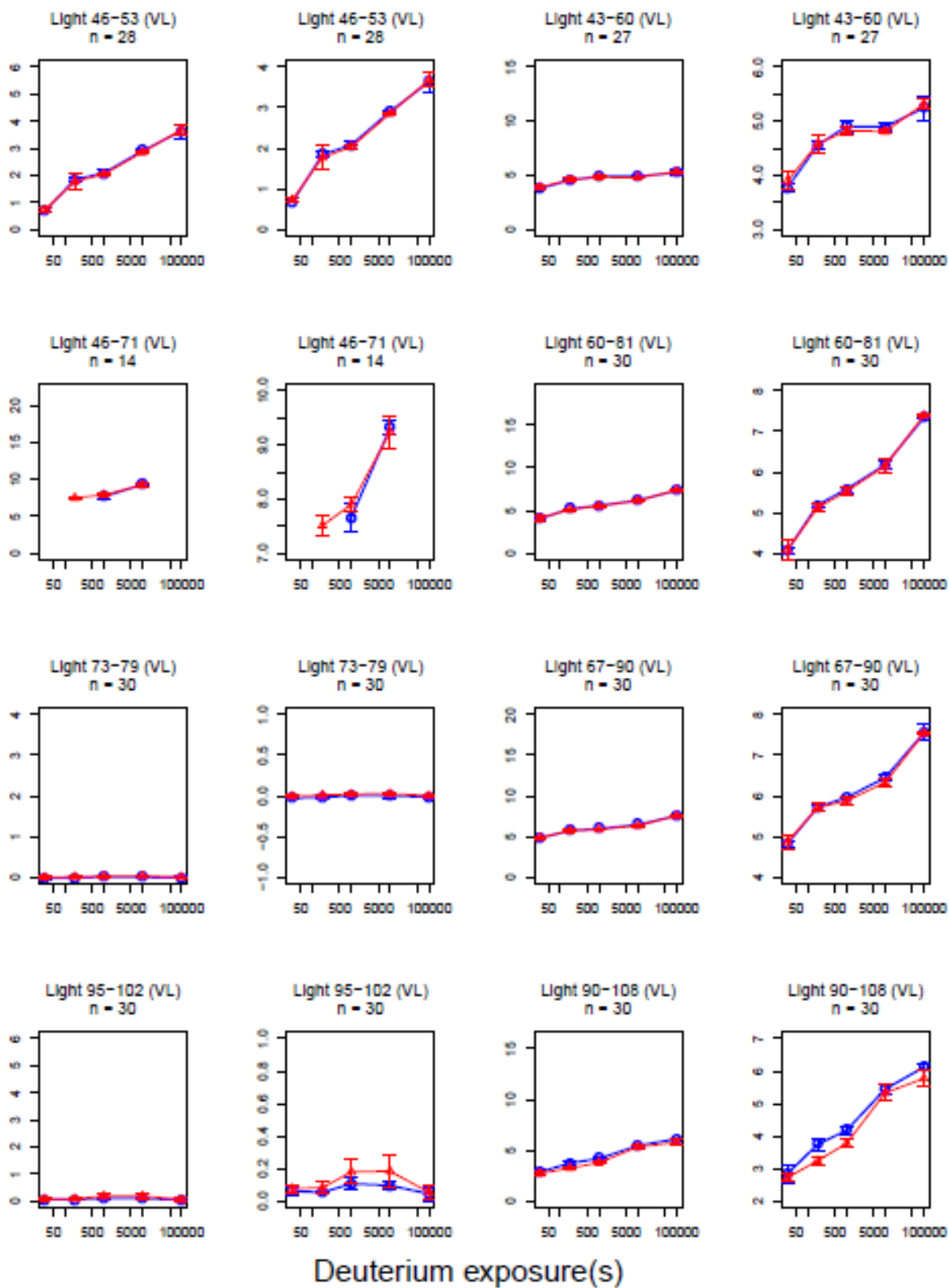
Mass Increase(Da)



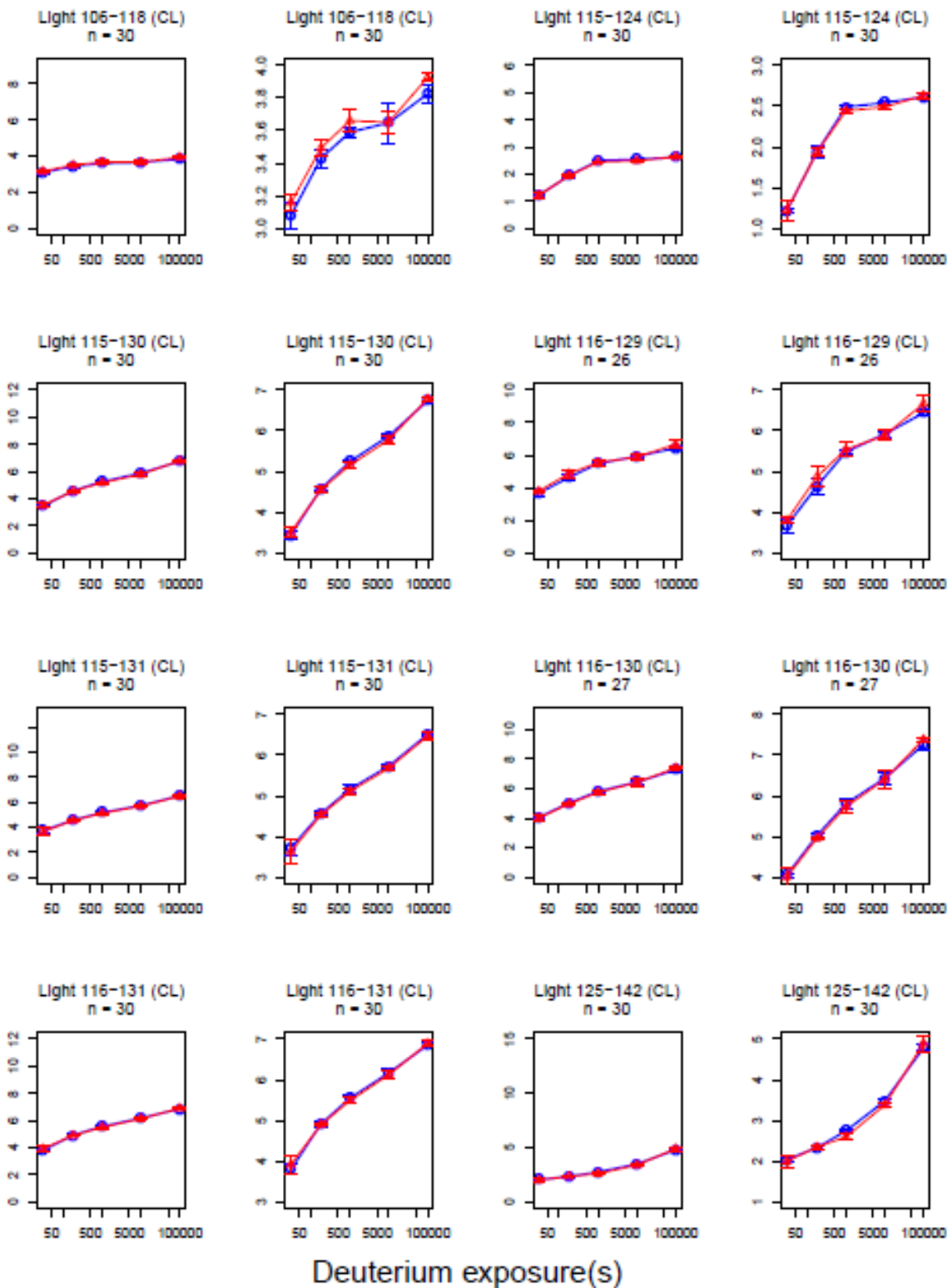
Mass Increase(Da)



Mass Increase(Da)

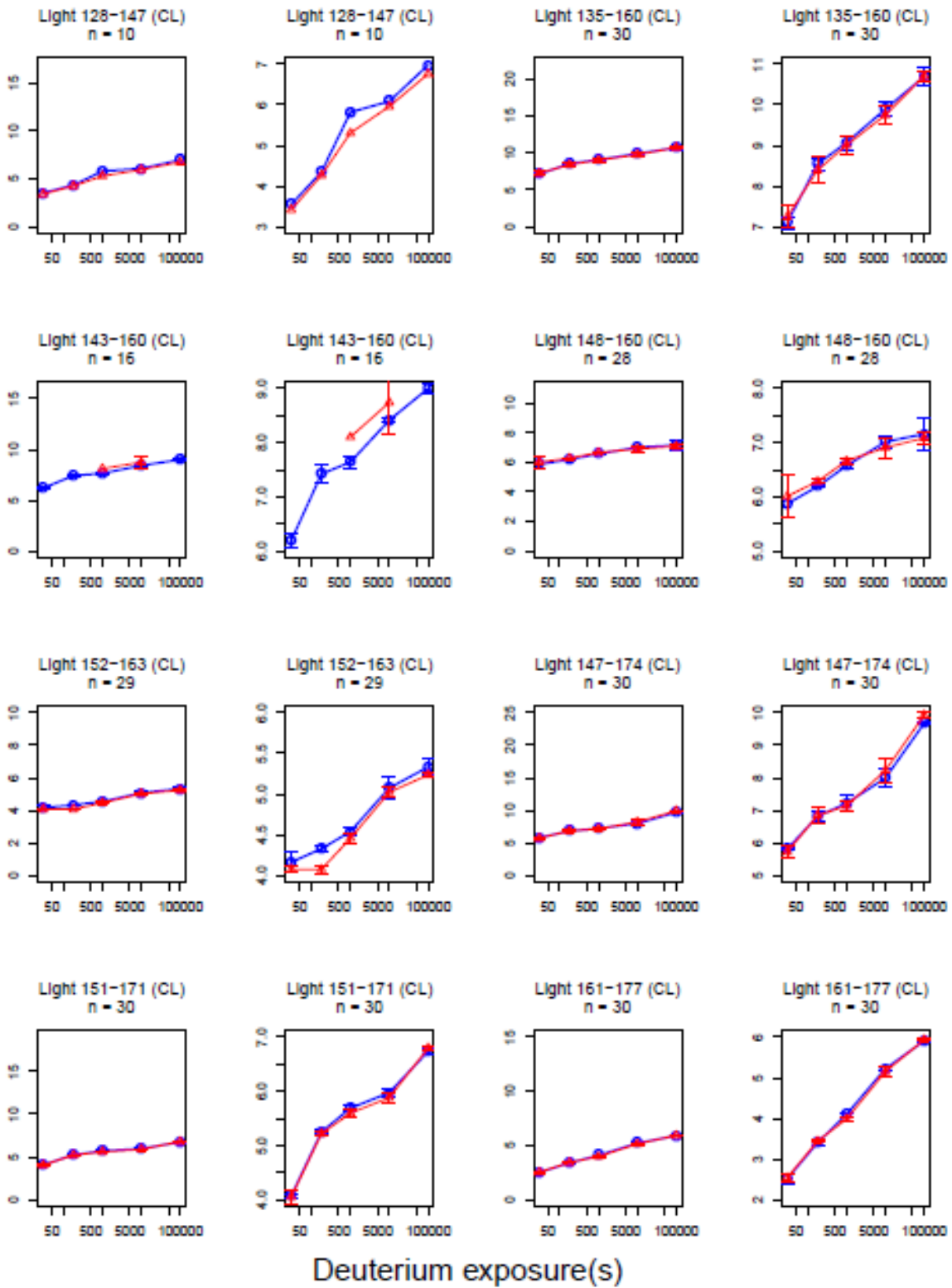


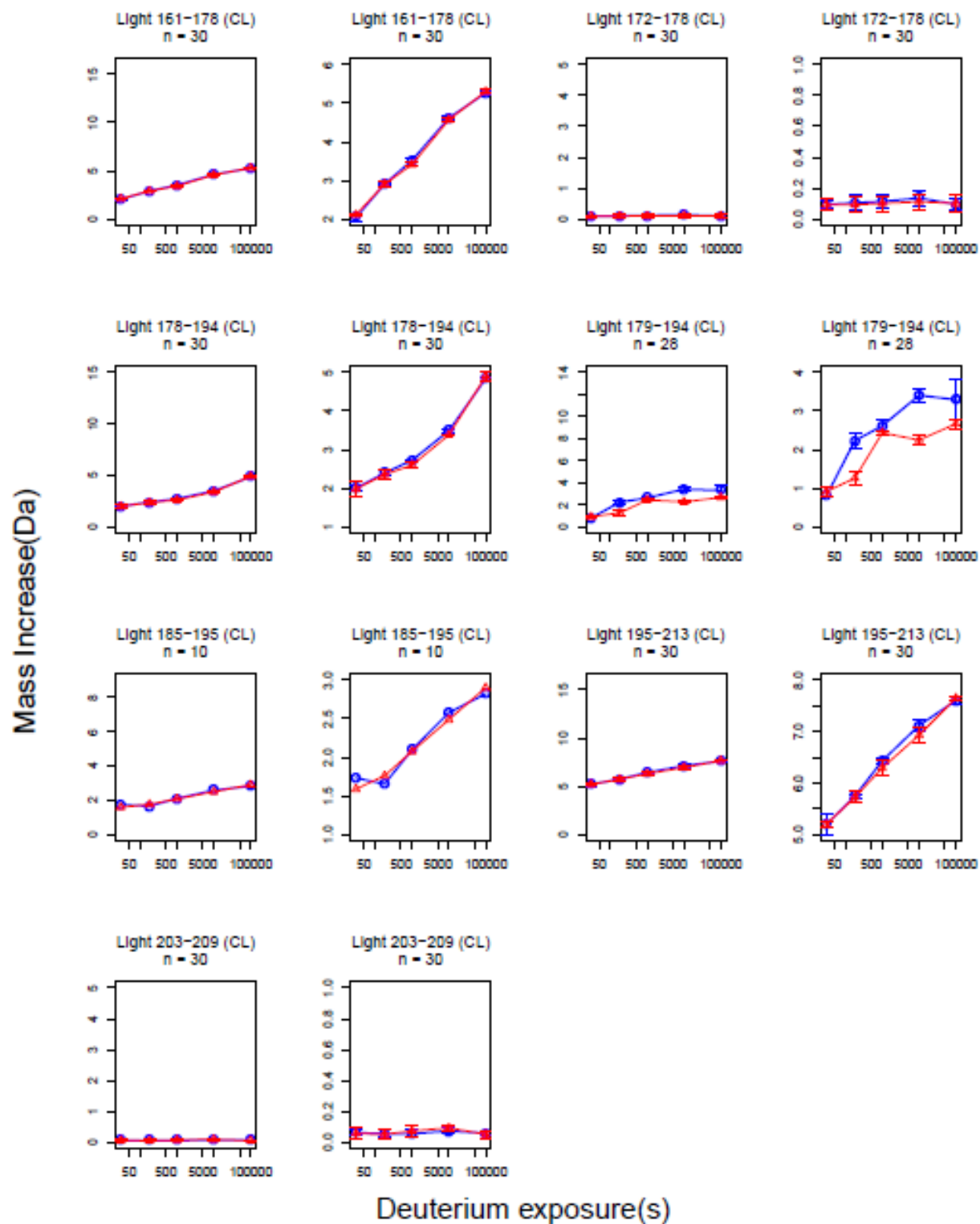
Mass Increase(Da)



Deuterium exposure(s)

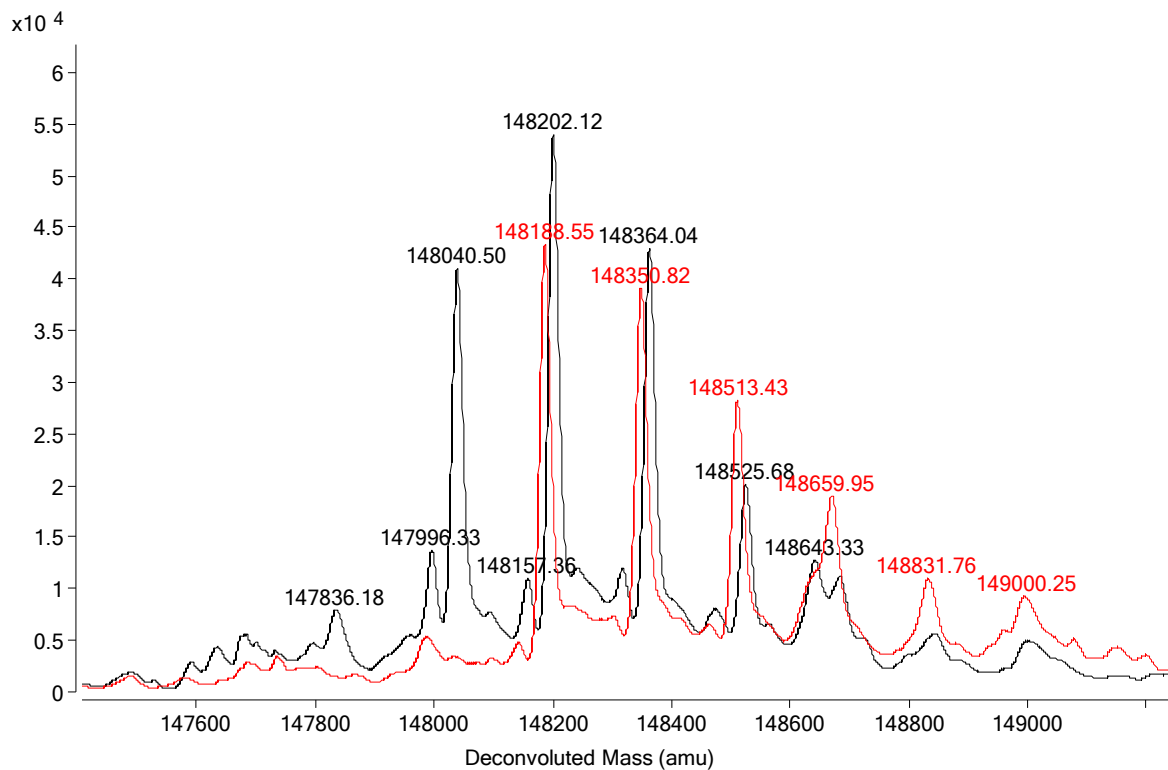
Mass Increase(Da)





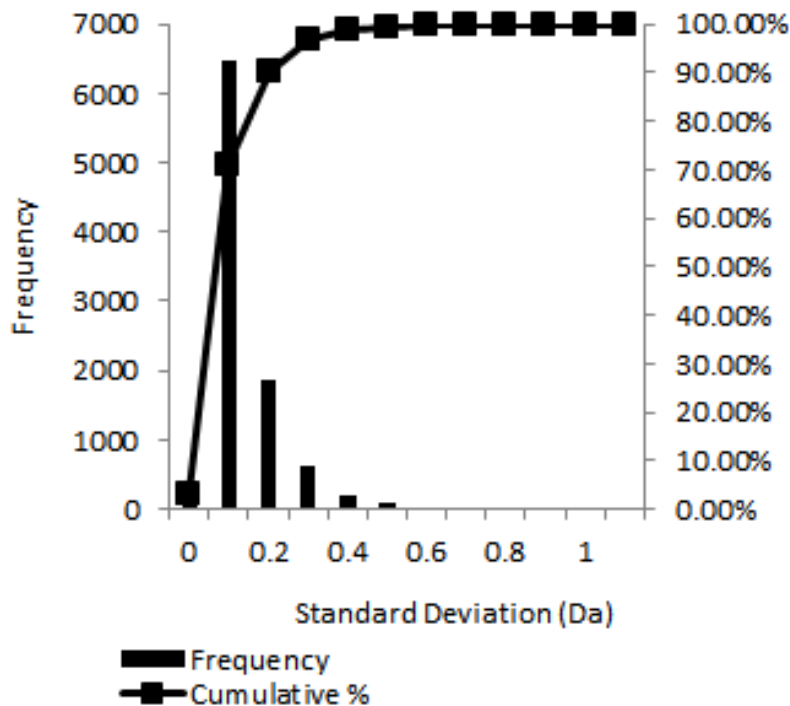
Deuterium uptake plots of 167 common segments between mAb-A and mAb-E at pH 7.4.

Figure 5.S4



Overlaid mass spectra of the two intact mAbs. The black and red traces correspond to mAb-A and mAb-E respectively. Both the mAbs were incubated with carboxypeptidase B for two hours at room temperature prior to injection into the mass spectrometer. The difference in mass between the two mAbs as seen in the figure is due to the YTE mutations. Possible glycosylation profiles for both mAbs corresponding to the mass values detected are shown in Table 5.S2.

Figure 5.S5



Reproducibility of H/D-MS data from our experimental setup as measured from standard deviations for the mass increase across all time points and peptides of mAb-B (chapters 3 and 4) and mAb-A (chapter 5) from triplicate experiments (run on different days, months and year, N = 9580). The 99th percentile for standard deviations was 0.42 Da.

Chapter 6

Conclusion and future work

6.1 Overview

Monoclonal antibodies (mAbs) and related antibody-based drugs are the largest class of biopharmaceuticals in clinical development. These protein drugs experience various types of stress during production, processing, shipping and administration and hence are susceptible to physical instability ranging from conformational instability, aggregation, low solubility and precipitation. Changes in stability of mAbs due to particular types of stress are generally monitored by long-term (18-24 months), accelerated and stressed stability studies. Approaches to predict the long-term storage stability of proteins have relied on integration of large amounts of short term stability data with some success but with certain limitations.¹ Recent work has shown that structural dynamics of mAbs are important for maintaining their stability.²⁻⁵ Hence changes in dynamics may potentially serve as indicators for changes in long term storage stability of mAbs. Furthermore, excipients may differentially alter the structural dynamics and physical stability of mAbs, as was shown with two different mAbs from the same IgG1 subclass in presence of excipients.^{6,7} However, the relation between dynamics and stability of proteins is complex,³ and not all changes in dynamics will correspond to changes in stability for all mAbs.

This dissertation explored potential mechanisms of changes in physical stability of IgG1 mAbs by examining changes in local backbone dynamics of IgG1 mAbs and correlating the results to physical stability changes. Changes in protein physical stability were monitored by biophysical techniques such as differential scanning calorimetry (DSC) and aggregation measuring techniques such as size exclusion chromatography (SEC). Changes in protein backbone dynamics were monitored by hydrogen-deuterium exchange mass spectrometry (H/D-MS).

6.2 Chapter summaries and future work

6.2.1 Chapter 2

As part of initial H/D-MS method development work for an IgG1 mAb, significant amounts of carry-over were observed. Here carry-over indicated elution of peptides in subsequent blank LC-MS injections after the mAb sample injection. Carry-over arises due to the large number of peptides generated by online pepsin digestion of the mAb that are rapidly separated (~ 5 min) at low pH (~ 2.5) and 0 °C prior to mass analyses. Carry-over is particularly problematic due to back-exchange of deuterated peptides which, when elute during subsequent sample injections, give rise to bimodal isotopic distribution, falsely indicating EX1 kinetics.⁸ We identified the online pepsin digestion step as the major source of carry-over. An online wash protocol consisting of subsequent injections of two wash cocktails was designed that significantly reduced carry-over, but at the same time, did not harm the enzymatic activity of the protease. Analysis of the physicochemical properties such as mass, pI, hydrophobicity, and MS response could not distinguish between carried-over and non-carried over peptides.

Other acidic proteases⁹ may also give rise to carry-over during H/D-MS experiments if immobilized on a column. Hence similar studies as described in this chapter may be required to explore carry-over in other protease columns for H/D-MS. Moreover, it will be interesting to explore if other IgG1 mAbs and other classes of IgG mAbs (IgG 2 or IgG4) are also prone to carry-over problems during typical H/D-MS experiments.

6.2.2 Chapter 3

This chapter explores the effects of two excipients (arginine and sucrose) on the thermal stability (T_{onset} and T_m by DSC), aggregation propensity under accelerated as well as long-term storage conditions (SEC), and local backbone dynamics (H/D-MS) of an IgG1 mAb. Changes in

physical stability were then compared with changes in dynamics of local segments of the mAb. Sucrose increased the thermal stability of the mAb, decreased mAb monomer loss, and caused a global trend of small decreases in backbone dynamics. Although most of the decreases in backbone dynamics were less than significant, these overall trends are consistent with earlier observations on the preferential hydration mechanism of sucrose induced stabilization of proteins.¹⁰ Arginine decreased the thermal stability of the mAb most notably for the C_{H2} domain, accelerated the loss of mAb monomer and formation of soluble and insoluble aggregates during storage at elevated temperature, and increased backbone dynamics of few specific segments of the mAb most notably in the C_{H2} domain. Results from Chapter 4 below also showed physical destabilization of the same IgG1 mAb as well as significantly increased dynamics of specific segments (241-252 and 300-306) in the C_{H2} domain caused by sodium thiocyanate. Hence, decreased conformational stability of the C_{H2} domain in presence of arginine correlated with increased dynamics of a specific aggregation hotspot segment, 241-252 of the heavy chain in the C_{H2} domain of the mAb. However, sucrose had no effect on the dynamics of this segment of the C_{H2} domain. These results indicate that change in dynamics of specific sequences in the C_{H2} domain of a mAb induced by destabilizing excipients may dictate its overall physical stability of at least some percentage of IgG1 mAbs.

Arginine is generally included in protein formulations to improve efficiency of protein refolding and to decrease aggregation.^{11,12} Although in this study, arginine caused increased aggregation of the mAb stored at a high temperature, it will be interesting to explore arginine effects on a mAb due to other forms of stress such as agitation, freeze-thaw, etc. It will also be interesting to confirm if arginine cause similar effects in terms of changes in dynamics and stability of the constant domains in other IgG1 mAbs under heat stress.

No significant changes were observed in local dynamics of the IgG1 mAb at three different concentrations (0.5, 1.0, and 1.35 M) of arginine and sucrose compared to a 0.1 M sodium chloride control as described in chapters 3 and 4. It will be interesting to repeat this experiment with arginine and sucrose concentration in the 0 - 0.5 M concentration range, to explore if the results are similar or different than what are discussed in Chapter 3.

Experiments to explore the effects of a wide variety of additives, selected from the different classes of pharmaceutical excipients, on the local dynamics of key segments in the C_{H2} domain and the variable domains including the CDR motifs, of an IgG1 mAb using pulsed H/D exchange mass spectrometry experiments (at one or two exchange times in a high throughput fashion) is in progress in the laboratory. The results will be compared with changes in conformational stability, aggregation propensity and types of aggregates formed under identical formulation conditions. Such experiments can potentially indicate if H/D-MS can be used a predictive tool in a high throughput manner to screen for stabilizing excipients for specific mAbs.

This work explored changes in only the physical stability of the mAb. However, mAbs are also known to degrade due to various different types of chemical degradation pathways. Hence, changes in chemical stability of monoclonal antibodies may be explored upon long-term storage and/or stressed conditions in a variety of excipient and salt containing liquid formulations. The observed changes in chemical stability of specific amino acid residues may be compared with changes in local dynamics of the same residues within the intact mAb using H/D-MS in the same formulation conditions. This future work may help better explain and understand the inter-relationships between changes in protein higher order structure and protein instability from a local dynamics, chemical and physical stability perspective.

6.2.3 Chapter 4

This chapter explores the effects of three sodium salts from the Hofmeister series (sulfate, chloride, and thiocyanate) on the physical stability and backbone dynamics of an IgG1 mAb. Physical stability of the mAb was tested in formulations containing 0.5 M of the different salts. Sulfate increased the thermal stability of the mAb as measured by DSC, decreased mAb monomer loss, and increased local dynamics of several segments in the F_{ab} and the C_H3 domain compared to 0.1 M sodium chloride control. In comparison to the control, 0.5 M chloride caused similar changes in physical stability, and small, uniform decreases in dynamics across all segments of the mAb. The small decreases in dynamics in presence of 0.5 M sodium chloride were not statistically significant, but showed a global trend similar to what was observed with sucrose as described above. In contrast, thiocyanate decreased the thermal stability of the mAb, accelerated mAb monomer loss, resulted in formation of insoluble aggregates, and increased local dynamics of multiple segments across all domains of the mAb. Effects of thiocyanate were most pronounced on the C_H2 domain. Thiocyanate decreased the thermal unfolding transition temperature of the C_H2 domain by 9 °C, and caused the highest increases in dynamics in two segments HC 241-252 and HC 300-306 of the C_H2 domain. As discussed in Chapter 3, physical destabilization of the IgG1 mAb induced by arginine correlated with increased dynamics of the 241-252 segment of the heavy chain in the C_H2 domain. Hence, thiocyanate induced destabilization of the IgG1 mAb correlated with increased dynamics of the same apolar segment HC 241-252, further supporting that this segment may act as a hotspot initiating aggregation events in this IgG1 mAb. On the contrary, sulfate induced changes in local dynamics had no similarities with changes in dynamics observed in presence of sucrose as outlined in Chapter 3. Moreover, sulfate and thiocyanate increased the backbone dynamics of several common

segments in the F_{ab} and C_{H3} domains. Such observations further highlight the complex interrelationships between stability and dynamics of proteins.³

These results indicate that dynamics of specific segments may dictate overall physical stability of a multi-domain protein such as a mAb. Correlation between physical stability of the mAb and dynamics for specific segments may not only help to better understand how salts may destabilize proteins, but may help predict changes in long-term stability induced by various salts depending upon their effects on local dynamics of hotspot sequences.

Molecular dynamics simulations of an IgG1 mAb in presence of the different anions may provide further mechanistic insights into anion induced stability changes in mAbs and thus could complement the experimental results from H/D-MS experiments as discussed in this work. Moreover, anion induced effects on the dynamics and stability of other IgG1 mAbs as well as other subclasses of mAbs (IgG2, and IgG4) may further unravel the universality of sequence specificity of aggregation hotspots across different mAbs.

6.2.4 Chapter 5

YTE mutations (S255Y/S257T/T259E) in the C_{H2} domain of an IgG1 mAb have been shown previously to increase in-vivo half-life by 4 fold, FcRn binding by 10 fold, and tissue bioavailability by 4 fold in non-human primates,¹³ but marginally decreased the physical stability of the mAb.¹⁴ This chapter explored the nature of relative differences in physical stability between an IgG1 mAb and its YTE mutant by examining changes in thermal stability by DSC, changes in aggregation propensity under accelerated conditions measured by SEC, and changes in backbone dynamics measured by H/D-MS at pH 6.0 and 7.4. The YTE mutation decreased the thermal unfolding temperature of the C_{H2} domain only, and increased aggregation propensity of

the mAb when tested under accelerated storage conditions. The YTE mutation induced changes in backbone dynamics at few local segments away from the mutation sites as well as away from the FcRn binding sites. The highest magnitude of increase in local backbone dynamics was detected for the 244-255 segment of the heavy chain in the C_H2 domain. Increased dynamics of this particular segment has been shown to correlate with arginine and thiocyanate induced destabilization of an IgG1 mAb in Chapters 3 and 4 respectively of this thesis, as well as destabilization of IgG1 mAbs due to deglycosylation,¹⁵ and methionine oxidation¹⁶⁻¹⁸. In this study, increased dynamics of the 244-255 segment in the C_H2 domain correlates with decreased thermal stability of the C_H2 domain, and higher aggregation propensity induced by the YTE mutation. Hence this study provides mechanistic insights on the physical destabilization of an IgG1 mAb due to YTE mutations.

The results from this chapter as well as Chapters 3 and 4 suggest that the possible mechanism for changes in physical stability of the mAbs examined in this thesis is by disruption in packing of the heterogeneous glycan structures within a key hydrophobic segment in the C_H2 domain of the mAb. As a continuation of this research, the nature of interactions between glycan chains and segments of the C_H2 domain can be explored to gain more mechanistic insights into changes in physical stability of mAbs. To serve this purpose, Fc proteins with well-defined homogenous glycan structures are being produced in various ways by enzymatic treatments. The changes in local dynamics due to changes in glycan structures can then be explored using H/D exchange mass spectrometry and compared to changes in physical stability of the Fc glycoproteins. This approach is currently being tested in our laboratory.

6.2.5 References

1. Maddux NR, Iyer V, Cheng W, Youssef AM, Joshi SB, Volkin DB, Ralston JP, Winter G, Middaugh CR 2014. High throughput prediction of the long-term stability of pharmaceutical macromolecules from short-term multi-instrument spectroscopic data. *J Pharm Sci* 103(3):828-839.
2. Kamerzell TJ, Middaugh CR 2007. Two-Dimensional Correlation Spectroscopy Reveals Coupled Immunoglobulin Regions of Differential Flexibility that Influence Stability. *Biochemistry* 46(34):9762-9773.
3. Kamerzell TJ, Middaugh CR 2008. The complex inter-relationships between protein flexibility and stability. *J Pharm Sci* 97(9):3494-3517.
4. Kamerzell TJ, Ramsey JD, Middaugh CR 2008. Immunoglobulin Dynamics, Conformational Fluctuations, and Nonlinear Elasticity and Their Effects on Stability. *The Journal of Physical Chemistry B* 112(10):3240-3250.
5. Ramsey JD, Gill ML, Kamerzell TJ, Price ES, Joshi SB, Bishop SM, Oliver CN, Middaugh CR 2009. Using empirical phase diagrams to understand the role of intramolecular dynamics in immunoglobulin G stability. *J Pharm Sci* 98(7):2432-2447.
6. Thakkar SV, Joshi SB, Jones ME, Sathish HA, Bishop SM, Volkin DB, Middaugh CR 2012. Excipients differentially influence the conformational stability and pretransition dynamics of two IgG1 monoclonal antibodies. *J Pharm Sci* 101(9):3062-3077.
7. Thakkar SV, Kim JH, Samra HS, Sathish HA, Bishop SM, Joshi SB, Volkin DB, Middaugh CR 2012. Local dynamics and their alteration by excipients modulate the global conformational stability of an IgG1 monoclonal antibody. *J Pharm Sci* 101(12):4444-4457.

8. Fang J, Rand KD, Beuning PJ, Engen JR 2011. False EX1 signatures caused by sample carryover during HX MS analyses. *Int J Mass Spectrom* 302(1-3):19-25.
9. Kadek A, Mrazek H, Halada P, Rey M, Schriemer DC, Man P 2014. Aspartic protease nepenthesin-1 as a tool for digestion in hydrogen/deuterium exchange mass spectrometry. *Anal Chem* 86(9):4287-4294.
10. Arakawa T, Timasheff SN 1982. Stabilization of protein structure by sugars. *Biochemistry* 21(25):6536-6544.
11. Arakawa T, Tsumoto K 2003. The effects of arginine on refolding of aggregated proteins: not facilitate refolding, but suppress aggregation. *Biochem Biophys Res Commun* 304(1):148-152.
12. Lange C, Rudolph R 2009. Suppression of protein aggregation by L-arginine. *Curr Pharm Biotechnol* 10(4):408-414.
13. Oganessian V, Damschroder MM, Woods RM, Cook KE, Wu H, Dall'Acqua WF 2009. Structural characterization of a human Fc fragment engineered for extended serum half-life. *Mol Immunol* 46(8-9):1750-1755.
14. Tavakoli-Keshe R, Phillips JJ, Turner R, Bracewell DG 2014. Understanding the relationship between biotherapeutic protein stability and solid-liquid interfacial shear in constant region mutants of IgG1 and IgG4. *J Pharm Sci* 103(2):437-444.
15. Houde D, Arndt J, Domeier W, Berkowitz S, Engen JR 2009. Characterization of IgG1 Conformation and Conformational Dynamics by Hydrogen/Deuterium Exchange Mass Spectrometry. *Anal Chem* 81(7):2644-2651.

16. Burkitt W, Domann P, O'Connor G 2010. Conformational changes in oxidatively stressed monoclonal antibodies studied by hydrogen exchange mass spectrometry. *Protein Sci* 19(4):826-835.
17. Houde D, Peng Y, Berkowitz SA, Engen JR 2010. Post-translational Modifications Differentially Affect IgG1 Conformation and Receptor Binding. *Molecular & Cellular Proteomics* 9(8):1716-1728.
18. Zhang A, Hu P, MacGregor P, Xue Y, Fan H, Suchecki P, Olszewski L, Liu A 2014. Understanding the conformational impact of chemical modifications on monoclonal antibodies with diverse sequence variation using hydrogen/deuterium exchange mass spectrometry and structural modeling. *Anal Chem* 86(7):3468-3475.